Understanding the molecular determinants of IFITM resistance in viral entry glycoproteins

Winstone, Helena

Awarding institution:
King's College London

Understanding the molecular determinants of IFITM resistance in viral entry glycoproteins

Helena Winstone

A thesis submitted to the University of London for the degree of Doctor of Philosophy

Department of Infectious Disease
King's College London
Faculty of Life Sciences & Medicine
School of Immunology & Microbial Sciences

Declaration

I, Helena Winstone, confirm that the work presented in my thesis is my own. Where information has been derived from other sources, I confirm that this has been indicated in the thesis.

Helena Winstone

London, 03 October 2022

Abstract

Severe acute respiratory syndrome coronavirus 2 (SARS-CoV-2) and human immunodeficiency virus 1 (HIV-1) are enveloped viruses that mediate viral entry via class I fusion glycoproteins. Both of these viruses demonstrate significant sequence variability in their entry glycoproteins, a result of adaptation to escape both adaptive and innate immunity intra-host. Interferon-Induced TransMembrane (IFITM) proteins are antiviral proteins that inhibit viral entry and previous reports demonstrate varying IFITM sensitivity in coronaviruses. HIV-1 has also been reported to be varyingly susceptible to IFITM-mediated inhibition in an isolate-dependent manner.

This thesis evaluates the IFITM sensitivity of the ancestral Wuhan SARS-CoV-2 virus and SARS-CoV-2 variants of concern (VOCs) that emerged between 2020 and 2022. We found that the Wuhan SARS-CoV-2 was IFITM2-sensitive in the A549-ACE2 system, however this can be overcome by overexpression of TMPRSS2. Deletion of the polybasic cleavage site of spike renders Wuhan SARS-CoV-2 pseudotyped lentiviral vectors even more IFITM2 sensitive, which cannot be rescued by TMPRSS2 overexpression, demonstrating that the polybasic cleavage site of SARS-CoV-2 spike can modulate IFITM2 sensitivity. The IFITM sensitivity of D614G, alpha, beta, gamma, kappa, delta, and omicron (BA.1 and BA.2) variants was also investigated. Strikingly, the alpha variant was resistant to IFITMs in TMPRSS2-negative cells which contributes a significant component of the resistance of the alpha virus to IFNβ. Additionally, we show here that the P681H mutation in alpha is a major determinant of both IFITM and IFNβ resistance.

We also investigated the IFITM sensitivity of 24 CCR5-tropic HIV-1 Envelopes isolated from a single anti-retroviral therapy negative patient over nine years of infection in order to define the determinants of IFITM sensitivity and resistance of Env. Transmitted/founder (T/F) viruses, and viruses which emerge following ART interruption, have previously been reported to be more resistant to both IFITMs and type I IFN. Here, it is shown that sensitivity to both IFITMs and IFNα fluctuate over the course of infection and isolates present at the same timepoint exhibit differing sensitivity to IFITMs and IFNα. By utilising a pair of Envs that are the most related but

differentially sensitive to IFITM3, the determinant of IFITM sensitivity/resistance of both Envs was traced to the V1/V2 loop.

Overall, this piece of work highlights the complexity of the relationship between viral entry and IFITM sensitivity. The data presented here demonstrate that although different regions of spike and Env can alter IFITM sensitivity, there are also commonalties in the relationships between two unrelated viruses and IFITM-mediated restriction. The priming cleavage of both HIV-1 Env and SARS-CoV-2 spike can impact IFITM sensitivity. Additionally, the cytoplasmic tail of spike and Env appears to play a role in restriction by IFITM2, and also in enhancement of entry by IFITM3. Altogether, IFITM sensitivity of unrelated viral entry proteins can be governed by both similar and distinct mechanisms.

Acknowledgements

Firstly, I would like to thank my supervisor **Stuart "the trouble is…" Neil** for his support, advice, mentorship, motivation, knowledge, and humour over the course of my PhD. You may have been right at least once. Genuinely, thank you for your guidance, good humour, and encouragement. You have supported me through the good and less good times of my PhD, and I am very thankful for it.

I would like to thank my second supervisor **Katie Doores** for her advice, support and corridor chats, and my Thesis Committee **Juan Martin-Serrano, Maddy Parsons** and **Sergi Padilla Parra** for their advice and guidance. Thank you to the technical support **Terry, Rose**, and **Ian** for making things in the department work while still having time for a laugh and a chat.

Thank you to the "SwanGaNeil" lab past and present: **Pedro Matos, Claire Kerridge, Max Handley, Franka Debeljak, Kristina Schierhorn, Dorota Kmiec, Suzy Pickering, Harry Wilson, Alisha Reid, Piotr Kwiatkowski, Clement Bouton, Enrico Bravo, Thomas Courty, Marianne Perera,** and last but certainly not least, a big thank you to my lab wife **María José Lista Brotos** (désolé Flo, elle est à moi). Thank you also to **Rui Pedro Galao** and **Chad Swanson.** Thank you all for the advice, laughs, beers, snacks, and just being lovely.

Thank you to my friends who have provided distraction from the lab over the last few years: Thank you **Ruth, MaJo,** and **Alisha** for beer, bread, and gym-based stress relief (and thanks **Ruth** for keeping me relatively sane during lockdown). Thank you **Chloe, Georgia, Jaz, Emma, Katie, Henry, Pete** and **Adrian** for the many pints, jokes about microlitres, and for getting sympathetically outraged at Western blots/the CL3/whatever was not working that day. **Adam,** thank you for your remarkably unwavering support and being there for me throughout the most stressful part of the PhD. And for ensuring I didn't die of malnutrition.

And lastly, a big thank you to my family. Thank you to my parents **Nikki** and **Graham**, for their continually amazing support and endless supply of advice, humour, food, and gin. Thank you to my siblings **Rowena** and **George** for the pints, laughs, gigs, and the lectures I didn't subscribe to (and yes George, I have written my thesis now).

PS – thank you to my GCSE biology teacher, for telling me I wasn't very good at biology and consequently fuelling me with enough spite to do a PhD in the first place.

Table of Contents

Abbreviations

ACE2 angiotensin converting enzyme 2

ADAM	a disintegrin and metalloproteinase
ADCC	antibody dependent cellular toxicity
AIDS	acquired immunodeficiency syndrome
ART	anti retroviral therapy
CA	capsid
CD4	cluster of differentiation 4
CH25H	cholesterol 25 hydroxylase
CIL	intracellular loop
COPI	coatomer protein I
CPE	cytopathic effect
CSXW	firefly luciferase expressing vector
CTD	C-terminal domain
CT	cytoplasmic tail
DMEM	Dulbecco's modified eagle medium
DMV	double membrane vesicle
ER	endoplasmic reticulum
ERGIC	endoplasmic reticulum Golgi intermediate compartment
ERRS	endoplasmic reticulum retention signal
ESCRT	endosomal sorting complex required for transport
FP	fusion peptide
GBP	guanylate binding protein
GD	Guangdong
gp	glycoprotein
HIV	human immunodeficiency virus
HPV	human papilloma virus
HR	heptad repeat
IAV	Influenza A virus
IC50	inhibitory concentration to achieve 50% reduction
IFITM	interferon-induced transmembrane protein
IDT	integrated DNA technologies
IFN	interferon
IN	integrase
ISG	interferon induced gene
ISRE	interferon-stimulated response element

LRA	latency reversing agents
LTR	long terminal repeat
LY6E	lymphocyte antigen 6 complex, locus E
MA	matrix
MLV	murine leukemia virus
MMP	matrix metalloproteinase
MSM	men who have sex with men
NC	nucleocapsid
Nef	negative factor
NEB	New England biolabs
Nsp	non-structural protein
NTD	N-terminal domain
ORF	open reading frame
PAMP	pathogen associated molecular patterns
PDB	protein data base
PLV	pseudotyped lentiviral vector
PNG	potential glycosylation site
PR	protease
PRR	pattern recognition receptor
RBD	receptor binding domain
Rev	RNA splicing regulator
RLU	relative luminescence units
rSAP	shrimp alkaline phosphatase
RSV	respiratory syncytial virus
RT	reverse transcriptase
RTC	replication and transcription complex
SARS-CoV	severe acute respiratory syndrome coronavirus
SERINC	serine incorporator
SIV	simian immunodeficiency virus
SPARTAC	short pulse anti-retroviral therapy at seroconversion
SNP	single nucleotide polymorphism
Tat	transactivator protein
T/F	transmitted/founder
TLR	toll-like receptor

TM	transmembrane
TMPRSS2	transmembrane protease serine 2
TRS	transcription regulatory sequence
VAPA	vesicle-associated protein associated protein A
vATPase	vaculoar ATPase
VLP	virus like particle
VOC	variant of concern
Vif	viral infectivity factor
Vpr	viral protein r
Vpu	viral protein u
VSV	vesicular stomatisis virus
WHO	world health organization
YFV	yellow fever virus
ZMPSTE24	zinc metallopeptidase STE24

Table of figures

Table of tables

Chapter 1: Introduction

1.1 Enveloped viral entry

Viruses are obligate parasites that infect host cells to hijack aspects of their biology in order to replicate. The first step of viral infection is traversal of the cell membrane. For viruses with a lipid bilayer surrounding the viral capsid or genome (enveloped viruses), this involves correctly timing the activation of viral proteins that mediate fusion of the cellular and viral membranes, thereby permitting the viral capsid to enter the cytoplasm. This is a complex process that for enveloped viruses involves non-specific membrane attachment, host receptor recognition, and the release of the viral fusion peptide (Figure 1.1). For class I fusion glycoproteins, this also involves receptor binding induced changes to conformation, proteolytic cleavage or pH-dependent conformational changes in order to prime and trigger the viral entry protein, allowing the transition from a metastable state into a lower energy, post-fusion conformation [1]. Due to the need to regulate the triggering of viral entry proteins such that this does not occur prematurely, the activation of these proteins is intrinsically linked to host factors at the cell membrane such as cleavage by certain proteases or acidic pH.

The fusion of the viral and cell membranes can either occur directly at the plasma membrane at neutral pH, or later in endosomal compartments following endocytic uptake in either a pH-dependent or independent manner (Figure 1.2). The plasma membrane is not a homogenous landscape, and the concentration of attachment factors and receptors required for viral entry on lipid rafts has been implicated as a factor that assists entry for some viral families [2]. The kinetics of viral entry vary enormously between different viral families, with the fusion of influenza virus occurring in less than a minute once it has reached the required pH and the fusion of human immunodeficiency virus 1 (HIV-1) taking up to 15 minutes [3, 4]. As well as viral entry occurring through infection by cell free virions, several viruses can enter neighbouring cells via “cell to cell” transmission through tight cellular junctions, thereby reducing the risk of inhibition by humoral immunity in the extracellular space [5]. The viral entry protein of enveloped viruses is usually the main target of neutralising antibodies in the host and therefore it is not only important to mediate the viral entry step itself, but also to escape humoral immunity. In addition to antibody escape, there are a plethora of

steady state and interferon (IFN) -induced antiviral proteins that can inhibit viral entry [6]. The poor proofreading capacity of many viral polymerases can result in mutations that may be either beneficial or detrimental to viral fitness [7]. Beneficial mutations that improve viral entry, antibody escape, or escape from innate immunity may then become fixed and provide the virus an advantage over the host. Consequently, antibodies that bind different sites of viral glycoproteins can be produced intra-host, and over the course of many generations the innate immune system can also undergo positive selection to better restrict viral infection. In turn the virus can then adapt, and over time this cycle drives both host and viral evolution. Viral entry proteins must therefore be able to mediate the step of entry itself, escape antibody-mediated inhibition, and escape innate immunity in order to successfully infect a cell. For viruses that cause chronic infection the virus has the chance to adapt intra-host, this can give rise to multiple viral variants with differing abilities to combat these distinctive selective pressures.

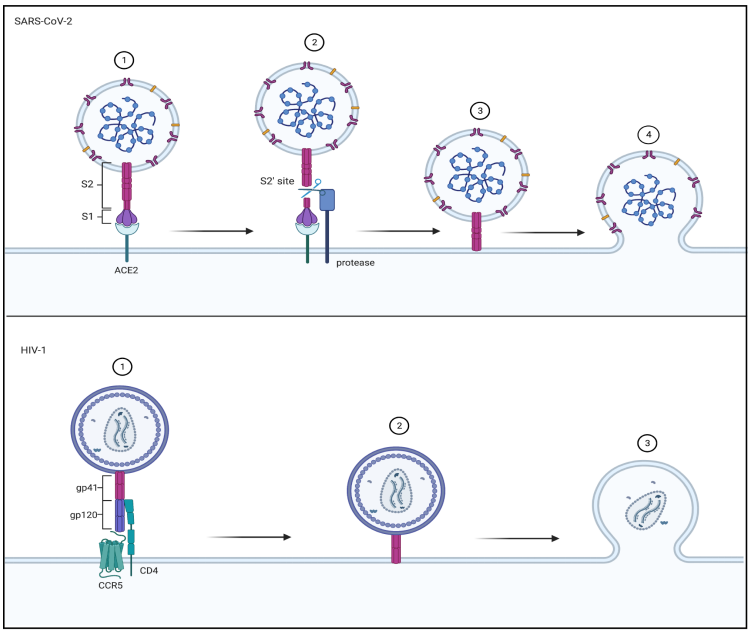

Figure 1.1. Viral entry comparison of enveloped viruses SARS-CoV-2 and HIV-1. A) SARS-CoV-2 binds to its receptor ACE2 and is cleaved by a protease on the target cell at the S2' site to trigger the release of the fusion peptide (1) and (2). The fusion peptide inserts into the membrane and brings the membranes closer together (3), finally permitting fusion of the cellular and viral membranes (4). B) HIV-1 binds to its receptor CD4 and is stabilised by either CCR5 or CXCR4. This allows conformational changes which expose the fusion peptide, and this is inserted into the cell membrane (2). This brings the membranes closer together until the viral and cellular membranes can fuse (3). Figure created in BioRender.

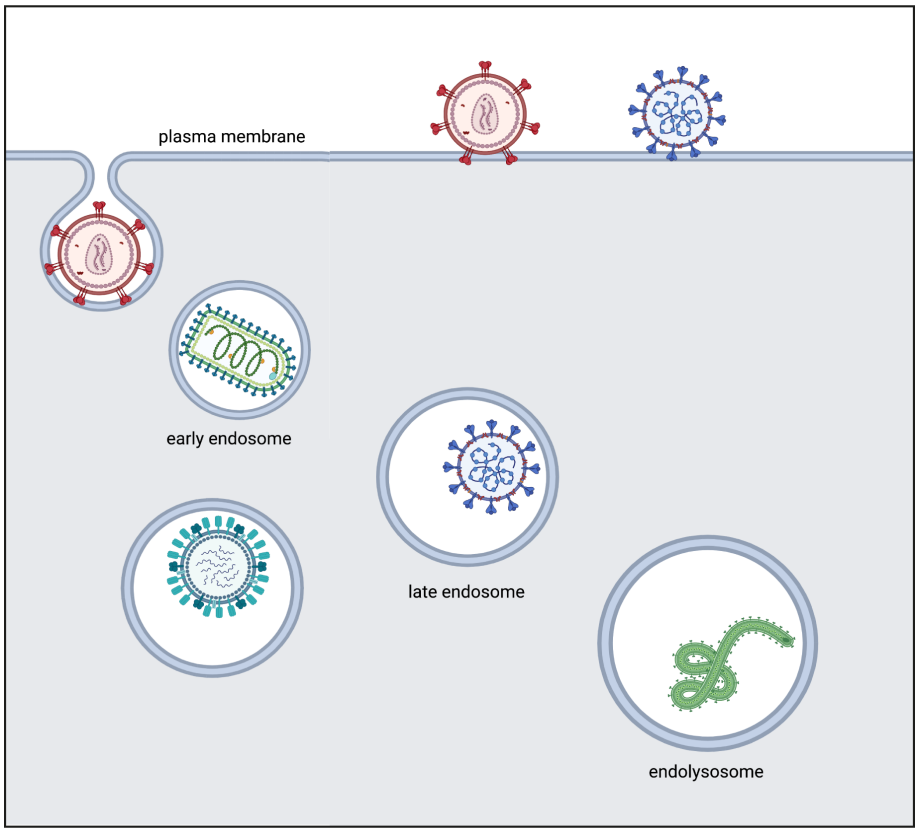

Figure 1.2. Viruses fuse in different subcellular compartments. Some viruses can fuse directly at the plasma membrane in a pH-independent manner, including HIV-1 and SARS-CoV-2. Viruses can also be endocytosed and fuse at various stages of the endocytic pathway. VSV-G does not require a very low pH to fuse and therefore fuses in early endosomes. Influenza requires a low pH, and subsequently fuses in late endosomes. SARS-CoV-2 can also fuse in endosomal compartments depending on protease bioavailability. Ebola, which requires a very low pH in order to mediate membrane fusion, fuses in endolysosomes. Figure created in BioRender.

1.1.1 Priming of type I fusion protein viral entry

The crux of enveloped viral entry is the exposure of the hydrophobic fusion peptide of the entry protein which can be achieved through several common mechanisms. The priming requirements for enveloped viral entry vary; some require protease-mediated cleavage, pH changes, or both. In essence, either proteolytic cleavage or pH changes result in the release of the hydrophobic fusion peptide, which can interact with the host membrane and ultimately bring the cellular and viral membranes together to form a fusion pore and permit the entry of the viral capsid or genome [8]. All class I fusion glycoproteins have a fusion protein primarily comprised of alpha helices and require proteolytic cleavage to prime the glycoprotein for entry [1]. This can be achieved during viral replication in the producer cell, by proteases in the extracellular matrix, or in the

target cell either by proteases on the plasma membrane surface or in endosomes. Common proteases that mediate the cleavage of class I fusion glycoproteins include furin, which can prime some influenza strains, HIV-1 and severe acute respiratory syndrome virus 2 (SARS-CoV-2), trypsin, which cleaves the HA of influenza and coronavirus spikes, and cathepsins, which can also prime coronavirus spikes and the filovirus glycoprotein [1].

Differences in priming can be linked to pathogenicity and transmissibility. Most strains of influenza are usually cleaved by trypsin-like proteases in the extracellular matrix. However, more pathogenic strains of influenza such as the H5N1 strain have mutations that enable cleavage by furin-like proteases in the Golgi [9]. Additionally, a key difference between the spikes of SARS-CoV-1 and SARS-CoV-2 is the presence of four amino acids at the S1/S2 cleavage site in SARS-CoV-2. These amino acids permit spike to be cleaved by furin-like proteases in the producer cell rather than this priming step being limited to only serine proteases and cathepsins in the target cell. This difference in priming is suggested to be a major reason why SARS-CoV-2 is more transmissible than SARS-CoV-1 and why it displays different cellular tropism in the host [10]. The purpose of the priming step is to separate the glycoprotein into a receptor binding subunit and a subunit that contains the fusion peptide that remains associated through non-covalent interactions. This priming essentially converts the glycoprotein into a fusion-competent state, during which it can be triggered to expose the hydrophobic fusion peptide, therefore mediating membrane fusion. Triggering can occur through receptor binding, a second protease cleavage event, low pH, or a combination of these factors [1].

1.1.2 Triggering of class I fusion glycoprotein viral entry

The triggering of viral entry proteins exposes the fusion peptide such that it can penetrate the host cell membrane and begin the process of membrane fusion. For some enveloped viruses, for example HIV-1, binding of receptors such as CD4 and the coreceptors CCR5/CXCR4 is sufficient to trigger conformational changes of the glycoprotein Env that expose the fusion peptide, therefore triggering membrane fusion [11]. This allows HIV-1 to fuse directly at the plasma membrane at neutral pH, although

it has also been observed that HIV-1 can fuse in endosomal compartments in certain cell-types in a pH-independent manner [12, 13]. The immense diversity in HIV-1 across strains, and intra-host, may mean that there are Env-dependent differences in viral entry that require further investigation with physiologically relevant strains. For other enveloped viruses, receptor binding is needed in conjunction with low pH, proteolytic cleavage, or a combination of the two. Enveloped viruses that require a relatively high pH such as VSV, can fuse in early endosomes [14], unlike influenza, which requires a lower pH to trigger exposure of the HA protein fusion peptide, and therefore needs to fuse in late endosomes [15]. The triggering of filovirus entry has been found to require a lower pH than that of influenza, and therefore fusion occurs in endolysosomes (Figure 1.2). The triggering of the Ebola glycoprotein requires both receptor binding and cathepsin mediated cleavage [16, 17]. Coronaviruses, including SARS-CoV-2, require a second proteolytic cleavage in the S2 subunit to release the fusion peptide [18]. This can be mediated by either serine proteases on the plasma membrane, or cathepsins in endosomes, dependent on the relative availability of these pathways in the cell [10].

While some viruses require low pH for membrane fusion, others can enter in either a pH-dependent or independent manner. SARS-CoV-1 and SARS-CoV-2 can enter cells in either a pH dependent or independent manner, depending on the bioavailability of serine proteases at the surface or cathepsins in endosomal compartments. It has however recently been shown that although SARS-CoV-2 can fuse at the plasma membrane, a majority of fusion events appear to take place in endosomes, dependent on acidic pH [19]. This suggests there may be more of a pH dependency for SARS-CoV-2 viral entry than previously thought. Ultimately, the site of endosomal fusion depends on the availability of the proteases or pH required for entry.

1.1.3 Membrane fusion

Upon completion of priming and triggering, the steps of membrane fusion are essentially identical for enveloped viruses containing a class I fusion glycoprotein (Figure 1.3). Triggering, whether that be through receptor binding, proteolytic cleavage, or low pH, results in the exposure of the fusion peptide. An extended

intermediate complex is then formed whereby the fusion peptide inserts into the cell membrane, known as the pre-hairpin. This is followed by the collapse of this extended intermediate, caused by a C-terminal part of the protein collapsing back on itself, forming a trimer of hairpins conformation containing a six helix bundle, bringing the membranes in close proximity. Once this collapse has proceeded to the extent that the cellular and viral membranes are close enough together, the lipids in the membranes mix and form a hemifusion stalk. Finally, the refolded trimer snaps into its post fusion conformation that prevents the fusion pore from resealing, permitting the contents of the virion to traverse into the cytoplasm and the later stages of viral infection to proceed. The postfusion conformation of class I fusion glycoproteins contains a heptad repeat derived six helix bundle core structure.

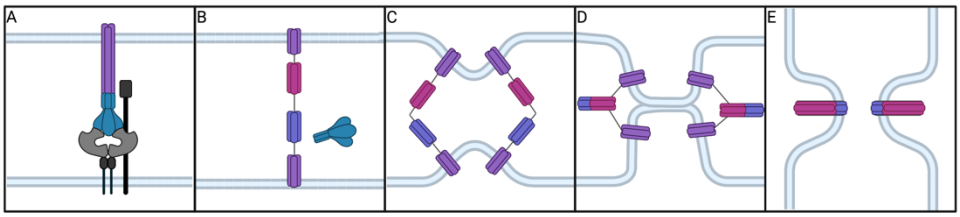

Figure 1.3. Membrane fusion of SARS-CoV-2 A) The RBD of spike engages ACE2 and the S2' site is cleaved by an available protease. B) The S1 subunit is shed and the hydrophobic fusion peptide of the S2 domain inserts itself in the cellular membrane. C) The prehairpin complex is formed where the fusion peptide brings the cellular membrane closer to the viral membrane. D) The prehairpin folds back on itself causing the helical heptad repeats to form a six helix bundle which pulls the membranes closer together, allowing hemifusion to occur E) The spike snaps into the postfusion complex and a fusion pore is formed in the membrane permitting the contents of the virion to enter the cell. Figure created in BioRender.

1.1.4 Commonalities of SARS-CoV-2 and HIV-1 entry proteins

Both SARS-CoV-2 and HIV-1 are enveloped viruses with typical class I fusion glycoproteins, namely spike and Env (Figure 1.4). These proteins share several structural similarities. The NTD of spike and the V1/V2 loop of Env are both flexible N-terminal structures that are major sites of antibody neutralisation [20, 21]. Both glycoproteins also share very similar alpha helical structures in their S2/gp41 domains with which they operate membrane fusion [22]. Both these proteins are primed by

proteolytic cleavage and mediate viral entry by transitioning from a metastable state to an intermediate state, and finally to a stable post fusion state. Both viruses have significant mutations and variations in their entry proteins that impact infectivity, antibody escape, and innate immune escape. In singular patients with chronic infection, both these viruses exhibit marked diversity and evolution in the glycoproteins. SARS-CoV-2 spike and HIV-1 Env are also heavily glycosylated [23-25]. Lastly, both glycoproteins are primed by furin in the Golgi during viral production due to the presence of multi-basic cleavage sites between the receptor binding domain and the fusion peptide-containing domains of these proteins. However, spike and Env differ in their triggering requirements for viral entry, with SARS-CoV-2 triggered by receptor binding and further target cell proteolytic cleavage, and HIV-1 triggered by receptor/co-receptor binding alone. Despite this difference, it has been documented that both of these glycoproteins are capable of fusing either directly at the plasma membrane, or in endosomal compartments [10, 12, 13, 26]. Finally, both of these viruses demonstrate glycoprotein-dependent differences across variants in their sensitivity to interferon and interferon-induced genes (ISGs) [27-30].

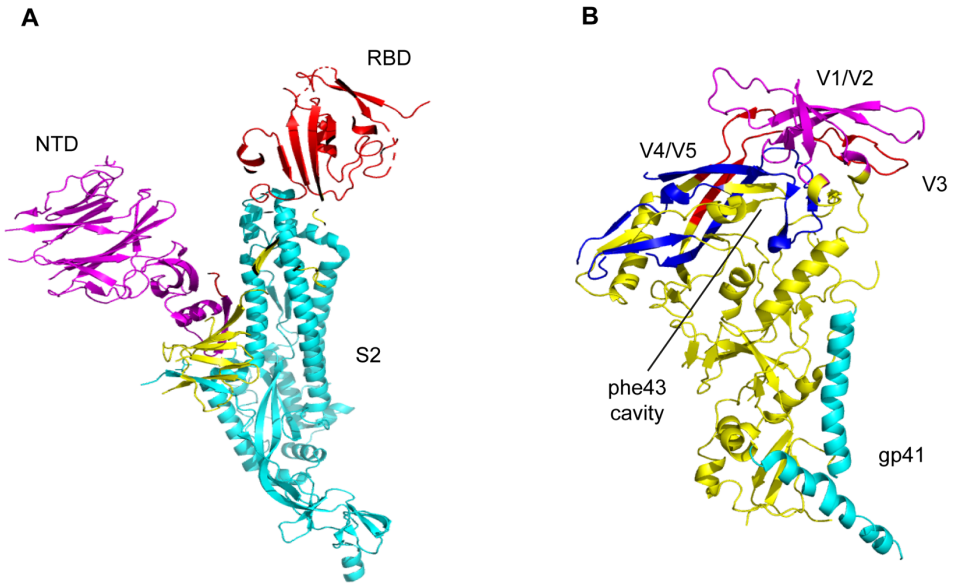

Figure 1.4. Commonalities in SARS-CoV-2 spike and HIV-1 Env structures. A, B) Structures of SARS-CoV-2 spike PDB:6VXX (A) and HIV-1 Env PDB:5ACO (B), coloured by domain in ribbon structure. NTD and V1/V2 loop are coloured in purple, RBD and V3 loop coloured in red, and S2/gp41 coloured in cyan. The Phe43 cavity in gp120 where CD4 binds is labelled. Structures made in PyMOL.

1.2 IFN and ISGs that inhibit viral entry

1.2.1 Induction of IFN

Interferons (IFNs), a conserved family of proinflammatory cytokines, are the cell's first line of antiviral defence. Cells express pattern-recognition receptors (PRRs), which detect conserved components of bacteria or viruses known as pathogen-associated molecular patterns (PAMPs). This includes lipids, proteins, and nucleic acids. Different PRRs recognise different types of PAMPs, as outlined in Figure 1.5 A. The recognition of PAMPs by PRRs activates a cascade of intracellular signalling which ultimately results in the expression of proinflammatory cytokines, including IFNs. The binding of IFNs to IFN receptors then triggers another signalling cascade which results in the induction of hundreds of ISGs that can inhibit multiple stages of viral infection [31]. Because IFNs trigger these changes in both an autocrine and paracrine fashion, this results in an antiviral state in the cell itself and surrounding cells. ISGs can also be expressed in a low but constitutive manner in certain areas of the body to provide a barrier to infection, as well as in direct response to antiviral infection.

There are three human families of IFNs, type I, comprising IFN$\alpha 1-13$, IFNβ, IFNε, IFNτ, IFNκ, IFNδ, IFNω, and IFNξ; Type II comprises IFNγ; and type III, which is comprised of IFNλ $1-4$. Of the type I family, IFNα and IFNβ are the most well expressed and characterised so far in terms of their antiviral effects. Both IFNα and IFNβ bind to the IFNAR receptor, which is a heterodimeric transmembrane receptor comprised of IFNAR1 and IFNAR2 [32]. The binding of IFNα or IFNβ to the IFNAR results in the activation of receptor-associated tyrosine kinases, JAK1 and TYK2 (Figure 1.5 B). These then phosphorylate signal transducer and activator of transcription 1 (STAT1) and 2 (STAT2) in the cytosol which leads to their dimerization. STAT1/STAT2 heterodimers translocate to the nucleus and form the ISG3 complex with IRF9. This complex subsequently binds to interferon-stimulated response elements (ISRE) in the promoters of ISGs, and transcription of hundreds of ISGs is activated. Described so far is the canonical pathway of IFNα/β signalling, however signalling can also occur through the non-canonical pathway. In the non-canonical pathway, STAT1 homodimers, and dimers of other STAT proteins 3-5 form [32]. The

diversity of the downstream signalling of the IFNAR likely contributes to the subsequent diversity in effects of IFNα/β.

IFNs and the ISGs they upregulate play an important role in controlling viral infections. This is demonstrated by autoantibodies against IFN being associated with increased severity of COVID-19, and the linking of single nucleotide polymorphisms (SNPs) in ISGs to an increased severity of several viral infections including influenza and SARS-CoV-2 *in vivo* [33-35]. For HIV-1, the ability to evade the restrictive capacity of type I IFNs is correlated with whether a virus can transmit or not, and transmitted/founder viruses have been shown to be more resistant to type I IFNs when compared to viruses from six months into infection [27]. ISGs can block many aspects of the viral lifecycle, with numerous ISGs targeting viral entry through distinct mechanisms.

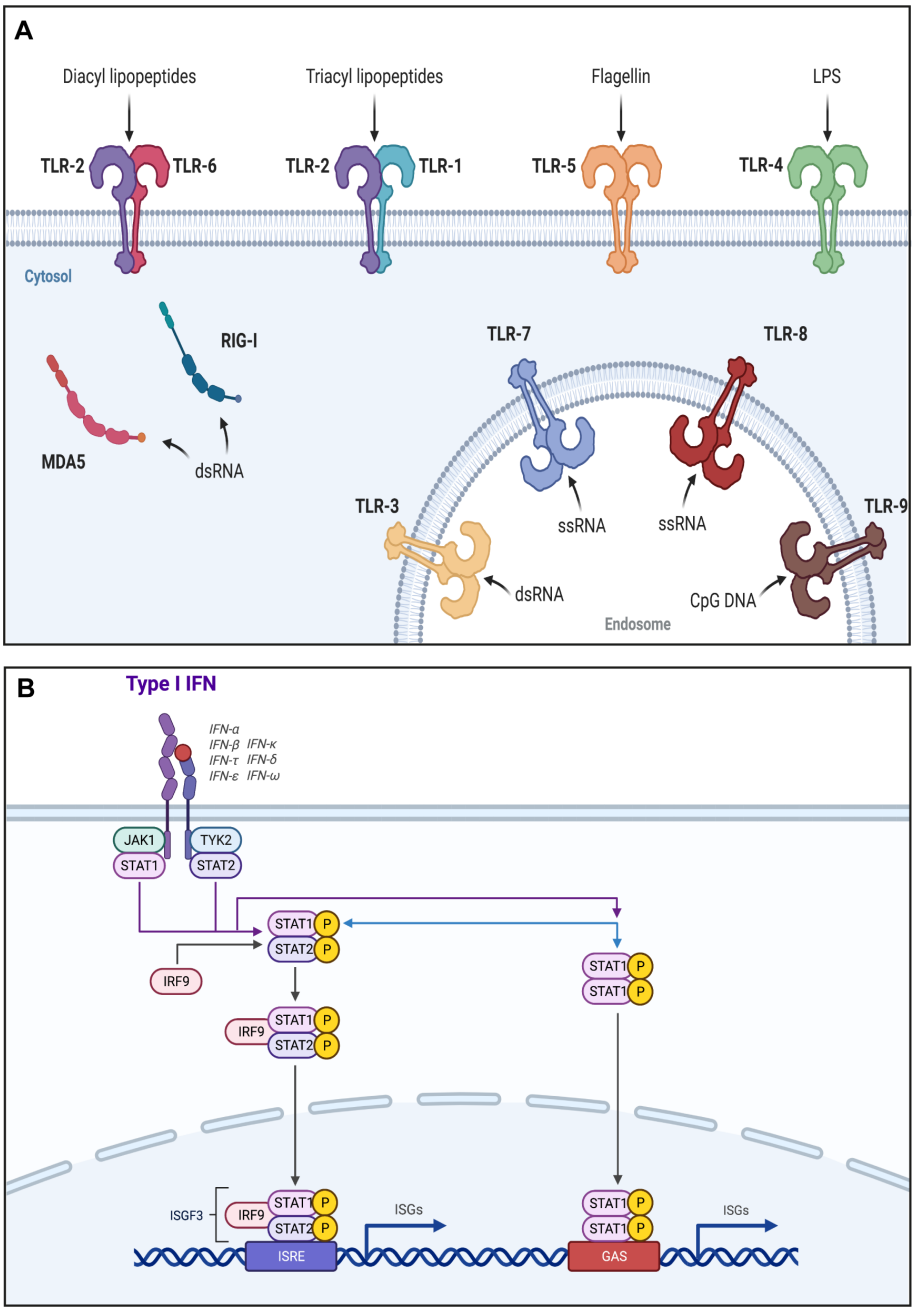

Figure 1.5. Sensing of viral infection triggers IFN signalling. A) PAMPs are recognised by an array of PRRs at the plasma membrane (TLRs 1/2, TLR2/6, TLR4, TLR5), in endosomal compartments (TLR3, TLR7, TLR8, TLR9), and in the cytoplasm (RIG-I, MDA5). B) IFNα/β bind the IFNAR which activates JAK1 and TYK2 kinases. These phosphorylate STAT1 and STAT2 which leads to their dimerization and translocation across the nucleus. These form an ISG3 complex with IRF9 which binds ISRE elements in the promoters of ISGs, resulting in the transcription of ISGs. Figure created in BioRender.

1.2.2 IFITMs

1.2.2.1 IFITMs inhibit viral entry

IFN-induced transmembrane (IFITM) proteins are the some of the earliest acting ISGs. IFITMs are membrane spanning proteins that inhibit the entry of a range of enveloped viruses, including HIV-1, influenza, Ebola, SARS-CoV-1, and SARS-CoV-2 [6, 36-42]. There are three IFITMs that exert antiviral effects in humans: IFITM1, IFITM2, and IFITM3. IFITM1 localises predominantly to the plasma membrane, and IFITMs 2 and 3 to endosomal compartments [41, 43]. All three IFITMs are highly homologous, with only ten amino acids different between IFITM2 and IFITM3.

The mechanism of action of IFITMs is still not fully understood. They do not inhibit interactions with viral receptors, impede endocytosis, or inhibit low pH-mediated triggering of glycoproteins [37, 44]. They are also capable of inhibiting both pH-dependent and independent viruses, suggesting they do not restrict endosomal access. The first, and most favoured model of IFITM-mediated inhibition of entry, proposes that they alter the positive curvature of host membranes and thereby prevent the fusion of the cellular and viral membranes [45, 46]. It has been shown that despite influenza accessing endosomal compartments with no change to entry kinetics, influenza cannot fuse with the endosomal membrane in the presence of IFITM3 [39]. It has been shown that this is due to inhibiting the transition from hemifusion to full membrane fusion, or the process of hemifusion itself. Treatment with chlorpromazine, a drug which promotes the transition from hemifusion to full membrane fusion, is unable to rescue IFITM-mediated restriction, suggestive of inhibition prior to hemifusion [44]. Other reports have suggested that IFITMs inhibit the transition from hemifusion to full fusion [47]. Nevertheless, IFITMs have been found to decrease membrane fluidity and membrane curvature in the compartments in which they reside [44, 47]. An amphipathic helix has also been reported to be essential for IFITM function, further supporting their role in directly altering membrane properties [38, 48]. Amphipathic helices are protein sequences that fold into helical structures when they come into contact with polar/non polar interfaces and have previously been identified to trigger membrane curvature [49, 50]. The process of oligomerisation, whereby individual IFITM proteins interact with each other, has been found to be essential for

IFITM antiviral activity [51]. A $_{91}$GxxxG$_{95}$ motif was recently identified as essential for both IFITM3 oligomerisation and antiviral activity against influenza [45]. The authors demonstrate that the glycine at position 95 of this motif is also essential to the membrane rigidification caused by IFITM3. Furthermore, treatment with the anti-fungal amphotericin B can rescue viruses from IFITM3-mediated inhibition through decreasing the stiffness of IFITM3-containing membranes [45]. The S-palmitoylation of IFITMs, the process whereby fatty acids are added onto cysteine residues, is also an essential aspect of IFITM function; suggested to be through contributing to their appropriate subcellular localisation and stability [37, 52] [53].

Another model for IFITM-mediated restriction suggests they exert antiviral activity indirectly through interactions with other host proteins. Increased endosomal cholesterol has been reported in IFITM3 overexpression cells due to the interaction of IFITM3 with the vesicle-associated protein-associated protein A (VAPA) [54]. The role of VAPA in the antiviral activity of IFITM3 has however been disputed, and it has also been demonstrated that IFITMs can modulate the trafficking of the vacuolar ATPase (vATPase) and therefore restrict viral entry by modifying the acidic environment of endosomes [55]. Additionally, it has been shown that IFITMs can exert antiviral effects through interactions with other antiviral proteins, such as zinc metallopeptidase STE24 (ZMPSTE24), which has recently been implicated in the restriction of arenavirus entry [56]. There is debate in the literature about whether IFITMs only exert their antiviral activity when present in the target cell, or whether they can also inhibit viral infectivity through their incorporation into virions during production [57, 58]. There is more evidence for the former than the latter, however IFITMs certainly get incorporated into viral particles during production in the presence of IFN or IFITM overexpression, and IFITM incorporation has been demonstrated to reduce infectivity of some viruses [59]. The decrease in infectivity of virions with incorporated IFITM could further suggest that the antiviral mechanism of these proteins is due to effects on membrane curvature.

1.2.2.2 IFITM structure

IFITMs are transmembrane proteins that belong to the larger family of dispanin proteins. These proteins are organised into a hydrophobic N-terminal domain (NTD), a conserved and hydrophobic intramembrane domain (M1), a conserved intracellular loop (CIL), a second hydrophobic transmembrane domain (M2), and a C-terminal domain (CTD) [37]. The NTD, M2, and CTD regions are variable in sequence. IFITMs are defined by the presence of a highly conserved region, the CD225 domain, (located at residues 58-108 in IFITM3). Although highly homologous, IFITM1 contains a shorter N-terminal domain and longer C-terminal domain than IFITM2 or 3 (Figure 1.6 A).

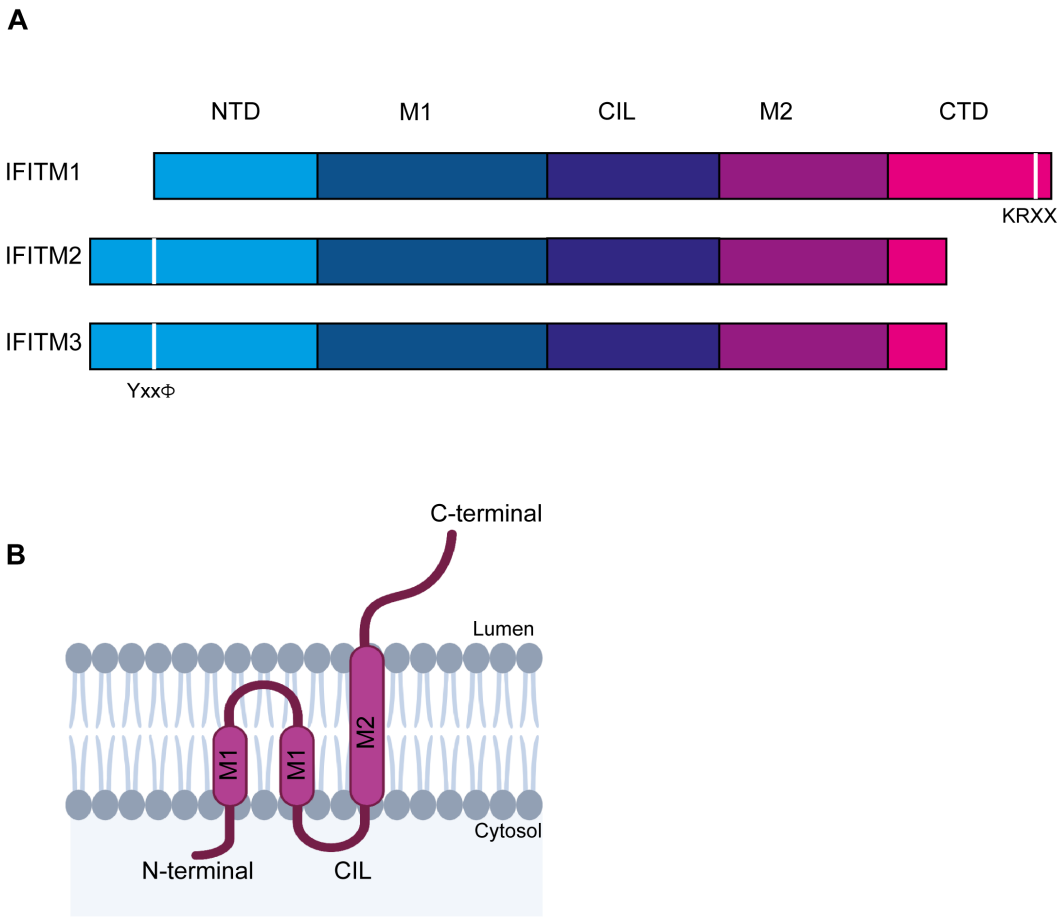

Figure 1.6. IFITM structure and regions of interest. A) Schematic of IFITMs 1, 2 and 3 with NTD, M1, CIL, M2, and CTD labelled. Endocytic/sorting signals are highlighted in white. B) Most accepted topology of IFITMs in the membrane with a luminal C-terminal and cytosolic N-terminal and intervening regions labelled. Panel B was created in BioRender.

There is debate about the most commonly adopted topology of these transmembrane proteins in the cellular membrane. Immunofluorescent staining and flow cytometry based assays demonstrate that both the N and C terminals can face the lumen or extracellular space [60], however other studies show that the N and C terminal, or N terminal only, localises in the cytoplasm [61] [52]. There are three different topology models currently suggested for the orientation of IFITM2 and 3 domains in membranes, and five for the domains of IFITM1. For IFITM2/3: the Type III transmembrane model proposes that both the N and C terminals face the lumen, intramembrane model posits that both N and C terminal face the cytosol, and the most accepted model, the Type II transmembrane model, suggests the N terminal faces the cytosol and the C terminal faces the lumen with the first transmembrane domain not fully penetrating the membrane. The NTD located ubiquitylation and phosphorylation sites demonstrate that the N-terminal of IFITM3 must be accessible to cytosolically located enzymes [43, 52]. For IFITM1, there are five models of topology, of which type II proposes that the C terminal is luminal/extracellular and the N terminal is in the cytosol, similar to the most accepted model for IFITMs 2 and 3 [62] (Figure 1.6 B).

There are several post-translational modifications of IFITMs imperative to their function (highlighted in Figure 1.7). As previously mentioned, S-palmitoylation is essential to IFITM function; There are two conserved palmitoylation sites in the intramembrane domain and a less conserved palmitoylation site in between the intracellular loop and transmembrane domain. Additionally, there are four potential ubiquitination sites – one in the NTD, and the remaining three in the intracellular loop. Although ubiquitination has been suggested to be important to regulating IFITM expression, it has been reported that mutation of all four ubiquitination sites to alanines does not impact on the antiviral activity of IFITM3 [52]. The NTDs of IFITMs 2 and 3 contain a potential phosphorylation site (position 19 in IFITM2 and 20 in IFITM3), that sits within a canonical PPxY motif that regulates the ubiquitination of IFITM3 via recruitment of NEDD4-like HECT ubiquitin ligases and thereby target it for endosomal sorting complex required for transport (ESCRT)-dependent degradation [63].

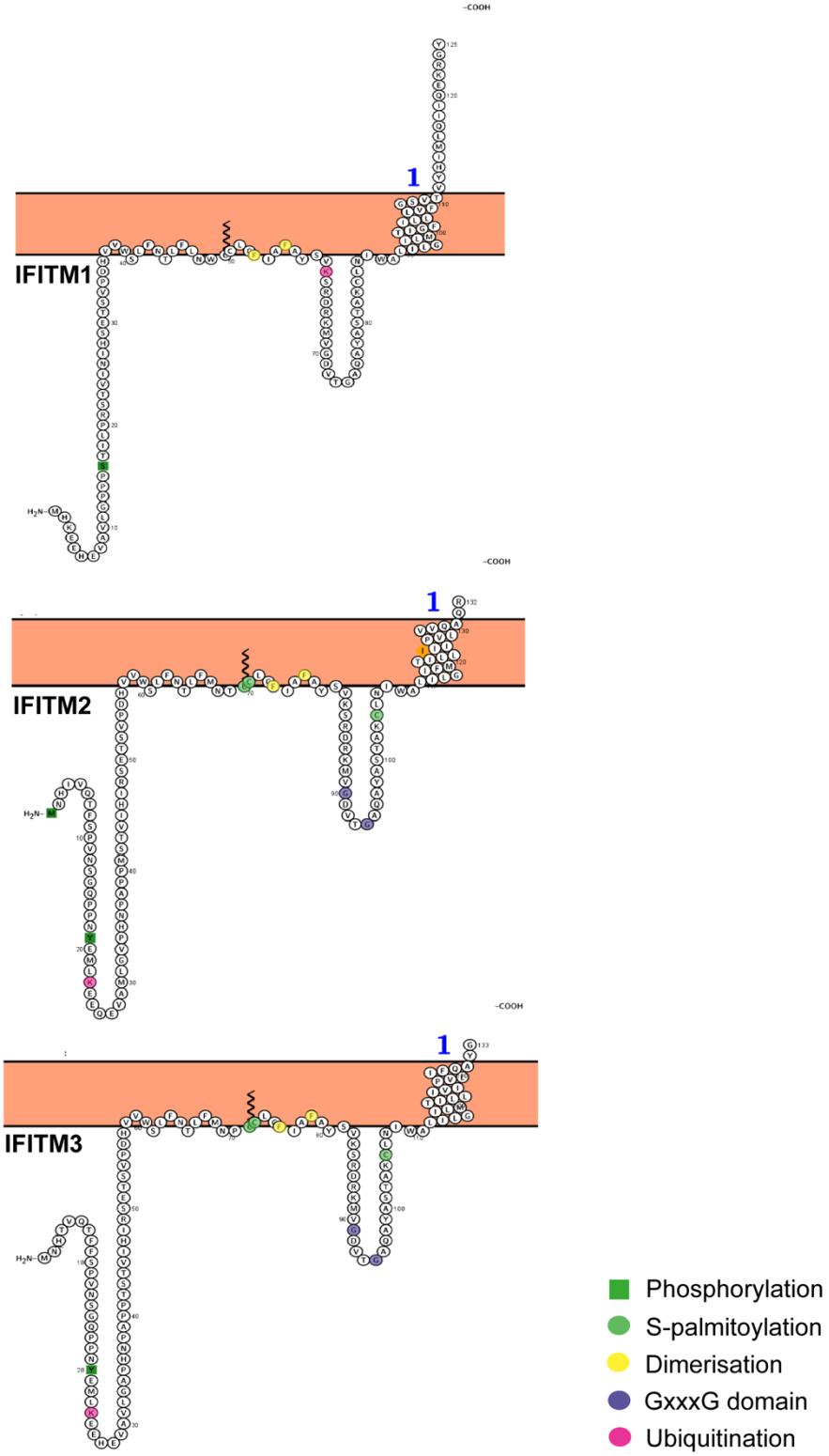

Figure 1.7. Snake diagrams of IFITMs 1, 2, and 3. IFITM1, IFITM2 and IFITM3 snake diagrams were generated in Protter. Phosphorylation sites are highlighted in green boxes, ubiquitination sites in pink circles, S-palmitoylation sites in green circles, the GxxxG domain in purple circles, and residues thought to be involved in dimerization in yellow circles.

1.2.2.3 IFITM localisation

Despite their similar homology IFITMs 1, 2, and 3 localise to different membranes. IFITM1 localises predominantly to the plasma membrane and IFITM2/3 to endosomal membranes [37]. However, subcellular localisation of IFITMs varies between cell-types, and despite the predominant localisation of IFITM2/3 on endosomal membranes they cycle through the plasma membrane. IFITM2/3 localise to endosomal compartments due to their NTDs containing a Yxxφ endocytic signal motif which regulates their sorting into endosomal compartments from the plasma membrane via binding to the μ-subunits of clathrin adaptor AP-2 (Figure 1.8) [43, 64]. However, all three IFITMs have been observed to partially colocalise with the endolysosomal marker CD63 [36]. However, phosphorylation of the tyrosine of this motif by Fyn kinases inhibits IFITM3 internalisation which could result in prolonged IFITM3 localisation at the surface [43].

This tyrosine is an important aspect of IFITM biology, as this tyrosine also forms the PPxY motif which regulates IFITM3 ubiquitination. Mutation of this site therefore can potentially modulate antiviral activity through multiple ways. IFITM1 does not contain the Yxxφ motif, and therefore must internalise through an independent method. IFITM1 has been shown to colocalise with caveolin at the plasma membrane and may therefore utilise caveolin-mediated endocytosis [65]. However, the C-terminal of IFITM1 has been shown to affect the subcellular localisation of IFITM1, demonstrated by deletion of this region conferring restrictive capacity to IFITM1 to NL4.3, an HIV-1 isolate which enters through endosomal compartments [66]. IFITM localisation can also be affected in other ways. S-palmitoylation is also essential to IFITM antiviral activity by virtue of localisation as this enhances the clustering of IFITM3 in endosomal compartments [53]. Deletion of the S-palmitoylation domain in IFITM3 results in a more diffuse rather than punctate localisation of IFITM3 in HeLa cells and abolishes antiviral activity against influenza [53].

IFITM localisation dictates which viruses they restrict and is regulated by several aspects of their biology. The localisation of IFITM3 to endosomes, due to the Yxxφ motif, correlates with its ability to restrict influenza entry which fuses in

endosomal compartments [39]. It has also been proposed that CCR5-tropic HIV-1 viruses that are suspected to fuse at the plasma membrane are more restricted by IFITM1, while CXCR4-tropic viruses that are thought to utilise the endosomal route are more restricted by IFITMs 2 and 3 [67]. However, another group has disputed this and shown no correlation between coreceptor usage and IFITM sensitivity for HIV-1 isolates, suggesting that the route of entry may be more complex than simply the use of CCR5 or CXCR4, therefore requiring study of more HIV-1 isolates [68]. Additionally, the C-terminal of IFITM1 can regulate its antiviral activity by altering subcellular localisation. IFITM1 does not usually restrict the lab-adapted HIV-1 strain NL4.3, however, a deletion of the C-terminal domain of IFITM1 (∆117-125) mislocalises IFITM1 and grants the capacity to restrict NL4.3 [66]. Similarly, mislocalising IFITM3 with a Y20A/F mutation, which retains IFITM3 at the plasma membrane, abolishes the ability of this to restrict influenza [43]. There does appear to be a cell-type dependent effect of IFITM-restriction however, as IFITM Y20A does not rescue infection of influenza or Zika virus in WeBo cell lines [69]. IFITM localisation has been reported to vary in the heterogenous tissues of the lung, with IFITM3 reported to localise at the apical plasma membrane and cilia of the ciliated columnar cells in the upper airways, and in endosomal compartments in type II pneumocytes [37, 70]. Although generally IFITM3 is considered an endosomally located protein, it appears there are caveats to this rule.

A majority of studies investigating the link between viral entry and IFITM-mediated inhibition utilise overexpression, transient transfection and cell-free infection. However, whether this recapitulates the role of IFITMs *in vivo* is contested. Expression of overly high levels of exogenous IFITMs has been suggested to overwhelm the internalisation of these proteins and therefore result in a more predominant presence of IFITMs at the plasma membrane which could affect their antiviral function [37]. Additionally, many viruses have been suggested to utilise cell-cell transmission *in vivo,* possibly to avoid the effects of neutralising antibodies but a mechanism that could also escape IFITM-mediated inhibition. Cell-cell transmission has also been shown to be adopted by HIV-1 to escape the antiviral effects of tetherin, an ISG that inhibits viral egress [71, 72]. Although it has been shown that IFITMs can inhibit syncytia formation, whether these also effectively inhibit cell-cell transmission has not yet been thoroughly

investigated [73]. IFITM-mediated inhibition of syncytia has consequences for infections during pregnancy. The activation of IFITMs in response to viral infection *in utero* has been linked to foetal demise through inhibiting trophoblast syncytia formation which is a vital stage in early pregnancy [69, 74]. Interestingly, both wild-type IFITM3 and the mislocalisation of Y20A-IFITM3 were found to reduce trophoblast syncytia formation, despite the predominantly intracellular localisation of IFITM3 [69]. Inhibition of syncytia may also have consequences for SARS-CoV-2 infection. SARS-CoV-2 spike binding to ACE2 at the cell surface on neighbouring cells mediates syncytia formation which has been linked to the disruption of lung tissue following infection [75]. It has been shown that IFITM1 can block syncytia formation, suggesting that the role of IFITMs in SARS-CoV-2 infection can go beyond direct antiviral effects [76].

1.2.2.4 SNPs in IFITMs and disease

In vivo studies have demonstrated the importance of IFITMs in controlling infections. Knocking out IFITM3 in mice results in enhanced severity and pathogenicity of influenza, West Nile Virus and Respiratory Syncytial Virus infections [70, 77, 78]. In addition to animal models, correlative evidence from humans also highlights the role of IFITMs in infection. The single nucleotide polymorphisms (SNP) in the IFITM3 allele named rs12252-C has also been linked to increased influenza severity in humans, with the SNP being more prevalent in patients hospitalised with the H1N1/2009 influenza virus than in the general population [79]. The rs12252-C SNP is rare in Caucasians, but more frequent in Han Chinese. Zhang and colleagues examined the genotypes of patients from a Chinese hospital during the H1N1 2009 pandemic and found that 69% of patients who experienced severe infection were found to be homozygous for the SNP, while only 25% of those who experienced mild infection were homozygous [80]. The rs12252-C SNP has been suggested to result in a truncated form of IFITM3 that lacks the first 21 amino acids at the N-terminal due to this mutation creating a novel splice acceptor site [37]. However, the shorter variant of IFITM3 was not found in cell lines homozygous for rs12252-C and an *in vitro* link between the rs12252-C SNP and its effect on IFITM3 function has yet to be identified [79].

The severity of other viral infections has more recently been linked to the rs12252-C SNP, namely HIV-1 and SARS-CoV-2 [81, 82]. A higher frequency of homo- and heterozygotes for the rs12252-C allele was found in patients rapidly progressing to AIDS, however was not found to be associated with increased susceptibility to HIV-1 infection itself [81]. In the context of COVID-19, homozygosity for rs12252-C was associated with more severe disease in an age-dependent manner [82]. Of the hospitalised patients studied, 35% were homozygous for rs12252-C. IFITM3 has also recently been implicated in the regulation of CD4+ T cell helper differentiation, suggesting that the impact of the rs12252 SNP may not be attributed to the direct antiviral effects of IFITM3 on entry, but due to consequences for the adaptive response [83].

1.2.2 SERINCs

IFITMs are not the only antiviral protein family that inhibits viral entry. Serine incorporators (SERINC) 3 and 5, although SERINC3 to a lesser extent than SERINC5, can inhibit viral entry via incorporation into budding virions in the producer cell which prevents viral fusion in the target cell [84, 85]. SERINC3/5 are transmembrane proteins that have been thought to be involved in the incorporation of serine into the phosphatidylserine and sphingolipids [86]. Unlike IFITMs and many antiviral proteins, SERINC3/5 are not upregulated by IFN, but are constitutively expressed restriction factors [84]. SERINC5 is highly expressed in certain cell lines and was found to significantly block Nef-deficient HIV-1 infection [84, 85]. This is due to the role of Nef in excluding SERINCs from the site of HIV-1 assembly [84].

The mechanism of SERINC-mediated inhibition is still not entirely understood. SERINC5 has been reported to not affect the lipid order of pseudotyped lentiviral vectors (PLVs) bearing SERINC-sensitive HIV-1 Envs [87]. However, a recent preprint showed that SERINC5 results in exposure of phosphatidylserines which correlates with the impairment of infectivity [88]. It has also been reported that SERINC5-mediated disruption of viral fusion correlates with its ability to indirectly prevent the clustering of Env, which is important in regulating HIV-1 entry [89]. Additionally, it has been found that deletion of the cytoplasmic tail of HIV-1 Env can render Env resistant

to SERINC3/5 without altering the incorporation of SERINC5 into virions [90]. It has been proposed that IFITMs and SERINCs exert differential selection pressures during HIV-1 infection, as HIV-1 Envs that become sensitive to IFITM3 over chronic infection retain resistance to SERINC5 [91]. While HIV-1 does not encode a protein to antagonise the inhibition by IFITMs, HIV-1 encodes Nef, which prevents SERINC incorporation into nascent virions [84].

It has also recently been demonstrated that SERINC5 can block the entry step of SARS-CoV-2 infection and is counteracted by the viral protein orf7a [92]. SARS-CoV-2 does not assemble and bud at the plasma membrane, where SERINC5 is incorporated into retroviral virions, but instead egresses via the exocytic and endolysosomal secretory pathways. It has been proposed that SERINC5 and SARS-CoV-2 spike encounter each other in the endoplasmic reticulum-Golgi intermediate compartment (ERGIC) and that orf7a blocks this interaction [92]. To date, SARS-CoV-2 is the only non-retroviral virus that has been found to be restricted by SERINC5. Intriguingly, Timilsina et al describe the alpha, beta, gamma, and delta variants, which have different mutations in their spike proteins, as equally restricted by SERINC5. However, the authors utilise spikes that have their cytoplasmic tails deleted, commonly done to increase PLV infectivity. Given that the cytoplasmic tail of Env has been linked to modulating SERINC restriction, it could be that differential sensitivity to SERINCs is conferred by using full-length spikes with cytoplasmic tails.

1.2.3 GBP2/GBP5

Restriction factors can also inhibit viral entry through inhibition of the priming step of viral entry proteins. The guanylate binding protein (GBP) family encompasses seven GBP proteins which hydrolyse GTP to GDP and GMP [93]. Of the seven proteins, only GBP2 and GBP5 are antiviral; these two proteins inhibit viral infectivity by reducing the proteolytic activity of the host protein furin [93]. By reducing the activity of furin, GBP2/5 block the priming cleavage step of viral entry glycoproteins, resulting in glycoproteins that are not fully processed. Many enveloped viruses rely on furin to prime class I fusion glycoproteins for viral entry, including HIV-1 and SARS-CoV-2. Therefore, inhibition of this step reduces the amount of primed glycoprotein available

on viral particles, meaning that either these proteins cannot fuse or require priming by another protein that may have lower bioavailability in the target cell. GBP2 and 5 have been found to exert the most antiviral activity of the GBP family and are reported to inhibit a range of enveloped viruses including Zika, influenza, measles, HIV-1, and SARS-CoV-2 [93, 94].

1.2.4 Other antiviral proteins which inhibit entry

IFITMs and SERINCs block the same step of viral infection, albeit by inhibiting viral entry through purportedly distinct mechanisms. LY6E has also recently been found to inhibit the entry step of several coronaviruses, including SARS-CoV-2, and influenza [95, 96]. Lymphocyte antigen 6 complex, locus E (LY6E) is a GPI-anchored protein which inhibits the entry of OC43, NL63, 229E, HKU1, and SARS-CoV-2, but not SARS-CoV-1 [96]. Inhibition by LY6E could not be overcome by the expression of TMPRSS2 or treatment with amphotericin B, both of which can rescue IFITM-mediated restriction of influenza virus [95, 97]. This suggests that the inhibitory effects of LY6E appears to be distinct from IFITM-mediated restriction, however the exact mechanism is still not understood. Interestingly, LY6E has been found to enhance, rather than restrict, infection by HIV-1 [98]. This is also exemplified by the association of a SNP in LY6E with rapid progression to AIDS, further implying that this antiviral protein can assist HIV-1 infection [99]. LY6E has also been found to enhance an early step of viral replication of both yellow fever virus (YFV) and influenza virus [100]. The mechanism of LY6E enhancing viral infectivity is not entirely understood; LY6E does not alter binding to target cells, but LY6E knockdown does impede membrane fusion of HIV-1 and LY6E overexpression increases YFV viral entry and IAV uncoating [98, 100]. The finding that both IFITMs and LY6E can increase SARS-CoV-2 and HIV-1 infection, respectively, implies that despite their antiviral properties, these proteins can be hijacked to aid viral entry under certain conditions.

Cholesterol-25-hydroxylase (CH25H), which converts cholesterol to 25-hydroxycholesterol, has also been found to inhibit the membrane fusion of a range of enveloped viruses, including HIV-1 and SARS-CoV-2 [101, 102]. CH25H has been implicated in inhibiting the replication of multiple RNA viruses including Zika virus,

hepatitis C, and SARS-CoV-2 [102-104]. CH25H is upregulated by both IFNα and IFNβ, and knockout of CH25H results in increased Zika infection in mice [101]. It has been found that in the context of SARS-CoV-2, the 25HC derivative activates the ER-localised-acyl CoA acyltransferase which leads to the depletion of cholesterol from the cell membrane [102]. It has also been reported that CH25H can inhibit stages of viral replication downstream of entry, with CH25H having been found to inhibit the formation of double membrane vesicles that hide hepatitis C replication from innate sensing [104]. The number of antiviral proteins and significant redundancy by the host to inhibit the earliest stage of infection demonstrates the importance of blocking this step of viral replication to control viral infection (Figure 1.8).

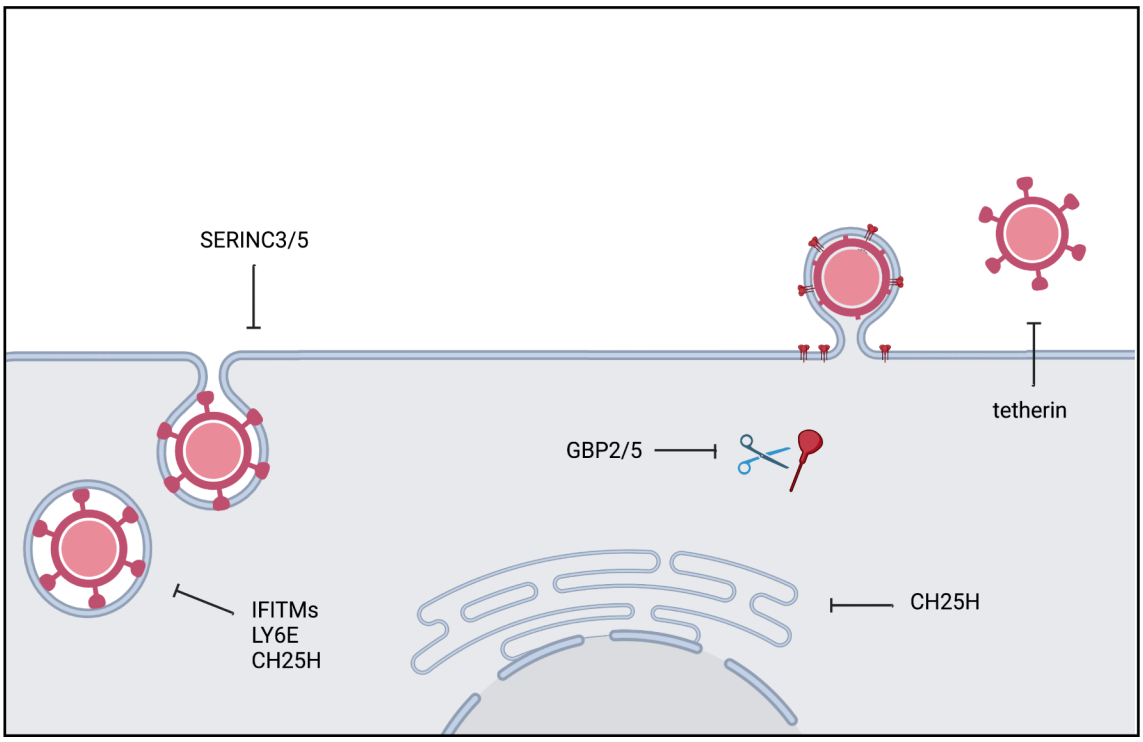

Figure 1.8. Antiviral proteins that inhibit early and late viral replication. SERINCs 3 and 5 inhibit viral entry through their incorporation into budding viral particles in the producer cell, and have been reported to inhibit both HIV-1 and SARS-CoV-2. This inhibits viral entry at the next target cell. IFITMs inhibit viral entry through altering positive membrane curvature and preventing viral and cellular membranes from fusing, and inhibit both HIV-1 and SARS-CoV-2. LY6E and CH25H also inhibit viral entry through preventing viral fusion. CH25H and LY6E have been reported to inhibit SARS-CoV-2, while LY6E has been suggested to enhance infection by HIV-1. CH25H can also inhibit the formation of double membrane vesicles where hepatitis C replicates, and could theoretically also inhibit SARS-CoV-2 in this compartment. GBP2 and GBP5 inhibit furin-mediated processing of glycoproteins. In terms of inhibiting later stages of viral replication, tetherin inhibits viral release by tethering budding virions to the plasma membrane, and has been shown to inhibit both HIV-1 and more recently SARS-CoV-2. IFITMs have also been suggested to be incorporated into nascent virions, which can in turn inhibit entry at the next cell as well as their expression on the target cell. Figure created in BioRender.

1.3 The SARS-CoV-2 pandemic

In late 2019, several patients with severe pneumonia were identified in Wuhan, a city in the Hubei province of China. A novel coronavirus was isolated from patient samples and identified as being phylogenetically related to the betacoronaviruses SARS-CoV-

1 and MERS-CoV [105, 106]. This novel coronavirus was temporarily called 2019-nCoV and was later named as SARS-CoV-2, and the symptoms caused by SARS-CoV-2 infection termed COVID-19. On the 30th of January 2020, the World Health Organisation (WHO) declared the outbreak of COVID-19 as a Public Health Emergency of International Concern. By the 11th of March 2020, COVID-19 was a pandemic and by the end of the month many governments across the planet elected to implement social distancing in public spaces, mandate mask wearing, and implemented national lockdowns to manage the spread and impact of the virus. The majority of international travel was halted. Despite these interventions, COVID-19 cases continued to rise globally and by the end of 2020 there were over 79 million cases worldwide with 1.7 million deaths [107]. During this stage of the pandemic, several independent vaccines for SARS-CoV-2 were developed and vaccine rollout began in early 2021. Since the initial rollout of the vaccine, many countries relaxed lockdown restrictions and curfews. Some countries managed to temporally eliminate COVID-19 cases through strict lockdown procedures and border shutdown. However, to date no country has successfully eliminated COVID-19 permanently. As of September 2022, over 6 million people are confirmed to have died of COVID-19 [108].

1.4 Origin of SARS-CoV-2

SARS-CoV-2 demonstrated high sequence homology to bat coronaviruses isolated from the same region of China; and given previous zoonoses of coronaviruses to humans, it is suggested that SARS-CoV-2 moved from bats to humans potentially through a currently unidentified intermediate host [109, 110]. Although not yet identified, this intermediate has been postulated to be pangolins due to their trade in the food markets in Wuhan and viral sequence homology. However, more recently it has been proposed the intermediate was either racoon dogs or civets [110-112]. There have been speculations on the emergence of SARS-CoV-2 as a consequence of laboratory manipulation. Although impossible to fully rule out, there is more evidence suggesting natural selection in animal hosts prior to transmission to humans, or a zoonotic event and subsequently natural selections in humans [113].

Given the proximity of humans and animals in the food markets in Wuhan, and the genetic similarities between SARS-CoV-2 and bat and pangolin viruses, it is highly possible that SARS-CoV-2 emerged from one of these animals and was transferred through close contact at wet markets. Coronaviruses detected in pangolins illegally imported and trafficked in the Guangdong province show strong similarities in the key ACE2-binding RBD residues in SARS-CoV-2 [110]. This is suggestive of intermediate passage in these animals prior to jumping to humans rather than the passage of a bat virus in human cells in laboratory conditions. The presence of potential O-linked glycosylation sites at the polybasic cleavage site in the spike protein has also been implied to be a result of passage in the presence of adaptive immunity [114]. Recently published analyses of samples from the Huanan Seafood Market in Wuhan are indicative of there being two separate jumping events of SARS-CoV-2 from animals to humans [115]. This is consistent with the emergence of other coronaviruses, i.e. a result of multiple zoonotic events and an analysis of the transcriptome of 18 different species across China recently identified 21 viruses that could potentially transmit to humans [116].

1.5 Genomic organisation of SARS-CoV-2

SARS-CoV-2 is categorised under the *coronaviridae* family, the subfamily *orthocoronaviridae*, and the genus *betacoronaviruses* [117]. It finally belongs to the subgenus *sarbecoviruses*, along with SARS-CoV-1. SARS-CoV-2 is the seventh coronavirus to infect humans. OC43, HKU1, SARS-CoV-1 and MERS-CoV are also *betacoronaviruses,* however MERS-CoV falls under the subgenus of *merbecoviruses*. 229E and NL63 are closely related viruses from the *alphavirus* genus of *orthocoronaviridae*. OC43, HKU1, 229E and NL63 cause seasonal colds, whereas SARS-CoV-1 caused an outbreak in South East Asia in 2003, and MERS-CoV caused an outbreak in the Middle East in 2012, with several cases recorded since [118]. The spike of the original ancestral Wuhan SARS-CoV-2 is estimated to be 73% homologous to that of SARS-CoV-1, and highly homologous to the bat virus RaTg13 and the pangolin Guangdong virus from the *sarbecovirus* subgenus.

Coronaviruses are single-stranded positive-sense RNA enveloped viruses. Coronaviruses have the largest genomes of RNA viruses, with the genome of SARS-

CoV-2 measuring 29.9kb with 14 ORFs (Figure 1.9) [119]. This encodes for the four structural proteins nucleocapsid (N), spike (S), envelope (E) and membrane (M), 16 non-structural proteins, and up to six accessory proteins [120]. The SARS-CoV-2 virion has a diameter of approximately 60-140 nm and the viral particle consists of the N protein encapsulating the viral genome, surrounded by a lipid bilayer studded with spike, E and M [121]. N is the only structural protein that is inside the virion, which is associated with the viral genomic RNA via electrostatic interactions [122]. Spike, E, and M, are studded in the lipid bilayer obtained from the host membrane in the producer cell, with M being the most abundant protein, followed by spike, then E [123].

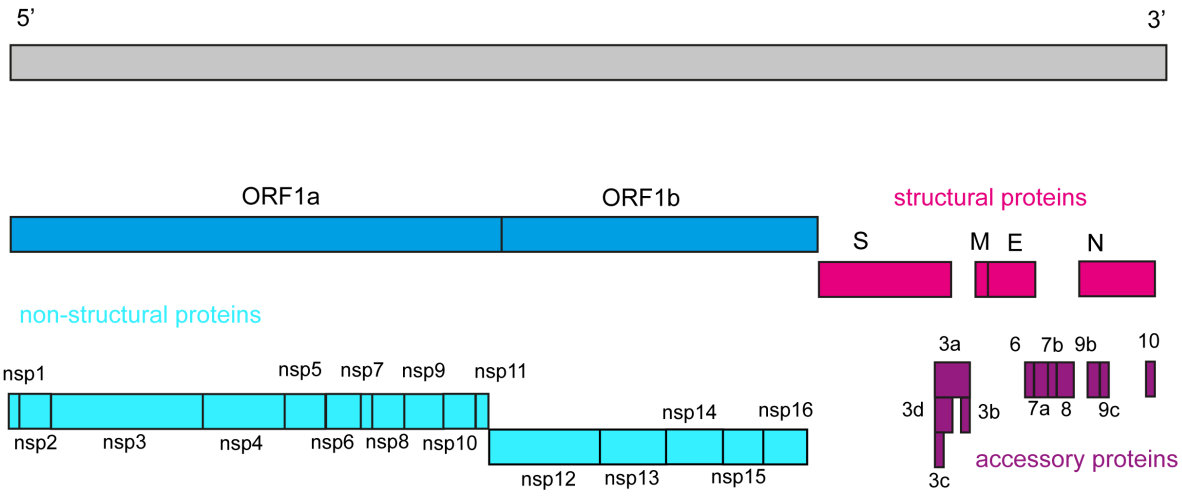

Figure 1.9. SARS-CoV-2 genome. Schematic of SARS-CoV-2 genome with structural proteins (pink) non-structural proteins (light blue) and accessory proteins (purple) labelled.

1.6 Viral entry of SARS-CoV-2

Entry of SARS-CoV-2 into the target cell is initiated by the spike glycoprotein. As with all enveloped viral entry, non-specific attachments between the virion and the cell surface is the first step of viral interaction. Heparan sulfate proteoglycans and DC-SIGN/lectins have been found to enhance SARS-CoV-2 infection by promoting virus attachment [124, 125] [126]. Following attachment to the membrane, spike binds to its receptor angiotensin converting enzyme 2 (ACE2) (Figure 1.10) [10]. ACE2 is a carboxypeptidase that removes a single amino acid from the C-terminus of its

substrates, however the catalytic activity of ACE2 is not required for viral entry [18]. In addition to binding its receptor, spike must be proteolytically cleaved in order to trigger viral entry. The priming cleavage at the S1/S2 boundary ($_{681}$PRRARS$_{686}$) is mediated by furin in the producer cell, and the second cleavage which occurs during viral entry on the target cell is presumed to be located at the S2' site ($_{815}$RS$_{816}$) adjacent to the fusion peptide. The S2' cleavage can be mediated by TMPRSS2 at the plasma membrane or cathepsins B and L in endosomes [10]. Recently, several other proteases have been implicated in S2' cleavage, including members of the a disintegrin and metalloproteinase (ADAM) and matrix metalloproteinase (MMP) families, in addition to other TMPRSS proteases [127-129].

Binding of ACE2 and S2' cleavage are both required to trigger structural rearrangements which permit S1 shedding, the release of the fusion peptide in the S2 domain, and ultimately membrane fusion [18]. The fusion peptide is inserted into the host membrane that forms the intermediate state. This is quickly and irreversibly refolded into the stable post fusion state bringing the host cell membrane and viral membrane into close proximity, which ultimately results in fusion of the two membranes. Depending on the availability of proteases and the relative pH, this fusion can happen at the plasma membrane directly (early pathway), or more commonly on endosomal membranes (late pathway). However, it has recently been established that an acidic pH is still required for a majority of SARS-CoV-2 fusion events, even when TMPRSS2 mediates the S2' cleavage [19]. This suggests there is more of a pH-dependence for SARS-CoV-2 entry than previously understood, which may have consequences for antiviral proteins that target entry.

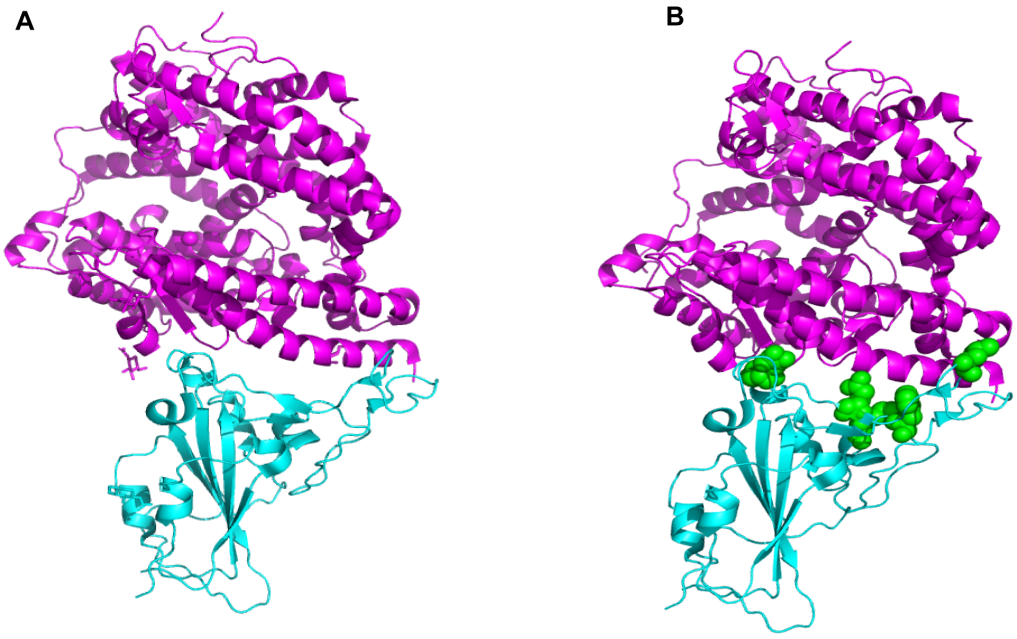

Figure 1.10. RBD and ACE2 interaction. Structural model of the RBD of SARS-CoV-2 spike RBD (cyan) interacting with ACE2 (magenta) (7EKE:PDB) unlabelled (A) and with labels of the six key ACE2 binding residues in the RBD labelled (B) Model made in PyMOL.

1.7 Replication of SARS-CoV-2

Following fusion, the contents of the viral particle are released into the cytoplasm and the positive-sense RNA is translated (Figure 1.11). The components of the viral replication and transcription complex (RTC) are immediately translated, allowing viral replication to begin [130]. Double membrane vesicles (DMVs) are formed by nsps 3, 4 and 6 which shield the viral intermediates from host sensing whilst also functioning to concentrate the host factors needed for replication [131]. The RNA dependent RNA polymerase transcribes a full-length negative-sense RNA. There are two distinct processes of RNA synthesis in coronavirus replication, the first being the continuous transcription of the negative-sense template to produce positive-sense genomic RNAs to be packaged into nascent virions [122]. Secondly, there is discontinuous transcription of the sub genomic mRNAs from the negative-sense template [122]. The RTC encounters transcription regulatory sequences (TRS) in the 3' end of the last third of the SARS-CoV-2 ORFs at the 3' end of the genome and RNA synthesis is stopped when these sequences are encountered and reinitiated at a leader sequence at the 5' end of the genome. This results in the generation of a nested set of sub genomic mRNAs from which the structural proteins spike, M, E and N are translated [118]. These are inserted into the ER membrane and transported through the ERGIC. Newly synthesised genomic RNA and N proteins interact with E, M and spike to assemble viral particles that bud through the lumen of the secretory pathway [118].

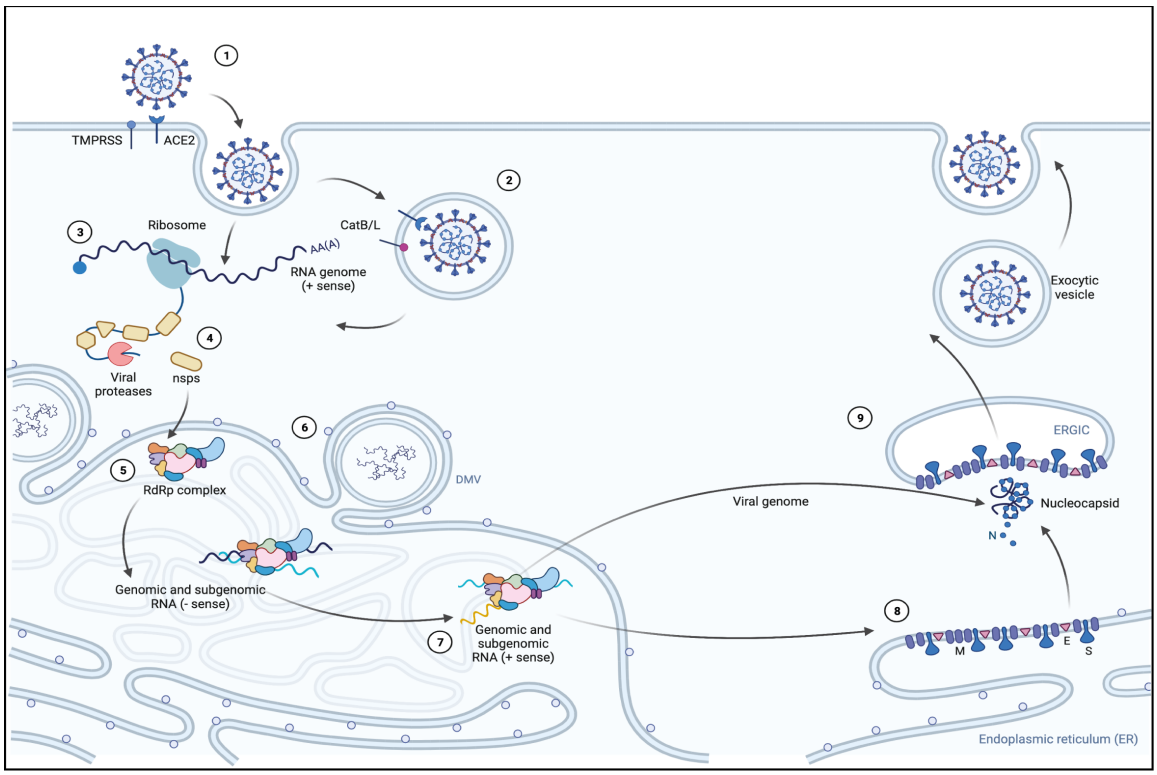

Figure 1.11. SARS-CoV-2 viral replication. SARS-CoV-2 virions initially attach to the cell surface using non-specific attachment factors. Subsequently, SARS-CoV-2 spike binds to the ACE2 receptor, triggering conformational changes which result in the exposure of the S2' cleavage site. This permits binding by TMPRSS proteins such as TMPRSS2, TMPRSS1D, or TMPRSS13 at the plasma membrane (1), or by cathepsins B/L in endosomes (2). Cleavage at the S2' releases the fusion peptide and allows spike to mediate the fusion of the cellular and viral membranes, releasing the contents of the virion into the cytoplasm. The positive sense RNA ORF1a and ORF1b are immediately translated, resulting in the polyproteins pp1a and pp1b (3). Due to a ribosomal frameshift, pp1a is expressed1.4-2.2x more than pp1b. Pp1a and pp1b are processed into the non-structural proteins (4). This includes the formation of the replication and transcription complex (5). In parallel, double-membrane vesicles are formed for viral replication to occur in, thought to shield the replication components from host sensing (6). In this protective environment, the viral genomic RNA is replicated and subgenomic RNAs used as a template for transcription of new viral genomes and for translation of viral proteins (7). Structural proteins are translated and trafficked through the ER to the ERGIC where they encounter the N-encapsuled genomic RNA (8). Nascent virions bud into the lumen of the secretory pathway and eventually secreted from the producer cell by exocytosis (9). Figure created in BioRender.

1.8 SARS-CoV-2 tropism

ACE2 expression predominantly determines the tropism of SARS-CoV-2. ACE2 expression has been found in the nasal passages and lungs, as well as the small intestine, testis, heart, kidney, colon, and thyroid gland [132]. The presence of ACE2 in the gastrointestinal tract and kidney may explain some of the gastrointestinal and renal complications from SARS-CoV-2 infection, and infection of cardiac tissue has also been documented in COVID-19 autopsies [133]. There is debate about whether other receptors besides ACE2 can facilitate SARS-CoV-2 infection; It is highly possible other host transmembrane proteins play a role in SARS-CoV-2 viral entry, however infection of ACE2-negative cells has not yet been convincingly observed. The furin cleavage site of SARS-CoV-2 spike is key to its different tropism to SARS-CoV-1 in the lungs. While SARS-CoV-1 is limited to the lower respiratory tract due to insufficient expression of the proteases to cleave both the priming and triggering cleavage steps in the upper airways, the use of a ubiquitously expressed protease by SARS-CoV-2 for the priming step has been suggest to expand its tropism into the upper airways [134].

1.9 SARS-CoV-2 spike structure

SARS-CoV-2 spike exists as a highly glycosylated heterotrimer of S1 and S2 embedded in the lipid bilayer of the viral membrane. The S1 domain contains the N-terminal domain (NTD) and receptor binding domain (RBD). The S2 domain contains the fusion peptide, transmembrane domain and cytoplasmic tail of spike. The S1/S2 boundary is bridged by a polybasic cleavage site which permits cleavage by furin-like proteases in the producer cell during spike synthesis (Figure 1.12).

Spike is not the only viral protein in the viral membrane. M is actually the most abundant protein present in the mature viral particle, followed by spike, then E (Snake diagrams of each in Figure 1.13) [135]. M is a triple-spanning membrane protein, with an extra-virion N terminal and a luminal C terminal domain and has been suggested

to function as a sugar transporter based on its structure [123]. M and E are the minimal required proteins to form virus-like-particles with coronavirus morphology, demonstrated by the co-expression of just M, E, and spike [136]. Although a majority of antibodies against SARS-CoV-2 target spike, several have also been identified that bind the M protein, possibly due to the large presence of M in the viral particle [137].

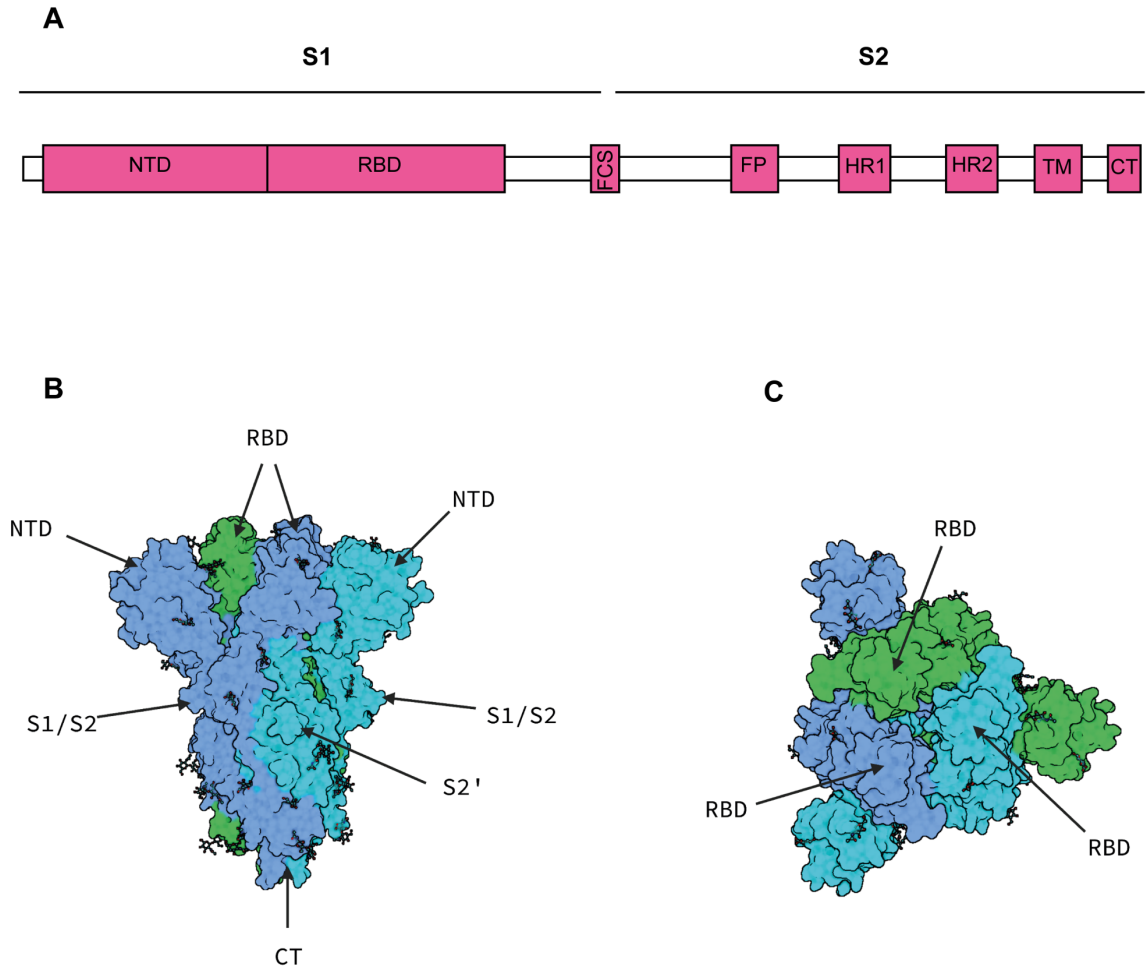

Figure 1.12. SARS-CoV-2 spike schematic. A) Schematic of spike highlighting the NTD (N-terminal domain), RBD (receptor binding domain), polybasic cleavage site, FP (fusion peptide), heptad repeats (HR1 and HR2), transmembrane (TM) and CT (cytoplasmic tail). B) Trimeric spike (PDB:6VXX) labelled with NTD, RBD, S1/S2 cleavage site, S2' site, and CT. C) Trimeric spike (PDB:6VXX) viewed from above. Figure B and C created in BioRender.

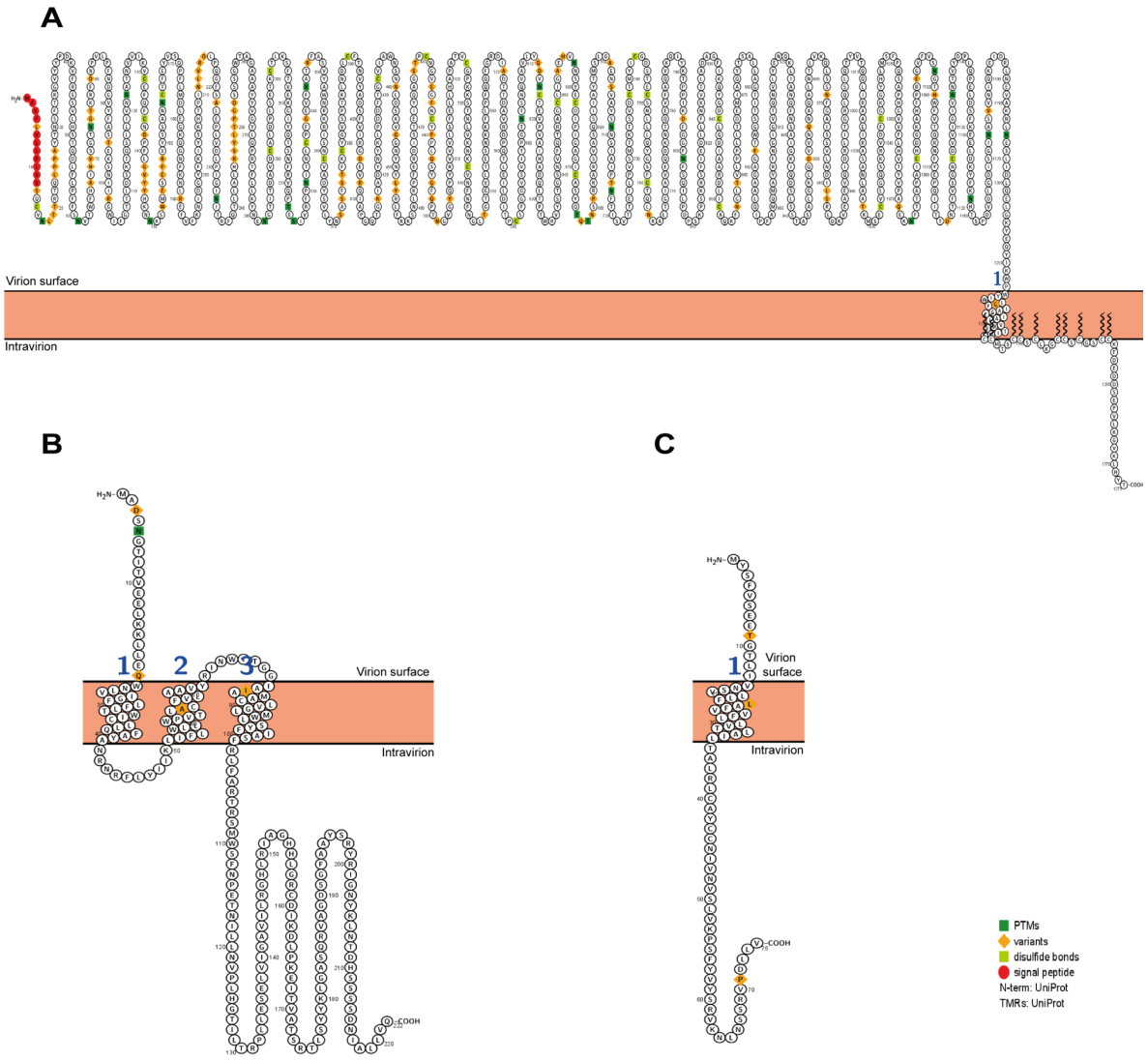

Figure 1.13. Snake diagrams of SARS-CoV-2 spike, membrane and envelope proteins. A, B, C) Snake diagrams of spike (A), membrane (B), and envelope (E) were generated in Protter. Post-translational modifications highlighted in green and variant mutation locations highlighted in orange.

1.9.1 Spike NTD

The NTD of the S1 domain of spike is located at the top of the spike trimer and contains several N-linked glycans. The NTD has previously been suggested to facilitate the binding of spike to attachment factors on the cell surface for a bovine coronavirus [138], however whether this is also the case for SARS-CoV-2 has not yet been confirmed. It has however been suggested that the NTD can modulate TMPRSS2-dependent viral entry and allosterically affect the accessibility of the RBD [139, 140]. The NTD is also a target for neutralising antibodies to spike, as several mutations that have arisen in SARS-CoV-2 variants have been found to escape antibody

neutralisation [141-143]. An antibody “supersite” has been identified which comprises of a beta-hairpin loop surrounded by the glycan N17, N74, N122, and N149 [20].

1.9.2 Spike RBD

The spike RBD mediates the interaction with ACE2. There are six amino acid residues that are critical for ACE2 binding: K417, F456, F486, Q493, Q498, and N501 [144, 145]. Spike exists as a trimer, and when all three RBDs are “down”, the spike is in the closed conformation. Prior cleavage at the S1/S2 boundary of the SARS-CoV-2 spike is essential to the RBD adopting the “up” conformation and being able to bind ACE2. When one RBD is “up”, this is a partially open conformation that could theoretically mediate receptor binding (Figure 1.14). Although spike is a homotrimer with three RBDs per spike unit, the movement of only one of these into the “up” conformation is sufficient to mediate the transition from a closed to an open conformation of spike [146]. It has been suggested that an interaction between spike and heparan sulfates may promote the open conformation [126]. This allows the accessibility of the second cleavage site to be accessed by TMPRSS proteases, cathepsins B/L, or matrix metalloproteinases (MMPs) dependent on the bioavailability [10, 128, 129].

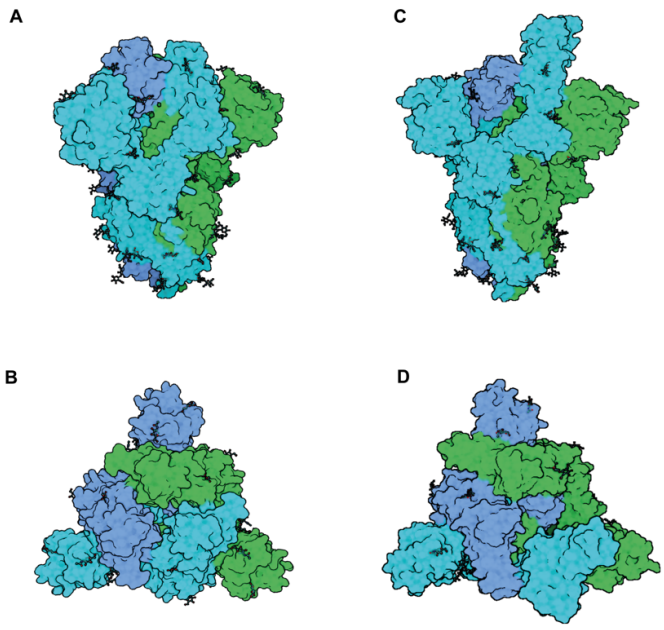

Figure 1.14. Effect of RBD up on spike conformation. A, B) Spike trimer coloured by chain in the closed conformation (PDB: 6VXX) from side on (A) and above (B). C, D) Spike trimer coloured by chain in the one RBD up conformation (PDB: 6XM4) with the cyan chain in the up position from the side on (C) and above (D). Figure made in BioRender.

There are 24 +/-9 spikes estimated per virion and surprisingly cryo-EM studies have shown that not all spikes per virion are in the prefusion conformation [147, 148]. One paper estimated that 97% of spikes were in the prefusion conformation, 3% in the post fusion conformation, and that these were evenly distributed across virions [148]. Another report found a similar majority of spikes in prefusion conformation, but that virions that contained fewer spikes overall also contained more in a post fusion conformation, and that these were closer together. This indicates a tendency for post fusion spikes to "bundle" onto the virus surface [147]. Across a single virion, spikes have been found to be a mix of totally closed RBDs, two RBDs "up", or one RBD "up" in addition to some spikes in the post fusion conformation [148]. The factors involved in dictating the propensity to find more post fusion spikes on a particle are yet to determined. The relative availability of furin and other proteases in the producer cell may be a factor, as more priming spike cleavage could result in premature activation of spike.

1.9.3 Spike polybasic cleavage site

The canonical cleavage sites in the SARS-CoV-2 spike are located at the S1/S2 boundary ($_{681}$PRRA/RS$_{686}$), and at the S2' site ($_{815}$RS$_{816}$) located upstream of the fusion peptide. However, whether the S2' site is the only location the triggering cleavage can occur is still up for debate. It has recently been demonstrated that there are two additional sites in spike which can be cleaved by cathepsin L, located at position 259 in the NTD, and position 636 in the CTD of the S1 unit [149]. Both of these sites are conserved amongst SARS-CoV-2 variants to date, and the authors demonstrate that these sites lead to functional spike cleavage and entry *in vitro.*

The presence of four amino acids at the S1/S2 boundary and the creation of a polybasic cleavage site at this position represents a major difference between the spikes of SARS-CoV-1, SARS-CoV-2 and the related bat RATG13 and Pangolin Guangdong viruses (Figure 1.15). In SARS-CoV-1, this can only be cleaved by TMPRSS or cathepsin proteins, necessitating that the priming step happens on or in the target cell. However, the presence of these four amino acids in SARS-CoV-2 results in this priming site being cleaved by furin, TMPRSS, or cathepsins as

mentioned earlier. In addition to conferring polybasic cleavage properties, the presence of these four amino acids led to the acquisition of 3 potential O-linked glycosylation sites around the site, S673, T678, and S686 [113]. The polybasic cleavage site is important for transmission in animal models, with viruses lacking the polybasic cleavage site being shed to lower titres in infected ferrets, and not transmitted to other animals [150]. Loss of the polybasic cleavage site also attenuates pathogenicity in hamster models [151]. It has also been reported that trypsin treatment of MERS-like coronaviruses from bats confers the ability to infect human cells, implying that overcoming the barrier of S1/S2 cleavage is an important factor in transmitting to humans [152]. As previously mentioned, the acquisition of polybasic cleavage sites in the HA protein of influenza has been linked to the conversion of low, to high pathogenicity viruses [153]. This demonstrates that in multiple viral species the acquisition of polybasic cleavage sites results in increased transmission and/or pathogenicity.

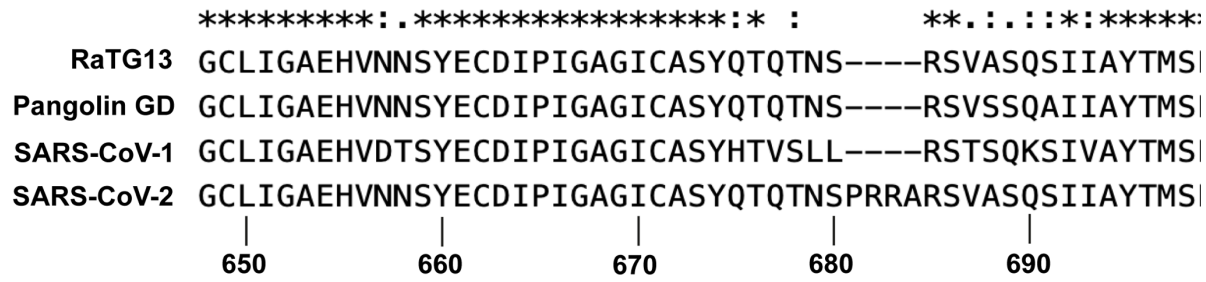

Figure 1.15. SARS-CoV-2 has a polybasic cleavage site. Sequence alignment of RaTG13, Guangdong Pangolin, SARS-CoV-1 and SARS-CoV-2 spikes between amino acids 657-704. Sequences aligned in DNA Dynamo.

Although this site has been implicated in the increased transmission of SARS-CoV-2 relative to other coronaviruses that infect humans, the polybasic S1/S2 cleavage site is rapidly lost in passage of the original Wuhan-like virus in Vero-E6 cells, which have high expression levels of cathepsins B and L, but low TMPRSS2 [154]. Similar mutations have also been reported in patients in the early waves of the pandemic [155, 156]. Since then, mutations have emerged adjacent to the polybasic cleavage site that can enhance the efficiency of cleavage [157-159]. Of note, whilst cleavage of the S2' site by TMPRSS2 requires the S1/S2 cleavage site to already have been cleaved, cathepsins on endosomal membranes can achieve both the priming cleavage as well

as the activation cleavage [160]. This could suggest why viruses can lose the polybasic cleavage site so rapidly in culture of cells that are high in cathepsins and low in TMPRSS2. It is also becoming apparent that other proteases besides furin, TMPRSS2, and cathepsins B/L play a role in spike cleavage, with other TMPRSS and MMPs being demonstrated to mediate spike cleavage (Figure 1.16). Additionally, differences in cell culture conditions have been shown to affect spike cleavage, with higher serum concentrations found to mimic trypsin-like effects and result in increased spike cleavage [161]. The furin-mediated cleavage of the S1/S2 boundary has also been found to create substrates for other host factors. The cleaved end of the S1 domain can be bound by neuropilin, which has been demonstrated to increase viral entry *in vitro* [162, 163]. Neuropilin-1 and 2 are abundantly expressed transmembrane receptors in the respiratory and olfactory epithelium. Daly et al report blocking of neuropilin with a small molecule inhibitor decreases SARS-CoV-2 entry by inhibiting the interaction between the cleaved S1 C-terminal and neuropilin [163]. However, the relevance of this *in vivo* has not yet been established.

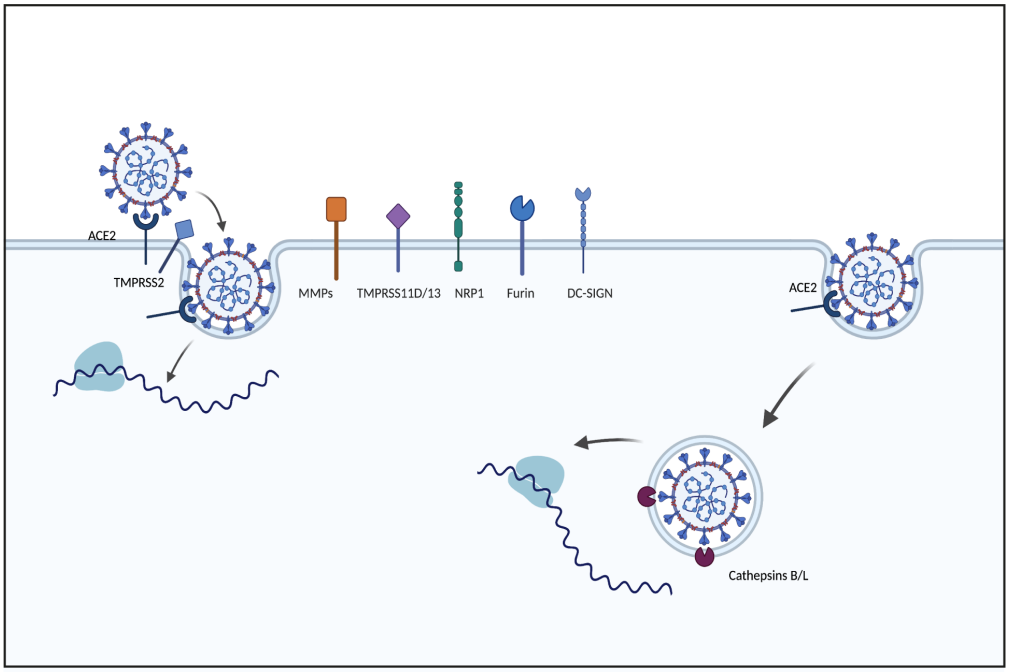

Figure 1.16. Different proteases and entry factors. DC-SIGN has been shown to facilitate binding of SARS-CoV-2 to target cells. TMPRSS2 has been the mainly characterised protease to mediate S2' cleavage and early entry of SARS-CoV-2. Other TMPRSS proteins including TMPRSS11D/13 have also been shown to cleave spike. MMPs have been demonstrated to cleave spike and permit entry. Neuropilin has been shown to bind the cleaved end of the S1 of spike and facilitate entry. Cathepsins B and L, and now potentially G, are found on endosomal membranes and can also cleave the S2' site.

1.10 Spike synthesis

The SARS-CoV-2 spike protein is synthesised as a polyprotein precursor that requires two proteolytic cleavages, priming and triggering, prior to mediating the viral entry of SARS-CoV-2. Spike translation begins in the cytoplasm, however the presence of an ER signal in the N-terminal signal peptide of spike results in transport of the spike transcript to the ER, where translation is completed [164]. The N terminal is removed by proteases in the ER lumen, and spike translation and post-translational modifications occur concomitantly. During the transport of spike through the ER, N-linked high mannose oligosaccharides are added which are then modified to become a mix of complex and high mannose oligosaccharides. O-linked oligosaccharides are added once spike has been transported from the ER to the Golgi [164]. During spike synthesis, furin-like proteases can cleave the S1/S2 cleavage site, with the S1 and S2 domains remaining associated via non-covalent interactions. O-linked glycosylation has been proposed to decrease furin-mediated cleavage, which may be another factor in determining SARS-CoV-2 tropism [165]. Although furin is likely the main protease to mediate the S1/S2 cleavage in spike, it has been demonstrated that some spike cleavage occurs in furin knock-out cells, showing that other proteases can also cleave this site, albeit less efficiently [166]. Additionally, as furin is a membrane bound protease produced in the ER and transported through the secretory pathway, it is also possible that furin can cleave the S1/S2 cleavage site during other steps of spike synthesis, or even once virions have egressed from the producer cell. The exact timing of furin-mediated cleavage in spike biosynthesis is not yet known. It is possible that the serine protease patriptase that activates the HA of H9N2 influenza virus may also be a candidate for cleaving the polybasic cleavage site of SARS-CoV-2 [167].

The presence of an inefficient endoplasmic reticulum retention signal (ERRS) at the C terminal of spike retrieves spike from the face of the cis-Golgi by recruiting the COPI coatomer and facilitates the return of spike to the ER [168]. The inefficiency of this signal has been proposed to serve several functions: it retains spike in the ER which is the site of coronavirus assembly, it allows some spike to leak to the membrane to mediate syncytia formation, and may also be important in ensuring spike has undergone the appropriate post-translational modifications in the ERGIC [169]. The ERRS sequence is important for mediating the interaction of spike with the M protein.

The M protein assists incorporation of mature spike into virus particles and the trafficking of spike to the site of viral assembly [170, 171]. Additionally, the leaky ERRS ensures that some spike protein travels to the plasma membrane through the secretory pathway and forms syncytia with ACE2 on neighbouring cells. This allows SARS-CoV-2 to spread between cells whilst avoiding neutralising antibodies and syncytia formation is a major factor in the pathology of SARS-CoV-2 in lung tissue [75, 169, 172]. The ability to form syncytia has been reported to be variable amongst SARS-CoV-2 variants, likely due to differences in cleavage efficiency at the S1/S2 boundary [173]. Some coronavirus spike proteins do not have an intracellular localisation signal and may accumulate more rapidly at the membrane which may contribute to differential pathogenesis across different coronavirus infections [174]. Deletion of the spike cytoplasmic tail, including the ERRS, has been found to increase viral titre of PLVs by increasing the amount of spike that reaches the plasma membrane, where lentiviral vectors assemble [175]. However, the rate of trafficking of spike through the ERGIC has been found to be important for post-translational modifications such as glycosylation. There are 22 N-linked glycosylation sites in the ancestral Wuhan SARS-CoV-2, several of which are important for determining spike conformation and altering infectivity. N343 is a “glycan gate” that can modulate the propensity of the RBD to adopt the ‘up’ conformation [176]. Additionally, removal of other N-linked glycosylation sites such as N165 and N234 have been found to reduce infectivity [177]. There are more complex high mannose N-linked glycans in the S2 domain than the S1 domain, which are added during cleaved spike cycling through the Golgi [168]. Whether these complex glycans are also added to spikes with cytoplasmic deletions that do not cycle back to the ER, is unknown.

1.11 Variants of SARS-CoV-2

It was initially expected early on in the COVID-19 pandemic that SARS-CoV-2 would not exhibit a high rate of mutation due to the error-correcting capacity in the nsp14 exonuclease protein in the RdRp complex [178]. Contrary to this, it became apparent that despite this error-reading capacity, SARS-CoV-2 does indeed accumulate mutations which are then selected for due to conferring advantages for replication and/or transmission, resulting in multiple variants of SARS-CoV-2. During Wave 1 of

the pandemic, the D614G mutation became the first identified mutation in spike to become fixed [179]. Since then, a myriad of other mutations in the spike protein have been documented, and viruses that demonstrated enhanced transmission or immune evasion characteristics designated as variants of concern (VOCs) (Table 1.1). The first of these was the alpha variant (also known as B.1.1.7), which arose in the autumn of 2020 in the South-East of England. This appeared more transmissible than wave 1 isolates and rapidly spread around the globe in early 2021 [180-182]. Several other, less prevalent variants also emerged at the end of 2020, with the beta variant in South Africa in December of 2020, and the gamma variant in Brazil in January of 2021. In February of 2021, the kappa and delta variants emerged in India. While the kappa variant did not take off to the same extent and was not classified as a variant of concern, the delta variant became more prevalent and dominant worldwide by the end of 2021. This was in turn displaced by the emergence of the omicron BA.1 variant in winter of 2021, and since then several other omicron sub-variants have emerged.

1.11.1 D614G

Due to the high sequence homology, several studies utilised SARS-CoV-1 as a comparator when assessing the viral properties of the original SARS-CoV-2 strain. As previously mentioned, SARS-CoV-2 contains a polybasic cleavage site which SARS-CoV-1 does not, however there were several other differences in viral phenotypes. Firstly, SARS-CoV-2 demonstrated 10x higher affinity for the ACE2 receptor than SARS-CoV-1 [183]. Additionally, SARS-CoV-2 exhibited a differential tropism for the upper airways, whereas SARS-CoV-1 was previously found to preferentially infect the tissues of the lower airways [106]. Lastly, the ancestral strain of SARS-CoV-2 was initially found to be more sensitive to the effects of type I IFNs, despite similar viral replication kinetics, compared to SARS-CoV-1 [184].

In March 2020, 2 months after the documentation of SARS-CoV-2, the first mutation in the SARS-CoV-2 spike protein was identified, D614G [185]. The 614 site is in a pocket adjacent to the S2' cleavage site (Figure 1.17). The rapid dominance of this mutation, with nearly every sequence across Europe containing the D614G mutation by May of 2020, led to concerns that it was both more transmissible and perhaps more

pathogenic. Clinically however, although the viral load was found to be increased in G614-carrying patients relative to D614 patients, there did not appear to be any link between D614G and disease severity [185, 186]. Biologically, this mutation has been found to alter several properties of spike. The location of this mutation adjacent to the S2' site was suggested to impact the propensity of spike to utilise TMPRSS2 for entry. Accordingly, it was demonstrated that the D614G mutation increased infectivity in a TMPRSS2-dependent manner [185, 187]. It has also been shown that this mutation can increase S1/S2 processing, and may also alter the glycosylation at the 616 site adjacent to D614G [185, 188]. In addition to increasing S1/S2 processing, it has been found that D614G increases both spike incorporation and reduces S1 shedding [189]. Both increased incorporation and reduced shedding are likely to contribute to the increased stability of the D614G spike relative to the Wuhan spike [189].

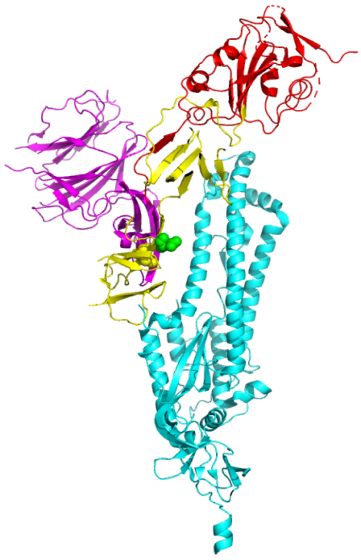

Figure 1.17. The D614G mutation sits adjacent to the cleavage loop in spike. SARS-CoV-2 spike coloured in pink (NTD), red (RBD), cyan (S2), and yellow for the intervening region. D614G mutation highlighted in green. PDB:6VXX. Structure made in PyMOL.

1.11.2 The alpha variant

In late 2020, the alpha variant was first detected in the UK. At the time, three sets of primer/probe sets were used in PCR diagnostic testing to confirm SARS-CoV-2 infection, one in spike, and two in nucleocapsid. The serendipitous location of the

primers for spike coincides with a mutation in the alpha spike, Δ69/70, resulting in the spike "drop out" phenomenon in PCR testing, whereby samples were positive for nucleocapsid but not for spike. Sequencing of these spike drop out results led to the discovery of a SARS-CoV-2 variant with seven substitutions and two deletions: Δ69/70 and Δ144 in the NTD, N501Y in the RBD, A570D and D614G in the CTD, P681H in the polybasic cleavage site, and T716I, S982A and P1118H in the S2 domain (Figure 1.18). Several of the mutations in the alpha variant have now been characterised. The Δ69/70 mutation has been found to increase spike incorporation and has been suggested to compensate for other mutations which may decrease spike fitness [190]. The Δ144 mutation has been found to escape neutralising antibodies that target the NTD [143]. The N501Y mutation increases the affinity of the RBD for ACE2 [191]. The P681H mutation increases S1/S2 cleavage, and as described later in this thesis escapes IFITM2-mediated restriction in TMPRSS2-negative cells [30, 159, 192]. The alpha variant was also found to be more resistant to the effects of exogenous IFN, and also demonstrated enhanced ability to escape innate immunity through increased expression of orf6 and orf9 [29, 193].

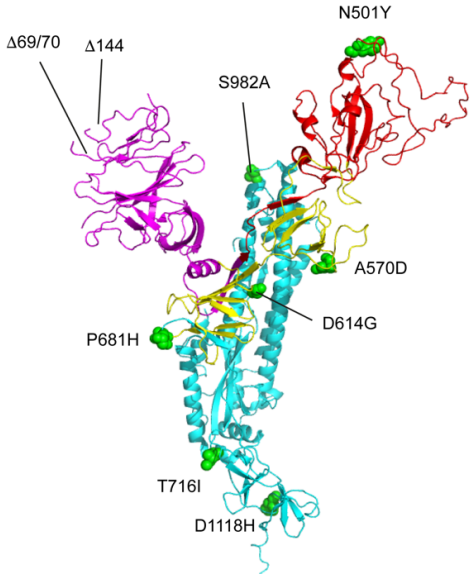

Figure 1.18. The alpha variant has seven mutations and two deletions in spike. NTD (purple), RBD (red), and S2 domain (cyan) coloured on the 7FET (PDB) alpha spike monomer. Mutations are highlighted in green. Deletions are marked with arrows.

Table 1.1. Spike mutations in variants of concern/interest. Spikes highlighted in red are used in this thesis.

Variant	Lineage	Origin date	Origin location	Spike mutations
D614G	B.1	March 2020	Europe	D614G
Alpha	B.1.1.7	Dec 2020	UK	Δ69-70, Δ144, N501Y, A570D, D614G, P681H, T716I, S982A, D1118H
Beta	B.1.351	Dec 2020	South Africa	D80A, D215G, Δ242-244, K417N, E484K, N501Y, D614G, A701V
Gamma	P1	Jan 2021	Brazil	L18F, T20N, P26S, D138Y, R190S, K417T, E484K, N501Y, D614G, H655Y, T1027I
Eta	B.1.525	March 2021	North America	Q52R, A67V, Δ69/70, Δ144, E484K, D614G, Q677H, F888L
Iota	B.1.526	Late 2020	New York	L5F, T95I, D253G, E484K, D614G, A701V
Lambda	C.37	Late 2020	South America	G75V, T76I, ΔR246, ΔS247, ΔY248, ΔL249, ΔT250, ΔP251, ΔG252, D253N, L452Q, F490S, D614G, T859N
Mu	B.1.621	Early 2021	South America	T95I, Y144S, Y145N, R346K, E484K, N501Y, D614G, P681H, D950N
Kappa	B.1.617.1	Late 2021	India	G142D, E154K, L452R, E484Q, P681R, D614G, Q1071H
Delta	B.1.617.2	Late 2021	India	T19R, Δ156-157, R158G, L452R, T478K, P681R, D614G, D950N
Omicron	B.1.1529 BA.1	November 2021	South Africa	A67V, Δ69/70, T95I, ins 214EPE, G142D, Δ143-145, NL211-212I, G339D, S371L, S373P, S375F, K417N, N440K, G446S, S477N, T478K, E484A, Q493R, G496S, Q498R, N501Y, Y505H, T547K, D614G, H655Y, N679K, P681H, N764K, D796Y, N858K, Q954H, N969K, L981F
Omicron	B.1.1529 BA.2			T19I, Δ24-26, A27S, G142D, V213G, G339D, S371F, S373P, T376A, S375F, D405N, R408S, K417N, S477N, T478K, E484A, N501Y, Y505H, Q493R, Q498R, D614G, H655Y, N679K, P681H, N764K, D796Y, Q954H, N969K

Omicron	B.1.1529 BA.4/5			T19I, ∆24-26, **∆69/70**, A37S, G142D, V213G, G339D, S371F, S373P, S375F, T376A, D405N, R408S, K417N, N440K, **L452R**, E484A, **F486V**, N501Y, Y505H, Q498R, D614G, H655Y, N679K, P681H, N674K, D796Y, Q954H, N969K

1.11.3 Spike mutations across variants of interest

The evolution of SARS-CoV-2 spike has demonstrated significant convergent evolution, with multiple divergent strains adopting similar or the same mutations to escape antibody neutralisation and alter spike properties (Figure 1.19, Table 1.2). The ∆69/70 mutation, which increases spike incorporation as mentioned earlier, has been documented in the alpha, eta, and in the omicron BA.1 and BA.4/5 variants. This mutation has also been documented in long-term COVID-19 patients unable to clear infection, and has been found to co-occur with both the D796H and Y453F mutations [190, 194]. Mutations at D796 and Y453 have been found to escape antibody neutralisation, and it has been suggested that the increased spike incorporation of the ∆69/70 mutation is required to compensate for the detrimental effect of these escape mutations [190]. Deletions in other regions of the NTD, including ∆144/145 mutations, have also been reported in other persistently infected COVID patients [195, 196]. In addition to chronic patients, the ∆69/70 and D796Y combination is present in the omicron BA.1 and BA.4/5 variants.

Another mutation that has been found in several variants to date is the N501Y mutation in the RBD. This mutation is present in the alpha, beta, gamma, mu and omicron variants. This mutation has been found to increase affinity for ACE2 [191]. Interestingly, this mutation has also been reported to permit antibody escape mutations in the RBD, which would otherwise be detrimental, to be tolerated without overall negative consequences for ACE2 binding and spike structure [197]. Deep mutational scanning of VOC spikes has revealed the epistatic role of the N501Y mutation in permitting future antibody escape mutations to be tolerated by spike; the N501Y mutation affects not only the direct contacting residues of Q498 and 491-496,

but also the 446-447, 449, and 403, 505, 506, and 406 residues [197]. Starr et al report that although the Q498R mutation weakens ACE2 interaction, incorporation of the N501Y mutation increases the Q498R binding affinity 25-fold. This double mutant is present in the omicron spike. The recurrent theme of the N501Y across multiple VOCs is likely due to its impact on ACE2 binding of not only itself but other residues. A combination of the K417N/T, E484A/Q/K and N501Y mutations is seen in several variants to date, and has been suggested to be favourable because of the N501Y mutation compensating for the K417 and E484 antibody escape mutations which are more detrimental alone [198].

Since the alpha variant, several other VOCs have emerged with mutations in the spike protein. Of particular interest, several of the variants also contained mutations within the polybasic cleavage site: kappa, delta, and omicron all contain P681R or P681H mutations [126, 199]. The location of these mutations was suggested to enhance the efficiency of S1/S2 cleavage, as mentioned earlier. However there has been discrepancy in the literature over which of these spikes are better cleaved than others, with some claims the P681R in kappa and delta is better cleaved, and others claiming the P681H mutation found in alpha and omicron confers enhanced S1/S2 cleavage [30, 157-159, 188, 192]. It is likely that cleavage efficiency is also a function of cell type, and the cells used to grow virus can alter the level of spike cleavage achieved.

It is also possible that mutations outside of the polybasic cleavage site itself can influence the efficiency of both the S1/S2 cleavage and the S2' site. The H655Y mutation has also been found in unrelated lineages (gamma and omicron) and documented in both persistent human infection and during infection of African green monkeys [200, 201]. This mutation has been found to outcompete a H655 virus in hamster models, suggesting this mutation enhances transmission [202]. Additionally, the H655Y mutation has been identified as a determinant of endosomal entry, which is consistent with evidence so far of the omicron variant being less TMPRSS2-dependent [203, 204]. There are also many mutations in the S2 domain which have not yet been thoroughly investigated in their function or impact on spike conformation. It has however been demonstrated that the S2 domain of omicron is a determinant of

both its decreased utilisation of the TMPRSS2-dependent route of entry and relatively closed conformation compared to earlier variants [204]. It is highly possible that mutations in the S2 domain may stabilise or destabilise the pre- or post- fusion conformation, and therefore have knock-on effects on viral entry.

A majority of the mutations emerging in spike variants to date have been identified as antibody escape mutations, especially in the NTD and RBD which are the most accessible parts of spike to neutralising antibodies. A “supersite” has been identified in the NTD where many antibodies can bind, which several mutations present in variants can escape [20, 142]. (Table 1.3). Of the antibodies that bind the RBD, there are antibodies that only bind the RBD ‘up’ structure and block ACE2 binding, antibodies that bind both the RBD ‘up’ and RBD ‘down’ structure and block ACE2 binding, antibodies that bind both RBD ‘up’ and RBD ‘down’ but block outside of the ACE2 binding site, and antibodies that bind the RBD ‘up’ structure but do not block ACE2 binding [205].

There are other selective pressures on SARS-CoV-2 spike besides adaptive immunity escape and several mutations thus far alter spike incorporation and restriction by innate immunity. The D614G mutation, the first to become fixed, improves spike incorporation and subsequently infectivity in a TMPRSS2-dependent manner [189]. This mutation also enhances syncytia formation, which could indirectly aid escape from neutralising antibodies, and may also contribute to evasion of IFITMs [76, 206]. D614G has also been found to reduce sensitivity to GBP2 and GBP5, which inhibit furin-mediated cleavage, which may represent a relatively early adaptation to escape from innate immunity [94].

	alpha	beta	gamma	kappa	delta	eta	lamba	mu	omicron BA.1	omicron BA.2	omicron BA.4/5
NTD		L18F	L18F								
					T19R					T19I	T19I
			T20N								
										L24-	L24-
										P25-	P25-
			P26S							P26-	P26-
										A27S	A27S
						E52R					
						A67V			A67V		
	H69-					H69-			H69-		H69-
	V70-					V70-			V70-		V70-
							G75V				
							T76I				
		D80A									
								T95I	T95I		
			D138Y								
					G142D				G142D	G142D	G142D
	Y144-					Y144-		Y144S	Y144-		
								Y145N	Y145D		
				E154K							
					F157-						
			R190S								
									N211-		
									L212I		
										V213G	V213G
		D215G									
		L242-									
		L243-									
		L244-									
							R246-				
							S247-				
							Y248-				
							L249-				
							T250-				
							P251-				
							G252-				
							D253N				
RBD									G339D	G339D	G339D
								R346K			
									S371F	S371F	S371F
									S373P	S373P	S373P
									S375F	S375F	S375F
										T376A	T376A
										D405N	D405N
										R408S	R408S
			K417N		K417T				K417N	K417N	K417N
									N440K	N440K	N440K
									G446S		
				L452R	L452R		L452Q				L452R
									S477N	S477N	S477N
					T478K				T478K	T478K	T478K
				E484Q		E484K		E484K	E484A	E484A	E484A
											F486V
							F490S				
									Q493R	Q493R	
									G496S		
									Q498R	Q498R	Q498R
	N501Y	N501Y	N501Y					N501Y	N501Y	N501Y	N501Y
									Y505H	Y505H	Y505H
									T547K		
S1/S2 boundary	A570D										
	D614G	D614G	D614G	D614G	D614G	D614G	D614G	D614G	D614G	D614G	D614G
			H655Y						H655Y	H655Y	H655Y
						Q677H					
									N679K	N679K	N679K
		A701V									
	P681H			P681R	P681R			P681H	P681H	P681H	P681H
S2	T716I										
									N764K	N764K	N764K
									D796Y	D796Y	D796Y
									N856K		
							T859N				
						F888L					
					D950N			D950N			
									Q954K	Q954K	Q954K
									N969K	N969K	N969K
	S982A										
			T1027I								
				Q1071H							
	D1118H										
			V1176F								

Figure 1.19. Many mutations, or site of mutation, are shared across the major variants. Table created with information from Covariants.org. Mutations are grouped by spike region.

Table 1.2 Spike mutations of interest within VOCs to date

Mutation	Effects	Variant
L18F	Located in NTD supersite, likely affects antibody binding [142] Destabilises ACE2 interaction [207]	Beta, gamma
T19R/I	Located in NTD supersite [142] T19I reduces syncytia formation as a singular mutation [208]	BA.2, BA.4/5
T20N	Introduces a potential glycosylation site [209]	Gamma
∆24-26	Reduces syncytia formation as a singular mutation [208]	BA.2, BA.4/5
A27S	No reported effect to date	BA.2, BA.4/5
P26S	No reported effect to date	Zeta, gamma
A67V	No reported effect to date	BA.1
∆69/70	Increases spike incorporation [190]	Alpha, BA.1
T95I	No reported effect to date	BA.1, delta plus
D138Y	No reported effect to date	Gamma
D80A	Located in NTD supersite [142]	Beta
G142D	Located in NTD supersite [142]	Delta plus
∆143-145	Likely affects antibody binding [142]	BA.1
E154K	No reported effect to date	Kappa
∆156-157	Antibody escape [141]	Delta
G158R	Located in NTD supersite [142] Antibody escape [141]	Delta
R190S	No reported effect to date	Gamma
∆144	Antibody escape [143]	Alpha
211L/212I	Escapes T cell response [210]	BA.1

V213G	Escapes T cell response [210]	BA.2, BA.4/5
Ins 214 EPE	Escapes T cell response [210]	BA.1
D215G	Emerges in NHP models of SARS-CoV-2 with H655Y [201]	Beta
A222V	Small increase in PLV titre [211]	Delta plus
∆242-244/ ∆243-244	Antibody escape [143, 212]	Beta
R246I/∆	Located in NTD supersite [142] Likely affects antibody binding [142]	Lambda
G339D	Evades the T cell response [213]	Omicron
S371F/L	Reduces infectivity as a singular mutation, reduces syncytia formation [208]	Omicron
S373P/F	Increases spike stability [214]	Omicron
S375F	Reduces infectivity as a singular mutation [208]	Omicron
T376A	Reduces infectivity as a singular mutation, reduces syncytia formation [208]	BA.2
D405N	D405 is a key residue in the opening of the RBD [215]	BA.2, BA.4/5
R408S	R408 is a key residue in the opening of the RBD [215]	BA.2, BA.4/5
K417N/T	Antibody escape [18]	Beta, gamma, delta, omicron
N440K	Antibody escape Destabilises T cell response [213]	Omicron
G446S/V	Antibody escape [216]	BA.1
Y449H	Antibody escape [197]	C.1.2
L452R	Antibody escape [18, 217]	Kappa, delta
S477N	Increases binding to ACE2 [218]	Omicron
T478K	Enhances entry into mouse/koala ACE2 expressing cells [219]	Delta, omicron

E484K/Q/A	Antibody escape [18, 143] E484K enhances entry into mouse/koala ACE2 expressing cells [219]	Beta, kappa, gamma, omicron
F486V	Antibody escape [217]	BA.4/5
Q493R	Drug resistance [220]	BA.1, BA,2
Q498K/R	Q498R increases ACE2 affinity in the context of N501Y [197]	Omicron
N501Y	Increases affinity to ACE2, and allows tolerance of other mutations in the RBD [197] Does not increase binding to mouse ACE2 [219]	Alpha, beta, gamma, omicron
H505Y	Increases ACE2 affinity [221]	Omicron
T547K	T547 stabilises the down state of the RBD [222]	BA.1
A570D	Reduces trimeric affinity in combination with S982A and D614G [223] May also interact with D950N and D1118H [222] Stabilises interactions between HR1 and SD1 [224] Enhances ACE2 interaction	Alpha
D614G	Orders the 630 loop, increases virion spike density, increases infectivity, reduces s1 shedding [189] Abolishes a salt bridge with K854 which may reduce the folding of the 833-854 loop [148]	All variants to date
N764K	No reported effect to date	Omicron
A701V	Likely affects antibody binding	Beta
H655Y	Increases endosomal entry dependence [203] Emerges in NHP models with D215G [201]	Gamma, omicron
Q677H	Could influence the S1/S2 cleavage [225]	Eta
P681H	Enhances S1/S2 cleavage by furin [159, 192]	Alpha, omicron
P681R	Enhances S1/S2 cleavage by furin [157, 158, 188] Increases binding by HLA [210]	Kappa, delta
T716I	Destabilises the prefusion spike conformation [224]	Alpha
N679K	Creates a cathepsin G cleavage site in combination with P681H [226]	Omicron

D796H/Y	In fusion peptide, increases hydrophobicity [222] Antibody escape [227]	Alpha
N856K	No reported effect to date	BA.1
D950N	In the HR1 region Enhances S1/S2 cleavage with P681R [228]	Delta
Q954H	In HR1 region	Omicron
S982A	In the HR1 region Reduces trimeric affinity in combination with D614G and A570D [223] Increases the 'up' of the RBD by eliminating interaction with T547, however is counteracted by A570D [222]	Alpha
N969K	At end of HR1 region Promotes endosomal entry [229] Reduces infectivity as a singular mutation [208]	Omicron
L981F	In between HR regions Moderately increases syncytia formation as singular mutation [208]	BA.1
T0127I	In between HR regions No reported effect to date	Gamma
Q1071H	In between HR regions No reported effect to date	Kappa
D1118H	In between HR regions Stabilises the prefusion spike conformation [224]	Alpha
V1176F	In HR2 region No reported effect to date	Gamma

1.11.4 Mutations in other SARS-CoV-2 viral proteins

Although spike is a hotspot for mutations, some have been found in other viral proteins, mostly in the accessory proteins (orfs), N, and intriguingly some mutations have emerged in M, the most abundant protein in the viral membrane (Figure 1.20). M is well conserved amongst related coronaviruses, with the pangolin Guangdong coronavirus sharing 98.2 % and SARS-CoV-1 sharing 90 % homology with SARS-

CoV-2 M [123]. There are 4 mutations known in M to date, I82S (kappa), I82T (delta) and the D3G/Q19E/A63T combination (omicron). The D3G and Q19E mutations of omicron are in the N terminal domain of M, which is postulated to be facing out towards the virion surface [123]. The A63T and I82S/T mutations are in the second and third transmembrane domains of the predicted M structure [123]. The location of these mutations may therefore directly alter the interactions between M and spike or how M is located in the viral membrane. The C-terminal of M has been shown to interact with spike in other coronaviruses, however no mutations in the C-terminal of SARS-CoV-2 have been reported to date [230]. The presence of two N-terminal mutations in omicron is therefore perhaps surprising, however these could be antibody escape mutations as antibodies against M have been documented in patient sera [137].

In addition to mutations in viral proteins, differential expression levels of SARS-CoV-2 accessory proteins have also been reported. The alpha virus has been found to express higher levels of orf9b, which reduces innate immune sensing and therefore mediates the effects of interferon [193]. Additionally, an independent study identified that emerging variants of SARS-CoV-2 are less sensitive to IFN than the ancestral strain, and that of those tested, the alpha variant was the least sensitive to IFN inhibition [29]. Overall, the sequence differences in variants to date are indicative of both adaptive and innate immunity mediated selection pressures.

	alpha	beta	gamma	kappa	delta	eta	lamba	mu	omicron BA.1	omicron BA.2	omicron BA.4/5
ORF1a										S135R	S135R
		T265I									
										T842I	T842I
									K856R		
	T1001I										
								T1055A			
			S1188L								
							T1246I				
										G1307S	G1307S
								T1538I			
				T1567I							
		K1655N									
	A1780D										
			K1795Q								
						T2007I					
									S2083-		
									L2084I		
	I2230T						P2287S				
							F2387V				
									S2710T		
							L3201P				
										L3027F	L3027S
										T3090I	T3090I
							T3255I	T3255I	T3255I	T3255I	T3255I
		K3353R									
							G3278S				
									I3578V		
									P3395H	P3395H	P3395H
									L3674-		
				T3646A							
	S3675-	S3675-	S3675-			S3675-	S3675-		S3675-	S3675-	S3675-
	G3676-	G3676-	G3676-			G3676-	G3676-		G3676-	G3676-	G3676-
	F3677-	F3677-	F3677-			F3677-	F3677-			F3677-	F3677-
								Q3729R			
ORF1b	P314L	P314L	P314L	P314L	P314L	P314L	P314L	P314L	P314L	P314L	P314L
					G662S						
					P1000L						
				G1229C							
			E1264D								
										R1315C	R1315C
								P1342S			
				M1352I							
									I1566V	I1566V	I1566V
				K2310R							
				S2313A							
										T2163I	T2163I
ORF3a				S26L	S26L						
		Q57H						Q57H			
										T223I	T223I
			S253P								
								V256I			
								N257Q			
								P258*			
ORF6						F2-					
										D61L	
ORF7a					T20I						
				V82A	V82A						
ORF8								T11K			
	Q27*										
								P38S			
	R52I										
								S67F			
	Y73C										
			E92K								
					D119-						
					F120-						
ORF9b									P10S	P10S	P10S
									E27-	E27-	E27-
									N28-	N28-	N28-
									A29-	A29-	A29-
					T60A						
N						S2-					
						D3Y					
						A12G					
							P13L		P13L	P13L	P13L
									E13-	E13-	E13-
											R32-
									S33-	S33-	S33-
					D63G						
			P80R								
	R203K		R203K	R203M	R203M		R203K		R203K	R203K	R203K
	G204R		G204R				G204R		G204R	G204R	G204R
		N205I				N205I		N205I			
							G214C				
	S235F										
				D377Y	D377Y						
										S413R	S413R
M									D3G	D3G	D3N
									Q19E	Q19E	Q19E
									A63T	A63T	A63T
				I82S	I82T	I82T					
E									T9I	T9I	T9I
						L21F					
		P71L									

Figure 1.20. Mutations in non-spike proteins in SARS-CoV-2 VOCs. Table created with information from Covariants.org.

1.11.5 Impact of variant mutations on tropism

Mutations in SARS-CoV-2 variants have been found to impact on viral tropism and the preferential routes of viral entry. The P681R and P681H mutations that arose in the kappa, delta, alpha and omicron variants have been argued to improve the efficiency of the furin cleavage site of spike, and for alpha and delta this correlates with increased usage of TMPRSS2 [157-159, 231]. Although the early alpha and delta variants appeared to be more dependent on TMPRSS2 for cleavage, the omicron variants BA.1 and BA.2 that emerged in late 2021 have been found to be less TMPRSS2-dependent and more reliant on cathepsins to mediate viral entry [204]. Omicron's increased tropism, and viral load, for the upper respiratory tract could have provided omicron with an advantage over variants in terms of transmission. It has been reported that the recent BA.5 variant may now again be more reliant on TMPRSS2 for entry and reflect another shift in tropism [232]. The apparent pattern of alternating TMPRSS2 tropism could suggest that variants which utilise a differential entry pathway to the previous variant have an evolutionary advantage.

The polybasic cleavage site itself has been shown to quickly be lost and re-emerge, depending on cell culture conditions. Polybasic cleavage site deletions have also been documented in some COVID-19 patients and it is likely that these are more endosomal pathway dependent and exhibit a different tropism to the initial transmitted virus [233-236]. The polybasic cleavage site deletions in patient samples and shift of entry preference by omicron variants suggests that benefits of TMPRSS2 mediated route of entry are not as clear-cut as initially demonstrated in animal transmission studies [150]. Instead, route of viral entry by SARS-CoV-2 appears to be a flexible variable that can be rapidly be gained, lost, and adapted.

1.11.6 Origins of SARS-CoV-2 variants

The similarities between mutations emerging from persistently infected patients and those that are present in SARS-CoV-2 variants adds weight to the theory of variants emerging from persistent infections of SARS-CoV-2. Chronic SARS-CoV-2 infections in immunocompromised patients can persist for hundreds of days, allowing the virus time to adapt to both adaptive and innate immunity in a host with a compromised

immune system. Over the course of one long-term COVID-19 infection, the authors identified 12 mutations in spike occurring in 152 days of infection [195]. Since then even longer persistent infections have been identified, with the longest persistent infection documented to date covering 254 days and over 20 mutations in spike [237]. Infections of this length of time provide the virus ample time to adapt to a partially competent immune system, and given the number of antibody escape mutations in VOCs to date, it is highly plausible that SARS-CoV-2 variants could have emerged from persistently infected patients.

It has also been suggested that some mutations that have been found in variants could be due to SARS-CoV-2 spillover back into animals and subsequently back into humans [238]. In this theory, the passage of the virus in a species such as mink, which are susceptible to SARS-CoV-2 infection, could accrue mutations to adapt to mink ACE2 and immune systems, resulting in a distinct virus which could then reinfect humans. The Y453F mutation, identified in long-term patients, was also found in a population of mink infected with SARS-CoV-2 in Denmark and shows increased ACE2 affinity [190, 194, 239]. Coronavirus-to-human zoonoses are not rare events, with SARS-CoV-2 being the seventh documented coronavirus zoonosis. Jumps between humans, animals and back again are therefore possible. Additionally, recombination between SARS-CoV-2 variants, or SARS-CoV-2 and other *sarbecoviruses*, is also possible, with the former already having been documented. Recombination is common in coronaviruses and occurs due to switching of the RNA-dependent RNA polymerase from one RNA template to another in a cell infected by two genetically distinct CoVs [240]. A patient co-infected with beta and delta has been identified and sequencing indicated a high chance of recombination [241]. Additionally there has been evidence of recombination, and onward transmission of a recombinant virus lineage, for at least nine weeks in the UK [242]. There are several potential sources of SARS-CoV-2 variants, and it could be that persistent infection, reverse zoonoses and recombination all contribute to the emergence of variants in combination.

1.12 The HIV-1 pandemic

In the early 1980s, increasing numbers of young men who have sex with men (MSM) were presenting in clinics in the United States with unusual opportunistic infections and malignancies [243]. By 1981, the disease acquired immunodeficiency syndrome (AIDS) was described in New York and San Francisco to encompass these symptoms, and within a few years the causative agent identified as a retrovirus which is now termed HIV-1 [244-246]. By 1992, AIDS had become the leading cause of death of American men aged 25–44 [247]. A few years later in 1999, AIDS had become the fourth-leading cause of death worldwide and the leading cause of death in Africa [247]. As of 2021, 84.2 million people have become infected with HIV and 40.1 million people have died of AIDS-related illnesses since the start of the pandemic [248].

Several different forms of anti-retroviral therapy (ART) were developed over the late 1980s which target several different stages of HIV-1 replication. The administration of a combination of two or three antiretroviral agents targeting different steps of the viral lifecycle was found to be the optimal way of achieving viral suppression in HIV-infected people [249]. Successful ART can suppress the viral load of an HIV-infected person to undetectable levels, to the point where HIV can no longer be transmitted [250]. However, there is still no effective vaccine against HIV-1, and there are still issues in terms of global access to ART. The Joint United Nations Programme on HIV/AIDS launched the 95-95-95 targets in 2014; These targets aim for 95% of people with HIV-1 to have been diagnosed, for 95% of that category to be provided with ART, and for 95% of that category to achieve viral suppression by 2030. In 2019 however, only 67% of people living with HIV were accessing treatment, and major barriers to these targets are access to diagnostics and treatment for people living with HIV [251].

The integration of retroviruses into their hosts genomes combined with their ability to establish latent proviral reservoirs that can stochastically produce infectious virus makes curing HIV-1 difficult [252, 253]. Efforts to cure HIV-1 infection have centred around the “shock and kill” strategy, where viral transcription is induced with latency reversing agents (LRA) and subsequent aggressive antiretroviral therapy to eradicate the latent reservoir of virus and eliminate infection; or more recently the “block and lock” strategy to inhibit viral transcription permanently [253]. However, to date there

has not been significant success with either of these strategies. There are issues with achieving sufficient viral reactivation, insufficient killing of the reactivated pool, and the significant heterogeneity of the latent pool. HIV has no proofreading capacity, resulting in rapid accumulation of mutations that can be beneficial or detrimental to viral replication. Mutations which are beneficial to viral replication, antibody escape and drug escape are selected for. This results in hundreds of quasispecies in an HIV-infected person, which causes issues for not only HIV eradication strategies, but also for HIV vaccine attempts and antibody-based therapies.

1.13 Origins of HIV-1

HIV-1 originated from a zoonotic transmission from chimpanzees to humans, with at least four independent cross-species transmissions of HIV-1, which have been categories into groups M, N, O, and P [243]. Another retrovirus which can infect humans, however found to be less pathogenic, was discovered after HIV-1 and designated as HIV-2 [254]. The M group of HIV-1 accounts for over 98 % of HIV-1 infections globally. This group can be further divided into nine clades: A, B, C, D, E, F, G, H, I, J, and K. Subtype C of group M is responsible for almost half of infections globally; with subtypes A and B the next most common. HIV-1 subtypes have varying penetration across the globe, with subtype C highly prevalent in South Africa, West Africa and India, subtype B most common in the Americas, UK and Australia, and subtype A prevalent in Russia and Eastern Europe [255]. Several recombinant clades have also been recognised. Epidemiological and phylogenetic analyses suggest that HIV was introduced into humans in between 1920–1940 [256]. HIV most likely had the opportunity to transmit to humans through the bushmeat trade in Africa, where cuts on the hands of butchers would provide opportunity for the mixing of blood and transmission of HIV. This is supported by analysis of bushmeat in Cameroon demonstrating Simian immunodeficiency virus (SIV) positive samples in several different non-human primate species from geographically distinct areas [257, 258].

1.14 HIV-1 genomic organisation

HIV-1 belongs to the *retroviridae* family, the subfamily *orthoretrovirinae* and finally to the *lentivirus* genus [117]. As a retrovirus, HIV-1 has an RNA genome which is reverse transcribed into DNA as part of its viral lifecycle. HIV-1 has a 9.7kb RNA genome encoding 9 ORFs that produce 15 proteins (Figure 1.21). Two copies of the HIV-1 single stranded RNA genome are enclosed within the viral capsid, which is in turn surrounded by the lipid bilayer studded with the viral entry protein, Env. The genome is flanked at the 5' and 3' ends by long terminal repeat (LTR) sequences, which encodes for the promoter sequence which permit active transcription once the RNA genome has been reverse transcribed and integrated into the host's DNA. The gag and pol ORFs encode multiple proteins: gag encodes matrix (MA), capsid (CA) and nucleocapsid (NC). The pol ORF encodes protease (PR), reverse transcriptase and RNase H (RT/p66), and integrase (IN). The Env reading frame encodes the gp160 precursor which is later cleaved by the host protein furin into gp120 and gp41. In addition to these structural proteins, HIV-1 encodes several accessory proteins. transactivator protein (tat) and RNA splicing regulator (rev) are required for the initiation of HIV replication. Negative factor (nef), viral infectivity factor (vif), virus protein r (vpr) and virus protein unique (vpu) are not essential for HIV replication *per se* but instead are involved in viral pathogenesis [256].

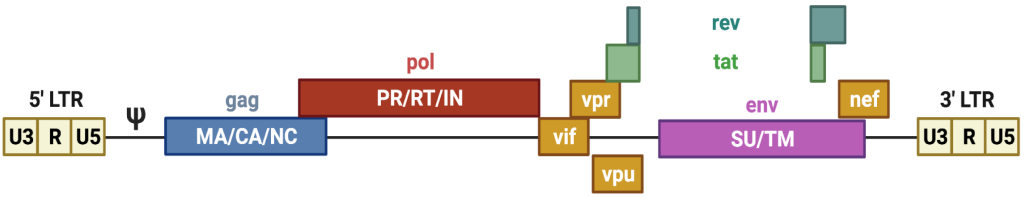

Figure 1.21. HIV-1 genome. Schematic showing location of the structural genes gag, pol and env, and the accessory proteins tat, rev, vpu, vpr, vif and nef. Figure created, using BioRender.

1.15 Entry of HIV-1

HIV-1 entry is mediated by the viral entry protein Env binding to non-specific attachment factors, followed by the primary receptor CD4, and a coreceptor of either CCR5 or CXCR4. Before the CD4 receptor is engaged, Env attaches to the cell by interacting with a range of host factors including negatively charged heparan sulfate

proteoglycans, intergrins, or DC-SIGN on the cell surface [259]. Following attachment to the cell surface, Env can now bind its primary receptor, CD4, a member of the immunoglobulin super-family (Figure 1.22). The CD4 binding site in Env is located in a cavity between the inner and outer domains of gp120 [260, 261]. The presence of a bulky residue at position 375 of Env, which forms part of this cavity, has been shown to predispose Env to adopt a more open conformation of Env akin to the CD4-bound conformation, demonstrating that the filling of this cavity is an important step in the triggering of Env [260]. The binding of Env and CD4 triggers structural rearrangements in the V1/V2 and V3 loop of Env that expose the binding site for the coreceptor. Either CCR5 or CXCR4, depending on the tropism of the virus, is now accessible to Env and coreceptor binding. CCR5 is the primary coreceptor in HIV-1 transmission, and CXCR4-tropic viruses, or dual-tropic viruses, tend to emerge later in about 50% of subtype B infections [262]. The binding of the coreceptor brings Env closer to the target membrane and stabilises the complex, the fusion peptide is released, and membrane fusion can now occur resulting in viral entry [263].

It was previously suggested that the binding of the coreceptor permitted further structural rearrangements in Env that triggered release of the membrane fusion machinery [259]; however more recent evidence shows that coreceptor binding stabilises the entry complex and does not result in allosteric changes in gp120 [263]. HIV-1 entry is pH-independent and it has been demonstrated that viral fusion occurs at the plasma membrane in T cells [12, 264]. This suggests that endocytosis is not required for HIV-1 entry, however, the sensitivity of HIV-1 entry to both endocytosis inhibitors in certain cell lines and to endosomally located antiviral proteins implies that HIV-1 can utilise endosomal entry despite not requiring acidic pH [13, 91]. It has been shown for some HIV-1 strains that CCR5-tropic Envs preferentially fuse at the plasma membrane, while CXCR4-tropic Envs fuse in endosomes [67]. However, it has been shown that for some viral strains coreceptor tropism and location of viral entry do not correlate [68]. The use of different HIV-1 strains and different cell lines likely determines much of the differences in the literature regarding plasma versus endosome fusion.

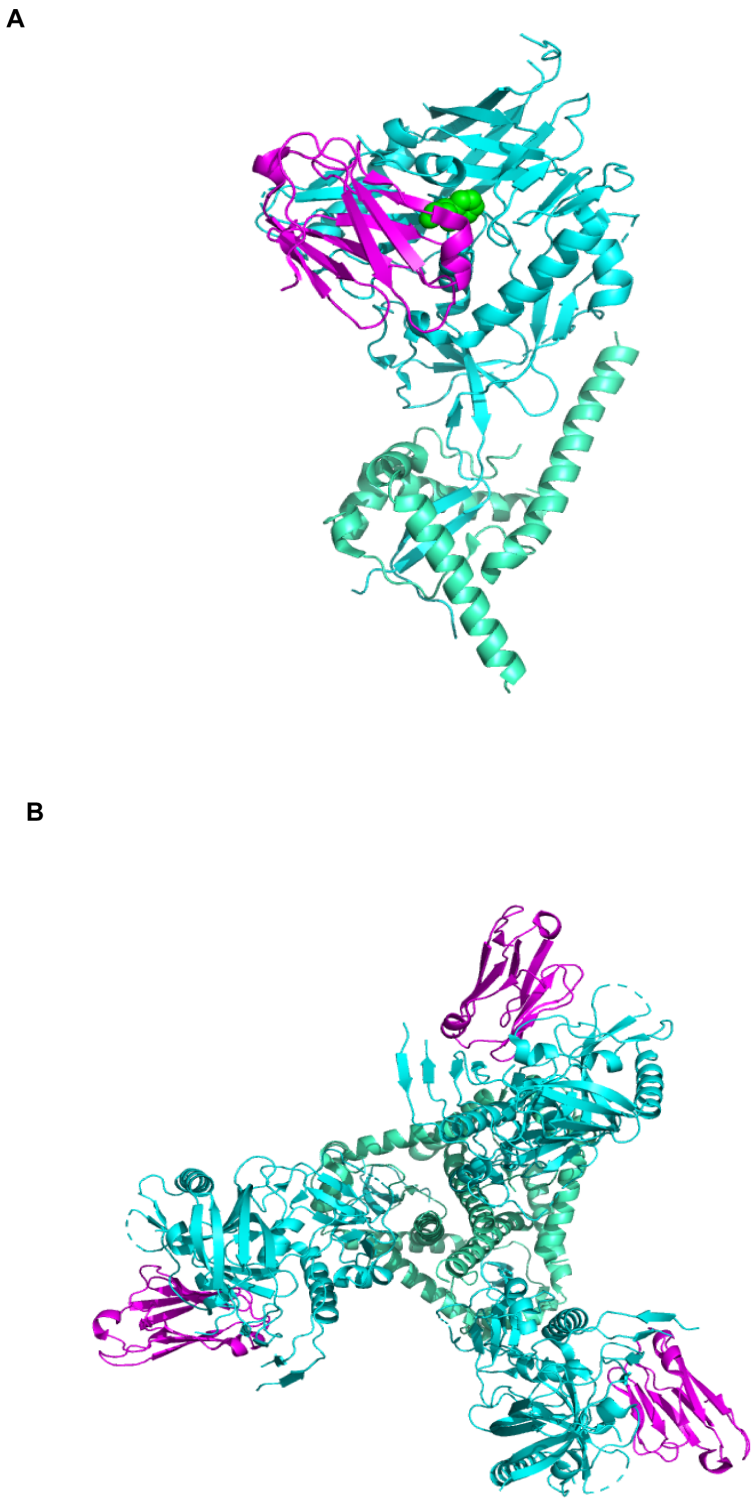

Figure 1.22. HIV-1 Env in complex with CD4. A) Single chain of Env (cyan) in complex with CD4 (pink) with the Phe43 of CD4 coloured in green. B) Trimeric Env cyan) in the CD4-bound open conformation in complex with CD4 (pink) from a top down view. PDB:6OPN. Structures made in PyMOL.

1.16 HIV-1 replication

Following fusion, the viral capsid is released into the cytoplasm and the capsid migrates across the cytoplasm to the nuclear pore [265, 266] (Figure 1.23). Reverse transcription occurs inside the capsid during the journey to the nuclear pore [267] and the capsid interacts with nucleoporins at the nuclear rim to mediate import of the capsid into the nucleus [268, 269]. The pre-integration complex assembles inside the nucleus and the reverse transcribed genome is integrated into the host genome [252]. Following integration, proviral transcription is initiated and viral mRNAs are exported from the nucleus [270]. These mRNAs serve as templates for protein production and genome RNAs are packaged into nascent viral particles. The ESCRT pathway mediates viral budding and following release from the host membrane, the viral protease cleaves Gag to result in the fully mature virion [271, 272]. In addition to cells which actively produce virus, HIV-1 can establish a non-productive state of infection termed latency. These cells do not actively produce virus but harbour intact integrated proviruses which can stochastically produce virus [273].

1.17 HIV-1 Env tropism

The primary targets of HIV-1 infection are CD4 T cells, macrophages, and dendritic cells which express CD4 and the CCR5 coreceptor. CCR5-tropism appears to be a requirement for HIV-1 transmission, however a switch to CXCR4 usage, or dual coreceptor usage has been associated with rapid disease progression [274]. Although the exact recipe for a CXCR4 tropic Env has not yet been established, CXCR4-tropic Envs have been found to have longer and higher charged V3 loops [275].

Due to the high mutation rate of HIV-1 and the targeting of Env by adaptive immunity, Env is highly variable. This can lead to hundreds of quasispecies of Env circulating in the same patient with very different Env sequences, presenting a problem for the adaptive immune system in terms of generating neutralising antibodies. It has also been found that a majority of infection of new cellular targets *in vivo* is estimated to occur through cell-cell transmission at virological synapses rather than through cell-free virus [71]. The use of cell-cell transmission likely assists in escaping adaptive immunity and may also overcome stability constraints of the Env glycoprotein.

However, much of HIV-1 viral entry research utilises *in vitro* tissue culture models of cell-free infection, and there may be disparities in viral entry as measured by cell-free infection and cell-cell infection.

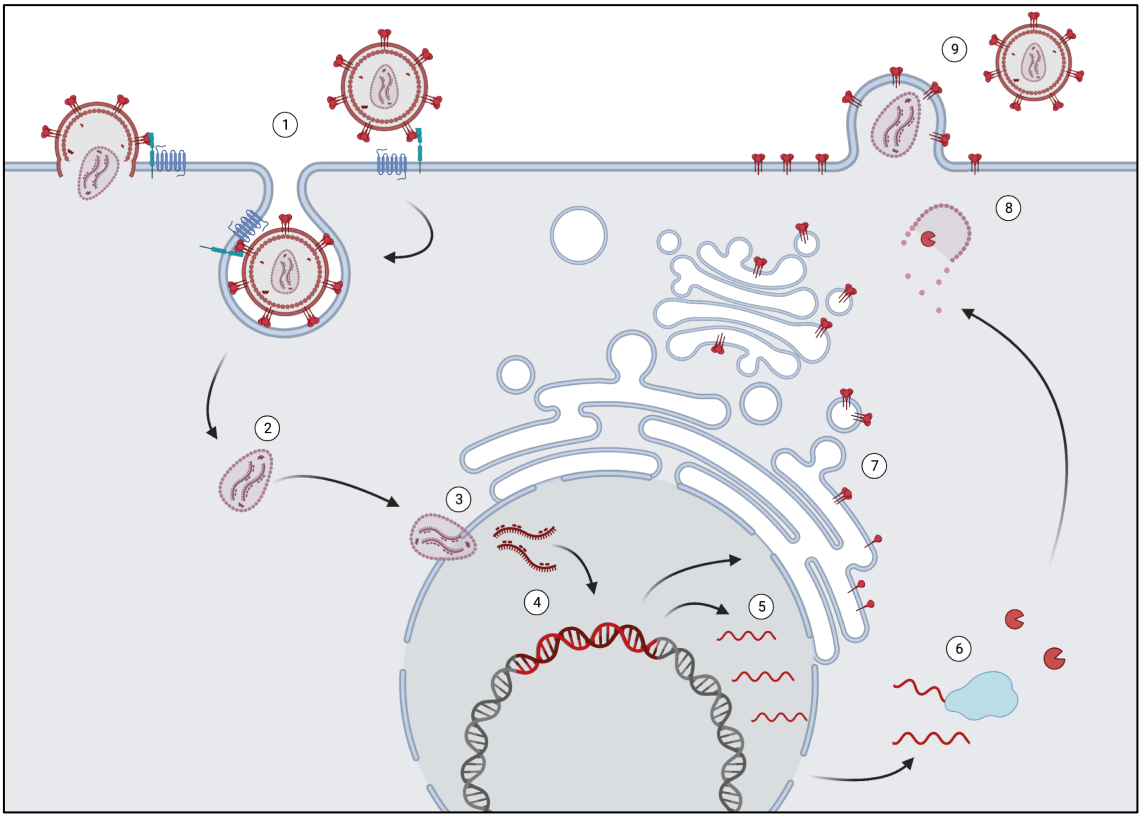

Figure 1.23. HIV-1 viral replication. HIV-1 associates with non-specific attachment factors at the cell surface. Envelope binds to CD4, which triggers conformational changes allowing Env to bind the coreceptor CCR5 or CXCR4 to stabilise the complex (1). The fusion peptide is released which results in the fusion of the viral and cellular membranes and the release of the capsid into the cytoplasm. This can happen at the plasma membrane, or in endosomes. The capsid migrates across the cytoplasm to the nuclear pore (2). Reverse transcription occurs inside the capsid or once inside the nuclear pore (3). The reverse transcribed genome is then integrated into the host genome (4). Viral genes are transcribed and exported from the nucleus by Rev (5). Viral transcripts are translated (6), in parallel Env is translated in the ER and trafficked through the ER and Golgi and post translationally modified (7). Viral assembly occurs at the plasma membrane where the p6 protein of Gag binds the viral genome and incorporates it into assembling capsids (8). Immature viruses bud from the plasma membrane and Gag cleavage results in mature virus particles (9). Figure created in BioRender.

1.18 HIV-1 Env synthesis and processing

Like SARS-CoV-2, Env is synthesised as a full-length precursor. Translation of Env begins in the cytoplasm and is translocated to the ER once an ER signal sequence is encountered at the N-terminal of Env. This signal peptide is then co-translationally removed by signal peptidases within the ER. The transmembrane domain of gp41 contains a membrane anchor which stops gp160 from being fully released into the lumen of the ER, allowing the gp120 portion to extend into the ER lumen and the gp41 portion to reside in the cytoplasm [276]. Through Env's journey in the ER, N-linked and O-linked oligosaccharides are added and the gp160 monomers oligomerise into trimers [277]. This facilitates the trafficking of gp160 through the Golgi and trans-Golgi network. More high-mannose modifications are made and the gp160 precursor is processed into gp120 and gp41.

Env requires proteolytic processing by furin at the gp120/gp41 boundary to prime the protein for entry. Furin-mediated cleavage is vital for viral entry and deletion of this site produces viruses that adopt non-native conformations and are non-fusiogenic [278] [279]. The gp120-gp41 boundary contains a highly conserved furin cleavage site motif, REKR, at the bridge of gp120 and gp41. The furin motif is highly conserved amongst HIV-1 isolates, although given the sequence variability in contact resides around the REKR site, it is possible there are differences in the efficiency of gp160 processing across HIV-1 strains. A second putative furin cleavage site has also been identified (KAKR) a few residues upstream of the canonical furin cleavage site [280]. However whether this second site is of physiological relevance is unclear; although it has been suggested that conformational differences may explain the preference for the canonical site over the second upstream KAKR site [281]. Following cleavage, the gp120 and gp41 subunits remain associated through non-covalent interactions. Complexes of gp120-gp41 are subsequently trafficked through the secretory pathway to the plasma membrane for viral assembly. Most Env at the surface is endocytosed and either trafficked to lysosomes, or back to the plasma membrane. Because of the relatively weak interactions between gp120 and gp41, some gp120 is also shed from the plasma membrane, which may be a factor in the relatively low levels of Env that are incorporated onto nascent virions [282]. It has recently been described that un-

cleaved HIV-1 Env takes a different secretory pathway to the cell surface, bypassing the Golgi and site of furin cleavage, and is excluded from virion incorporation [283]. Combined with the rapid recycling of Env back into endosomes and away from the plasma membrane, this is another potential mechanism through which Env can evade neutralising antibodies; antibodies against the un-cleaved form of Env will likely bind different epitopes and not the cleaved, fusion competent form of Env.

At the plasma membrane, Env is incorporated into nascent virions. Several models for Env incorporation into virions have been proposed: the passive incorporation model, the Gag-Env interaction model, the Gag-Env co-targeting model, and the indirect Gag-Env interaction model (Figure 1.24). The passive incorporation model is based on observations that several host proteins are packaged into retroviral virions, and that non-retroviral glycoproteins can also be packaged, which can be leveraged to "pseudotype" lentiviral vectors with different viral glycoproteins to examine viral entry [277]. Additionally, deletion of the cytoplasmic tail of Env does not significantly reduce viral titre, demonstrating some Env incorporation can occur in a cytoplasmic tail and Gag independent manner [284]. Truncation of the cytoplasmic tail of Env has however been found to increase Env incorporation and has also been reported to overcome the antiviral effects of the SERINC proteins [90, 285].

Evidence for the Gag-Env interaction model is derived from observations that deletions or mutations in the matrix of Gag can reduce Env incorporation into virions [286]. If Gag is not cleaved, and therefore matrix and gp41 cannot interact, these virions are fusion defective, therefore a lack of interaction between matrix and Gag may prevent Env from forming a fusiogenic state [287]. This can be rescued by gp41 truncation, implying a mix of passive and Gag-Env interacting incorporation can occur at the membrane. The Gag-Env co-targeting model relies on evidence from gp41 truncation studies and Env incorporation. In some cell types, cytoplasmic tail deletion does reduce PLV titre, which indicates Env and Gag are targeted to the correct site for viral assembly by a host factor [284]. This would explain the cell-type dependency of gp41 truncation, as this factor may not be present in all cell lines and be associated with their relative permissivity to cytoplasmic tail truncation. Finally, a host protein may indirectly bridge a Gag and Env interaction, similarly to the co-targeting model.

Distinguishing which of these models is predominantly utilised, or whether in fact a mix of them occur concomitantly, remains to be elucidated.

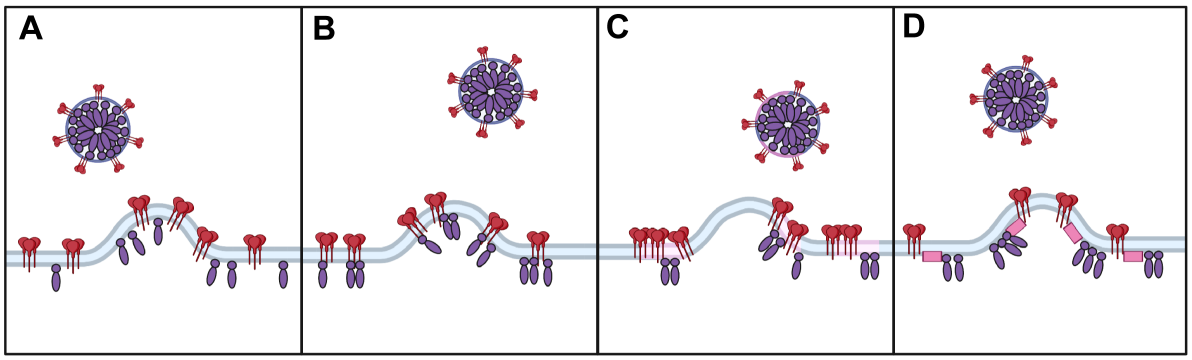

Figure 1.24. Models of Env incorporation into virions. A) Passive incorporation model. Env is passively incorporated into virions due to its presence at the plasma membrane through no interaction with Gag. B) Gag-Env interaction model. The cytoplasmic tail of Env interacts with the MA of Gag to incorporate Env into virions. C) Gag-Env co-targeting model. Both Gag and Env are targeted to a host motif on the plasma membrane which is packaged into virions. D) Gag-Env indirect interaction model. Gag and Env interact indirectly through a third-party host protein.

1.19 HIV-1 Env structure and conformation

HIV-1 Env, similarly to other class I fusion glycoproteins, consists of two subunits; one contains the receptor binding domain (gp120), and one the fusion machinery (gp41) (Figure 1.25). HIV-1 Env is primed by furin cleavage in the Golgi and triggered to mediate viral entry by binding to CD4 and either CCR5 or CXCR4 as a coreceptor. The Env trimer is a highly dynamic structure that primarily exists in a metastable, closed state termed “state 1”. A significant energy barrier must be overcome for Env to transition to state 2 (CD4 bound conformation) and the final postfusion conformation (state 3). HIV-1 strains demonstrate a varying propensity to sample the downstream states (Figure 1.26 A). If Envs sample state 2 and state 3, they can functionally inactivate by prematurely reaching the postfusion conformation, and are also more susceptible to neutralising antibodies that target the open conformation of Env [288]. More open Envs are also more susceptible to functional inactivation by the presence of a CD4-mimetic [289].

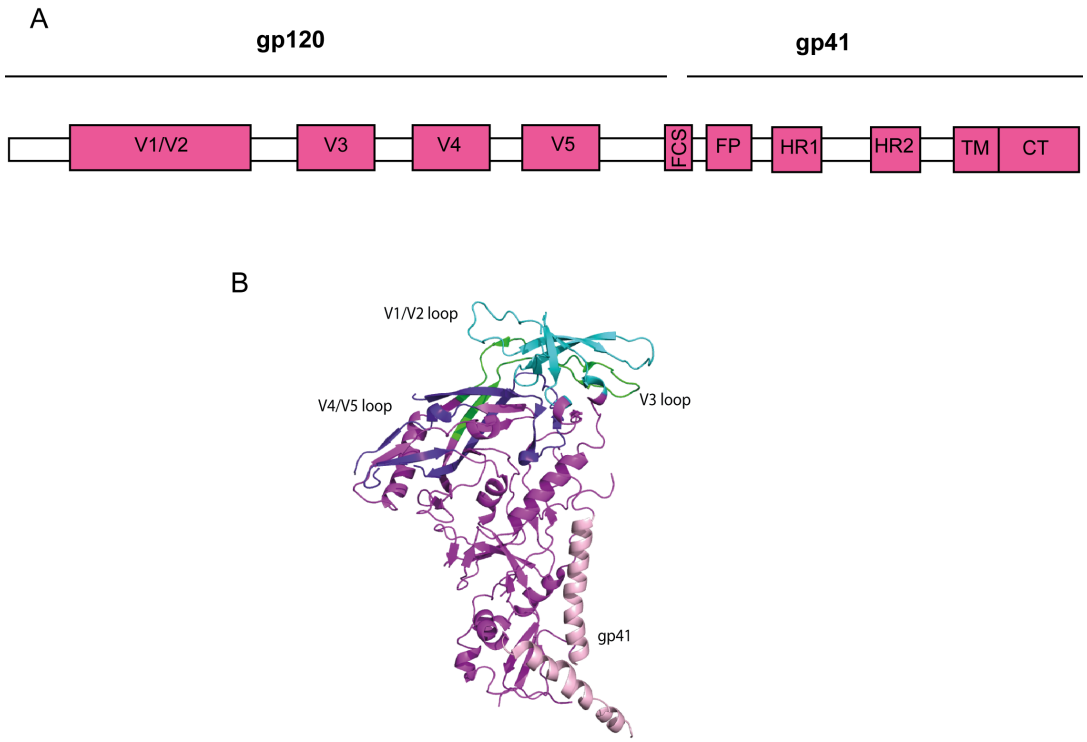

Figure 1.25. HIV-1 Env schematic. A) Schematic of Env with variable regions, furin cleavage site (FCS), fusion peptide (FP), heptad repeats (HR), transmembrane domain ™ and cytoplasmic tail (CT)abelled. B) Single chain of HIV-1 Env (PDB:5ACO) with variable loops and gp41 coloured in. Structure made in PyMOL.

The propensity of an Env to functionally inactivate by sampling state 2 and irreversibly achieving state 3 can be measured by cold inactivation. This assay measures how much infectivity a virus or PLV loses when incubated on ice and is then frozen. If the Env adopts a more open conformation, water molecules can enter and form crystals, which break the Env during the freezing process. Envs which adopt the more open conformation are more sensitive to cold inactivation, and Envs which are more stably in the closed conformation are more resistant to cold inactivation [290, 291]. Env conformation can also be stabilised with small molecule inhibitors. The inhibitor Temsavir stabilises the closed conformation of Env, while mimetics of CD4 can stabilise the open conformation of Env [292]. It has been found that processing of gp160 to gp120 and gp41 stabilises the closed conformation of Env [279, 293]. In addition to preventing premature firing and functional inactivation of Env, full

processing may also assist in escape from antibody mediated cellular toxicity (ADCC) by reducing the transitioning of Env to the open conformation where ADCC epitopes are accessible at the cell surface [292]. Structures of the closed, partially open and open conformations of Env are shown in Figure 1.26 B.

In addition to intrinsic reactivity, the clustering of Env trimers on the virion surface is important in determining the infectivity of an HIV-1 particle [294]. The clustering of Env increases local Env density, which therefore overcomes the energy barrier required for membrane fusion. This is especially important due to the low number of Envs per virion which has been estimated as low as 7-14 Env particles per virion [295]. Mature, infectious particles display fewer clusters of Env trimers than non-infectious particles where gag has not matured, signifying a link between Env clustering and gag maturation [294].

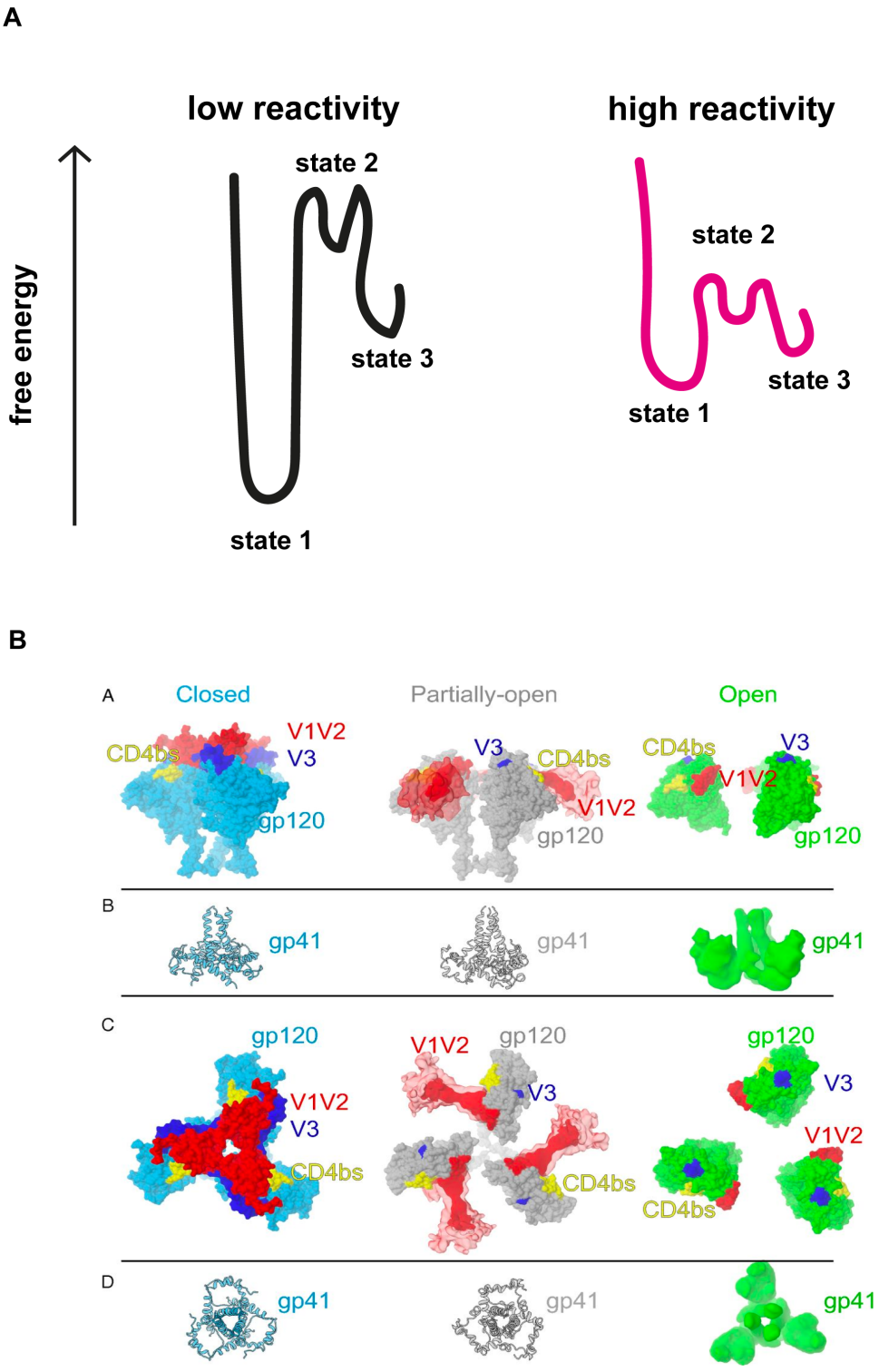

Figure 1.26. Reaching the CD4 bound conformation requires overcoming a significant energy barrier for Env. A) A significant amount of free energy is required to transition from state 1 to state 2, and finally down to the lowest energy state, state 3. B) In Envs with a more open conformation also known as high reactivity, require lower energy to transition from state 1 to state 2. B) Structures of gp120 and gp41 in the closed (blue), partially open (grey) and open (green) conformations from a side view and a top view, taken from Wang et al 2016 [296].

1.19.1 V1/V2 loop

There are five sequence variable loops in Env, demarcated by the presence of disulphide bonds (Figure 1.27). The V1/V2 loop is located at the apex of the Env trimer and stabilises the trimeric gp120 on the surface of virions whilst also shielding the coreceptor binding site in the closed conformation. The V1/V2 loop forms a five stranded beta-barrel in structure [297]. The V1/V2 loop is the most sequence and length diverse of the variable regions. Roughly one in ten of the residues of the V1/V2 loop are glycosylated, with the putative glycosylation sites numbered according to HxB2: N133, N142, N156, N160, and N181 [298, 299]. The V1/V2 loop is vital to Env structure and function and deletion of the V1/V2 loop abolishes viral infectivity [300].

The L193 site in the V1/V2 loop has been found to be an important constraint on the maintenance of the closed conformation of Env [288]. It has been reported that mutation of this site to an alanine or arginine results in Env adopting a more open conformation, suggesting that the L193 site constrains Env in the closed conformation [288]. The importance of this constraint is again not only for preventing premature functional inactivation of Env, but to also protect Env from being neutralised by antibodies at epitopes that are only vulnerable in the open conformation.

1.19.2 V3 loop

The V3 loop is located underneath the V1/V2 loop and is a major determinant of coreceptor usage [301, 302]. The importance of the V3 loop is exemplified by the fact that deletion of this region completely abrogates viral infectivity [300]. The V3 loop is more conserved than the V1/V2 loop and tolerates less variation in its sequence. It also contains notable glycosylation sites, the N301 and N332 sites [298]. The N332 glycosylation site is at the base of the V3 loop, and is a major target of neutralising antibodies [303].

The V4 and V5 loops are not as well characterised as the V1/V2 and V3 loops. These loops do contain a number of glycosylation sites (N392, N408 and N411 in the V4 and N463 and N466 in the V5), and deletion of either of these loops impairs virion infectivity [298, 300]. The V4 and V5 loops are the most tolerant in gp120 to insertion of labelling

components, such as GFP, and are frequently used to label HIV-1 Env for microscopy [304].

1.19.3 gp41

Gp41 contains the fusion machinery of Env. It can be divided into an ectodomain, comprising the heptad repeats 1 and 2, and an endodomain containing the transmembrane domain and the cytoplasmic tail of Env. The conversion of the prefusion to postfusion conformation of gp41 and anchoring of the fusion peptide in the host membrane is integral to membrane fusion. As such, gp41 is relatively conserved in sequence across HIV-1 strains compared to gp120. Additionally, gp41 bears structural similarities to other class I fusion glycoproteins from influenza, respiratory syncytial virus (RSV), and Ebola and is comprised of two long helices which sit at the base of the trimer [305]. Residues in gp41 have been found to be key to modulating Env clustering, with the residues 751-854 in particular regulating clustering of Env by interacting with cholesterol [306]. Additionally, a conserved region between A582 and L587 of gp41 is an important regulator of Env conformation, which decreases the transition from state 1 to state 2. A582T and L587A can increase the closed conformation of the trimer [307]. Incorporation of the A582T and L587A mutations into HxB2 reduces the effects of cold inactivation, demonstrating that this stabilises the trimer [307].

Gp41 also contains the cytoplasmic tail, which interacts with gag during Env incorporation. Of the gp41 ectodomain and endodomain, the endodomain has slightly more sequence diversity compared to the ectodomain [308]. The cytoplasmic tail of HIV-1 is relatively longer than that of other retroviruses, with average HIV-1 cytoplasmic tails comprising of approximately 150 amino acids, while other retroviruses cytoplasmic tails are usually around 50 amino acids on average [309].

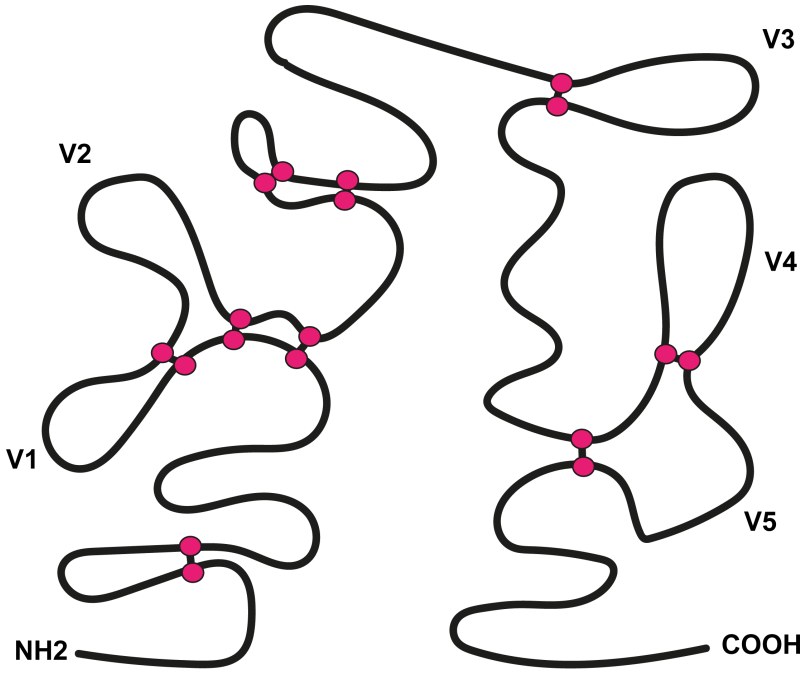

Figure 1.27. The variable regions of HIV-1 Env are demarcated by disulphide bonds. Schematic shows the location of disulphide bonds in HIV-1 Env which separate the variable loops.

1.19.5 Env glycosylation

Env is one of the most heavily glycosylated proteins identified. A major proposed function of the high density of glycans is to shield the protein from antibody neutralisation [310]; That said, several broadly neutralising antibodies have been identified that target glycan patches on Env [310]. Env glycans also help with correct protein folding and can impact viral infectivity. Depending on the HIV-1 strain, there are approximately 25 N-linked glycan sites on each chain of Env [311]. Gp120 is more heavily glycosylated than gp41, with gp41 on average only having four N-linked potential glycosylation sites (PNGs). A high proportion of the glycans on Env have been found to be surprisingly under processed relative to other viruses, due to enzymes that would process these into complex sugars being unable to access the glycans due to steric hinderance from the Env conformation [312]. The site of 29 of the N-linked glycans in the HxB2 Env are shown in Figure 1.28.

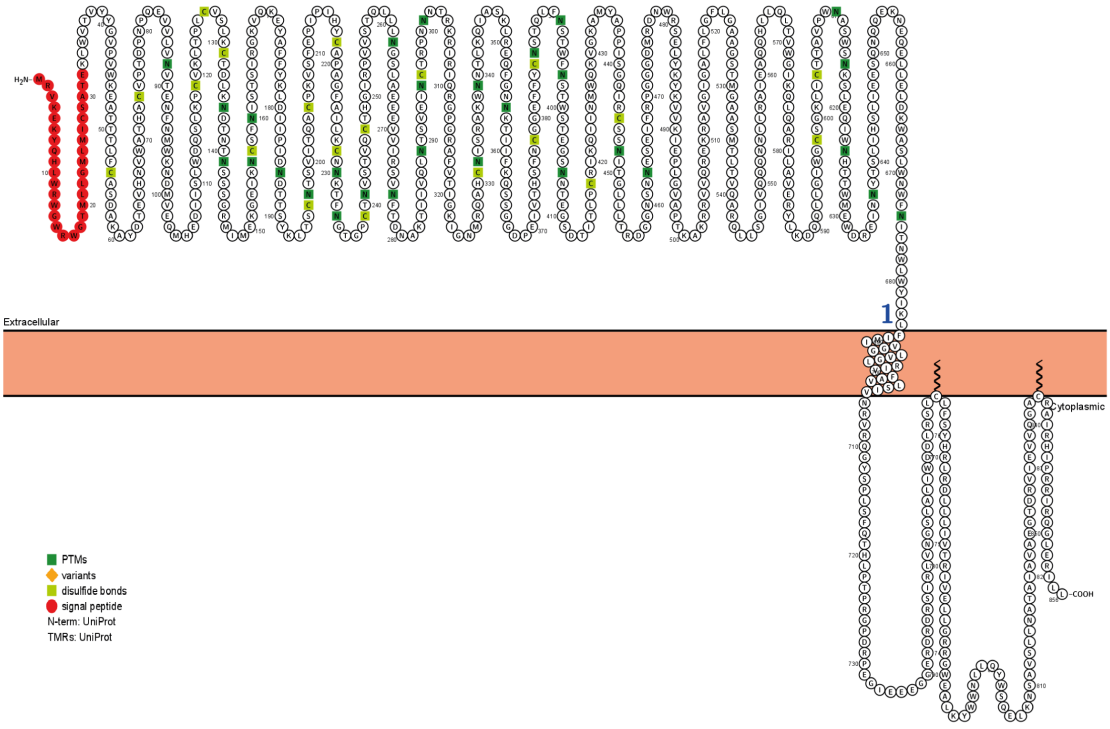

Figure 1.28. Snake diagram of HIV-1 Envelope. A) Snake diagram of HIV-1 Envelope HxB2 generated in Protter. Glycosylation sites are shown in dark green and disulphide bonds in light green.

As mentioned earlier, there are several glycosylation sites in the V1/V2 loop and V3 loops of Env, the N133, N142, N156, N160, N181, N301 and N332 sites. In particular, the N332 glycan has been found to represent an antibody targeting supersite on Env, with several neutralising antibodies targeting the N332, including the broadly neutralising antibody 2G12 and PGT121 [313, 314]. Loss of the N332 site during chronic infection has been documented as an escape mechanism from broadly neutralising antibodies [315]. In addition to mutation of the site to escape neutralising antibodies, it has been documented that increasing V1/V2 loop length and mutation of sites distal to the N332 site itself can also result in escape from N332-targeting antibodies [303]. This demonstrates that interplay between the variable regions can affect Env conformation, in particular how altering the more variable V1/V2 loop can cause allosteric changes to the V3 loop.

1.20 HIV-1 transmitted/founder viruses

The majority of HIV-1 transmission worldwide results from heterosexual contact. HIV-1 transmission is a relatively inefficient process, with a single virion being responsible for HIV-1 transmission in 80% of heterosexual transmissions and 60% of MSM transmissions [316]. For HIV-1 transmitted intravenously through needles, up to 16 transmitted virions have been found to be responsible for productive infection [317]. Additionally, it is estimated that 98 % of sexual exposure events do not result in transmission of HIV-1 [318]. The likelihood of HIV-1 transmission is however increased by high infecting partner's viral load, decreased mucosal integrity, and increased immune activation and target cell availability in the new host [319]. The low success of HIV-1 transmission suggests there is a considerable bottleneck for HIV-1 transmission with significant constraints on which virions can transmit. An alternative view of this is rapid selection of one of several virions that transmit occurs in the new host (Figure 1.29). The viruses that are either capable of transmitting, or are rapidly selected for in the new host, are termed transmitted/founder (T/F) viruses. The apparent constraints on HIV-1 transmission mean that T/Fs have garnered significant attention to attempt to characterise their properties.

The chief characteristic of T/F viruses is their utilisation of CCR5 as a coreceptor compared to viruses from chronic infection that can either utilise both receptors or fully switch to CXCR4 use [320]. It has been suggested that the predominance of CCR5-tropic T/Fs is due to differences in the infection of resting memory versus active CD4 T cells by CXCR4-tropic viruses. Zhou et al found that CXCR4-tropic infection peripheral memory CD4 T cells, those that are likely to be infected at transmission, result in abortive infection; however activated CD4 T cells, which are found in later infection when CXCR4-tropic viruses emerge are not as susceptible to abortive infection [321]. The requirement for CCR5-tropic viruses at transmission has been linked to the decreased susceptibility of people who are homozygous for the Δ32 CCR5 gene, which results in no expression of CCR5 at the cell surface, to HIV-1 infection [322]. However, it has been found that although protective against HIV-1 infection, this mutation increases susceptibility to West Nile Virus through a currently unknown mechanism [323]. Other phenotypic differences of T/Fs have been debated, with some reports of increased Env incorporation, increased cell-free infectivity, IFNα

resistance, and resistance to fusion inhibitors and neutralising antibodies [324-326]. It has also been suggested that T/F Envs have shorter variable loops and fewer potential glycosylation sites than Envs from chronic infection [327, 328].

While some of the characteristics have not been found to be broadly qualifying, the resistance to type I IFNs appears to be a significant characteristic of T/F viruses and suggests that type I IFN may impose a significant constraint on viral transmission [27, 325]. Viruses isolated from chronic infection, or constructed from consensus sequences from chronic infection, have been found to be more sensitive to inhibition by IFN and in particular, IFITMs [27, 67]. Reversion of the mutations that were hypothesised to provide escape from neutralising antibodies reverted the IFN and IFITM sensitivity of chronic Envs [67]. This is suggestive of the interplay between adaptive and innate immunity over the course of infection, and indicative that while IFN imposes a constraint on transmission, evasion of neutralising antibodies is relatively more important in chronic infection.

Interestingly however, while IFN resistance has been characterised as a property of T\Fs, viruses isolated from the interruption of ART have also been found to be highly IFN resistant [28]. This demonstrates that IFN is also a selection pressure in chronic infection. It has been questioned whether IFN resistance is a true property of T/F viruses, or simply an artefact of faster replication kinetics to viruses from chronic infection [329]. This is supported by observations that there are ISGs that can inhibit both T/F and chronic viral isolates [329], suggesting that perhaps a combination of IFN resistance and rapid replication kinetics are important to overcome the transmission bottleneck.

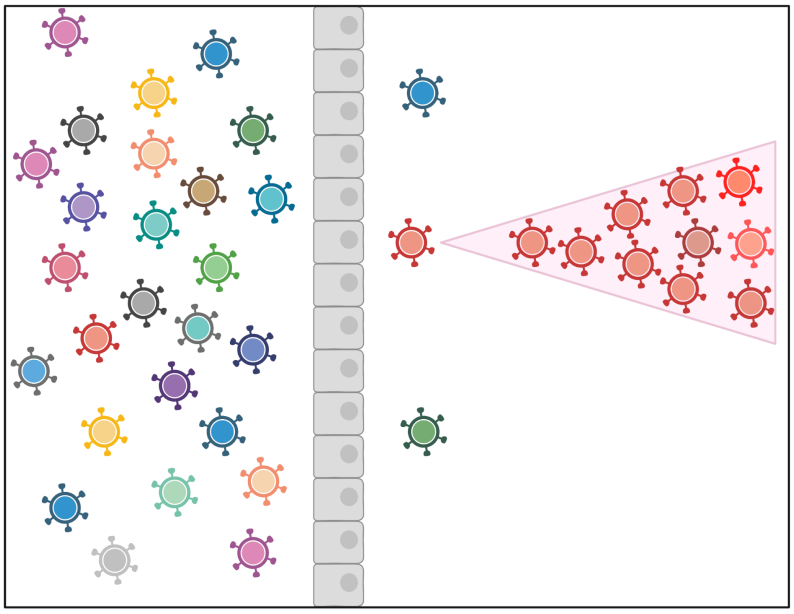

Figure 1.29. Transmitted/founder effect in HIV-1 transmission. Hundreds of quasispecies of HIV-1 can be present in the donor. In mucosal transmission, a bottleneck effect results in only a few viruses traversing the mucosa. Of these viruses, some are capable of replicating in the recipient and further diversifying (orange) while others are defective or not fit for the new environment and rapidly lost (blue, green). Figure created in BioRender.

HIV-1 Env is the only viral protein exposed on the outside of the virus and is therefore the prime target for neutralising antibodies. However due to the poor proofreading capacity of HIV-1, there is a rapid rate of mutation and accumulation of mutations during infection; these mutations may be either detrimental or beneficial for viral transmission and replication [330]. The need of HIV-1 to escape neutralising antibodies means Env is a hotspot for mutation, to escape both antibody-mediated immunity, and also to escape innate immunity. Reversion of neutralising antibody escape mutations in six month viruses has been reported to confer IFITM resistance to previously sensitive viruses, suggesting that these selective pressures compete during chronic infection [67]. It has also been found that Envs which are IFITM3 and SERINC5 resistant in acute infection gradually lose resistance to IFITM3 but not SERINC5 [91]. This suggests that antiviral proteins which inhibit entry exert differential selection pressures over chronic infection and a further layer of complexity to the selection pressures of intra-host viral evolution.

1.21 IFITM antagonism of HIV-1 and SARS-CoV-2 entry

IFITMs have been found to inhibit a broad range of viruses; their importance *in vivo* has been demonstrated by mouse knock-out studies, and association of SNPs with increased disease severity for influenza, SARS-CoV-2, and HIV-1 [79, 81, 82]. However, there are also some viruses which can escape IFITM restriction. Lassa virus entry is entirely unaffected by IFITM overexpression, thought to be due to accessing endosomal compartments where IFITM3 is absent [331]. The unrelated human papilloma virus (HPV) has also found to be entirely resistant to IFITM overexpression [332]. Furthermore, it has also been found that even within the same virus, viral subtypes can vary in their susceptibility to IFITM restriction.

Different HIV-1 isolates exhibit differential sensitivity to IFITMs [333]. T/Fs have been found to be more resistant to IFITM overexpression than their counterparts from six months into infection [67]. Reversion of mutations in the six-month viruses can re-confer IFITM sensitivity, demonstrating that IFITM resistance can be lost due to the selection pressure of adaptive immune escape. Differential IFITM sensitivity for HIV-1 has been previously linked to the V3 loop of Env [333]. Additionally, IFITM-mediated inhibition of HIV-1 has been reported to be distinct from that of SERINC-mediated Env inhibition, as Envs can be sensitive to one and not the other [91]. It has also been shown that IFITMs can reduce the infectivity of nascent virions through their incorporation into virions in producer cells [58, 59]. It has however been shown that this form of IFITM-mediated inhibition does not appear to be dependent on Env, whereas IFITM-mediated inhibition through their expression in target cells varies in an Env-dependent manner [59, 67].

The interplay between IFITMs and SARS-CoV-2 entry is debated in the literature, with some groups demonstrating that SARS-CoV-2 is IFITM sensitive in particular cell lines [40, 94, 150, 334]. However, other groups show that IFITMs can actually enhance SARS-CoV-2 infection under certain circumstances; It has been reported that IFITMs can enhance the infection of the Wuhan SARS-CoV-2 spike when IFITM3 is mis-localised by incorporating a Y20A/F mutation [40]. We can recapitulate these findings with IFITM2, and find that mis-localisation of IFITM2 also results in enhancement of

Wuhan virus and PLVs in A549-ACE2 cells [334]. Additionally, it has been reported that knockdown of IFITMs in Calu-3lu3 cells results in enhancement of SARS-CoV-2 infection; IFITMs 2 and 3 have also been shown to enhance the entry of the coronavirus OC43 [335, 336]. This suggests a common mechanism utilising the hijacking of antiviral proteins for entry. There have also been discrepancies about which IFITMs can inhibit SARS-CoV-2; some articles report IFITM1 being the most inhibitory [94], and others demonstrate more inhibition by IFITM2 or IFITM3 [94, 334]. The overexpression of TMPRSS2 has been shown to reduce IFITM-mediated restriction of SARS-CoV-2, and that IFITM3-mediated inhibition of SARS-CoV-2 can be abolished by treatment with amphotericin B [150]. IFITMs have also been reported to inhibit the formation of syncytia, a pathophysiological hallmark of SARS-CoV-2 infection *in vitro* and *in vivo*. IFITM1 has been shown to inhibit syncytia formation, in contrast to TMPRSS2 overexpression which promotes syncytia formation [69, 75, 76]. In addition to directly inhibiting entry, these findings further demonstrate there are additional indirect antiviral properties of IFITMs.

IFITMs can play an important role in controlling viral infection and may be a constraint on viral transmission. Understanding the glycoprotein-dependent factors involved in why some viral envelopes are restricted by IFITMs and others are not, is therefore of interest.

1.22 Aims of this thesis

Traversing the cellular membrane is the first essential step of viral infection and common solutions to mediate viral entry have been utilised by multiple unrelated viruses. Not only must a virus mechanistically mediate the fusion of the cellular and viral membranes, but there are numerous antiviral proteins that can inhibit viral entry. Perhaps the most well characterised of these thus far are the IFITM proteins that inhibit the entry of a broad range of enveloped viruses, including SARS-CoV-2 and HIV-1. Many strains and variants of both SARS-CoV-2 and HIV-1 exist due to their capacity to mutate when replicating, resulting in strains with significant differences in the sequences of their viral entry proteins. The need to evade IFITM proteins in order to mediate viral entry confers one of the several selective pressures on the evolution of viral glycoproteins intra- and inter-host. Understanding the determinants of the relative sensitivity of viral glycoproteins to IFITMs can shed light on these host-virus interactions and assist our understanding of viral evolution.

The data presented in this thesis aims to investigate the molecular determinants of IFITM resistance and sensitivity in both the SARS-CoV-2 and HIV-1 entry glycoproteins. The results section of this thesis is divided into four chapters:

1. IFITM2 sensitivity of the Wuhan spike can be modulated by deletion of the polybasic cleavage site.
2. The SARS-CoV-2 alpha variant is IFNβ resistant in an IFITM-dependent manner.
3. Spike cleavage by TMPRSS2 and matrix metalloproteinases alters IFITM sensitivity.
4. The V1/V2 loop of HIV-1 Env can confer IFITM resistance or sensitivity.

Chapter 2: Methods

2.1 Plasmids

Main plasmids and their origins are listed in Table 2.1. Primers used to make mutants of said plasmids used in this thesis are listed in Table 2.2.

Table 2.1 Plasmids used in this thesis

Plasmid	Backbone	Source/cloning
ACE2	pcDNA.31	Dr Nigel Temperton
ACE2	Pcms28 puromycin	Cloned with NotI/XhoI
ACE2	Pcms28 blasticidin	Cloned with NotI/XhoI
TMPRSS2	RRL.sin.cPPT.SFFV/IRES-neo.WPRE	Dr Caroline Goujon
Wuhan-1	pcDNA3.1	Dr Nigel Temperton
D614G	pcDNA3.1	SDM
D614G ΔCT	pcDNA3.1	SDM
Alpha (B.1.1.7)	pcDNA3.1	Dr Katie Doores
Alpha (B.1.1.7) ΔCT	pcDNA3.1	Prof Wendy Barclay
Beta	pcDNA3.1	Dr Katie Doores
Gamma	pcDNA3.1	Prof Wendy Barclay
Kappa	pcDNA3.1	Prof Wendy Barclay
Delta	pcDNA3.1	Prof Wendy Barclay
Omicron (BA.1)	pcDNA3.1	Prof Wendy Barclay
Omicron (BA.2)	pcDNA3.1	Prof Wendy Barclay
Pangolin Guangdong	pD603	Dr Joe Grove
pLHCX	pLHCX	Neil lab
IFITM1	pLHCX	Neil lab
IFITM2	pLHCX	Neil lab
IFITM3	pLHCX	Neil lab
CSXW		Neil lab
p8.91	pCRV1	Neil lab
MLV gag-pol	pCRV1	Neil lab
VSV-G	pMDG	Neil lab
SARS-CoV-2 M	pLVX-EF1alpha-IRES-Puro	Prof Michael Malim

Table 2.2 Mutants generated in this thesis

Mutant	Primer 1	Primer 2
Spike mutants		
ΔPRRA	AGAAGCGTGGCCAGCCAG	GCTATTGGTCTGGGTCTGGTAG
Ins PRRA	AGAGCCCGGAGCACCAGCCAGAAA	TCTAGGCAGCAGAGACACGGTGTG
Ins “Y2Y”	cagaagcgtggccagccagagcatcatcGCCTACACCATGAGCCTG	gctcttctagggctattggtctgggtctgGTAAGAGGCACAGATGCC
Ins PRRA pangolin	agagccagAAGCGTGTCCAGCCAAGC	tctaggggAGTTGGTCTGTGTCTGATAGC

ΔS2'	TTCATCGAGGACCTGCTG	CTTGCTAGGCTTGCTTGG
D614G	GCTGTACCAGGGCGTGAATTGCA	ACGGCCACCTGATTGCTG
ΔHRRA	AGAAGCGTGGCCAGCCAG	GCTATTGGTCTGGGTCTGGTAG
P681H	GACCAATAGCcacAGAAGAGCCAGAAGC	TGGGTCTGGTAGCTGGCG
H681P	GACCAATAGCcccAGAAGAGCCAG	TGGGTCTGGTAGCTGGCG
P681R	GACCAATAGCagaAGAAGAGCCAGAAGCGTG	TGGGTCTGGTAGCTGGCG
R681P	GACAAACAGCcctAGACGGGCCAG	TGTGTCTGGTAGCTGGCA
Δ69/70	AGCGGCACCAATGGCACC	GATGGCGTGGAACCAGGTC
Δ144	CATAAGAACAACAAGAGC	ATAAACACCCAGGAAAGG
N501Y	CCAGCCTACCtacGGCGTGGGCT	AAGCCGTAGCTCTGCAGAG
E484K	TAATGGCGTGAAGGGCTTCAATTGCTACTT	CACGGTGTGCTGCCGGCC
ΔCT	GTCCTGCTGCtgatgaGACGAGGACGACAGCG	CCACACGAACAACACCCT
ΔCT reversion	CAGCTGCTGCaagTTCGACGAGG	CCACAGCTACAACAGCCC
Env mutants		
B5 In	TTAGGCATCTCCTATGGCAGGAAGAAG	
B3 In	GTCTCGAGATACTGCTCCCACCC	
BamHI In	ATCATCGCATCCTTAGGCATCTCCTATGGC	
XbaI In	GCGCATTCTAGAGTGTCGAGATACTGCTCC	
C1 V1 V2 F	ACCCCACTCTGTGTTACTTTAAAT	
C1 V1 V2 R	AGTTAAAGTAACACAGAGTGGGGT	
C2 V3 F	GTAATTAATTGTACAAGACCCGGC	
C2 V3 R	GCCGGGTCTTGTACAATTAATTAC	
C5 TM F	GAGAAAAAAGAGGAGCGGGACTAG	
C5 TM R	CTAGTCCCACTGCTCTTTTTTCTC	
TM CT F	GTCTTTACTGTACTTTCTGTAGTGAATAGA	
TM CT R	CCCTGCCTAACTCTATTCACTACAGAAAGT	
V1 V2 C2 F	GAAGCTATATGTTGATAAATTGTAACACCTCAGTCATTACACAGGCC	
V1 V2 C2 R	GGCCTGTGTAATGACTGAGGTGTTACAATTTATCCAACATATAGCTTC	
57 N332S	AGCACATTGCAGCCTTAGTAGGG	TGTCTTATATCTCCTACTATGTCTC
113 S332N	AGCACATTGCAACCTTAGTGGGG	TGTCTTATATCTCCTACTATGTCTCCTG

57 N186/187	aataatGATAATAGAAGCTATATGTTGATAAATTG	AATTGGTACTACATCAAGTTTATTAAAAATTG
113 ∆186/187	GATAATAGAAGCTATATGTTGATAAATTG	AATTGGTACTACATCAAGTTTATTAAAAATTG
113 L193R	AAGCTATATGcgaATAAATTGTAATACCTCAG	CTATTATCATTATTAATTGGTACTAC
113 ATLA	agatacgctCAGGATCAACAGCTCCTAG	ttccacagtCAGGACTCTTGCCTGGAG
Receptors and IFITMs		
ACE2 pcms28	ATCATCGCGGCCGCGCCACCATGTCAAGCTCTTCCTGG	GCGCATCTCGAGCTAAAAGGAGGTCTGAACATC
IFITM1 ∆117-125	TATTATGTTAtgatgaATACAGGAAAAACGGGGTTACTAG	TGGTAGACTGTCACAGAG
IFITM2 Y19F	GCCTCCCAACtttGAGATGCTCAAGGAG	TGGCCGCTGTTGACAGGA
IFITM3 Y20F	GCCCCCCAACtttGAGATGCTCA	TGGCCACTGTTGACAGGAG

2.2 PCR and sequencing

Enzymes used during PCR reactions were all purchased from New England Biolabs (NEB). Primers were designed using SnapGene software and synthesised by MWG Eurofins or IDT. Plasmids were at least partially sequenced prior to use to confirm correct plasmid, and sequenced post-cloning. For sequencing, 15μl of a miniprep was sent for sequencing with Eurofins MWG or Genewiz Azenta along with 10pmol of the relevant primers. Sequencing results were aligned to the reference sequence using SnapGene. For standard PCR, the below cycle template was used with the extension time altered depending on the plasmid size.

Table 2.3 Standard PCR cycle

Standard PCR cycle					
98ºC	98ºC	60ºC	72ºC	72ºC	4ºC
30s	10s	30s	2min	2min	Hold
	X30 cycles				

2.3 Generation of Envelope mutants by overlapping PCR and ligation independent cloning

HIV Envelope chimeras were generated by overlapping PCR. Primers overlapping the junction to be switched were designed and fragments amplified with the PCR reaction outlined in the table below. The PCR products were run on a 1% agarose gel and following extraction and purification of the fragments, 1μl of each fragment was then mixed and put into a second PCR reaction to make the next fragment.

Table 2.4 Overlapping PCR cycles for Env chimeras

PCR cycle 1					
98ºC	98ºC	60ºC	72ºC	72ºC	4ºC
30s	10s	30s	2min	2min	Hold
	X35 cycles				
PCR cycle 2					
98ºC	98ºC	60ºC	72ºC	72ºC	4ºC
30s	10s	30s	2min30sec	2min	Hold
	X35 cycles				

Table 2.5 Env chimera constructs generated in this thesis

Construct	Primer set 1	Primer set 2	Primer set 3
57_S9H(V1V2-CT 113_S8D)	B5 In	C1 V1 V2 F	
	C1 V1 V2 R	B3 In	
57_S9H(V3-CT 113_S8D)	B5 In	C2 V3 F	
	C2 V3 R	B3 In	
57_S9H(TM-CT 113_S8D)	B5 In	C5 TM F	
	C5 TM R	B3 In	
57_S9H(113_S8D CT)	B5 In	TM CT F	
	TM CT R	B3 In	
57_S9H(V1V2 113_S8D) 113_S8D(V1V2 57_S9H)	B5 In	C1 V1 V2 F	V1 V2 C2 F
	C1 V1 V2 R	V1 V2 C2 R	B3 In

Next, depending on the number of fragments to be stitched in the chimera, the outer Env B3 In and Env B5 In primers were used to amplify the final fragment. In parallel, pCDNA3.1 was cut with SSpI for 2 hours at 37ºC and 1μl of shrimp alkaline phosphatase (rSAP, NEB) to remove 5' and 3' end phosphates. The linearised SSpI and final PCR products were run on a 1% agarose gel and extracted again. Next,

ligation mixtures were prepared according to the table below and incubated as per the ligation-independent PCR cycle below.

Table 2.6 Ligation independent cloning ligation mix

Vector ligation mix	
Reagent	**Volume/amount**
pcDNA3	100-150ng
dGTPs	2μl
2.1 buffer	2μl
T4 Polymerase	0.5μl
H2O	Remaining volume to 20μl TV
Insert ligation mix	
Reagent	**Volume/amount**
Insert DNA	100ng
dCTPs	2μl
2.1 buffer	2μl
T4 Polymerase	0.5μl
H2O	Remaining volume to 20μl TV

Table 2.7 Ligation-independent PCR cycle

Ligation-independent PCR		
25ºC	80ºC	4ºC
30min	5min	Hold

After the PCR, 1:1, 2:1, and vector only mixes of vector and insert were prepared in 10μl volumes and incubated at 37ºC for 30 minutes, or overnight if you forgot about them. These were then transformed into competent cells and screened by colony PCR and sequencing prior to MIDI prepping.

Some of the Envelope chimeras were cloned using a slightly different method. The previously described PCR cycles 1 and 2 were used with the Env B3 In-BamHI and Env B5 In-XbaI primers, and the pcDNA3.1 vector cut with BamHI and XBaI for 2 hours. The final PCR product and digested 3.1 backbone were run on a 1% agarose gel and extracted as before. The insert was then digested with BamHI and XbaI for 1-2 hours, and insert ligated using the Quick Ligation kit (NEB, M2200).

2.4 DNA extraction and purification

DNA fragments were separated based on molecular weight using agarose gel electrophoresis. A majority of agarose gels were prepared at 1% agarose by adding 1g of electrophoresis grade agarose (Invitrogen) to 100ml of 1X TAE buffer (MP Biomedicals) and heated until dissolved. When cool, 5μl of ethidium bromide (Sigma) per 100ml of buffer was added and the gel poured and left to set at "room temperature". DNA samples were then loaded with a 2-log DNA ladder (NEB) and run at 50-150volts in a tank containing 1x TAE buffer. After sufficient separation the DNA was visualised under ultraviolet using the Chemi Doc UV system (BioRad). Fragments of the desired size were excised and then extracted as per the QIAGEN Gel Extraction Kit instructions.

2.5 Ligation

Digested plasmids were ligated using Quick Ligase (NEB, M2200). 50ng of the vector was used with a 2:1 or 1:1 ratio of insert calculated using the NEB online calculator along with H20 and 2x Quick Ligase buffer (NEB), and 1μl of Quick Ligase (NEB). The ligation mix was incubated for 5-10 minutes at 25ºC. 5μl of this mix was then transformed into competent cells, along with a control ligation mix containing no insert to confirm the amount of background empty annealing. Colonies were picked the next day and screen by colony PCR, or miniprepped and screened by diagnostic digest and sequencing.

2.6 Transformation and preparation of competent bugs

2.6.1 Transformation of plasmid DNA into competent cells

NEB Stbl 3 E. coli (NEB) were thawed on ice. 5μl of ligation mixture (10μl for LIC) was mixed with 45μl of thawed cells and incubated on ice for 20 minutes before undergoing heat shock at 42ºC for 45 seconds. Following a further 2 minute incubation, 250μl of LB with no antibiotic was added and the mix incubated in a shaking incubator at 30ºC

for 30 minutes to 2 hours. 50-300μl of this mix was then pipetted onto agar plates containing 100μg/ml ampicillin and incubated at 32ºC overnight. The next day, 2mls of LB broth containing ampicillin were inoculated with individual colonies picked with pipette tips from the agar plates and this was incubated at 30ºC with shaking, either overnight if the DNA was then purified with a Qiagen Miniprep kit or for 6 hours before being added to a 100ml culture for overnight shaking and purification with a Qiagen Midiprep kit. Alternatively, colonies were picked directly into a 100ml culture and incubated at 30ºC overnight prior to purification with a Qiagen Midiprep kit.

2.6.2 Preparation of Chemically competent NEB Stbl 3 E. Coli

NEB Stbl 3 E. coli purchased from NEB were inoculated into a 1ml LB broth starter culture overnight at 30ºC with shaking. The next day, this was added to an 250ml flask of LB broth and incubated at 30ºC with shaking until the optical density measured at 550nm reached 0.45-0.5. Cells were incubated on ice for 10 minutes and then pelleted at 3000 g at 4ºC for 10 minutes. Pellets were resuspended in 100ml of Buffer 1 (see table below) and incubated on ice for 10 minutes. Cells were then pelleted at 3000 g at 4ºC for 10 minutes again and resuspended in 10ml of Buffer 2 and incubated on ice for a further 10 minutes. Cells were then aliquoted into 100-200μl aliquots on dry ice and stored at -80ºC. 1 vial was used to test the competency of the cells by retransforming a plasmid alongside a vial of older competent cells and the number of colonies counted the next day.

Table 2.8 Competent bug buffers

Buffer 1	Buffer 2
KAc 30mM	PIPES 10mM
RbCl 100mM	CaCl2 75mM
CaCl2 10mM	RbCl 10mM
MnCl2 50mM	Glycerol 15%
Glycerol 15%	-

2.7 Colony PCR

Colony PCR was used to screen for positive ligation independent cloning colonies or when a gene had been amplified by PCR and inserted into a new backbone to reduce the number of samples to send for sequencing. 20μl of mastermix (as specified in the table below) was added to each PCR tube. Each colony was picked, briefly stirred in the tube and then placed into a culture tube with 2mls of ampicillin LB broth for culturing overnight and mini prepping. The below PCR cycle was then ran, and positive cloning identified by the presence of a band of the right size by running the PCR product on a 1% agarose gel.

Table 2.9 Colony PCR mastermix

Colony PCR mastermix	
Reagent	**Volume**
Water	17.05μl
10x buffer	2μl
dNTPs	0.4μl
Primer forward	0.2μl
Primer reverse	0.2μl
Taq polymerase	0.15μl

Table 2.10 Colony PCR cycle

Colony PCR cycle					
1	2	3	4	5	6
95ºC	94ºC	60ºC	72ºC	72ºC	4ºC
3 min	30 sec	30 sec	2 min	15 min	Hold
	X25 cycles				

2.8 Restriction digest cloning

Table 2.11 Restriction digest

Reagent	**Volume**
Cutsmart buffer	5μl
Enzyme 1	0.5-1μl
Enzyme 2	0.5-1μl
Water	35-40μl
DNA	50ng-5μg

Reactions were incubated at the recommended temperature for 2 hours, with 1μl of rSAP (NEB) if required, and run on a 1% agarose to separate bands and excised and gels extracted as per the manufacturer's instructions of the Qiagen Gel Extraction Kit.

2.9 Mutagenesis

To introduce small substitutions, insertions, or deletions, mutagenesis was completed using the NEB Site-Directed Mutagenesis Kit (E0554) as per the manufacturer's instructions. Primers were designed using the NEB base changer website (https://nebasechanger.neb.com). Following PCR with the selected primers and appropriate elongation time, 5μl of the PCR product was run on an agarose gel to confirm concatenation of the DNA. 1μl of PCR product was then mixed with 5μl of the KLD buffer, 1μl of KLD enzyme and 3μl of H2O at 25ºC for 5 minutes and then 5μl of this mix transformed into NEB stables as previously described. Colonies were mini prepped and screened by sequencing to confirm success of cloning.

2.10 Cell culture

The majority of cell lines were incubated in Dulbecco's modified Eagle Medium (DMEM, Gibco) containing 10% heat-inactivated Foetal Calf Serum (FCS) and 20μg/ml of gentamicin (Invitrogen) or 5ml/500ml of Penstrep (Gibco). All cells were maintained at 37ºC with 5% CO_2. For adherent cells, 2ml of Trypsin (TryplE, Invitrogen) was used to detach cells. For the passaging of Calu-3 cells, cells were washed twice with 1X PBS and then incubated with 1X PBS for 5 minutes at 37ºC. Cells were then trypsinised and treated with excessive swearing for 20-30 minutes. Cell line originations and antibiotic requirements are detailed below.

Table 2.12 Stable cell lines

Cell line	Antibiotic	Origin/details
293T-17	-	ATCC
TZM-Bl HeLa	-	ATCC
U87-CD4-CCR5	1μg/ml puromycin, 100μg/ml G418	Generated by Dr Toshana Foster
U87-CD4-CCR5-PLHCX	1μg/ml puromycin, 100μg/ml G418, 100μg/ml hygromycin	Generated from U87-CD4-CCR5 cells
U87-CD4-CCR5-IFITM1	1μg/ml puromycin, 100μg/ml G418, 100μg/ml hygromycin	Generated from U87-CD4-CCR5 cells
U87-CD4-CCR5-IFITM2	1μg/ml puromycin, 100μg/ml G418, 100μg/ml hygromycin	Generated from U87-CD4-CCR5 cells
U87-CD4-CCR5-IFTIM3	1μg/ml puromycin, 100μg/ml G418, 100μg/ml hygromycin	Generated from U87-CD4-CCR5 cells
U87-CD4-CCR5-IFITM1 Δ117-125	1μg/ml puromycin, 100μg/ml G418, 100μg/ml hygromycin	Generated from U87-CD4-CCR5 cells
U87-CD4-CCR5-IFITM2 Y19F	1μg/ml puromycin, 100μg/ml G418, 100μg/ml hygromycin	Generated from U87-CD4-CCR5 cells
U87-CD4-CCR5-IFITM3 Y20F	1μg/ml puromycin, 100μg/ml G418, 100μg/ml hygromycin	Generated from U87-CD4-CCR5 cells
U87-CD4-CXCR4	1μg/ml puromycin, 100μg/ml G418	Generated by Dr Toshana Foster
293T-17-M	1μg/ml puromycin	Generated from 293T17 ATCC cells
A549-ACE2	1μg/ml puromycin	Generated from A549 cells obtained from ATCC
A549-ACE2-TMPRSS2	1μg /ml puromycin, 400μg/ml G418	Generated from A549-ACE2
A549-ACE2-PLHCX	1μg/ml puromycin, 100μg/ml hygromycin	Generated from A549-ACE2
A549-ACE2-IFITM1	1μg/ml puromycin, 100μg/ml hygromycin	Generated from A549-ACE2
A549-ACE2-IFITM2	1μg/ml puromycin, 100μg/ml hygromycin	Generated from A549-ACE2
A549-ACE2-IFITM3	1μg/ml puromycin, 100μg/ml hygromycin	Generated from A549-ACE2
A549-ACE2-IFITM1 Δ 117-125	1μg/ml puromycin, 100μg/ml hygromycin	Generated from A549-ACE2
A549-ACE2-IFITM2 Y19F	1μg/ml puromycin, 100μg/ml hygromycin	Generated from A549-ACE2
A549-ACE2-IFITM3 Y20F	1μg/ml puromycin, 100μg/ml hygromycin	Generated from A549-ACE2
A549-ACE2-TMPRSS2-PLHCX	1μg/ml puromycin, 400μg/ml G418, 100μg/ml hygromycin	Generated from A549-ACE2-TMPRSS2
A549-ACE2-TMPRSS2-IFITM1	1μg/ml puromycin, 400μg/ml G418, 100μg/ml hygromycin	Generated from A549-ACE2-TMPRSS2
A549-ACE2-TMPRSS2-IFITM2	1μg/ml puromycin, 400μg/ml G418, 100μg/ml hygromycin	Generated from A549-ACE2-TMPRSS2
A549-ACE2-TMPRSS2-IFITM3	1μg/ml puromycin, 400μg/ml G418, 100μg/ml hygromycin	Generated from A549-ACE2-TMPRSS2

A549-ACE2-TMPRSS2-IFITM1 117-125	1μg/ml puromycin, 400μg/ml G418, 100μg/ml hygromycin	Generated from A549-ACE2-TMPRSS2
A549-ACE2-TMPRSS2-IFITM2 Y19F	1μg/ml puromycin, 400μg/ml G418, 100μg/ml hygromycin	Generated from A549-ACE2-TMPRSS2
A549-ACE2-TMPRSS2-IFITM3 Y20F	1μg/ml puromycin, 400μg/ml G418, 100μg/ml hygromycin	Generated from A549-ACE2-TMPRSS2
Calu-3	-	ATCC
Vero-E6	-	ATCC
Vero-E6-TMPRSS2	400μg/ml G418	Generated from Vero-E6 cells

2.11 Generation of stable cells

2.11.1 Transduction of stable cells lines

Cells were plated 24h prior to transduction for 50-90% confluence the next day. Cells were transduced with 0.5ml-1ml of lentiviral or retroviral vectors packaged with HIV gag-pol (p8.91) or murine-leukaemia virus (MLV) gag-pol and vesicular stomatitis virus G protein (VSVG) for 4-24h. Antibiotic selection was added to transduced cells and a sacrificial control well that had not been transduced 24h later. Cells were split in the 6-well or expanded to a 10cm once the well was confluent and split in selection until the sacrificial well/plate had died. Cells were then deemed stable and Western blotted for the protein of interest to confirm sufficient expression.

2.11.2 Kill curve

If the antibiotic required for a stable cell line was new to the cell line used, a kill curve would be set up to determine the appropriate amount of antibiotic selection. Cells were plated to be confluent in a 24 well plate 24h before antibiotic treatment. The next day cells were treated with increasing amounts of antibiotic depending on the range suggested in the specification sheet. Cells were monitored for the next 96h for cell death and the concentration one above the concentration that killed all cells was selected for generating a stable cell line.

2.12 Generation of SARS-CoV-2 viral stocks

In 2020, England-02 stocks were made in Vero-E6 cells. When VOCs began emerging that appeared to be more dependent on TMPRSS2 for viral entry, this protocol was updated to use Vero-E6-TMPRSS2 cells. These were used to generate all stocks from then on for consistency. Vero-E6-TMPRSS2 cells were plated at 6x10^6 in a T75 flask in 30ml of 10% FCS DMEM 24h prior to infection. The next day, media was changed for 20ml of 2% FCS DMEM and cells inoculated with 100-200μl of SARS-CoV-2 virus. Higher volumes of inoculation were used for strains with poor replicative capacity. Cells were monitored for cytopathic effect (CPE) for the next 48-72h, and supernatant harvested and filtered through a 0.45μm filter and frozen when appropriate CPE had occurred, deemed by microscopy. Viruses were then titred by plaque assay to determine pfu/ml, or copies of E/ml calculated by qPCR of viral stock.

Table 2.13 Viral stocks used in this thesis

Virus	Original source of stock	Stock generated in
England-02 (D614) used in Chapter 3	Public Health England	Vero-E6
England-02 (D614) used in Chapter 4	Public Health England	Vero-E6-TMPRSS2
3.20 (G614)	Dr Suzy Pickering	Vero-E6-TMPRSS2
Alpha (B.1.1.7)	Prof Wendy Barclay	Vero-E6-TMPRSS2
Delta (B.1.6.7.2)	Prof Wendy Barlcay	Vero-E6-TMPRSS2
Omicron BA.1 (, B.1.1529)	Prof Wendy Barclay	Vero-E6-TMPRSS2
Wuhan-alpha spike	Prof Massimo Palmarini	Vero-E6-TMPRSS2
Wuhan-alpha spike H681P	Prof Massimo Palmarini	Vero-E6-TMPRSS2

2.13 Titrating SARS-CoV-2 viral stocks

2.13.1 Plaque assay of viral stocks

Vero-E6-TMPRSS2 were plated in 6 well plates to be fully confluent the next day with no gaps between cells. 24h later, viral stocks were diluted appropriately, usually at 10-fold dilutions for titreing viral stocks, or 2-fold dilutions for determining titer of supernatant off infected cells. Dilutions were prepared in 2% FCS DMEM and cells

infected in 1ml for 1h. 2ml of completely warm 2x overlay (DMEM, 2% FBS, and 0.1% agarose) was then gently applied over the top and cells incubated at 37ºC for 72h. 1ml of 4% PFA was then added to the cells and plates fixed for 30 minutes at room temperature. Plates were aspirated and 1ml of crystal violet added for 5 minutes at room temperature. Crystal violet was aspirated and wells washed with PBS, allowed to dry, and plaques counted.

2x warm overlay was prepared by fully warming a bottle of DMEM in the water bath at 37ºC for 6h to prevent clumping of agarose when added. 0.6g of agarose was added to 30ml of water and microwaved until dissolved. 25ml of the melted agarose was added to the prewarmed media, along with 10ml of FCS and 5ml of Pen/Strep in a TC hood. The media was vigorously shaken to ensure minimal clumping of agarose. Before use, overlay was warmed at 37ºC in the incubator for 1 hour. Crystal violet was prepared by adding 700ml of water, 200ml of ethanol and 100ml of Crystal Violet (2.3%, Sigma, HT90132).

2.13.2 Calculation of E copies/ml of viral stocks

In the CL3, 140μl of viral supernatant was mixed with 560μl of buffer AVL with carrier RNA and samples removed to an RNA hood. The samples were processed with the QIAamp Viral RNA kit (Qiagen, 52904) as per the manufacturer's instructions. Briefly, 560μl of 100% ethanol was added to the sample and the tube vortexed. 630μl was then added to a column and spun at 6000g for 1 minute. Elutant was discarded and 630μl of sample added and spun at 6000g for 1 minute again. Elutant was discarded and 500μl of RW1 buffer added and column spun at 6000g for 1 minute. The collection tube was changed and 500μl of RW2 added and column spun at maximum speed for 2 minutes. The collection tube was changed again and the column spun at maximum speed for 1 minute. The collection tube was discarded and replaced with a fresh 1.5ml Eppendorf. 100μl of buffer AVE was added and column spun at 6000g for 1 minute. RNA was used immediately or stored at -80ºC until use.

To calculate the number of E copies/ml, a 10-fold dilution series was generated of the extracted RNA and of an E copy standard kindly gifted by the Barclay group. 1μl of each dilution and standard was used to perform one-step RT-qPCR using the TaqMan fast virus one-step mastermix (Invitrogen), using the CDC qPCR probes against E (IDT DNA Technologies). The number of E copies was then calculated in Prism by generation of a standard curve.

2.14 SARS-CoV-2 infection assays

A549 cell lines were plated at 1.5x10^5/ml in 24-well plates in 10% FCS DMEM. Calu-3 cells were plated at 2-2.5x10^5/ml in 24-well plates in 10% FCS DMEM. The next day, cells were infected with SARS-CoV-2 in 10% FCS DMEM for 1 hour in 500μl TV per well. Media was then changed for fresh 10% FCS DMEM without virus and cells incubated for 48 hours. Cells were then harvested for quantification of infection by inoculation of Vero cells, N staining intracellularly, or qPCR of cell or supernatant.

For PLV infection assays, cells were plated at 1-1.5x10^5/ml 24h prior to transduction. Media was aspirated and 100μl of PLVs added to each well. Cells were incubated at 37ºC for 48 hours and readout measured using the Promega Steady-Glo luciferase assay system (E2250). 45μl of Steady-Glo was added to 45μl of media and plates incubated in the dark at RT for 10 minutes. 70μl of Steady-Glo-media was then added to a 96-well white plate and read on the Perkin Elmin Luminometer.

2.15 N staining of Vero-E6/Vero-E6-TMPRSS2 cells inoculated with infected supernatant

Vero-E6, or Vero-E6-TMPRSS2 from early 2021 onwards, were plated at 1x10^5/ml in a 96 well plate. The next day, SARS-CoV-2 infected supernatant, either fresh or thawed, was used to inoculate the cells both neat and diluted 1:2 in 2%FCS DMEM for 1 hour, in 50μl TV. After 1 hour, 50μl of warm 2x overlay media was gently added

and cells incubated at 37ºC for 24 hours. Media was aspirated and cells were washed with PBS prior to fixing in 50μl of 4% PFA for 30 minutes at RT. 100μl of PBS was added to wells and plate removed from the CL3. In a tissue culture hood, cells were washed with PBS again, and permeabilized with 0.1% Triton for 15 minutes at RT. Cells were then blocked with 3% milk for 15 minutes and incubated with anti-human anti-SARS-CoV-2 N antibody (CR3009) for 45 minutes. Following this, cells were washed twice with PBS and incubated with goat anti-human IgG (Fc) peroxidase conjugate (Sigma A0170) for 45 minutes. Cells were washed with PBS twice again, and finally presence of N was detected using the 1 step Ultra TMB-ELISA substrate solution (ThermoFisher). After sufficient detection, cells were quenched with sulfuric acid and the luminescence detected with Perkin Elmer EnVision multimode plate reader at 405nm absorbance.

2.16 N staining of intracellular N by flow cytometry

48 hours post-infection, cells were trypsinised with 150μl of trypsin for 5 minutes at 37ºC. 150μl of 4% PFA was added and cells fixed for 30 minutes at RT. 300μl was then transferred to a round-bottom 96 well plate and the plate removed from CL3. Cells were centrifuged at 500g for 5 minutes. Supernatant was removed with a multichannel pipette in a TC hood, and 150μl of PBS 0.5% tritonX100 added for 10 minutes at RT. Cells were centrifuged at 500g for 5 minutes and supernatant removed with a multichannel pipette. Cells were washed with 150μl PBS and centrifuged again as before. Supernatant was removed and 200μl of PBS with 5% FCS added for 20 minutes. Cells were centrifuged and supernatant removed. 100μl of anti-N (human, CR3009, 1:1000) added for 30 minutes at RT. Cells were then centrifuged and supernatant removed. Cells were washed with 150μl of PBS and centrifuged. Supernatant was removed and 100μl of anti-mouse secondary antibody (1:750) added for 25 minutes at RT. Cells were again centrifuged and supernatant removed. Cells were washed with 150μl of PBS once more, centrifuged, and pellet resuspended in 100μl of PBS for flow cytometry. Flow cytometry data was analysed using FlowJo.

2.17 Generation of PLVs

293T-17 cells were split 1:4 into 10cm plates or plated at $3x10^5$/ml in 6 well plates the day before transfection. 24h later cells were transfected with firefly luciferase-expressing vector (CSXW), HIV gag-pol (8.91) and either HIV Envelope or SARS-CoV-2 Spike at a ratio of 3:2:1 for HIV-1, or 3:2:2 for SARS-CoV-2, using 4x PEI-MAX per μg of DNA. Media was changed 6-16 hours later for fresh DMEM 10% FCS, and supernatant harvested and filtered through 0.45μm 48 hours after transfection. Viral supernatant was stored at -80ºC until use. PLVs were used to transduce each cell line of interest for 48h. Equal volumes of PLVs were used to infect the cell line of interest.

2.18 IFN assays

Cells were plated in the morning at the same confluency for infection and treated with IFNα (Invitrogen, 111001) IFNβ (PBL Assay Science, 11415-1), IFNγ (Peprotech, 300-02) or IFNλ (Peprotech, 300-02L) 6-8h later. IFN dilutions were made up in a five-fold series from 0.1 to 62.5ng/μl or U/ml in DMEM 10%FCS. Cells were treated with IFN for 16-24h and then media replaced for PLVs or infectious virus as previously described.

2.19 Drug assays

To determine route of SARS-CoV-2 viral entry, cells were treated with various drugs that inhibited TMPRSS-mediated (Camostat), Cathepsin B/L-mediated (E64d) or MMP2/MMP9-mediated (MMP2/MMP9 inhibitor II). Cells were plated at $1.5x10^5$/ml the day prior, and treated with Camostat mesylate (Sigma, SML0057), E64d (Sigma, E8640), or MMP2/MMP9 inhibitor (444249 Merck MMP2/MMP9 inhibitor II) for 1h at 37ºC. Cells were then transduced with SARS-CoV-2 PLVs, with the drug remaining on, for 48h and infection determined by luciferase activity as previously described. Infectivity was normalised to the DMSO control per cell line for these experiments.

2.20 RNA extractions and qPCR

2.20.1 RNA extractions

For infected cells, cells were lysed in 350μl of RLT lysis buffer (Qiagen) containing freshly added β-mercaptoethanol (Sigma) in the CL3. Samples were immediately processed or stored at -80ºC. RNA extractions were performed using the RNeasy Mini Kit (Qiagen) as per the manufacturer's instructions in an RNA extraction hood. RNA was eluted in 30-50μl of RNase-free H20 which was subsequently used for cDNA synthesis or Fast-Virus qPCR.

For infected supernatant, 140μl of viral supernatant was mixed with 560μl of buffer AVL with carrier RNA in the CL3 and samples subsequently removed to an RNA hood. The samples were processed with the QIAamp Viral RNA kit (Qiagen, 52904) as per the manufacturer's instructions and described in section 2.12.2. RNA was used immediately or stored at -80ºC until use.

2.20.2 cDNA synthesis

After RNA extraction, cDNA was synthesised using the High Capacity cDNA Reverse Transcription Kit (ThermoFisher) as per the manufacturer's instructions. 12.5μl of RNA was mixed with 12.5μl of the master mix (see below) and reaction placed inside a PCR machine for 2 hours at 37ºC. A negative control where water was used instead of RNA was also run in the same plate to check for contamination. cDNA was used immediately for qPCR or stored at -80ºC until qPCR.

Table 2.14 cDNA master mix

Reagent	Volume for 1x reaction
10x reaction buffer	1.25μl
10x primers	1.25μl
dNTPs	1μl
Reverse transcriptase	0.5μl
Nuclease free water	8.5μl

2.20.3 Regular qPCR

1μl of cDNA was used to perform qPCR for the SARS-CoV-2 E gene. A master mix of the TaqMan 2x PCR mix, water and primers for GAPDH (Hs99999905_m1 GAPDH Applied Biosystems) or E (IDT DNA Technologies) was prepared and 9ul added to each well of a 384 well plate. In a separate hood, 1μl of sample was added to each well and the plate sealed and placed in a qPCR machine (Quant studio 5).

Table 2.15 qPCR cycle for cell

Hold stage		**PCR stage**	
50ºC	95ºC	95ºC	60ºC
2min	10min	15sec	1min
		40x cycles	

Table 2.16 qPCR cycle for supernatant

Hold stage		**PCR stage**	
50ºC	95ºC	95ºC	60ºC
5min	20sec	3sec	30sec
		40x cycles	

2.20.4 Fast virus qPCR

Alternatively, Fast-Virus qPCR was used. 1μl of extracted RNA was used to perform one-step RT-qPCR using the TaqMan fast virus one-step master mix (Invitrogen), using the CDC qPCR probe assay (IDT DNA Technologies) against nucleocapsid (N1 and N2).

2.21 siRNA knockdown of IFITMs

Cells were reverse transfected using 20pmol of nontargeting siRNA (Dharmacon catalog no. D-001206-13-20) or IFITM2 siRNA (Dharmacon catalog no. M-020103-02-0010), or IFITM3 siRNA (Dharmacon catalog no. L-014116-01-0010) and 1 μl of RNAi Max (Invitrogen) diluted in Optimem. This was added to the bottom of plates while cells were trypsinising, and then 1x10^5 cells added on top of the transfection mix in

a 24-well plate. Cells were incubated for 24h and then treated to a second round of reverse transfection as before. 8h later, cells were treated with different doses of IFN as previously described.

2.22 Western blotting

To detect proteins of interest in cells, cells were lysed in 2x Laemelli buffer (20% glycerol, 4% SDS, 100mM Tris-HCL pH6.8, 200mM betamercaptoethanol, 0.2% bromophenol blue). The lysis mixture was then denatured at 100ºC for 10-15 minutes. To detect proteins of interest in viruses or vectors, filtered supernatant from viral transfections were layered on top of 20% sucrose in eppendorfs and centrifuged at 18000 G for 60-120 minutes at 4ºC. After removal of sucrose, the pellets were resuspended in 50μl of 2x Laemelli buffer and boiled for 10 minutes at 96ºC. Samples were then run on 8-16% precast gels (Biorad), or homemade poured gels. For homemade gels, the resolving gel was poured between two western blotting glass plates held together using a BioRad casting frame. Isopropanol was immediately layered on top of the resolving gel to ensure a smooth transition from stacking gel to resolving gel. After the resolving gel had solidified, the isopropanol layer was poured off and the top of the gel was washed with double distilled water. The stacking gel was then prepared and poured on top of the resolving gel and a plastic comb (BioRad) inserted into the top of the stacking gel to create wells. Once the stacking gel had set, gels were wrapped in wet blue roll and kept at 4ºC until the gel was run. 10μl of sample was loaded into each well alongside 4μl of a pre-stained protein ladder (NEB), and gels were ran in the BioRad Protean Tetra Cell electrophoresis system with running buffer (0.1% SDS, 25mM Tris, 200mM glycine). Gels were run at 80-150v to separate proteins until the bottom of the ladder had reached the bottom of the gel.

Separated proteins were then blotted onto a nitrocellulose membrane (Amersham Protran 0.45 NC) using Criterion Blotters from BioRad containing transfer buffer (20% ethanol, 25mM Tris, 200mM glycine). The transfer was run at 400mAmp for 1 hour on ice. Following transfer, membranes were blocked at room temperature with 1x PBS 0.1% Tween 5% Milk (Marvel) with rolling or 1x PBS 0.1% Tween 3% BSA (A7906 SIGMA). Membranes were then incubated in primary antibodies overnight at 4ºC with rolling. The next day, membranes were washed with 1x PBS 0.1% Tween 3x for 10

minutes and incubated with relevant secondary antibodies in 1x PBS 0.1% Tween 5% Milk or 3% BSA for 1 hour at room temperature with rolling. Membranes were then again washed with 1 PBS 0.1% Tween 3x for 10 minutes and analysed with either the LICOR odyssey infrared imaging system or the ImageQuant LAS 400 mini system or the Amersham Imagequant 800. Membranes that had been incubated with a horseradish peroxidase conjugated secondary antibody were incubated with Super Signal West Pico Chemiluminescent solutions (Thermofisher) or ECL Prime Western Blotting Reagent Amersham GE Healthcare (RPN2232) before visualisation. Band intensities were analysed with LICOR Lite imaging software.

Table 2.17 Antibody list

Primary Antibody	**Species**	**Source**	**Dilution**
Gp120	Rabbit	NISBC ARP421	1:3000
Gag	Mouse	Neil lab	1:100
HSP90	Mouse	sc-515081 Santa Cruz	1:3000
HSP90	Rabbit	GTX109753 Genetex	1:3000
Beta actin	Mouse	ab8226 Abcam	1:3000
Beta actin	Rabbit	20536-1-AP Proteintech	1:3000
GAPDH	Mouse	60004-1-Ig Proteintech	1:3000
GAPDH	Rabbit	WH139831 Abclonal	1:3000
GAPDH	Rabbit	ab9485 Abcam	1:3000
αtubulin	Rabbit	Ab15246 Abcam	1:3000
IFITM1	Mouse	60073-I-Ig Proteintech	1:2000
IFITM2	Rabbit	12769-I-AP Proteintech	1:2000
IFITM3	Rabbit	11714-I-AP Proteintech	1:2000
ACE2	Rabbit	ab108209 Abcam	1:2000
SARS-CoV-2 spike	Mouse	GTX632604 Genetex	1:1000
Strep tag II	Rabbit	ab76950 Abcam	1:2000
Phospho STAT1	Mouse	612133 BD Transduction Laboratories	1:2000
STAT1	Rabbit	9172S Cell Signalling	1:2000
Secondary antibody	**Species**	**Source**	**Dilution**

Anti-Rabbit 800	Goat	LICOR	1:5000
Anti-Mouse 680	Goat	LICOR	1:5000
Anti-Rabbit HRP	Goat	Cell signalling	1:5000
Anti-Mouse HRP	Goat	Cell signalling	1:5000

Chapter 3: The sensitivity of the early wave Wuhan spike to IFITM2 can be modulated by the polybasic cleavage site

Some of the data presented in this chapter have been published under the title “The Polybasic Cleavage Site in SARS-CoV-2 Spike Modulates Viral Sensitivity to Type I Interferon and IFITM2” [334] and “The P681H Mutation in the Spike Glycoprotein of the Alpha Variant of SARS-CoV-2 Escapes IFITM Restriction and Is Necessary for Type I Interferon Resistance” [30].

3.1 Introduction

In January of 2020 a novel coronavirus, SARS-CoV-2, was identified from patient samples following an outbreak of pneumonia cases in Wuhan, China. The spike sequence of this novel virus contained 67% homology to SARS-CoV-1, a coronavirus which caused an outbreak in the early 2000s [337]. The receptor for SARS-CoV-2 was identified as ACE2, which SARS-CoV-1 and NL63, a coronavirus which causes seasonal colds, also utilise for viral entry [10, 338]. One major distinction between the spikes of SARS-CoV-1 and SARS-CoV-2 however is the presence of four amino acids at the S1/S2 boundary of SARS-CoV-2 spike, $_{681}$PRRA$_{684}$, which creates a polybasic cleavage site that can be cleaved by furin-like proteases [10]. Two cleavage events in spike are required in order to achieve viral entry, a priming cleavage at the S1/S2 boundary, and a secondary triggering cleavage, presumed to be at the S2’ site ($_{815}$RS$_{816}$) which releases the fusion peptide. The PRRA in the SARS-CoV-2 spike means this site can be cleaved by furin-like proteases in the producer cell during virion assembly, meaning that only one proteolytic cleavage event, the S2’ cleavage, is required to mediate viral entry on the surface of the target cell. For SARS-CoV-1, the necessity of both cleavage events on the target cell may limit the tropism of this virus relative to SARS-CoV-2.

Several papers early in the pandemic suggested that this polybasic cleavage site was key to entering lung cells which express high levels of TMPRSS2 and key to SARS-

CoV-2 transmitting between ferrets in animal models which may explain the increased transmissibility of SARS-CoV-2 relative to SARS-CoV-1 [10, 150]. Blocking of the TMPRSS2-dependent pathway of entry with Camostat, a TMPRSS inhibitor, reduced SARS-CoV-2 infectivity. Inhibition of the cathepsins B/L with E64d was also found to inhibit SARS-CoV-2 entry, suggesting that in the absence of TMPRSS2 spike cleavage could be mediated by endosomal cathepsins [10]. Additionally, passage of SARS-CoV-2 in TMPRSS2-negative cells rapidly results in deletions in the polybasic cleavage site of spike [154]. However, infection of non-human primates with a polybasic cleavage site deleted virus results in the rapid re-emergence of the polybasic cleavage site, suggesting this site is important for *in vivo* infection [201].

It has previously been found that SARS-CoV-1 is sensitive to IFITM-mediated inhibition [36, 37, 62]. Given the differences in the spike protein between SARS-CoV-1 and SARS-CoV-2, especially the presence of a polybasic cleavage site, we were interested in whether the differences in the SARS-CoV-2 spike would result in changes in IFITM sensitivity. It has previously been found that more pathogenic influenza strains have mutations in their HA proteins which permit furin-mediated cleavage, suggesting a link between cleavage and altered pathogenicity [339]. In this chapter, I describe our initial work in understanding the sensitivity of the ancestral Wuhan spike and England-02 virus, an early Wave 1 isolate with an identical spike sequence to Wuhan, to IFITMs and IFNβ in the A549-ACE2 system. Additionally, the role of the D614G mutation that became fixed in early 2020 and the role of cytoplasmic tail deletions on viral entry and IFITM sensitivity is examined. ΔCT spikes are commonly used in SARS-CoV-2 research because deletion of the suboptimal endoplasmic retention signal (ERRS) results in increased spike accumulation at the cell surface where it is packaged into PLVs, increasing PLV infectivity [94, 175]. However, it has been suggested that ΔCT spikes do not behave similarly as full-length spike and that this can mask the effects of individual mutations [175]. Coronavirus assembly usually happens in replication complexes near the endoplasmic reticulum, and the suboptimal ERRS keeps spike in the endoplasmic reticulum and the Golgi to ensure required post-translational modifications and packaging into nascent virions [164, 340], however because of the inefficiency of this signal sequence some spike can leak to the surface and promote syncytia formation [169]. Therefore, ensuring sufficient spike remains in

the ER to be modified and incorporated onto coronavirus particles is an important aspect of coronavirus biology, that deletion of the cytoplasmic tail will alter. The impact of deleting the cytoplasmic tail on PLV viral entry and IFITM sensitivity is therefore also investigated in this chapter. For simplicity, the original SARS-CoV-2 spike described in this chapter will be referred to as Wuhan (for PLVs) and England-02 (virus).

3.2 Results

3.2.1 The polybasic cleavage site in the SARS-CoV-2 Wuhan virus is detrimental for entry into TMPRSS2-negative cells, but beneficial for entry into TMPRSS2-positive cells

The importance of ACE2 and TMPRSS2 was established early on in the pandemic as the receptor for SARS-CoV-2 infection and as a factor which can increase viral entry into cells respectively [10]. The polybasic cleavage site bridging the S1/S2 domains was suggested to improve titre on TMPRSS2+ cells, as being cleaved by furin-like proteases in the producer cell necessitates only the cleavage of the S2' site on the target cell. To examine the role of the polybasic cleavage site in entry, pseudotyped lentiviral vectors (PLVs) were utilised due to their ease in incorporating mutations into the spike protein. PLVs were produced in 293T17s using the 3-plasmid system, with a Luciferase reporter, HIV 8.91, and the spike of interest. The polybasic cleavage site (PRRA) was deleted from the Wuhan spike and infectivity tested on 293T17s transiently transfected with ACE2 (Figure 3.2.1 A, B). Infectivity increased with ACE2 expression as expected; However, surprisingly little ACE2 was sufficient to render these cells permissive to infection with viral entry 10-fold over background for Wuhan and 40-fold for the WuhanΔPRRA PLVs with 5ng of ACE2. Also surprisingly, was the increased infectivity of the WuhanΔPRRA relative to the Wuhan spike.

Next the infectivity of these PLVs was tested on a range of cell lines either endogenously or stably overexpressing ACE2 and TMPRSS2 (Figure 3.2.2 A – E). Both Calu-3 and Huh7.5 cells endogenously express ACE2, with Calu-3 cells being considered the most representative cell line of the airway epithelia which also endogenously express TMPRSS2 [160]. However, we also included A549 and Hela cells, stably overexpressing ACE2, due to these being much easier to manipulate than Calu-3. TMPRSS2 was also overexpressed on the A549-ACE2 cells, which are naturally TMPRSS2 negative. The WuhanΔPRRA PLVs had higher infectivity in A549-ACE2, Hela-ACE2 and Huh7.5, however comparable infectivity to Wuhan in the A549-ACE2-TMPRSS2 and slightly lower infectivity than Wuhan in the Calu-3 cells. The higher infectivity of Wuhan in TMPRSS2+ cells suggests the polybasic cleavage site is beneficial in this context, however is detrimental in the absence of TMPRSS2 (A549-ACE2, Hela-ACE2, Huh7.5).

Cleavage of the S2' site, at $_{815}$RS$_{816}$ has been suggested to be essential for release of the fusion peptide in the S2 domain and the final step of viral entry. To test whether deletion of this site abolished viral infectivity, the S2' site was deleted from both Wuhan and WuhanΔPRRA spikes, and infectivity measured in A549-ACE2 cells and Huh7.5 cells (Figure 3.2.3 A). The S2' deletion in the Wuhan spike decreased infectivity 4-fold and by 100-fold in the double mutant WuhanΔPRRAΔS2', however surprisingly this did not totally abolish infection (Figure 3.2.3 B, C). This could suggest that there are other potential cleavage sites besides the S2' site that can be cleaved by cathepsins. This is consistent with the recent suggestion of multiple cathepsin L cleavage sites being found in the SARS-CoV-2 spike, however whether this results in release of the fusion peptide is not yet clear [149]. These data do however suggest that if another site is being cleaved in WuhanΔS2', it is much less efficient than cleavage at the S2' site.

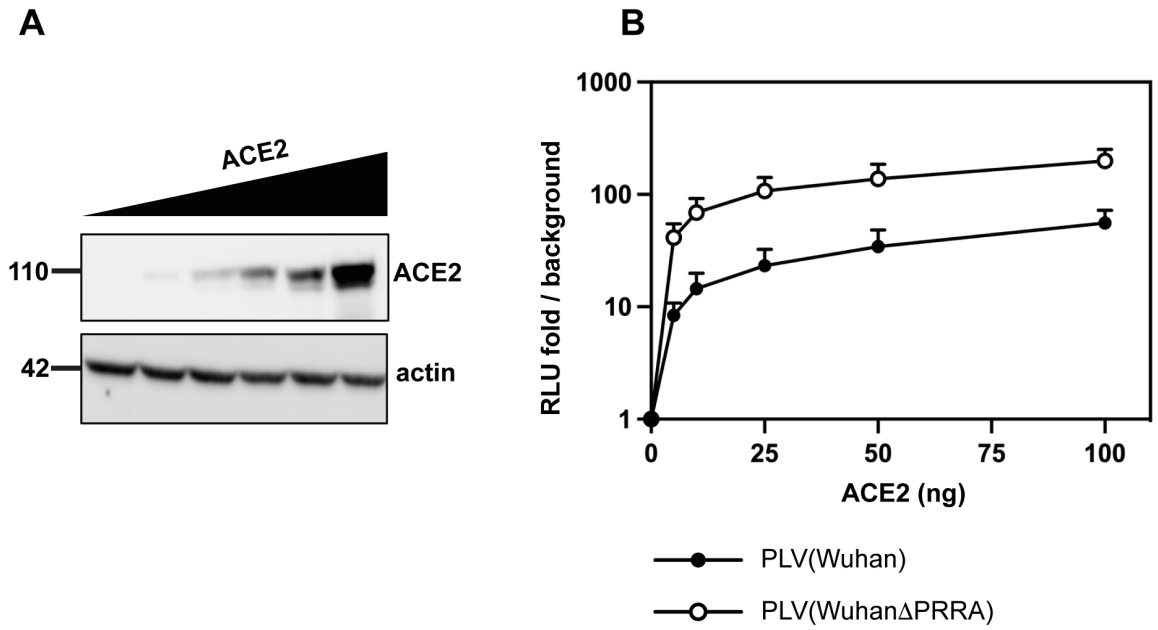

Figure 3.2.1. Low amounts of ACE2 are sufficient to mediate entry for Wuhan PLVs. A, B) 293T17s were transfected with ACE2 for 18 hours and immunoblotted for ACE2 (A) or infected with Wuhan or WuhanΔPRRA PLVs and infection quantified by luciferase activity 48 hours later. Infection is plotted as fold over background. N=3, Mean±SEM shown.

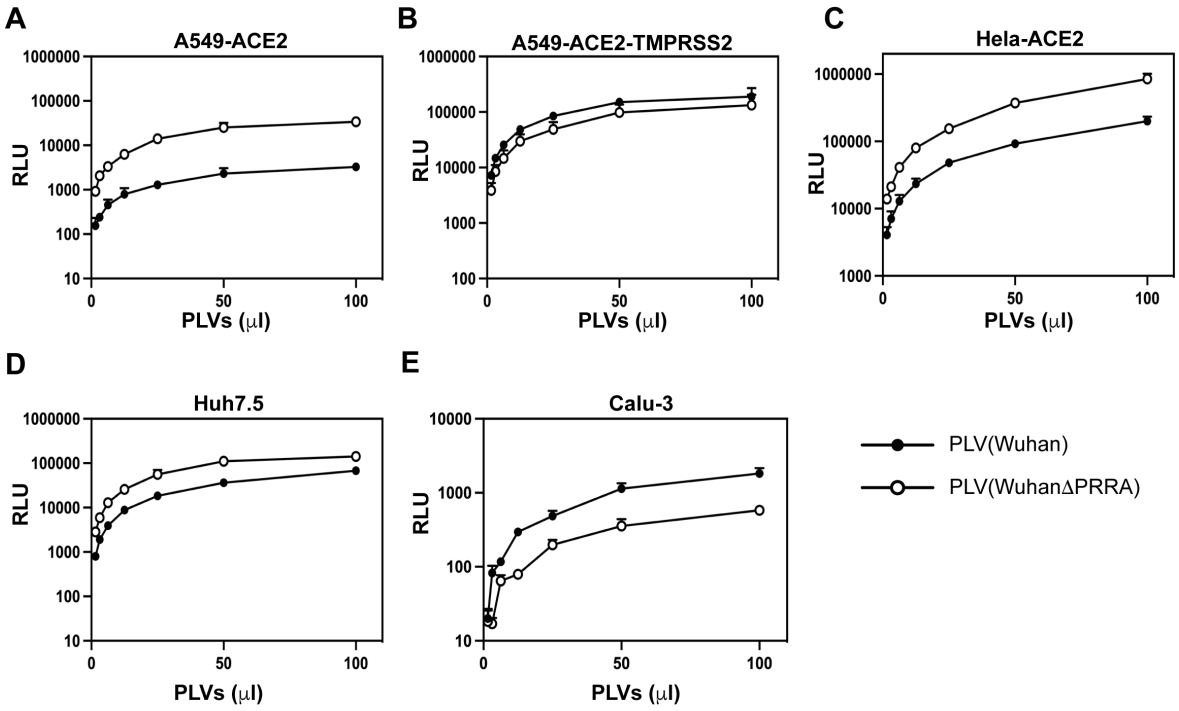

Figure 3.2.2. The polybasic cleavage site confers an advantage in TMPRSS2-positive cells, but is detrimental in TMPRSS2-negative cells. A, B, C, D, E) Cells were infected with Wuhan or WuhanΔPRRA PLVs and infection measured by luciferase activity 48 hours later. Relative Luminescence Units (RLUs) with background subtracted are plotted. N=3, Mean±SEM shown.

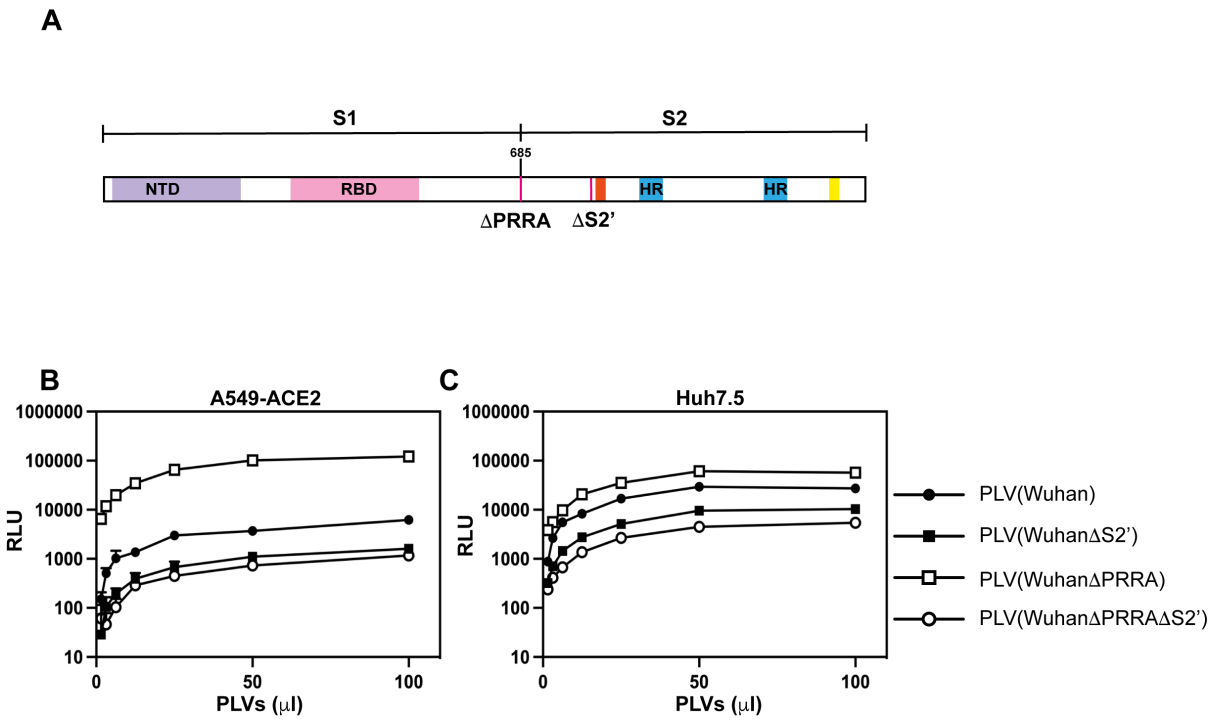

Figure 3.2.3. Deletion of the S2' site reduces infectivity of Wuhan PLVs. A) Schematic of deletion mutations created in spike. NTD=N-terminal domain, RBD=receptor binding domain, HR=heptad repeat. Fusion peptide is shown in orange and transmembrane domain in yellow. B) A549-ACE2 (B) or Huh7.5 (C) were infected with Wuhan, WuhanΔPRRA, WuhanΔS2', or WuhanΔPRRAΔS2' PLVs and infection quantified by luciferase activity 48 hours later. Raw RLUs with background subtracted are plotted. N=3, Mean±SEM shown.

3.2.2 Insertion of a polybasic cleavage site into SARS-CoV-1 spike permits furin-like protease cleavage and alters PLV infectivity

As previously mentioned, SARS-CoV-1 spike does not contain a polybasic cleavage site and cannot be cleaved by furin in the producer cell. To test whether the insertion of a polybasic cleavage site into SARS-CoV-1 spike could alter the route of viral entry, a PRRA motif was inserted into the SARS-CoV-1 S1/S2 boundary (Figure 3.2.4 A). PLVs of SARS-CoV-1 and SARS-CoV-1-PRRA were Western blotted for spike and gag to confirm whether the addition of this site altered spike cleavage (Figure 3.2.4 B). The SARS-CoV-1 PLVs spike was not cleaved into S2 on the purified virions, consistent with furin-like proteases not being able to cleave this site in the producer cell. However, addition of the PRRA site into SARS-CoV-1 resulted in some cleavage of the SARS-CoV-1 spike into S2, but not to quite the same extent as in the Wuhan spike. This could suggest the surrounding sequence of the SARS-CoV-1 S1/S2 boundary does not permit as much accessibility to furin. As expected, deletion of the PRRA site from the Wuhan spike abolished cleavage to the level of the SARS-CoV-1 spike.

The titre of these mutants was tested on A549-ACE2-, A549-ACE2-TMPRSS2, Huh7.5 and Calu-3 cells as before (Figure 3.2.5 A – D). The SARS-CoV-1-PRRA mutant had lower infectivity than SARS-CoV-1 in all the cell lines tested, except Calu-3s where it was comparable. This suggested that while the polybasic cleavage site was beneficial for entry into TMPRSS2+ cells, consistent with the literature and the previous data on the Wuhan spike, it was dispensable and even detrimental for entry into the TMPRSS2- cell lines [10, 150]. SARS-CoV-1 and 2 can also take an endosomal route of entry with the secondary cleavage step being triggered by cathepsins B/L.

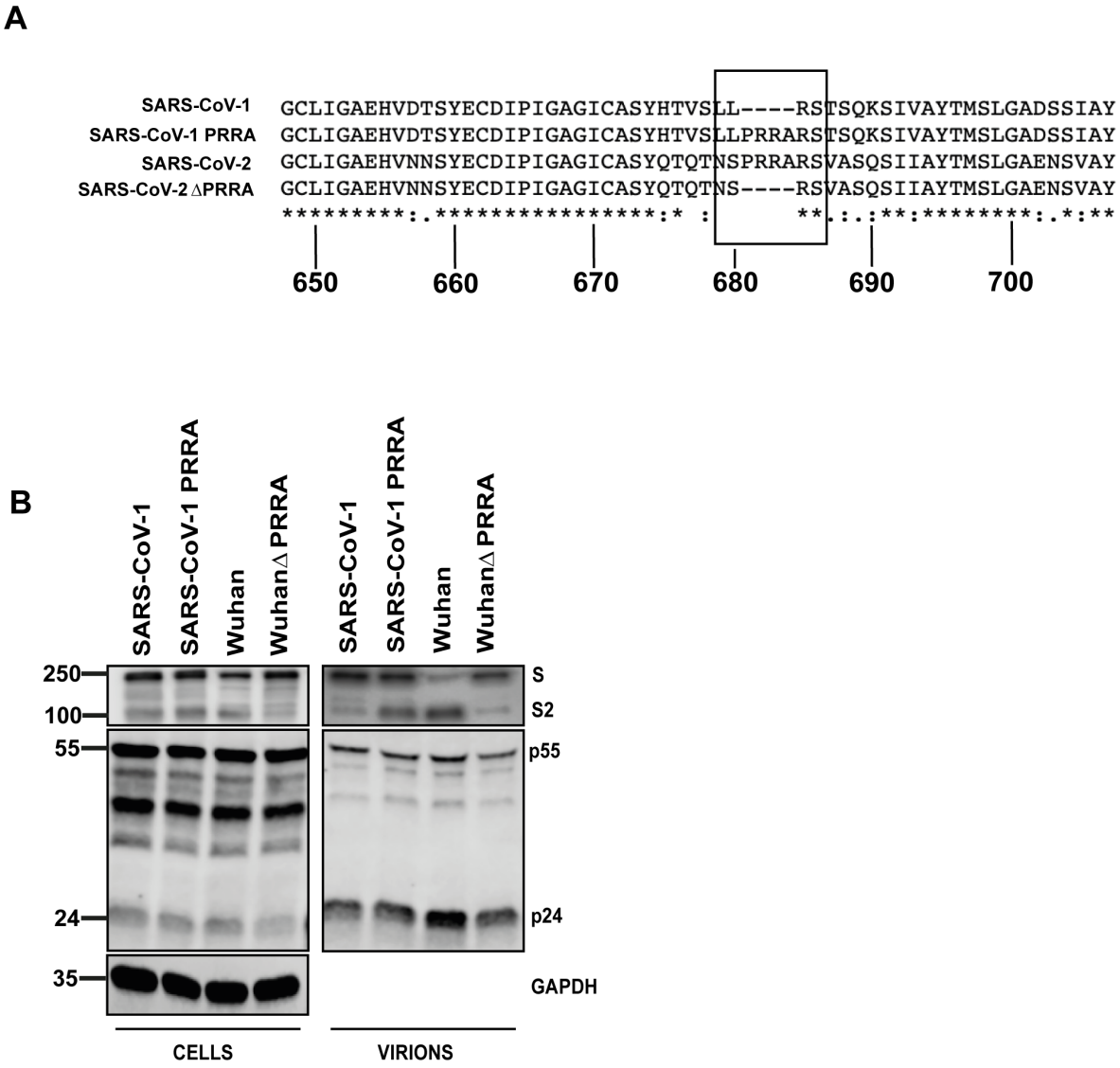

Figure 3.2.4. The PRRA motif at the S1/S2 boundary modulates S1/S2 processing in the producer cell. A) Alignment of SARS-CoV-1, SARS-CoV-2, and PRRA swap mutants generated. B) Cellular lysates and purified supernatant of PLVs generated in 293T17s were immunoblotted for spike and gag.

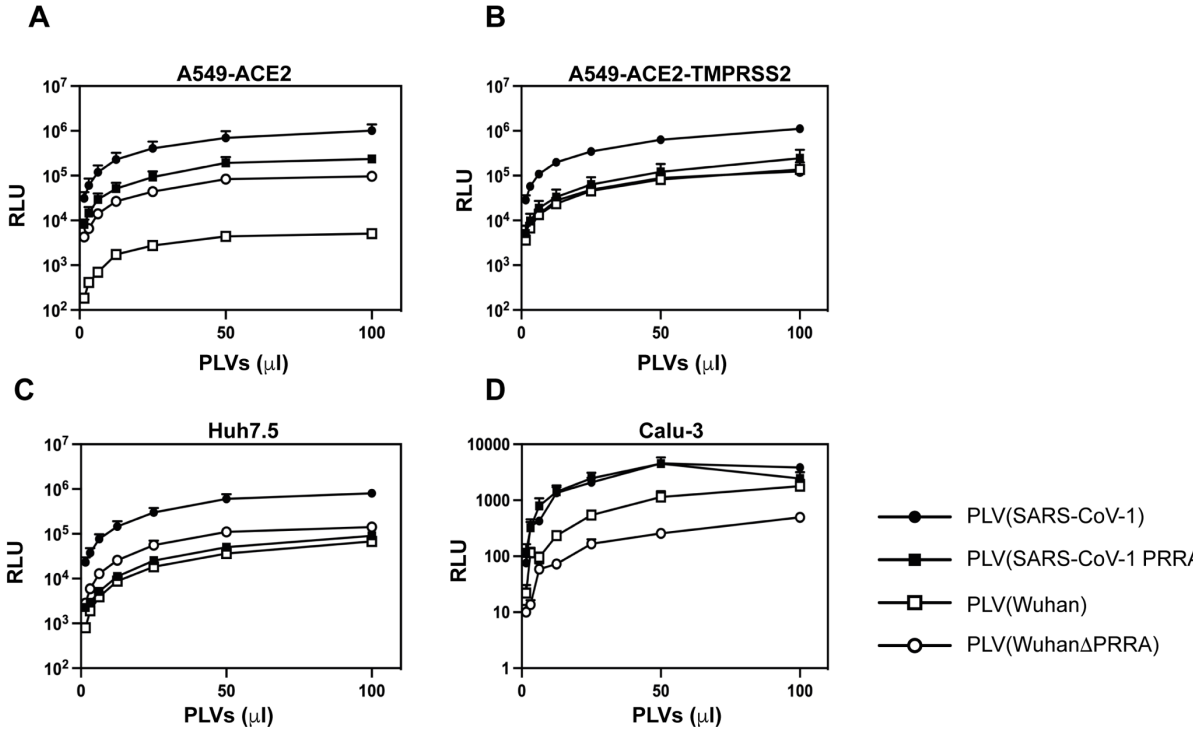

Figure 3.2.5. The PRRA site reduces SARS-CoV-1 entry into TMPRSS2- cell lines. A-D) SARS-CoV-1, Wuhan, and PRRA mutant swaps were titrated onto A549-ACE2s (A), A549-ACE2-TMPRSS2 (B), Huh7.5 (C) or Calu-3 (D) cells and infection quantified by luciferase activity 48 hours later. Raw RLUs with background subtracted are plotted. N=3, Mean±SEM shown.

As the WuhanΔPRRA spike was at a clear advantage for viral entry in TMPRSS2- cells relative to the Wuhan spike, we hypothesised that the WuhanΔPRRA was utilising the cathepsin-dependent route of entry. To test this, A549-ACE2 and A549-ACE2-TMPRSS2 cells were pre-treated with concanamycin, an inhibitor of the endosomal vATPase which prevents endosomal acidification and entry of a range of enveloped viruses which fuse in these compartments [341] [342]. In A549-ACE2 cells, SARS-CoV-1, SARS-CoV-1 PRRA and WuhanΔPRRA PLVs were very sensitive to Concanamycin (Figure 3.2.6). For SARS-CoV-1 and SARS-CoV-1-PRRA, this could be rescued slightly by the presence of TMPRSS2, with SARS-CoV-1-PRRA being rescued to a similar level of inhibition as Wuhan. The WuhanΔPRRA PLVs however did not demonstrate much rescue in the TMPRSS2+ cells, consistent with its inability

to utilise the pathway triggered by TMPRSS2-mediated cleavage. The Wuhan PLVs were the least sensitive in either TMPRSS2-negative or TMPRSS2-positive cells. This suggests that the presence of the polybasic cleavage site can decrease the level of endosomal usage of both SARS-CoV-1 and Wuhan PLVs for viral entry.

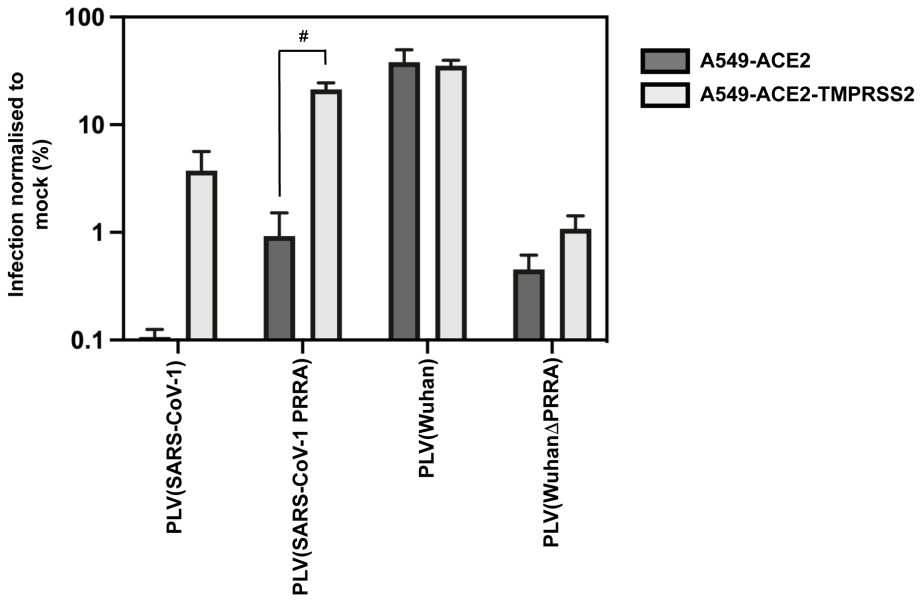

Figure 3.2.6. TMPRSS2 rescues SARS-CoV-1 and SARS-CoV-1 PRRA PLVs from Concanamycin treatment. A549-ACE2 or A549-ACE2-TMPRSS2 cells were pre-treated with 100nM of Concanamycin for 1 hour prior to infection with PLVs. Data is plotted as infection in the presence of concanamycin as a percentage of the infection in the DMSO control (for each cell line). Experiment performed by Alisha Reid. #=P>0.05 and indicate statistical significance between cell line for each PLV determined by ANOVA. N=3, Mean±SEM shown.

3.2.3 Deletion of the polybasic cleavage site forces Wuhan SARS-CoV-2 to take the endosomal route of viral entry

To further examine whether the WuhanΔPRRA was indeed reliant on the cathepsin-dependent “late pathway” of infection in TMPRSS2-negative cells, A549-ACE2 or A549-ACE2-TMPRSS2 cells were pre-treated with E64d (cathepsin B/L inhibitor) or Camostat (TMPRSS inhibitor) prior to infection with SARS-CoV-1, Wuhan, and the cleavage site swap mutant PLVs. It should be noted that Camostat is not entirely specific to TMPRSS2, and likely inhibits a broad range of serine proteases that could cleave the S2’ site. As expected, the WuhanΔPRRA was much more sensitive to

inhibition by E64d than the Wuhan PLVs. Conversely, Wuhan PLVs were more inhibited by Camostat on TMPRSS2-overexpression cells than WuhanΔPRRA (Figure 3.2.7 A – D), further implying that deletion of the polybasic cleavage site forces the spike to utilise the cathepsin-dependent route of entry. The reciprocal mutation in SARS-CoV-1 however, does not alter the route of viral entry to the same extent, with the SARS-CoV-1-PRRA mutant only becoming slightly more sensitive to Camostat in the A549-ACE2-TMPRSS2 cells (Figure 3.2.7 E – H). Both SARS-CoV-1 and SARS-CoV-1-PRRA were similarly sensitive to E64d, in the absence and presence of TMPRSS2. Given that the SARS-CoV-1-PRRA spike was not as well cleaved as Wuhan when detected by Western blot, this is likely a factor in why differences in viral entry is minimal for SARS-CoV-1 and SARS-CoV-1-PRRA.

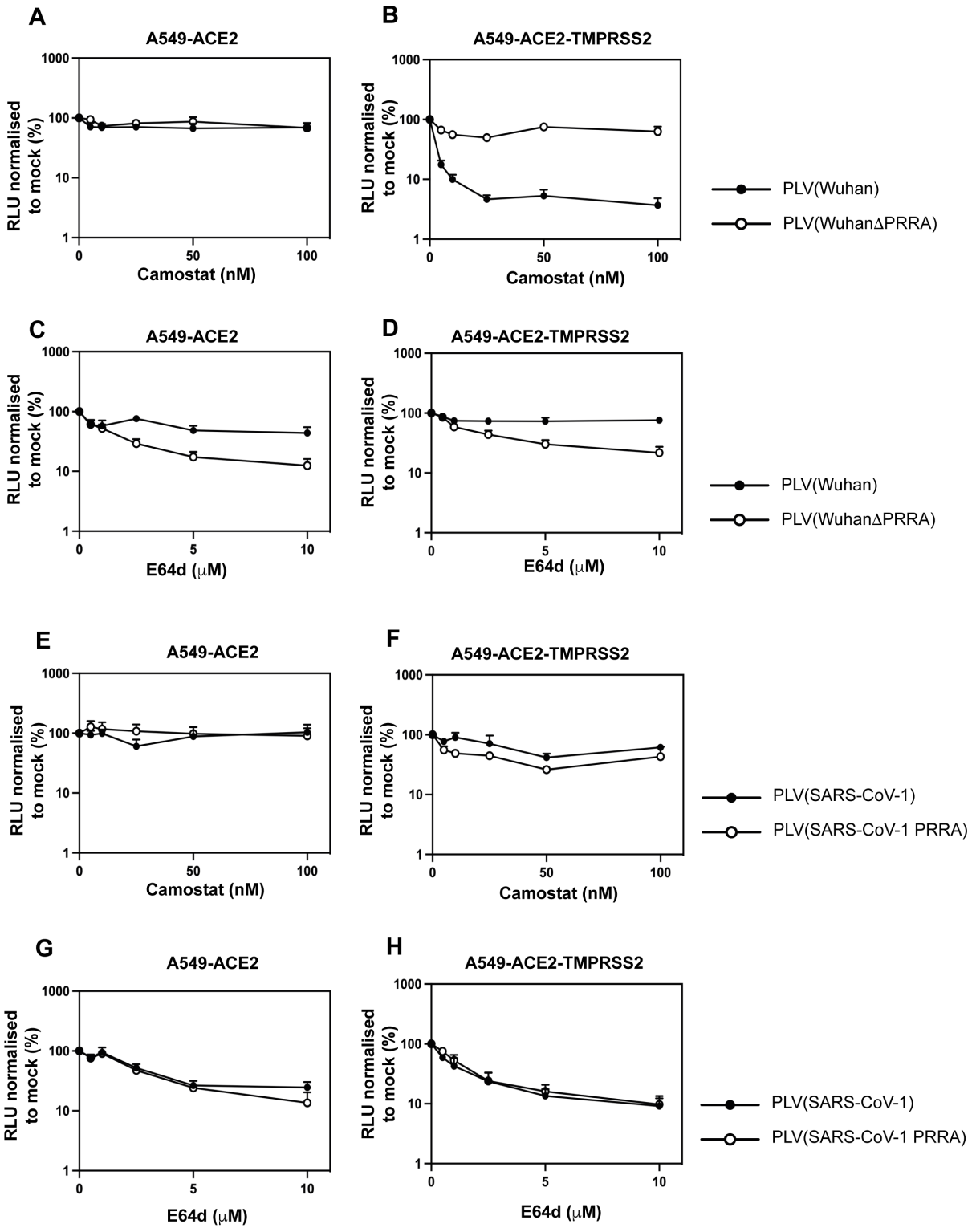

Figure 3.2.7. The presence or absence of a polybasic cleavage site dictates whether SARS PLVs can take a TMPRSS or cathepsin mediated route of entry. A, B, C, D) A549-ACE2 or A549-ACE2-TMPRSS2 were pre-treated with increasing concentrations of E64d or Camostat prior to infection with equal volumes of Wuhan or WuhanΔPRRA PLVs. E, F, G, H) A549-ACE2 or A549-ACE2-TMPRSS2 were pre-treated with E64d or Camostat prior to infection with SARS-CoV-1 or SARS-CoV-1-PRRA PLVs. N=3, Mean±SEM shown.

3.2.4 Differences in viral entry preference between Wuhan and WuhanΔPRRA correlate with IFITM2 sensitivity

It has previously been demonstrated that SARS-CoV-1 is sensitive to IFITM restriction tested by IFITM overexpression [36]. As SARS-CoV-1 lacks a polybasic cleavage site and the polybasic cleavage site in the Wuhan spike permits this virus to be less reliant on the cathepsin-mediated route of entry, we hypothesised that this may be an adaptation to escape IFITM2 restriction encountered in the “late pathway”. To test this, A549-ACE2 cells overexpressing each individual IFITM were generated (Figure 3.2.8 A). Due to the high degree of homology between IFITM2 and IFITM3, there is significant cross-reactivity between the antibodies for these proteins when detected by Western blot. First, these cells were infected with Wuhan PLVs (Figure 3.2.8 B) or England-02 virus (Figure 3.2.8 C) at an MOI of 0.005, 0.05 or 0.01. Indeed, Wuhan appeared to show some sensitivity to IFITMs 1 and 2, but little sensitivity to IFITM3. Both PLVs and virus showed a similar extent of IFITM sensitivity, suggesting that the PLVs, with only spike, phenocopy native viral sensitivity to IFITMs in this system.

Next, to confirm whether the IFITM sensitivity of SARS-CoV-1 PLVs could be recapitulated in this system, A549-ACE2-IFITM cells were infected with SARS-CoV-1 or Wuhan PLVs (Figure 3.2.9 A). SARS-CoV-1 PLVs showed some sensitivity to IFITMs 1, 2 and 3. Additionally, SARS-CoV-1 PLVs were more sensitive to IFITM2 than Wuhan PLVs, consistent with our hypothesis on the role of the presence of the polybasic cleavage site in determining sensitivity to IFITM2 in endosomal entry. Next, to establish whether the polybasic cleavage site could indeed modulate IFITM2 sensitivity, the IFITM sensitivity of the SARS-CoV-1, SARS-CoV-1 PRRA, Wuhan, and WuhanΔPRRA PLVs were tested. SARS-CoV-1 and WuhanΔPRRA PLVs were the most sensitive to IFITM2 (Figure 3.2.9 B). SARS-CoV-1 PRRA PLVs were minimally less IFITM2 sensitive than SARS-CoV-1 PLVs, consistent with the similar E64d sensitivity of these PLVs and the incomplete cleavage of SARS-CoV-1-PRRA PLVs. However, WuhanΔPRRA PLVs were 3-fold more restricted by IFITM2 than Wuhan PLVs (Figure 3.2.9 B). These data suggest that the polybasic cleavage site can modulate IFITM2 sensitivity by decreasing the dependence on the cathepsin-mediated

route of entry and likely encountering IFITM2 on endosomal membranes. Given that the SARS-CoV-1-PRRA spike was not rescued to the same extent as Wuhan in terms of cleavage, drug sensitivity or IFITM sensitivity, it was tested whether swapping a larger section of the Wuhan S1/S2 boundary into SARS-CoV-1 spike could further rescue this spike from IFITM2. This swap contained Y674–Y695 of the Wuhan spike inserted into the SARS-CoV-1 spike, termed the "Y2Y" mutant. However, the Y2Y mutant was similarly IFITM2 sensitive as SARS-CoV-1-PRRA PLVs (Figure 3.2.9 C), suggesting that a region outside of the S1/S2 boundary may be mediating the relative inaccessibility of the SARS-CoV-1 cleavage site.

The polybasic cleavage site modulates the sensitivity of the Wuhan spike to IFITM2. Additionally, insertion of a polybasic cleavage site into SARS-CoV-1 spike mildly reduced the sensitivity of this to IFITM2. The pangolin Guangdong (GD) coronavirus, which has been found in Malayan pangolins, shares 91.2% spike homology with the Wuhan spike, but lacks a polybasic cleavage site at the S1/S2 boundary [343]. To test whether insertion of the PRRA motif into the pangolin GD spike could also alter IFITM2 sensitivity, a pangolin-PRRA mutant was created. The relative cleavage of the pangolin-PRRA spike was assessed by Western blot (Figure 3.2.10 A). Again, the cleavage of the pangolin-PRRA spike did not appear to be as complete compared to the Wuhan spike, however was more cleaved than the parental pangolin spike. Next, the IFITM sensitivity of pangolin and pangolin-PRRA PLVs was tested. The pangolin GD PLVs appeared sensitive to all three IFITMs in A549-ACE2 cells (Figure 3.2.10 B). To test whether the PRRA could alleviate the IFITM sensitivity of the pangolin spike, this was inserted into the pangolin spike and the IFITM sensitivity tested (Figure 3.2.10 A, B). Although there was not a significant change in IFITM2 sensitivity, the PRRA site rescued sensitivity to IFITMs 1 and 3. Although surprising that IFITM2 sensitivity was largely unaffected, this does confirm that S1/S2 cleavage in the producer cell can alleviate IFITM sensitivity. Which IFITM this specifically alters is likely dependent on other conformational attributes of the spike.

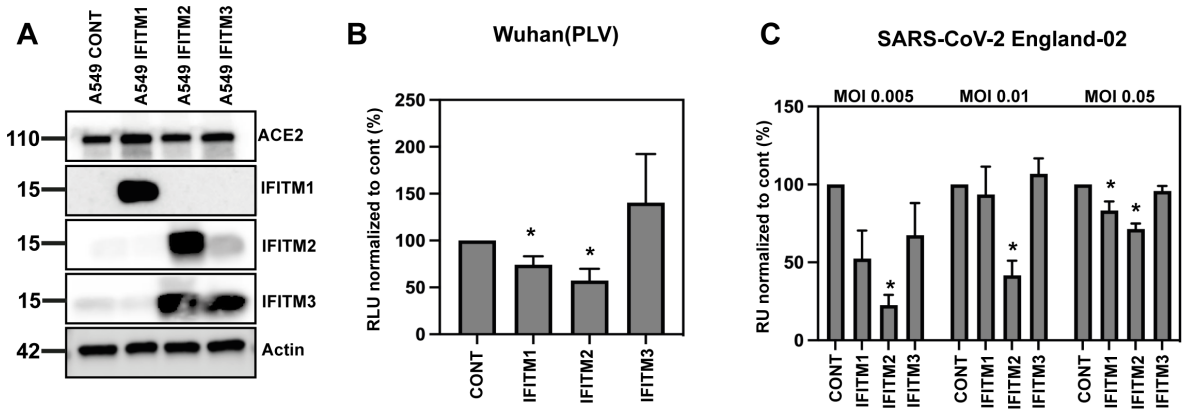

Figure 3.2.8. The England-02/Wuhan virus shows some sensitivity to IFITMs 1 and 2. A) Immunoblot of A549-ACE2 cells expressing each individual IFITM. B) PLVs bearing Wuhan spike were used to infect A549-ACE2-IFITM cells and infection quantified by luciferase activity and normalised to infection in empty vector control cells. C) A549-ACE2-IFITM cells were infected with England-02 at MOI 0.005, 0.01 or 0.05 for 48 hours and infection quantified by inoculating Vero-E6 cells with the infected supernatant and staining for N colorimetrically. *=P>0.05 and indicate statistical significance of each individual IFITM condition versus the control for each PLV determined by ANOVA. N=3, Mean±SEM shown.

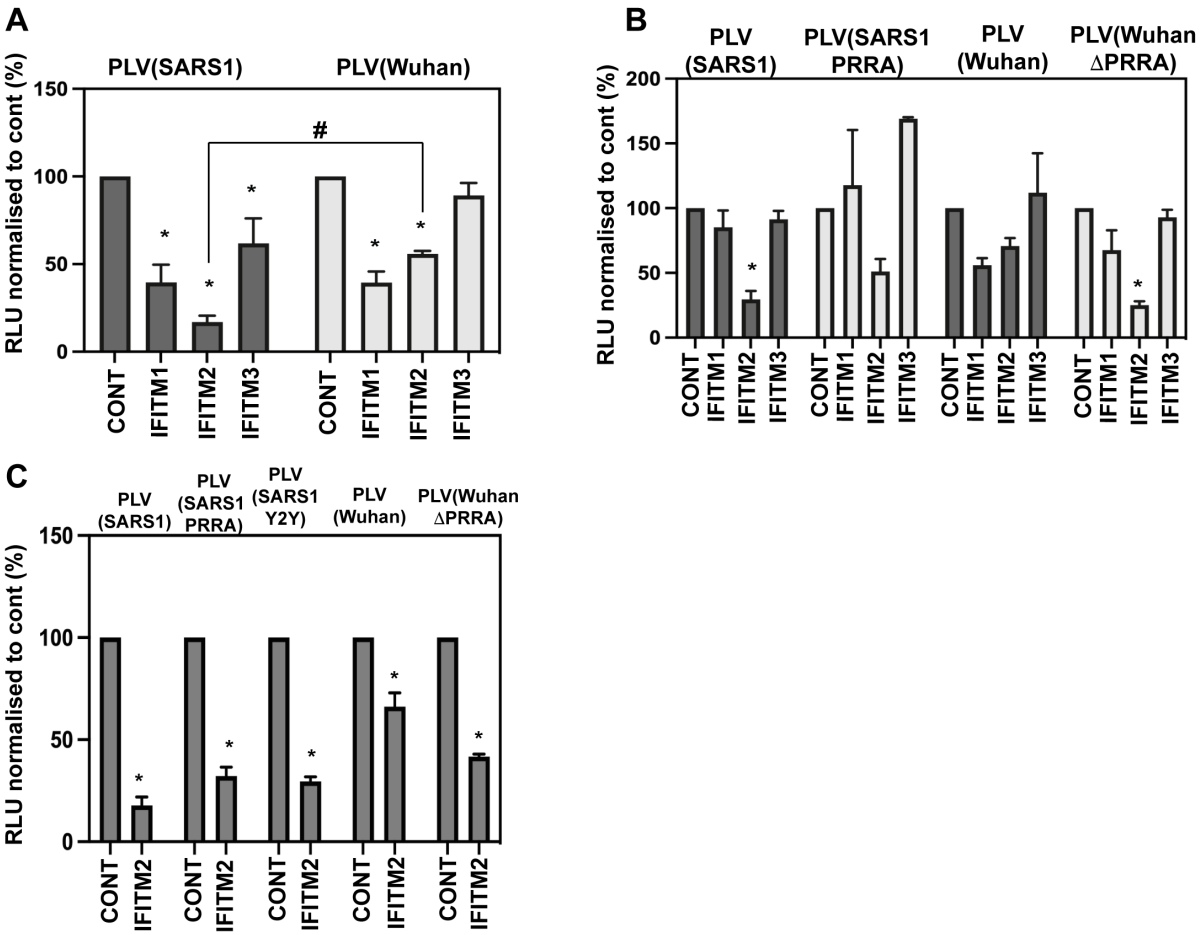

Figure 3.2.9. The polybasic cleavage site alters IFITM sensitivity in A549-ACE2 cells. A) A549-ACE2 cells were infected with equal volumes of SARS-CoV-1 or Wuhan PLVs and infection quantified by luciferase activity 48 hours later. B) A549-ACE2 cells were infected with equal volumes of SARS-CoV-1, SARS-CoV-1-PRRA, Wuhan, or WuhanΔPRRA PLVs and infection quantified by luciferase activity 48 hours later. C) PLVs with mutant spikes of SARS-CoV-1 and SARS-CoV-2 were used to infect A549-ACE2-CONTROL or A549-ACE2-IFITM2 cells and % infection normalised to the control cells. *=P<0.05 and indicate statistical significance between each IFITM and the control cell line for each PLV determined by two-way ANOVA. # indicate statistical significance between different PLVs for the same IFITM condition determined by two-way ANOVA. N=3, Mean±SEM shown.

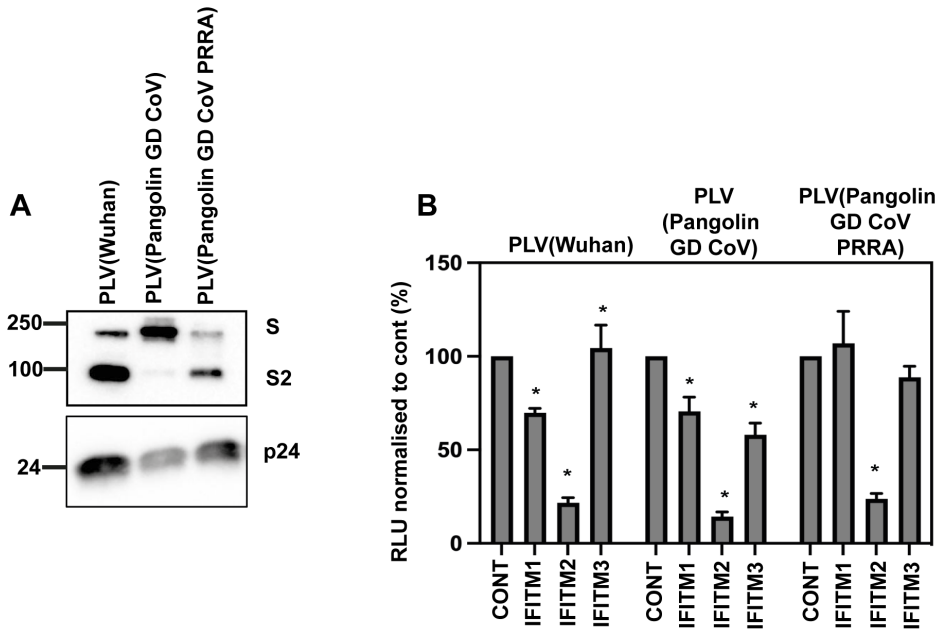

Figure 3.2.10. The polybasic cleavage site alters IFITM1 and 3 sensitivity of pangolin GD CoV PLVs in A549-ACE2 cells. A) PLVs bearing Wuhan, Pangolin Guangdong (GD), or Pangolin-PRRA GD spikes were purified through 20% sucrose and Western blotted for spike and gag. B) A549-ACE2 were infected with equal volumes of Wuhan, Pangolin GD, or Pangolin-PRRA GD PLVs. Infection was quantified by luciferase. *=P<0.05 and indicate statistical significance between each IFITM and the control cell line for each PLV determined by ANOVA. N=3, Mean±SEM shown.

3.2.5 The Wuhan SARS-CoV-2 spike and virus is sensitive to the effects of IFNβ in the A549-ACE2 system, which can be rescued by IFITM2 knockdown

Several early reports in the pandemic demonstrated that SARS-CoV-2 was sensitive to pre-treatment with IFN, and that IFN-autoantibodies were correlated with poor prognosis for COVID-19 patients [33, 184, 344-346]. Given that SARS-CoV-2 virus and PLVs appeared IFITM sensitive in A549-ACE2s, whether SARS-CoV-2 was sensitive to IFN was next tested. To investigate the sensitivity of the Wuhan virus to IFNs in this system, A549-ACE2 cells were pre-treated with Type I, II and III IFNs: α (i), β (ii), λ (iii) and γ (iv) prior to infection. A549-ACE2 cells were infected with England-02 virus 18 hours later and infection quantified by both intracellular N RNA 48 hours later (Figure 3.2.11 A), and by measuring N in the infected supernatant by inoculating Vero-E6 cells for 24 hours and staining these cells for N colorimetrically (Figure 3.2.11 B). In both readouts of infection, IFNβ and IFNγ strongly inhibited England-02 infection (Figure 3.2.11 A, B, ii and iv). This confirmed that IFNβ and γ inhibited both intracellular RNA, and the release of infectious virus. Next, to confirm whether these results could be recapitulated with PLVs and viral entry only, the IFN sensitivity of Wuhan PLVs to IFN α, β, λ and γ was tested (Figure 3.2.11 C). Again, both IFNβ and IFNγ showed the strongest inhibition of Wuhan PLV infection, although to not the same extent as with native virus (IC50s shown in Figure 3.2.11 D – G). However, a similar trend of inhibition by IFNβ was observed across viral infection, measured by qPCR and infectious virus release, and in the PLVs. This suggested that IFNβ and IFNγ were likely inhibiting an early entry step of infection.

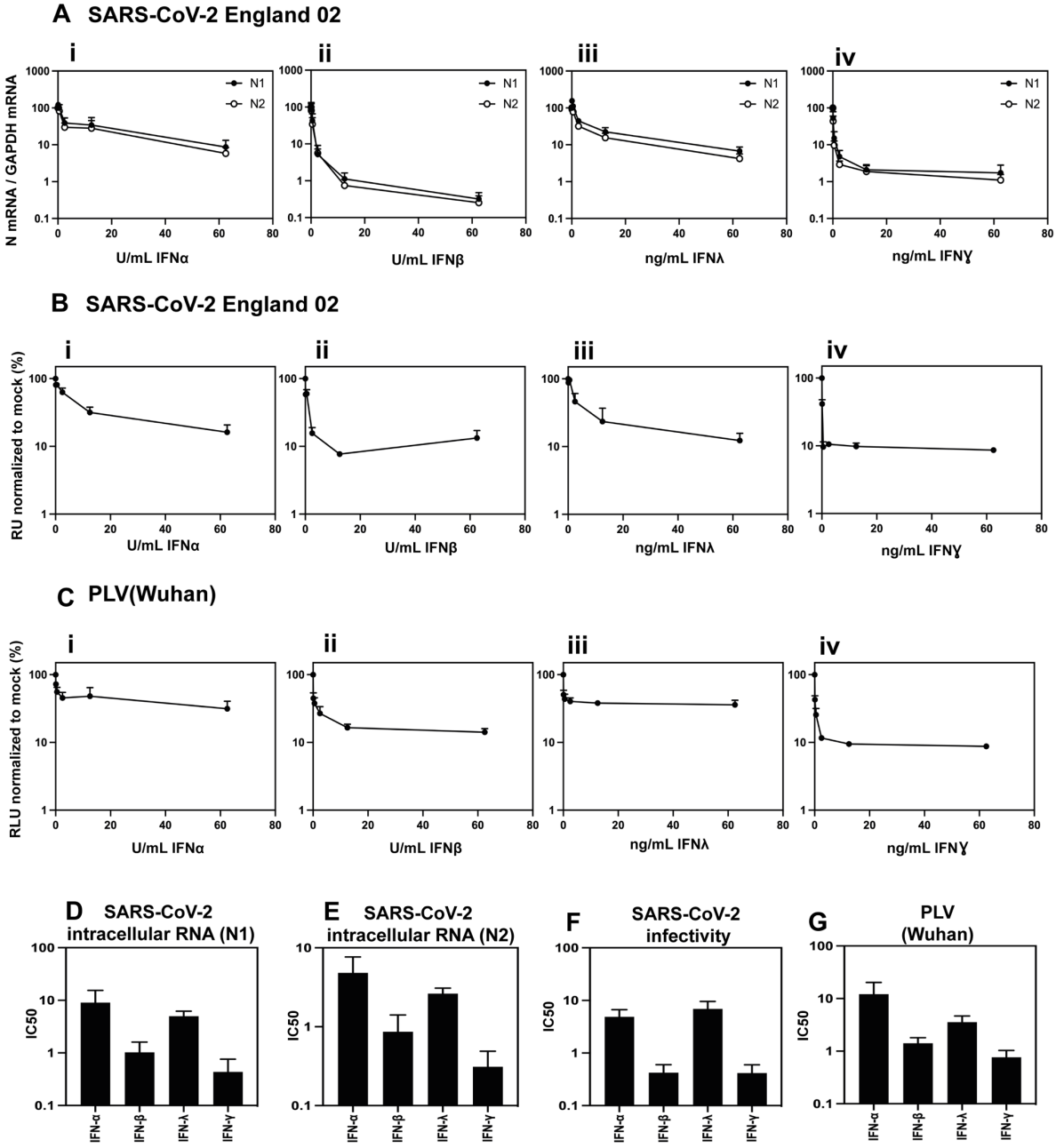

Figure 3.2.11. The SARS-CoV-2 England-02 virus and Wuhan PLVs are inhibited by IFNβ and IFNɣ. A, B) A549-ACE2 cells were pre-treated with IFN α, β, λ, or ɣ for 18 hours prior to infection with England-02 virus at an MOI of 0.005. Infection was quantified 48 hours later by intracellular N RNA and infection normalised to the no IFN condition. B) A549-ACE2 were pre-treated with IFN and infected as in (A) and infected supernatant harvested at 48 hours post infection. Supernatant was used to inoculate Vero-E6 cells and cells stained for N colorimetrically 24 hours later. C) Wuhan PLVs were used to infect A549-ACE2 cells that had been pre-treated with IFN as in A and B and infection quantified by luciferase activity 48 hours later. D) IC50 of N1 primer probe set. E) IC50 of N2 primer probe set. F) IC50 of B (viral infectivity). G) IC50 of C (PLV infectivity). IC50s calculated in GraphPad Prism. N=3, Mean±SEM shown.

IFNβ upregulates an array of antiviral proteins, including IFITMs. To test whether the IFNβ-mediated inhibition of Wuhan was linked to the previously observed IFITM2 sensitivity, the relative upregulation of IFITMs 2 and 3 following IFNβ and IFNγ treatment in A549-ACE2s was first measured by Western blot (Figure 3.2.12 A). IFITM3 was upregulated similarly between IFNβ and IFNγ, however IFITM2 was more strongly upregulated by IFNβ than IFNγ. It should be noted however that the high homology between IFITM2 and 3 makes distinguishing these proteins by Western blot difficult. Importantly, ACE2 expression was not affected by IFNβ or IFNγ, confirming that the effect on infection we see is not due to receptor downregulation. Next, A549-ACE2s were pre-treated with either siRNA against IFITM2 or a non-targeting control prior to IFNβ treatment. To confirm the efficiency of knockdown and whether this altered the expression of other ISGs or STAT1 signalling, both IFITM2 and viperin were immunoblotted for after siRNA knockdown (Figure 3.2.12 B). Even at the highest concentration of IFNβ, IFITM2 could not be observed after knockdown whilst viperin was similarly expressed in the control and IFITM2 knockdown. Additionally, samples were taken 30 minutes and 2h after IFNβ treatment, confirming that IFITM2 knockdown did not alter STAT1 signalling by immunoblotting for pSTAT1 and STAT1 (Figure 3.2.12 C, D).

Next, A549-ACE2 cells knocked down for IFITM2 or the control and treated with IFNβ were infected with England-02 virus and supernatant harvested 48 hours later. This was used to inoculate Vero-E6 cells for 24 hours and the Vero-E6 cells stained for intracellular N as before (Figure 3.2.13 A). This resulted in a substantial rescue of the IFNβ sensitivity. Next, A549-ACE2 cells were knocked down for IFITM2 as before but this time pre-treated with IFNγ prior to infection (Figure 3.2.13 B). While a 10-fold increase in IC50 was observed when IFITM2 was knocked down in the context of IFNβ, IFITM2 knockdown did not yield a significant rescue from IFNγ-mediated inhibition, suggesting that the inhibitory effect of IFNγ on England-02 infectivity is independent of IFITM2 upregulation. Next, it was tested whether IFITM3, which did not exert much inhibition of SARS-CoV-2 when overexpressed alone, played any part in the IFNβ-mediated inhibition of England-02 (Figure 3.2.13 C). IFITM3 was knocked down prior to IFNβ treatment as before, and consistent with the overexpression data,

IFITM3 knockdown did not significantly rescue IFNβ-mediated inhibition of England-02 infection. Overall, these data suggest that a significant part of the IFNβ-mediated inhibition of England-02 is due to IFITM2 upregulation, not IFITM3, and that IFNγ inhibits England-02 infectivity through an independent mechanism (IC50s shown in Figure 3.2.13 D). Next, given that overexpression of TMPRSS2 can permit SARS-CoV-2 to utilise the early entry pathway, IFITM2 was knocked down in the context of A549-ACE2-TMPRSS2 cells. Strikingly, the combination of IFITM2 knockdown and TMPRSS2 overexpression resulted in a full rescue of infectivity in the presence of IFNβ (Figure 3.2.13 E). Interestingly, even the sensitivity of England-02 to IFNβ in the presence of TMPRSS2 was reduced 2-fold compared to the TMPRSS2-negative cells. These data suggest that the presence of TMPRSS2 alone reduces the antiviral effects of IFNβ, possibly through reducing the amount of entry via the late pathway where IFITM2 is present.

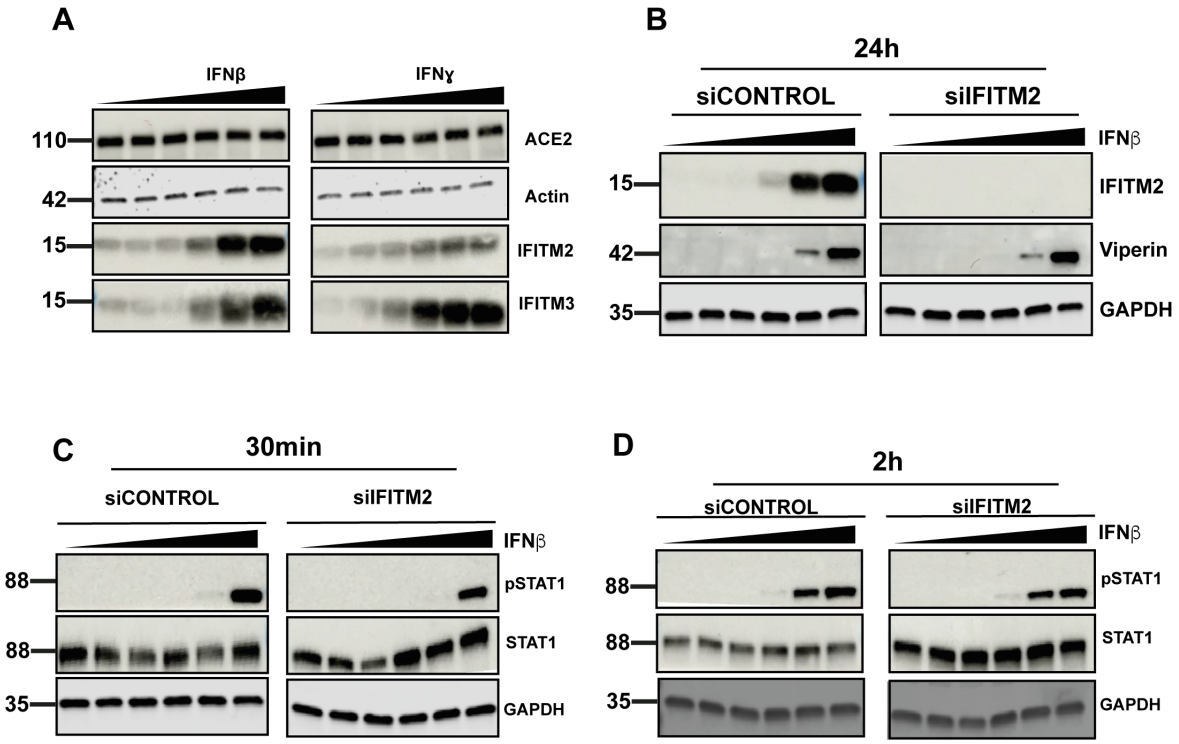

Figure 3.2.12. IFNβ upregulates IFITM2 knockdown. IFITM2 knockdown does not alter STAT1 signalling. A) A549-ACE2 cells were treated with IFNβ or IFNɣ for 18 hours and immunoblotted for IFITMs 2 and 3. B) A549-ACE2 cells were transfected with control or IFITM2 siRNA and treated with IFNβ as before. Samples were immunoblotted for IFITM2 and viperin to confirm knockdown efficiency. C, D) A549-ACE2 cells were transfected with siRNAs and IFNβ treated as in B, and samples taken for immunoblot 30 minutes (C) or 2h (D) after IFNβ treatment and immunoblotted for pSTAT1 and STAT1.

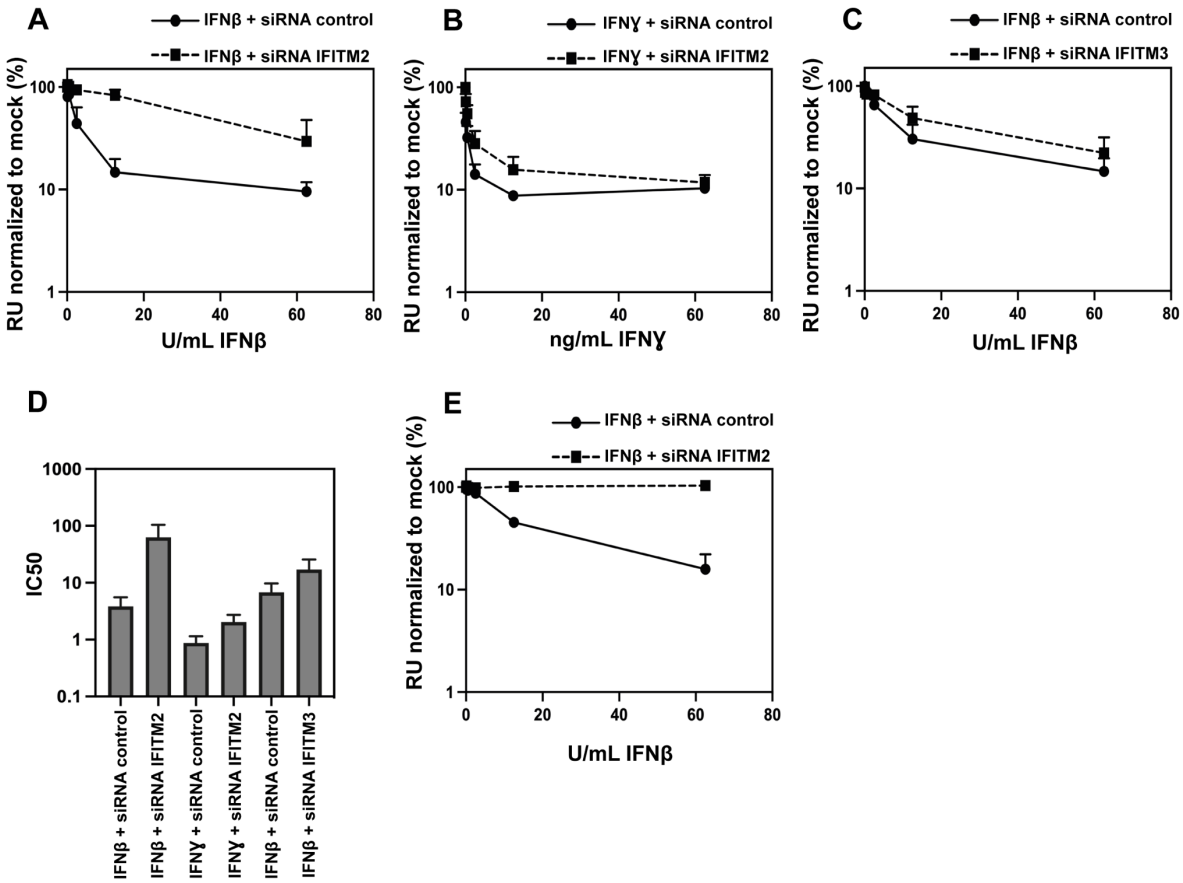

Figure 3.2.13. IFITM2 knockdown rescues IFNβ mediated inhibition of England-02. A, B) A549-ACE2 cells were transfected with a control or IFITM2 targeting siRNA and treated with IFNβ (A) or IFNɣ (B). 18 hours later, cells were infected with SARS-CoV-2 England-02 virus at an MOI of 0.005 and infection measured 48 hours later by inoculated of Vero-E6 cells with the infected supernatant and measuring for intracellular N. C) IC50s of A and B were calculated in GraphPad Prism. D) A549-ACE2-TMPRSS2 cells were transfected with a control or IFITM2 targeting siRNA and treated with IFNβ. 18 hours later cells were infected with SARS-CoV-2 England-02 and infection quantified 48 hours later as in A. E) A549-ACE2 cells were transfected with a control or IFITM3 targeting siRNA and treated with IFNβ. 18 hours later cells were infected with England-02 and infection quantified 48 hours later as in A. N=3, Mean±SEM shown.

3.2.6 The D614G mutation increases infectivity and spike processing

The dominance of the D614G mutation early in the pandemic implied that this mutation altered viral infectivity or transmissibility. To establish whether there were any differences in single-round infectivity between Wuhan and D614G, the impact of this mutation was tested using PLVs on A549-ACE2 and A549-ACE2-TMPRSS2 cells (Figure 3.2.14 A and B). The D614G mutation resulted in a 2-fold increase in infectivity in the A549-ACE2 cells, and a 9-fold increase in infectivity in the A549-ACE2-TMPRSS2 cells. This suggested the D614G mutation does increase infectivity, especially in the context of the TMPRSS2-dependent entry pathway. D614G could therefore represent an early adaptation of the virus to utilise the TMPRSS2 pathway more efficiently. Next, to characterise the effects of the D614G mutation on IFITM sensitivity, Wuhan and D614G PLVs were tested on A549-ACE2-IFITM cells as before (the interplay between TMPRSS2 and IFITMs are further explored in chapter 5). Despite the increased infectivity of D614G, the IFITM2 sensitivity of Wuhan and D614G PLVs were remarkably similar (Figure 3.2.14 C). Interestingly however, D614G did appear to be less sensitive to IFITM1 than the Wuhan spike. This could suggest that D614G is not only an early adaptation to TMPRSS2 usage, but also an early adaptation to escape IFITM1.

An early report suggested that the D614G mutation increased spike incorporation and reduced S1 shedding [189]. To investigate the relative incorporation of spike, England-02 or an early wave isolate which contained the D614G mutation, 3.20, were purified through sucrose and immunoblotted for spike and N (Figure 3.2.14 D). Using an anti-S2 antibody, it was apparent that higher amounts of the cleaved S2 domain were present on D614G virions compared to England-02, despite comparable amounts of N. This may explain the increased infectivity of D614G into TMPRSS2+ cells, as relatively more of the S1/S2 priming cleavage has occurred prior to encountering the target cell. Additionally, total spike also appeared slightly higher in the D614G virus compared to England-02, consistent with this mutation resulting in increased spike incorporation, which could also be linked to D614G's higher infectivity. These results were recapitulated using purified PLVs, and again there were higher quantities of both total S and S2 on the particle, to the extent that this made it difficult to even visualise

the total S band of the Wuhan spike (Figure 3.2.14 E). Given the effect of the D614G mutation on spike processing and incorporation, we wondered whether there would be any difference in the sensitivity of Wuhan and D614G to the GBP family, an IFN-upregulated antiviral protein that inhibits furin-mediated processing of the glycoproteins of several enveloped viruses [93]. This was briefly investigated by transfecting 293T17s with Wuhan and D614G spike and treating these cells with 500U/ml of IFNβ 6 hours later and subsequently Western blotting for the spike protein after 24 hours (Figure 3.2.14 F). While the Wuhan spike is less well processed in the presence of IFNβ, the processing of the D614G spike did not appear to be affected by the presence of IFNβ (quantified in 3.2.14 G). This was not however tested in terms of whether PLVs produced in the presence of IFNβ showed any decreased infectivity. It has recently been suggested that the D614G mutation does indeed confer increased resistance to the effects of both GBP2 and GBP5 on spike by the Jolly lab relative to Wuhan [94]. In light of this preprint, this suggests that the effect of IFNβ on Wuhan spike processing found here could indeed be mediated by GBP-family proteins. It is tempting to speculate whether the D614G mutation represented an early adaptation to human innate immunity in the form of IFITM1 and GBP2/5 in TMPRSS2-negative cells.

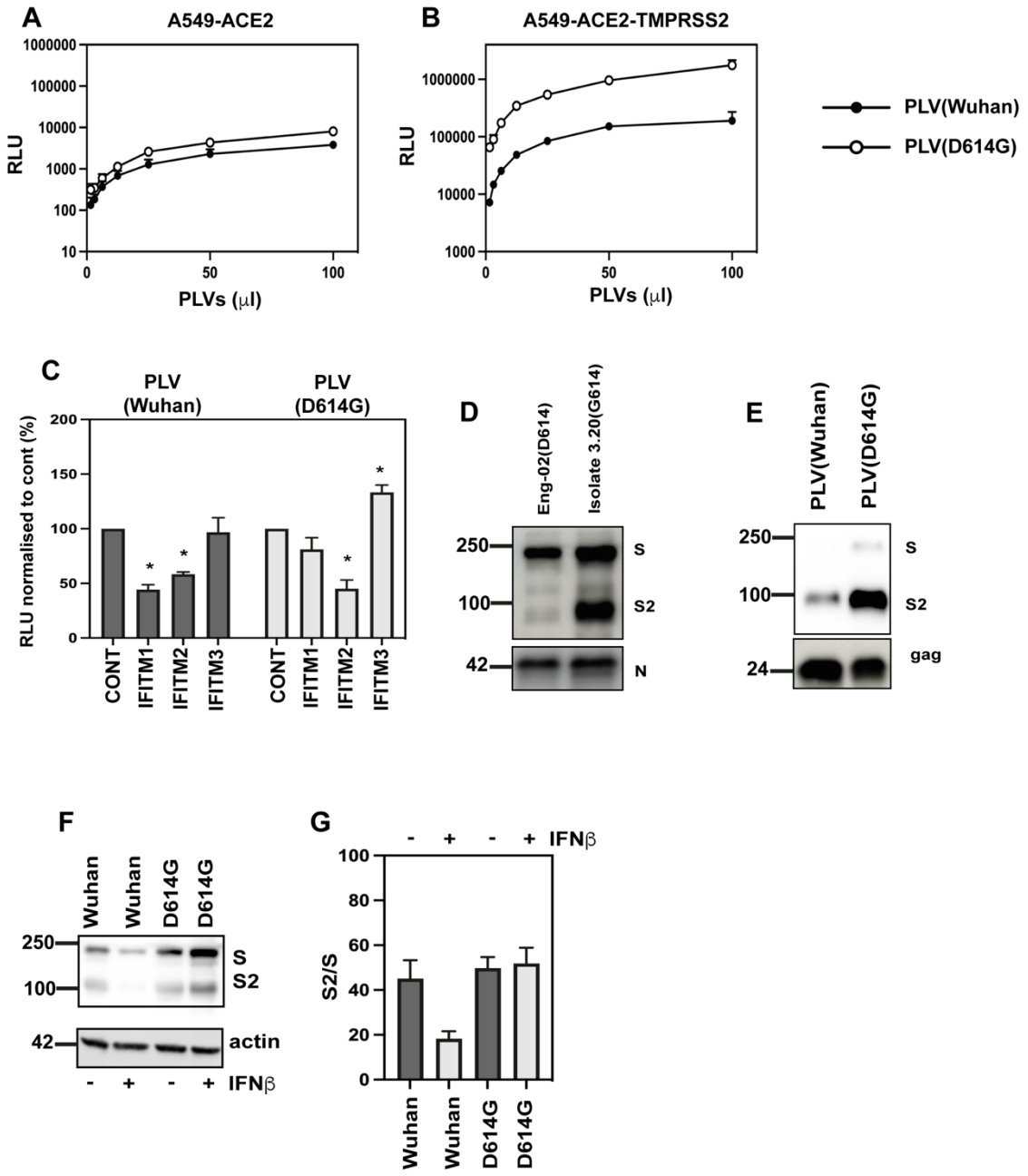

Figure 3.2.14. Characterising the differences of the D614G mutation on the Wuhan spike. A, B) Equal volumes of Wuhan and D614G PLVs were used to infect A549-ACE2 or A549-ACE2-TMPRSS2 cells. Infectivity was determined by luciferase activity 48 hours later. C) Wuhan or D614G PLVs were used to infect A549-ACE2-IFITM cells and infectivity determined by luciferase activity 48 hours later. *=P>0.05 and indicate statistical significance between control and individual IFITM for each PLV determined by two-way ANOVA. N=3, Mean±SEM shown. D) England-02 or a D614G isolate were purified through a 20% sucrose cushion for 1 hour at 18000 g and Western blotted for spike and N. E) PLVs of Wuhan or D614G were purified and Western blotted for spike and gag. F) representative Western blot of 293T-17 which were pre-treated with 500U/ml of IFNβ and transfected with spike prior to blotting for spike and actin. G) quantification of S2 relative to all spike of blot in E from three independent experiments.

3.2.7 Deletion of the cytoplasmic tail from spike results in increased E64d and IFITM2 sensitivity

The cytoplasmic tail of spike contains an inefficient ERRS signal which results in some spike leaking to the surface where this can facilitate syncytia formation [175]. Deletion of the last 19 amino acids, which contains this sequence, boosts PLV titre because it results in increased leaking of spike to the plasma membrane where this can be picked up by budding PLVs. Consequently, it is common practice in many labs to use ΔCT spikes when preparing PLVs. In our hands, deleting the last 19 amino acids of spike results in a 28-fold boost in titre on A549-ACE2 cells (Figure 3.2.15 A). However, SARS-CoV-2 virions do not usually assemble at the plasma membrane in native virus production and retention in the endoplasmic reticulum is important for determining appropriate post-translational modifications and glycosylation [169]. Therefore, we wanted to confirm whether the ΔCT mutant behaved similarly to full-length spike on PLVs in terms of IFITM sensitivity. D614G and D614GΔCT PLVs were generated and IFITM sensitivity tested in A549-ACE2s as before (Figure 3.2.15 B). The ΔCT PLVs had similar IFITM1 and IFITM3 resistance in these cells compared to the full-length spike counterpart. Surprisingly however, the ΔCT D614G PLVs were 2-fold more sensitive to IFITM2 than the full-length spike PLVs.

Given what we knew so far about route of viral entry and IFITM2 sensitivity in this system, the sensitivity of the D614G and ΔCT PLVs to the cathepsin inhibitor E64d was tested next to determine if the increased IFITM2 sensitivity was due to increased cathepsin-dependence (Figure 3.2.15 C). As expected, the ΔCT was 2-fold more sensitive to E64d at both 2.5 and 10μM, with a 5-fold decrease in IC50 (Figure 3.2.15 D). This suggests that the D614GΔCT spike is more cathepsin-dependent than wild-type full-length D614G. To determine if there were any differences in spike incorporation or processing, the PLVs were immunoblotted for spike and gag in both the producer cell lysates and purified supernatant (Figure 3.2.15 E). Intracellular spike expression was comparable between D614G and D614GΔCT, however there was 10-fold more S2 compared to S in the D614GΔCT mutant than full-length D614G spike on purified PLVs (3.2.15 F). Although unexpected that more S2 on the surface would

result in increased IFITM2 sensitivity, overall this data could suggest that deletion of the cytoplasmic tail could have knock-on effects on spike conformation or glycosylation, altering the accessibility of the S2' site. These data also suggest that interpreting the route of viral entry from ΔCT spikes should be done with caution.

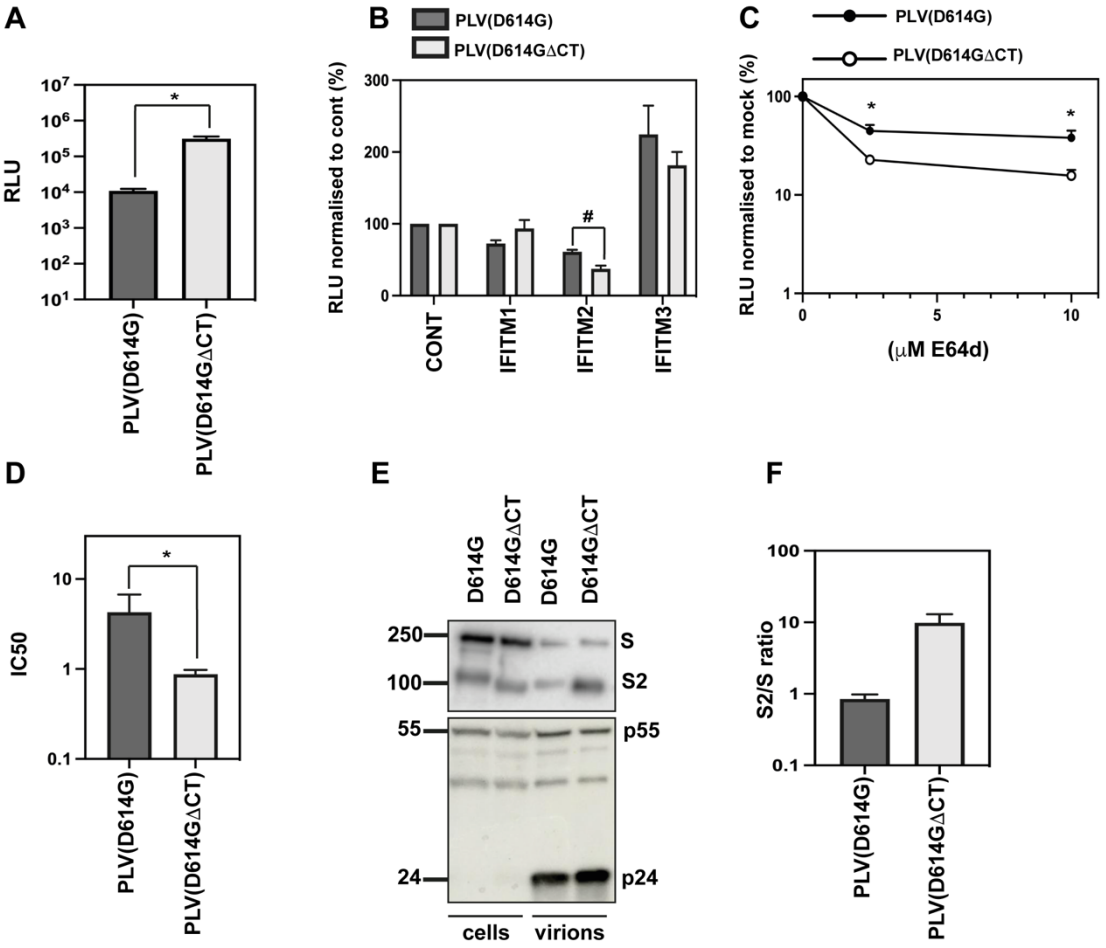

Figure 3.2.15. Deleting the cytoplasmic tail of spike on PLVs increases IFITM2 sensitivity by increasing cathepsin-dependent entry. A) A549-ACE2 cells were infected with equal volumes of D614G or D614GΔCT PLVs and infection quantified by luciferase activity 48 hours later. *=P>0.05 indicating statistical significance between D614G and D614GΔCT determined by two-tailed unpaired t test. B) A549-ACE2-IFITM cells were infected with D614G or D614GΔCT PLVs and infection quantified by luciferase activity. *=P>0.05 indicating statistical significance between the IFITM2 condition of D614G and D614GΔCT determined by two-way ANOVA. C) A549-ACE2 cells were pre-treated with 2.5μM or 10μM of E64d for 1 hour and infected with D614G or D614GΔCT PLVs and infection quantified by luciferase activity 48 hours later. *=P>0.05 and indicate statistical significance between D614G and D614GΔCT at 2.5 and 10μM E64d determined by ANOVA. D) IC50 of C calculated in GraphPad Prism. *=P>0.05 indicating statistical significance between IC50s determined by two-tailed unpaired t test. E) Cellular lysates and purified supernatant of PLVs of D614G and D614GΔCT were Western blotted for spike and gag. F) quantification of band intensity of S2 over total S from three independent experiments of F. N=3, Mean±SEM shown.

3.3 Discussion

In this chapter, I discuss how removal of the polybasic cleavage site in the Wuhan spike skews viral entry towards the cathepsin-dependent late entry pathway, which cannot be rescued by TMPRSS2 overexpression. Comparatively, the polybasic cleavage site is beneficial to entering TMPRSS2-positive cells, however is detrimental in TMPRSS2-negative cells. This is consistent with the findings from several groups that the polybasic cleavage site is rapidly lost in culture of TMPRSS2-negative cells [233, 347]. Deletions of the polybasic cleavage site have also been reported in some clinical samples from COVID-19 patients, albeit at a low frequency [234]. Cleavage of the S1/S2 boundary has been reported to decrease the stability of the spike trimer [172]. It is possible that in the absence of TMPRSS2, it is advantageous for the S1/S2 boundary to remain uncleaved until the target cell as this would confer increased stability of spike. The SARS-CoV-1 and pangolin GD PLVs are also more efficient at entering TMPRSS2-negative cells, and insertion of a polybasic cleavage site into the SARS-CoV-1 spike mildly reduces infectivity in the TMPRSS2-negative cells. The spikes tested here which lack a polybasic cleavage site, SARS-CoV-1, pangolin and Wuhan∆PRRA, are all very sensitive to IFITM2. Insertion or restoration of the polybasic cleavage site slightly alleviates the IFITM2 sensitivity for SARS-CoV-1 and Wuhan, however only rescues IFITM1 and IFITM3 sensitivity for the pangolin spike. It is therefore tempting to speculate whether the polybasic cleavage site is an adaptation to more efficient viral entry through the avoidance of endosomal antiviral proteins that inhibit entry. Additionally, the early emergence of the D614G mutation and the finding this decreases IFITM1 sensitivity in A549-ACE2 cells could further suggest an early adaptation of the virus to escape IFITM restriction. IFITMs are key antiviral proteins in the airways to protect against respiratory infection and have been found to be highly upregulated in the airways relative to the nasal cavity of mice. Additionally, the rs2155c mutant of IFITM3, which results in decreased antiviral activity of IFITM3, has previously been found to be associated with increased severity of influenza infections in humans, demonstrating the importance of IFITMs in controlling viral infection *in vivo* [35, 348, 349].

It is however surprising that IFITM3 does not inhibit the Wuhan or ΔPRRA spike to the same extent as IFITM2, considering these proteins only have ten amino acids different between them. This could imply that in these cell lines at least, stably overexpressed IFITM2 and IFITM3 are occupying distinct subcellular compartments and pathways of viral entry. IFITM2 is thought to localise to late endosomes coexpressing rab5, while IFITM3 localises to early endosomes expressing rab7 [62, 350]. Analysis of the subcellular localisation of IFITMs in these cells and whether this differs to other commonly used cell lines in SARS-CoV-2 research, such as Calu-3 and Caco-2 cells, would aid in understanding the relative restriction of IFITMs 2 and 3 shown here. Under IFN-stimulated conditions, IFITMs have been shown to interact with each other heterologously and cycle through multiple cellular compartments [351]. By overexpressing these individually, it could also be that we are missing an aspect of IFITM biology that would be seen when all IFITMs are expressed at once. That said, the knockdown of IFITM2 prior to IFNβ treatment does seem to suggest that of all the IFITMs, IFITM2 is having the most significant effect on viral infection by SARS-CoV-2 in A549 cells. When we knock down IFITM3, we find that this does not rescue England-02 from IFNβ mediated inhibition. There do appear to be multiple mechanisms inhibiting SARS-CoV-2 entry however, as IFNγ inhibits both England-02 and Wuhan PLVs in an IFITM-independent manner. It has previously been suggested that IFNγ can inhibit viral entry through downregulation of hepatitis and HIV-1 receptors [352, 353]; however we did not observe any decreases in ACE2 by Western blot following 48 hours of IFNγ treatment. This suggests that IFNγ is inhibiting SARS-CoV-2 entry through another mechanism. Alternatively, there could be other antiviral proteins upregulated by IFNγ inhibiting entry. it has recently been reported that LY6E can inhibit the coronaviruses 229E, OC43, MERS-CoV, SARS-CoV-1 and SARS-CoV-2 by blocking membrane fusion [95, 96]. Zhao et al show that LY6E inhibition of SARS-CoV-2 cannot be overcome by TMPRSS2 overexpression, meanwhile IFITM-mediated inhibition of SARS-CoV-2 could be overcome by TMPRSS2, suggesting these are distinct mechanisms of entry restriction [95]. Additionally, CH25H has been suggested to also inhibit an early step of SARS-CoV-2 replication through an incompletely understood mechanism [102].

The data in this chapter also characterise the IFITM sensitivity of the first known mutation to become fixed in spike, D614G. Compared to the Wuhan spike, the D614G is similarly IFITM2 sensitive, but less sensitive to IFITM1. This could suggest that the D614G spike is taking a slightly different route of viral entry to evade IFITM1 relative to the Wuhan spike. Additionally, the D614G spike is less sensitive to the effects of IFNβ on S1/S2 cleavage. This is consistent with the findings from the Jolly lab that the D614G spike is less sensitive to restriction by GBP2 and 5, an IFN-upregulated inhibitor of furin-mediated cleavage [94]. It is possible that the enhanced cleavage of the D614G mutation represents an early adaptation to escaping two independent forms of innate immunity, IFTIM1 and GBP2/5; this could suggest that inhibition of furin cleavage by GBP2/5 could sensitise a spike to IFITM-mediated inhibition. However, GBP5-induced sensitisation to IFITM restriction has been ruled out by the Jolly group in Caco-2 cells [94]. Caco-2 cells do express TMPRSS2 endogenously, and whether GBP2/5 induced sensitisation to IFITMs occurs in TMPRSS2-negative cells remains to examined. However, it is worth noting that in the context of viral infection with native virus, many of the viruses non-structural proteins counteract IFN signalling. The relevance of GBP5 and IFITM inhibition *in vivo* could therefore potentially be smaller than in the context of spike-only PLVs without the viral nsps, in single round infections [354]. Nevertheless, it would be interesting to further investigate the interplay between GBP5 and IFITM restriction.

I also demonstrate in this chapter that deletion of the cytoplasmic tail of D614G increases IFITM2 sensitivity and sensitivity to E64d. Cytoplasmic tail deletion also increases the S2/S ratio on the particle of D614G PLVs. Another group has also reported that deletion of the cytoplasmic tail can mask the interpretation of differential spike properties when examining the D614G mutation [175]. The increased sensitivity of ΔCT PLVs to IFITM2, but also increased spike cleavage, indicates that the relationship between cleavage and IFITM sensitivity is not as clear cut as implied by the initial data presented in this chapter with the Wuhan virus. Because the spike of ΔCT PLVs will have prematurely leaked to the cell surface due to the deletion of the ERRS, it could be that consequently these spikes are improperly glycosylated or adopt a different conformation. It has been suggested that a “glycan gate” at the N343 site of spike can modulate spike adopting the open conformation, suggesting that glycosylation can have an important role in spike dynamics [176]. It would be

interesting to test if the increased sensitivity to IFITMs of ΔCT mutants can be overcome by TMPRSS2 overexpression or exogenous protease treatment. Overall, these data suggest that interpreting certain phenotypes from ΔCT spikes should be done with caution.

Altogether, the data in this chapter confirm that the polybasic cleavage site can alter the route of viral entry which SARS-CoV-2 can take. Deletion of the polybasic cleavage site results in increased IFITM2 sensitivity, and may therefore be an adaptation to avoid antiviral restriction late endosomes. However, this has only been explored in the context of TMPRSS2-negative cells in this chapter. Given what is now known about the role of TMPRSS2 in reducing cathepsin-dependent entry, it is reasonable to ask whether TMPRSS2 affects IFITM sensitivity. The role of TMPRSS2+ on IFITM-mediated inhibition will be further explored in Chapter 5.

Chapter 4: SARS-CoV-2 variants of concern vary in route of viral entry and IFITM sensitivity

Some of the data presented in this chapter have been published under the title “The P681H Mutation in the Spike Glycoprotein of the Alpha Variant of SARS-CoV-2 Escapes IFITM Restriction and Is Necessary for Type I Interferon Resistance” [30].

4.1 Introduction

Many RNA viruses lack effective proofreading capacity in their polymerase proteins, resulting in the accumulation of mutations that may then be selected for due to being advantageous for replication or transmission. The nsp14 exonuclease protein of SARS-CoV-2 has error-correcting capacity, which was expected to result in a low mutational rate of SARS-CoV-2; thus it was initially considered that this virus would not exhibit a high rate of mutation [178]. However, the first documented positively selected mutation in SARS-CoV-2 spike, D614G, became fixed relatively early in the pandemic [185]. Early reports suggested this may reduce S1 shedding, improving virion stability, and thereby increase transmissibility [186, 187, 189]. This mutation is present in every variant of concern (VOC) tested to date.

In late 2020, the alpha variant was identified in the UK. The first mutation in the NTD of alpha, the Δ69/70 mutation, happened to be in the probe binding site of the spike primer/probe set used in RT-qPCR diagnostics, leading to positive N and Orf1b samples but “drop out” for spike. This resulted in the rapid identification of the alpha variant, which has seven mutations and two deletions in the spike gene. Over the next two years of the pandemic, several other VOCs emerged across the globe, with the beta variant in South Africa, gamma in Brazil, kappa and delta in India, and omicron again in South Africa. More recently, several sub-variants of omicron have emerged, with up to 30 mutations in the spike protein [355] (Figure 4.1.1). BA.4 and BA.5 have been excluded because they are not examined in this thesis due to becoming dominant after this thesis was written. Several of the mutations present in these spikes

have arisen independently in distinct lineages, suggesting that they provide a fundamentally adaptive advantage to virus replication or transmission [356]. A major concern is whether the number of spike changes across multiple VOCs alters vaccine efficacy. The spike protein is the most important target of neutralisation by antibodies and the sole viral component of most vaccines used worldwide. Importantly it appears that many of these mutations, especially in the RBD, have been linked to evading the antibody response [357]. Additionally, many mutations in the RBD have been found to increase or decrease ACE2 affinity, for example the N501Y mutation - which increases ACE2 affinity - is found in the alpha, gamma, kappa and delta VOCs [358].

Several mutations have also emerged in spike which improve spike incorporation or compensate for fitness costs associated with antibody escape mutations. The ∆69/70 mutation, which is present in alpha and omicron, has been suggested to increase spike incorporation into the virus particle [190]. It has also been suggested that in the alpha variant, this mutation arose to compensate for the reduction in infectivity mediated by the D796H mutation in the S2 domain which reduces antibody neutralisation [227]. Many mutations have arisen in the RBD which are likely to mediate antibody escape, as the RBD is a hotspot for neutralising antibodies [205]. An “antibody supersite” has also been identified in the NTD which is recognised by all known NTD-targeting antibodies [142]. This likely explains the number of NTD mutations present in VOCs to date. Additionally, mutations near and in the polybasic cleavage site have arisen in multiple lineages which have been shown to improve S1/S2 processing, which has been suggested to be an adaptation to better utilisation of TMPRSS2 [159, 203, 359]. Given the number of changes in spike across these variants, in this chapter I investigate whether any of the VOCs tested to date have a different IFITM sensitivity compared with the wave 1 virus due to the presence of spike mutations, with a focus on the polybasic cleavage site. In particular, I focus on the first VOC to emerge, the alpha variant. The D614G mutation is present in every VOC to date, and as such, for the rest of this thesis will be used as the control spike for comparison.

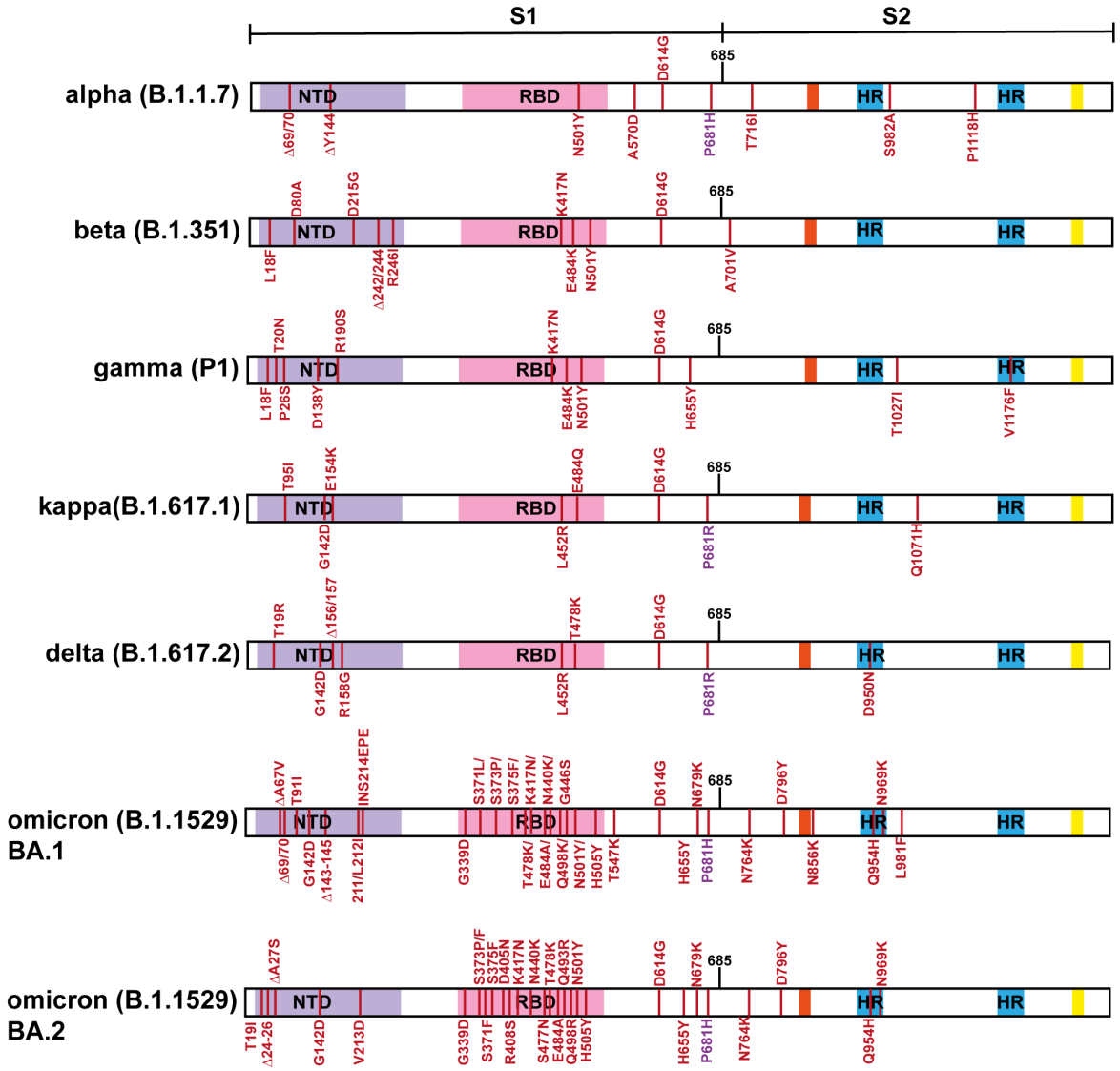

Figure 4.1.1. Schematic of major variants of concern 2020-2022 tested in this chapter. Spike sequences of variants of concern with N-terminal domain (NTD) highlighted in purple, receptor binding domain (RBD) highlighted in pink, fusion peptides in orange, heptad repeats in blue, and transmembrane domain in yellow. Spikes have been ordered chronologically by emergence. For simplicity, only the sequence of VOCs that have been tested in this chapter have been included in this schematic.

4.2 Results

4.2.1 The alpha variant is type I IFN resistant in A549-ACE2 and Calu-3 cells

The alpha variant was identified in late 2020 in the UK, and with seven mutations and two deletions in the spike protein there were early concerns that this virus may be more transmissible. To test if any of the changes in spike in the alpha variant impacted IFN sensitivity, A549-ACE2 cells were pre-treated with increasing doses of IFNβ, as before (Figure 3.2.12) and infected with England-02 (an early wave isolate in the UK) or an isolate of alpha (Figure 4.2.1 A). Infectivity was measured by the number of E copies in the supernatant 48 hours later. Interestingly, alpha was much less sensitive to pre-treatment with IFNβ than the England-02 virus. To confirm if this could be recapitulated in another cell line, this was tested in Calu-3 cells, which are considered to be a more relevant lung epithelial cell line for SARS-CoV-2 and endogenously express ACE2 (Figure 4.2.1 B). Again, alpha was less inhibited by IFNβ than England-02 when measuring the viral RNA present in the supernatant of infected cells, confirming that the alpha isolate is more IFNβ resistant in two different cell lines.

However, measuring viral RNA in the supernatant does not necessarily confirm whether there has been a reduction of infectivity. To investigate this, Calu-3 cells that had been pre-treated with IFNβ were again infected with England-02 or alpha virus and the supernatant taken after 48 hours. This was used to inoculate Vero-E6-TMPRSS2 cells and infectivity measured by plaque assay (Figure 4.2.1 C). Surprisingly, when measured by plaque assay we observed an increase in infectivity for both England-02 and alpha with 0.1 and 0.5 U/ML of IFN. However, at higher concentrations of IFN this confirmed there were more plaque forming units/ml from the alpha virus than England-02 following IFNβ pre-treatment and that alpha is indeed resistant to the effects of IFNβ on viral infectivity.

Next, to confirm whether this was a spike-dependent phenotype, we utilised reverse genetics-engineered viruses based on Wuhan-1, in which the spike gene was exchanged for that of the alpha virus (designated Wuhan(alpha), kindly provided by

the Palmarini and Patel groups in Glasgow) (Figure 4.2.1 D). This virus contains an entirely Wuhan-1 background except for the spike protein. Indeed, the Wuhan(alpha) virus phenocopied the alpha isolate, demonstrating significant resistance to pre-treatment with IFNβ. This established that the IFNβ resistance of alpha is determined by the spike protein. This suggests that the mutations within the alpha virus spike alter IFNβ sensitivity.

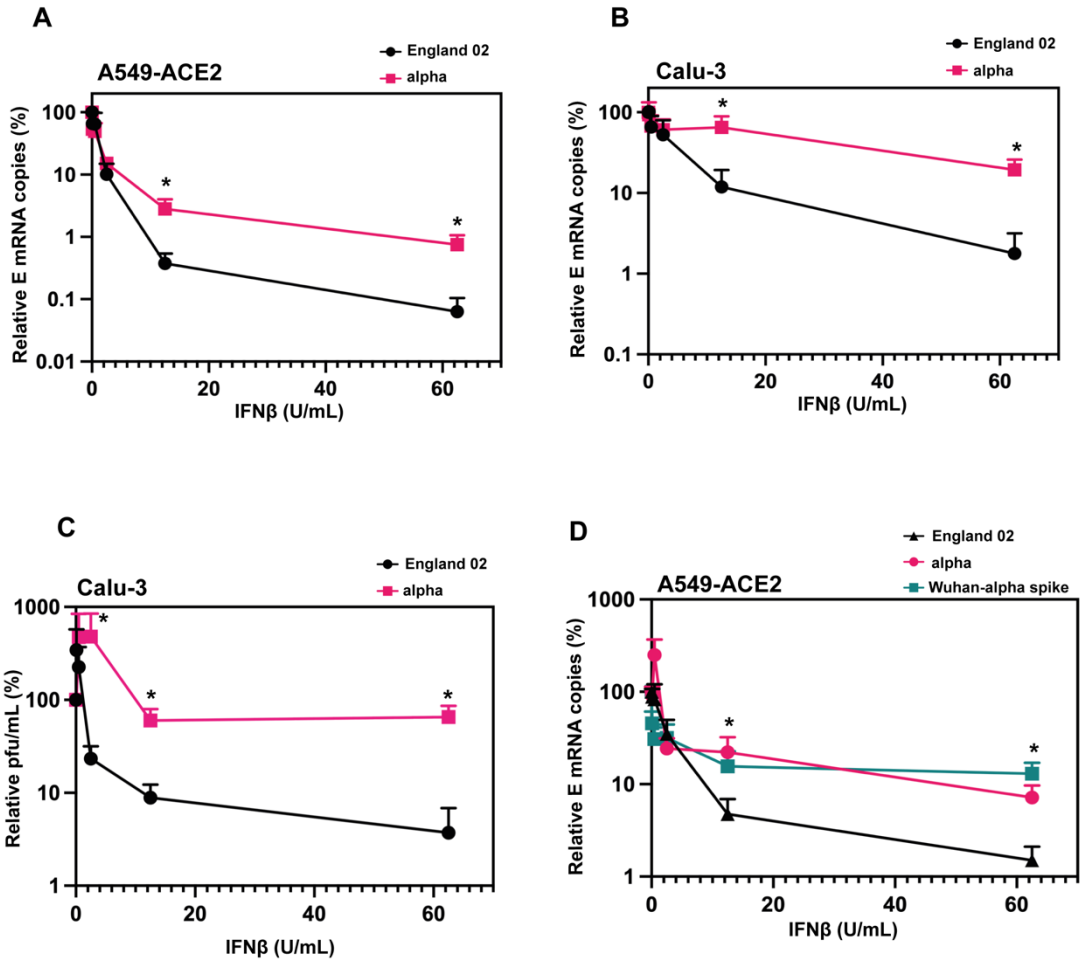

Figure 4.2.1. The alpha virus is IFNβ resistant in A549-ACE2 and Calu-3 cells in a spike-dependent manner. A) A549-ACE2 were pre-treated with IFNβ for 18 hours prior to infection with 500 copies/cell England-02 or alpha virus. Infection was quantified 48 hours later by E mRNA copies in the supernatant using a standard curve. B) Calu-3 cells were pre-treated with IFNβ for 18 hours prior to infection with 5000 copies/cell England-02 or alpha virus. Infection was quantified 48 hours later by E mRNA copies in the supernatant. C) Calu-3 cells were IFNβ treated and infected as in A and B but infection quantified by plaque assay of infected supernatant on Vero-E6-TMPRSS2 cells. D) A549-ACE2 were IFNβ pre-treated and infected with England-02, alpha or Wuhan(alpha spike) viruses and infection quantified 48 hours later by E mRNA copies in the supernatant. *=P>0.05 and indicate statistical significance between the viruses at each IFNβ concentration determined by two-tailed unpaired t test. N=3, Mean±SEM shown.

4.2.2 The alpha variant is IFITM resistant in A549-ACE2 cells

As the alpha virus was less sensitive to the effects of IFNβ, we reasoned that it may also be less sensitive to restriction by IFITMs based on our previous work linking the IFNβ sensitivity of the England-02 virus to IFITM2-mediated restriction. To test this, A549-ACE2-IFITM cells were infected with England-02, virus 3.20, and alpha. Virus 3.20 is an early wave 1 isolate containing the D614G mutation. Infection was measured by percentage of intracellular N by flow cytometry (Figure 4.2.2 A). Both England-02 and the D614G isolate retained IFITM2 sensitivity, consistent with the previous PLV data. However, the alpha virus was entirely resistant to IFITMs 1, 2 and 3, with a surprising but marked enhancement of infection in the presence of IFITM3. To confirm whether the IFITM resistance of alpha could be recapitulated using PLVs, PLVs of D614G or alpha were used to transduce A549-ACE2-IFITM cells and infection measured by luciferase as before (Figure 4.2.2 B). Again, the alpha PLVs were IFITM resistant with a 3-fold increase in the presence of IFITM3. This demonstrates that the alpha virus is resistant to both IFNβ and IFITMs in A549-ACE2s, and that the IFITM resistance of alpha is spike-dependent. Surprisingly, IFITM1 also enhanced infection by the alpha virus, suggesting that other IFITMs can enhance entry by alpha. However, this could not be recapitulated by PLV infection while IFITM3 enhancement was clear in both native viral infection and PLV infection. This suggests there is perhaps a subtle but important difference in the entry of alpha virus and PLVs.

4.2.3 Deletion of the cytoplasmic tail overcomes the IFITM resistance of the alpha spike in A549-ACE2s

Having established in the previous chapter that deletion of the cytoplasmic tail of spike increased the IFITM2 sensitivity of D614G, the effect of the cytoplasmic tail on the IFITM resistance of the alpha spike was also tested. Both D614G ΔCT and alpha ΔCT PLVs were used to transduce A549-ACE2-IFITM cells as before along with their full-

length spike controls (Figure 4.2.3). In accordance with the D614GΔCT data in the previous chapter, D614GΔCT was more sensitive to IFITM2 than its full-length counterpart. Additionally, the alpha spike was now rendered IFITM2 sensitive by the cytoplasmic tail deletion and also no longer enhanced by IFITM3. This suggests that the ΔCT mutation not only confers IFITM2 sensitivity, but also overcomes factors involved in IFITM3 enhancement. The ΔCT mutation has been suggested previously to mask the effects of the D614G mutation in PLVs [175], and these data here confirm that the ΔCT mutation can also mask the IFITM resistance of the alpha spike in PLVs. Overall, these data suggest that use of ΔCT spikes when investigating IFITM sensitivity can result in differing phenotypes, likely due to altering the route of viral entry or potentially due to altered spike conformation. This makes it difficult to differentiate viral entry phenotypes, which has consequences for antiviral proteins that target the entry step.

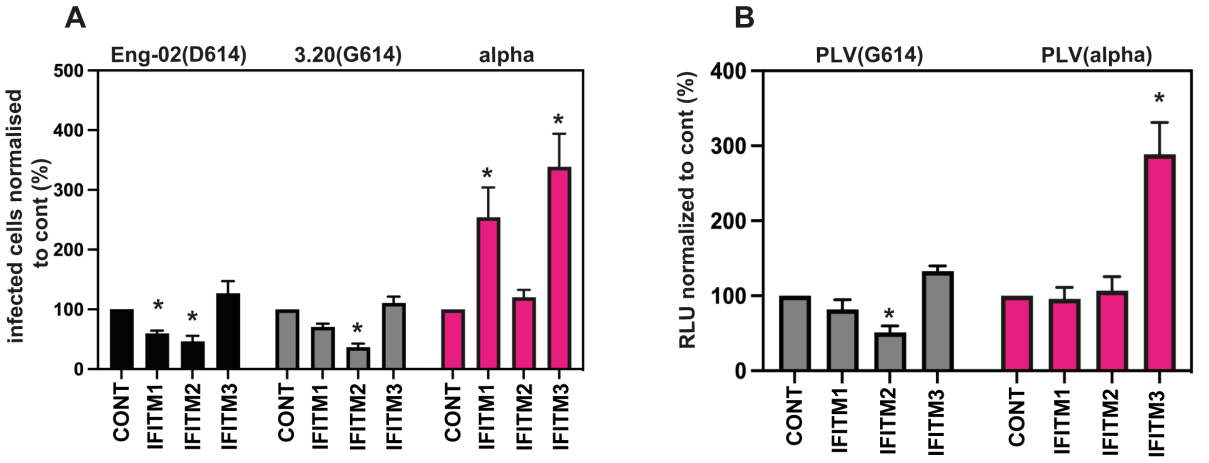

Figure 4.2.2. The alpha virus is IFITM resistant in A549-ACE2 cells. A) A549-ACE2-IFITM cells were infected with England-02, 3.20(D614G), or alpha virus and infection quantified by % intracellular N 48 hours later by flow cytometry. B) A549-ACE2-IFITM cells were infected with PLVs of D614G or alpha and infection quantified by luciferase activity 48 hours later. *=P>0.05 and indicate statistical significance between control and individual IFITM conditions determined by one-way ANOVA. N=3, Mean±SEM shown.

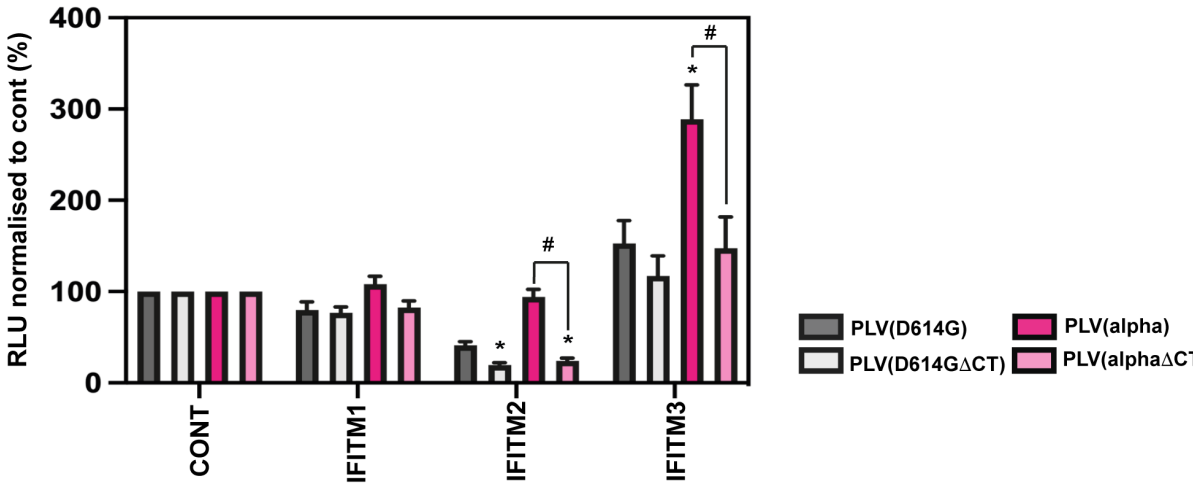

Figure 4.2.3. Deleting the spike cytoplasmic tail of spike on alpha PLVs masks the effect of IFITM2 resistance and IFITM3 enhancement. A549-ACE2-IFITM cells were infected with equal volumes of D614G, D614GΔCT, alpha, or alpha ΔCT PLVs and infection was quantified by luciferase activity 48 hours later. Infection is normalised to infection in the empty vector control cells for each PLV. * indicates statistical significance between IFITMs of each PLV and control, and # indicate statistical significance between IFITM conditions of different PLVs determined by two-way ANOVA. N=3, Mean±SEM shown.

4.2.4 Mutations in the NTD or RBD of alpha do not affect IFITM sensitivity

Having confirmed that the alpha spike is IFITM resistant, determining which mutations are important in this phenotype was next investigated. The alpha spike contains seven mutations and two deletions (both in the NTD). The Δ69/70 mutation has been suggested to increase spike incorporation, while the Δ144 mutation has been found to reduce antibody neutralisation [143, 190]. The RBD of alpha also contains the N501Y mutation, which increases the affinity for ACE2 [360]. Additionally, the alpha variant contains a P681H mutation which has been suggested to increase the efficiency of the polybasic cleavage site [192, 361]. There are three other mutations in the alpha spike S2 domain that were not investigated here, namely the T716I, S982A and P1118H mutations.

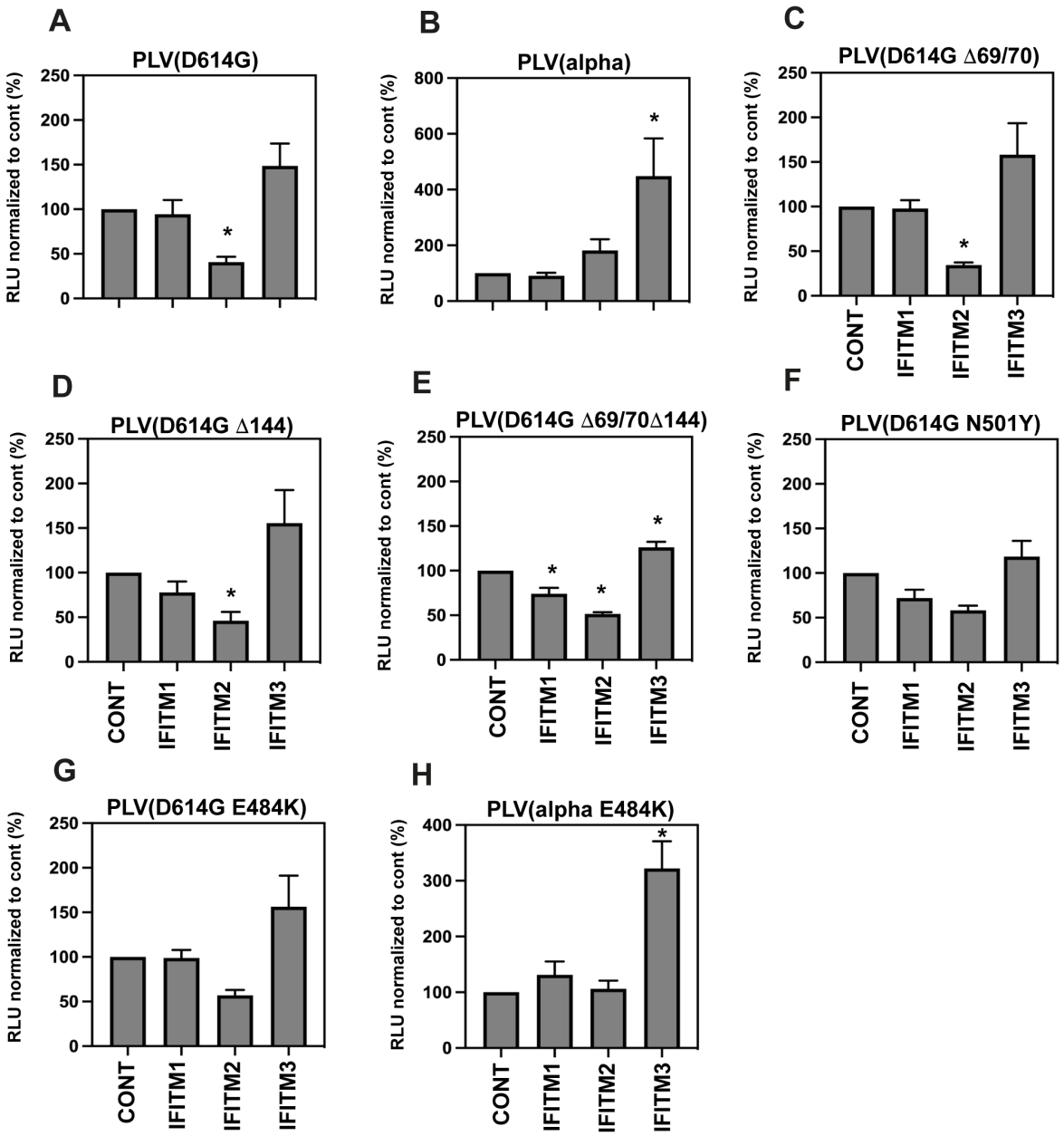

Figure 4.2.4. Neither the alpha NTD or RBD mutations alter IFITM sensitivity in the D614G spike. A-F) PLVs bearing each mutant spike were used to infect A549-ACE2-IFITM cells and infection was quantified by luciferase activity 48 hours later. *=P>0.05 and indicate statistical significance between the control and individual IFITM conditions determined by one-way ANOVA. N=3, Mean±SEM shown. Panels A and B have been reproduced for ease of reading.

To test the impact of the individual mutations in the NTD and RBD on IFITM sensitivity, spikes were generated with Δ69/70, Δ144, Δ69/70 Δ144, or N501Y alone in the D614G background. Additionally, the effect of the E484K mutation in D614G and in alpha were tested, as this mutation arose in some alpha isolates at the time. PLVs of these spikes were used to infect A549-ACE2-IFITM cells (Figure 4.2.4 A – F). Neither of the NTD mutations alone, or in combination appeared to impact IFITM2 sensitivity with IFITM2 still inhibiting transduction 2-2.5-fold. Additionally, neither N501Y or E484K appeared to enhance or reduce IFITM2 sensitivity of D614G. Lastly, the E484K mutation in the alpha context had no impact on the IFITM resistance of alpha, suggesting the emergence of this mutation in some alpha lineages was unrelated to IFITM evasion and likely due to other selection pressures, including antibody evasion.

4.2.5 The P681H mutation confers IFITM resistance in PLVs and alters IFNβ sensitivity of the alpha virus

Having confirmed that none of the NTD or RBD alpha-defining mutations reduced the IFITM sensitivity of D614G, the role of the P681H mutation in the polybasic cleavage site was investigated. First, the polybasic cleavage sites of D614G and alpha were deleted (ΔPRRA and ΔHRRA respectively) to confirm that total ablation of the alpha polybasic cleavage site rendered the spike IFITM2 sensitive (Figure 4.2.5 A), as previously demonstrated for the Wuhan spike (Figure 3.2.9 B). Indeed, ΔPRRA/HRRA conferred even more IFITM2 sensitivity to D614G, and conferred IFITM2 sensitivity to the previously resistant alpha PLVs. Next, to test whether reverting the P681H mutation alone in the alpha spike could reduce the IFITM resistance, an alpha H681P spike was generated. Although not as sensitive as the ΔHRRA mutant, this conferred some IFITM2 sensitivity to alpha. Interestingly, both the ΔHRRA and H681P mutations also abolished the IFITM3 enhancement of alpha, suggesting the P681H mutation is necessary for IFITM3 enhancement of the alpha PLVs. Finally, whether the P681H mutation alone could confer IFITM resistance to a D614G spike was tested. Indeed, the P681H mutation reduced IFITM2 sensitivity for the D614G spike, with transduction

in the presence of IFITM2 being indistinguishable from the empty vector control cells. However, this mutation did not confer IFITM3 enhancement to the same extent as alpha, suggesting that the IFITM3 enhancement of alpha is dependent on other contextual mutations in the spike. Thus, the P681H mutation is necessary for IFITM resistance in A549-ACE2 cells, but not sufficient to confer IFITM3 enhancement alone.

We hypothesised that the P681H mutation may be reducing the dependency on cathepsin-dependent entry and thereby reducing IFITM2 sensitivity, the inverse of what we had observed so far with the ΔPRRA and ΔCT mutations. To test this, A549-ACE2 cells were pre-treated with the cathepsin inhibitor E64d and the mutants described above used to infect these cells. Consistent with what we have previously shown, the D614G-ΔPRRA was extremely sensitive to E64d-mediated inhibition, consistent with its increased restriction by IFITM2 (Figure 4.2.5 B). The alpha PLVs were less sensitive to E64d than D614G, however alpha ΔHRRA and H681P alpha were significantly sensitised to inhibition by E64d. Lastly, the D614G P681H mutation reduced the inhibition of E64d relative to D614G 2-fold. These data suggest that the P681H mutation can reduce the cathepsin dependence in D614G in A549-ACE2 cells and reversion of this mutation in alpha can increase its cathepsin dependence. This is likely a factor in determining alpha's resistance to IFITMs in this system. This does not however shed any light on the mechanism behind the IFITM3 enhancement of alpha. Additionally, as described earlier alpha and D614G are similarly Camostat sensitive, yet here alpha is less sensitive to E64d than D614G. This suggests other proteases are involved in the priming S2' cleavage besides cathepsins and TMPRSS2.

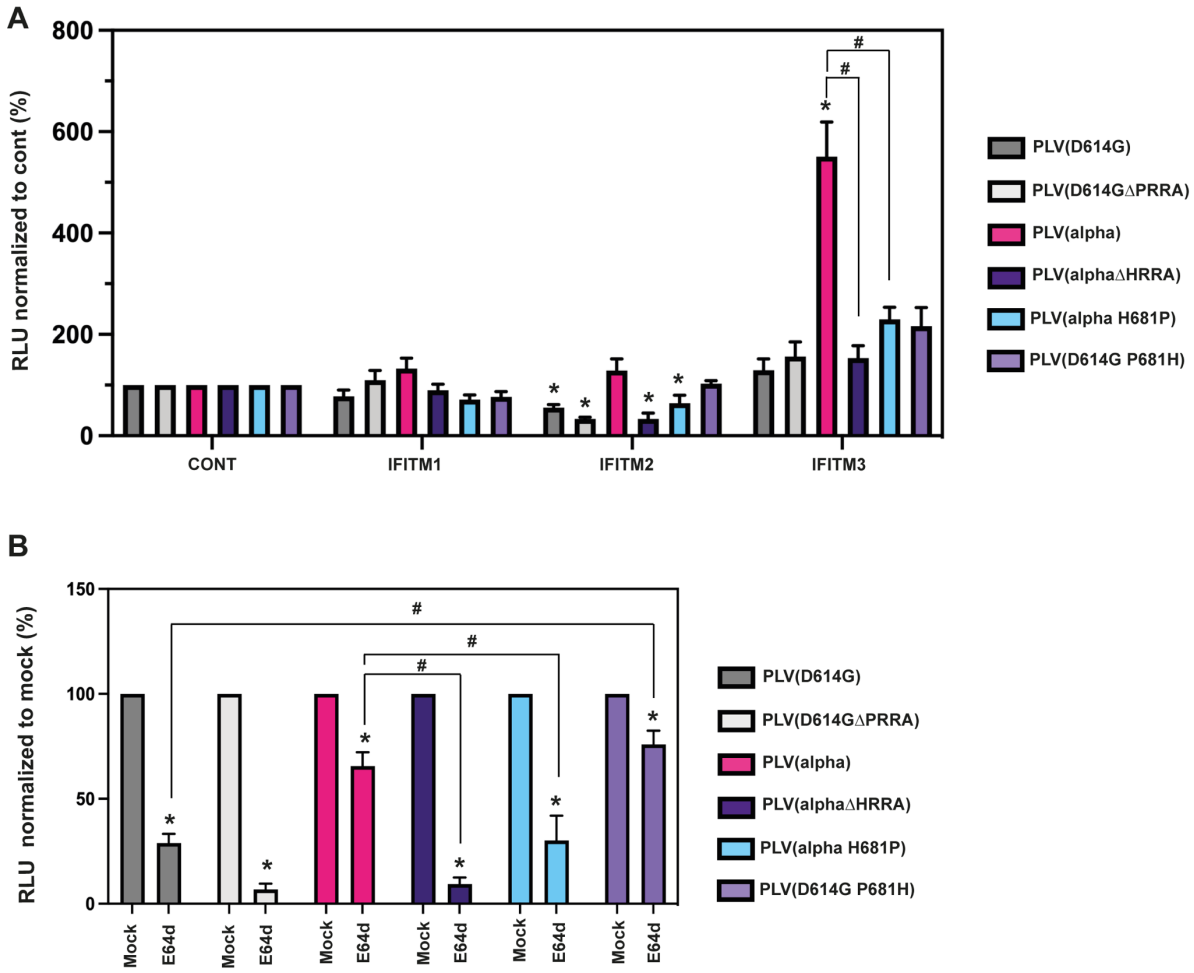

Figure 4.2.5. The P681H mutation reduces IFITM sensitivity by reducing cathepsin dependence. A) A549-ACE2-IFITM cells were infected with equal volumes of D614G, D614GΔPRRA, alpha, alphaΔHRRA, P681H or alpha H681P PLVs and infection quantified by luciferase 48 hours later. * indicate statistical significance between the IFITM and the control condition for each PLV, # indicate statistical significance between different PLV conditions determined by two-way ANOVA. B) A549-ACE2 cells were pre-treated with 10μM E64d prior to infection with PLVs and infection quantified by luciferase 48 hours later. #=P>0.05 and indicate statistical significance between the E64d condition of each PLV and other PLVs determined by two-way ANOVA. N=3, Mean±SEM shown.

To investigate whether the P681H mutation could also contribute to the overall IFNβ resistance of alpha, we again utilised viruses kindly gifted from the University of Glasgow engineered to contain only the spike of the alpha variant in the background of the Wuhan-1 virus. Palmarini and colleagues generated an H681P mutant of the alpha spike in the Wuhan background, and this was used to infect A549-ACE2 cells as before that had been pre-treated with IFNβ (Figure 4.2.6 A). It has now been identified that the alpha virus antagonises IFNβ production through Orf6 and Orf9b [193]. Therefore, in this assay we ensured that we were measuring the effects of IFNβ on alpha prior to any antagonism of IFN by providing exogenous IFN before infection. The H681P mutant virus was much more sensitive to IFNβ pre-treatment than the Wuhan(alpha) virus, confirming that the P681H did indeed confer IFNβ resistance to alpha. Finally, to link this to IFITM2, we performed RNAi by transfecting siRNAs of either a non-targeting control or against IFITM2 prior to IFNβ treatment and infection. While the Wuhan(alpha) virus was virtually unaffected by IFITM2 knockdown, the Wuhan (alpha H681P) virus was rescued by IFITM2 knockdown (Figure 4.2.6 B). This suggests that IFITM2 mediates a significant portion of the IFNβ-mediated inhibition of the Wuhan (alpha H681P virus), while the Wuhan(alpha) virus is insensitive to IFITM2 in the context of IFNβ. Interestingly, when viral stocks of England-02, alpha, Wuhan(alpha), and Wuhan (alpha H681P) were immunoblotted for spike and N, the H681P reversion did not alter the cleavage phenotype of Wuhan(alpha) (Figure 4.2.6 C). Adding to the finding that the D614GΔCT spike is better cleaved, but this does not correlate with IFITM resistance, this further exemplifies that increased S1/S2 processing may not necessarily be the determinant of IFITM resistance.

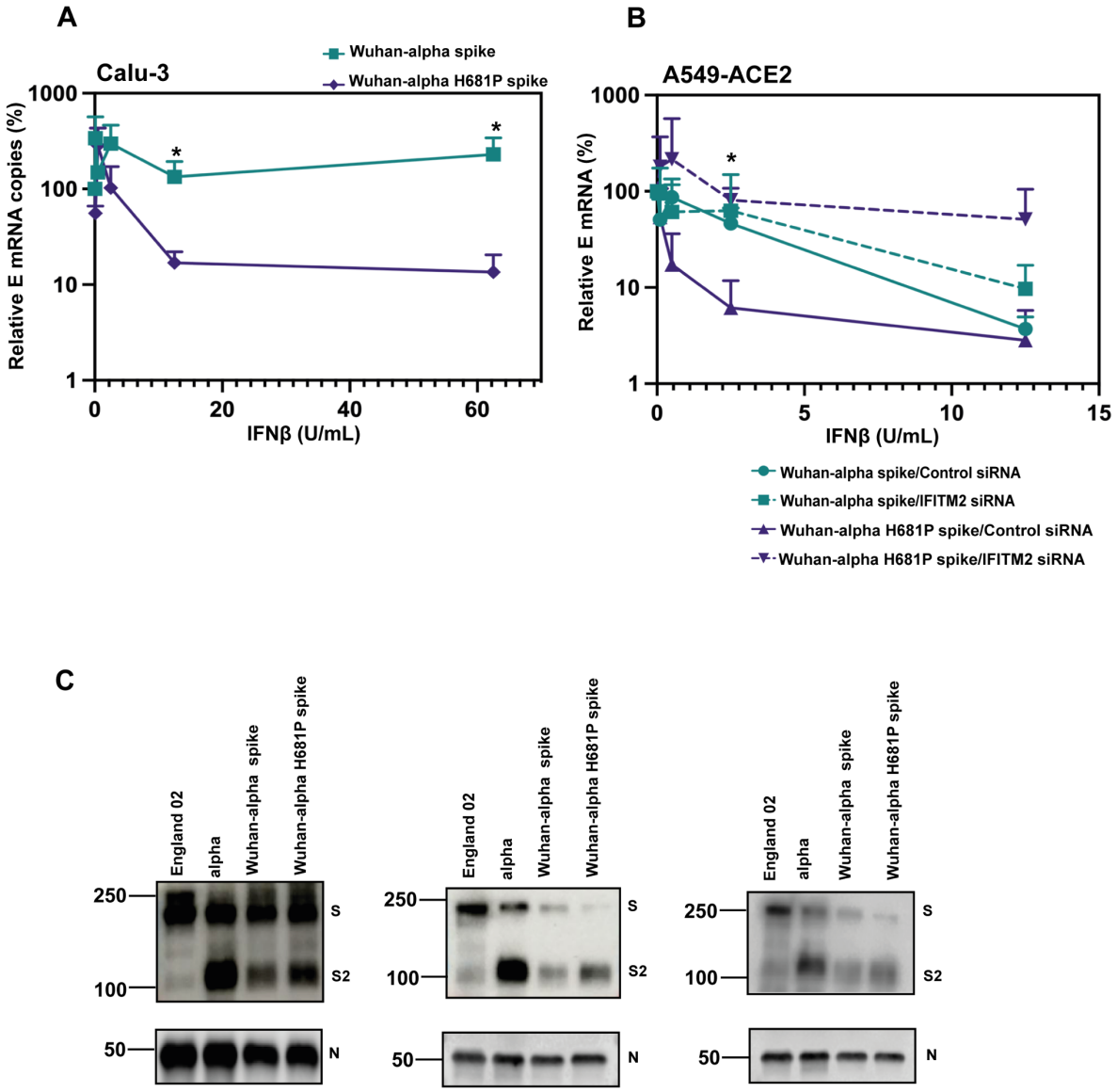

Figure 4.2.6. The H681P mutation confers IFNβ sensitivity to the Wuhan(alpha) virus in an IFITM2-dependent manner. A) Calu-3 cells were pre-treated with IFNβ for 18 hours prior to infection with Wuhan-alpha or Wuhan-alpha H681P virus for 48 hours. Infection was quantified by relative E mRNA copies in the supernatant. B) A549-ACE2 cells were transfected with non-targeting or IFITM2 siRNAs and treated with IFNβ for 18 hours prior to infection with Wuhan-alpha or Wuhan-alpha H681P viruses for 48 hours. Infection was quantified by intracellular E mRNA. N=3, Mean±SEM shown. C) Three independent Western blots of viral stocks of England-02, alpha, Wuhan-alpha and Wuhan-alpha H681P. Viral stocks were purified through a 20% sucrose cushion for 1 hour before Western blotting for spike and N.

4.2.6 Other VOCs to date are not IFITM resistant in A549-ACE2s

Since the emergence of the alpha variant in late 2020, a multitude of other variants have emerged, all with significant changes in the spike protein. Interestingly, the kappa, delta, and omicron VOCs all have polybasic cleavage site mutations, with P681R in kappa and delta, and P681H in omicron. Given that the P681H mutation conferred IFITM resistance to alpha in A549-ACE2 cells, whether other VOCs to date had any differential IFITM sensitivity was tested next. The IFITM phenotypes of the VOCs beta, gamma, kappa, delta, and omicron BA.1 and BA.2 were assessed as PLVs on A549-ACE2s as before, with Wuhan, D614G and alpha as controls (Figure 4.2.7 A – I). As before, Wuhan was IFITM1 and 2 sensitive, while D614G was only sensitive to IFITM2. The alpha PLVs were the only PLVs tested that exhibited IFITM resistance, however interestingly the delta PLVs also showed some mild IFITM3 enhancement. However, the kappa, delta and omicron PLVs retained some sensitivity to IFITM2 and some sensitivity to IFITM1. This suggested that perhaps a P681H/R mutation can only confer IFITM resistance in the context of a D614G or alpha spike, and that other mutations within the spike can overcome the effects of this mutation.

To confirm that delta and omicron were truly IFITM sensitive, authentic virus infection in A549-ACE2-IFITM cells was quantified by qPCR or flow cytometry (Figure 4.2.7 J, K). Measured by E mRNA copies intracellularly 48 hours after infection, the delta virus was still sensitive to IFITMs 1, 2, and 3 in A549-ACE2 cells. The delta PLVs displayed a small degree of IFITM3 enhancement as PLVs, however this was not observed when measuring native viral infection. Additionally, omicron infectivity measured by percentage of intracellular N showed that this virus is still IFITM2 sensitive. The finding that the omicron virus appeared entirely IFITM1 resistant while the omicron PLVs showed a small degree of sensitivity further shows that there can be discrepancies between native virus and PLV sensitivity to IFITMs. Nevertheless, these data demonstrate that in A549-ACE2 cells neither delta nor omicron virus are IFITM resistant despite their polybasic cleavage site mutations.

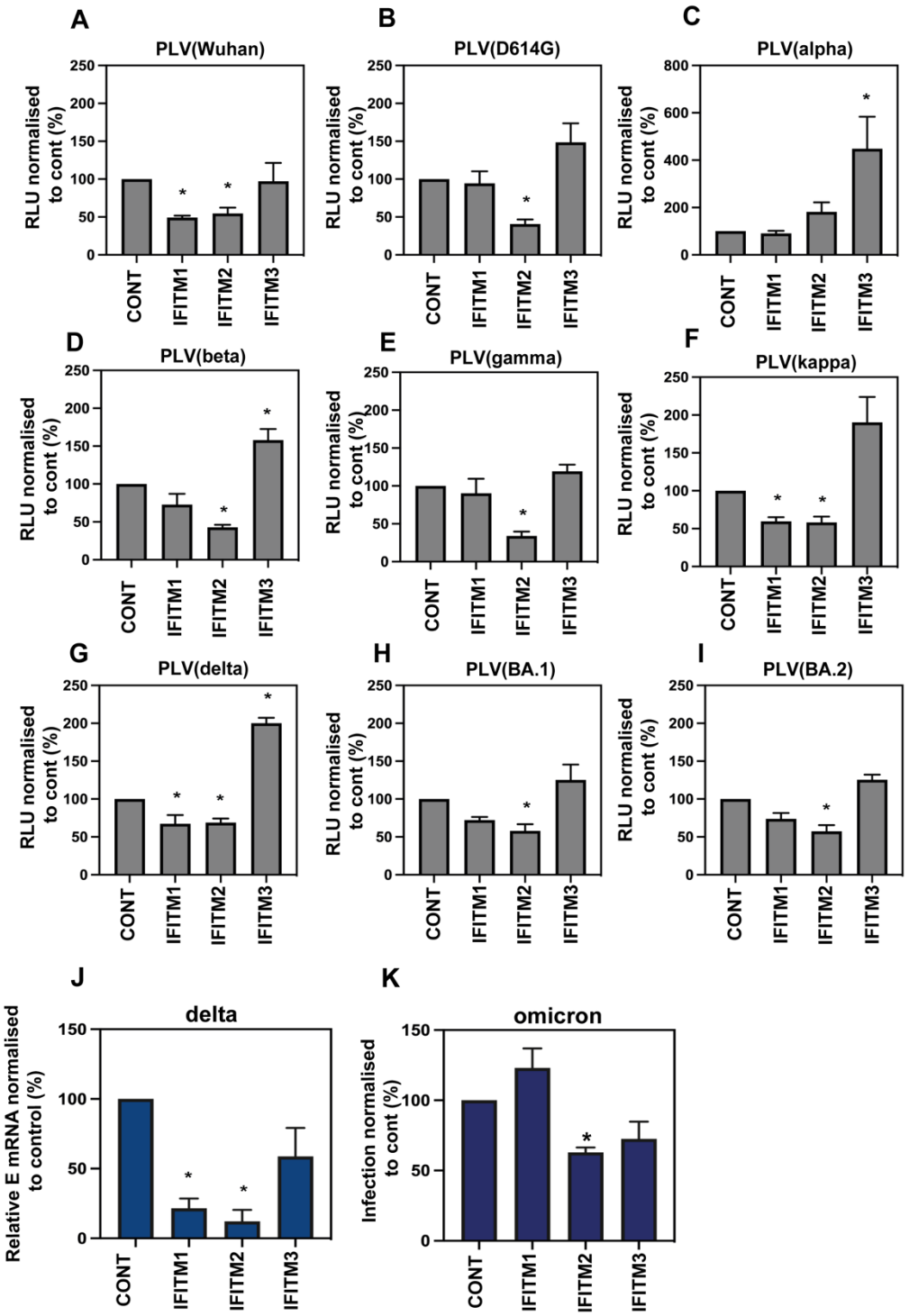

Figure 4.2.7. Of the VOCs tested to date, only the alpha variant is IFITM resistant in A549-ACE2 cells. A - I) A549-ACE2-IFITM cells were infected with equal volumes of PLVs bearing spikes of Wuhan, D614G, alpha, beta, gamma, kappa, delta, omicron (BA.1) and omicron (BA.2). Infection was quantified by luciferase activity 48 hours later. J) A549-ACE2-IFITM cells were infected with delta virus for 48 hours and infection quantified by intracellular E mRNA levels. K) A549-ACE2-IFITM cells were infected with omicron BA.1 virus for 48 hours and infection quantified by % N infected cells by flow cytometry. *=P<0.05 indicating statistical significance between the control and each IFITM determined by one-way ANOVA. N=3, Mean±SEM shown.

4.2.7 Delta and omicron differ in their cathepsin dependency

The majority of this work was carried out prior to the emergence and dominance of delta and omicron. The advent of these two variants containing P681R and P681H mutations, but retaining IFITM sensitivity, added some perplexity to exactly how the P681H mutation can alter IFITM sensitivity in a D614G background. It has been suggested that the omicron variant is cathepsin dependent and that this may be due to the constellation of mutations in the RBD of omicron conferring a more closed conformation of spike [204]. Whether the delta and omicron spikes are still somehow cathepsin dependent would explain their lack of IFITM resistance. To investigate this, A549-ACE2s or A549-ACE2-TMPRSS2 cells were pre-treated with E64d and infected with D614G, D614GΔPRRA, alpha, delta, or omicron PLVs (Figure 4.2.8). D614G PLVs were reasonably sensitive to E64d, but this could be rescued to a degree by TMPRSS2 overexpression. As expected, the D614G ΔPRRA PLVs were very sensitive to E64d in A549-ACE2 cells, which could not be rescued by TMPRSS2. However, the sensitivity of both alpha and delta to E64d was comparable in both A549-ACE2 and A549-ACE2-TMPRSS2 cells.

While this does not explain why delta is IFITM2 sensitive, the fact that both alpha and delta are E64d-resistant in the absence of TMPRSS2 does suggest that other proteases besides TMPRSS2 and cathepsins can cleave these spikes. Finally, the omicron PLVs were moderately sensitive to E64d inhibition in both A549-ACE2 and A549-ACE2-TMPRSS2 cells, with the difference between alpha/delta and omicron nearing but not reaching statistical significance. These data confirm, as shown by others, that omicron is more cathepsin dependent than the alpha and delta variants [204].

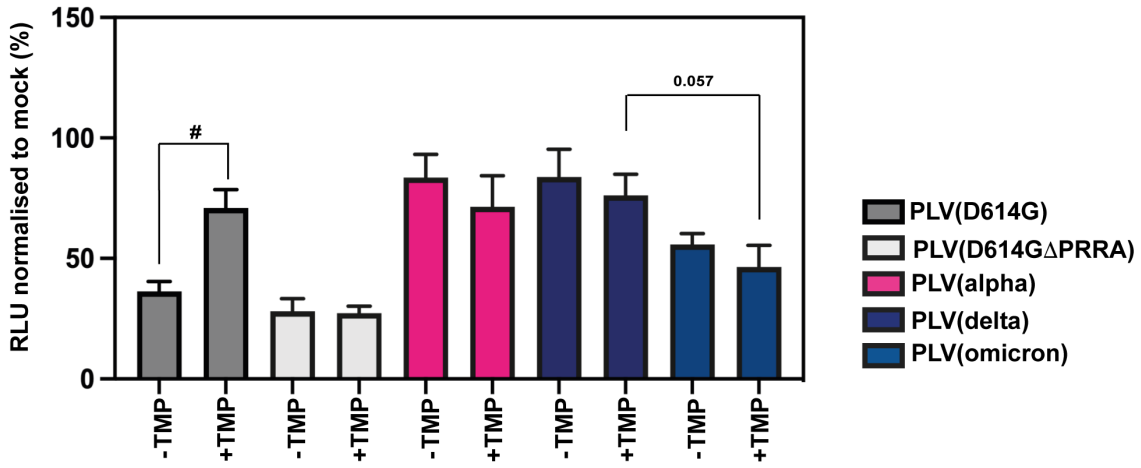

Figure 4.2.8. Alpha and delta are less sensitive to inhibition by E64d in both A549-ACE2 and A549-ACE2-TMPRSS2 cells. A549-ACE2 (-TMP) A549-ACE2-TMPRSS2 (+TMP) cells were pre-treated with 2.5μM E64d for 1 hour prior to infection with PLVs and infection quantified by luciferase activity 48 hours later. Infection is normalised to the DMSO control for each cell line and each PLV. #=P>0.05 indicating statistical significance between conditions determined by one-way ANOVA. N=3, Mean±SEM shown.

To delve further into this, the role of the P681R mutation (found in delta) was compared to the P681H mutation (found in alpha and omicron) in a D614G spike. PLVs were used to infect A549-ACE2-IFITM cells as before (Figure 4.2.9 A). The P681H mutation, as before, reduced IFITM sensitivity. The P681R mutation however was essentially indistinguishable from the wild-type D614G PLVs. Furthermore, while the H681P reversion conferred some IFITM2 sensitivity to the alpha spike previously (Figure 4.2.5 A), the R681P mutation in the delta spike did not significantly alter IFITM2 sensitivity (Figure 4.2.9 B). The R681P mutation did however reduce any IFITM3 enhancement by delta, suggesting that other amino acids besides a proline at this position can alter IFITM3 enhancement. The H681P mutation in omicron also did not affect the IFITM2 sensitivity of this spike, suggesting that the P681R and P681H in delta and omicron are not the main determinants of IFITM2 sensitivity in these spikes.

Finally, to test whether the P681R mutation affected cathepsin dependence, cells were pre-treated with E64d and infected with D614G, P681H or P681R PLVs (Figure 4.2.9 C). In both A549-ACE2 and A549-ACE2-TMPRSS2 cells, the P681H was the least sensitive to E64d. However, the P681R mutation was similarly sensitive to E64d as D614G. This suggests a differential use of protease pathways between P681R and P681H.

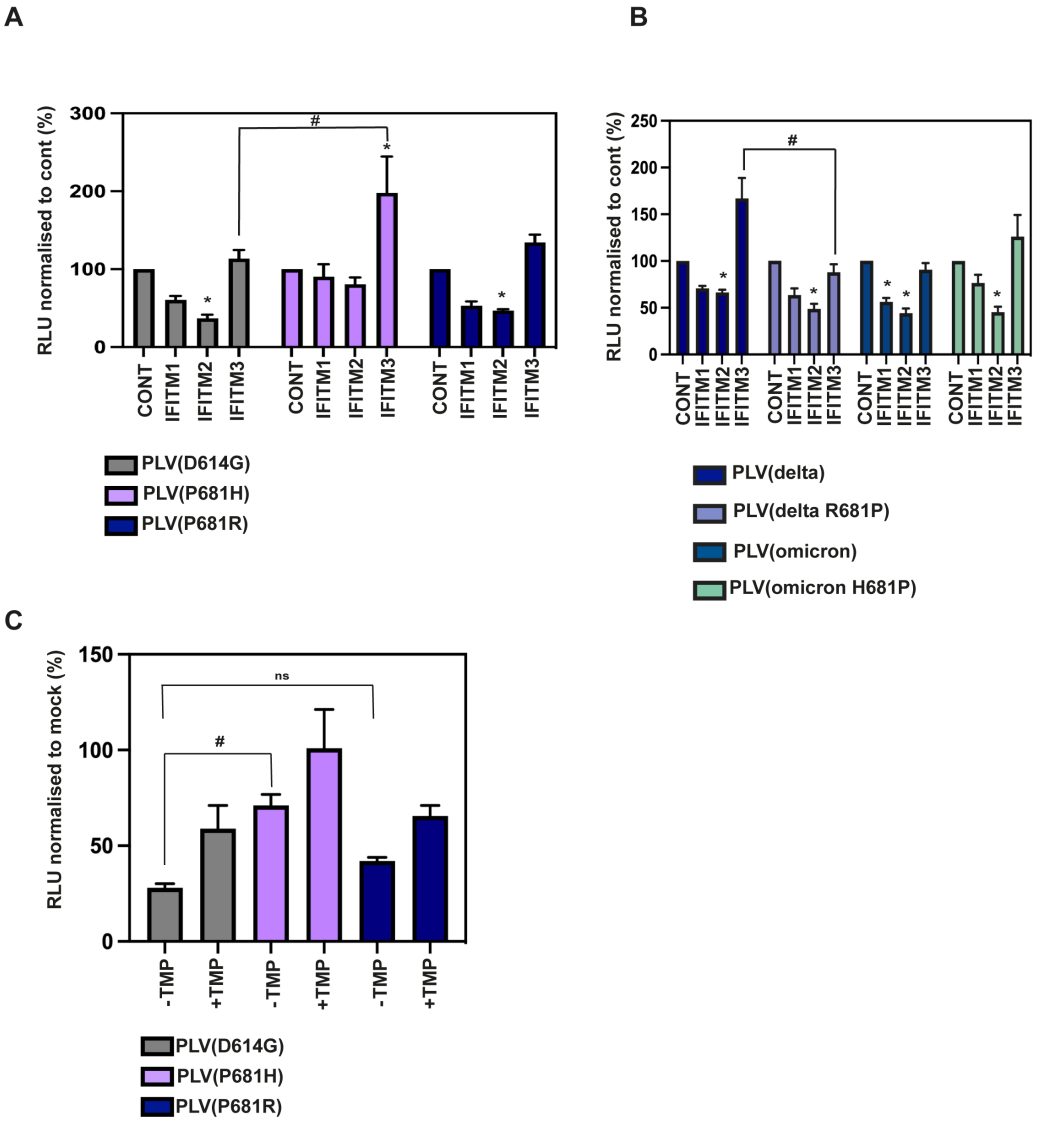

Figure 4.2.9. The P681R mutation does not significantly reduce endosomal-mediated entry. A) A549-ACE2-IFITM cells were infected with equal volumes of D614G, P681H, P681R PLVs and infection quantified by luciferase activity 48 hours later. B) A549-ACE2-IFITM cells were infected with delta, delta R681P, omicron, or omicron H681P PLVs and infection measured by luciferase 48 hours later. #= P>0.05 and indicates statistical significance between delta IFITM3 and delta R681P IFITM3 determined by two-way ANOVA. C) Either A549-ACE2 (-TMP) or A549-ACE2-TMPRSS2 (+TMP) cells were pre-treated with 10μM E64d for 1 hour prior to infection with D614G, P681H or P681R PLVs and infection measured by luciferase activity 48 hours later. Infection is normalised to the untreated control for each PLV for each cell line. #= P>0.05 and indicates statistical significance between each PLV in the -TMP condition and other PLVs determined by one-way ANOVA. N=3, Mean±SEM shown.

4.2.8 IFITM2 sensitivity in A549-ACE2 cells is generally predicted by E64d sensitivity

In the spikes tested so far, there appeared to be a relationship between IFITM2 sensitivity and E64d sensitivity. This makes logical sense in terms of cellular organisation: IFITM2 and cathepsins are all endosomal proteins, and the propensity of a spike to utilise cathepsins to mediate viral fusion should in theory correlate with the sensitivity of a spike to inhibition by IFITM2. Indeed, when IFITM2 and E64d sensitivity are plotted against each other for the VOC and mutant spikes tested so far, a correlation between IFITM2 and E64d sensitivity is apparent for most of the spikes tested, with an R^2 of 0.66 and a slope of 0.74 (Figure 4.2.10). The alpha and P681H PLVs are IFITM2 and E64d insensitive, while the ΔPRRA, gamma, and ΔCT spikes are the most IFITM2 and E64d sensitive. It is worth noting that the gamma PLVs were as sensitive to E64d as D614GΔPRRA, consistent with data suggesting that the H655Y mutation, which is present in the gamma and omicron spikes, promotes cathepsin dependence [203]. Omicron has the same H655Y mutation but is less E64d sensitive than gamma, further exemplifying the complex interplay between multiple mutations in spike. However, when the data are visualised in this manner it is clear that the delta spike is the only one tested so far that bucks this trend, retaining some IFITM2 sensitivity whilst being insensitive to inhibition by E64d. As A549-ACE2 cells do not express TMPRSS2, the insensitivity of delta to E64d in these cells begs the question of which protease is delta using to mediate entry, and how is this spike still restricted by IFITM2?

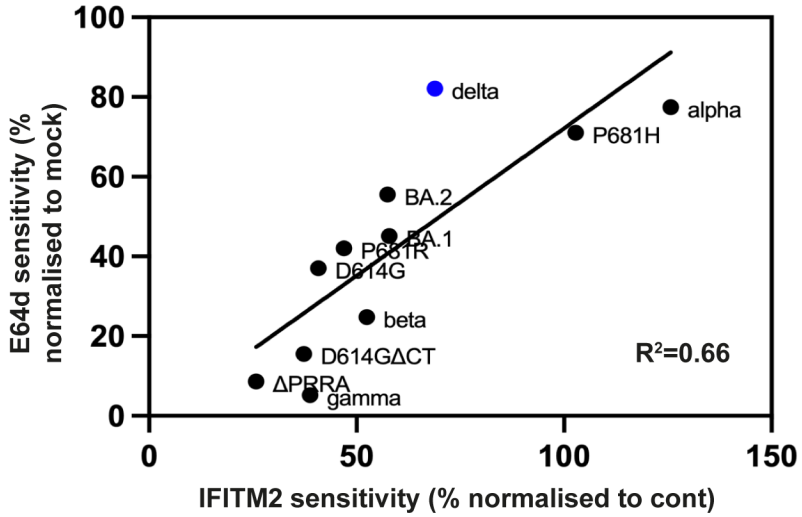

Figure 4.2.10. E64d sensitivity correlates with IFITM2 sensitivity for most of the SARS-CoV-2 spike PLVs tested to date. Graph shows E64d sensitivity plotted against IFITM2 sensitivity, both of which are plotted as percentage of inhibition relative to the empty vector control cell line for IFITM2, and as a percentage of infection of the DMSO control for E64d sensitivity. Line plotted using simple linear regression in GraphPad Prism. Slope=0.74. R^2=0.66. The outlier delta is highlighted in blue.

4.2.9 The delta spike is more sensitive to inhibition of MMP2/MMP9 that alpha or omicron

The second cleavage event in the SARS-CoV-2 spike triggers the release of the fusion peptide and is essential for the fusion of the cellular and viral membranes. The S2' site is postulated to be at R815-S816, however other potential cleavage sites have also been identified in the protein, and it is possible other cleavage sites could compensate for the R815-S816 site [149]. It has also been shown that the S2' site can be cleaved by other TMPRSS proteins besides TMPRSS2, and also by other proteinases including members of the MMP family [128, 129]. The delta spike has been shown to utilise the MMP2/MMP9 pathway to mediate entry independent of TMPRSS2 [129]. We hypothesised that perhaps the utilisation of the MMP2/MMP9-mediated pathway could assist in understanding why the delta spike is sensitive to IFITM2 in TMPRSS2-negative cells, despite its lack of dependence on cathepsins. To test this, A549-ACE2 and A549-ACE2-TMPRSS2 cells were treated with an MMP2/9 inhibitor for 1 hour prior to infection with D614G, D614GΔPRRA, alpha, delta and omicron PLVs and the effect on infectivity measured (Figure 4.2.11). Consistent with the literature [128, 129],

the delta PLVs were more sensitive to inhibition of entry by MMP2/MMP9 inhibitor treatment than alpha, and indeed omicron, PLVs. This is consistent with delta being able to preferentially use this pathway relative to alpha and omicron. The presence of TMPRSS2 did not really alter the sensitivity of any of the PLVs tested to MMP2/9 inhibition. It is however likely that this inhibitor does not only inhibit MMP2/9, and likely inhibits other MMPs, or indeed other proteinases, as well. Interestingly, the D614GΔPRRA and D614G spikes were similarly sensitive to MMP2/9 inhibition as the delta spike. This could suggest that D614G and D614GΔPRRA can utilise either the cathepsin or MMP pathway in these cells, however delta cannot utilise the cathepsin pathway but can utilise the MMP pathway. Alpha is therefore the only spike tested so far which is insensitive to cathepsin and MMP inhibition, while delta and omicron retain sensitivity to inhibition of at least one of these proteinases. Altogether, these data could suggest that usage of the cathepsin or MMP pathway for viral entry results in exposure to IFITM2 compartments. However, this does not answer the question of which proteinase the alpha spike is using for viral entry in TMPRSS2-negative cells, as it appears to only use cathepsins or MMPs to a small extent.

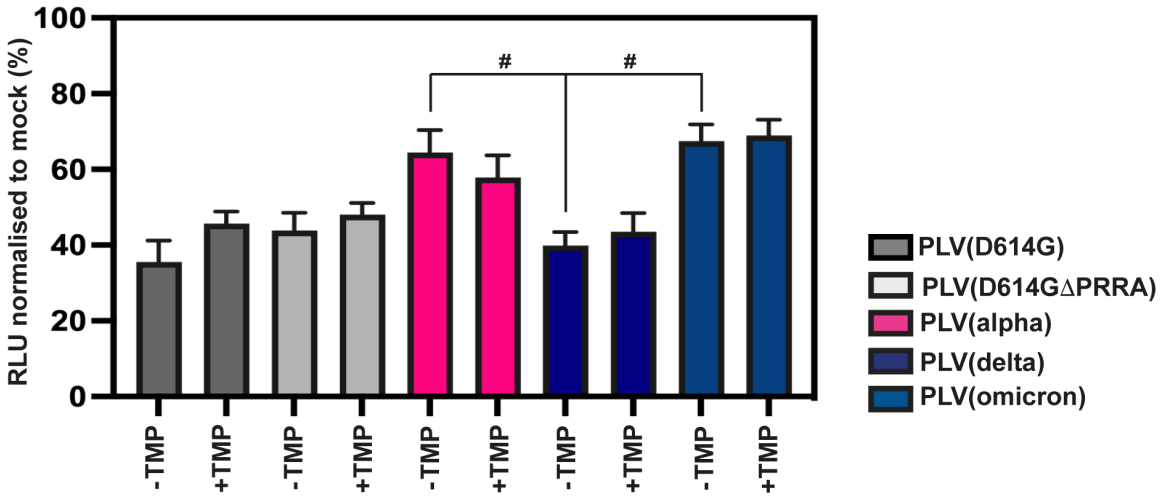

Figure 4.2.11. Delta is more sensitive to an MMP2/9 inhibitor than alpha or omicron. A549-ACE2 (-TMP) A549-ACE2-TMPRSS2 (+TMP) cells were pre-treated with 20μM MMP2/MMP9 inhibitor II for 1 hour prior to infection with PLVs and infection quantified by luciferase activity 48 hours later. Infection is plotted as percentage infectivity as a percentage of the DMSO control for each PLV. #=P>0.05 indicating statistical significance between conditions determined by one-way ANOVA. N=3, Mean±SEM shown.

4.2.10 Inhibition of MMP2/MMP9 confers alpha-like properties to delta in A549-ACE2 cells

Having established that delta can utilise the MMP pathway, it was next tested whether this had any consequences for IFITM-mediated restriction. A549-ACE2-IFITM cells were pre-treated with the MMP2/MMP9 Inhibitor II again for 1 hour prior to infection with D614G, D614GΔPRRA, alpha, delta and omicron PLVs (Figure 4.2.12 A-E). Inhibition of the MMP pathway mildly reduced IFITM1 and 2 inhibition of D614G, and conferred a small degree of IFITM3 enhancement. The D614GΔPRRA mutant showed a small degree of IFITM3 enhancement in the presence of the inhibitor. Additionally, although alpha was already IFITM resistant, the inhibitor increased the IFITM2 and IFITM3 enhancement of the alpha PLVs. Most intriguingly, the MMP2/MMP9 inhibition resulted in the delta spike becoming more “alpha like”, with enhancement by IFITM2 and IFITM3 to a similar extent as the alpha spike. Finally, the omicron PLVs were ultimately unaffected by MMP2/MMP9 inhibition, further suggesting these PLVs do not utilise this pathway. This could suggest that MMP-based cleavage of spike is distinct from cathepsin-based cleavage, however confers a less favourable pathway in terms of exposure to IFITMs.

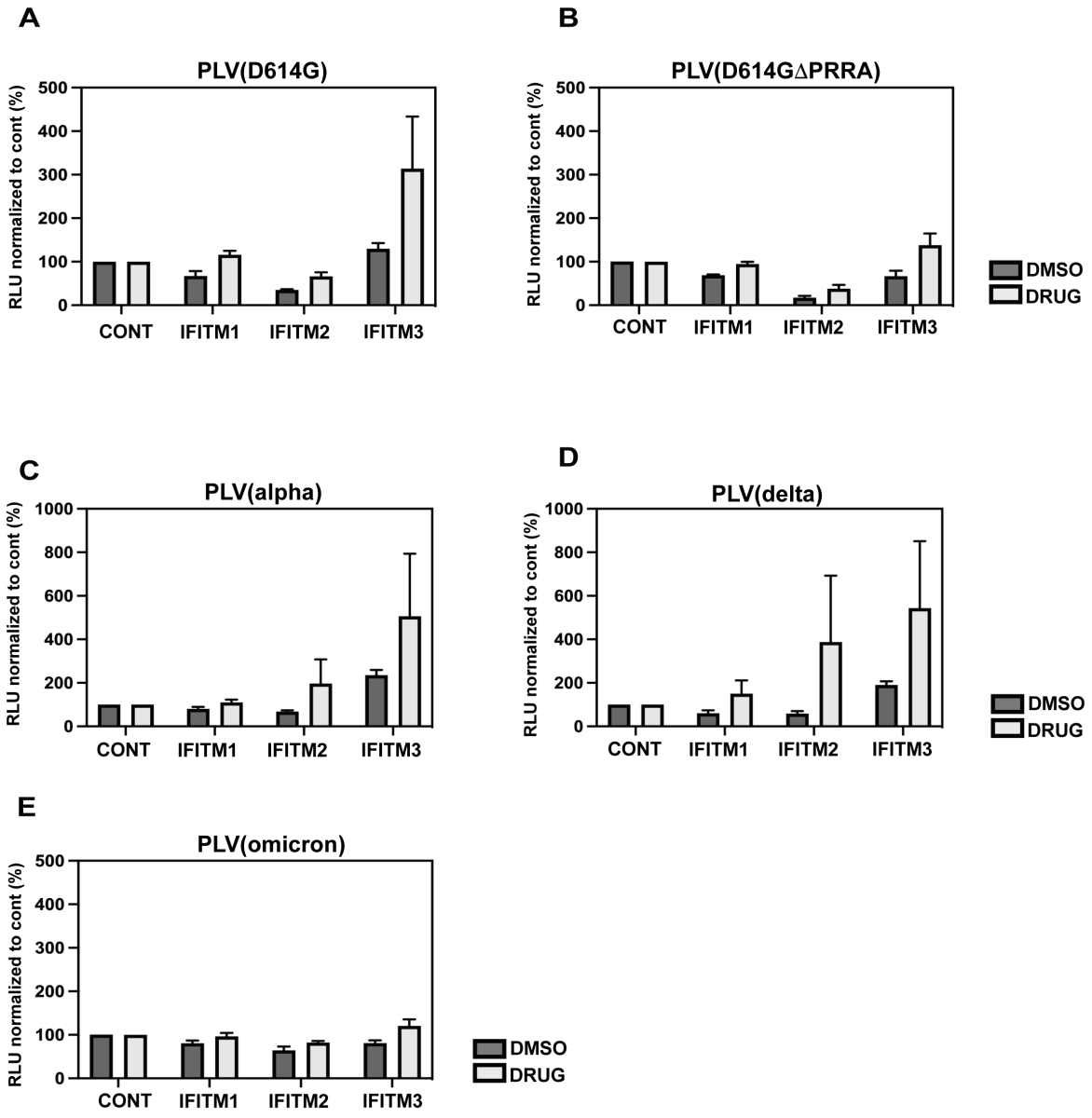

Figure 4.2.12. Inhibition of MMP2/MMP9 in A549-ACE2 cells confers alpha-like properties to delta. A-E) A549-ACE2-IFITM were pre-treated with 20μM of MMP2/MMP9 inhibitor II for 1 hour prior to infection with PLVs and infection quantified by luciferase activity 48 hours later. Infection is plotted as percentage infectivity as a percentage of the DMSO control for each PLV #=P>0.05 indicating statistical significance between conditions determined by one-way ANOVA. N=3, Mean±SEM shown.

4.2.11 Polybasic cleavage site mutations alter spike processing but not in all cell types

The location of the P681H and P681R mutations led to the suggestion that these mutations could increase the efficiency of S1/S2 cleavage and contribute to the increased transmissibility of alpha and delta. Indeed, several groups have shown that alpha and delta are better cleaved at the S1/S2 compared to an ancestral virus [157, 359, 361] [129]. Whether this contributes to the increased transmissibility of omicron is open to debate and there are conflicting results in the literature as to whether a P681H or a P681R enhances cleavage more than the other. To test this, Vero-E6-TMPRSS2 cells were infected with England-02, D614G, alpha, delta and omicron viruses and immunoblotted for the cellular and purified supernatants 30 hours post infection (Figure 4.2.13 A). In our hands, we found that the alpha, delta and omicron were all more cleaved in the cellular lysates and supernatant compared to England-02 and D614G. As discussed in the previous chapter, the D614G isolate was more cleaved than the England-02 spike, suggesting that this mutation alone, which is outside of the polybasic cleavage site, has knock-on effects on increasing S1/S2 cleavage.

Additionally, the alpha variant appeared more cleaved than delta or omicron in the viral supernatant, suggesting that in this cell type at least, this spike is more efficiently cleaved at the S1/S2 boundary. We tried to recapitulate these findings with PLVs, and to our surprise found that we could not discern differential cleavage in the purified supernatant of PLVs made in 293T-17 cells for alpha, delta and omicron (Figure 4.2.13 D). Probing the omicron PLVs for spike proved difficult, and we had to expose this sample for much longer than the others. We concluded from these data that effects on S1/S2 cleavage are likely to be highly dependent on the cell type the virus or PLVs are produced in, and that this may facilitate understanding why there are differential results on cleavage in the literature. Additionally, despite all of the VOCs, including D614G, being better cleaved than the England-02 virus at the S1/S2 boundary, this does not correlate with IFITM2 sensitivity. This further suggests that there is not a simple relationship between the degree of S1/S2 cleavage and IFITM sensitivity.

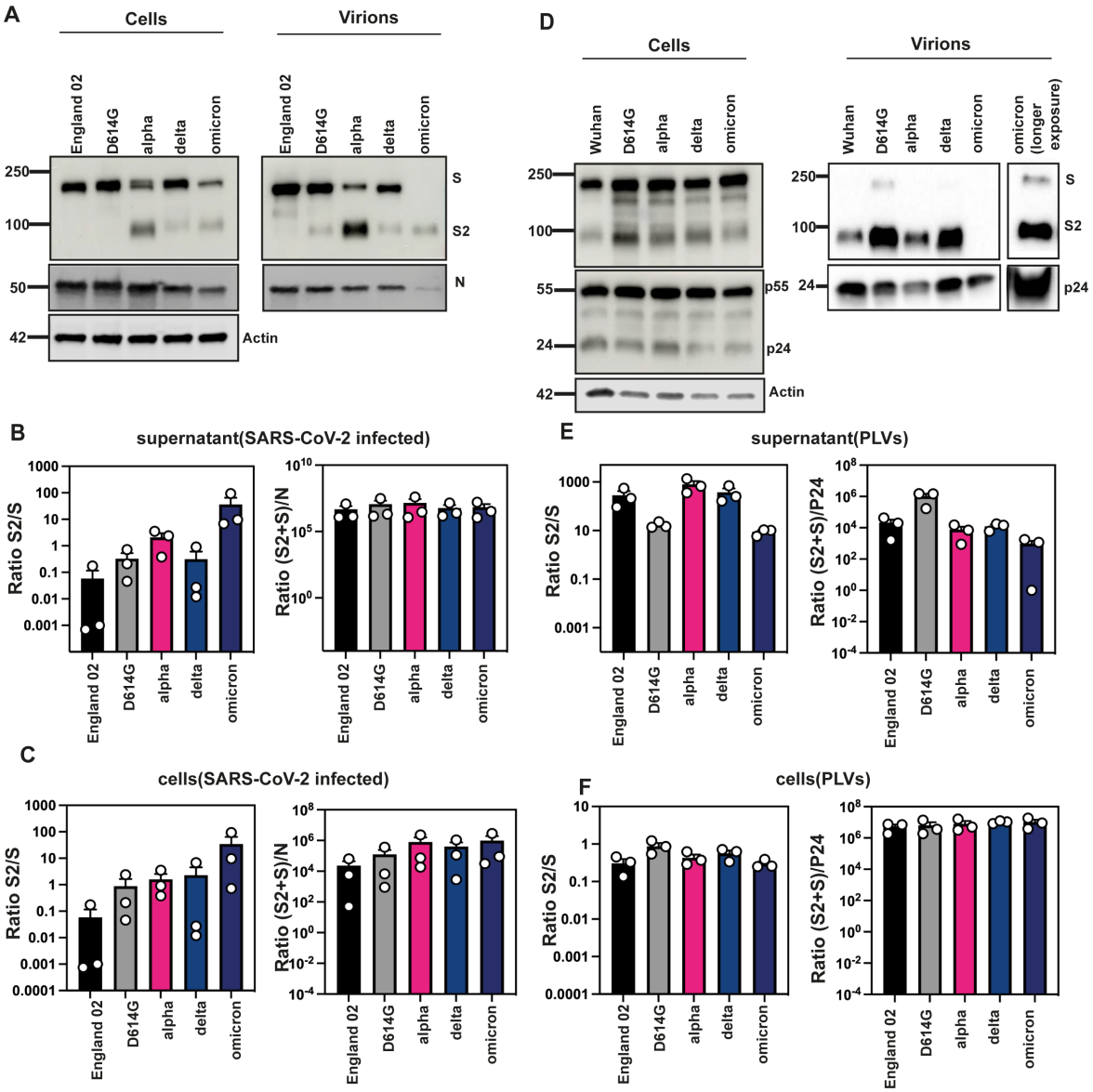

Figure 4.2.13. Virus produced in Vero-E6-TMPRSS2 and PLVs produced in 293T17s differentially process spike. A) England-02, D614G, alpha, delta and omicron viruses were used to infect Vero-E6-TMPRSS2 for 30 hours. Cellular lysates were harvested and supernatant purified through a 20% sucrose cushion at 18 000 g prior to lysis. Samples were Western blotted for spike and N. B) Quantification of spike in cell lysates of infected Vero-E6-TMPRSS2 cells after 30h. Graph shows ratio of S2 over total S, and ratio of S2 and total S over N. C) Quantification of spike in purified supernatant from infected Vero-E6-TMPRSS2 cells after 30h. Graph shows ratio of S2 over total S, and ratio of S2 and total S over N. D) PLVs were produced in 293T17s and cellular lysates harvested after 48 hours and supernatant purified as in A. Samples were immunoblotted for spike and gag. Blots are representative of three independent experiments. E) Quantification of spike in cell lysates of 293T/17 cells used to produce PLVs. Graph shows ratio of S2 over total S, and ratio of S2 and total S over p55. F) Quantification of spike in purified PLVs produced in 293T/17 cells. Graph shows ratio of S2 over total S, and ratio of S2 and total S over p24.

4.3 Discussion

In this chapter I show that the alpha variant is IFNβ resistant in A549 and Calu-3 cells, and that this tracks to the spike protein and specifically to the P681H mutation. Additionally, reversion of this mutation can confer IFNβ sensitivity to the alpha virus, and IFITM sensitivity to alpha PLVs. Furthermore, I show that, of the alpha, beta, gamma, kappa, delta and omicron variants BA.1 and BA.2 VOCs, only the alpha variant is IFITM resistant in A549-ACE2s with the remaining VOCs demonstrating varying IFITM sensitivity. Interestingly, there is also a 3-6-fold enhancement of infection by IFITM3 for the alpha virus, in both viral and PLV infection. An element of IFITM3 enhancement is also seen with delta PLVs, however this cannot be recapitulated with native viral infection. This could suggest that while the spike of delta can be enhanced by IFITM3, there are other factors in full viral infection which overcome any enhancing effects of the spike. For instance, the delta variant has a mutation in the intramembrane domain of the M protein, I82T. The role of this mutation on M has not been investigated to date, but given that M and spike interact it is possible that this could alter some properties of spike in viral entry. It could also be that either more or less spike is packaged onto pseudotyped lentiviral vectors relative to native virus, resulting in an artefact of IFITM3 enhancement on some PLVs.

However, the IFITM3 enhancement of alpha is a consistent phenotype between both PLVs and viral infection in A549-ACE2s. There is also some enhancement of alpha by IFITM1 or IFITM2 in some experiments, suggesting that perhaps these IFITMs can also enhance infection under certain circumstances. The P681H mutation in the alpha spike appears to be necessary for this IFITM3 enhancement phenotype, as when we revert this mutation the IFITM3 enhancement is abolished. Addition of a P681H mutation into a D614G spike does not however confer IFITM3 enhancement, suggesting that other contextual mutations are required to confer this enhancement. Deletion of the cytoplasmic tail from alpha also abolishes IFITM3 enhancement, as well as reducing the resistance of alpha to IFITM2. The deletion of the cytoplasmic tail reducing IFITM3 enhancement suggests that there is a favourable conformation of spike required for IFITM3 enhancement and may assist in determining the mechanism of IFITM3 enhancement. Although surprising that an antiviral protein can enhance

rather than restrict infection, IFITM enhancement has previously been shown for the coronavirus OC43 [336]. Additionally, the Yount group has reported that mutations that alter the endocytic recycling of IFITMs 2 and 3, thereby retaining them at the plasma membrane, can turn them into enhancers of SARS-CoV-2 rather than restrictors [40]. The Kirchhoff lab has also suggested that in Calu-3 cells IFITMs 2 and 3 can enhance SARS-CoV-2 infection, and that knocking IFITMs down in this cell line inhibits infection [335]. Overall, this suggest that IFITMs can enhance infection under certain conditions which remain to be fully elucidated.

The P681H mutation appears to be key in the IFITM and IFNβ resistance of the alpha variant, and the fact that this mutation alone reduces E64d and IFITM2 sensitivity of D614G in A549-ACE2s demonstrates this singular mutation can alter the route of viral entry and thereby exposure to antiviral proteins. However, the omicron variant, which also has a P681H mutation, is still dependent on cathepsins for entry and sensitive to IFITM restriction. It has been suggested that the omicron spike adopts a more closed conformation than other variants to date which reduces its ability to utilise TMPRSS2, and that this maps to the RBD and S2 domain of omicron [94, 362]. The closed conformation of omicron could override the benefits of the P681H mutation, and it would be interesting to investigate if generating chimeras of alpha and omicron is sufficient to switch the IFITM sensitivity of these two spikes. Additionally, the omicron variant contains the H655Y mutation which has been demonstrated to confer endosomal entry [203]. This mutation is also present in the gamma variant, which as shown here has similar E64d sensitivity to the ΔPRRA mutant, further confirming the role of this mutation in directing endosomal entry.

Given that the P681R mutation has been shown to enhance S1/S2 cleavage, the question arises of why this mutation does not confer IFITM resistance? The delta variant has a similar E64d insensitivity to the alpha variant, however the P681R mutation alone does not significantly alter the cathepsin dependence of a D614G spike. This indicates that there are other factors involved in the preference of the delta spike for cathepsin independent entry. The insensitivity of delta to E64d is at odds with the fact it is restricted by IFITM2, unlike the rest of the spikes tested so far which demonstrate a clear correlation between IFITM2 sensitivity and E64d sensitivity. It has

recently been suggested that MMPs can also mediate the S2' cleavage for the delta spike and permit an additional route of entry [129]. Indeed, consistent with recent literature, I demonstrate here that delta is more sensitive to the inhibition of MMPs than alpha or omicron, and that inhibition of this pathway rescues the IFITM2 sensitivity of the delta PLVs in TMPRSS2-negative cells. This suggests that sensitivity to either E64d, MMP inhibitors, or both, is a determinant for IFITM2 sensitivity in TMPRSS2-negative cells; alpha is fairly insensitive to both E64d and the MMP2/9 inhibitor. Meanwhile, delta is insensitive to E64d but sensitive to MMP inhibition, and omicron shows sensitivity to E64d but insensitivity to MMP inhibition. These data also suggest that D614G and the D614GΔPRRA spikes can also utilise the MMP pathway. It would be interesting to investigate whether the P681H of alpha and omicron dictates the decreased usage of the MMP pathway by these spikes.

There may also be other unknown proteases that can mediate this cleavage process that remain to be examined. The data presented here suggest that the MMP pathway is utilised by VOCs to a varying extent, however that this may be an "unfavourable" pathway in terms of escaping IFITM restriction, as inhibition of MMP2/MMP9 resulted in reduced IFITM sensitivity. It cannot be ruled out that the MMP2/MMP9 inhibitor used here may not be specific, and likely inhibits other MMPs and potentially other proteinases outside of this family. Yamamato and colleagues reported that there was much variability amongst MMP9 inhibitors, which again could be due to unknown effects on other proteinases or non-specific effects of these inhibitors [128]. They also suggest that furin cleavage was a pre-requisite for mediating MMP-dependent entry, however in the data presented here the D614GΔPRRA PLVs were also inhibited by the MMP2/MMP9 inhibitor, suggesting that MMPs can mediate the S1/S2 cleavage [128]. It has also recently been shown that SARS-CoV-2 entry requires more of an acidic pH component than previously appreciated [19]. These findings suggest that there is still an acidic pH requirement, even in the context of TMPRSS2-mediated S2' cleavage in a cell-type dependent manner.

It is also becoming apparent that there may be more potential cleavage sites in spike than simply the S1/S2 boundary and the S2' site. Two additional sites which could be cleaved by cathepsin L (at positions 259 and 636 of spike) have been identified [149].

If these additional sites are used during infection, this could further explain why viruses can so rapidly lose the polybasic cleavage site in culture and become less TMPRSS2-dependent [154].Furthermore, with many reports suggesting that alpha and delta prefer a cell-surface adjacent route of viral entry via TMPRSS2 mediated cleavage, testing IFITM sensitivity in TMPRSS2-negative cells may be different to the phenotypes observed in the presence of TMPRSS2. The impact of TMPRSS2, and other factors proteinases which may be involved in SARS-CoV-2 entry will be discussed further in Chapter 5.

The data presented here also demonstrate differential cleavage efficiency between native virus grown in Vero-E6-TMPRSS2 cells, and in PLVs produced in 293T-17s, whereby virus grown in Vero-E6-TMPRSS2 cells shows disparity in cleavage between variants, whereas variant-dependent cleavage is fairly indistinguishable in PLVs produced in 293T-17s. This is in contrast to a report showing that delta is better cleaved than alpha in Vero-E6-TMPRSS2 cells [157], and another demonstrating that omicron is less well cleaved than delta in hNEC and Calu-3 cells [204]. Additionally, it has been shown that the P681H mutation alone increases spike cleavage [231]. Given the disparity between the data shown here and the literature over which spikes are better cleaved, it is likely that the cell type used to produce virus or lentiviral vectors has a large impact on the cleavage efficiency of the spike. It would be interesting to compare if growing virus in TMPRSS2-negative cell lines, or other ACE2+ TMPRSS2+ cell lines like Caco-2, has any impact on differential spike processing.

The fact that the H681P reversion of alpha in the real virus does not revert the cleavage phenotype further suggests that the IFITM resistance from a P681H mutation may be separate from cleavage efficiency *per se*. Based on the data presented in Chapter 3, it is clear that some S1/S2 cleavage is required in order to reduce the impact of IFITM2 on entry. However, it may be that actually a small amount of cleavage at the S1/S2 site is enough and the P681H mutation is conferring IFITM resistance through a distinct mechanism separated from cleavage. Additionally, increased cleavage of ΔCT spike but increased IFITM sensitivity also suggests that the relationship between cleavage and IFITM sensitivity may not be quite so clear cut. This further suggests that increased cleavage may not always necessitate increased

IFITM resistance, and that the P681H is conferring IFITM resistance through a different mechanism to S1/S2 processing. PLVs are produced in a system where virion assembly is not at the site it would be in the context of native virus production and it has previously been shown that producing VLPs in the presence of M, E, and N affects the processing and glycosylation of spike [170]. Overall, these data suggest that inferring spike biology from a single cell-type may be misleading, and studying spike cleavage in multiple cell-types will be informative for further understanding factors that affect cleavage.

Chapter 5: TMPRSS2 expression and altering IFITM localisation affects IFITM-mediated restriction

5.1 Introduction

Other groups have suggested that IFITMs can enhance, rather than restrict, the entry of SARS-CoV-2 spike: a variety of systems suggest that IFITMs enhance SARS-CoV-2 infection in Calu-3 cells, and that the Y20A mutation in IFITM3 also results in the enhancement of infection in 293T-17s [40, 94, 335]. Additionally, another report suggests that IFITM1 is more restrictive than IFITM2 or 3 in Caco-2 cells [94]. The contradictions in the literature regarding the antiviral effects of IFITMs on SARS-CoV-2 is likely a function of IFITMs behaving differently in different cell types. Additionally, as both Calu-3 and Caco-2 cells endogenously express TMPRSS2, in contrast to A549s which do not endogenously express, the presence or absence of TMPRSS2 likely plays a role in the antiviral properties of IFITMs.

The role of TMPRSS2, which we know can alter routes of viral entry, has been suggested to be able to overcome IFITM3-mediated restriction of SARS-CoV-1, MERS and SARS-CoV-2 [96]. TMPRSS2 has been focussed on as the main serine protease capable of cleaving the S2' site to mediate viral entry near the cell surface [10, 188]. However, several other TMPRSS proteins [127] and other proteinases [128, 129] have been found to cleave this step and may provide an alternative route of viral entry. TMPRSS11D and 13 have been reported to cleave the S2' site and are expressed in the airways, especially in the nasal passageways [127]. Finally, it has recently been shown that even after TMPRSS2 cleavage, a majority of SARS-CoV-2 entry still requires acidic pH, which may explain why ability to use TMPRSS does not always track with IFITM sensitivity [19]. Both the current literature and data presented in the previous chapter suggest that the omicron variant utilises cathepsins to mediate viral entry to a greater extent than the previous variants alpha or delta. This demonstrates a shift away from TMPRSS2 usage for the most recent SARS-CoV-2 variants and underlines the importance of investigating viral entry phenotypes in different cell types. However, given what we know about TMPRSS2 in providing an

alternate route of viral entry, in this chapter I investigate the impact of TMPRSS2 overexpression on the IFITM sensitivity of alpha, delta, and omicron. Additionally, I also explore the role of mutations which mislocalise IFITMs on the sensitivity of the major VOCs to IFITMs in both TMPRSS2-negative and TMPRSS2-positive cells.

SARS-CoV-2 PLVs only contain the spike protein, despite the fact that in native SARS-CoV-2 virions, the lipid bilayer is also studded with Membrane (M) and Envelope (E). M and E are involved in viral assembly, and M in particular is involved in both trafficking and post-translational modifications of spike. Unsurprisingly, inclusion of these proteins during VLP production has been found to alter spike properties, including virion shape [170]. It has also been suggested from in silico analyses that the M protein may also function as a sugar transporter, which in turn has been hypothesised to alter spike glycosylation [123]. Mutations in the E and M proteins have not been as frequent as those in spike, however several mutations in M have emerged in the kappa, delta and omicron variants. In this chapter, I also investigate the role of producing PLVs in the presence of the Wuhan M protein on PLV infectivity and IFITM sensitivity in A549-ACE2 cells.

5.2 Results

5.2.1 Overexpression of TMPRSS2 rescues spike from IFITM2 mediated inhibition

Overexpression of the TMPRSS2 protease, as previously demonstrated, can confer decreased dependence on cathepsin-mediated cleavage and entry [334]. Additionally, we had previously observed that over-expression of TMPRSS2 in conjunction with IFITM2 knockdown resulted in almost total rescue of IFNβ-mediated inhibition of Wuhan virus in Chapter 3 (Figure 3.2.13 D). To test whether overexpression of TMPRSS2 alone could also therefore rescue Wuhan from IFITM2-mediated inhibition, A549-ACE2-TMPRSS2-IFITM cells were generated and the IFITM sensitivity of Wuhan and WuhanΔPRRA PLVs tested (Figure 5.2.1 A, B). In A549-ACE2s, the Wuhan PLVs were mildly sensitive to IFITM1 and most sensitive to IFITM2 (Figure 3.2.8 B, C). However, in the context of TMPRSS2, Wuhan PLVs were now completely insensitive to IFITMs 1, 2 and 3, suggesting that TMPRSS2 over-expression could rescue both IFITM1 and IFITM2 sensitivity for this spike. The insensitivity to IFITM1 was intriguing, as this IFITM predominantly localises to the plasma membrane and an increased use of cell-surface fusion would perhaps logically result in increased IFITM1 sensitivity. This could therefore suggest that in these cells IFITM1 and TMPRSS2 occupy distinct areas of the membrane, and TMPRSS2-mediated cleavage does not direct viral infection towards IFITM1 compartments. However, the WuhanΔPRRA PLVs, which are even more sensitive to IFITM2 than Wuhan PLVs in A549-ACE2s (Figure 3.2.9 B), were still very sensitive to the presence of IFITM2 when TMPRSS2 was overexpressed. This is consistent with the fact that the WuhanΔPRRA PLVs do not exhibit reduced sensitivity to E64d in the presence of TMPRSS2, and most likely cannot utilise this pathway. Overall, this suggests that TMPRSS2 can rescue IFITM-inhibition dependent on whether the spike can utilise this protease spike cleavage, however it remains unclear whether this is S1/S2 cleavage, S2' cleavage, or another currently unknown site.

These observations were extended to the D614G, alpha, delta and omicron PLVs (Figure 5.2.2 A-D). Similarly to the Wuhan PLVs, the D614G and delta PLVs were no longer sensitive to IFITM2 in the presence of TMRPSS2. The omicron PLVs still

exhibited a degree of sensitivity to all three IFITMs, however not to statistical significance (Figure 5.2.2 D). Interestingly, for D614G, alpha and delta, the overexpression of TMPRSS2 opened up IFITM1 sensitivity, when D614G and alpha had previously been insensitive to IFITM1. This is contrary to what was observed with the Wuhan PLVs, however it could be that TMPRSS2 can alter IFITM1 sensitivity in a D614G-dependent manner. Additionally, although TMPRSS2 rescued all of the spikes except omicron and D614GΔPRRA from IFITMs 2 and 3, the overexpression of TMPRSS2 did reduce the IFITM3 enhancement exhibited by the alpha PLVs previously.

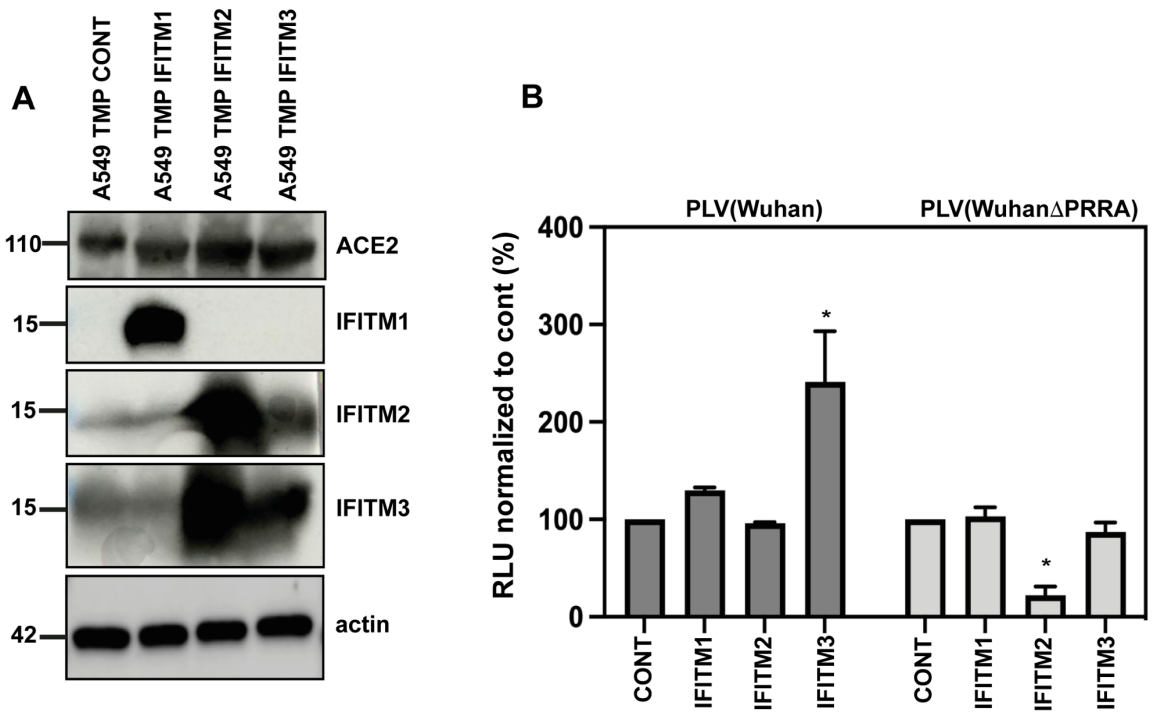

Figure 5.2.1. Overexpression of TMPRSS2 rescues the Wuhan spike from IFITM-mediated inhibition. A) Representative immunoblot of A549-ACE2-TMPRSS2 cells stably expressing the individual IFITMs. B) A549-ACE2-TMPRSS2 cells were infected with PLVs and infection measured by luciferase activity 48 hours later. *=P>0.05 indicating statistical significance between control and IFITM for each PLV determined by ANOVA. N=3, Mean±SEM shown.

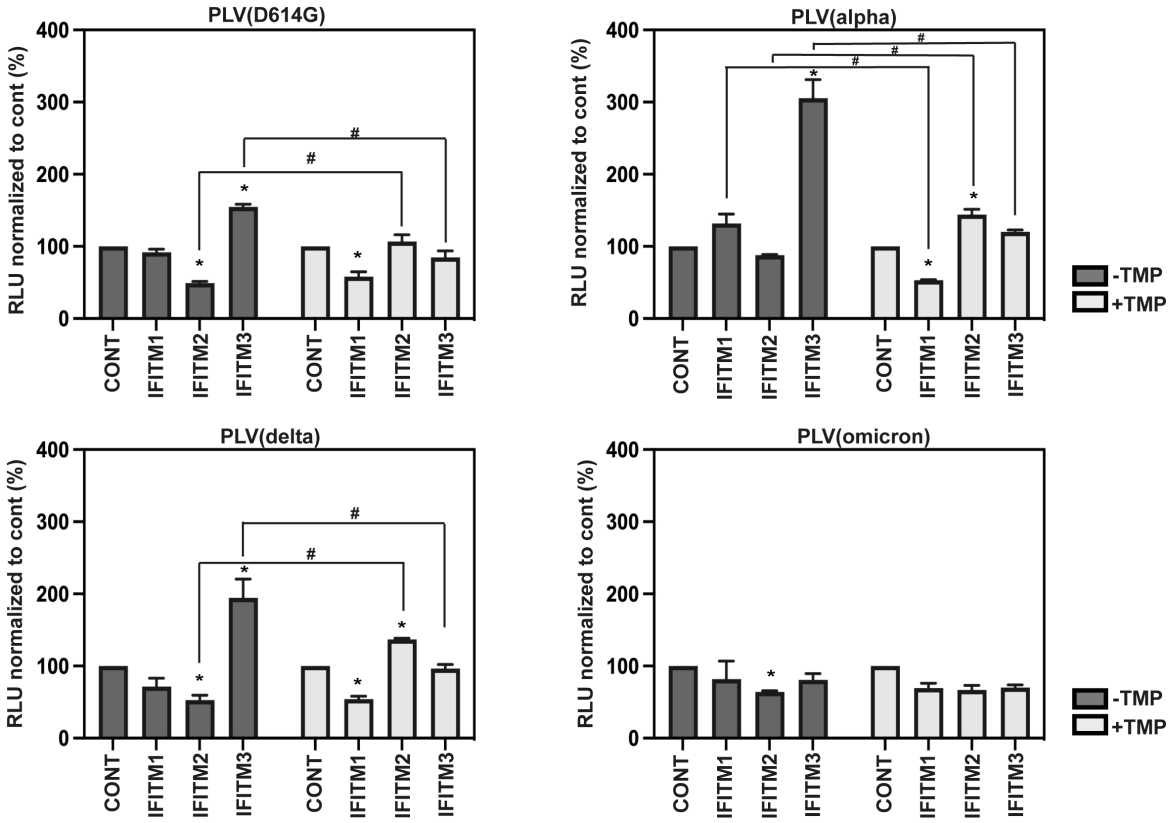

Figure 5.2.2. Overexpression of TMPRSS2 rescues D614G and delta spikes from restriction by IFITM2. A-D) A549-ACE2 or A549-ACE2-TMPRSS2 cells expressing the individual IFITMs were infected with equal volumes of PLVs and infection measured by luciferase activity 48 hours later. *=P>0.05 indicating statistical significance between control and IFITM for each PLV, #=P>0.05 indicating statistical significance between the -/+ TMPRSS2 conditions for each PLV determined by two-way ANOVA. N=3, Mean±SEM shown.

5.2.2 IFITM mutants can enhance or restrict infection in a TMPRSS2-dependent manner

Thus far, the alpha spike was the only spike tested that exhibited significant IFITM3 enhancement in A549-ACE2s as both a PLV and native virus. However, IFITM enhancement in the context of coronaviruses is not novel, as the coronavirus OC43 hijacks IFITM2 and IFITM3 to enter cells [336]. Additionally, mislocalising IFITMs by mutating the endocytic YxxΦ motif which should result in increased accumulation at the plasma membrane had also been shown to result in IFITM enhancement of infection [40]. To further examine factors that dictate enhancing versus restrictive

abilities of IFITMs, the mutant IFITM2 Y19F was generated, as in the A549-ACE2 system this IFITM appeared to have the most restrictive effect on SARS-CoV-2 entry (Figure 5.2.3 A). The Y19F mutant was similarly expressed compared to the wild-type, and the effect of this mutant on Wuhan PLVs and native virus was tested next (Figure 5.2.3 B, C). In accordance with the Yount groups findings, IFITM2 Y19F converted IFITM2 into an enhancer of infection for both the Wuhan PLVs and virus by 2-fold. These data suggest that the localisation of IFITM2 to endosomal membranes is essential for its restriction of the England-02/Wuhan SARS-CoV-2, and further confirms the results to date suggesting SARS-CoV-2 can be enhanced by IFITMs under certain conditions.

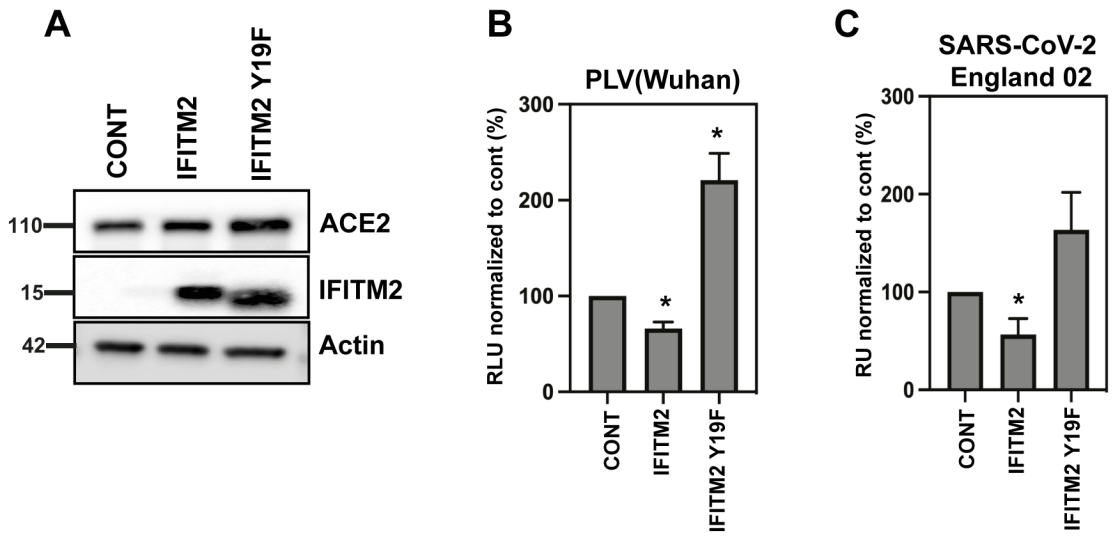

Figure 5.2.3. IFITM2 Y19F rescues restriction of Wuhan and England-02 SARS-CoV-2. A) representative Western blot of A549-ACE2 cells stably expressing IFITM2 or IFITM2 Y19F. B) PLVs of Wuhan were used to infect A549-ACE2 control, IFITM2, or IFITM2 Y19F cells and infectivity quantified by luciferase activity 48 hours later. Infection was normalised to control. C) England-02 virus was used to infect A549-ACE2 control, IFITM2, or IFITM2 Y19F cells at an MOI of 0.005 for 48 hours. Infection was quantified by using the infected supernatant to inoculate Vero-E6 cells and measuring intracellular N colorimetrically 24 hours later. *= $P<0.05$, indicating statistical significance between control and each IFITM condition determined by ANOVA. N=3, Mean±SEM shown.

Given that the IFITM2 Y19F mutation can rescue inhibition of the previously IFITM2-sensitive Wuhan spike and TMPRSS2 rescued IFITM2 restriction, whether IFITM2 Y19F behaved differently in the presence of TMPRSS2 was tested next. The N-terminal of IFITM3 also contains a YxxΦ motif, and an IFITM3 Y20F mutant was also generated. IFITM3 has shown minimal restriction of the spikes tested in this thesis, however this mutant was generated to assess whether mislocalisation of IFITM3 could alter the IFITM3 enhancement phenotype observed with the alpha variant. Additionally, the C-terminal of IFITM1 has previously been shown to regulate its antiviral properties in the context of certain coronaviruses and HIV-1 by altering its subcellular localisation [66, 363]. Based on this, a C-terminal deletion mutant of IFITM1 was also created to test whether altering the localisation of IFITM1 could also affect antiviral properties in the context of SARS-CoV-2. A549-ACE2 and A549-ACE2-TMPRSS2 cells stably expressing these mutants were generated to confirm expression of the IFITM mutants (Figure 5.2.4). The IFITM1Δ117-125 mutant appeared to express slightly less well than the wild-type, however IFITM2 Y19F and IFITM3 Y20F appeared similarly well expressed.

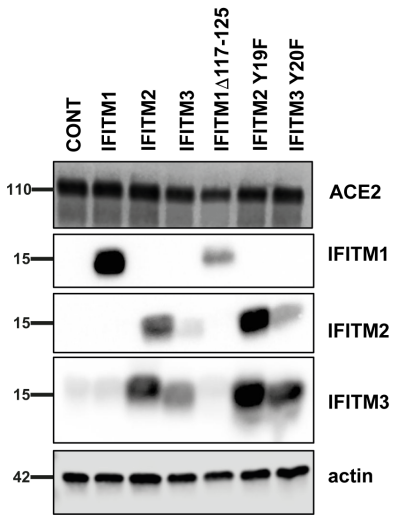

Figure 5.2.4. **Expression of IFITM mutants in A549-ACE2 cells.** A) Western blot of cell lysates from A549-ACE2 cells stably expressing individual IFITMs and mutants thereof.

Next, the IFITM sensitivity of D614G, alpha, delta and omicron was tested in these cells (Figure 5.2.5 A-D). Surprisingly, in the A549-ACE2 cells, the IFITM1∆117-125 mutant enhanced infection 5-8-fold for D614G, alpha and delta PLVs. This mutant had less of an effect on omicron, with at most a 2-fold enhancement. Consistent with the previous results for Wuhan, the IFITM2 Y19F mutant also enhanced infection, from 4-6-fold for D614G, alpha and delta. Again, this mutant did not enhance the infection of omicron significantly. IFITM3 still enhanced the alpha PLVs 3-fold, and interestingly this was reduced by the Y20F mutation in A549-ACE2 cells. This suggests that the localisation of IFITM3 is imperative to its ability to enhance alpha infection under steady-state conditions.

Conversely, in the A549-ACE2-TMPRSS2 cells, the IFITM1∆117-125 mutation rescued IFITM1 inhibition, but did not enhance infection like it did in the TMPRSS2-negative cells. The IFITM2 Y19F mutation in the TMPRSS2-positive context no longer enhanced infection, and interestingly actually conferred a small amount of restriction on D614G, alpha and delta. This suggests that localising IFITM2 to the plasma membrane in the context of TMPRSS2 confers restrictive capacity to IFITM2, and that SARS-CoV-2 restriction by IFITM2 is essentially a function of its localisation. Lastly, the Y20F mutation in IFITM3 now had little to no effect on infection, with only a slight rescue in restriction for the omicron variant. These data suggest that the enhancing capacity of an IFITM is highly dependent on its subcellular localisation, and also demonstrates that the Y19F IFITM2 mutant can restrict SARS-CoV-2 infection in the context of TMPRSS2-positive cells. This suggests that this mutant is likely in the same pathway as that conferred by TMPRSS2 cleavage, while IFITM2, IFITM1∆117-125 and IFITM3 Y20F are not. Additionally, this suggest IFITM2 Y19F, IFITM3 Y20F and IFITM1 behave differently even in the same subcellular compartment; as IFITM1 and IFITM2 Y19F restrict infection in the presence of TMPRSS2, while IFITM3 Y20F does not. Overall, these data suggest that the conflict in the literature regarding which IFITMs restrict infection is in part due to the presence or absence of TMPRSS2.

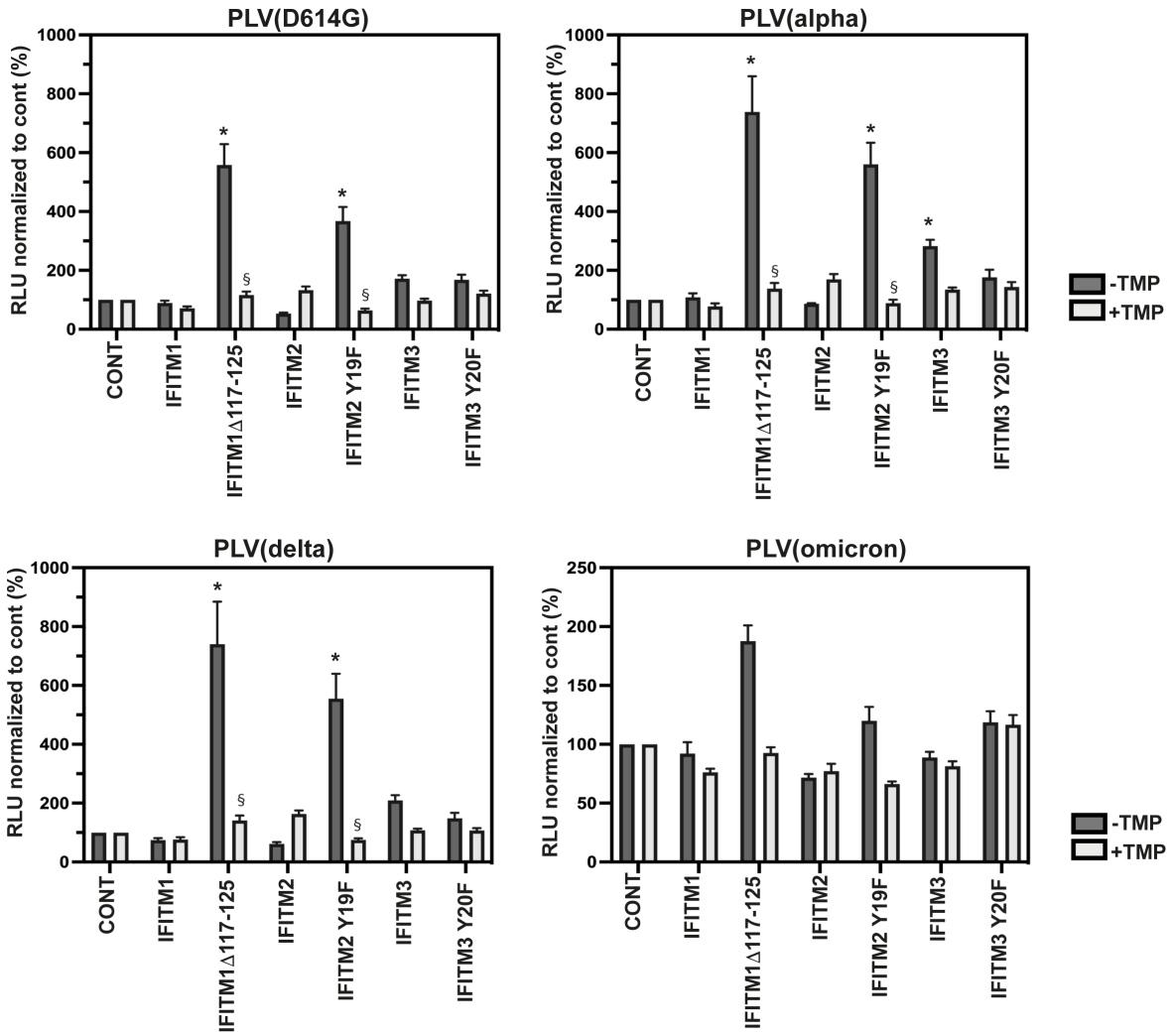

Figure 5.2.5. IFITM mutations that enhance in A549-ACE2 cells can restrict in A549-ACE2-TMPRSS2 cells. A-D) PLVs were used to infect A549-ACE2 (-TMP) or A549-ACE2-TMPRSS2 (+TMP) cells stably expressing IFITMs or mutant IFITMs and infection quantified by luciferase activity 48 hours later. Infection is normalised to the empty vector control (in each cell line). *=P>0.05 indicating statistical significance between different IFITMs relative to the control of each PLV, and § indicates P=>0.05 statistical significance between an IFITM and the mutant of that IFITM determined by two-way ANOVA. N=3, Mean±SEM shown.

5.2.3 Inhibition of MMP2/MMP9 in the presence of TMPRSS2 confers IFITM2 and IFITM3 enhancement

TMPRSS2 overexpression rescues D614G and delta spikes from IFITM2 inhibition but cannot rescue D614GΔPRRA or omicron which are more dependent on the cathepsin pathway (Figure 3.2.7). In the previous chapter I demonstrated how inhibition of MMP2/MMP9 rescued delta PLVs from IFITM2 inhibition in A549-ACE2 cells. To test whether inhibition of MMP2/MMP9 in TMPRSS2+ cells could rescue the IFITM1 sensitivity of D614G, alpha and delta, A549-ACE2-TMPRSS2 IFITM cells were pre-treated with the MMP2/MMP9 inhibitor II prior to infection as before (Figure 5.2.6 A-D). Although not reaching statistical significance, MMP2/MMP9 inhibitor treatment reduced the IFITM1 sensitivity of all the spikes except omicron. Additionally, MMP2/MMP9 inhibition resulted in IFITM2 and IFITM3 enhancement up to 3-fold for the alpha and delta PLVs. Consistent with the data in the previous chapter, this could suggest that utilisation of the MMP pathway is not conducive to IFITM enhancement. This also suggests that even in the presence of TMPRSS2, the MMP pathway can be used for viral entry.

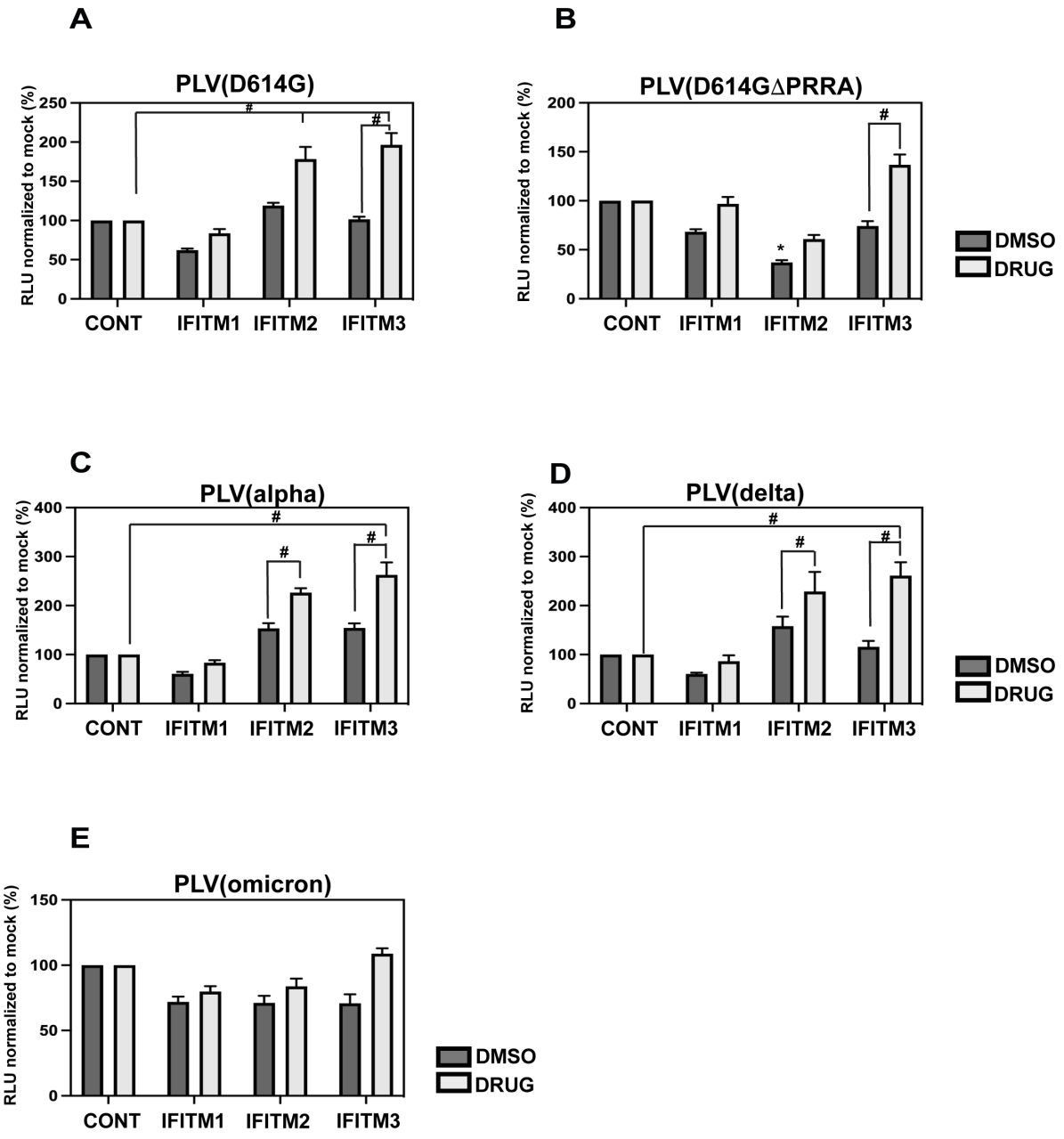

Figure 5.2.6. Inhibition of MMP2/MMP9 protease in A549-ACE2-TMPRSS2 IFITM cells confers enhancement by IFITM2 and IFITM3 to D614G, alpha and delta. A-E) A549-ACE2-TMPRSS2-IFITM cells pre-treated with 20μM of MMP2/MMP9 inhibitor II for 1 hour prior to infection with PLVs and infection quantified 48 hours later by luciferase activity. #=P>0.05 indicating statistical significance between different IFITM conditions determined by ANOVA. N=3, Mean±SEM shown.

5.2.4 Overexpression of M during PLV production results in increased S1/S2 processing in a cytoplasmic tail-dependent manner

Generation of SARS-CoV-2 PLVs usually only utilises the spike protein, despite the fact that in native virions coronaviruses lipid bilayers also contain M and E. M and E interact with spike during native viral assembly, and it has been reported that M and E induce specific maturation of N-linked glycans in spike [170, 230]. Analysis of SARS-CoV-1 M has found there are two functionally distinct forms of M when producing virus-like particles of just the coronavirus structural proteins [364]. Formation of a particle with uniform curvature and a rigid membrane is associated with one of these forms of M (M_{LONG}) rather than the other, and interestingly also associated with spike incorporation and clustering [364]. Additionally, coronavirus M proteins have previously been reported to interact with each other which can exclude host proteins from the viral envelope [230]. Until now, we had observed IFITM3 mediated enhancement of alpha entry, and enhancement of CoV PLV entry when IFITMs 1 and 2 were mislocalised. Separately, the clustering of HIV-1 Env has been found to be important for HIV-1 infectivity [294]. The mechanism of IFITM enhancement for OC43 and SARS-CoV-2 has not yet been elucidated and given that a link between M and altered VLP properties has been found, I wanted to test whether overexpression of M had any impact on the effects of IFITMs on SARS-CoV-2 entry. To test this, 293T17s expressing the Wuhan M protein C-terminally tagged with a strep ii tag were generated and expression of M confirmed (Figure 5.2.7 A).

To confirm whether overexpression of M resulted in incorporation into PLVs, D614G PLVs were generated in 293T17s, or in 293T17s stably overexpressing M and supernatant purified and Western blotted for spike, gag and strep tag ii. Indeed, M was incorporated into PLVs (5.2.7 B). Interestingly, the proportion of S2 on the D614G-M particles was approximately 2-fold higher (quantified in 5.2.7 C) than in the D614G PLVs without M, despite a similar expression of M in the cell lysates. It has been suggested that the cytoplasmic tail of spike interacts with M and that this retains spike in the ERGIC compartment [170]. To test whether the D614GΔCT spike, which lacks the ERRS, is altered in the quantity of spike on the particle, these PLVs were also

generated in 293T-17-M cells and S1/S2 processing quantified. D614GΔCT spike was increased relative to full length D614G spike on the PLVs as previously found. However, there did not appear to be any differences in spike incorporation in the presence or absence of M (Figure 5.2.7 C). This is consistent with M interacting with the cytoplasmic tail of spike and suggests that the increased incorporation of spike in 293T17s stably overexpressing M is due to a direct interaction between spike and M. However, the lack of increased spike incorporation in the +M condition for the D614GΔCT spike could also be an artefact due to the amount of spike incorporated onto a ΔCT PLV already being at the maximal incorporation.

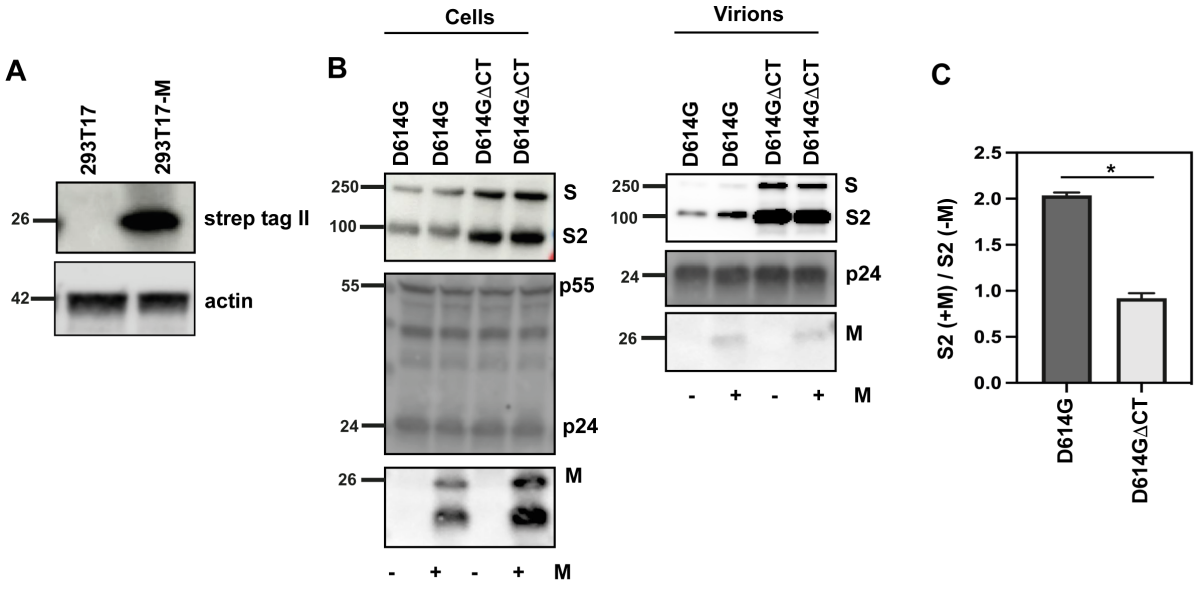

Figure 5.2.7. Overexpression of M in 293T17s when producing D614G PLVs results in increased S1/S2 processing in a cytoplasmic tail dependent manner. A) Representative immunoblot of 293T17 and 293T17 cells stably overexpressing the Wuhan M C-terminally tagged with strep tag ii blotted for actin and the strep tag II of M. B) Representative immunoblot of PLVs generated in 293T17s (-M) or in 293T17s stably overexpressing Wuhan M (+M). Supernatant was purified through a 20% sucrose cushion prior to lysis. C) Quantification of S2 (293T17-M) over S2 (293T17). *=P>0.05 indicating statistical significance between D614G and D614GΔCT S2 quantification.

5.2.5 Overexpression of M during PLV production results in IFITM3 enhancement

Next, having confirmed that overexpression of M results in M incorporation and may also impact on spike properties in a cytoplasmic tail dependent manner, whether this affect viral titre and IFITM sensitivity was next tested. PLVs of Wuhan, D614G, alpha, beta, gamma, delta, omicron (BA.1) and the pangolin Guangdong (GD), were produced in 293T17 or 293T17-M cells and used to infect A549-ACE2 cells. There was no noticeable effect on baseline infectivity when PLVs were produced in the presence of M (Figure 5.2.8). However, when these PLVs were used to infect A549-ACE2-IFITM cells as before, all PLVs demonstrated a statistically significant increase in IFITM3 enhancement when produced in the presence of M (Figure 5.2.9). This ranged from 2-3-fold, with the pangolin and omicron PLVs showing the least IFITM3 enhancement in the presence of M. Additionally, the alpha variant which is already enhanced by IFITM3 only showed a small increase in IFITM3 enhancement. There was little impact of M on IFITM1 sensitivity, and only a small decrease in IFITM2 sensitivity for some of the PLVs. Overall, this suggests that the overexpression of M in the producing cell can affect PLV biology in some way that confers IFITM3 enhancement to PLVs that were previously not enhanced by IFITM3 in TMPRSS2-negative cells. Whether this alters IFITM3 enhancement in the context of TMPRSS2-positive cells remains to be tested.

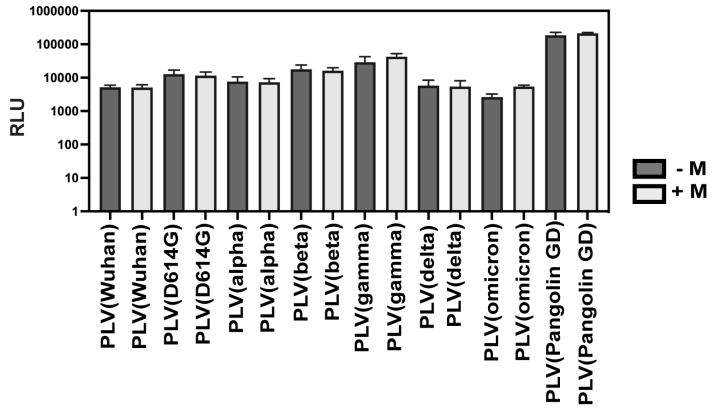

Figure 5.2.8. Producing PLVs in the presence of M does not significantly alter infectivity. PLVs produced in 293T17s (-M) or 293T17s stably overexpressing M (+M) were used to infect A549-ACE2s and infection measured by luciferase activity 48 hours later. Infection is plotted as RLUs with background subtracted. GD= Guangdong. N=3, Mean±SEM shown.

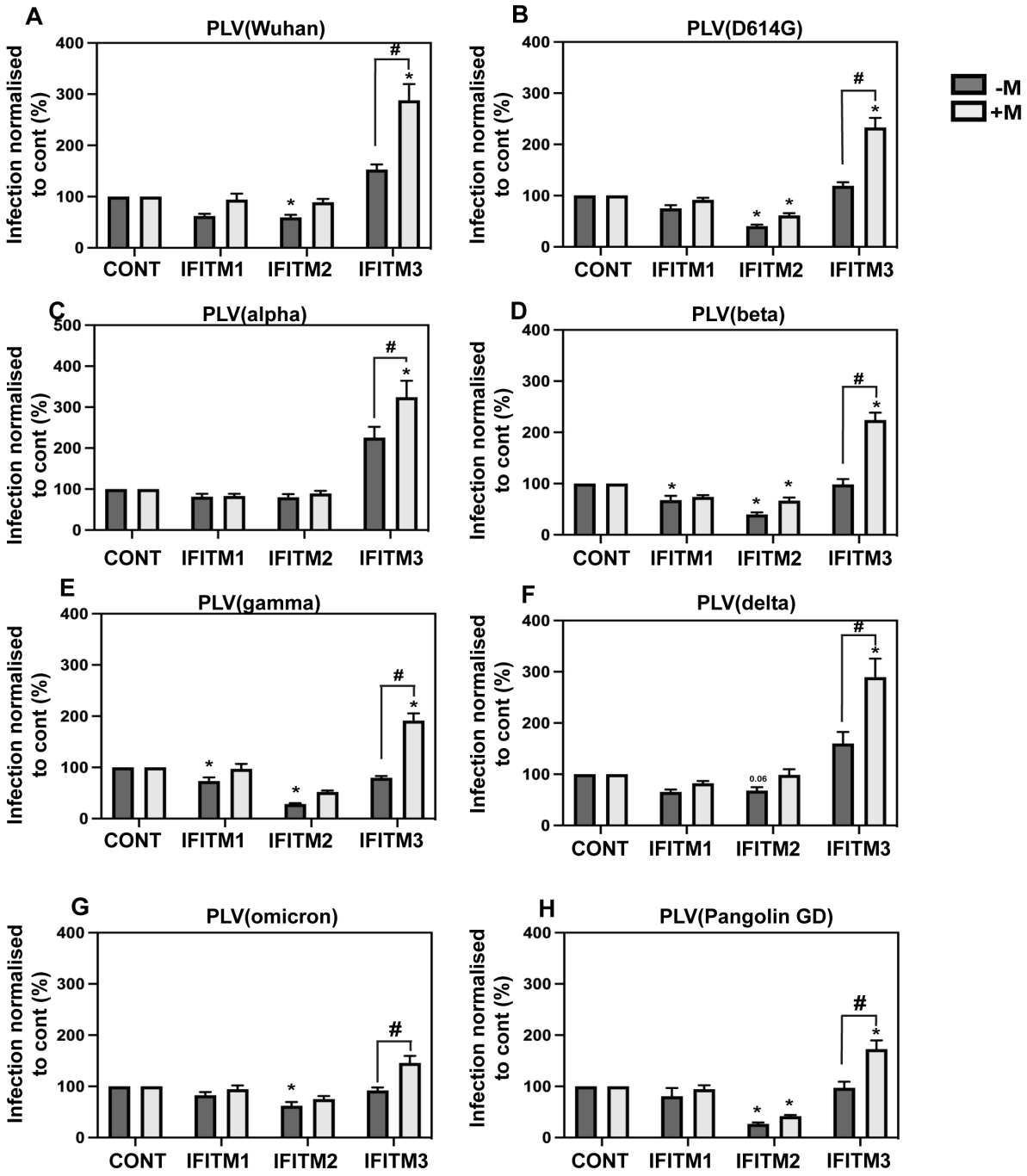

Figure 5.2.9. PLVs produced in M overexpression cells are enhanced by IFITM3. A, B, C, D, E, F, G, H) PLVs were generated in 293T17s (-M) or in 293T17s stably overexpressing Wuhan M C-terminally tagged with a strep tag II (+M) and were used to infect A549-ACE2-IFITM cells and infection quantified by luciferase activity 48 hours later. Infection is normalised to empty control for PLV or PLV-M. GD=Guangdong. †=P>0.05 and indicate statistical significance between PLV and PLV-M for IFITM3 determined by ANOVA. N=3, Mean±SEM shown.

5.2.6 Overexpression of M during PLV production does not alter E64d sensitivity

Having established that M overexpression alters IFITM3 enhancement whether this altered cathepsin-dependence was next tested. Given that there is a correlation broadly between E64d sensitivity and IFITM2 sensitivity (Figure 4.2.10), we hypothesised that perhaps there was also a link between IFITM3 enhancement and route of viral entry. To test this, A549-ACE2 cells were pre-treated with E64d prior to infection with -/+ M PLVs as before (Figure 5.2.10). Surprisingly, given the slight reduction in IFITM2 sensitivity for some of the spikes tested and significant IFITM3 enhancement, there was no statistically significant difference in cathepsin-dependence of -M or +M PLVs following E64d treatment. This implies that although there is a correlation between IFITM2 sensitivity and E64d sensitivity, E64d sensitivity does not appear to be linked to IFITM3 enhancement. Nevertheless, with further study this may assist in understanding the determinants of IFITM3 enhancement.

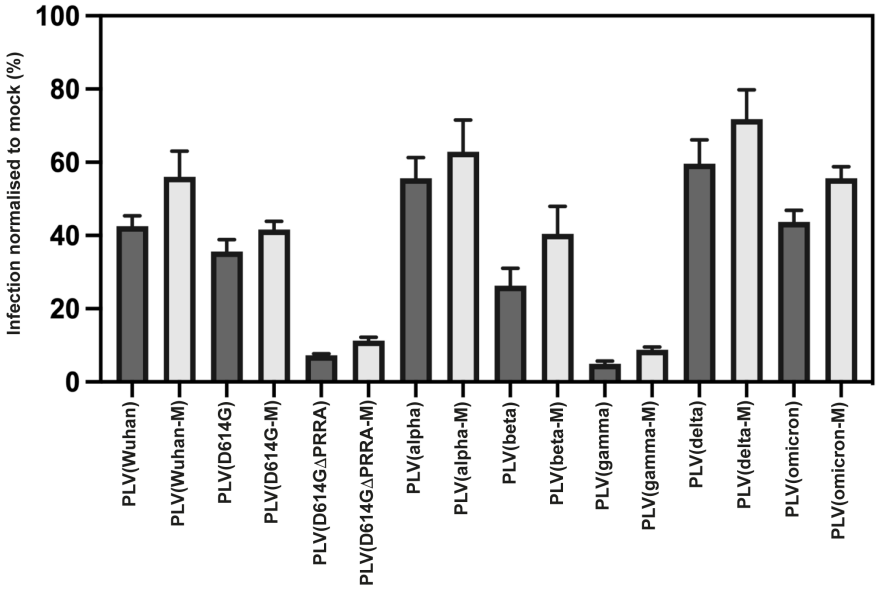

Figure 5.2.10. PLVs produced in M overexpression cells do not display altered dependence on cathepsin-mediated entry. A) PLVs were generated in 293T17s (-M) or in 293T17s stably overexpressing Wuhan M C-terminally tagged with a strep tag II (+M). PLVs were used to infect A549-ACE2 that had been pre-treated with 10μM E64d prior to infection. Infection was quantified 48 hours by luciferase activity. Infection is plotted as percentage of infection in the DMSO control for each PLV. N=3, Mean+/-SEM.

5.3 Discussion

In this chapter I explore the role of TMPRSS2 in altering IFITM sensitivity and demonstrate that TMPRSS2 can overcome IFITM-mediated restriction to a certain extent. For Wuhan PLVs, TMPRSS2 overexpression can overcome inhibition by IFITMs 1 and 2. For D614G, TMPRSS2 overexpression overcomes IFITM2 restriction but actually confers IFITM1 restriction. TMPRSS2 overexpression however cannot overcome the IFITM2 sensitivity of the ΔPRRA mutant. This further demonstrates the role of the polybasic cleavage site in evading IFITM restriction and could suggest that the presence of the polybasic cleavage site is an important adaptation to escape restriction by IFITM2. It has been suggested that TMPRSS2 can also accelerate syncytia formation, suggesting that the adaptation to utilise TMPRSS2 has multiple roles for escaping innate and adaptive immunity [76]. While TMPRSS2 can alter the effects of IFITM2/3 for D614G, alpha and delta, TMPRSS2 overexpression cannot overcome the IFITM sensitivity of omicron, again furthering the evidence that omicron has adapted away from TMPRSS2 usage and perhaps represents a trade-off between escaping adaptive immunity at the cost of being more sensitive to innate immunity.

In a previous chapter, I showed that Wuhan was partially IFITM1 sensitive, while D614G loses almost all IFITM1 sensitivity in A549-ACE2 cells. The fact that Wuhan loses IFITM1 sensitivity in the context of TMPRSS2, but that D614G now becomes IFITM1 sensitive, suggests that even the D614G mutation confers a subtle change in viral entry, and perhaps a trade-off in terms of IFITM1 sensitivity versus RBD conformation and fusion efficiency [179]. The delta variant shows some IFITM1 and IFITM2 sensitivity in A549-ACE2s, however TMPRSS2 overexpression results in the delta variant losing IFITM2 sensitivity. The moderate IFITM1 sensitivity of the delta variant when the D614G spike was previously resistant again indicates the context-dependency of other mutations in spike, suggesting other mutations in delta mask the IFITM1 resistance of the D614G mutation. Further to this, despite previously showing that the P681H mutation can reduce cathepsin-dependence in either A549-ACE2 or A549-ACE2-TMPRSS2 cells, omicron is similarly cathepsin-dependent in both, suggesting that other mutations can mask the effect of P681H. It has been suggested that the H655Y mutation is a key determinant in omicron's endosomal entry

preference, a mutation which is shared with the gamma spike which is very E64d sensitive [203].

The role of TMPRSS2 in determining the restrictive capacity of IFITMs 2 and 3 may partially explain some of the discrepancies in the literature regarding IFITM restriction of SARS-CoV-2. It has been reported that in Calu-3 and Caco-2 cells, which both express high levels of TMPRSS2, that IFITMs 2 and 3 do not restrict SARS-CoV-2 spike or variants thereof, but can even enhance infection [94, 335]. This is consistent with the data presented here showing that in A549-ACE2-TMPRSS2 cells, only IFITM1 can restrict D614G, alpha and delta, whilst IFITM2 and IFITM3 do not inhibit infectivity. Meanwhile, in A549-ACE2 cells without TMPRSS2, IFITM2 does restrict all variants except alpha. The interplay between TMPRSS2 and IFITMs highlights the need to study IFITM-mediated restriction in multiple cell types and to acknowledge cell-type dependent effects. The lung epithelium is not homogenous and TMPRSS2 expression is not constant across the varying cell types in the airways [365]. Additionally, the emergence of VOCs which are less reliant on TMPRSS2-mediated viral entry, such as the omicron variants, highlights the need to study antiviral proteins in the context of TMPRSS2-negative cells as well as TMPRSS2-positive cells. Moreover, multiple serine proteases including TMPRSS11D and TMPRSS13 have been shown to be able to mediate spike cleavage and whether these TMPRSS proteins have the same impact on IFITM sensitivity remains to be examined [127].

IFITMs 2 and 3 cycle through the plasma membrane despite their predominant retention on endosomal membranes. As SARS-CoV-2 can mediate membrane fusion at both the plasma and endosomal membranes, understanding differential properties of IFITMs at the plasma membrane is therefore of importance. Additionally, the rs12252c SNP in IFITM3, which results in an N-terminally truncated version, has been found in patients and tentatively linked to COVID-19 severity [79] [82]. Here, I show that mutations in IFITMs that affect their localisation have differential effects on IFITMs in viral entry in TMPRSS2-negative and TMPRSS2-positive cells. The IFITM1Δ117-125 mutant does not inhibit SARS-CoV-2 PLVs in the presence or absence of TMPRSS2, and is the only mutant to reduce the antiviral effects of the IFITM in both TMPRSS2-negative and TMPRSS2-positive cells. This mutation also results in

significant enhancement of entry for the D614G, alpha and delta PLVs. I also show that the Y19F IFITM2 mutation rescues Wuhan, D614G, and delta from restriction in TMPRSS2- cells. Additionally, this mutant results in 3-6-fold enhancement for Wuhan, D614G, alpha and delta. In the context of TMPRSS2 however, the IFITM2 Y19F mutant restricts D614G, D614GΔPRRA, delta and omicron. Alpha exhibits the least restriction by Y19F. This suggests that when the TMPRSS2 pathway is available and IFITM2 is at the plasma membrane, this can now restrict viral entry. This furthers the evidence for IFITM2 sensitivity and resistance simply being a function of access to IFITM2-containing compartments. However, it is surprising that this mutant still restricts D614GΔPRRA and omicron, which do not utilise TMPRSS2 for S2' cleavage. It could be that some IFITM2 Y19F is still cycling through endosomes and sufficient to still restrict these spikes. Additionally, it could be that Y19F is still recruited to the endocytic pits that D614GΔPRRA and omicron bypass the plasma membrane via.

It is worth noting that the omicron variant is still IFITM restricted even in the presence of TMPRSS2, unlike the other spikes tested where IFITM2 sensitivity can be rescued by TMPRSS2 overexpression. Additionally, IFITM mutants such as IFITM1Δ117-125 and IFITM2 Y19F which enhance the other VOCs tested, cannot enhance the omicron variant. This suggests there is something fundamentally different about the omicron spike which warrants further investigation, especially considering the dominance of the omicron subvariants globally as of summer 2022. Which regions of the omicron spike determine its IFITM sensitivity remain to be elucidated. The effects of mutations in the S2 domain of spike have not been tested here, however given the effects some of these mutations can have on spike conformation, it is possible that investigating these mutations could assist understanding what is different about omicron.

In this chapter I also explore how the overexpression of M in PLV production can result in IFITM3 enhancement. This is concordant with an increase in S1/S2 processing on the virion for the D614G spike, however whether this is the case for all of the VOC spikes remains to be tested. Additionally, increased S1/S2 processing in 293T17-M produced PLVs may not be the direct cause of IFITM3 enhancement. As M is present in the native virus, yet the native virus of alpha phenocopies spike only PLVs, this suggests that M itself is not the determinant of IFITM3 enhancement. Additionally, England-02 and D614G were certainly not IFITM3 enhanced when native virus was

tested on IFITM overexpression cells in the previous chapter, yet become IFITM3 enhanced when M is overexpressed in PLV production. However, the M protein may not function in the same when overexpressed alone in 293T-17s as it does during native viral infection. Whether the amount of M present in the 293T-17 overexpression cells used here is similar to that of an infected Vero-E6-TMPRSS2 cell, and whether this results in a similar amount of M incorporation, was not established here and remains to be tested. Nevertheless, overexpression of M in this system appears to have effects on spike that result in IFITM3 enhancement and further investigation of this may assist in shedding light on the mechanism behind IFITM3 enhancement of SARS-CoV-2. It would be interesting to investigate if M impacts IFITM phenotypes at all in the context of TMPRSS2+ cells, as TMPRSS2 overexpression appears to reduce the magnitude of IFITM enhancement. Additionally, whether co-expression of E, or expression of E alone, sheds any light on the IFITM3 enhancement phenotype has not yet been tested. Several mutations in M have been documented in the kappa, delta and omicron variants. As M-targeted antibodies are directed against the N-terminal of M, it is possible that two of the mutations in the M of the omicron variant are antibody escape mutations [137]. However, the kappa, delta, and omicron variants all have M mutations in the transmembrane region of M, and whether this has any implications on viral biology has not yet been tested.

Chapter 6: The V1/V2 loop regulates IFITM sensitivity in a closely related pair of HIV-1 Envs

6.1 Introduction

The speed and mutation-prone nature of HIV-1 replication results in many viral quasispecies of HIV-1 being present in a single patient [316]. These quasispecies can vary immensely in the Env protein due to the competing selective pressures of escape from humoral and innate immunity. HIV-1 transmission however is a relatively inefficient process with 80% of heterosexual and 60% of MSM sexual transmissions being established by just one HIV-1 virion [325]. This implies that there are significant constraints on which HIV-1 virions can successfully transmit, or which HIV-1 virions get rapidly selected for in the new host, and it has previously been demonstrated that evading the antiviral consequences of type I IFNs is a major factor in HIV-1 transmission. Specifically, whether HIV-1 is type I IFN resistant has been shown to be the key determinant of whether an HIV-1 quasispecies can transmit to another host [27]. Our lab has previously demonstrated that one of the IFN-mediated constraints on the HIV-1 Env is evasion of IFITM proteins. Transmitted/founder Envs (T/Fs) have been found to be more resistant to restriction by IFITM1, IFITM2, and IFITM3 than Envs constructed from six-month consensus sequences [67]. By reverting the nAb escape mutations in the 6 month Envs, the IFITM sensitivity could be rescued, suggesting that escape from neutralising antibodies became the driving selection pressure in chronic infection [67]. Furthermore, Envs from acute and chronic infection differ in their IFITM3 sensitivity with T/F Envs being resistant to IFITM3, and Envs from chronic infection becoming sensitive to IFITM3 [91]. Interestingly, viruses that rebound after ART withdrawal during chronic infection have also been found to be interferon resistant, suggesting continual interplay between innate immunity and viral evolution during chronic infection [28].

Env is a dynamic structure which varies in its propensity to sample the “open” conformation prior to receptor binding and viral entry. The “open” and “closed” nature of the trimer can impact on IFN and IFITM sensitivity, with several studies suggesting that the propensity of an Env trimer to sample the open conformation of Env is linked

to its sensitivity to IFITM3 [91, 333]. Additionally, adopting the more closed conformation of Env may be an escape from ADCC-mediated inhibition, as exposure of ADCC epitopes requires the transition from the unliganded closed conformation to the CD4-bound open state [292]. This suggests that there are multiple advantages and selection pressures that could confer adoption of a more closed conformation. It has also been suggested that the more IFITM3 resistant Envs are more highly processed in the producer cell, which could have knock-on effects on Env conformation and open conformation sampling [333].

Determining which regions of Env dictate IFITM resistance or sensitivity is an important question in further understanding the constraints on HIV-1 transmission, and due to their high tolerance for mutation, the hypervariable V1/V2 and V3 loops of Env are prime candidates. It has previously been suggested that the V3 loop can govern IFITM sensitivity [333]. However, mutations outside of the variable regions of Env may also contribute to determining IFITM resistance and sensitivity. For example, NL4.3 is sensitive to restriction by the IFITM1 Δ117-125 mutant which localises differently to wild-type IFITM1, but after passage in culture has been shown to obtain a mutation in gp41 that decreases its sensitivity to inhibition by this mutant [58]. Gp41 has also been implicated in determining restriction by other antiviral proteins that affect entry, with the Jolly lab demonstrating that the cytoplasmic tail of T/F Envs is key to their resistance to SERINC5 [90]. They report that deletion of the cytoplasmic tail of T/F Envs renders them more sensitive to SERINC5 restriction, again indicating that regions outside of the variable loops of Env can impact the interaction of Env with antiviral proteins.

In this chapter, the molecular determinants of HIV-1 Env resistance and sensitivity to IFITMs are investigated through the use of a panel of Envs isolated from one HIV-infected patient sequentially over nine years of chronic infection. These Envs were isolated from Patient 29/SUT036022 of the SPARTAC trial by Dr Luke Granger (Luke Granger thesis, 2019; [315], (Figure 6.1.1). 24 CCR5-tropic Envs from this patient, that were considered representative from each timepoint, were selected for the investigation of IFNα and IFITM sensitivity as PLVs. This chapter explores the IFITM

sensitivity of these 24 Envs and aims to identify which region of Env determines IFITM sensitivity and resistance.

6.2 Results

6.2.1 HIV-1 Envs derived from a chronically infected patient vary in IFITM and IFNα sensitivity

Over 80 Envs were previously isolated from the SUT036022 patient of the control arm of the SPARTAC trial by Luke Granger. The SPARTAC trial (Short Pulse Anti-Retroviral Therapy at SeroConversion trial) was a randomised controlled trial that aimed to test whether a short period of ART in the early stages of HIV-1 infection delayed the need for longer-term ART treatment [366]. As part of the control arm of the trial, plasma samples were banked longitudinally for each patient. As part of Luke Granger's thesis, 84 Env sequences were isolated from patient SUT036022 (also known as patient 29). SUT036022 was infected with a clade B virus, and samples were isolated from 9 different timepoints spanning 247 weeks: Week 3, 26, 57, 113, 142, 172, 185, 213 and 250. It should be noted that Week 3 samples are not true T/F viruses, and were isolated from approximately 10 weeks after estimated seroconversion. Amongst other patients from the trial, Dr Granger investigated resistance of PLVs bearing the Envs from patient SUT036022 to broadly neutralising antibodies and autologous serum, demonstrating that this patient followed a classic model of sequential escape to the previous autologous serum, and also documented the emergence of escape from antibodies targeting the N332 site. 24 of the SUT036022 Envs that were deemed fairly representative of each timepoint were selected for investigation of IFITM and type I IFN sensitivity (Figure 6.1.1).

To investigate the IFITM sensitivity of these Envs, U87-CD4-CCR5 cells stably expressing the individual IFITMs or empty vector control were generated and IFITM expression confirmed by Western blot (Figure 6.2.1 A). Next, PLVs bearing each Env were generated and used to infect the U87-CD4-CCR5 cells, and infectivity measured by luciferase activity 48 hours later. The infectivity in each IFITM condition was normalised to cells transduced with the empty vector control, shown as percentage of infection relative to control cells (Figure 6.2.1 B–Y). Although the Envs demonstrated

differential sensitivity to IFITMs 1, 2, and 3, interestingly there were Envs that were isolated from the same week exhibiting markedly different sensitivity to IFITMs. For example, the Envs from week 113 included two Envs that were sensitive to all 3 IFITMs (6.2.1 J, L), an Env with intermediate sensitivity (6.2.1 M) which exhibited resistance to IFITM1, and 113_S8D (6.2.1 K), which was entirely resistant to all three IFITMs. This is despite these Envs clustering closely together on the phylogenetic tree, suggesting that small differences in Env sequence can impact IFITM sensitivity. Interestingly, out of all 24 Envs assayed, only two appeared to be completely resistant to IFITM overexpression: 113_S8D (6.2.1 K) and 185_S5G (Figure 6.2.1 S). Envs 57_S9H (6.2.1 H) and 113_S8D (6.2.1 K) are highlighted in blue and red because these Envs were chosen for further analysis later in the Chapter.

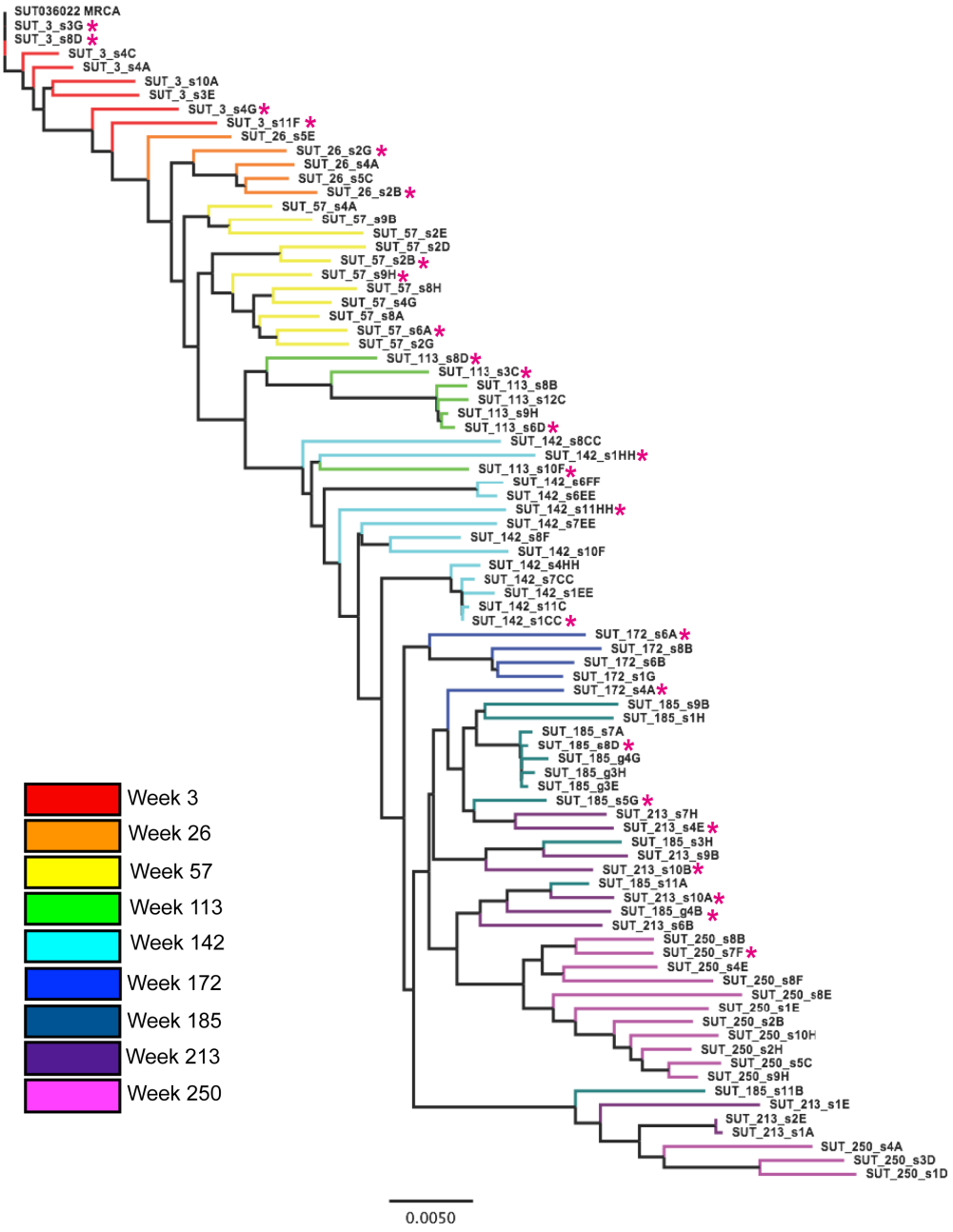

Figure 6.1.1 Phylogenetic tree of all Envs isolated from SUT036022. A rooted uncorrected pairwise distances phylogenetic tree of isolated Env orf HxB2 (6225-8795). Colours correlate to Week of sample as per the key. Week 3 refers to week number of the study, estimated to 10 weeks post seroconversion. Sequences were aligned using DNAstar MegAlign Pro running MUSCLE and rooted to the MRCA which was determined through analysis of Week 3 sample sequences. Phylogenetic tree provided by Dr Luke Granger (Luke Granger thesis, 2019). Sequences used in this chapter are highlighted with pink stars. Key specifies week of sample.

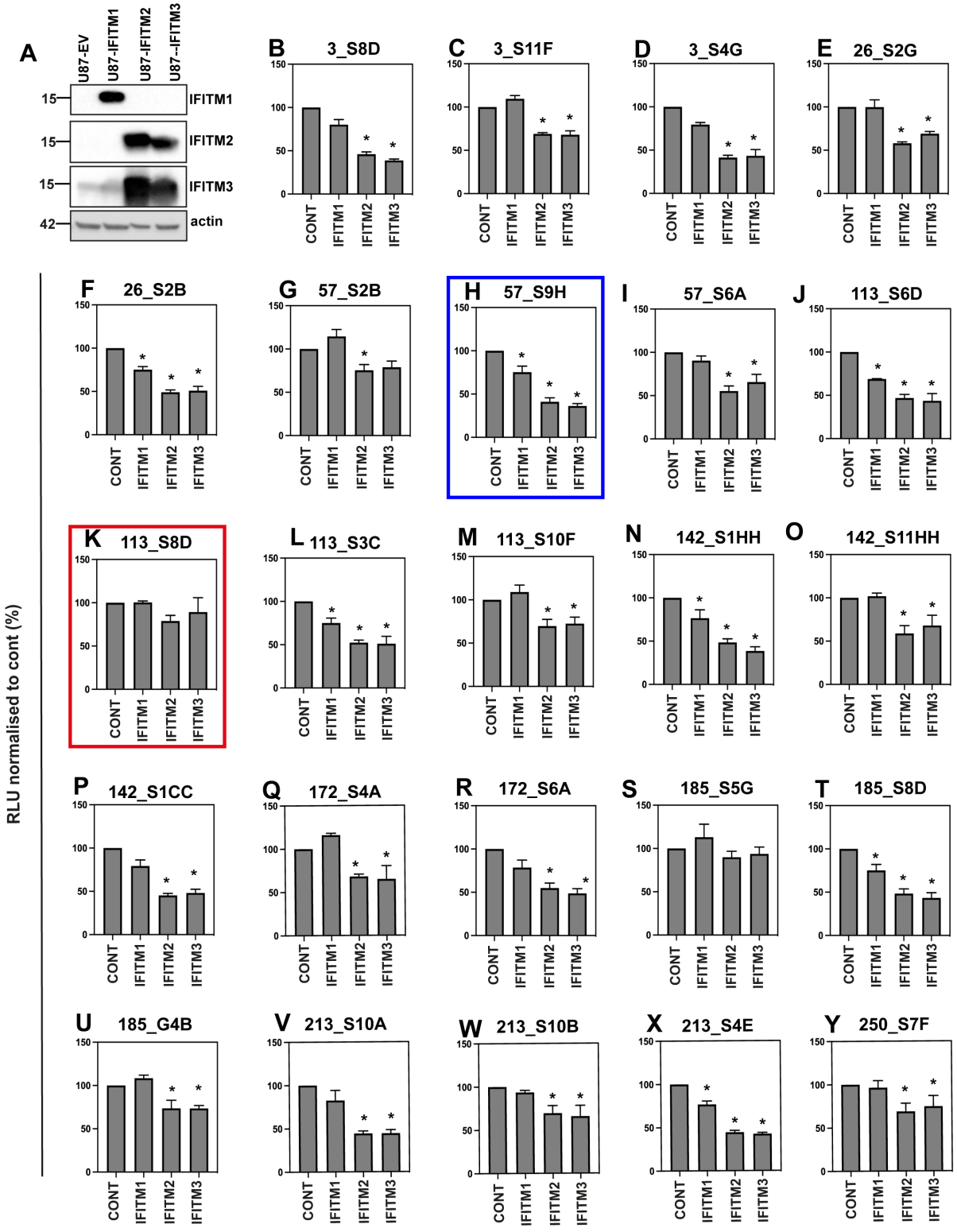

Figure 6.2.1. IFITM sensitivity of Envs from SUT036022. PLVs pseudotyped with each Env were generated in 293T-17s and used to infect U87-CD4-CCR5 stably expressing the individual IFITMs (A). Infectivity was measured by luciferase activity 48 hours later. Infection was normalised to infection levels in the empty vector control. *= P<0.05 using a two-way ANOVA indicating statistical significance between cells transduced with empty vector control and IFITM cells. 57_S9H (blue and 113_S8D (red) are highlighted as these were chosen for further analysis later. N=3, Mean+/-SEM shown.

Next, the sensitivity of the 24 Envs to IFNα was assayed to investigate whether this correlated with IFITM sensitivity, as IFITMs are upregulated by type I IFNs (Figure 6.2.2 A). U87-CD4-CCR5 were pre-treated with increasing doses of IFNα for 18 hours, IFNα removed, and infected with PLVs as before (Figure 6.2.2 B-Y). Again, there appeared to be variability in IFNα sensitivity even from the same timepoint, however to a lesser extent than observed with IFITM overexpression. IC50s were calculated for each Env and ranked in order of sensitivity to IFNα (Figure 6.2.3). This demonstrated that while the IFITM sensitivity of these Envs only varied by 2-fold when investigated by IFITM overexpression in Figure 6.2.1, the IC50 of each Env varied over a 20-fold range. This could suggest that other antiviral proteins that inhibit entry are contributing to the increased inhibition of these Envs after IFNα treatment. Additionally, as IFITMs interact with each other it is likely that IFITM-mediated inhibition is stronger following IFN-mediated upregulation rather than single IFITM overexpression.

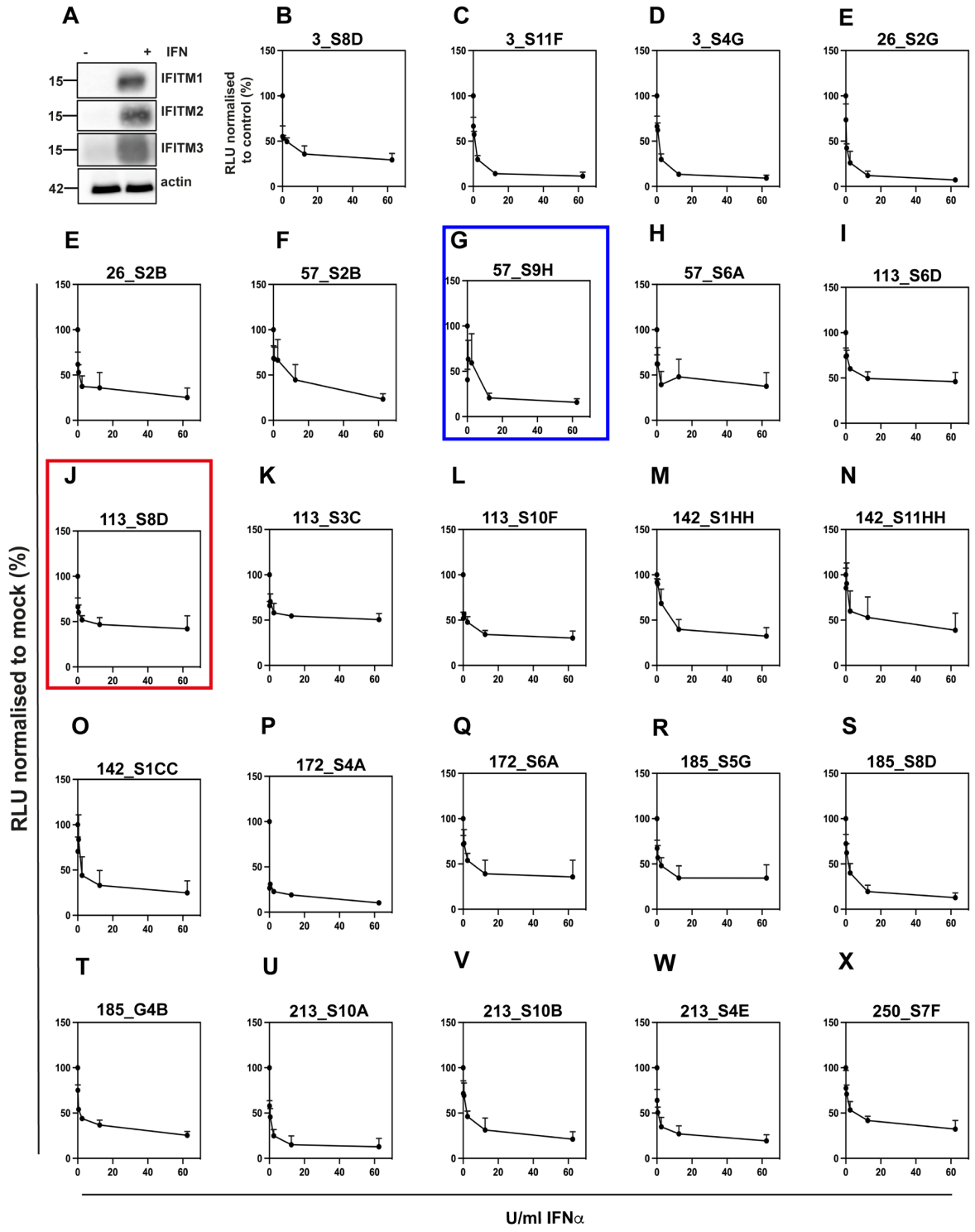

Figure 6.2.2. IFNα sensitivity of SUT036022 Envs. A) U87-CD4-CCR5 were pre-treated with increasing concentrations of IFNα for 18 hours prior to infection with PLVs. Infectivity was measured by luciferase activity 48 hours later. Infection is normalised as a percentage of infection in mock-treated cells. N=3, Mean+/-SEM shown.

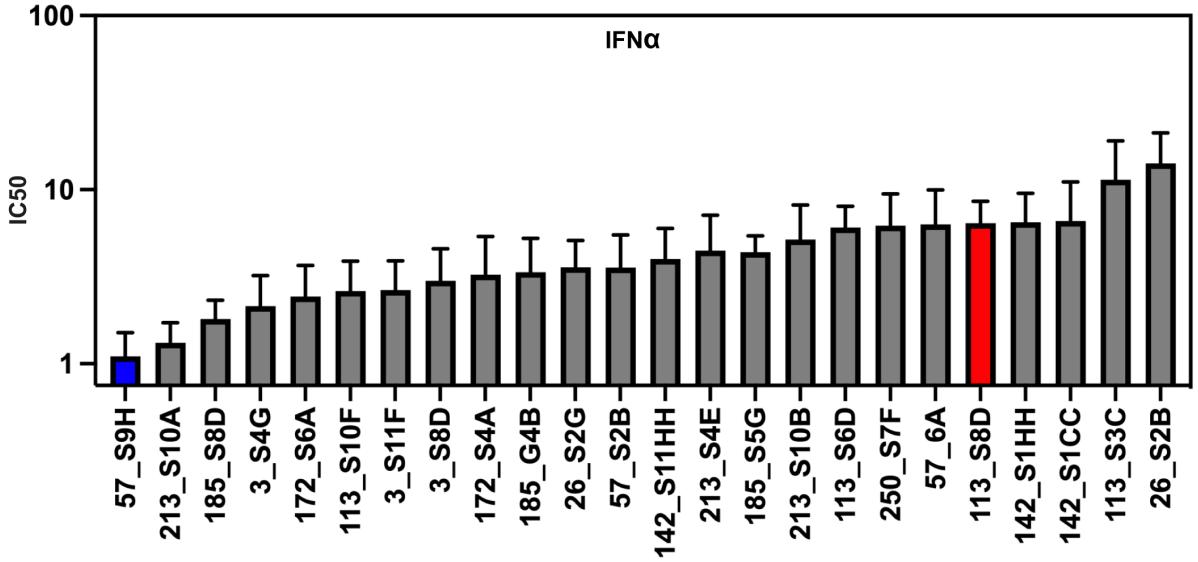

Figure 6.2.3. SUT036022 Envs ranked by IFNα IC50. A) U87-CD4-CCR5 were pre-treated with increasing concentrations of IFNα for 18 hours prior to infection with PLVs. Infectivity was measured by luciferase activity 48 hours later. IC50s were calculated in GraphPad Prism. N=3, Mean+/-SEM.

6.2.2 Envs from SUT036022 vary in cold inactivation

The propensity to adopt the open conformation has previously been linked to IFITM and IFN sensitivity of Env [333]. Therefore, it was next tested whether the Envs from patient SUT036022 varied in their sensitivity to cold inactivation. The cold inactivation assay is a surrogate for testing the open/closed conformation of Env. PLVs are incubated at 4°C on ice for different amounts of time and then frozen at -80°C. PLVs are then thawed, along with a control vial that was not subjected to cold incubation, and used to infect cells. If an Env samples the open conformation frequently, water will be able to get inside the Env which then forms ice crystals when stored at -80°C, which can crack open the Env and result in a loss of infectivity when then used to infect target cells after the second thawing. When these 24 Envs were tested, some Envs appeared essentially insensitive to even 48 hours incubation on ice, whilst others already lost 50% infectivity by 6 hours incubation (Figure 6.2.4 A-X). Again, even at the same timepoint there appeared to be little consensus on similarities between cold inactivation of the Envs tested, however cold inactivation varied over a 0-3-fold range. This could suggest differences in the propensity to sample the CD4-bound open conformation of Env.

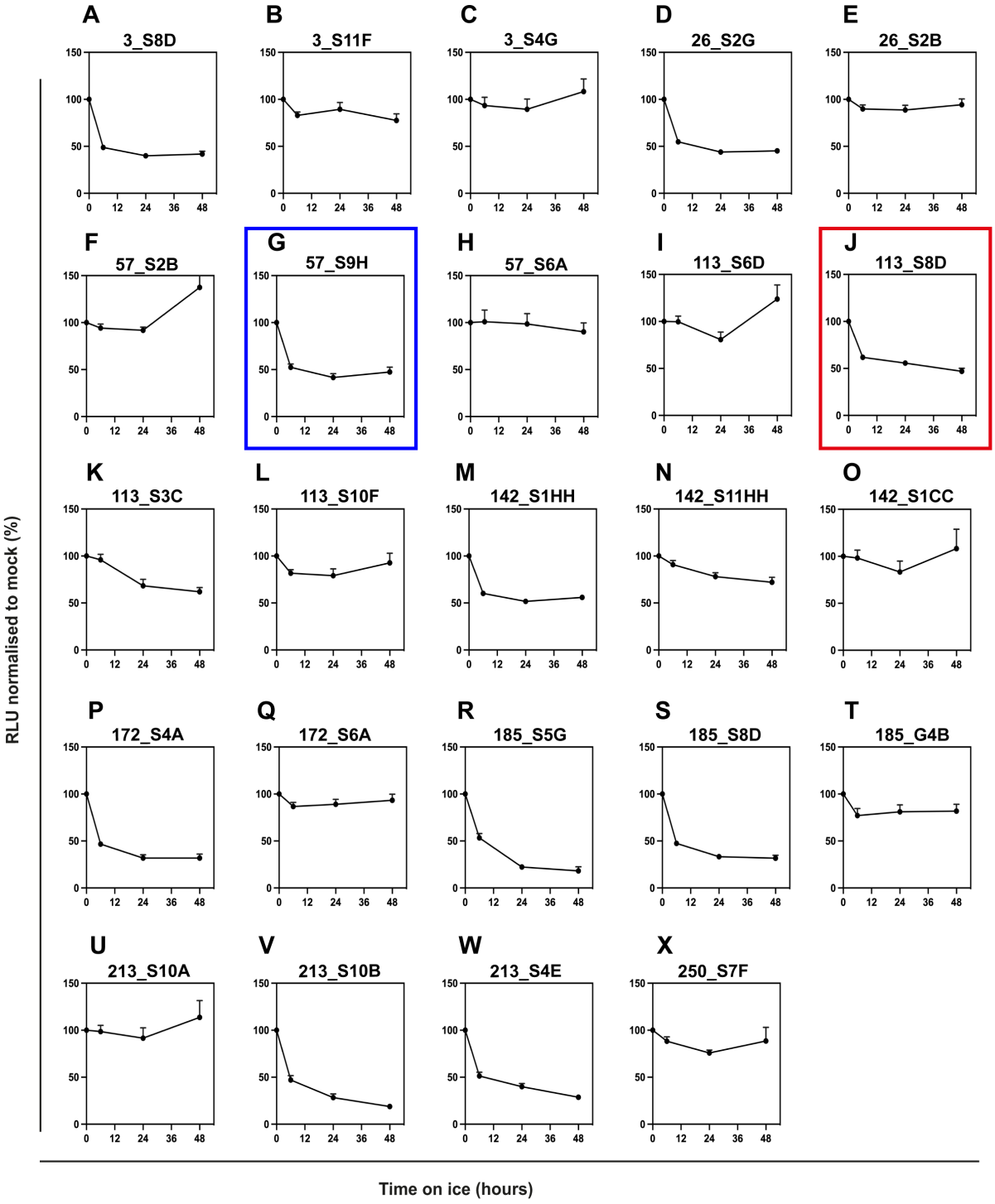

Figure 6.2.4. Cold inactivation of Envs from SUT036022 varies. A-X) PLVs were produced in 293T-17s and stored at -80ºC. PLVs were thawed and incubated at 4oC on ice for 6, 24 or 48 hours before being refrozen at -80ºC. Samples were thawed, along with an aliquot that had not been incubated on ice, and used to infect U87-CD4-CCR5 cells for 48 hours. Infectivity was measured by luciferase activity and normalised to the sample that had not been incubated on ice. N=3, Mean+/-SEM.

6.2.3 IFITM3 correlates with IFN sensitivity, however timepoint of sample or cold inactivation do not

Thus far the IFITM sensitivity, IFNα sensitivity, and the cold inactivation of the 24 Env samples from patient SUT036022 had been tested. However, the IFNα sensitivity of Envs did not appear to correlate with either the timepoint of the samples, with large variability in IC50 between Envs that were isolated in the same week and would very likely have been circulating at the same time, or cold inactivation (Figure 6.2.5 A, B).

Multiple species circulating at the same time with differing sensitivity to IFN further suggests that multiple selection pressures from not just adaptive but also innate immunity pervade during chronic infection. Additionally, the lack of correlation between IFN sensitivity and cold inactivation suggests that for these Envs at least, the propensity to sample the open conformation is not the main determinant of IFN resistance, with some Envs having high IC50s but still being sensitive to cold inactivation and vice versa. There also appeared to be no correlation between cold inactivation and IFITM3 sensitivity, with the most and least IFITM3 sensitive Envs having similar sensitivity to cold inactivation (Figure 6.2.5 C).

Interestingly, when plotting IFITM3 sensitivity against cold inactivation, Envs formed clusters that had similar sensitivity to IFITM3 and cold inactivation, with one cluster being IFITM3 and cold inactivation sensitive and a second cluster that was also IFITM3 sensitive but cold inactivation insensitive. This suggests than an open conformation can result in IFITM3 sensitivity for some Envs, but is certainly not the case for all the Envs tested here.

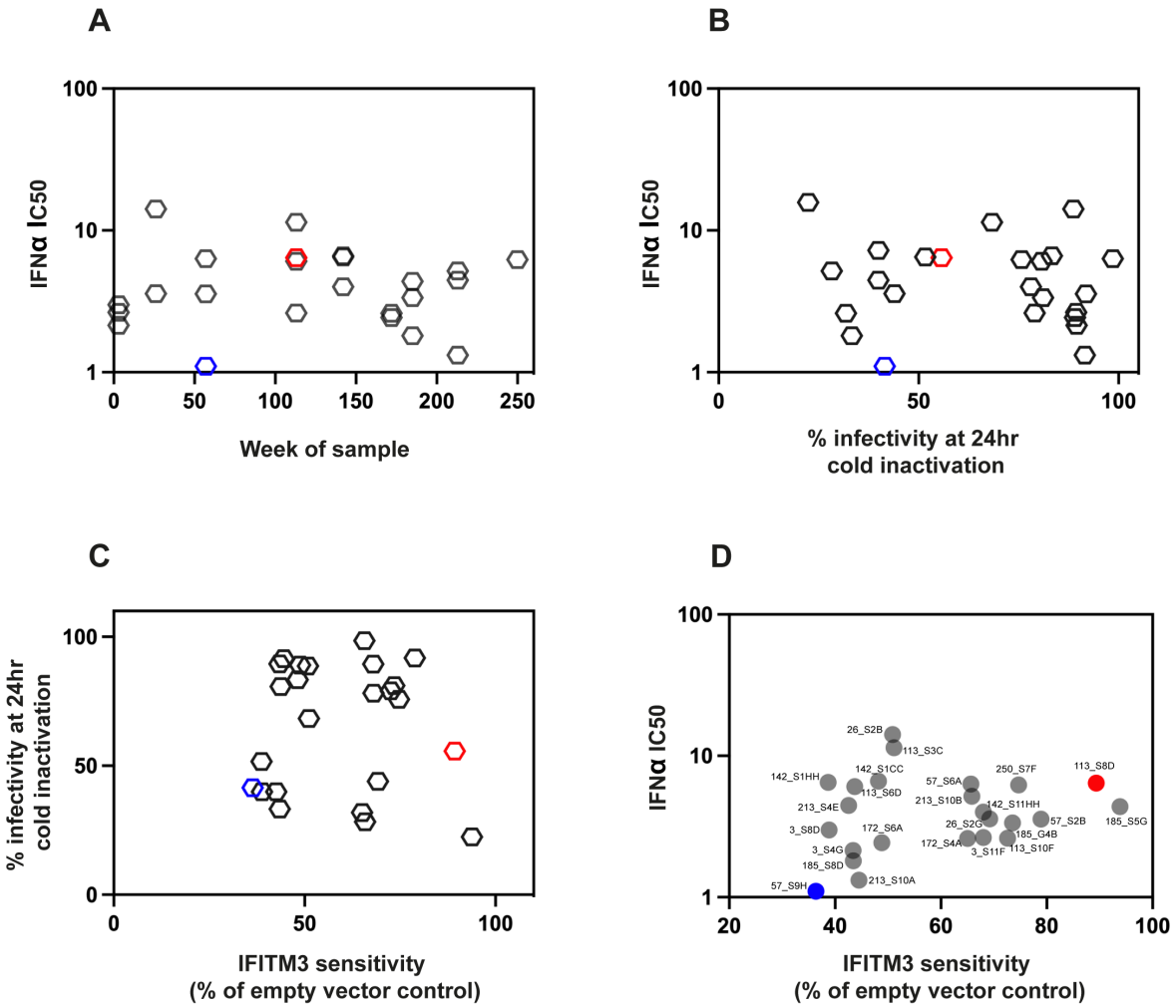

Figure 6.2.5. Timepoint and cold inactivation do not correlate with IFNα sensitivity. A) IC50 plotted against the week of sample. B) IC50 plotted against % infectivity of PLVs at 24 hours of cold inactivation. C) % infectivity at 24 hours of cold inactivation plotted against IFITM3 sensitivity (% of empty vector control). D) IC50 plotted against IFITM3 sensitivity (% of empty vector control). 57_S9H (blue) and 113_S8D (red) are highlighted. N=3, Mean+/-SEM.

Next, we wanted to investigate the determinants of IFITM sensitivity and resistance in Env utilising this set of closely related Envs. Two Envs that were the most differentially sensitive to both IFNα and IFITM3, but the most closely related, were selected (57_S9H highlighted in blue and 113_S8D highlighted in red in Figure 6.2.5 D). IFNα and IFITM3 sensitivity broadly correlated with each other, however there were some Envs that did not fit the trend, suggesting that there may be another IFN-upregulated protein active in the target cell inhibiting the entry of these Envs. Additionally, this could also be a product of the interaction of IFITMs with each other versus single IFITM overexpression.

6.2.4 57_S9H and 113_S8D are differentially processed in producer cells

To further examine which regions of Env determine relative sensitivity to IFITMs, the two Envs that were most differentially sensitive to IFNα and IFITMs but most closely related on the phylogenetic tree were selected for further characterisation. 57_S9H and 113_S8D differ in their IFNα sensitivity (Figure 6.2.6 A) and IFITM sensitivity (Figure 6.2.6 B), with 113_S8D being significantly less sensitive to all three IFITMs. This could suggest these Envs utilise distinct routes of viral entry, where 113_S8D can evade the presence of IFITMs and 57_S9H cannot.

Next, cell lysates of producer cells and purified PLVs of 57_S9H and 113_S8D PLVs were Western blotted for relative incorporation of Env to test if this was a factor in their differential IFITM sensitivity (Figure 6.2.6 C). Similar amounts of gp120 were incorporated onto both 57_S9H and 113_S8D PLVs. Interestingly however, in the producer cells 57_S9H appeared to be less efficiently processed from gp160 to gp120 than 113_S8D. Although this did not appear to affect the incorporation of gp120 into 57_S9H PLVs, this could potentially have knock on effects on Env conformation or glycosylation.

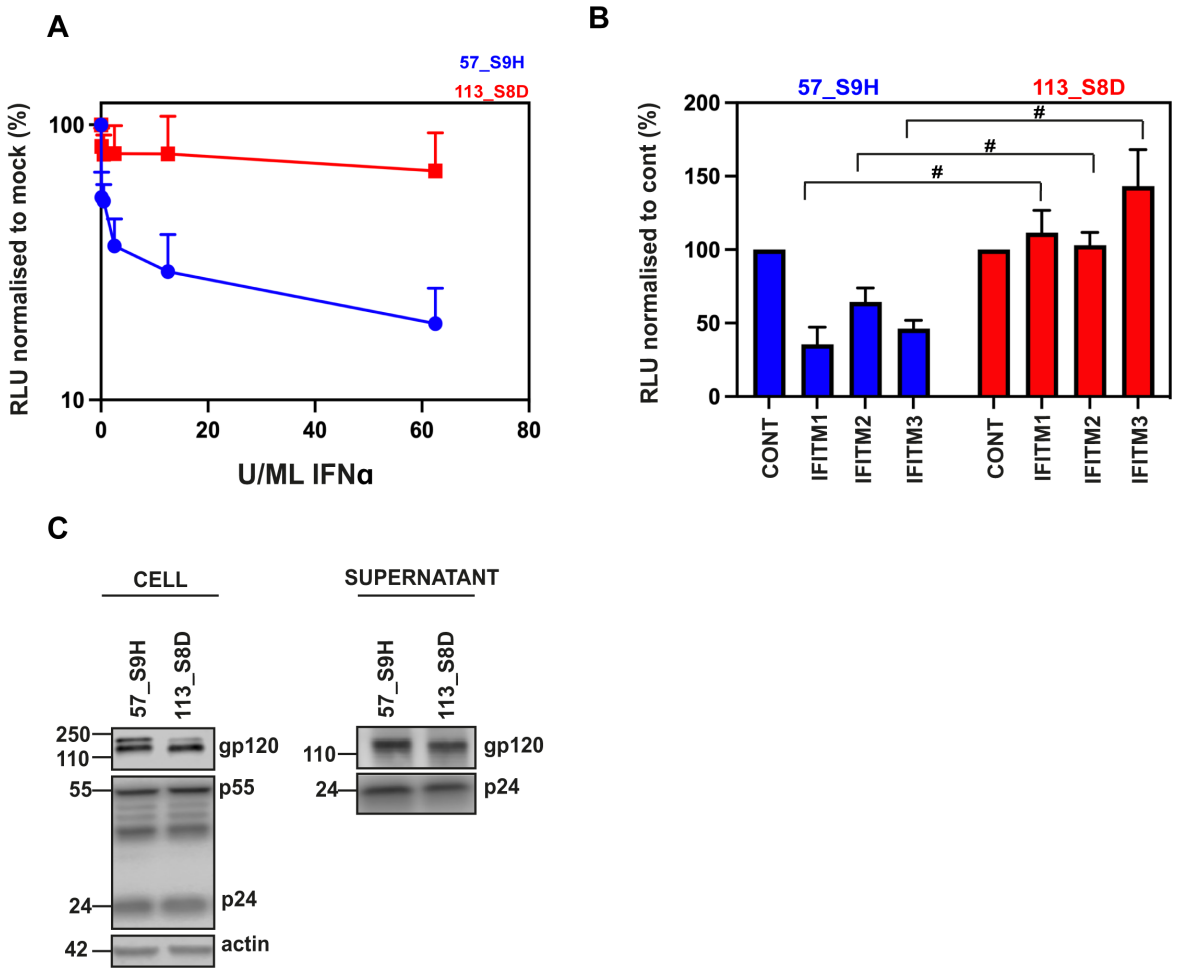

Figure 6.2.6. 57_S9H and 113_S8D have differential IFNα and IFITM sensitivity. **A**) U87-CD4-CCR5 cells were pre-treated with IFNα for 18 hours prior to infection with PLVs and infection quantified by luciferase 48 hours later. B) 57_s9H and 113_S8D PLVs were used to infect U87-CD4-CCR5-IFITM cells and infectivity measured by luciferase activity 48 hours later. #= P=>0.05 and indicate statistical significance between PLVs of the same IFITM condition determined by two-way ANOVA. C) Representative Western blot of cellular lysates and purified supernatant of 57_S9H and 113_S8D PLVs produced in 293T-17s. N=3, Mean+/-SEM shown.

6.2.5 IFITM overexpression in producer cells has a small impact on 57_S9H infectivity

It has previously been suggested that IFITMs can inhibit Env through their incorporation into viral particles in the producer cell. This has been suggested to impair viral infectivity through IFITMs directly targeting Env, and through negative imprinting due to their incorporation into particles [57-59]. To test whether IFN was having any effect in the producer cell on 57_S9H and 113_S8D, 293T-17s were treated with IFNβ 6h after transfection and these PLVs used to infect U87-CD4-CCR5 cells as before and % of infected cells measured by flow cytometry (Figure 6.2.7 A). The addition of IFNβ mildly reduced the viral infectivity of 57_S9H by 1.5-fold, however not to as great an extent as pre-treatment of the target cells with IFN. 113_S8D remained unaffected by the presence of IFNβ in the producer cells. The cell lysates were immunoblotted for IFITM1, and a significant amount of IFITM1 upregulation observed, suggesting that any diminished inhibition was not due to a lack of IFITM upregulation (Figure 6.2.7 B). Although not all 24 Envs were screened for inhibition by IFN in the producer cell, given that there was not a strong phenotype with 57_S9H and 113_S8D the effects of IFN and IFITMs were focused upon in the target cell.

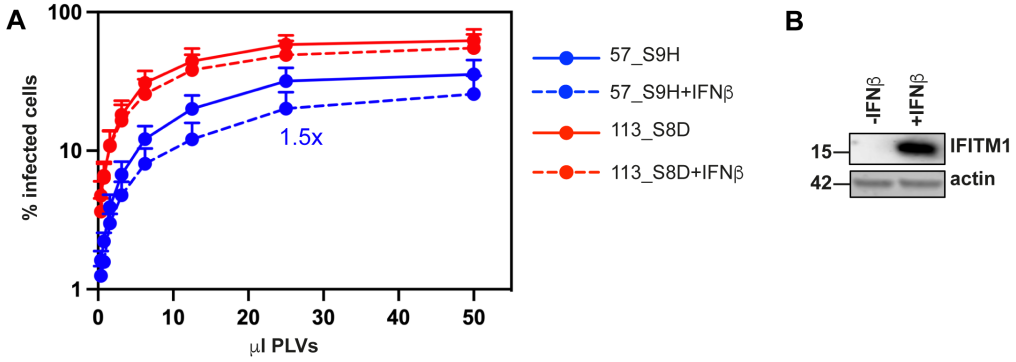

Figure 6.2.7. IFNβ added at transfection does not reduce infectivity of 57_S9H and 113_S8D. A) 500U/ML of IFNβ was added 6h after transfection of 293T-17s and infectivity of PLVs measured by flow cytometry 48 hours post infection of U87-CD4-CCR5. B) Cell lysates of the 293T-17s from A were Western blotted for IFITM1 and actin. N=3, Mean+/-SEM shown.

6.2.6 The V1/V2 loop of 57_S9H and 113_S8D confers their relative IFITM sensitivities

There are 37 amino acid differences between 57_S9H and 113_S8D in total across the V1/V2 region, V3, and gp41. To narrow down the region of interest in terms of determining IFITM phenotypes, chimeras were generated of 57_S9H containing the V1/V2 loop onwards, V3 loop onwards, the transmembrane domain onwards, or just the cytoplasmic tail of 113_S8D (Figure 6.2.8 A). PLVs of these chimeras were produced and both the cell lysates and purified supernatant Western blotted for Env (Figure 6.2.8 B). Interestingly, the decreased processing phenotype of 57_S9H was rescued by both the V1/V2-CT and V3-CT chimeras, but not the TM-CT or CT alone. This suggests that V3 loop confers the enhanced processing phenotype to 113_S8D. Next, these chimeras were tested for IFITM sensitivity as before on U87-CD4-CCR5 cells (Figure 6.2.9 A). The V1/V2-CT swap fully rescued the IFITM sensitivity of 57_S9H. The V3-CT swap did not rescue any IFITM sensitivity of 57_S9H, and both the TM-CT and CT swaps rescued IFITM2/3 sensitivity, but not IFITM1 sensitivity. This suggests that the V1/V2 loop of 113_S8D is key to its IFITM resistance. However, it appears that some properties of the cytoplasmic tail are also able to regulate IFITM 2 and 3 resistance to some degree. However, despite rescuing a degree of IFITM2 and 3 sensitivity, the TM-CT and CT only chimeras were reduced in infectivity (not shown), suggesting this came at a fitness cost for the Env.

Interestingly, the V1/V2-CT and V3-CT chimeras had differing phenotypes when tested for IFITM sensitivity and for IFN sensitivity. U87-CD4-CCR5 cells were pre-treated with IFN and infected with the chimera PLVs (Figure 6.2.9 B). The V1/V2-CT chimera rescued the IFN sensitivity of 57_S9H, suggesting this region dictates both the IFITM only and IFN resistance of 113_S8D. However, whilst the V3-CT chimera could not rescue IFITM sensitivity, this could rescue the IFN sensitivity of 57_S9H. This could suggest that the V3-CT chimera can overcome some level of IFN-upregulated antiviral proteins, however somehow cannot overcome individual IFITM-mediated restriction. Additionally, despite the TM-CT and CT chimeras being able to overcome IFITM2/3 restriction, both of these chimeras could not rescue the IFN sensitivity of 57_S9H.

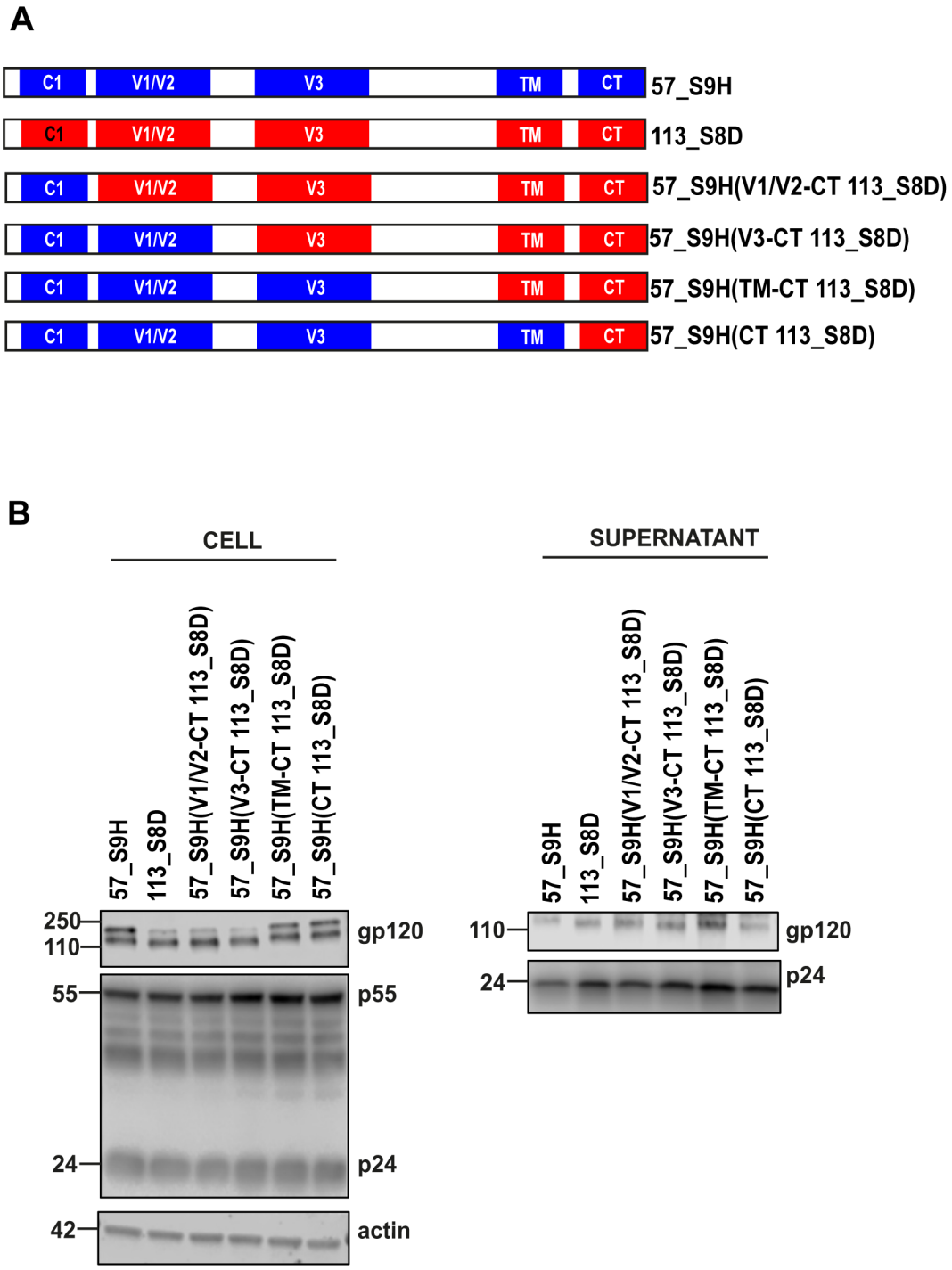

Figure 6.2.8. Chimeric Envs with the V1/V2 loop onwards of 113_S8D confer processing phenotype to 57_S9H. A) Schematic of chimeras generated of 57_S9H (blue) and 113_S8D (red). B) Representative Western blot of cell lysates and purified supernatant of PLVs as described in A produced in 293T-17s. N=3, Mean+/-SEM.

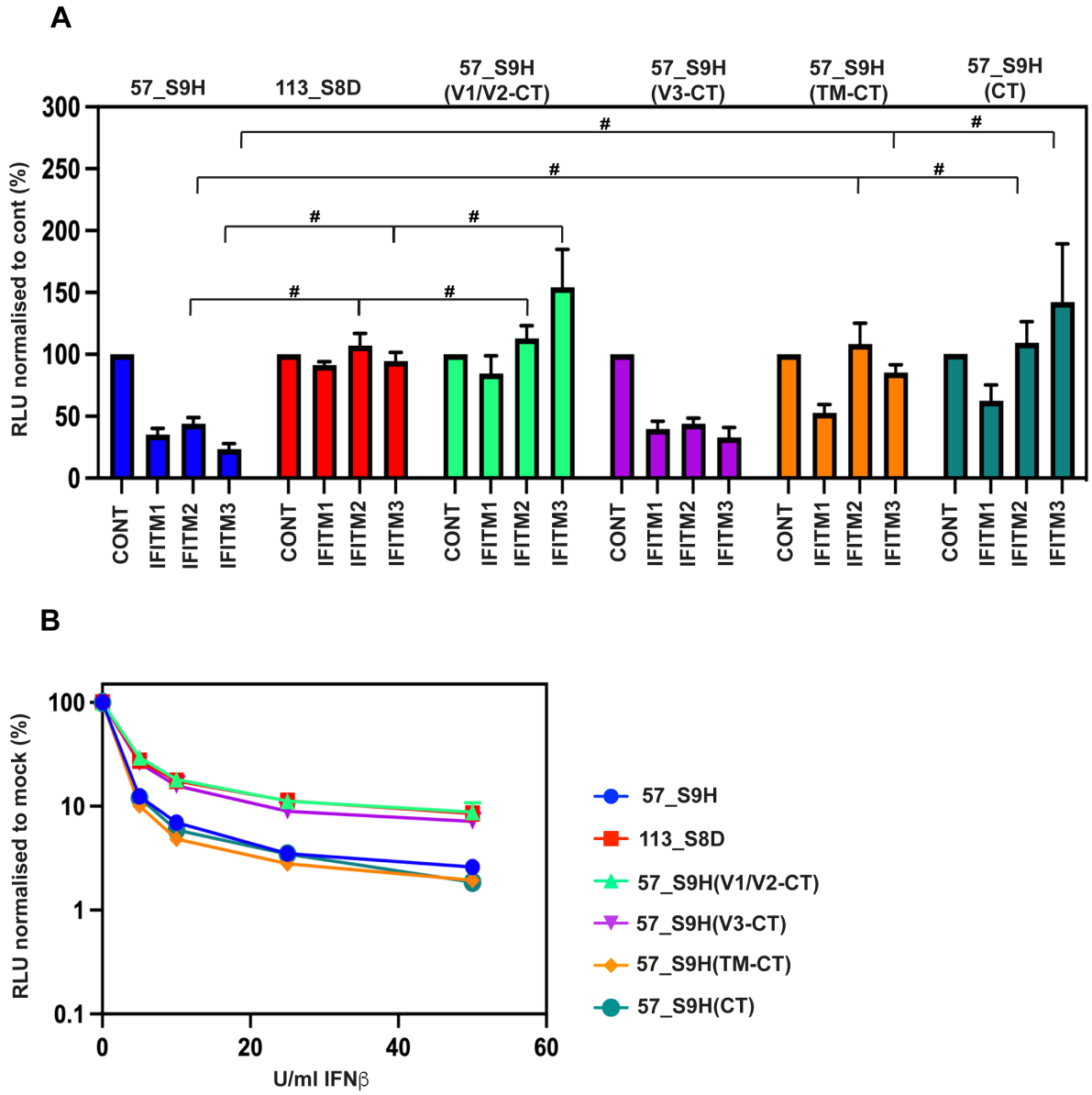

Figure 6.2.9. The transmembrane domain and cytoplasmic tail of 113_S8D cannot fully confer IFITM resistance to 57_S9H. A) PLVs bearing chimeric Envs were used to infect U87-CD4-CCR5-IFITM as before. #= P<0.05 using a two-way ANOVA indicating statistical significance between the PLVs for the same IFITM condition. B) U87-CD4-CCR5 cells were pre-treated with IFNβ for 18 hours and then infected with PLVs as in A. Infectivity was measured 48 hours later and normalised to mock treated cells. N=3, Mean+/-SEM.

There are six differences in the sequence of the V1/V2 loop of 57_S9H and 113_S8D (Figure 6.2.10 A), and only one in the V3 loop, the presence or absence of the N332 glycan site (Figure 6.2.10 B). 57_S9H possesses the N332, while 113_S8D has lost this potential glycan site. To ascertain whether the V1/V2 loop alone could confer IFITM resistance to 57_S9H, V1/V2 loop swaps between 57_S9H and 113_S8D were generated (Figure 6.2.10 C). As the V3-CT chimera rescued the IFN sensitivity but not IFITM sensitivity of 57_S9H, single swaps of just the V3 loop between 57_S9H and 113_S8D were also generated. This comprised of mutating just the N332 residue, to N332S in 57_S9H and S332N in 113_S8D.

These V1/V2 loop and V3 loop swaps were tested for IFITM sensitivity as before (Figure 6.2.10 D). Confirming the previous result, the V1/V2 loop of 113_S8D in the 57_S9H background was sufficient to rescue this Env and confer IFITM resistance. Conversely, the V1/V2 loop of 57_S9H into 113_S8D conferred IFITM sensitivity to the previously resistant 113_S8D. Consistent with the previous experiments, this suggests that the V1/V2 loop of 113_S8D confers its IFITM resistance, and conversely that this is also the determinant of 57_S9H's IFITM sensitivity. However, the V3 loop swaps did not confer relative IFITM sensitivity/resistance in both directions. Surprisingly, the V3 loop of 113_S8D into 57_S9H did rescue IFITM sensitivity and make 57_S9H resistant to IFITMs. However, the reciprocal swap did not confer IFITM sensitivity to 113_S8D. This suggests that, consistent with the literature, the V3 loop can govern IFITM sensitivity, but in a context-specific manner. In this pair of Envs however, the V1/V2 domain appears to be the main determinant of IFITM sensitivity and resistance.

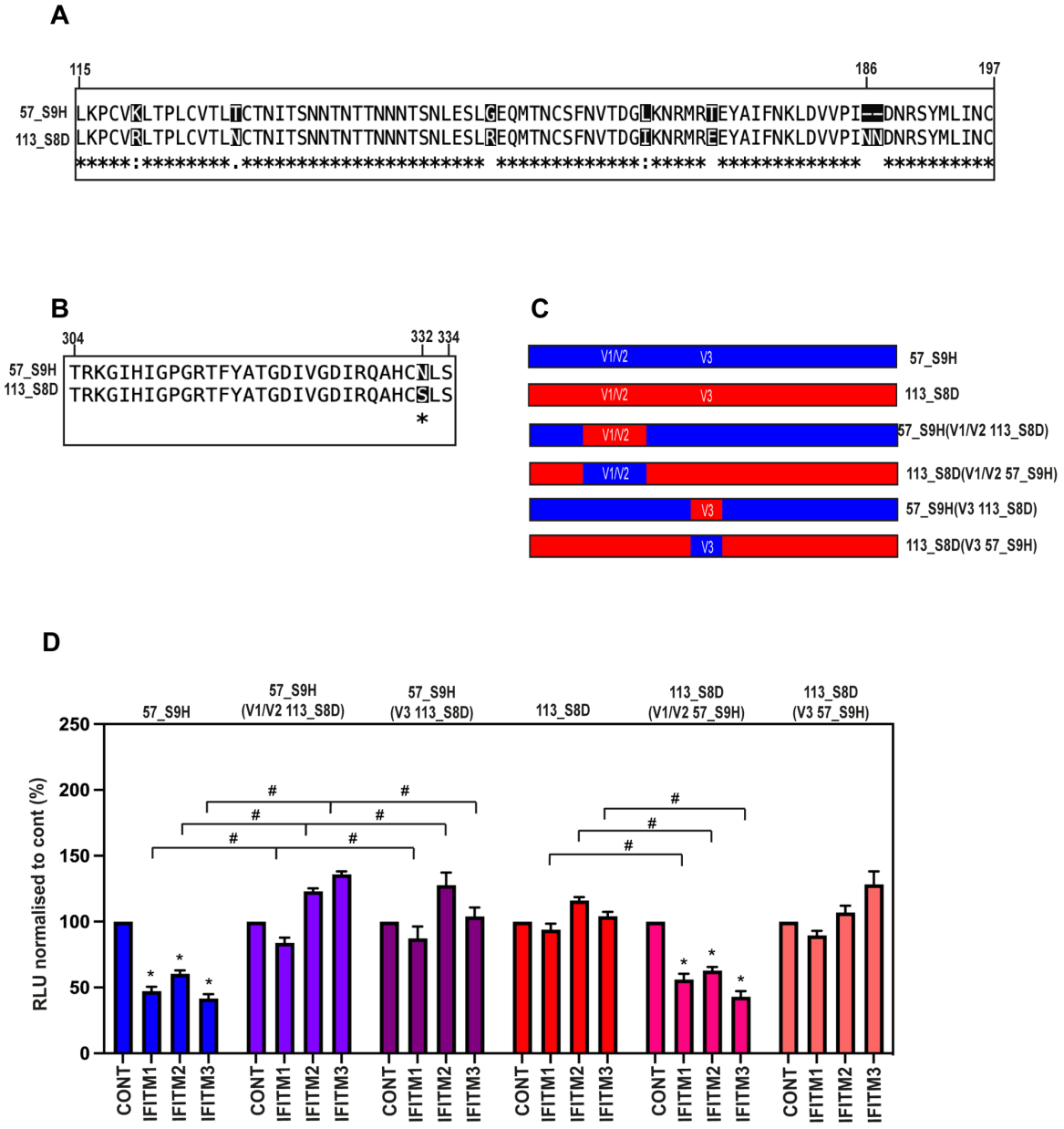

Figure 6.2.10. The V1/V2 loop confers IFITM resistance and sensitivity for 57_S9H and 113_S8D. A) Alignment of the V1/V2 loop of 57_S9H and 113_S8D, numbered according to HxB2. B) Alignment of the V3 loop of 57_S9H and 113_S8D, numbered according to HxB2. C) Schematic describing V1/V2 and V3 loop swaps between 57_S9H (blue) and 113_S8D (red). D) 57_S9H, 113_S8D andV1/V2 loop and V3 loop swap PLVs were used to infect U87-CD4-CCR5-IFITM cells and infectivity measured by luciferase activity 48 hours later. *= P<0.05 using a two-way ANOVA indicating statistical significance between the IFITM condition and control for each PLV, #=P>0.05 indicating statistical significance using a two-way ANOVA between different PLVs for the same IFITM condition. N=3, Mean+/-SEM.

6.2.7 Altering V1/V2 loop length alters IFITM sensitivity in 57_S9H and 113_S8D

As previously mentioned, there are six amino acid differences in the V1/V2 loop between 57_S9H and 113_S8D. One of these is a difference in loop length by two amino acids caused by the presence or absence of two asparagines at positions 186 and 187 (relative to HxB2). 57_S9H is lacking two amino acids here relative to 113_S8D. To investigate if this change in loop length could contribute to conformational changes that alter IFITM sensitivity, mutants swapping these residues at N186/187 only were generated (Figure 6.2.11 A). These were tested for IFITM sensitivity and again a one-way rescue was observed, with the 57_S9H being rescued by the addition of these two asparagines and becoming IFITM resistant. However, deletion of these two amino acids did not confer sensitivity to the 113_S8D Env. These data suggest that this mutation in the V1/V2 loop of 57_S9H is sufficient to rescue IFITM sensitivity. Meanwhile, to reduce the IFITM resistance of 113_S8D, swapping the whole V1/V2 loop of 57_S9H is required, perhaps suggesting interplay between mutations upstream.

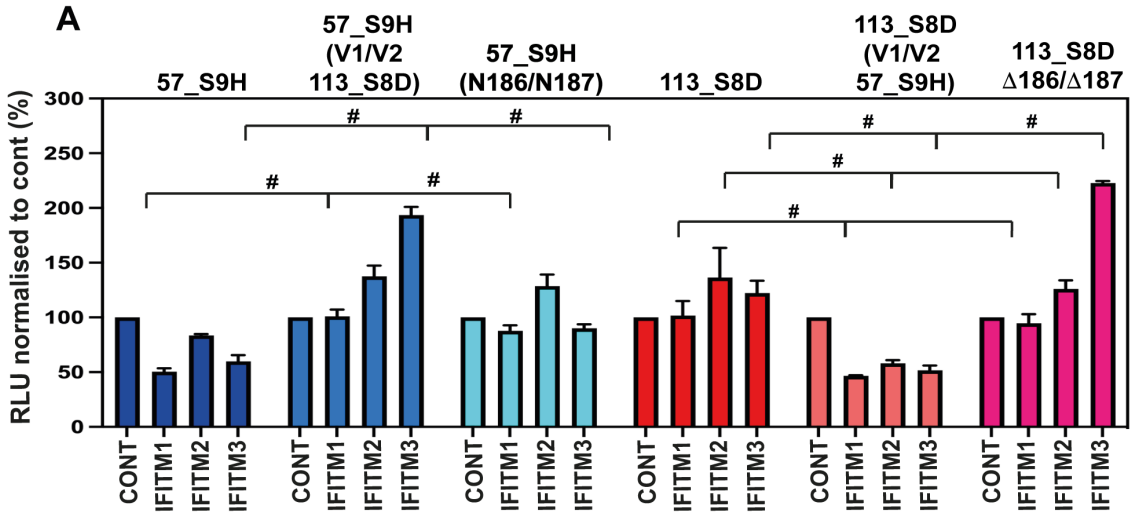

Figure 6.2.11. Altering V1/V2 loop length between 57_S9H and 113_S8D confers IFITM resistance to 57_S9H but does not confer sensitivity to 113_S8D. A) PLVs of 57_S9H and 113_S8D where two additional asparagines were added into 57_S9H at position 186, or were deleted from the corresponding position in 113_S8D were generated and used to infect U87-CD4-CCR5-IFITM as before. #= P<0.05 using a two-way ANOVA indicating statistical significance between the PLVs for the same IFITM condition. N=3, Mean+/-SEM.

6.2.8 Opening up the conformation of the 113_S8D Env confers IFITM sensitivity

Along with V3 loop mutations, mutations that alter the "openness" of Env have previously been suggested to alter IFITM sensitivity (Dr Toshana Foster, unpublished data). We hypothesised that the conformation of 113_S8D may be more closed than that of 57_S9H, conferring reduced sensitivity to IFITMs. To test this, a mutation that has previously been shown to open up the conformation of Env, L193R, and two mutations shown to close the conformation of Env, A582T and L587A, were introduced into the 113_S8D Env. The L193R mutation is located at the end of the V1/V2 loop, and the A582T/L587A mutations in gp41 (Figure 6.2.12 A). The IFITM sensitivity of these mutants was then tested (Figure 6.2.12 B). The L193R mutation did indeed increase the sensitivity of 113_S8D to IFITMs 1, 2 and 3, while the A582T/L587A mutations did not increase IFITM sensitivity. Interestingly, the A582T/L587A mutations did result in a small but significant degree of IFITM3 enhancement by 2-fold. It should be noted that these mutations did reduce 113_S8D infectivity, and reduced the infectivity of 57_S9H to the extent that the reciprocal experiment could not be interpreted. This does however suggest that opening up the conformation of 113_S8D confers IFITM sensitivity on this Env, and taken together, that the swapping of the V1/V2 loops between 57_S9H and 113_S8D may be altering conformational dynamics which alters IFITM sensitivity.

This is at a slight disparity with the cold inactivation data which suggested that both 57_S9H and 113_S8D were similarly likely to sample the CD4-bound conformation of Env, however 57_S9H is IFITM sensitive. Additionally, there were other Envs which were entirely resistant to cold inactivation, however were IFITM sensitive. It would be interesting to test if introducing the L193R and A582T/L587A mutations into other Envs from this panel and testing IFITM sensitivity correlates with the cold inactivation data.

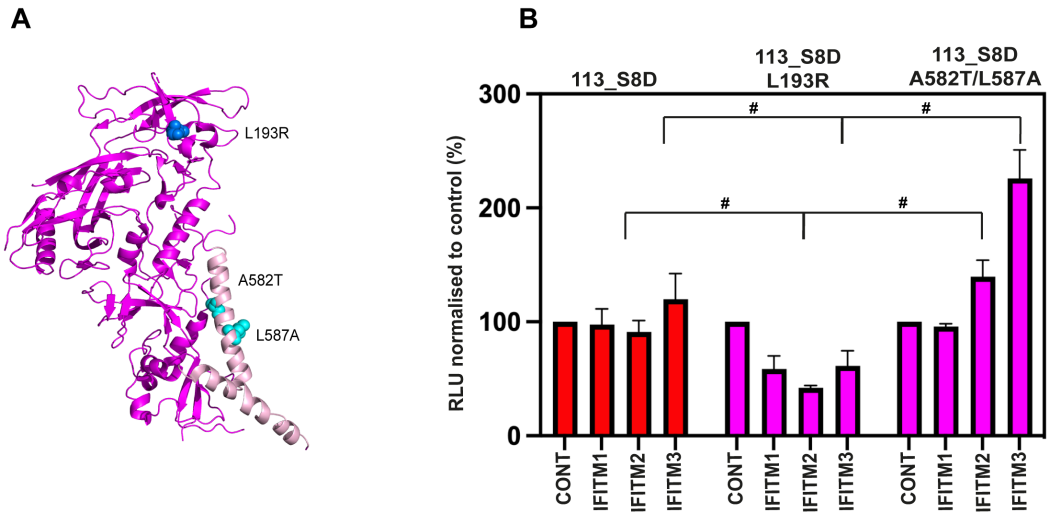

Figure 6.2.12. The opening L193R mutation in 113_S8D can confer IFITM sensitivity. A) Structure of Env (PDB:5ACO) with L193R (blue) and A582T/L587A (cyan) highlighted. B) PLVs of 113_S8D with the L193R or A582T/L587A mutations were used to infect U87-CD4-CCR5-IFITM cells and infectivity measured by luciferase activity 48 hours later. #= $P<0.05$ using ANOVA indicating statistical significance between the PLVs for the same IFITM condition. N=3, Mean±SEM.

6.2.9 IFITM3 Y20F restricts both 57_S9H and 113_S8D

Finally, the impacts of mislocalising IFITM3 on the IFITM sensitivity of 57_S9H and 113_S8D was briefly investigated. The Y20F mutation in IFITM3 alters the endocytic trafficking of this protein, effectively mislocalising it to the plasma membrane. However, these mutants appear to adopt distinct patterns of viral restriction at the plasma membrane, as viruses with intermediate IFITM1 sensitivity can still be highly sensitive to IFITM3 Y20A/F restriction [69]. To test whether this mutant could therefore still inhibit 113_S8D despite its general IFITM resistance, IFITM3 Y20F U87-CD4-CCR5 cells were generated. PLVs of 57_S9H and 113_S8D were used to infect U87-CD4-CCR5-IFITM or U87-CD4-CCR5 IFITM3 Y20F cells (Figure 6.2.13). As expected, 57_S9H was sensitive to IFITMs 1 2 and 3 as before, and indeed even more sensitive to IFITM3 Y20F restriction. However, surprisingly the 113_S8D PLVs were equally sensitive to IFITM3 Y20F, despite this Env being resistant to the three wild-type IFITMs. This demonstrates that although 113_S8D is insensitive to IFITM1 usually, introduction of the Y20F mutation into IFITM3 localises IFITM3 such that it can now restrict 113_S8D. Further investigation of this may yield further insights into the mechanism of 113_S8D's IFITM resistance.

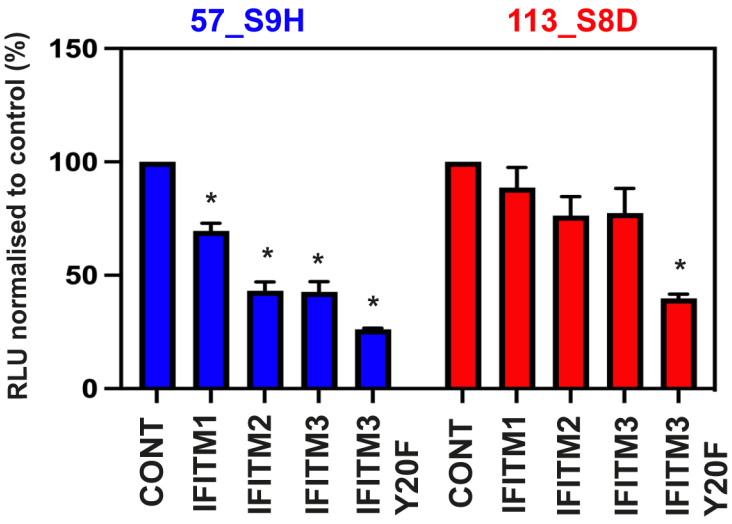

Figure 6.2.13. The Y20F mutation in IFITM3 restricts both 57_S9H and 113_S8D. A) 57_S9H and 113_S8D PLVs were used to infect U87-CD4-CCR5-IFITM cells and infectivity measured by luciferase activity 48 hours later. *=P>0.05 indicating statistical significance between control and each IFITM. N=3, Mean+/-SEM.

6.3 Discussion

In this chapter I discuss the IFITM sensitivity of a panel of Envs isolated from a single HIV-1 infected patient over chronic infection and the role of the V1/V2 and V3 loops in determining these phenotypes. It has previously been reported that the Envs of T/F viruses have thus far been found to be more resistant to the effects of type I IFNs and IFITMs than consensus viruses from six months into chronic infection [27, 67]. Additionally, withdrawal of ART has been found to result in rebound of viruses that are IFN-resistant [28]. Patient SUT036022 was not on ART therapy at any of the timepoints samples were taken; across all nine time points examined here there appeared to be Envs circulating at the same time in chronic infection with varying sensitivity to both IFN and IFITMs. This further suggests that innate immunity is a continuing selection pressure during chronic infection. For example at week 113, the 113_S8D Env is present which is IFITM resistant, however the other three Envs tested from this week exhibit moderate IFITM sensitivity. This suggests that although the majority of chronic Envs display IFITM sensitivity, IFITM-resistant viruses can still circulate during chronic infection. However, of over 80 sequences from patient SUT036022, only 24 were tested here. This could be under or overrepresenting the relative balance of IFITM-sensitive and IFITM-resistant Envs.

Several of the Envs investigated here were IFITM sensitive but had relatively high IC50s, suggestive of these Envs being resistant to or enhanced by other IFN-upregulated proteins that could apply a selective pressure during chronic infection. This patient exhibited an N332-escape response around week 113, where the N332 potential glycan site is lost from all Envs of that Week except 113_S10F [315]. Within the samples from the same week where this antibody escape mutation is present however, several still exhibit high IC50s and 113_S8D is IFITM resistant. This demonstrates that there is still a relative balance of selective pressures of both innate and adaptive immunity at this time point. Additionally, mutations to escape antibody neutralisation could perhaps sometimes confer beneficial structural changes that also impact IFITM sensitivity.

It would be interesting to determine what causes the relatively high IC50s of some of these Envs that is not IFITM resistance. There are also other antiviral proteins that can

inhibit entry through their effects or incorporation in the producer cell, such as the SERINC and GBP families, as well as LY6E and CH25H. SERINC3/5 also inhibit viral entry through their incorporation into viral particles during production [84, 85]. This panel of Envs would provide an interesting resource to further interrogate the mechanism of SERINC3/5 resistance, especially due to the differences in gp41 across these Envs and the fact that SERINC resistance in T/F viruses has thus far been ascribed to the cytoplasmic tail of Env [90]. Swapping of the cytoplasmic tail of 113_S8D into 57_S9H conferred IFITM2 and IFITM3 resistance. Additionally, the A582T/L587A mutations in 113_S8D conferred a small amount of IFITM3 enhancement. These data suggest there could be a role for the cytoplasmic tail determining sensitivity to antiviral proteins that block entry for this panel of Envs. Recently, cholesterol-25-hydroxylase (CH25H) has also been demonstrated to inhibit the entry of a broad range of enveloped viruses by blocking membrane fusion [101]. LY6E has recently been implicated to inhibit SARS-CoV-2 viral entry through an independent mechanism to IFITM3, however has also been suggested to enhance, rather than restrict HIV-1 infection [95, 367]. Whether these findings also apply to primary isolates, and could contribute to the IFN resistance of some of the Envs tested here, remains to be elucidated.

Only CCR5-tropic Envs were tested here, with IFITM2 and 3 generally exhibiting the most inhibition. Some Envs were sensitive to all three IFITMs, and some were IFITM1 resistant while still being sensitive to IFITMs 2 and 3. It is disputed whether IFITMs block HIV-1 entry in a coreceptor dependent manner, with some reports suggesting that IFITM1 blocks CCR5-tropic viruses and IFITMs 2 and 3 inhibit CXCR4-tropic viruses, and others proposing that IFITM-mediated inhibition is independent of coreceptor usage [67, 68]. There is likely a component of cell-type dependency, however this panel of Envs demonstrates that at least in this cell type, several of these CCR5-tropic Envs are sensitive to restriction by IFITMs 2 and 3. Whether this correlates with utilisation of the endocytic route of entry in these cells, or whether IFITM2 and 3 localise differently in these cells, has not been tested yet. HIV-1 does not require acidic pH to mediate viral fusion, however it has been documented to adopt the endocytic pathway in some cell types [13]. Further exploration of the Y20F mutant may assist in shedding some light on the differential sensitivity of these Envs to IFITMs as well, as both 57_S9H and 113_S8D were sensitive to inhibition by IFITM3 Y20F,

despite 113_S8D being IFITM1 resistant. It could be that despite the Y20F mutation mislocalising IFITM3 away from endosomes, this does not localise IFITM3 to the same subcellular location as IFITM1. Additionally, it has previously been shown for a CCR5-tropic lab strain which is IFITM3 resistant, that the IFITM3 Y20F mutation renders this isolate IFITM3 sensitive [67]. Taken together, this further suggests that "IFITM resistant" Envs can be rendered sensitive through IFITM mislocalisation. It is also worth noting that the effect of IFITMs on HIV-1 entry here has only been tested in the context of cell-free infection, and this may be irrelevant in the context of cell-cell transmission which constitutes 60% of infection *in vivo* for HIV-1 and can overcome tetherin-mediated inhibition of infection [71, 368]. It has been suggested that cell-cell transmission can overcome the inhibitory effects of IFITM1, and therefore measuring IFITM1 sensitivity in cell-free infection may be misleading [369]. Additionally, these experiments have all been conducted with pseudotyped lentiviral vectors, and whether these can be recapitulated with full length virus in spreading infection needs to be confirmed. Only the Envs of these viruses from patient 29 were isolated, and it is therefore unknown whether mutations in other HIV-1 proteins would also affect IFN resistance.

The V3 loop has previously been suggested to play a role in determining the IFITM resistance or sensitivity of lab isolates AD8 and NL43, likely through affecting the conformation of Env [333]. For the 57_S9H and 113_S8D pair of Envs studied here, the V3 loop swap confers a one-way rescue where the N332S mutation in 57_S9H can rescue this Env from IFITM restriction. However, the S332N mutation in 113_S8D does not confer IFITM sensitivity to this Env. This suggests that the V3 loop can alter IFITM sensitivity in a context-dependent manner. Only switching the entire V1/V2 loop of 57_S9H and 113_S8D fully switched their relative IFITM sensitivities, while the N186/N187 switch rescued 57_S9H but did not confer sensitivity to 113_S8D. The N186/N187 residues are only a few amino acids upstream of the L193 site which when mutated to an arginine can open up the IFITM sensitivity of 113_S8D. It would be interesting to confirm if the A582T/L587A mutation in the 57_S9H can rescue the IFITM sensitivity of this Env and further solidify the link between open/closed conformation and IFITM sensitivity, however the L193R and A582T/L587A mutations in 57_S9H significantly reduce viral infectivity, making interpretation of these experiments difficult. The L193R mutation, which opens up the conformation of Env,

sensitises 113_S8D to IFITM restriction. However, the cold inactivation data suggest that both 57_S9H and 113_S8D are amongst the most sensitive Envs to cold inactivation, losing approximately 2-fold infectivity by 24 hours, and therefore more likely to sample the CD4-bound open state. The general lack of correlation between cold inactivation and IFITM sensitivity could suggest that there is a certain tolerance of open sampling by these Envs, and that fully opening the Env with the L193R mutation would be required to open up an IFITM resistant Env to the point of IFITM sensitisation. Whether the V1/V2 swaps demonstrate altered cold inactivation, or sensitivity to a CD4-mimetic, remains to be tested.

It has previously been suggested that the overexpression of IFITMs in the producer cell can affect gp160 processing and that this can impact infectivity [333]. No impact of IFN on gp160 processing in the producer cell was observed here, however 57_S9H did appear to be processed less efficiently than 113_S8D at steady state. This processing phenotype was conferred to 57_S9H by generating chimeras from the V1/V2 loop onwards or V3 loop onwards, suggesting that the V3 loop is the determinant of this change in accessibility of the furin cleavage site. It would be interesting to assess whether the V1/V2 loop and N332 swaps between 57_S9H and 113_S8D also correlate with changes any changes in gp160 processing and if this may explain why the S332N mutation in 113_S8D does not alter IFITM sensitivity. It has previously been shown that uncleaved Envs are more able to sample the downstream open conformations of Env and it could be that the differences in gp160 processing between 57_S9H and 113_S8D correlate with conformational changes [292]. However, the amount of gp120 incorporated onto virions is similar for 57_S9H and 113_S8D, and there does not appear to be a significant difference in cold inactivation between the 57_S9H and 113_S8D Envs. Further investigating differences in Env conformation between 57_S9H and 113_S8D using more sensitive techniques than cold inactivation are likely required. Additionally, it would be interesting to further investigate the relevance of this differential processing to IFITM sensitivity for some of the other mutants generated, and the other Envs in this panel.

Chapter 7: Final discussion

The HIV-1 and SARS-CoV-2 pandemics have both spurred significant advances in virology. In particular, the SARS-CoV-2 pandemic resulted in rapid advances in diagnostic testing, development and rollout of vaccines, and understanding of the virus' molecular biology in the span of two years. While our knowledge of the molecular biology of these viruses has developed immensely, there are still many unanswered questions surrounding the relationship between SARS-CoV-2 and evasion of innate immunity. There is much necessary focus on how mutations in spike and Env allow evasion of the antibody response. However, there are multiple selection pressures *in vivo* that also play a role in viral evolution and it has been shown in HIV-1 that the innate immune system can enforce significant constraints on viral transmission and impose a selective pressure following ART interruption [27, 28]. It has also been demonstrated that the emerging SARS-CoV-2 VOCs B.1, alpha and beta strains are more IFN resistant than the ancestral Wuhan strain [29]. Understanding the impact of innate antiviral proteins that target early viral replication not only informs our understanding of viral entry, but has consequences for our understanding of intra-host viral evolution.

HIV-1 and SARS-CoV-2 are completely unrelated viruses. However, these viruses have similarities in the structure of their entry proteins, require priming of their glycoproteins by furin, and demonstrate significant glycoprotein-dependent differences in IFN and IFITM sensitivity. The regions of these glycoproteins that dictate their relative IFITM sensitivity differs. The polybasic cleavage site confers IFITM sensitivity for SARS-CoV-2, while the V1/V2 loop is responsible for IFITM sensitivity of the HIV-1 Envs studied here. Despite these differences, altering the cytoplasmic tail of either virus has consequences for IFITM sensitivity, in particular IFITM3 enhancement. Deletion of the cytoplasmic tail of both SARS-CoV-2 and HIV-1 has been found to improve PLV titre [175, 285], and deletion of the HIV-1 Env cytoplasmic tail has also been found to overcome SERINC restriction [90]. The SARS-CoV-2 alpha virus and PLVs are both enhanced by IFITM3. This enhancement can be abolished by the H681P mutation or ablation of the polybasic cleavage site, demonstrating the polybasic cleavage site is necessary for IFITM3 enhancement. Deletion of the

cytoplasmic tail also reduces IFITM3 enhancement for the alpha spike in PLVs. Additionally, deletion of the cytoplasmic tail increases IFITM2 sensitivity for both D614G and alpha PLVs. In HIV-1, the introduction of the A582T/L587A mutation in gp41 of the 113_S8D Env results in a small but significant enhancement by IFITM3, and inserting the 113_S8D cytoplasmic tail into the 57_S9H Env rescues IFITM2 and IFITM3 sensitivity. This suggests that the cytoplasmic tail can alter the level of enhancement by IFITM3 in completely unrelated viruses, which could suggest a common mechanism of IFITM3 enhancement. This is however at odds with the finding that deletion of the cytoplasmic tail of Env rescues Env from restriction by SERINC5, suggesting that the relationship between cytoplasmic tails of glycoproteins and sensitivity to antiviral proteins may not be clear cut [90]. It has been proposed that IFITMs and SERINCs exert a block on viral entry through distinct mechanisms, which could explain the differential relevance of the cytoplasmic tail in resistance and sensitivity to these antiviral proteins [91]. SARS-CoV-2 PLVs of several VOCs with deleted cytoplasmic tails have been found to be similarly sensitive to SERINC5 [92]. Whether increased differences in sensitivity are observed with full-length spikes remains to be elucidated. Overall, these data suggest interplay between glycoprotein cytoplasmic tails and IFITM restriction, and that the use of ΔCT SARS-CoV-2 spikes to investigate viral entry should be interpreted with caution. Additionally, further understanding of how deletion of the SARS-CoV-2 spike cytoplasmic tail mechanistically results in an altered conformation of spike that increases E64d sensitivity warrants further examination.

Another similarity between SARS-CoV-2 and HIV-1 IFITM sensitivities is that both viruses have distinct routes of viral entry implicated in patterns of IFITM restriction (see Figure 7.1.1. for a model of SARS-CoV-2 entry pathways and IFITM-mediated inhibition). 57_S9H is IFITM1 sensitive while 113_S8D is IFITM1 resistant, yet both are sensitive to IFITM3 Y20F. This is suggestive of differential routes of viral entry. In the VOCs of SARS-CoV-2 tested thus far, there are disparities in the sensitivity to TMPRSS, cathepsin, and MMP2/9 inhibitors. For the VOC spikes tested in this thesis, the sensitivity to IFITM2 and E64d correlate, with the exception of the delta spike. The delta spike retains IFITM2 sensitivity despite being insensitive to the effects of E64d. The delta spike is however sensitive to inhibition by the MMP2/9 inhibitor, implying

that perhaps the delta spike is IFITM2 sensitive because the MMP pathway results in access to IFITM2-encompassing endosomes. Meanwhile, the alpha variant is not sensitive to either E64d or MMP inhibition. The data here suggest that viral entry and susceptibility to IFITMs is not simply a function of early or late entry but in fact a function of multiple proteases. This, combined with the recent findings that a majority of SARS-CoV-2 viral entry requires an acidic pH component, regardless of the protease used for viral entry, suggests much more complex requirements of viral entry for SARS-CoV-2 than appreciated in the early stages of the pandemic [19].

The mechanism of IFITM3 enhancement itself, and of the enhancing features of IFITM2 Y19F and IFITM1Δ117-125 in TMPRSS2-negative cells, also warrants further investigation. It could be that the presence of IFITM3 somehow creates an environment that permits viral fusion, despite increasing membrane curvature as per the current model of IFITM-mediated inhibition. The recurrent theme of IFITM enhancement under certain conditions for coronaviruses is not new; OC43 has been reported to be enhanced by IFITMs 2 and 3, and has been found for SARS-CoV-2 in Calu-3 cells [335, 336]. Additionally, mislocalisation of IFITM3 has been shown to also enhance SARS-CoV-2 infection [40]. The deletion of the C terminal of IFITM1 has also been found to result in the enhancement of SARS-CoV-1, MERS-CoV, and OC43 [363]. To date, the exact mechanism of IFITM enhancement has not yet been elucidated. The N-terminal of IFITMs 2 and 3 fine tune their localisation and restrictive capacity in the cell, and during IFITM biosynthesis the IFITM will traffic via the plasma membrane [57]. Understanding how IFITMs have differential antiviral effects in different subcellular compartments is therefore still important in the context of *in vivo* infection. The IFITM mutants made here are artificial, however the SNP rs12252-C has been suggested to result in a truncated form of IFITM3 lacking its Yxxϕ domain that would localise to the plasma membrane [79]. It has also previously been reported that N-terminal mutants of IFITM3 are present in old world monkeys and that these mutations alter their viral restriction capacity [370]. In addition to the existence of mislocalisation SNPs, IFITMs cycle through multiple cellular compartments and understanding the variable effects of these proteins at different subcellular localisations is important to further understanding of how viruses can hijack and bypass IFITM restriction.

Mislocalisation of IFITM1 resulted in the largest enhancement phenotype in TMPRSS2-negative cells for all except the omicron variant, which was not considerably enhanced by IFITMs under any of the conditions tested so far. The fact that the ∆117-125 mutation in IFITM1 does not enhance infection to the same degree in TMPRSS2+ cells further infers a complex interplay between proteases and IFITMs. The ∆117-125 mutant has previously been found to restrict the NL4.3 strain of HIV-1, which was previously insensitive to IFITM1 [66]. Understanding how exactly the ∆117-125 mutant toggles IFITM1's restrictive capacity will help understand the differences in viral entry for these viruses, and the relationship between membrane properties and viral entry.

IFITMs may localise differently in different cell-types, and it is entirely reasonable to consider that discrepancies in the literature about which IFITMs inhibit both SARS-CoV-2 and HIV-1 depend on the cell-type used. A common factor thus far appears to be the presence of TMPRSS2, which abolishes the restrictive capacity of IFITM2 and IFITM3. Results from A549-ACE2-TMPRSS2-IFITM cells shown in Chapter 5 display similar trends (although not magnitude) consistent with data from the Kirchhoff lab in Calu-3 IFITM knockdown cells [335]. Additionally, the finding that TMPRSS2 confers IFITM1 sensitivity is consistent with findings from other labs using cells that endogenously express TMPRSS2, such as Caco-2 cells [94]. The Calu-3 cell line is considered the gold standard cell line in SARS-CoV-2 research which is TMPRSS2-positive [160]. It is, however, becoming clearer that SARS-CoV-2 infection is not restricted to only TMPRSS2+ lung epithelia; The most recent variants that were studied in this thesis, BA.1 and BA.2, are less dependent on TMPRSS2 than its predecessors alpha or delta [26]. This further reinforces the need to study SARS-CoV-2 and its interactions with antiviral proteins that could influence transmission and pathology in multiple cell types. Additionally, SARS-CoV-2 infection is clearly not limited to the lung tissue itself, having been found in the trachea, brain, cardiac tissue, intestines, male genitals, and the kidneys [371].

There are also discrepancies in the literature regarding which VOC spikes are better or worse cleaved at the S1/S2 boundary [157, 159, 188, 192]. It is shown here in Chapter 4 that spike cleavage in virus grown in Vero-E6-TMPRSS2 exhibits differential processing at the S1/S2 boundary to PLVs produced in 293T17, suggesting that the cell type SARS-CoV-2 is grown in, or in which PLVs are produced, has a large impact on spike processing. It has also been shown that serum concentration can impact cleavage of SARS-CoV-2, with higher concentrations mimicking trypsin-like effects in Vero-E6 cells [161]. In Chapter 4, whether spike processing of PLVs was altered when 2% FCS rather than 10% FCS was not tested, and the higher serum concentration in PLV preparation may be a factor in the differential cleavage observed. The myriad of factors that can alter spike processing highlights the need for comparisons between cell types and culture conditions. In terms of cleavage and IFITM phenotypes, it is clear that the presence or absence of a polybasic cleavage site can modulate IFITM2 sensitivity. However, the emerging mutations in VOCs which alter cleavage do not necessarily correlate with IFITM phenotypes. Despite differences in relative cleavage between native virus and PLVs, IFITM sensitivity is comparable, suggesting that cleavage itself may not be mediating the difference in IFITM sensitivity between alpha and other VOCs. This implies that the mechanism through which the P681H mutation confers IFITM resistance may be via a pathway entirely unrelated to cleavage. With that said, the GBP family has been shown to inhibit furin-mediated cleavage for SARS-CoV-2 spikes [94]. The Wuhan spike is sensitive to GBP5, however it appears that the D614G mutation alone confers GBP5 resistance [94]. It would be interesting to test the effects of the GBP family in other cell lines in the absence of TMPRSS2 and determine whether this can impact IFITM sensitivity. There is likely a limit to the trade-off between S1/S2 cleavage and spike stability, and it will be intriguing to see if any future VOCs beyond alpha, delta, and omicron have increased S1/S2 cleavage or if this is the upper limit of S1/S2 cleavage without a total loss of stability.

It has been suggested that incorporation of IFITMs into virions in the producer cells can subsequently impact viral infectivity and that IFITMs can exert antiviral effects during viral production [57, 58]. Here, testing the antiviral effects of IFITMs in the target cells was tested rather than the in context of producer cells. When 293T17s were pre-treated with IFNβ during HIV-1 PLV production, there appeared to be a small impact

on viral infectivity for 57_S9H, and no impact at all for 113_S8D. Meanwhile, IFN pre-treatment of target cells resulted in much greater decreases in viral infectivity, and although small, IFITM overexpression consistently resulted in 2-fold inhibition of IFITM-sensitive Envs. This suggests that for these Envs tested, the effects of IFITM on infectivity are larger in the target cell than the producer cell. In the context of SARS-CoV-2, expression of IFNβ at transfection during PLV production was only tested to assess effects of IFNβ on spike S1/S2 cleavage, and not on infectivity. Measuring if IFITM overexpression in producer cells altered infectivity of PLVs or native virus would rule out whether IFITMs impact infectivity in the producer cell. Data presented here suggest that evasion of IFITMs, especially by SARS-CoV-2, is implicit with route of viral entry; as shown by the use of TMPRSS and cathepsin inhibitors. However, it cannot be ruled out that the IFNβ pre-treatment of A549 and Calu-3 prior to infection with replicative SARS-CoV-2 encompasses the effects of IFITMs on the producer cell and negative imprinting of SARS-CoV-2 virions. Furthermore, in the context of IFN-treated cells there are multiple antiviral proteins that can impact infectivity of the viral particle in addition to IFITMs, including the already mentioned GBP5 and SERINC3/5 [92, 94]. The effects of GBP5 and SERINC5 on SARS-CoV-2 spike and HIV-1 Env have not been explored here, and it is important to not rule out the impact these antiviral proteins may have in the context of IFN or *in vivo.*

In summary, the data presented here highlight the complexity of the relationship between viral entry and sensitivity to IFITMs. Route of viral entry is an important factor in determining IFITM sensitivity, however, for SARS-CoV-2 it is becoming apparent that there is more complexity than an early or late pathway, and more proteases and entry factors involved than initially thought. The relationship between spike cleavage and IFITM restriction is also not clear cut. The presence of a polybasic cleavage site does reduce sensitivity to IFITM2 in both TMPRSS2-negative and positive cells. However, the increased S1/S2 cleavage of the alpha variant does not appear to be the determinant of the IFITM resistance of this variant in TMPRSS2-negative cells, but is in fact the P681H mutation itself. Exactly how the P681H mutation mediates IFITM resistance independent of S1/S2 cleavage remains to be understood. While the regions of HIV-1 Env that dictate IFITM resistance and sensitivity are different to those of SARS-CoV-2 spike, there are commonalities in the relationships between these

glycoproteins and IFITM restriction. For both spike and Env, the cytoplasmic tail of the glycoprotein appears to play a role in IFITM2 sensitivity. Deletion of the cytoplasmic tail of spike sensitises the previously IFITM resistant alpha spike to IFITM2. Swapping of the cytoplasmic tail of the IFITM resistant 113_S8D Env rescues the previously IFITM2 and 3 sensitivity of the 57_S9H Env. Lastly, IFITMs can enhance the entry of both of these glycoproteins through mechanisms that are not currently understood and require further exploration.

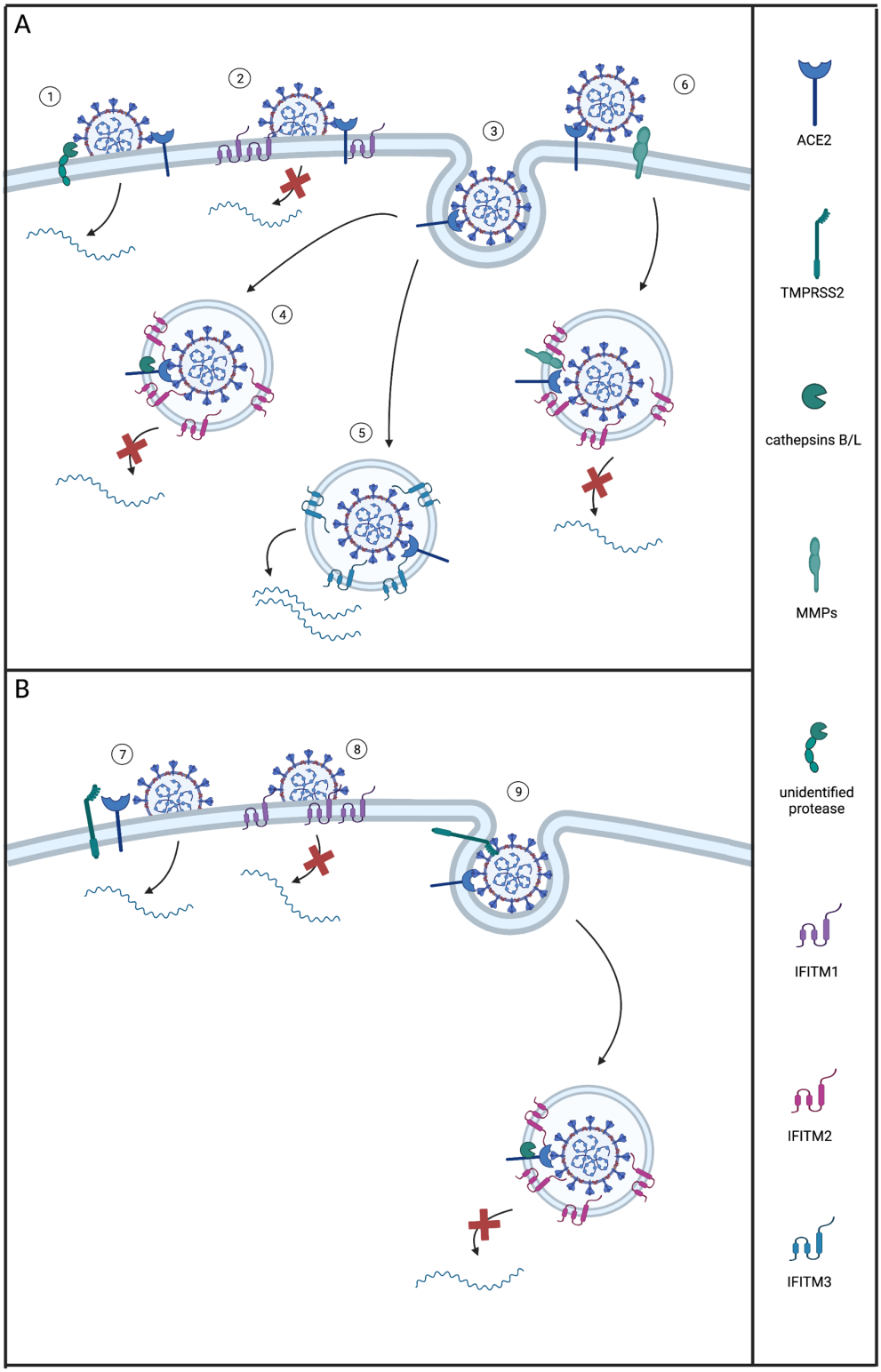

Figure 7.1.1. Model of SARS-CoV-2 viral entry and IFITM-mediated inhibition in TMPRSS2-negative and TMPRSS2-positive cells.

Figures from this thesis which support the presented model are referenced throughout. **A)** In A549-ACE2 cells, SARS-CoV-2 entry can be mediated at the cell surface by ACE2 binding and cleavage by either trace amounts of TMPRSS proteins or a currently unknown protease **(1)** (Figure 3.2.7). For some SARS-CoV-2 variants such as the ancestral Wuhan, delta and kappa, using this route results in a degree of IFITM1-mediated inhibition **(2)** (Figures 3.2.8, 4.2.7). The more prevalent entry pathway in the A549-ACE2 system involves ACE2 binding followed by endocytosis and cleavage at the S2' site by cathepsins B/L **(3, 4)** (Figure 3.2.7). However, usage of this entry pathway renders SARS-CoV-2 more susceptible to IFITM2-mediated inhibition due to accessing IFITM2 containing compartments **(4)** (Figures 3.2.8, 3.2.13, 3.2.15, 4.2.10). Spikes lacking the polybasic cleavage site such as SARS-CoV-1, pangolin GD, and the Wuhan/D614GΔPRRA are the most sensitive to IFITM2 due to being entirely reliant on this pathway for entry (Figures 3.2.7. 3.2.9, 3.2.10). Meanwhile, a majority of the VOCs exhibit at least a degree of IFITM2 sensitivity and demonstrate partial utilisation of this pathway in A549-ACE2s, however can also use the early pathway depending on bioavailability (Figure 4.2.7). The alpha and delta variants are the least dependent on cathepsins B/L for S2' cleavage, consistent with these spikes utilising other proteases for this cleavage (Figure 4.2.8). IFITM3 does not significantly inhibit any of the SARS-CoV-2 VOCs, suggesting that SARS-CoV-2 virions do not tend to access IFITM3-containing endosomes in this system (Figures 4.2.2, 4.2.7). However, the alpha variant is actively enhanced by the presence of IFITM3, suggesting that for the alpha variant accessing these compartments may increase viral entry **(5)** (Figure 4.2.2, 4.2.5). In addition to TMPRSS and cathepsins B/L, viral entry can also be achieved by utilising MMPs, and in particular the delta variant appears to use this pathway more relative

to the alpha and omicron variants **(6)** (Figure 4.2.11). Utilisation of the MMP pathway however appears to result in access to IFITM2-containing endosomes and a block to viral entry (Figure 4.2.12). **B)** In A549-ACE2-TMPRSS2 cells, the presence of TMPRSS2 permits more viral entry near the plasma membrane due to TMPRSS2 cleaving the S2' site (Figures 3.2.6, 3.2.7). This results in viral entry near the plasma membrane, rather than in IFITM2-containing endosomes, and rescues the Wuhan, D614G, and delta variants from IFITM2-mediated restriction **(7)** (Figures 3.2.13, 5.2.1, 5.2.2). However, utilisation of the TMPRSS2 pathway does sensitise D614G, alpha and delta to inhibition by IFITM1 which is present at/near the plasma membrane (Figure 5.2.2) **(8)**. Additionally, spikes which require both the S1/S2 and S2' cleavages to occur on the target cell, such as WuhanΔPRRA, are still sensitive to IFITM2 in A549-ACE2-TMPRSS2 cells because these spikes are still dependent on cathepsins B/L for spike cleavage **(9)** (Figure 5.2.1). Additionally, the omicron BA.1 variant also retains IFITM2 sensitivity in the presence of TMPRSS2 due to its preference for cleavage by cathepsins B/L in endosomes (Figure 5.2.2, Figure 4.2.8). Overall, the relative availability of and dependence on these entry pathways for each variant appears to determine its relative sensitivity to the different IFITMs. Figure created in BioRender.

References

1. White JM, Whittaker GR. Fusion of Enveloped Viruses in Endosomes. Traffic. 2016;17(6):593-614. Epub 20160407. doi: 10.1111/tra.12389. PubMed PMID: 26935856; PubMed Central PMCID: PMCPMC4866878.
2. Chazal N, Gerlier D. Virus entry, assembly, budding, and membrane rafts. Microbiol Mol Biol Rev. 2003;67(2):226-37, table of contents. doi: 10.1128/MMBR.67.2.226-237.2003. PubMed PMID: 12794191; PubMed Central PMCID: PMCPMC156468.
3. Lowy RJ, Sarkar DP, Chen Y, Blumenthal R. Observation of single influenza virus-cell fusion and measurement by fluorescence video microscopy. Proc Natl Acad Sci U S A. 1990;87(5):1850-4. doi: 10.1073/pnas.87.5.1850. PubMed PMID: 2308945; PubMed Central PMCID: PMCPMC53581.
4. Dimitrov DS, Willey RL, Martin MA, Blumenthal R. Kinetics of HIV-1 interactions with sCD4 and CD4+ cells: implications for inhibition of virus infection and initial steps of virus entry into cells. Virology. 1992;187(2):398-406. doi: 10.1016/0042-6822(92)90441-q. PubMed PMID: 1347667.
5. Zeng C, Evans JP, King T, Zheng YM, Oltz EM, Whelan SPJ, et al. SARS-CoV-2 spreads through cell-to-cell transmission. Proc Natl Acad Sci U S A. 2022;119(1). doi: 10.1073/pnas.2111400119. PubMed PMID: 34937699; PubMed Central PMCID: PMCPMC8740724.
6. Foster TL, Pickering S, Neil SJD. Inhibiting the Ins and Outs of HIV Replication: Cell-Intrinsic Antiretroviral Restrictions at the Plasma Membrane. Front Immunol. 2017;8:1853. Epub 2018/01/23. doi: 10.3389/fimmu.2017.01853. PubMed PMID: 29354117; PubMed Central PMCID: PMCPMC5758531.
7. Domingo E, Garcia-Crespo C, Lobo-Vega R, Perales C. Mutation Rates, Mutation Frequencies, and Proofreading-Repair Activities in RNA Virus Genetics. Viruses. 2021;13(9). Epub 20210921. doi: 10.3390/v13091882. PubMed PMID: 34578463; PubMed Central PMCID: PMCPMC8473064.
8. Harrison SC. Viral membrane fusion. Virology. 2015;479-480:498-507. Epub 20150410. doi: 10.1016/j.virol.2015.03.043. PubMed PMID: 25866377; PubMed Central PMCID: PMCPMC4424100.
9. Kido H, Okumura Y, Takahashi E, Pan HY, Wang S, Chida J, et al. Host envelope glycoprotein processing proteases are indispensable for entry into human cells by seasonal and highly pathogenic avian influenza viruses. J Mol Genet Med. 2008;3(1):167-75. Epub 20081129. PubMed PMID: 19565019; PubMed Central PMCID: PMCPMC2702071.
10. Hoffmann M, Kleine-Weber H, Pohlmann S. A Multibasic Cleavage Site in the Spike Protein of SARS-CoV-2 Is Essential for Infection of Human Lung Cells. Mol Cell. 2020;78(4):779-84 e5. Epub 2020/05/05. doi: 10.1016/j.molcel.2020.04.022. PubMed PMID: 32362314; PubMed Central PMCID: PMCPMC7194065.
11. Chen B. Molecular Mechanism of HIV-1 Entry. Trends Microbiol. 2019;27(10):878-91. Epub 20190628. doi: 10.1016/j.tim.2019.06.002. PubMed PMID: 31262533; PubMed Central PMCID: PMCPMC6744290.
12. Herold N, Anders-Osswein M, Glass B, Eckhardt M, Muller B, Krausslich HG. HIV-1 entry in SupT1-R5, CEM-ss, and primary CD4+ T cells occurs at the plasma membrane and does not require endocytosis. J Virol. 2014;88(24):13956-70. Epub 20140924. doi: 10.1128/JVI.01543-14. PubMed PMID: 25253335; PubMed Central PMCID: PMCPMC4249123.

13. Miyauchi K, Kim Y, Latinovic O, Morozov V, Melikyan GB. HIV enters cells via endocytosis and dynamin-dependent fusion with endosomes. Cell. 2009;137(3):433-44. doi: 10.1016/j.cell.2009.02.046. PubMed PMID: 19410541; PubMed Central PMCID: PMCPMC2696170.
14. White JM, Delos SE, Brecher M, Schornberg K. Structures and mechanisms of viral membrane fusion proteins: multiple variations on a common theme. Crit Rev Biochem Mol Biol. 2008;43(3):189-219. Epub 2008/06/24. doi: 10.1080/10409230802058320. PubMed PMID: 18568847; PubMed Central PMCID: PMCPMC2649671.
15. Luo M. Influenza virus entry. Adv Exp Med Biol. 2012;726:201-21. doi: 10.1007/978-1-4614-0980-9_9. PubMed PMID: 22297515; PubMed Central PMCID: PMCPMC7123407.
16. Schornberg K, Matsuyama S, Kabsch K, Delos S, Bouton A, White J. Role of endosomal cathepsins in entry mediated by the Ebola virus glycoprotein. J Virol. 2006;80(8):4174-8. doi: 10.1128/JVI.80.8.4174-4178.2006. PubMed PMID: 16571833; PubMed Central PMCID: PMCPMC1440424.
17. Brecher M, Schornberg KL, Delos SE, Fusco ML, Saphire EO, White JM. Cathepsin cleavage potentiates the Ebola virus glycoprotein to undergo a subsequent fusion-relevant conformational change. J Virol. 2012;86(1):364-72. Epub 20111026. doi: 10.1128/JVI.05708-11. PubMed PMID: 22031933; PubMed Central PMCID: PMCPMC3255896.
18. Jackson CB, Farzan M, Chen B, Choe H. Mechanisms of SARS-CoV-2 entry into cells. Nat Rev Mol Cell Biol. 2022;23(1):3-20. Epub 20211005. doi: 10.1038/s41580-021-00418-x. PubMed PMID: 34611326; PubMed Central PMCID: PMCPMC8491763.
19. Kreutzberger AJB, Sanyal A, Saminathan A, Bloyet LM, Stumpf S, Liu Z, et al. SARS-CoV-2 requires acidic pH to infect cells. bioRxiv. 2022. Epub 20220614. doi: 10.1101/2022.06.09.495472. PubMed PMID: 35702155; PubMed Central PMCID: PMCPMC9196115.
20. Cerutti G, Guo Y, Zhou T, Gorman J, Lee M, Rapp M, et al. Potent SARS-CoV-2 neutralizing antibodies directed against spike N-terminal domain target a single supersite. Cell Host Microbe. 2021;29(5):819-33 e7. Epub 20210312. doi: 10.1016/j.chom.2021.03.005. PubMed PMID: 33789084; PubMed Central PMCID: PMCPMC7953435.
21. O'Connell RJ, Kim JH, Excler JL. The HIV-1 gp120 V1V2 loop: structure, function and importance for vaccine development. Expert Rev Vaccines. 2014;13(12):1489-500. Epub 20140828. doi: 10.1586/14760584.2014.951335. PubMed PMID: 25163695.
22. Wu Zhang X, Leng Yap Y. Structural similarity between HIV-1 gp41 and SARS-CoV S2 proteins suggests an analogous membrane fusion mechanism. Theochem. 2004;677(1):73-6. Epub 20040402. doi: 10.1016/j.theochem.2004.02.018. PubMed PMID: 32287546; PubMed Central PMCID: PMCPMC7141560.
23. Tian W, Li D, Zhang N, Bai G, Yuan K, Xiao H, et al. O-glycosylation pattern of the SARS-CoV-2 spike protein reveals an "O-Follow-N" rule. Cell Res. 2021;31(10):1123-5. Epub 20210802. doi: 10.1038/s41422-021-00545-2. PubMed PMID: 34341488; PubMed Central PMCID: PMCPMC8326647.
24. Zhao X, Chen H, Wang H. Glycans of SARS-CoV-2 Spike Protein in Virus Infection and Antibody Production. Front Mol Biosci. 2021;8:629873. Epub 20210413. doi: 10.3389/fmolb.2021.629873. PubMed PMID: 33928117; PubMed Central PMCID: PMCPMC8076860.
25. Cao L, Diedrich JK, Kulp DW, Pauthner M, He L, Park SR, et al. Global site-specific N-glycosylation analysis of HIV envelope glycoprotein. Nat Commun. 2017;8:14954. Epub

20170328. doi: 10.1038/ncomms14954. PubMed PMID: 28348411; PubMed Central PMCID: PMCPMC5379070.
26. Meng B, Abdullahi A, Ferreira I, Goonawardane N, Saito A, Kimura I, et al. Altered TMPRSS2 usage by SARS-CoV-2 Omicron impacts infectivity and fusogenicity. Nature. 2022;603(7902):706-14. Epub 20220201. doi: 10.1038/s41586-022-04474-x. PubMed PMID: 35104837; PubMed Central PMCID: PMCPMC8942856.
27. Fenton-May AE, Dibben O, Emmerich T, Ding H, Pfafferott K, Aasa-Chapman MM, et al. Relative resistance of HIV-1 founder viruses to control by interferon-alpha. Retrovirology. 2013;10:146. Epub 20131203. doi: 10.1186/1742-4690-10-146. PubMed PMID: 24299076; PubMed Central PMCID: PMCPMC3907080.
28. Gondim MVP, Sherrill-Mix S, Bibollet-Ruche F, Russell RM, Trimboli S, Smith AG, et al. Heightened resistance to host type 1 interferons characterizes HIV-1 at transmission and after antiretroviral therapy interruption. Sci Transl Med. 2021;13(576). doi: 10.1126/scitranslmed.abd8179. PubMed PMID: 33441429; PubMed Central PMCID: PMCPMC7923595.
29. Guo K, Barrett BS, Morrison JH, Mickens KL, Vladar EK, Hasenkrug KJ, et al. Interferon resistance of emerging SARS-CoV-2 variants. Proc Natl Acad Sci U S A. 2022;119(32):e2203760119. Epub 20220722. doi: 10.1073/pnas.2203760119. PubMed PMID: 35867811; PubMed Central PMCID: PMCPMC9371743.
30. Lista MJ and Winstone H WH, Dyer AM, Pickering S, Pedro Galao R, De Lorezno G, Cowton V, Furnon W, Suarez NM, Orton R, Palmirini M, Patel AH, Snell LB, Nebbia G, Swanson CM, Neil SJD. The P681H Mutation in the Spike Glycoprotein of the Alpha Variant of SARS-CoV-2 Escapes IFITM Restriction and Is Necessary for Type I Interferon Resistance. J Virol. 2022. doi: 10.1128/jvi.01250-22. PubMed Central PMCID: PMCPMC9749455.
31. Hoffmann HH, Schneider WM, Rice CM. Interferons and viruses: an evolutionary arms race of molecular interactions. Trends Immunol. 2015;36(3):124-38. Epub 20150220. doi: 10.1016/j.it.2015.01.004. PubMed PMID: 25704559; PubMed Central PMCID: PMCPMC4384471.
32. McNab F, Mayer-Barber K, Sher A, Wack A, O'Garra A. Type I interferons in infectious disease. Nat Rev Immunol. 2015;15(2):87-103. doi: 10.1038/nri3787. PubMed PMID: 25614319; PubMed Central PMCID: PMCPMC7162685.
33. Bastard P, Gervais A, Le Voyer T, Rosain J, Philippot Q, Manry J, et al. Autoantibodies neutralizing type I IFNs are present in ~4% of uninfected individuals over 70 years old and account for ~20% of COVID-19 deaths. Sci Immunol. 2021;6(62). doi: 10.1126/sciimmunol.abl4340. PubMed PMID: 34413139; PubMed Central PMCID: PMCPMC8521484.
34. Gomez J, Albaiceta GM, Cuesta-Llavona E, Garcia-Clemente M, Lopez-Larrea C, Amado-Rodriguez L, et al. The Interferon-induced transmembrane protein 3 gene (IFITM3) rs12252 C variant is associated with COVID-19. Cytokine. 2021;137:155354. Epub 2020/10/29. doi: 10.1016/j.cyto.2020.155354. PubMed PMID: 33113474.
35. Prabhu SS, Chakraborty TT, Kumar N, Banerjee I. Association between IFITM3 rs12252 polymorphism and influenza susceptibility and severity: A meta-analysis. Gene. 2018;674:70-9. Epub 20180622. doi: 10.1016/j.gene.2018.06.070. PubMed PMID: 29940276.
36. Huang IC, Bailey CC, Weyer JL, Radoshitzky SR, Becker MM, Chiang JJ, et al. Distinct patterns of IFITM-mediated restriction of filoviruses, SARS coronavirus, and influenza A virus. PLoS Pathog. 2011;7(1):e1001258. Epub 20110106. doi: 10.1371/journal.ppat.1001258. PubMed PMID: 21253575; PubMed Central PMCID: PMCPMC3017121.

37. Bailey CC, Zhong G, Huang IC, Farzan M. IFITM-Family Proteins: The Cell's First Line of Antiviral Defense. Annu Rev Virol. 2014;1:261-83. Epub 2015/01/20. doi: 10.1146/annurev-virology-031413-085537. PubMed PMID: 25599080; PubMed Central PMCID: PMCPMC4295558.
38. Chesarino NM, Compton AA, McMichael TM, Kenney AD, Zhang L, Soewarna V, et al. IFITM3 requires an amphipathic helix for antiviral activity. EMBO Rep. 2017;18(10):1740-51. Epub 20170823. doi: 10.15252/embr.201744100. PubMed PMID: 28835547; PubMed Central PMCID: PMCPMC5623871.
39. Feeley EM, Sims JS, John SP, Chin CR, Pertel T, Chen LM, et al. IFITM3 inhibits influenza A virus infection by preventing cytosolic entry. PLoS Pathog. 2011;7(10):e1002337. Epub 20111027. doi: 10.1371/journal.ppat.1002337. PubMed PMID: 22046135; PubMed Central PMCID: PMCPMC3203188.
40. Shi G, Kenney AD, Kudryashova E, Zani A, Zhang L, Lai KK, et al. Opposing activities of IFITM proteins in SARS-CoV-2 infection. EMBO J. 2021;40(3):e106501. Epub 20201221. doi: 10.15252/embj.2020106501. PubMed PMID: 33270927; PubMed Central PMCID: PMCPMC7744865.
41. Weston S, Czieso S, White IJ, Smith SE, Wash RS, Diaz-Soria C, et al. Alphavirus Restriction by IFITM Proteins. Traffic. 2016;17(9):997-1013. Epub 2016/05/25. doi: 10.1111/tra.12416. PubMed PMID: 27219333; PubMed Central PMCID: PMCPMC5025721.
42. Narayana SK, Helbig KJ, McCartney EM, Eyre NS, Bull RA, Eltahla A, et al. The Interferon-induced Transmembrane Proteins, IFITM1, IFITM2, and IFITM3 Inhibit Hepatitis C Virus Entry. J Biol Chem. 2015;290(43):25946-59. Epub 20150909. doi: 10.1074/jbc.M115.657346. PubMed PMID: 26354436; PubMed Central PMCID: PMCPMC4646249.
43. Jia R, Pan Q, Ding S, Rong L, Liu SL, Geng Y, et al. The N-terminal region of IFITM3 modulates its antiviral activity by regulating IFITM3 cellular localization. J Virol. 2012;86(24):13697-707. Epub 20121010. doi: 10.1128/JVI.01828-12. PubMed PMID: 23055554; PubMed Central PMCID: PMCPMC3503121.
44. Li K, Markosyan RM, Zheng YM, Golfetto O, Bungart B, Li M, et al. IFITM proteins restrict viral membrane hemifusion. PLoS Pathog. 2013;9(1):e1003124. Epub 20130124. doi: 10.1371/journal.ppat.1003124. PubMed PMID: 23358889; PubMed Central PMCID: PMCPMC3554583.
45. Rahman K, Coomer CA, Majdoul S, Ding SY, Padilla-Parra S, Compton AA. Homology-guided identification of a conserved motif linking the antiviral functions of IFITM3 to its oligomeric state. Elife. 2020;9. Epub 20201028. doi: 10.7554/eLife.58537. PubMed PMID: 33112230; PubMed Central PMCID: PMCPMC7665892.
46. Majdoul S, Compton AA. Lessons in self-defence: inhibition of virus entry by intrinsic immunity. Nat Rev Immunol. 2022;22(6):339-52. Epub 20211013. doi: 10.1038/s41577-021-00626-8. PubMed PMID: 34646033; PubMed Central PMCID: PMCPMC8511856.
47. Guo X, Steinkuhler J, Marin M, Li X, Lu W, Dimova R, et al. Interferon-Induced Transmembrane Protein 3 Blocks Fusion of Diverse Enveloped Viruses by Altering Mechanical Properties of Cell Membranes. ACS Nano. 2021;15(5):8155-70. Epub 20210303. doi: 10.1021/acsnano.0c10567. PubMed PMID: 33656312; PubMed Central PMCID: PMCPMC8159881.
48. Rahman K, Datta SAK, Beaven AH, Jolley AA, Sodt AJ, Compton AA. Cholesterol binds the amphipathic helix of IFITM3 and regulates antiviral activity. J Mol Biol. 2022:167759. Epub 20220721. doi: 10.1016/j.jmb.2022.167759. PubMed PMID: 35872070.

49. Gimenez-Andres M, Copic A, Antonny B. The Many Faces of Amphipathic Helices. Biomolecules. 2018;8(3). Epub 20180705. doi: 10.3390/biom8030045. PubMed PMID: 29976879; PubMed Central PMCID: PMCPMC6164224.
50. Drin G, Antonny B. Amphipathic helices and membrane curvature. FEBS Lett. 2010;584(9):1840-7. Epub 20091020. doi: 10.1016/j.febslet.2009.10.022. PubMed PMID: 19837069.
51. John SP, Chin CR, Perreira JM, Feeley EM, Aker AM, Savidis G, et al. The CD225 domain of IFITM3 is required for both IFITM protein association and inhibition of influenza A virus and dengue virus replication. J Virol. 2013;87(14):7837-52. Epub 20130508. doi: 10.1128/JVI.00481-13. PubMed PMID: 23658454; PubMed Central PMCID: PMCPMC3700195.
52. Yount JS, Karssemeijer RA, Hang HC. S-palmitoylation and ubiquitination differentially regulate interferon-induced transmembrane protein 3 (IFITM3)-mediated resistance to influenza virus. J Biol Chem. 2012;287(23):19631-41. Epub 20120417. doi: 10.1074/jbc.M112.362095. PubMed PMID: 22511783; PubMed Central PMCID: PMCPMC3365998.
53. Yount JS, Moltedo B, Yang YY, Charron G, Moran TM, Lopez CB, et al. Palmitoylome profiling reveals S-palmitoylation-dependent antiviral activity of IFITM3. Nat Chem Biol. 2010;6(8):610-4. Epub 20100704. doi: 10.1038/nchembio.405. PubMed PMID: 20601941; PubMed Central PMCID: PMCPMC2928251.
54. Amini-Bavil-Olyaee S, Choi YJ, Lee JH, Shi M, Huang IC, Farzan M, et al. The antiviral effector IFITM3 disrupts intracellular cholesterol homeostasis to block viral entry. Cell Host Microbe. 2013;13(4):452-64. doi: 10.1016/j.chom.2013.03.006. PubMed PMID: 23601107; PubMed Central PMCID: PMCPMC3646482.
55. Wee YS, Roundy KM, Weis JJ, Weis JH. Interferon-inducible transmembrane proteins of the innate immune response act as membrane organizers by influencing clathrin and v-ATPase localization and function. Innate Immun. 2012;18(6):834-45. Epub 20120330. doi: 10.1177/1753425912443392. PubMed PMID: 22467717.
56. Stott-Marshall RJ, Foster TL. Inhibition of Arenavirus Entry and Replication by the Cell-Intrinsic Restriction Factor ZMPSTE24 Is Enhanced by IFITM Antiviral Activity. Front Microbiol. 2022;13:840885. Epub 20220218. doi: 10.3389/fmicb.2022.840885. PubMed PMID: 35283811; PubMed Central PMCID: PMCPMC8915953.
57. Compton AA, Bruel T, Porrot F, Mallet A, Sachse M, Euvrard M, et al. IFITM proteins incorporated into HIV-1 virions impair viral fusion and spread. Cell Host Microbe. 2014;16(6):736-47. Epub 20141126. doi: 10.1016/j.chom.2014.11.001. PubMed PMID: 25464829; PubMed Central PMCID: PMCPMC7104936.
58. Yu J, Li M, Wilkins J, Ding S, Swartz TH, Esposito AM, et al. IFITM Proteins Restrict HIV-1 Infection by Antagonizing the Envelope Glycoprotein. Cell Rep. 2015;13(1):145-56. Epub 20150917. doi: 10.1016/j.celrep.2015.08.055. PubMed PMID: 26387945; PubMed Central PMCID: PMCPMC4602366.
59. Tartour K, Nguyen XN, Appourchaux R, Assil S, Barateau V, Bloyet LM, et al. Interference with the production of infectious viral particles and bimodal inhibition of replication are broadly conserved antiviral properties of IFITMs. PLoS Pathog. 2017;13(9):e1006610. Epub 20170928. doi: 10.1371/journal.ppat.1006610. PubMed PMID: 28957419; PubMed Central PMCID: PMCPMC5619827.
60. Brass AL, Huang IC, Benita Y, John SP, Krishnan MN, Feeley EM, et al. The IFITM proteins mediate cellular resistance to influenza A H1N1 virus, West Nile virus, and dengue

virus. Cell. 2009;139(7):1243-54. doi: 10.1016/j.cell.2009.12.017. PubMed PMID: 20064371; PubMed Central PMCID: PMCPMC2824905.
61. Bailey CC, Kondur HR, Huang IC, Farzan M. Interferon-induced transmembrane protein 3 is a type II transmembrane protein. J Biol Chem. 2013;288(45):32184-93. Epub 20130925. doi: 10.1074/jbc.M113.514356. PubMed PMID: 24067232; PubMed Central PMCID: PMCPMC3820858.
62. Zhao X, Li J, Winkler CA, An P, Guo JT. IFITM Genes, Variants, and Their Roles in the Control and Pathogenesis of Viral Infections. Front Microbiol. 2018;9:3228. Epub 20190108. doi: 10.3389/fmicb.2018.03228. PubMed PMID: 30687247; PubMed Central PMCID: PMCPMC6338058.
63. Chesarino NM, McMichael TM, Hach JC, Yount JS. Phosphorylation of the antiviral protein interferon-inducible transmembrane protein 3 (IFITM3) dually regulates its endocytosis and ubiquitination. J Biol Chem. 2014;289(17):11986-92. Epub 2014/03/15. doi: 10.1074/jbc.M114.557694. PubMed PMID: 24627473; PubMed Central PMCID: PMCPMC4002105.
64. Chesarino NM, McMichael TM, Hach JC, Yount JS. Phosphorylation of the antiviral protein interferon-inducible transmembrane protein 3 (IFITM3) dually regulates its endocytosis and ubiquitination. J Biol Chem. 2014;289(17):11986-92. Epub 20140313. doi: 10.1074/jbc.M114.557694. PubMed PMID: 24627473; PubMed Central PMCID: PMCPMC4002105.
65. Xu Y, Yang G, Hu G. Binding of IFITM1 enhances the inhibiting effect of caveolin-1 on ERK activation. Acta Biochim Biophys Sin (Shanghai). 2009;41(6):488-94. doi: 10.1093/abbs/gmp034. PubMed PMID: 19499152.
66. Jia R, Ding S, Pan Q, Liu SL, Qiao W, Liang C. The C-terminal sequence of IFITM1 regulates its anti-HIV-1 activity. PLoS One. 2015;10(3):e0118794. Epub 20150304. doi: 10.1371/journal.pone.0118794. PubMed PMID: 25738301; PubMed Central PMCID: PMCPMC4349745.
67. Foster TL, Wilson H, Iyer SS, Coss K, Doores K, Smith S, et al. Resistance of Transmitted Founder HIV-1 to IFITM-Mediated Restriction. Cell Host Microbe. 2016;20(4):429-42. Epub 20160915. doi: 10.1016/j.chom.2016.08.006. PubMed PMID: 27640936; PubMed Central PMCID: PMCPMC5075283.
68. Yu J, Liu SL. The Inhibition of HIV-1 Entry Imposed by Interferon Inducible Transmembrane Proteins Is Independent of Co-Receptor Usage. Viruses. 2018;10(8). Epub 20180807. doi: 10.3390/v10080413. PubMed PMID: 30087232; PubMed Central PMCID: PMCPMC6115839.
69. Zani A, Zhang L, McMichael TM, Kenney AD, Chemudupati M, Kwiek JJ, et al. Interferon-induced transmembrane proteins inhibit cell fusion mediated by trophoblast syncytins. J Biol Chem. 2019;294(52):19844-51. Epub 20191117. doi: 10.1074/jbc.AC119.010611. PubMed PMID: 31735710; PubMed Central PMCID: PMCPMC6937555.
70. Bailey CC, Huang IC, Kam C, Farzan M. Ifitm3 limits the severity of acute influenza in mice. PLoS Pathog. 2012;8(9):e1002909. Epub 20120906. doi: 10.1371/journal.ppat.1002909. PubMed PMID: 22969429; PubMed Central PMCID: PMCPMC3435252.
71. Jolly C, Booth NJ, Neil SJ. Cell-cell spread of human immunodeficiency virus type 1 overcomes tetherin/BST-2-mediated restriction in T cells. J Virol. 2010;84(23):12185-99. Epub 20100922. doi: 10.1128/JVI.01447-10. PubMed PMID: 20861257; PubMed Central PMCID: PMCPMC2976402.

72. Neil SJ, Zang T, Bieniasz PD. Tetherin inhibits retrovirus release and is antagonized by HIV-1 Vpu. Nature. 2008;451(7177):425-30. Epub 20080116. doi: 10.1038/nature06553. PubMed PMID: 18200009.
73. Michael Rajah M, Hubert M, Bishop E, Saunders N, Robinot R, Grzelak L, et al. SARS-CoV-2 Alpha, Beta and Delta variants display enhanced Spike-mediated Syncytia Formation. EMBO J. 2021:e108944. Epub 2021/10/04. doi: 10.15252/embj.2021108944. PubMed PMID: 34601723.
74. Buchrieser J, Degrelle SA, Couderc T, Nevers Q, Disson O, Manet C, et al. IFITM proteins inhibit placental syncytiotrophoblast formation and promote fetal demise. Science. 2019;365(6449):176-80. doi: 10.1126/science.aaw7733. PubMed PMID: 31296770.
75. Rajah MM, Bernier A, Buchrieser J, Schwartz O. The Mechanism and Consequences of SARS-CoV-2 Spike-Mediated Fusion and Syncytia Formation. J Mol Biol. 2022;434(6):167280. Epub 20211001. doi: 10.1016/j.jmb.2021.167280. PubMed PMID: 34606831; PubMed Central PMCID: PMCPMC8485708.
76. Buchrieser J, Dufloo J, Hubert M, Monel B, Planas D, Rajah MM, et al. Syncytia formation by SARS-CoV-2-infected cells. EMBO J. 2020;39(23):e106267. Epub 20201104. doi: 10.15252/embj.2020106267. PubMed PMID: 33051876; PubMed Central PMCID: PMCPMC7646020.
77. Gorman MJ, Poddar S, Farzan M, Diamond MS. The Interferon-Stimulated Gene Ifitm3 Restricts West Nile Virus Infection and Pathogenesis. J Virol. 2016;90(18):8212-25. Epub 20160826. doi: 10.1128/JVI.00581-16. PubMed PMID: 27384652; PubMed Central PMCID: PMCPMC5008082.
78. Everitt AR, Clare S, McDonald JU, Kane L, Harcourt K, Ahras M, et al. Defining the range of pathogens susceptible to Ifitm3 restriction using a knockout mouse model. PLoS One. 2013;8(11):e80723. Epub 20131121. doi: 10.1371/journal.pone.0080723. PubMed PMID: 24278312; PubMed Central PMCID: PMCPMC3836756.
79. Everitt AR, Clare S, Pertel T, John SP, Wash RS, Smith SE, et al. IFITM3 restricts the morbidity and mortality associated with influenza. Nature. 2012;484(7395):519-23. Epub 20120325. doi: 10.1038/nature10921. PubMed PMID: 22446628; PubMed Central PMCID: PMCPMC3648786.
80. Zhang YH, Zhao Y, Li N, Peng YC, Giannoulatou E, Jin RH, et al. Interferon-induced transmembrane protein-3 genetic variant rs12252-C is associated with severe influenza in Chinese individuals. Nat Commun. 2013;4:1418. doi: 10.1038/ncomms2433. PubMed PMID: 23361009; PubMed Central PMCID: PMCPMC3562464.
81. Zhang Y, Makvandi-Nejad S, Qin L, Zhao Y, Zhang T, Wang L, et al. Interferon-induced transmembrane protein-3 rs12252-C is associated with rapid progression of acute HIV-1 infection in Chinese MSM cohort. AIDS. 2015;29(8):889-94. doi: 10.1097/QAD.0000000000000632. PubMed PMID: 25784441; PubMed Central PMCID: PMCPMC4442129.
82. Zhang Y, Qin L, Zhao Y, Zhang P, Xu B, Li K, et al. Interferon-Induced Transmembrane Protein 3 Genetic Variant rs12252-C Associated With Disease Severity in Coronavirus Disease 2019. J Infect Dis. 2020;222(1):34-7. doi: 10.1093/infdis/jiaa224. PubMed PMID: 32348495; PubMed Central PMCID: PMCPMC7197559.
83. Yanez DC, Ross S, Crompton T. The IFITM protein family in adaptive immunity. Immunology. 2020;159(4):365-72. Epub 20191222. doi: 10.1111/imm.13163. PubMed PMID: 31792954; PubMed Central PMCID: PMCPMC7078001.

84. Rosa A, Chande A, Ziglio S, De Sanctis V, Bertorelli R, Goh SL, et al. HIV-1 Nef promotes infection by excluding SERINC5 from virion incorporation. Nature. 2015;526(7572):212-7. Epub 20150930. doi: 10.1038/nature15399. PubMed PMID: 26416734; PubMed Central PMCID: PMCPMC4861059.
85. Usami Y, Wu Y, Gottlinger HG. SERINC3 and SERINC5 restrict HIV-1 infectivity and are counteracted by Nef. Nature. 2015;526(7572):218-23. Epub 20150930. doi: 10.1038/nature15400. PubMed PMID: 26416733; PubMed Central PMCID: PMCPMC4600458.
86. Inuzuka M, Hayakawa M, Ingi T. Serinc, an activity-regulated protein family, incorporates serine into membrane lipid synthesis. J Biol Chem. 2005;280(42):35776-83. Epub 20050824. doi: 10.1074/jbc.M505712200. PubMed PMID: 16120614.
87. Raghunath G, Chen YC, Marin M, Wu H, Melikyan GB. SERINC5-Mediated Restriction of HIV-1 Infectivity Correlates with Resistance to Cholesterol Extraction but Not with Lipid Order of Viral Membrane. Viruses. 2022;14(8). Epub 20220727. doi: 10.3390/v14081636. PubMed PMID: 35893701; PubMed Central PMCID: PMCPMC9332783.
88. Susan A. Leonhardt MDP, Jonathan R. Grover, Ziwei Yang, Sandra Poulos, William E. McIntire, Elizabeth A. Tatham, Satchal Erramilli, Kamil Nosol, Kin Kui Lai, Shilei Ding, Maolin Lu, Pradeep D. Uchil, Andrés Finzi, Alan Rein, Anthony A. Kossiakoff, Walther Mothes, Mark Yeager. CryoEM Structures of the Human HIV-1 Restriction Factor SERINC3 and Function as a Lipid Transporter. bioRxiv. 2022.
89. Chen YC, Sood C, Marin M, Aaron J, Gratton E, Salaita K, et al. Super-Resolution Fluorescence Imaging Reveals That Serine Incorporator Protein 5 Inhibits Human Immunodeficiency Virus Fusion by Disrupting Envelope Glycoprotein Clusters. ACS Nano. 2020;14(9):10929-43. Epub 20200601. doi: 10.1021/acsnano.0c02699. PubMed PMID: 32441921; PubMed Central PMCID: PMCPMC8274448.
90. Haider T, Snetkov X, Jolly C. HIV envelope tail truncation confers resistance to SERINC5 restriction. Proc Natl Acad Sci U S A. 2021;118(21). doi: 10.1073/pnas.2101450118. PubMed PMID: 34001619; PubMed Central PMCID: PMCPMC8166163.
91. Beitari S, Pan Q, Finzi A, Liang C. Differential Pressures of SERINC5 and IFITM3 on HIV-1 Envelope Glycoprotein over the Course of HIV-1 Infection. J Virol. 2020;94(16). Epub 20200730. doi: 10.1128/JVI.00514-20. PubMed PMID: 32493821; PubMed Central PMCID: PMCPMC7394893.
92. Timilsina U, Umthong S, Ivey EB, Waxman B, Stavrou S. SARS-CoV-2 ORF7a potently inhibits the antiviral effect of the host factor SERINC5. Nat Commun. 2022;13(1):2935. Epub 20220526. doi: 10.1038/s41467-022-30609-9. PubMed PMID: 35618710; PubMed Central PMCID: PMCPMC9135752.
93. Braun E, Hotter D, Koepke L, Zech F, Gross R, Sparrer KMJ, et al. Guanylate-Binding Proteins 2 and 5 Exert Broad Antiviral Activity by Inhibiting Furin-Mediated Processing of Viral Envelope Proteins. Cell Rep. 2019;27(7):2092-104 e10. doi: 10.1016/j.celrep.2019.04.063. PubMed PMID: 31091448.
94. Dejan Mesner A-KR, Matthew V.X Whelan, Taylor Bronzovich, Tafhima Haider, Lucy G. Thorne, Greg J. Towers, Clare Jolly. SARS-CoV-2 Spike evolution influences GBP and IFITM sensitivity. bioRxiv. 2022.
95. Zhao X, Zheng S, Chen D, Zheng M, Li X, Li G, et al. LY6E Restricts Entry of Human Coronaviruses, Including Currently Pandemic SARS-CoV-2. J Virol. 2020;94(18). Epub 20200831. doi: 10.1128/JVI.00562-20. PubMed PMID: 32641482; PubMed Central PMCID: PMCPMC7459569.

96. Pfaender S, Mar KB, Michailidis E, Kratzel A, Boys IN, V'Kovski P, et al. LY6E impairs coronavirus fusion and confers immune control of viral disease. Nat Microbiol. 2020;5(11):1330-9. Epub 20200723. doi: 10.1038/s41564-020-0769-y. PubMed PMID: 32704094; PubMed Central PMCID: PMCPMC7916999.
97. Lin TY, Chin CR, Everitt AR, Clare S, Perreira JM, Savidis G, et al. Amphotericin B increases influenza A virus infection by preventing IFITM3-mediated restriction. Cell Rep. 2013;5(4):895-908. Epub 20131121. doi: 10.1016/j.celrep.2013.10.033. PubMed PMID: 24268777; PubMed Central PMCID: PMCPMC3898084.
98. Yu J, Liang C, Liu SL. Interferon-inducible LY6E Protein Promotes HIV-1 Infection. J Biol Chem. 2017;292(11):4674-85. Epub 20170127. doi: 10.1074/jbc.M116.755819. PubMed PMID: 28130445; PubMed Central PMCID: PMCPMC5377782.
99. Xu X, Qiu C, Zhu L, Huang J, Li L, Fu W, et al. IFN-stimulated gene LY6E in monocytes regulates the CD14/TLR4 pathway but inadequately restrains the hyperactivation of monocytes during chronic HIV-1 infection. J Immunol. 2014;193(8):4125-36. Epub 20140915. doi: 10.4049/jimmunol.1401249. PubMed PMID: 25225669.
100. Katrina B. Mar NRR, Ian N. Boys, Jennifer L. Eitson, Matthew B. McDougal, R. Blake Richardson, and John W. Schoggins. LY6E mediates an evolutionarily conserved enhancement of virus infection by targeting a late entry step. Nature Communications. 2018. doi: 10.1038/s41467-018-06000-y. PubMed Central PMCID: PMCPMC6127192.
101. Liu SY, Aliyari R, Chikere K, Li G, Marsden MD, Smith JK, et al. Interferon-inducible cholesterol-25-hydroxylase broadly inhibits viral entry by production of 25-hydroxycholesterol. Immunity. 2013;38(1):92-105. Epub 20121227. doi: 10.1016/j.immuni.2012.11.005. PubMed PMID: 23273844; PubMed Central PMCID: PMCPMC3698975.
102. Wang S, Li W, Hui H, Tiwari SK, Zhang Q, Croker BA, et al. Cholesterol 25-Hydroxylase inhibits SARS-CoV-2 and other coronaviruses by depleting membrane cholesterol. EMBO J. 2020;39(21):e106057. Epub 20201005. doi: 10.15252/embj.2020106057. PubMed PMID: 32944968; PubMed Central PMCID: PMCPMC7537045.
103. Li C, Deng YQ, Wang S, Ma F, Aliyari R, Huang XY, et al. 25-Hydroxycholesterol Protects Host against Zika Virus Infection and Its Associated Microcephaly in a Mouse Model. Immunity. 2017;46(3):446-56. Epub 20170314. doi: 10.1016/j.immuni.2017.02.012. PubMed PMID: 28314593; PubMed Central PMCID: PMCPMC5957489.
104. Anggakusuma, Romero-Brey I, Berger C, Colpitts CC, Boldanova T, Engelmann M, et al. Interferon-inducible cholesterol-25-hydroxylase restricts hepatitis C virus replication through blockage of membranous web formation. Hepatology. 2015;62(3):702-14. Epub 20150728. doi: 10.1002/hep.27913. PubMed PMID: 25999047.
105. Worobey M. Dissecting the early COVID-19 cases in Wuhan. Science. 2021;374(6572):1202-4. Epub 20211118. doi: 10.1126/science.abm4454. PubMed PMID: 34793199.
106. Zhou P, Yang XL, Wang XG, Hu B, Zhang L, Zhang W, et al. Addendum: A pneumonia outbreak associated with a new coronavirus of probable bat origin. Nature. 2020;588(7836):E6. doi: 10.1038/s41586-020-2951-z. PubMed PMID: 33199918.
107. WHO. Weekly epidemiological update https://www.who.int/publications/m/item/weekly-epidemiological-update---29-december-20202020.
108. WHO. COVID-19 dashboard https://covid19.who.int/?adgroupsurvey={adgroupsurvey}&gclid=Cj0KCQjwmouZBhDSARIs

ALYcouph8xIC0RoCuhjK9rARA19deS-JC0CFYEPpG_istZy1H4FwkD7pCWEaAuCpEALw_wcB2022.
109. Malaiyan J, Arumugam S, Mohan K, Gomathi Radhakrishnan G. An update on the origin of SARS-CoV-2: Despite closest identity, bat (RaTG13) and pangolin derived coronaviruses varied in the critical binding site and O-linked glycan residues. J Med Virol. 2021;93(1):499-505. Epub 20200714. doi: 10.1002/jmv.26261. PubMed PMID: 32633815; PubMed Central PMCID: PMCPMC7361880.
110. Lam TT, Jia N, Zhang YW, Shum MH, Jiang JF, Zhu HC, et al. Identifying SARS-CoV-2-related coronaviruses in Malayan pangolins. Nature. 2020;583(7815):282-5. Epub 20200326. doi: 10.1038/s41586-020-2169-0. PubMed PMID: 32218527.
111. Lopes LR, de Mattos Cardillo G, Paiva PB. Molecular evolution and phylogenetic analysis of SARS-CoV-2 and hosts ACE2 protein suggest Malayan pangolin as intermediary host. Braz J Microbiol. 2020;51(4):1593-9. Epub 20200626. doi: 10.1007/s42770-020-00321-1. PubMed PMID: 32592038; PubMed Central PMCID: PMCPMC7319214.
112. Wang W, Tian JH, Chen X, Hu RX, Lin XD, Pei YY, et al. Coronaviruses in wild animals sampled in and around Wuhan at the beginning of COVID-19 emergence. Virus Evol. 2022;8(1):veac046. Epub 20220604. doi: 10.1093/ve/veac046. PubMed PMID: 35769892; PubMed Central PMCID: PMCPMC9214087.
113. Andersen KG, Rambaut A, Lipkin WI, Holmes EC, Garry RF. The proximal origin of SARS-CoV-2. Nat Med. 2020;26(4):450-2. doi: 10.1038/s41591-020-0820-9. PubMed PMID: 32284615; PubMed Central PMCID: PMCPMC7095063.
114. Bagdonaite I, Wandall HH. Global aspects of viral glycosylation. Glycobiology. 2018;28(7):443-67. doi: 10.1093/glycob/cwy021. PubMed PMID: 29579213; PubMed Central PMCID: PMCPMC7108637.
115. Pekar JE, Magee A, Parker E, Moshiri N, Izhikevich K, Havens JL, et al. The molecular epidemiology of multiple zoonotic origins of SARS-CoV-2. Science. 2022:eabp8337. Epub 20220726. doi: 10.1126/science.abp8337. PubMed PMID: 35881005.
116. He WT, Hou X, Zhao J, Sun J, He H, Si W, et al. Virome characterization of game animals in China reveals a spectrum of emerging pathogens. Cell. 2022;185(7):1117-29 e8. Epub 20220216. doi: 10.1016/j.cell.2022.02.014. PubMed PMID: 35298912.
117. https://ictv.global/taxonomy [cited 2022].
118. Malik YA. Properties of Coronavirus and SARS-CoV-2. Malays J Pathol. 2020;42(1):3-11. PubMed PMID: 32342926.
119. Rastogi M, Pandey N, Shukla A, Singh SK. SARS coronavirus 2: from genome to infectome. Respir Res. 2020;21(1):318. Epub 20201201. doi: 10.1186/s12931-020-01581-z. PubMed PMID: 33261606; PubMed Central PMCID: PMCPMC7706175.
120. Brant AC, Tian W, Majerciak V, Yang W, Zheng ZM. SARS-CoV-2: from its discovery to genome structure, transcription, and replication. Cell Biosci. 2021;11(1):136. Epub 20210719. doi: 10.1186/s13578-021-00643-z. PubMed PMID: 34281608; PubMed Central PMCID: PMCPMC8287290.
121. Massimo Pizzato* CB, Giulia Boscato Sopetto†, Davide Finozzi†, Carmelo Gentile†, Michele Domenico Gentile†, Roberta Marconi†, Dalila Paladino†, Alberto Raoss†, Ilary Riedmiller†, Hamza Ur Rehman†, Annalisa Santini†, Valerio Succetti† and Lorenzo Volpini†. SARS-CoV-2 and the Host Cell: A Tale of Interactions. Frontiers in Virology. 2022.
122. V'Kovski P, Kratzel A, Steiner S, Stalder H, Thiel V. Coronavirus biology and replication: implications for SARS-CoV-2. Nat Rev Microbiol. 2021;19(3):155-70. Epub 20201028. doi:

10.1038/s41579-020-00468-6. PubMed PMID: 33116300; PubMed Central PMCID: PMCPMC7592455.
123. Thomas S. The Structure of the Membrane Protein of SARS-CoV-2 Resembles the Sugar Transporter SemiSWEET. Pathog Immun. 2020;5(1):342-63. Epub 20201019. doi: 10.20411/pai.v5i1.377. PubMed PMID: 33154981; PubMed Central PMCID: PMCPMC7608487.
124. Liu L, Chopra P, Li X, Bouwman KM, Tompkins SM, Wolfert MA, et al. Heparan Sulfate Proteoglycans as Attachment Factor for SARS-CoV-2. ACS Cent Sci. 2021;7(6):1009-18. Epub 20210602. doi: 10.1021/acscentsci.1c00010. PubMed PMID: 34235261; PubMed Central PMCID: PMCPMC8227597.
125. Lempp FA, Soriaga LB, Montiel-Ruiz M, Benigni F, Noack J, Park YJ, et al. Lectins enhance SARS-CoV-2 infection and influence neutralizing antibodies. Nature. 2021;598(7880):342-7. Epub 20210831. doi: 10.1038/s41586-021-03925-1. PubMed PMID: 34464958.
126. Araf Y, Akter F, Tang YD, Fatemi R, Parvez MSA, Zheng C, et al. Omicron variant of SARS-CoV-2: Genomics, transmissibility, and responses to current COVID-19 vaccines. J Med Virol. 2022;94(5):1825-32. Epub 20220123. doi: 10.1002/jmv.27588. PubMed PMID: 35023191; PubMed Central PMCID: PMCPMC9015557.
127. Kishimoto M, Uemura K, Sanaki T, Sato A, Hall WW, Kariwa H, et al. TMPRSS11D and TMPRSS13 Activate the SARS-CoV-2 Spike Protein. Viruses. 2021;13(3). Epub 20210228. doi: 10.3390/v13030384. PubMed PMID: 33671076; PubMed Central PMCID: PMCPMC8001073.
128. Yamamoto M, Gohda J, Kobayashi A, Tomita K, Hirayama Y, Koshikawa N, et al. Metalloproteinase-Dependent and TMPRSS2-Independent Cell Surface Entry Pathway of SARS-CoV-2 Requires the Furin Cleavage Site and the S2 Domain of Spike Protein. mBio. 2022:e0051922. Epub 20220616. doi: 10.1128/mbio.00519-22. PubMed PMID: 35708281.
129. Mehdi Benlarbi GL, Corby Fink, Kathy Fu, Rory P. Mulloy, Alexandra Phan, Ardeshir Ariana, Corina M. Stewart, Jérémie Prévost, Guillaume Beaudoin-Bussières, Redaet Daniel, Yuxia Bo, Julien Yockell-Lelièvre, William L. Stanford, Patrick M. Giguère, Samira Mubareka, Andrés Finzi, Gregory A. Dekaban, Jimmy D. Dikeakos, Marceline Côté. Identification of a SARS-CoV-2 host metalloproteinase-dependent entry pathway differentially used by SARS-CoV-2 and variants of concern Alpha, Delta, and Omicron. bioRxiv. 2022.
130. Lou Z, Rao Z. The Life of SARS-CoV-2 Inside Cells: Replication-Transcription Complex Assembly and Function. Annu Rev Biochem. 2022;91:381-401. doi: 10.1146/annurev-biochem-052521-115653. PubMed PMID: 35729072.
131. Angelini MM, Akhlaghpour M, Neuman BW, Buchmeier MJ. Severe acute respiratory syndrome coronavirus nonstructural proteins 3, 4, and 6 induce double-membrane vesicles. mBio. 2013;4(4). Epub 20130813. doi: 10.1128/mBio.00524-13. PubMed PMID: 23943763; PubMed Central PMCID: PMCPMC3747587.
132. Wang Y, Wang Y, Luo W, Huang L, Xiao J, Li F, et al. A comprehensive investigation of the mRNA and protein level of ACE2, the putative receptor of SARS-CoV-2, in human tissues and blood cells. Int J Med Sci. 2020;17(11):1522-31. Epub 20200618. doi: 10.7150/ijms.46695. PubMed PMID: 32669955; PubMed Central PMCID: PMCPMC7359402.
133. Lindner D, Fitzek A, Brauninger H, Aleshcheva G, Edler C, Meissner K, et al. Association of Cardiac Infection With SARS-CoV-2 in Confirmed COVID-19 Autopsy Cases. JAMA Cardiol. 2020;5(11):1281-5. doi: 10.1001/jamacardio.2020.3551. PubMed PMID: 32730555; PubMed Central PMCID: PMCPMC7385672.

134. Tang T, Jaimes JA, Bidon MK, Straus MR, Daniel S, Whittaker GR. Proteolytic Activation of SARS-CoV-2 Spike at the S1/S2 Boundary: Potential Role of Proteases beyond Furin. ACS Infect Dis. 2021;7(2):264-72. Epub 20210112. doi: 10.1021/acsinfecdis.0c00701. PubMed PMID: 33432808; PubMed Central PMCID: PMCPMC7839419.
135. Fischer F, Stegen CF, Masters PS, Samsonoff WA. Analysis of constructed E gene mutants of mouse hepatitis virus confirms a pivotal role for E protein in coronavirus assembly. J Virol. 1998;72(10):7885-94. doi: 10.1128/JVI.72.10.7885-7894.1998. PubMed PMID: 9733825; PubMed Central PMCID: PMCPMC110113.
136. Vennema H, Godeke GJ, Rossen JW, Voorhout WF, Horzinek MC, Opstelten DJ, et al. Nucleocapsid-independent assembly of coronavirus-like particles by co-expression of viral envelope protein genes. EMBO J. 1996;15(8):2020-8. PubMed PMID: 8617249; PubMed Central PMCID: PMCPMC450121.
137. Jorrissen P, Schutz P, Weiand M, Vollenberg R, Schrempf IM, Ochs K, et al. Antibody Response to SARS-CoV-2 Membrane Protein in Patients of the Acute and Convalescent Phase of COVID-19. Front Immunol. 2021;12:679841. Epub 20210804. doi: 10.3389/fimmu.2021.679841. PubMed PMID: 34421894; PubMed Central PMCID: PMCPMC8371319.
138. Schultze B, Gross HJ, Brossmer R, Herrler G. The S protein of bovine coronavirus is a hemagglutinin recognizing 9-O-acetylated sialic acid as a receptor determinant. J Virol. 1991;65(11):6232-7. doi: 10.1128/JVI.65.11.6232-6237.1991. PubMed PMID: 1920630; PubMed Central PMCID: PMCPMC250319.
139. Meng B, Datir R, Choi J, Collaboration C-NBC-, Bradley JR, Smith KGC, et al. SARS-CoV-2 spike N-terminal domain modulates TMPRSS2-dependent viral entry and fusogenicity. Cell Rep. 2022;40(7):111220. Epub 20220803. doi: 10.1016/j.celrep.2022.111220. PubMed PMID: 35963244; PubMed Central PMCID: PMCPMC9346021.
140. Qing E, Kicmal T, Kumar B, Hawkins GM, Timm E, Perlman S, et al. Dynamics of SARS-CoV-2 Spike Proteins in Cell Entry: Control Elements in the Amino-Terminal Domains. mBio. 2021;12(4):e0159021. Epub 20210803. doi: 10.1128/mBio.01590-21. PubMed PMID: 34340537; PubMed Central PMCID: PMCPMC8406164.
141. Planas D, Veyer D, Baidaliuk A, Staropoli I, Guivel-Benhassine F, Rajah MM, et al. Reduced sensitivity of SARS-CoV-2 variant Delta to antibody neutralization. Nature. 2021;596(7871):276-80. Epub 20210708. doi: 10.1038/s41586-021-03777-9. PubMed PMID: 34237773.
142. McCallum M, De Marco A, Lempp FA, Tortorici MA, Pinto D, Walls AC, et al. N-terminal domain antigenic mapping reveals a site of vulnerability for SARS-CoV-2. Cell. 2021;184(9):2332-47 e16. Epub 20210316. doi: 10.1016/j.cell.2021.03.028. PubMed PMID: 33761326; PubMed Central PMCID: PMCPMC7962585.
143. Chen L, Zody MC, Di Germanio C, Martinelli R, Mediavilla JR, Cunningham MH, et al. Emergence of Multiple SARS-CoV-2 Antibody Escape Variants in an Immunocompromised Host Undergoing Convalescent Plasma Treatment. mSphere. 2021;6(4):e0048021. Epub 20210825. doi: 10.1128/mSphere.00480-21. PubMed PMID: 34431691; PubMed Central PMCID: PMCPMC8386433.
144. Wan Y, Shang J, Graham R, Baric RS, Li F. Receptor Recognition by the Novel Coronavirus from Wuhan: an Analysis Based on Decade-Long Structural Studies of SARS Coronavirus. J Virol. 2020;94(7). Epub 20200317. doi: 10.1128/JVI.00127-20. PubMed PMID: 31996437; PubMed Central PMCID: PMCPMC7081895.

145. Jawad B, Adhikari P, Podgornik R, Ching WY. Key Interacting Residues between RBD of SARS-CoV-2 and ACE2 Receptor: Combination of Molecular Dynamics Simulation and Density Functional Calculation. J Chem Inf Model. 2021;61(9):4425-41. Epub 20210824. doi: 10.1021/acs.jcim.1c00560. PubMed PMID: 34428371; PubMed Central PMCID: PMCPMC8409146.
146. Wrobel AG, Benton DJ, Xu P, Roustan C, Martin SR, Rosenthal PB, et al. SARS-CoV-2 and bat RaTG13 spike glycoprotein structures inform on virus evolution and furin-cleavage effects. Nat Struct Mol Biol. 2020;27(8):763-7. Epub 2020/07/11. doi: 10.1038/s41594-020-0468-7. PubMed PMID: 32647346.
147. Yao H, Song Y, Chen Y, Wu N, Xu J, Sun C, et al. Molecular Architecture of the SARS-CoV-2 Virus. Cell. 2020;183(3):730-8 e13. Epub 20200906. doi: 10.1016/j.cell.2020.09.018. PubMed PMID: 32979942; PubMed Central PMCID: PMCPMC7474903.
148. Ke Z, Oton J, Qu K, Cortese M, Zila V, McKeane L, et al. Structures and distributions of SARS-CoV-2 spike proteins on intact virions. Nature. 2020;588(7838):498-502. Epub 20200817. doi: 10.1038/s41586-020-2665-2. PubMed PMID: 32805734; PubMed Central PMCID: PMCPMC7116492.
149. Zhao MM, Zhu Y, Zhang L, Zhong G, Tai L, Liu S, et al. Novel cleavage sites identified in SARS-CoV-2 spike protein reveal mechanism for cathepsin L-facilitated viral infection and treatment strategies. Cell Discov. 2022;8(1):53. Epub 20220606. doi: 10.1038/s41421-022-00419-w. PubMed PMID: 35668062.
150. Peacock TP, Goldhill DH, Zhou J, Baillon L, Frise R, Swann OC, et al. The furin cleavage site in the SARS-CoV-2 spike protein is required for transmission in ferrets. Nat Microbiol. 2021;6(7):899-909. Epub 2021/04/29. doi: 10.1038/s41564-021-00908-w. PubMed PMID: 33907312.
151. Johnson BA, Xie X, Bailey AL, Kalveram B, Lokugamage KG, Muruato A, et al. Loss of furin cleavage site attenuates SARS-CoV-2 pathogenesis. Nature. 2021;591(7849):293-9. Epub 20210125. doi: 10.1038/s41586-021-03237-4. PubMed PMID: 33494095; PubMed Central PMCID: PMCPMC8175039.
152. Menachery VD, Dinnon KH, 3rd, Yount BL, Jr., McAnarney ET, Gralinski LE, Hale A, et al. Trypsin Treatment Unlocks Barrier for Zoonotic Bat Coronavirus Infection. J Virol. 2020;94(5). Epub 20200214. doi: 10.1128/JVI.01774-19. PubMed PMID: 31801868; PubMed Central PMCID: PMCPMC7022341.
153. Alexander DJ, Brown IH. History of highly pathogenic avian influenza. Rev Sci Tech. 2009;28(1):19-38. doi: 10.20506/rst.28.1.1856. PubMed PMID: 19618616.
154. Sasaki M, Uemura K, Sato A, Toba S, Sanaki T, Maenaka K, et al. SARS-CoV-2 variants with mutations at the S1/S2 cleavage site are generated in vitro during propagation in TMPRSS2-deficient cells. PLoS Pathog. 2021;17(1):e1009233. Epub 20210121. doi: 10.1371/journal.ppat.1009233. PubMed PMID: 33476327; PubMed Central PMCID: PMCPMC7853460.
155. Wong YC, Lau SY, Wang To KK, Mok BWY, Li X, Wang P, et al. Natural transmission of bat-like SARS-CoV-2PRRA variants in COVID-19 patients. Clin Infect Dis. 2020. Epub 2020/07/11. doi: 10.1093/cid/ciaa953. PubMed PMID: 32649739; PubMed Central PMCID: PMCPMC7454488.
156. Xing Y, Li X, Gao X, Dong Q. Natural Polymorphisms Are Present in the Furin Cleavage Site of the SARS-CoV-2 Spike Glycoprotein. Front Genet. 2020;11:783. Epub 20200717. doi: 10.3389/fgene.2020.00783. PubMed PMID: 32765596; PubMed Central PMCID: PMCPMC7379507.

157. Liu Y, Liu J, Johnson BA, Xia H, Ku Z, Schindewolf C, et al. Delta spike P681R mutation enhances SARS-CoV-2 fitness over Alpha variant. Cell Rep. 2022;39(7):110829. Epub 20220429. doi: 10.1016/j.celrep.2022.110829. PubMed PMID: 35550680; PubMed Central PMCID: PMCPMC9050581.
158. Peacock TP, Sheppard CM, Brown JC, Goonawardane N, Zhou J, Whiteley M, et al. The SARS-CoV-2 variants associated with infections in India, B.1.617, show enhanced spike cleavage by furin. bioRxiv. 2021:2021.05.28.446163. doi: 10.1101/2021.05.28.446163.
159. Lubinski B, Fernandes MHV, Frazier L, Tang T, Daniel S, Diel DG, et al. Functional evaluation of the P681H mutation on the proteolytic activation of the SARS-CoV-2 variant B.1.1.7 (Alpha) spike. iScience. 2022;25(1):103589. Epub 20211210. doi: 10.1016/j.isci.2021.103589. PubMed PMID: 34909610; PubMed Central PMCID: PMCPMC8662955.
160. Bestle D, Heindl MR, Limburg H, Van Lam van T, Pilgram O, Moulton H, et al. TMPRSS2 and furin are both essential for proteolytic activation of SARS-CoV-2 in human airway cells. Life Sci Alliance. 2020;3(9). Epub 20200723. doi: 10.26508/lsa.202000786. PubMed PMID: 32703818; PubMed Central PMCID: PMCPMC7383062.
161. Lamers MM, Mykytyn AZ, Breugem TI, Wang Y, Wu DC, Riesebosch S, et al. Human airway cells prevent SARS-CoV-2 multibasic cleavage site cell culture adaptation. Elife. 2021;10. Epub 20210409. doi: 10.7554/eLife.66815. PubMed PMID: 33835028; PubMed Central PMCID: PMCPMC8131099.
162. Cantuti-Castelvetri L, Ojha R, Pedro LD, Djannatian M, Franz J, Kuivanen S, et al. Neuropilin-1 facilitates SARS-CoV-2 cell entry and infectivity. Science. 2020;370(6518):856-60. Epub 20201020. doi: 10.1126/science.abd2985. PubMed PMID: 33082293; PubMed Central PMCID: PMCPMC7857391.
163. Daly JL, Simonetti B, Klein K, Chen KE, Williamson MK, Anton-Plagaro C, et al. Neuropilin-1 is a host factor for SARS-CoV-2 infection. Science. 2020;370(6518):861-5. Epub 20201020. doi: 10.1126/science.abd3072. PubMed PMID: 33082294.
164. Duan L, Zheng Q, Zhang H, Niu Y, Lou Y, Wang H. The SARS-CoV-2 Spike Glycoprotein Biosynthesis, Structure, Function, and Antigenicity: Implications for the Design of Spike-Based Vaccine Immunogens. Front Immunol. 2020;11:576622. Epub 20201007. doi: 10.3389/fimmu.2020.576622. PubMed PMID: 33117378; PubMed Central PMCID: PMCPMC7575906.
165. Zhang L, Mann M, Syed ZA, Reynolds HM, Tian E, Samara NL, et al. Furin cleavage of the SARS-CoV-2 spike is modulated by O-glycosylation. Proc Natl Acad Sci U S A. 2021;118(47). doi: 10.1073/pnas.2109905118. PubMed PMID: 34732583; PubMed Central PMCID: PMCPMC8617502.
166. Papa G, Mallery DL, Albecka A, Welch LG, Cattin-Ortola J, Luptak J, et al. Furin cleavage of SARS-CoV-2 Spike promotes but is not essential for infection and cell-cell fusion. PLoS Pathog. 2021;17(1):e1009246. Epub 20210125. doi: 10.1371/journal.ppat.1009246. PubMed PMID: 33493182; PubMed Central PMCID: PMCPMC7861537.
167. Baron J, Tarnow C, Mayoli-Nussle D, Schilling E, Meyer D, Hammami M, et al. Matriptase, HAT, and TMPRSS2 activate the hemagglutinin of H9N2 influenza A viruses. J Virol. 2013;87(3):1811-20. Epub 20121128. doi: 10.1128/JVI.02320-12. PubMed PMID: 23192872; PubMed Central PMCID: PMCPMC3554176.
168. Jennings BC, Kornfeld S, Doray B. A weak COPI binding motif in the cytoplasmic tail of SARS-CoV-2 spike glycoprotein is necessary for its cleavage, glycosylation, and localization.

FEBS Lett. 2021;595(13):1758-67. Epub 20210526. doi: 10.1002/1873-3468.14109. PubMed PMID: 33991349; PubMed Central PMCID: PMCPMC8209879.
169. Cattin-Ortola J, Welch LG, Maslen SL, Papa G, James LC, Munro S. Sequences in the cytoplasmic tail of SARS-CoV-2 Spike facilitate expression at the cell surface and syncytia formation. Nat Commun. 2021;12(1):5333. Epub 20210909. doi: 10.1038/s41467-021-25589-1. PubMed PMID: 34504087; PubMed Central PMCID: PMCPMC8429659.
170. Boson B, Legros V, Zhou B, Siret E, Mathieu C, Cosset FL, et al. The SARS-CoV-2 envelope and membrane proteins modulate maturation and retention of the spike protein, allowing assembly of virus-like particles. J Biol Chem. 2021;296:100111. Epub 20201203. doi: 10.1074/jbc.RA120.016175. PubMed PMID: 33229438; PubMed Central PMCID: PMCPMC7833635.
171. McBride CE, Li J, Machamer CE. The cytoplasmic tail of the severe acute respiratory syndrome coronavirus spike protein contains a novel endoplasmic reticulum retrieval signal that binds COPI and promotes interaction with membrane protein. J Virol. 2007;81(5):2418-28. Epub 20061213. doi: 10.1128/JVI.02146-06. PubMed PMID: 17166901; PubMed Central PMCID: PMCPMC1865919.
172. Barrett CT, Neal HE, Edmonds K, Moncman CL, Thompson R, Branttie JM, et al. Effect of mutations in the SARS-CoV-2 spike protein on protein stability, cleavage, and cell-cell fusion function. bioRxiv. 2021. Epub 20210125. doi: 10.1101/2021.01.24.428007. PubMed PMID: 33532777; PubMed Central PMCID: PMCPMC7852270.
173. Rajah MM, Hubert M, Bishop E, Saunders N, Robinot R, Grzelak L, et al. SARS-CoV-2 Alpha, Beta, and Delta variants display enhanced Spike-mediated syncytia formation. EMBO J. 2021;40(24):e108944. Epub 20211025. doi: 10.15252/embj.2021108944. PubMed PMID: 34601723; PubMed Central PMCID: PMCPMC8646911.
174. Lontok E, Corse E, Machamer CE. Intracellular targeting signals contribute to localization of coronavirus spike proteins near the virus assembly site. J Virol. 2004;78(11):5913-22. doi: 10.1128/JVI.78.11.5913-5922.2004. PubMed PMID: 15140989; PubMed Central PMCID: PMCPMC415842.
175. Chen HY, Huang C, Tian L, Huang X, Zhang C, Llewellyn GN, et al. Cytoplasmic Tail Truncation of SARS-CoV-2 Spike Protein Enhances Titer of Pseudotyped Vectors but Masks the Effect of the D614G Mutation. J Virol. 2021;95(22):e0096621. Epub 20210908. doi: 10.1128/JVI.00966-21. PubMed PMID: 34495700; PubMed Central PMCID: PMCPMC8549521.
176. Li Q, Wu J, Nie J, Zhang L, Hao H, Liu S, et al. The Impact of Mutations in SARS-CoV-2 Spike on Viral Infectivity and Antigenicity. Cell. 2020;182(5):1284-94 e9. Epub 20200717. doi: 10.1016/j.cell.2020.07.012. PubMed PMID: 32730807; PubMed Central PMCID: PMCPMC7366990.
177. Casalino L, Gaieb Z, Goldsmith JA, Hjorth CK, Dommer AC, Harbison AM, et al. Beyond Shielding: The Roles of Glycans in the SARS-CoV-2 Spike Protein. ACS Cent Sci. 2020;6(10):1722-34. Epub 20200923. doi: 10.1021/acscentsci.0c01056. PubMed PMID: 33140034; PubMed Central PMCID: PMCPMC7523240.
178. Morales AC, Rice AM, Ho AT, Mordstein C, Muhlhausen S, Watson S, et al. Causes and Consequences of Purifying Selection on SARS-CoV-2. Genome Biol Evol. 2021;13(10). doi: 10.1093/gbe/evab196. PubMed PMID: 34427640; PubMed Central PMCID: PMCPMC8504154.
179. Bhattacharya M, Chatterjee S, Sharma AR, Agoramoorthy G, Chakraborty C. D614G mutation and SARS-CoV-2: impact on S-protein structure, function, infectivity, and immunity.

Appl Microbiol Biotechnol. 2021;105(24):9035-45. Epub 20211110. doi: 10.1007/s00253-021-11676-2. PubMed PMID: 34755213; PubMed Central PMCID: PMCPMC8578012.
180. Lindstrom JC, Engebretsen S, Kristoffersen AB, Ro GOI, Palomares AD, Engo-Monsen K, et al. Increased transmissibility of the alpha SARS-CoV-2 variant: evidence from contact tracing data in Oslo, January to February 2021. Infect Dis (Lond). 2021:1-6. Epub 2021/10/08. doi: 10.1080/23744235.2021.1977382. PubMed PMID: 34618665.
181. Tanaka H, Hirayama A, Nagai H, Shirai C, Takahashi Y, Shinomiya H, et al. Increased Transmissibility of the SARS-CoV-2 Alpha Variant in a Japanese Population. Int J Environ Res Public Health. 2021;18(15). Epub 2021/08/08. doi: 10.3390/ijerph18157752. PubMed PMID: 34360046; PubMed Central PMCID: PMCPMC8345780.
182. Mok BW, Liu H, Deng S, Liu J, Zhang AJ, Lau SY, et al. Low dose inocula of SARS-CoV-2 Alpha variant transmits more efficiently than earlier variants in hamsters. Commun Biol. 2021;4(1):1102. Epub 2021/09/22. doi: 10.1038/s42003-021-02640-x. PubMed PMID: 34545191; PubMed Central PMCID: PMCPMC8452646.
183. Wrapp D, Wang N, Corbett KS, Goldsmith JA, Hsieh CL, Abiona O, et al. Cryo-EM structure of the 2019-nCoV spike in the prefusion conformation. Science. 2020;367(6483):1260-3. Epub 20200219. doi: 10.1126/science.abb2507. PubMed PMID: 32075877; PubMed Central PMCID: PMCPMC7164637.
184. Lokugamage KG, Hage A, de Vries M, Valero-Jimenez AM, Schindewolf C, Dittmann M, et al. Type I Interferon Susceptibility Distinguishes SARS-CoV-2 from SARS-CoV. J Virol. 2020;94(23). Epub 20201109. doi: 10.1128/JVI.01410-20. PubMed PMID: 32938761; PubMed Central PMCID: PMCPMC7654262.
185. Korber B, Fischer WM, Gnanakaran S, Yoon H, Theiler J, Abfalterer W, et al. Tracking Changes in SARS-CoV-2 Spike: Evidence that D614G Increases Infectivity of the COVID-19 Virus. Cell. 2020;182(4):812-27 e19. Epub 20200703. doi: 10.1016/j.cell.2020.06.043. PubMed PMID: 32697968; PubMed Central PMCID: PMCPMC7332439.
186. Volz E, Hill V, McCrone JT, Price A, Jorgensen D, O'Toole A, et al. Evaluating the Effects of SARS-CoV-2 Spike Mutation D614G on Transmissibility and Pathogenicity. Cell. 2021;184(1):64-75 e11. Epub 20201119. doi: 10.1016/j.cell.2020.11.020. PubMed PMID: 33275900; PubMed Central PMCID: PMCPMC7674007.
187. Plante JA, Liu Y, Liu J, Xia H, Johnson BA, Lokugamage KG, et al. Spike mutation D614G alters SARS-CoV-2 fitness. Nature. 2021;592(7852):116-21. Epub 20201026. doi: 10.1038/s41586-020-2895-3. PubMed PMID: 33106671; PubMed Central PMCID: PMCPMC8158177.
188. Takeda M. Proteolytic activation of SARS-CoV-2 spike protein. Microbiol Immunol. 2022;66(1):15-23. Epub 20211012. doi: 10.1111/1348-0421.12945. PubMed PMID: 34561887; PubMed Central PMCID: PMCPMC8652499.
189. Zhang L, Jackson CB, Mou H, Ojha A, Peng H, Quinlan BD, et al. SARS-CoV-2 spike-protein D614G mutation increases virion spike density and infectivity. Nat Commun. 2020;11(1):6013. Epub 20201126. doi: 10.1038/s41467-020-19808-4. PubMed PMID: 33243994; PubMed Central PMCID: PMCPMC7693302.
190. Meng B, Kemp SA, Papa G, Datir R, Ferreira I, Marelli S, et al. Recurrent emergence of SARS-CoV-2 spike deletion H69/V70 and its role in the Alpha variant B.1.1.7. Cell Rep. 2021;35(13):109292. Epub 2021/06/25. doi: 10.1016/j.celrep.2021.109292. PubMed PMID: 34166617; PubMed Central PMCID: PMCPMC8185188.

191. Tian F, Tong B, Sun L, Shi S, Zheng B, Wang Z, et al. N501Y mutation of spike protein in SARS-CoV-2 strengthens its binding to receptor ACE2. Elife. 2021;10. Epub 20210820. doi: 10.7554/eLife.69091. PubMed PMID: 34414884; PubMed Central PMCID: PMCPMC8455130.
192. Mohammad A, Abubaker J, Al-Mulla F. Structural modelling of SARS-CoV-2 alpha variant (B.1.1.7) suggests enhanced furin binding and infectivity. Virus Res. 2021;303:198522. Epub 20210724. doi: 10.1016/j.virusres.2021.198522. PubMed PMID: 34314772; PubMed Central PMCID: PMCPMC8310422.
193. Thorne LG, Bouhaddou M, Reuschl AK, Zuliani-Alvarez L, Polacco B, Pelin A, et al. Evolution of enhanced innate immune evasion by SARS-CoV-2. Nature. 2022;602(7897):487-95. Epub 20211223. doi: 10.1038/s41586-021-04352-y. PubMed PMID: 34942634; PubMed Central PMCID: PMCPMC8850198.
194. Bazykin GA SO, Danilenko D, Fadeev A, Komissarova K, Ivanova A,, Sergeeva M SK, Nabieva E, Klink G, Garushyants S, Zabutova J, Kholodnaia A, Skorokhod I, Ryabchikova VV, Komissarov A, Lioznov D.
Emergence of Y453F and Δ69-70HV mutations in a lymphoma patient with long-term COVID-19. 2020. doi: https://virological.org/t/emergence-of-y453f-and-69-70hv-mutations-in-a-lymphoma-patient-with-long-term-covid-19/580.
195. Choi B, Choudhary MC, Regan J, Sparks JA, Padera RF, Qiu X, et al. Persistence and Evolution of SARS-CoV-2 in an Immunocompromised Host. N Engl J Med. 2020;383(23):2291-3. Epub 20201111. doi: 10.1056/NEJMc2031364. PubMed PMID: 33176080; PubMed Central PMCID: PMCPMC7673303.
196. Avanzato VA, Matson MJ, Seifert SN, Pryce R, Williamson BN, Anzick SL, et al. Case Study: Prolonged Infectious SARS-CoV-2 Shedding from an Asymptomatic Immunocompromised Individual with Cancer. Cell. 2020;183(7):1901-12 e9. Epub 20201104. doi: 10.1016/j.cell.2020.10.049. PubMed PMID: 33248470; PubMed Central PMCID: PMCPMC7640888.
197. Starr TN, Greaney AJ, Hannon WW, Loes AN, Hauser K, Dillen JR, et al. Shifting mutational constraints in the SARS-CoV-2 receptor-binding domain during viral evolution. Science. 2022;377(6604):420-4. Epub 20220628. doi: 10.1126/science.abo7896. PubMed PMID: 35762884; PubMed Central PMCID: PMCPMC9273037.
198. https://covariants.org/ [cited 2022].
199. Ostrov DA, Knox GW. Emerging mutation patterns in SARS-CoV-2 variants. Biochem Biophys Res Commun. 2022;586:87-92. Epub 20211122. doi: 10.1016/j.bbrc.2021.11.059. PubMed PMID: 34837837; PubMed Central PMCID: PMCPMC8606318.
200. Maia Kavanagh Williamson FH, Stephanie Hutchings, Hannah M. Pymont, Mark Hackett, David Arnold, Nick A Maskell, Alasdair MacGowan, Mahableshwar Albur, Megan Jenkins, Izak Heys, Francesca Knapper, Mustafa Elsayed, Rachel Milligan, The COVID-19 Genomics UK (COG-UK) Consortium, Peter Muir, Barry Vipond, David A Matthews, Ed Moran, Andrew D. Davidson. Chronic SARS-CoV-2 infection and viral evolution in a hypogammaglobulinaemic individual. medRxiv. 2021.
201. Rowe LA, Beddingfield BJ, Goff K, Killeen SZ, Chirichella NR, Melton A, et al. Intra-Host SARS-CoV-2 Evolution in the Gut of Mucosally-Infected Chlorocebus aethiops (African Green Monkeys). Viruses. 2022;14(1). Epub 20220101. doi: 10.3390/v14010077. PubMed PMID: 35062281; PubMed Central PMCID: PMCPMC8777858.
202. Escalera A, Gonzalez-Reiche AS, Aslam S, Mena I, Laporte M, Pearl RL, et al. Mutations in SARS-CoV-2 variants of concern link to increased spike cleavage and virus transmission. Cell

Host Microbe. 2022;30(3):373-87 e7. Epub 20220121. doi: 10.1016/j.chom.2022.01.006. PubMed PMID: 35150638; PubMed Central PMCID: PMCPMC8776496.
203. Mizuki Yamamoto KT, Youko Hirayama, Jun-ichiro Inoue, Yasushi, Gohda KaJ. SARS-CoV-2 Omicron spike H655Y mutation is responsible for enhancement of the endosomal entry pathway and reduction of cell surface entry pathways. bioRxiv. 2022.
204. Willett BJ, Grove J, MacLean OA, Wilkie C, De Lorenzo G, Furnon W, et al. SARS-CoV-2 Omicron is an immune escape variant with an altered cell entry pathway. Nat Microbiol. 2022;7(8):1161-79. Epub 20220707. doi: 10.1038/s41564-022-01143-7. PubMed PMID: 35798890; PubMed Central PMCID: PMCPMC9352574.
205. Barnes CO, Jette CA, Abernathy ME, Dam KA, Esswein SR, Gristick HB, et al. SARS-CoV-2 neutralizing antibody structures inform therapeutic strategies. Nature. 2020;588(7839):682-7. Epub 20201012. doi: 10.1038/s41586-020-2852-1. PubMed PMID: 33045718; PubMed Central PMCID: PMCPMC8092461.
206. Cheng YW, Chao TL, Li CL, Wang SH, Kao HC, Tsai YM, et al. D614G Substitution of SARS-CoV-2 Spike Protein Increases Syncytium Formation and Virus Titer via Enhanced Furin-Mediated Spike Cleavage. mBio. 2021;12(4):e0058721. Epub 20210727. doi: 10.1128/mBio.00587-21. PubMed PMID: 34311586; PubMed Central PMCID: PMCPMC8406174.
207. Aljindan RY, Al-Subaie AM, Al-Ohali AI, Kumar DT, Doss CG, Kamaraj B. Investigation of nonsynonymous mutations in the spike protein of SARS-CoV-2 and its interaction with the ACE2 receptor by molecular docking and MM/GBSA approach. Comput Biol Med. 2021;135:104654. Epub 20210716. doi: 10.1016/j.compbiomed.2021.104654. PubMed PMID: 34346317; PubMed Central PMCID: PMCPMC8282961.
208. Pastorio C, Zech F, Noettger S, Jung C, Jacob T, Sanderson T, et al. Determinants of Spike infectivity, processing, and neutralization in SARS-CoV-2 Omicron subvariants BA.1 and BA.2. Cell Host Microbe. 2022. Epub 20220718. doi: 10.1016/j.chom.2022.07.006. PubMed PMID: 35931073; PubMed Central PMCID: PMCPMC9289044.
209. Harvey WT, Carabelli AM, Jackson B, Gupta RK, Thomson EC, Harrison EM, et al. SARS-CoV-2 variants, spike mutations and immune escape. Nat Rev Microbiol. 2021;19(7):409-24. Epub 20210601. doi: 10.1038/s41579-021-00573-0. PubMed PMID: 34075212; PubMed Central PMCID: PMCPMC8167834.
210. Nersisyan S, Zhiyanov A, Zakharova M, Ishina I, Kurbatskaia I, Mamedov A, et al. Alterations in SARS-CoV-2 Omicron and Delta peptides presentation by HLA molecules. PeerJ. 2022;10:e13354. Epub 20220427. doi: 10.7717/peerj.13354. PubMed PMID: 35502206; PubMed Central PMCID: PMCPMC9055995.
211. Hodcroft EB, Zuber M, Nadeau S, Vaughan TG, Crawford KHD, Althaus CL, et al. Emergence and spread of a SARS-CoV-2 variant through Europe in the summer of 2020. medRxiv. 2021. Epub 20210324. doi: 10.1101/2020.10.25.20219063. PubMed PMID: 33269368; PubMed Central PMCID: PMCPMC7709189.
212. McCarthy KR, Rennick LJ, Nambulli S, Robinson-McCarthy LR, Bain WG, Haidar G, et al. Recurrent deletions in the SARS-CoV-2 spike glycoprotein drive antibody escape. Science. 2021;371(6534):1139-42. Epub 20210203. doi: 10.1126/science.abf6950. PubMed PMID: 33536258; PubMed Central PMCID: PMCPMC7971772.
213. Li Y, Wang X, Jin J, Ma Z, Liu Y, Zhang X, et al. T-cell responses to SARS-CoV-2 Omicron spike epitopes with mutations after the third booster dose of an inactivated vaccine. J Med Virol. 2022;94(8):3998-4004. Epub 20220506. doi: 10.1002/jmv.27814. PubMed PMID: 35474581; PubMed Central PMCID: PMCPMC9088599.

214. Bin Zheng YX, Bei Tong, Yutong Mao, Rui Ge, Fang Tian, Xianchi Dong, Peng Zheng. S373P Mutation of Spike Protein in SARS-CoV-2 Stabilizes Omicron. bioRxiv. 2022.
215. Sztain T, Ahn SH, Bogetti AT, Casalino L, Goldsmith JA, Seitz E, et al. A glycan gate controls opening of the SARS-CoV-2 spike protein. Nat Chem. 2021;13(10):963-8. Epub 20210819. doi: 10.1038/s41557-021-00758-3. PubMed PMID: 34413500; PubMed Central PMCID: PMCPMC8488004.
216. Rees-Spear C, Muir L, Griffith SA, Heaney J, Aldon Y, Snitselaar JL, et al. The effect of spike mutations on SARS-CoV-2 neutralization. Cell Rep. 2021;34(12):108890. Epub 20210306. doi: 10.1016/j.celrep.2021.108890. PubMed PMID: 33713594; PubMed Central PMCID: PMCPMC7936541.
217. Wang Q, Guo Y, Iketani S, Nair MS, Li Z, Mohri H, et al. Antibody evasion by SARS-CoV-2 Omicron subvariants BA.2.12.1, BA.4 and BA.5. Nature. 2022. Epub 20220705. doi: 10.1038/s41586-022-05053-w. PubMed PMID: 35790190.
218. Singh A, Steinkellner G, Kochl K, Gruber K, Gruber CC. Serine 477 plays a crucial role in the interaction of the SARS-CoV-2 spike protein with the human receptor ACE2. Sci Rep. 2021;11(1):4320. Epub 20210222. doi: 10.1038/s41598-021-83761-5. PubMed PMID: 33619331; PubMed Central PMCID: PMCPMC7900180.
219. Ren W, Ju X, Gong M, Lan J, Yu Y, Long Q, et al. Characterization of SARS-CoV-2 Variants B.1.617.1 (Kappa), B.1.617.2 (Delta), and B.1.618 by Cell Entry and Immune Evasion. mBio. 2022;13(2):e0009922. Epub 20220310. doi: 10.1128/mbio.00099-22. PubMed PMID: 35266815; PubMed Central PMCID: PMCPMC9040861.
220. Focosi D, Novazzi F, Genoni A, Dentali F, Gasperina DD, Baj A, et al. Emergence of SARS-COV-2 Spike Protein Escape Mutation Q493R after Treatment for COVID-19. Emerg Infect Dis. 2021;27(10):2728-31. Epub 20210727. doi: 10.3201/eid2710.211538. PubMed PMID: 34314668; PubMed Central PMCID: PMCPMC8462334.
221. Zhang S, Qiao S, Yu J, Zeng J, Shan S, Tian L, et al. Bat and pangolin coronavirus spike glycoprotein structures provide insights into SARS-CoV-2 evolution. Nat Commun. 2021;12(1):1607. Epub 20210311. doi: 10.1038/s41467-021-21767-3. PubMed PMID: 33707453; PubMed Central PMCID: PMCPMC7952905.
222. Magazine N, Zhang T, Wu Y, McGee MC, Veggiani G, Huang W. Mutations and Evolution of the SARS-CoV-2 Spike Protein. Viruses. 2022;14(3). Epub 20220319. doi: 10.3390/v14030640. PubMed PMID: 35337047; PubMed Central PMCID: PMCPMC8949778.
223. Ostrov DA. Structural Consequences of Variation in SARS-CoV-2 B.1.1.7. J Cell Immunol. 2021;3(2):103-8. doi: 10.33696/immunology.3.085. PubMed PMID: 33969357; PubMed Central PMCID: PMCPMC8104447.
224. Gobeil SM, Janowska K, McDowell S, Mansouri K, Parks R, Stalls V, et al. Effect of natural mutations of SARS-CoV-2 on spike structure, conformation, and antigenicity. Science. 2021;373(6555). Epub 20210624. doi: 10.1126/science.abi6226. PubMed PMID: 34168071; PubMed Central PMCID: PMCPMC8611377.
225. Hodcroft EB, Domman DB, Snyder DJ, Oguntuyo KY, Van Diest M, Densmore KH, et al. Emergence in late 2020 of multiple lineages of SARS-CoV-2 Spike protein variants affecting amino acid position 677. medRxiv. 2021. Epub 20210221. doi: 10.1101/2021.02.12.21251658. PubMed PMID: 33594385; PubMed Central PMCID: PMCPMC7885944.
226. Mustafa Z, Kalbacher H, Burster T. Occurrence of a novel cleavage site for cathepsin G adjacent to the polybasic sequence within the proteolytically sensitive activation loop of the SARS-CoV-2 Omicron variant: The amino acid substitution N679K and P681H of the spike protein. PLoS One. 2022;17(4):e0264723. Epub 20220418. doi:

10.1371/journal.pone.0264723. PubMed PMID: 35436320; PubMed Central PMCID: PMCPMC9015119.
227. Kemp SA, Collier DA, Datir RP, Ferreira I, Gayed S, Jahun A, et al. SARS-CoV-2 evolution during treatment of chronic infection. Nature. 2021;592(7853):277-82. Epub 20210205. doi: 10.1038/s41586-021-03291-y. PubMed PMID: 33545711; PubMed Central PMCID: PMCPMC7610568.
228. Singh P, Sharma K, Singh P, Bhargava A, Negi SS, Sharma P, et al. Genomic characterization unravelling the causative role of SARS-CoV-2 Delta variant of lineage B.1.617.2 in 2nd wave of COVID-19 pandemic in Chhattisgarh, India. Microb Pathog. 2022;164:105404. Epub 20220119. doi: 10.1016/j.micpath.2022.105404. PubMed PMID: 35065253; PubMed Central PMCID: PMCPMC8769534.
229. Thomas P. Peacock JCB, Jie Zhou, Nazia Thakur, Ksenia Sukhova, Joseph Newman, Ruthiran Kugathasan, Ada W.C. Yan, Wilhelm Furnon, Giuditta De Lorenzo, Vanessa M. Cowton, Dorothee Reuss, Maya Moshe, Jessica L. Quantrill, Olivia K. Platt, Myrsini Kaforou, Arvind H. Patel, Massimo Palmarini, Dalan Bailey, and Wendy S. Barclay. The altered entry pathway and antigenic distance of the SARS-CoV-2 Omicron variant map to separate domains of spike protein. bioRxiv. 2022.
230. de Haan CA, Smeets M, Vernooij F, Vennema H, Rottier PJ. Mapping of the coronavirus membrane protein domains involved in interaction with the spike protein. J Virol. 1999;73(9):7441-52. doi: 10.1128/JVI.73.9.7441-7452.1999. PubMed PMID: 10438834; PubMed Central PMCID: PMCPMC104271.
231. Jonathan C. Brown DHG, Jie Zhou, Thomas P. Peacock, Rebecca Frise, Niluka Goonawardane, Laury Baillon, Ruthiran Kugathasan, Andreia L. Pinto, Paul F. McKay, Jack Hassard, Maya Moshe, Aran Singanayagam, Thomas Burgoyne, the ATACCC Investigators, PHE Virology Consortium, Wendy S. Barclay. Increased transmission of SARS-CoV-2 lineage B.1.1.7 (VOC 2020212/01) is not accounted for by a replicative advantage in primary airway cells or antibody escape. bioRxiv. 2021.
232. Anupriya Aggarwal AA, Vanessa Milogiannakis, Mariana Ruiz Silva, Gregory Walker, Andrea Kidinger, Thomas Angelovich, Emily Waring, Supavadee Amatayakul-Chantler, Nathan Roth, Germano Coppola, Malinna Yeang, Tyra Jean, Charles Foster, Alexandra Carey Hoppe, C. Mee Ling Munier, David Darley, Melissa Churchill, Damian Starck, Daniel Christ, Gail Matthews, William Rawlinson, Anthony D. Kelleher, Stuart Turville. SARS-CoV-2 Omicron BA.5: Evolving tropism and evasion of potent humoral responses and resistance to clinical immunotherapeutics relative to viral variants of concern. medRxiv. 2022.
233. Chaudhry MZ, Eschke K, Hoffmann M, Grashoff M, Abassi L, Kim Y, et al. Rapid SARS-CoV-2 Adaptation to Available Cellular Proteases. J Virol. 2022;96(5):e0218621. Epub 20220112. doi: 10.1128/jvi.02186-21. PubMed PMID: 35019723; PubMed Central PMCID: PMCPMC8906416.
234. Liu Z, Zheng H, Lin H, Li M, Yuan R, Peng J, et al. Identification of Common Deletions in the Spike Protein of Severe Acute Respiratory Syndrome Coronavirus 2. J Virol. 2020;94(17). Epub 2020/06/24. doi: 10.1128/JVI.00790-20. PubMed PMID: 32571797; PubMed Central PMCID: PMCPMC7431800.
235. Andres C, Garcia-Cehic D, Gregori J, Pinana M, Rodriguez-Frias F, Guerrero-Murillo M, et al. Naturally occurring SARS-CoV-2 gene deletions close to the spike S1/S2 cleavage site in the viral quasispecies of COVID19 patients. Emerg Microbes Infect. 2020;9(1):1900-11. doi: 10.1080/22221751.2020.1806735. PubMed PMID: 32752979; PubMed Central PMCID: PMCPMC8284971.

236. Lau SY, Wang P, Mok BW, Zhang AJ, Chu H, Lee AC, et al. Attenuated SARS-CoV-2 variants with deletions at the S1/S2 junction. Emerg Microbes Infect. 2020;9(1):837-42. doi: 10.1080/22221751.2020.1756700. PubMed PMID: 32301390; PubMed Central PMCID: PMCPMC7241555.
237. L.B. Snell TC, A. Alcolea-Medina, S. Pickering, F. Flaviani, G. O'hara, L. O'connell, S. Douthwaite, J. Edgeworth, S. Neil, R. Ribeiro Galao, G. Nebbia. A longitudinal study of evolution of SARS-CoV-2 variants in immunocompromised individuals with persistent infection. ECCMID 2022 2022.
238. Burki T. The origin of SARS-CoV-2 variants of concern. Lancet Infect Dis. 2022;22(2):174-5. Epub 20220113. doi: 10.1016/S1473-3099(22)00015-9. PubMed PMID: 35033232.
239. Bayarri-Olmos R, Rosbjerg A, Johnsen LB, Helgstrand C, Bak-Thomsen T, Garred P, et al. The SARS-CoV-2 Y453F mink variant displays a pronounced increase in ACE-2 affinity but does not challenge antibody neutralization. J Biol Chem. 2021;296:100536. Epub 20210311. doi: 10.1016/j.jbc.2021.100536. PubMed PMID: 33716040; PubMed Central PMCID: PMCPMC7948531.
240. Worobey M, Holmes EC. Evolutionary aspects of recombination in RNA viruses. J Gen Virol. 1999;80 (Pt 10):2535-43. doi: 10.1099/0022-1317-80-10-2535. PubMed PMID: 10573145.
241. He Y, Ma W, Dang S, Chen L, Zhang R, Mei S, et al. Possible recombination between two variants of concern in a COVID-19 patient. Emerg Microbes Infect. 2022;11(1):552-5. doi: 10.1080/22221751.2022.2032375. PubMed PMID: 35081877; PubMed Central PMCID: PMCPMC8843165.
242. Jackson B, Boni MF, Bull MJ, Colleran A, Colquhoun RM, Darby AC, et al. Generation and transmission of interlineage recombinants in the SARS-CoV-2 pandemic. Cell. 2021;184(20):5179-88 e8. Epub 20210817. doi: 10.1016/j.cell.2021.08.014. PubMed PMID: 34499854; PubMed Central PMCID: PMCPMC8367733.
243. Sharp PM, Hahn BH. Origins of HIV and the AIDS pandemic. Cold Spring Harb Perspect Med. 2011;1(1):a006841. doi: 10.1101/cshperspect.a006841. PubMed PMID: 22229120; PubMed Central PMCID: PMCPMC3234451.
244. Barre-Sinoussi F, Chermann JC, Rey F, Nugeyre MT, Chamaret S, Gruest J, et al. Isolation of a T-lymphotropic retrovirus from a patient at risk for acquired immune deficiency syndrome (AIDS). Science. 1983;220(4599):868-71. doi: 10.1126/science.6189183. PubMed PMID: 6189183.
245. Gallo RC, Salahuddin SZ, Popovic M, Shearer GM, Kaplan M, Haynes BF, et al. Frequent detection and isolation of cytopathic retroviruses (HTLV-III) from patients with AIDS and at risk for AIDS. Science. 1984;224(4648):500-3. doi: 10.1126/science.6200936. PubMed PMID: 6200936.
246. Popovic M, Sarngadharan MG, Read E, Gallo RC. Detection, isolation, and continuous production of cytopathic retroviruses (HTLV-III) from patients with AIDS and pre-AIDS. Science. 1984;224(4648):497-500. doi: 10.1126/science.6200935. PubMed PMID: 6200935.
247. https://www.hiv.gov/hiv-basics/overview/history/hiv-and-aids-timeline.
248. https://www.unaids.org/sites/default/files/media_asset/UNAIDS_FactSheet_en.pdf 2021.
249. Maenza J, Flexner C. Combination antiretroviral therapy for HIV infection. Am Fam Physician. 1998;57(11):2789-98. PubMed PMID: 9636341.

250. Rodger AJ, Cambiano V, Bruun T, Vernazza P, Collins S, Degen O, et al. Risk of HIV transmission through condomless sex in serodifferent gay couples with the HIV-positive partner taking suppressive antiretroviral therapy (PARTNER): final results of a multicentre, prospective, observational study. Lancet. 2019;393(10189):2428-38. Epub 20190502. doi: 10.1016/S0140-6736(19)30418-0. PubMed PMID: 31056293; PubMed Central PMCID: PMCPMC6584382.
251. Heath K, Levi J, Hill A. The Joint United Nations Programme on HIV/AIDS 95-95-95 targets: worldwide clinical and cost benefits of generic manufacture. AIDS. 2021;35(Suppl 2):S197-S203. doi: 10.1097/QAD.0000000000002983. PubMed PMID: 34115649.
252. Craigie R, Bushman FD. HIV DNA integration. Cold Spring Harb Perspect Med. 2012;2(7):a006890. doi: 10.1101/cshperspect.a006890. PubMed PMID: 22762018; PubMed Central PMCID: PMCPMC3385939.
253. Abner E, Jordan A. HIV "shock and kill" therapy: In need of revision. Antiviral Res. 2019;166:19-34. Epub 20190323. doi: 10.1016/j.antiviral.2019.03.008. PubMed PMID: 30914265.
254. Huet T, Cheynier R, Meyerhans A, Roelants G, Wain-Hobson S. Genetic organization of a chimpanzee lentivirus related to HIV-1. Nature. 1990;345(6273):356-9. doi: 10.1038/345356a0. PubMed PMID: 2188136.
255. Hemelaar J, Gouws E, Ghys PD, Osmanov S, Isolation W-UNfH, Characterisation. Global trends in molecular epidemiology of HIV-1 during 2000-2007. AIDS. 2011;25(5):679-89. doi: 10.1097/QAD.0b013e328342ff93. PubMed PMID: 21297424; PubMed Central PMCID: PMCPMC3755761.
256. German Advisory Committee Blood SAoPTbB. Human Immunodeficiency Virus (HIV). Transfus Med Hemother. 2016;43(3):203-22. Epub 20160509. doi: 10.1159/000445852. PubMed PMID: 27403093; PubMed Central PMCID: PMCPMC4924471.
257. Aghokeng AF, Ayouba A, Mpoudi-Ngole E, Loul S, Liegeois F, Delaporte E, et al. Extensive survey on the prevalence and genetic diversity of SIVs in primate bushmeat provides insights into risks for potential new cross-species transmissions. Infect Genet Evol. 2010;10(3):386-96. Epub 20090423. doi: 10.1016/j.meegid.2009.04.014. PubMed PMID: 19393772; PubMed Central PMCID: PMCPMC2844463.
258. Peeters M, Courgnaud V, Abela B, Auzel P, Pourrut X, Bibollet-Ruche F, et al. Risk to human health from a plethora of simian immunodeficiency viruses in primate bushmeat. Emerg Infect Dis. 2002;8(5):451-7. doi: 10.3201/eid0805.010522. PubMed PMID: 11996677; PubMed Central PMCID: PMCPMC2732488.
259. Wilen CB, Tilton JC, Doms RW. HIV: cell binding and entry. Cold Spring Harb Perspect Med. 2012;2(8). Epub 20120801. doi: 10.1101/cshperspect.a006866. PubMed PMID: 22908191; PubMed Central PMCID: PMCPMC3405824.
260. Prevost J, Tolbert WD, Medjahed H, Sherburn RT, Madani N, Zoubchenok D, et al. The HIV-1 Env gp120 Inner Domain Shapes the Phe43 Cavity and the CD4 Binding Site. mBio. 2020;11(3). Epub 20200526. doi: 10.1128/mBio.00280-20. PubMed PMID: 32457241; PubMed Central PMCID: PMCPMC7251204.
261. Kwong PD, Wyatt R, Majeed S, Robinson J, Sweet RW, Sodroski J, et al. Structures of HIV-1 gp120 envelope glycoproteins from laboratory-adapted and primary isolates. Structure. 2000;8(12):1329-39. doi: 10.1016/s0969-2126(00)00547-5. PubMed PMID: 11188697.
262. Margolis L, Shattock R. Selective transmission of CCR5-utilizing HIV-1: the 'gatekeeper' problem resolved? Nat Rev Microbiol. 2006;4(4):312-7. doi: 10.1038/nrmicro1387. PubMed PMID: 16541138.

263. Shaik MM, Peng H, Lu J, Rits-Volloch S, Xu C, Liao M, et al. Structural basis of coreceptor recognition by HIV-1 envelope spike. Nature. 2019;565(7739):318-23. Epub 20181212. doi: 10.1038/s41586-018-0804-9. PubMed PMID: 30542158; PubMed Central PMCID: PMCPMC6391877.
264. McClure MO, Marsh M, Weiss RA. Human immunodeficiency virus infection of CD4-bearing cells occurs by a pH-independent mechanism. EMBO J. 1988;7(2):513-8. doi: 10.1002/j.1460-2075.1988.tb02839.x. PubMed PMID: 3259178; PubMed Central PMCID: PMCPMC454348.
265. Rasaiyaah J, Tan CP, Fletcher AJ, Price AJ, Blondeau C, Hilditch L, et al. HIV-1 evades innate immune recognition through specific cofactor recruitment. Nature. 2013;503(7476):402-5. Epub 20131106. doi: 10.1038/nature12769. PubMed PMID: 24196705; PubMed Central PMCID: PMCPMC3928559.
266. Zila V, Margiotta E, Turonova B, Muller TG, Zimmerli CE, Mattei S, et al. Cone-shaped HIV-1 capsids are transported through intact nuclear pores. Cell. 2021;184(4):1032-46 e18. Epub 20210210. doi: 10.1016/j.cell.2021.01.025. PubMed PMID: 33571428; PubMed Central PMCID: PMCPMC7895898.
267. Aiken C, Rousso I. The HIV-1 capsid and reverse transcription. Retrovirology. 2021;18(1):29. Epub 20210925. doi: 10.1186/s12977-021-00566-0. PubMed PMID: 34563203; PubMed Central PMCID: PMCPMC8466977.
268. Buffone C, Martinez-Lopez A, Fricke T, Opp S, Severgnini M, Cifola I, et al. Nup153 Unlocks the Nuclear Pore Complex for HIV-1 Nuclear Translocation in Nondividing Cells. J Virol. 2018;92(19). Epub 20180912. doi: 10.1128/JVI.00648-18. PubMed PMID: 29997211; PubMed Central PMCID: PMCPMC6146805.
269. Dharan A, Talley S, Tripathi A, Mamede JI, Majetschak M, Hope TJ, et al. KIF5B and Nup358 Cooperatively Mediate the Nuclear Import of HIV-1 during Infection. PLoS Pathog. 2016;12(6):e1005700. Epub 20160621. doi: 10.1371/journal.ppat.1005700. PubMed PMID: 27327622; PubMed Central PMCID: PMCPMC4915687.
270. Karn J, Stoltzfus CM. Transcriptional and posttranscriptional regulation of HIV-1 gene expression. Cold Spring Harb Perspect Med. 2012;2(2):a006916. doi: 10.1101/cshperspect.a006916. PubMed PMID: 22355797; PubMed Central PMCID: PMCPMC3281586.
271. Votteler J, Sundquist WI. Virus budding and the ESCRT pathway. Cell Host Microbe. 2013;14(3):232-41. doi: 10.1016/j.chom.2013.08.012. PubMed PMID: 24034610; PubMed Central PMCID: PMCPMC3819203.
272. Kohl NE, Emini EA, Schleif WA, Davis LJ, Heimbach JC, Dixon RA, et al. Active human immunodeficiency virus protease is required for viral infectivity. Proc Natl Acad Sci U S A. 1988;85(13):4686-90. doi: 10.1073/pnas.85.13.4686. PubMed PMID: 3290901; PubMed Central PMCID: PMCPMC280500.
273. Dufour C, Gantner P, Fromentin R, Chomont N. The multifaceted nature of HIV latency. J Clin Invest. 2020;130(7):3381-90. doi: 10.1172/JCI136227. PubMed PMID: 32609095; PubMed Central PMCID: PMCPMC7324199.
274. Connor RI, Sheridan KE, Ceradini D, Choe S, Landau NR. Change in coreceptor use correlates with disease progression in HIV-1--infected individuals. J Exp Med. 1997;185(4):621-8. doi: 10.1084/jem.185.4.621. PubMed PMID: 9034141; PubMed Central PMCID: PMCPMC2196142.

275. Coetzer M, Cilliers T, Ping LH, Swanstrom R, Morris L. Genetic characteristics of the V3 region associated with CXCR4 usage in HIV-1 subtype C isolates. Virology. 2006;356(1-2):95-105. Epub 20060830. doi: 10.1016/j.virol.2006.07.030. PubMed PMID: 16942785.
276. Haffar OK, Dowbenko DJ, Berman PW. Topogenic analysis of the human immunodeficiency virus type 1 envelope glycoprotein, gp160, in microsomal membranes. J Cell Biol. 1988;107(5):1677-87. doi: 10.1083/jcb.107.5.1677. PubMed PMID: 3053734; PubMed Central PMCID: PMCPMC2115321.
277. Checkley MA, Luttge BG, Freed EO. HIV-1 envelope glycoprotein biosynthesis, trafficking, and incorporation. J Mol Biol. 2011;410(4):582-608. doi: 10.1016/j.jmb.2011.04.042. PubMed PMID: 21762802; PubMed Central PMCID: PMCPMC3139147.
278. Hallenberger S, Bosch V, Angliker H, Shaw E, Klenk HD, Garten W. Inhibition of furin-mediated cleavage activation of HIV-1 glycoprotein gp160. Nature. 1992;360(6402):358-61. doi: 10.1038/360358a0. PubMed PMID: 1360148.
279. Ringe RP, Sanders RW, Yasmeen A, Kim HJ, Lee JH, Cupo A, et al. Cleavage strongly influences whether soluble HIV-1 envelope glycoprotein trimers adopt a native-like conformation. Proc Natl Acad Sci U S A. 2013;110(45):18256-61. Epub 20131021. doi: 10.1073/pnas.1314351110. PubMed PMID: 24145402; PubMed Central PMCID: PMCPMC3831437.
280. Dubay JW, Dubay SR, Shin HJ, Hunter E. Analysis of the cleavage site of the human immunodeficiency virus type 1 glycoprotein: requirement of precursor cleavage for glycoprotein incorporation. J Virol. 1995;69(8):4675-82. doi: 10.1128/JVI.69.8.4675-4682.1995. PubMed PMID: 7609032; PubMed Central PMCID: PMCPMC189271.
281. Pasquato A, Dettin M, Basak A, Gambaretto R, Tonin L, Seidah NG, et al. Heparin enhances the furin cleavage of HIV-1 gp160 peptides. FEBS Lett. 2007;581(30):5807-13. Epub 20071126. doi: 10.1016/j.febslet.2007.11.050. PubMed PMID: 18037384; PubMed Central PMCID: PMCPMC7125586.
282. Hammonds J, Chen X, Ding L, Fouts T, De Vico A, zur Megede J, et al. Gp120 stability on HIV-1 virions and Gag-Env pseudovirions is enhanced by an uncleaved Gag core. Virology. 2003;314(2):636-49. doi: 10.1016/s0042-6822(03)00467-7. PubMed PMID: 14554091.
283. Zhang S, Nguyen HT, Ding H, Wang J, Zou S, Liu L, et al. Dual Pathways of Human Immunodeficiency Virus Type 1 Envelope Glycoprotein Trafficking Modulate the Selective Exclusion of Uncleaved Oligomers from Virions. J Virol. 2021;95(3). Epub 20210113. doi: 10.1128/JVI.01369-20. PubMed PMID: 33148792; PubMed Central PMCID: PMCPMC7925103.
284. Murakami T, Freed EO. The long cytoplasmic tail of gp41 is required in a cell type-dependent manner for HIV-1 envelope glycoprotein incorporation into virions. Proc Natl Acad Sci U S A. 2000;97(1):343-8. doi: 10.1073/pnas.97.1.343. PubMed PMID: 10618420; PubMed Central PMCID: PMCPMC26665.
285. Mammano F, Salvatori F, Indraccolo S, De Rossi A, Chieco-Bianchi L, Gottlinger HG. Truncation of the human immunodeficiency virus type 1 envelope glycoprotein allows efficient pseudotyping of Moloney murine leukemia virus particles and gene transfer into CD4+ cells. J Virol. 1997;71(4):3341-5. doi: 10.1128/JVI.71.4.3341-3345.1997. PubMed PMID: 9060707; PubMed Central PMCID: PMCPMC191476.
286. Freed EO, Martin MA. Domains of the human immunodeficiency virus type 1 matrix and gp41 cytoplasmic tail required for envelope incorporation into virions. J Virol.

1996;70(1):341-51. doi: 10.1128/JVI.70.1.341-351.1996. PubMed PMID: 8523546; PubMed Central PMCID: PMCPMC189823.
287. Wyma DJ, Jiang J, Shi J, Zhou J, Lineberger JE, Miller MD, et al. Coupling of human immunodeficiency virus type 1 fusion to virion maturation: a novel role of the gp41 cytoplasmic tail. J Virol. 2004;78(7):3429-35. doi: 10.1128/jvi.78.7.3429-3435.2004. PubMed PMID: 15016865; PubMed Central PMCID: PMCPMC371074.
288. Herschhorn A, Ma X, Gu C, Ventura JD, Castillo-Menendez L, Melillo B, et al. Release of gp120 Restraints Leads to an Entry-Competent Intermediate State of the HIV-1 Envelope Glycoproteins. mBio. 2016;7(5). Epub 20161025. doi: 10.1128/mBio.01598-16. PubMed PMID: 27795397; PubMed Central PMCID: PMCPMC5080382.
289. Madani N, Princiotto AM, Zhao C, Jahanbakhshsefidi F, Mertens M, Herschhorn A, et al. Activation and Inactivation of Primary Human Immunodeficiency Virus Envelope Glycoprotein Trimers by CD4-Mimetic Compounds. J Virol. 2017;91(3). Epub 20170118. doi: 10.1128/JVI.01880-16. PubMed PMID: 27881646; PubMed Central PMCID: PMCPMC5244334.
290. Medjahed H, Pacheco B, Desormeaux A, Sodroski J, Finzi A. The HIV-1 gp120 major variable regions modulate cold inactivation. J Virol. 2013;87(7):4103-11. Epub 20130123. doi: 10.1128/JVI.03124-12. PubMed PMID: 23345516; PubMed Central PMCID: PMCPMC3624226.
291. Kassa A, Finzi A, Pancera M, Courter JR, Smith AB, 3rd, Sodroski J. Identification of a human immunodeficiency virus type 1 envelope glycoprotein variant resistant to cold inactivation. J Virol. 2009;83(9):4476-88. Epub 20090211. doi: 10.1128/JVI.02110-08. PubMed PMID: 19211747; PubMed Central PMCID: PMCPMC2668461.
292. Prevost J, Medjahed H, Vezina D, Chen HC, Hahn BH, Smith AB, 3rd, et al. HIV-1 Envelope Glycoproteins Proteolytic Cleavage Protects Infected Cells from ADCC Mediated by Plasma from Infected Individuals. Viruses. 2021;13(11). Epub 20211106. doi: 10.3390/v13112236. PubMed PMID: 34835042; PubMed Central PMCID: PMCPMC8625184.
293. Castillo-Menendez LR, Witt K, Espy N, Princiotto A, Madani N, Pacheco B, et al. Comparison of Uncleaved and Mature Human Immunodeficiency Virus Membrane Envelope Glycoprotein Trimers. J Virol. 2018;92(12). Epub 20180529. doi: 10.1128/JVI.00277-18. PubMed PMID: 29618643; PubMed Central PMCID: PMCPMC5974486.
294. Chojnacki J, Waithe D, Carravilla P, Huarte N, Galiani S, Enderlein J, et al. Envelope glycoprotein mobility on HIV-1 particles depends on the virus maturation state. Nat Commun. 2017;8(1):545. Epub 20170915. doi: 10.1038/s41467-017-00515-6. PubMed PMID: 28916807; PubMed Central PMCID: PMCPMC5601426.
295. Chertova E, Bess JW, Jr., Crise BJ, Sowder IR, Schaden TM, Hilburn JM, et al. Envelope glycoprotein incorporation, not shedding of surface envelope glycoprotein (gp120/SU), Is the primary determinant of SU content of purified human immunodeficiency virus type 1 and simian immunodeficiency virus. J Virol. 2002;76(11):5315-25. doi: 10.1128/jvi.76.11.5315-5325.2002. PubMed PMID: 11991960; PubMed Central PMCID: PMCPMC137021.
296. Wang H, Cohen AA, Galimidi RP, Gristick HB, Jensen GJ, Bjorkman PJ. Cryo-EM structure of a CD4-bound open HIV-1 envelope trimer reveals structural rearrangements of the gp120 V1V2 loop. Proc Natl Acad Sci U S A. 2016;113(46):E7151-E8. Epub 20161031. doi: 10.1073/pnas.1615939113. PubMed PMID: 27799557; PubMed Central PMCID: PMCPMC5135367.
297. Pan R, Gorny MK, Zolla-Pazner S, Kong XP. The V1V2 Region of HIV-1 gp120 Forms a Five-Stranded Beta Barrel. J Virol. 2015;89(15):8003-10. Epub 20150527. doi:

10.1128/JVI.00754-15. PubMed PMID: 26018158; PubMed Central PMCID: PMCPMC4505664.
298. Wang W, Nie J, Prochnow C, Truong C, Jia Z, Wang S, et al. A systematic study of the N-glycosylation sites of HIV-1 envelope protein on infectivity and antibody-mediated neutralization. Retrovirology. 2013;10:14. Epub 20130206. doi: 10.1186/1742-4690-10-14. PubMed PMID: 23384254; PubMed Central PMCID: PMCPMC3648360.
299. McLellan JS, Pancera M, Carrico C, Gorman J, Julien JP, Khayat R, et al. Structure of HIV-1 gp120 V1/V2 domain with broadly neutralizing antibody PG9. Nature. 2011;480(7377):336-43. Epub 20111123. doi: 10.1038/nature10696. PubMed PMID: 22113616; PubMed Central PMCID: PMCPMC3406929.
300. Yuan T, Li J, Zhang MY. HIV-1 envelope glycoprotein variable loops are indispensable for envelope structural integrity and virus entry. PLoS One. 2013;8(8):e69789. Epub 20130801. doi: 10.1371/journal.pone.0069789. PubMed PMID: 23936354; PubMed Central PMCID: PMCPMC3731308.
301. Lyumkis D, Julien JP, de Val N, Cupo A, Potter CS, Klasse PJ, et al. Cryo-EM structure of a fully glycosylated soluble cleaved HIV-1 envelope trimer. Science. 2013;342(6165):1484-90. Epub 20131031. doi: 10.1126/science.1245627. PubMed PMID: 24179160; PubMed Central PMCID: PMCPMC3954647.
302. Wu L, Gerard NP, Wyatt R, Choe H, Parolin C, Ruffing N, et al. CD4-induced interaction of primary HIV-1 gp120 glycoproteins with the chemokine receptor CCR-5. Nature. 1996;384(6605):179-83. doi: 10.1038/384179a0. PubMed PMID: 8906795.
303. van den Kerkhof TL, de Taeye SW, Boeser-Nunnink BD, Burton DR, Kootstra NA, Schuitemaker H, et al. HIV-1 escapes from N332-directed antibody neutralization in an elite neutralizer by envelope glycoprotein elongation and introduction of unusual disulfide bonds. Retrovirology. 2016;13(1):48. Epub 20160707. doi: 10.1186/s12977-016-0279-4. PubMed PMID: 27388013; PubMed Central PMCID: PMCPMC4936165.
304. Nakane S, Iwamoto A, Matsuda Z. The V4 and V5 Variable Loops of HIV-1 Envelope Glycoprotein Are Tolerant to Insertion of Green Fluorescent Protein and Are Useful Targets for Labeling. J Biol Chem. 2015;290(24):15279-91. Epub 20150424. doi: 10.1074/jbc.M114.628610. PubMed PMID: 25911103; PubMed Central PMCID: PMCPMC4463467.
305. Pancera M, Zhou T, Druz A, Georgiev IS, Soto C, Gorman J, et al. Structure and immune recognition of trimeric pre-fusion HIV-1 Env. Nature. 2014;514(7523):455-61. Epub 20141008. doi: 10.1038/nature13808. PubMed PMID: 25296255; PubMed Central PMCID: PMCPMC4348022.
306. Nieto-Garai JA, Arboleya A, Otaegi S, Chojnacki J, Casas J, Fabrias G, et al. Cholesterol in the Viral Membrane is a Molecular Switch Governing HIV-1 Env Clustering. Adv Sci (Weinh). 2021;8(3):2003468. Epub 20201221. doi: 10.1002/advs.202003468. PubMed PMID: 33552873; PubMed Central PMCID: PMCPMC7856888.
307. Pacheco B, Alsahafi N, Debbeche O, Prevost J, Ding S, Chapleau JP, et al. Residues in the gp41 Ectodomain Regulate HIV-1 Envelope Glycoprotein Conformational Transitions Induced by gp120-Directed Inhibitors. J Virol. 2017;91(5). Epub 20170214. doi: 10.1128/JVI.02219-16. PubMed PMID: 28003492; PubMed Central PMCID: PMCPMC5309946.
308. Steckbeck JD, Craigo JK, Barnes CO, Montelaro RC. Highly conserved structural properties of the C-terminal tail of HIV-1 gp41 protein despite substantial sequence variation among diverse clades: implications for functions in viral replication. J Biol Chem.

2011;286(31):27156-66. Epub 20110609. doi: 10.1074/jbc.M111.258855. PubMed PMID: 21659530; PubMed Central PMCID: PMCPMC3149309.
309. Hunter E, Swanstrom R. Retrovirus envelope glycoproteins. Curr Top Microbiol Immunol. 1990;157:187-253. doi: 10.1007/978-3-642-75218-6_7. PubMed PMID: 2203609.
310. Doores KJ. The HIV glycan shield as a target for broadly neutralizing antibodies. FEBS J. 2015;282(24):4679-91. Epub 20151023. doi: 10.1111/febs.13530. PubMed PMID: 26411545; PubMed Central PMCID: PMCPMC4950053.
311. Korber B, Gaschen B, Yusim K, Thakallapally R, Kesmir C, Detours V. Evolutionary and immunological implications of contemporary HIV-1 variation. Br Med Bull. 2001;58:19-42. doi: 10.1093/bmb/58.1.19. PubMed PMID: 11714622.
312. Doores KJ, Bonomelli C, Harvey DJ, Vasiljevic S, Dwek RA, Burton DR, et al. Envelope glycans of immunodeficiency virions are almost entirely oligomannose antigens. Proc Natl Acad Sci U S A. 2010;107(31):13800-5. Epub 20100719. doi: 10.1073/pnas.1006498107. PubMed PMID: 20643940; PubMed Central PMCID: PMCPMC2922250.
313. Sanders RW, Venturi M, Schiffner L, Kalyanaraman R, Katinger H, Lloyd KO, et al. The mannose-dependent epitope for neutralizing antibody 2G12 on human immunodeficiency virus type 1 glycoprotein gp120. J Virol. 2002;76(14):7293-305. doi: 10.1128/jvi.76.14.7293-7305.2002. PubMed PMID: 12072528; PubMed Central PMCID: PMCPMC136300.
314. Mouquet H, Scharf L, Euler Z, Liu Y, Eden C, Scheid JF, et al. Complex-type N-glycan recognition by potent broadly neutralizing HIV antibodies. Proc Natl Acad Sci U S A. 2012;109(47):E3268-77. Epub 20121030. doi: 10.1073/pnas.1217207109. PubMed PMID: 23115339; PubMed Central PMCID: PMCPMC3511153.
315. Granger LA, Huettner I, Debeljak F, Kaleebu P, Schechter M, Tambussi G, et al. Broadly neutralizing antibody responses in the longitudinal primary HIV-1 infection Short Pulse Anti-Retroviral Therapy at Seroconversion cohort. AIDS. 2021;35(13):2073-84. doi: 10.1097/QAD.0000000000002988. PubMed PMID: 34127581; PubMed Central PMCID: PMCPMC8505148.
316. Yu F, Wen Y, Wang J, Gong Y, Feng K, Ye R, et al. The Transmission and Evolution of HIV-1 Quasispecies within One Couple: a Follow-up Study based on Next-Generation Sequencing. Sci Rep. 2018;8(1):1404. Epub 20180123. doi: 10.1038/s41598-018-19783-3. PubMed PMID: 29362487; PubMed Central PMCID: PMCPMC5780463.
317. Bar KJ, Li H, Chamberland A, Tremblay C, Routy JP, Grayson T, et al. Wide variation in the multiplicity of HIV-1 infection among injection drug users. J Virol. 2010;84(12):6241-7. Epub 20100407. doi: 10.1128/JVI.00077-10. PubMed PMID: 20375173; PubMed Central PMCID: PMCPMC2876625.
318. Patel P, Borkowf CB, Brooks JT, Lasry A, Lansky A, Mermin J. Estimating per-act HIV transmission risk: a systematic review. AIDS. 2014;28(10):1509-19. doi: 10.1097/QAD.0000000000000298. PubMed PMID: 24809629; PubMed Central PMCID: PMCPMC6195215.
319. Joseph SB, Swanstrom R, Kashuba AD, Cohen MS. Bottlenecks in HIV-1 transmission: insights from the study of founder viruses. Nat Rev Microbiol. 2015;13(7):414-25. Epub 20150608. doi: 10.1038/nrmicro3471. PubMed PMID: 26052661; PubMed Central PMCID: PMCPMC4793885.
320. Parker ZF, Iyer SS, Wilen CB, Parrish NF, Chikere KC, Lee FH, et al. Transmitted/founder and chronic HIV-1 envelope proteins are distinguished by differential utilization of CCR5. J Virol. 2013;87(5):2401-11. Epub 20121226. doi: 10.1128/JVI.02964-12. PubMed PMID: 23269796; PubMed Central PMCID: PMCPMC3571396.

321. Zhou Y, Shen L, Yang HC, Siliciano RF. Preferential cytolysis of peripheral memory CD4+ T cells by in vitro X4-tropic human immunodeficiency virus type 1 infection before the completion of reverse transcription. J Virol. 2008;82(18):9154-63. Epub 20080702. doi: 10.1128/JVI.00773-08. PubMed PMID: 18596085; PubMed Central PMCID: PMCPMC2546913.
322. Ni J, Wang D, Wang S. The CCR5-Delta32 Genetic Polymorphism and HIV-1 Infection Susceptibility: a Meta-analysis. Open Med (Wars). 2018;13:467-74. Epub 20181016. doi: 10.1515/med-2018-0062. PubMed PMID: 30426084; PubMed Central PMCID: PMCPMC6227735.
323. Lim JK, Louie CY, Glaser C, Jean C, Johnson B, Johnson H, et al. Genetic deficiency of chemokine receptor CCR5 is a strong risk factor for symptomatic West Nile virus infection: a meta-analysis of 4 cohorts in the US epidemic. J Infect Dis. 2008;197(2):262-5. doi: 10.1086/524691. PubMed PMID: 18179388.
324. Parrish NF, Gao F, Li H, Giorgi EE, Barbian HJ, Parrish EH, et al. Phenotypic properties of transmitted founder HIV-1. Proc Natl Acad Sci U S A. 2013;110(17):6626-33. Epub 20130329. doi: 10.1073/pnas.1304288110. PubMed PMID: 23542380; PubMed Central PMCID: PMCPMC3637789.
325. Keele BF, Giorgi EE, Salazar-Gonzalez JF, Decker JM, Pham KT, Salazar MG, et al. Identification and characterization of transmitted and early founder virus envelopes in primary HIV-1 infection. Proc Natl Acad Sci U S A. 2008;105(21):7552-7. Epub 20080519. doi: 10.1073/pnas.0802203105. PubMed PMID: 18490657; PubMed Central PMCID: PMCPMC2387184.
326. Li M, Salazar-Gonzalez JF, Derdeyn CA, Morris L, Williamson C, Robinson JE, et al. Genetic and neutralization properties of subtype C human immunodeficiency virus type 1 molecular env clones from acute and early heterosexually acquired infections in Southern Africa. J Virol. 2006;80(23):11776-90. Epub 20060913. doi: 10.1128/JVI.01730-06. PubMed PMID: 16971434; PubMed Central PMCID: PMCPMC1642599.
327. Derdeyn CA, Moore PL, Morris L. Development of broadly neutralizing antibodies from autologous neutralizing antibody responses in HIV infection. Curr Opin HIV AIDS. 2014;9(3):210-6. doi: 10.1097/COH.0000000000000057. PubMed PMID: 24662931; PubMed Central PMCID: PMCPMC4068799.
328. Ping LH, Jabara CB, Rodrigo AG, Hudelson SE, Piwowar-Manning E, Wang L, et al. HIV-1 transmission during early antiretroviral therapy: evaluation of two HIV-1 transmission events in the HPTN 052 prevention study. PLoS One. 2013;8(9):e71557. Epub 20130924. doi: 10.1371/journal.pone.0071557. PubMed PMID: 24086252; PubMed Central PMCID: PMCPMC3782474.
329. Elena Sugrue AW, Nardus Mollentze, Muhamad Afiq Aziz, Vattipally B Sreenu, Sven Truxa, Lily Tong, Ana da Silva Filipe, David L Robertson, Joseph Hughes, Suzannah J Rihn, Sam J Wilson. The Interferon Resistance of Transmitted HIV-1 is a Consequence of Enhanced Replicative Fitness. bioRxiv. 2021.
330. Menendez-Arias L, Sebastian-Martin A, Alvarez M. Viral reverse transcriptases. Virus Res. 2017;234:153-76. Epub 20161230. doi: 10.1016/j.virusres.2016.12.019. PubMed PMID: 28043823.
331. Suddala KC, Lee CC, Meraner P, Marin M, Markosyan RM, Desai TM, et al. Interferon-induced transmembrane protein 3 blocks fusion of sensitive but not resistant viruses by partitioning into virus-carrying endosomes. PLoS Pathog. 2019;15(1):e1007532. Epub

20190114. doi: 10.1371/journal.ppat.1007532. PubMed PMID: 30640957; PubMed Central PMCID: PMCPMC6347298.
332. Warren CJ, Griffin LM, Little AS, Huang IC, Farzan M, Pyeon D. The antiviral restriction factors IFITM1, 2 and 3 do not inhibit infection of human papillomavirus, cytomegalovirus and adenovirus. PLoS One. 2014;9(5):e96579. Epub 20140514. doi: 10.1371/journal.pone.0096579. PubMed PMID: 24827144; PubMed Central PMCID: PMCPMC4020762.
333. Wang Y, Pan Q, Ding S, Wang Z, Yu J, Finzi A, et al. The V3 Loop of HIV-1 Env Determines Viral Susceptibility to IFITM3 Impairment of Viral Infectivity. J Virol. 2017;91(7). Epub 20170313. doi: 10.1128/JVI.02441-16. PubMed PMID: 28100616; PubMed Central PMCID: PMCPMC5355610.
334. Winstone H, Lista MJ, Reid AC, Bouton C, Pickering S, Galao RP, et al. The Polybasic Cleavage Site in SARS-CoV-2 Spike Modulates Viral Sensitivity to Type I Interferon and IFITM2. J Virol. 2021;95(9). Epub 2021/02/11. doi: 10.1128/JVI.02422-20. PubMed PMID: 33563656; PubMed Central PMCID: PMCPMC8104117.
335. Prelli Bozzo C, Nchioua R, Volcic M, Koepke L, Kruger J, Schutz D, et al. IFITM proteins promote SARS-CoV-2 infection and are targets for virus inhibition in vitro. Nat Commun. 2021;12(1):4584. Epub 20210728. doi: 10.1038/s41467-021-24817-y. PubMed PMID: 34321474; PubMed Central PMCID: PMCPMC8319209.
336. Zhao X, Guo F, Liu F, Cuconati A, Chang J, Block TM, et al. Interferon induction of IFITM proteins promotes infection by human coronavirus OC43. Proc Natl Acad Sci U S A. 2014;111(18):6756-61. Epub 20140421. doi: 10.1073/pnas.1320856111. PubMed PMID: 24753610; PubMed Central PMCID: PMCPMC4020042.
337. Zhong NS, Zheng BJ, Li YM, Poon, Xie ZH, Chan KH, et al. Epidemiology and cause of severe acute respiratory syndrome (SARS) in Guangdong, People's Republic of China, in February, 2003. Lancet. 2003;362(9393):1353-8. doi: 10.1016/s0140-6736(03)14630-2. PubMed PMID: 14585636; PubMed Central PMCID: PMCPMC7112415.
338. Hofmann H, Pyrc K, van der Hoek L, Geier M, Berkhout B, Pohlmann S. Human coronavirus NL63 employs the severe acute respiratory syndrome coronavirus receptor for cellular entry. Proc Natl Acad Sci U S A. 2005;102(22):7988-93. Epub 20050516. doi: 10.1073/pnas.0409465102. PubMed PMID: 15897467; PubMed Central PMCID: PMCPMC1142358.
339. Bogs J, Veits J, Gohrbandt S, Hundt J, Stech O, Breithaupt A, et al. Highly pathogenic H5N1 influenza viruses carry virulence determinants beyond the polybasic hemagglutinin cleavage site. PLoS One. 2010;5(7):e11826. Epub 20100727. doi: 10.1371/journal.pone.0011826. PubMed PMID: 20676399; PubMed Central PMCID: PMCPMC2910732.
340. Duverge A, Negroni M. Pseudotyping Lentiviral Vectors: When the Clothes Make the Virus. Viruses. 2020;12(11). Epub 20201116. doi: 10.3390/v12111311. PubMed PMID: 33207797; PubMed Central PMCID: PMCPMC7697029.
341. Guinea R, Carrasco L. Concanamycin A: a powerful inhibitor of enveloped animal-virus entry into cells. Biochem Biophys Res Commun. 1994;201(3):1270-8. doi: 10.1006/bbrc.1994.1842. PubMed PMID: 8024571.
342. Huss M, Ingenhorst G, Konig S, Gassel M, Drose S, Zeeck A, et al. Concanamycin A, the specific inhibitor of V-ATPases, binds to the V(o) subunit c. J Biol Chem. 2002;277(43):40544-8. Epub 20020816. doi: 10.1074/jbc.M207345200. PubMed PMID: 12186879.

343. Nie J, Li Q, Zhang L, Cao Y, Zhang Y, Li T, et al. Functional comparison of SARS-CoV-2 with closely related pangolin and bat coronaviruses. Cell Discov. 2021;7(1):21. Epub 20210406. doi: 10.1038/s41421-021-00256-3. PubMed PMID: 33824288; PubMed Central PMCID: PMCPMC8022302.
344. Bastard P, Rosen LB, Zhang Q, Michailidis E, Hoffmann HH, Zhang Y, et al. Autoantibodies against type I IFNs in patients with life-threatening COVID-19. Science. 2020;370(6515). Epub 20200924. doi: 10.1126/science.abd4585. PubMed PMID: 32972996; PubMed Central PMCID: PMCPMC7857397.
345. Felgenhauer U, Schoen A, Gad HH, Hartmann R, Schaubmar AR, Failing K, et al. Inhibition of SARS-CoV-2 by type I and type III interferons. J Biol Chem. 2020;295(41):13958-64. Epub 20200625. doi: 10.1074/jbc.AC120.013788. PubMed PMID: 32587093; PubMed Central PMCID: PMCPMC7549028.
346. Stanifer ML, Kee C, Cortese M, Zumaran CM, Triana S, Mukenhirn M, et al. Critical Role of Type III Interferon in Controlling SARS-CoV-2 Infection in Human Intestinal Epithelial Cells. Cell Rep. 2020;32(1):107863. Epub 20200619. doi: 10.1016/j.celrep.2020.107863. PubMed PMID: 32610043; PubMed Central PMCID: PMCPMC7303637.
347. Davidson AD, Williamson MK, Lewis S, Shoemark D, Carroll MW, Heesom KJ, et al. Characterisation of the transcriptome and proteome of SARS-CoV-2 reveals a cell passage induced in-frame deletion of the furin-like cleavage site from the spike glycoprotein. Genome Med. 2020;12(1):68. Epub 2020/07/30. doi: 10.1186/s13073-020-00763-0. PubMed PMID: 32723359; PubMed Central PMCID: PMCPMC7386171.
348. Pan Y, Yang P, Dong T, Zhang Y, Shi W, Peng X, et al. IFITM3 Rs12252-C Variant Increases Potential Risk for Severe Influenza Virus Infection in Chinese Population. Front Cell Infect Microbiol. 2017;7:294. Epub 20170630. doi: 10.3389/fcimb.2017.00294. PubMed PMID: 28713779; PubMed Central PMCID: PMCPMC5491636.
349. Hornick AL, Li N, Oakland M, McCray PB, Jr., Sinn PL. Human, Pig, and Mouse Interferon-Induced Transmembrane Proteins Partially Restrict Pseudotyped Lentiviral Vectors. Hum Gene Ther. 2016;27(5):354-62. doi: 10.1089/hum.2015.156. PubMed PMID: 27004832; PubMed Central PMCID: PMCPMC4840922.
350. Li C, Zheng H, Wang Y, Dong W, Liu Y, Zhang L, et al. Antiviral Role of IFITM Proteins in Classical Swine Fever Virus Infection. Viruses. 2019;11(2). Epub 20190130. doi: 10.3390/v11020126. PubMed PMID: 30704088; PubMed Central PMCID: PMCPMC6409519.
351. Shi G, Schwartz O, Compton AA. More than meets the I: the diverse antiviral and cellular functions of interferon-induced transmembrane proteins. Retrovirology. 2017;14(1):53. Epub 20171121. doi: 10.1186/s12977-017-0377-y. PubMed PMID: 29162141; PubMed Central PMCID: PMCPMC5697417.
352. Wei X, Jia ZS, Lian JQ, Zhang Y, Li J, Ma L, et al. Inhibition of hepatitis C virus infection by interferon-gamma through downregulating claudin-1. J Interferon Cytokine Res. 2009;29(3):171-8. doi: 10.1089/jir.2008.0040. PubMed PMID: 19196072.
353. Dhawan S, Heredia A, Wahl LM, Epstein JS, Meltzer MS, Hewlett IK. Interferon-gamma-induced downregulation of CD4 inhibits the entry of human immunodeficiency virus type-1 in primary monocytes. Pathobiology. 1995;63(2):93-9. doi: 10.1159/000163939. PubMed PMID: 8554705.
354. Lee JH, Koepke L, Kirchhoff F, Sparrer KMJ. Interferon antagonists encoded by SARS-CoV-2 at a glance. Med Microbiol Immunol. 2022. Epub 20220402. doi: 10.1007/s00430-022-00734-9. PubMed PMID: 35366686; PubMed Central PMCID: PMCPMC8976456.

355. Tegally H, Moir M, Everatt J, Giovanetti M, Scheepers C, Wilkinson E, et al. Emergence of SARS-CoV-2 Omicron lineages BA.4 and BA.5 in South Africa. Nat Med. 2022. Epub 20220627. doi: 10.1038/s41591-022-01911-2. PubMed PMID: 35760080.
356. Zahradnik J, Nunvar J, Schreiber G. Perspectives: SARS-CoV-2 Spike Convergent Evolution as a Guide to Explore Adaptive Advantage. Front Cell Infect Microbiol. 2022;12:748948. Epub 20220527. doi: 10.3389/fcimb.2022.748948. PubMed PMID: 35711666; PubMed Central PMCID: PMCPMC9197234.
357. Weisblum Y, Schmidt F, Zhang F, DaSilva J, Poston D, Lorenzi JC, et al. Escape from neutralizing antibodies by SARS-CoV-2 spike protein variants. Elife. 2020;9. Epub 20201028. doi: 10.7554/eLife.61312. PubMed PMID: 33112236; PubMed Central PMCID: PMCPMC7723407.
358. Zeng C, Evans JP, Faraone JN, Qu P, Zheng YM, Saif L, et al. Neutralization of SARS-CoV-2 Variants of Concern Harboring Q677H. mBio. 2021;12(5):e0251021. Epub 20211005. doi: 10.1128/mBio.02510-21. PubMed PMID: 34607452; PubMed Central PMCID: PMCPMC8527387.
359. Liu Y, Liu J, Johnson BA, Xia H, Ku Z, Schindewolf C, et al. Delta spike P681R mutation enhances SARS-CoV-2 fitness over Alpha variant. bioRxiv. 2021. Epub 20210905. doi: 10.1101/2021.08.12.456173. PubMed PMID: 34462752; PubMed Central PMCID: PMCPMC8404900.
360. Liu Y, Liu J, Plante KS, Plante JA, Xie X, Zhang X, et al. The N501Y spike substitution enhances SARS-CoV-2 transmission. bioRxiv. 2021. Epub 20210309. doi: 10.1101/2021.03.08.434499. PubMed PMID: 33758836; PubMed Central PMCID: PMCPMC7986995.
361. Lubinski B, Fernandes MHV, Frazier L, Tang T, Daniel S, Diel DG, et al. Functional evaluation of the P681H mutation on the proteolytic activation the SARS-CoV-2 variant B.1.1.7 (Alpha) spike. bioRxiv. 2021. Epub 20211101. doi: 10.1101/2021.04.06.438731. PubMed PMID: 33851153; PubMed Central PMCID: PMCPMC8043443.
362. Zeng C, Evans JP, Qu P, Faraone J, Zheng YM, Carlin C, et al. Neutralization and Stability of SARS-CoV-2 Omicron Variant. bioRxiv. 2021. Epub 20211220. doi: 10.1101/2021.12.16.472934. PubMed PMID: 34981053; PubMed Central PMCID: PMCPMC8722590.
363. Zhao X, Sehgal M, Hou Z, Cheng J, Shu S, Wu S, et al. Identification of Residues Controlling Restriction versus Enhancing Activities of IFITM Proteins on Entry of Human Coronaviruses. J Virol. 2018;92(6). Epub 20180226. doi: 10.1128/JVI.01535-17. PubMed PMID: 29263263; PubMed Central PMCID: PMCPMC5827390.
364. Neuman BW, Kiss G, Kunding AH, Bhella D, Baksh MF, Connelly S, et al. A structural analysis of M protein in coronavirus assembly and morphology. J Struct Biol. 2011;174(1):11-22. Epub 20101203. doi: 10.1016/j.jsb.2010.11.021. PubMed PMID: 21130884; PubMed Central PMCID: PMCPMC4486061.
365. Lukassen S, Chua RL, Trefzer T, Kahn NC, Schneider MA, Muley T, et al. SARS-CoV-2 receptor ACE2 and TMPRSS2 are primarily expressed in bronchial transient secretory cells. EMBO J. 2020;39(10):e105114. Epub 20200414. doi: 10.15252/embj.20105114. PubMed PMID: 32246845; PubMed Central PMCID: PMCPMC7232010.
366. Investigators ST, Fidler S, Porter K, Ewings F, Frater J, Ramjee G, et al. Short-course antiretroviral therapy in primary HIV infection. N Engl J Med. 2013;368(3):207-17. doi: 10.1056/NEJMoa1110039. PubMed PMID: 23323897; PubMed Central PMCID: PMCPMC4131004.

367. Yu J, Liang C, Liu SL. CD4-Dependent Modulation of HIV-1 Entry by LY6E. J Virol. 2019;93(7). Epub 20190321. doi: 10.1128/JVI.01866-18. PubMed PMID: 30674630; PubMed Central PMCID: PMCPMC6430548.
368. Iwami S, Takeuchi JS, Nakaoka S, Mammano F, Clavel F, Inaba H, et al. Cell-to-cell infection by HIV contributes over half of virus infection. Elife. 2015;4. Epub 20151006. doi: 10.7554/eLife.08150. PubMed PMID: 26441404; PubMed Central PMCID: PMCPMC4592948.
369. Ding S, Pan Q, Liu SL, Liang C. HIV-1 mutates to evade IFITM1 restriction. Virology. 2014;454-455:11-24. Epub 20140220. doi: 10.1016/j.virol.2014.01.020. PubMed PMID: 24725927; PubMed Central PMCID: PMCPMC4274668.
370. Compton AA, Roy N, Porrot F, Billet A, Casartelli N, Yount JS, et al. Natural mutations in IFITM3 modulate post-translational regulation and toggle antiviral specificity. EMBO Rep. 2016;17(11):1657-71. Epub 20160906. doi: 10.15252/embr.201642771. PubMed PMID: 27601221; PubMed Central PMCID: PMCPMC5090704.
371. Trypsteen W, Van Cleemput J, Snippenberg WV, Gerlo S, Vandekerckhove L. On the whereabouts of SARS-CoV-2 in the human body: A systematic review. PLoS Pathog. 2020;16(10):e1009037. Epub 20201030. doi: 10.1371/journal.ppat.1009037. PubMed PMID: 33125439; PubMed Central PMCID: PMCPMC7679000.

Appendix: Publications

Journal of Virology®

CELLULAR RESPONSE TO INFECTION

The Polybasic Cleavage Site in SARS-CoV-2 Spike Modulates Viral Sensitivity to Type I Interferon and IFITM2

Helena Winstone,[a] Maria Jose Lista,[a] Alisha C. Reid,[a] Clement Bouton,[a] Suzanne Pickering,[a] Rui Pedro Galao,[a] Claire Kerridge,[a] Katie J. Doores,[a] Chad M. Swanson,[a] Stuart J. D. Neil[a]

[a]Department of Infectious Diseases, School of Immunology and Microbial Sciences, King's College London, London, United Kingdom

Helena Winstone and Maria Jose Lista contributed equally to this work. The order of their authorship was agreed upon between the two authors.

ABSTRACT The cellular entry of severe acute respiratory syndrome-associated coronaviruses types 1 and 2 (SARS-CoV-1 and -2) requires sequential protease processing of the viral spike glycoprotein. The presence of a polybasic cleavage site in SARS-CoV-2 spike at the S1/S2 boundary has been suggested to be a factor in the increased transmissibility of SARS-CoV-2 compared to SARS-CoV-1 by facilitating maturation of the spike precursor by furin-like proteases in the producer cells rather than endosomal cathepsins in the target. We investigate the relevance of the polybasic cleavage site in the route of entry of SARS-CoV-2 and the consequences this has for sensitivity to interferons (IFNs) and, more specifically, the IFN-induced transmembrane (IFITM) protein family that inhibit entry of diverse enveloped viruses. We found that SARS-CoV-2 is restricted predominantly by IFITM2, rather than IFITM3, and the degree of this restriction is governed by route of viral entry. Importantly, removal of the cleavage site in the spike protein renders SARS-CoV-2 entry highly pH and cathepsin dependent in late endosomes, where, like SARS-CoV-1 spike, it is more sensitive to IFITM2 restriction. Furthermore, we found that potent inhibition of SARS-CoV-2 replication by type I but not type II IFNs is alleviated by targeted depletion of IFITM2 expression. We propose that the polybasic cleavage site allows SARS-CoV-2 to mediate viral entry in a pH-independent manner, in part to mitigate against IFITM-mediated restriction and promote replication and transmission. This suggests that therapeutic strategies that target furin-mediated cleavage of SARS-CoV-2 spike may reduce viral replication through the activity of type I IFNs.

IMPORTANCE The furin cleavage site in the spike protein is a distinguishing feature of SARS-CoV-2 and has been proposed to be a determinant for the higher transmissibility between individuals, compared to SARS-CoV-1. One explanation for this is that it permits more efficient activation of fusion at or near the cell surface rather than requiring processing in the endosome of the target cell. Here, we show that SARS-CoV-2 is inhibited by antiviral membrane protein IFITM2 and that the sensitivity is exacerbated by deletion of the furin cleavage site, which restricts viral entry to low pH compartments. Furthermore, we find that IFITM2 is a significant effector of the antiviral activity of type I interferons against SARS-CoV-2 replication. We suggest that one role of the furin cleavage site is to reduce SARS-CoV-2 sensitivity to innate immune restriction, and thus, it may represent a potential therapeutic target for COVID-19 treatment development.

KEYWORDS furin cleavage, IFITM2, innate immunity, SARS-CoV-2, spike, type 1 interferon

Severe acute respiratory syndrome coronavirus 2 (SARS-CoV-2) is a novel coronavirus that was identified in early 2020 (1). Entry of SARS-CoV-2 into the target cell is

Citation Winstone H, Lista MJ, Reid AC, Bouton C, Pickering S, Galao RP, Kerridge C, Doores KJ, Swanson CM, Neil SJD. 2021. The polybasic cleavage site in SARS-CoV-2 spike modulates viral sensitivity to type I interferon and IFITM2. J Virol 95:e02422-20. https://doi.org/10.1128/JVI.02422-20.

Editor Tom Gallagher, Loyola University Chicago

Address correspondence to Stuart J. D. Neil, stuart.neil@kcl.ac.uk.

Received 19 December 2020
Accepted 3 February 2021
Accepted manuscript posted online 9 February 2021
Published 12 April 2021

initiated by the spike glycoprotein binding to its receptor, angiotensin-converting enzyme 2 (ACE2) (2). Spike is a type I transmembrane protein that is synthesized as a polyprotein precursor and requires two steps of proteolytic cleavage at the S1/S2 boundary and at the S2′ site in order to mediate fusion of the viral and cell membranes. Due to the insertion of four amino acids (in bold) at the S1/S2 boundary of SARS-CoV-2 spike, with the sequence $_{681}$**PRRA**R/SV$_{687}$, SARS-CoV-2 spike contains a canonical furin-like protease cleavage site (2). This allows the SARS-CoV-2 spike to be cleaved by furin-like proteases intracellularly prior to virion release. TMPRSS2 on the target cell surface and cathepsins B and L in endosomes may then cleave the S2′ site and activate the fusion machinery, depending on the relative availability of these enzymes.

The presence of the furin cleavage site has been suggested to be important for determining viral tropism and transmission of SARS-CoV-2 (3–5). However, the necessity for this site is cell type dependent. It has been shown that this site can be lost after several passages in TMPRSS2-negative Vero E6 cells (6). Nevertheless, similar mutations have only been found rarely in a small number of patients (7, 8). This suggests a selective pressure to conserve the polybasic cleavage site for *in vivo* transmission but not necessarily *in vitro*, depending on the cell line used (5–8). Structural data for SARS-CoV-2 spike indicates that cleavage at the S1/S2 boundary results in exposure of the receptor-binding domain (RBD) of spike (9). It has been suggested that this exposure of the RBD facilitates binding to ACE2 and the secondary cleavage of the S2′ site of spike, facilitating membrane fusion.

Interferons (IFNs) upregulate the expression of a range of antiviral proteins, encoded by genes termed IFN-stimulated genes (ISGs), that inhibit various aspects of viral life cycles, including entry (10). One of these protein families, IFN-induced transmembrane proteins (IFITMs), are membrane-spanning proteins that inhibit the entry of several viruses, including HIV-1, influenza virus, Ebola virus, and SARS-CoV-1, through blocking the fusion of the cellular and viral membranes, possibly by decreasing membrane fluidity or affecting membrane curvature (11, 12). Three IFITMs demonstrate antiviral activity in humans: IFITM1, which localizes to the plasma membrane, and IFITM2 and -3, which localize to late and early endosomes, respectively (13, 14). Previous research has shown that the route of entry correlates with the restriction of both influenza virus and HIV-1 by IFITMs. Mislocalizing IFITM3 to the cell surface abrogates IFITM3 restriction of influenza virus (15). CCR5-tropic HIV-1 viruses that fuse at the plasma membrane are more restricted by IFITM1, while CXCR4-tropic viruses that utilize the endosomal route are more restricted by IFITM2 and -3 (13). It has been reported that SARS-CoV-2 is highly sensitive to type I and III IFNs and, more specifically, to IFITM3 (5, 16–18). Conversely, other authors have suggested that expression of IFITMs can enhance entry of SARS-CoV-2 (19). Given that entry is the first key step in viral transmission and IFITMs have been shown to be expressed in lung tissue, the interplay between IFITM restriction and the route of SARS-CoV-2 entry is likely to be fundamental to the ability of SARS-CoV-2 to infect and to be transmitted (20, 21). Here, we show the differential sensitivity of SARS-CoV-2 to IFITMs and how the presence of a polybasic cleavage site may affect entry in the context of IFITM restriction.

RESULTS

Sensitivity of SARS-CoV-2 and pseudotyped lentiviral vectors (PLVs) with SARS-CoV-2 spike to human type I, type II, and type III interferons in A549-ACE2 cells. In order to examine the restriction of SARS-CoV-2 replication by human antiviral proteins, we first sought to confirm the sensitivity of replication-competent SARS-CoV-2 (SARS-CoV-2 strain England 2) to type I (α and β), type II (γ), and type III (λ) IFNs in human A549 lung cancer cells stably expressing ACE2. We pretreated the cells with different doses of recombinant human IFN-α2, -β, -λ4, and -γ overnight and then challenged them with SARS-CoV-2 (multiplicity of infection [MOI] of 0.005 based on Vero E6 cells). Then, 48 h later we measured the levels of viral RNA by reverse transcription-quantitative PCR (RT-qPCR) using the N1 and N2 primer probe sets from Centers for

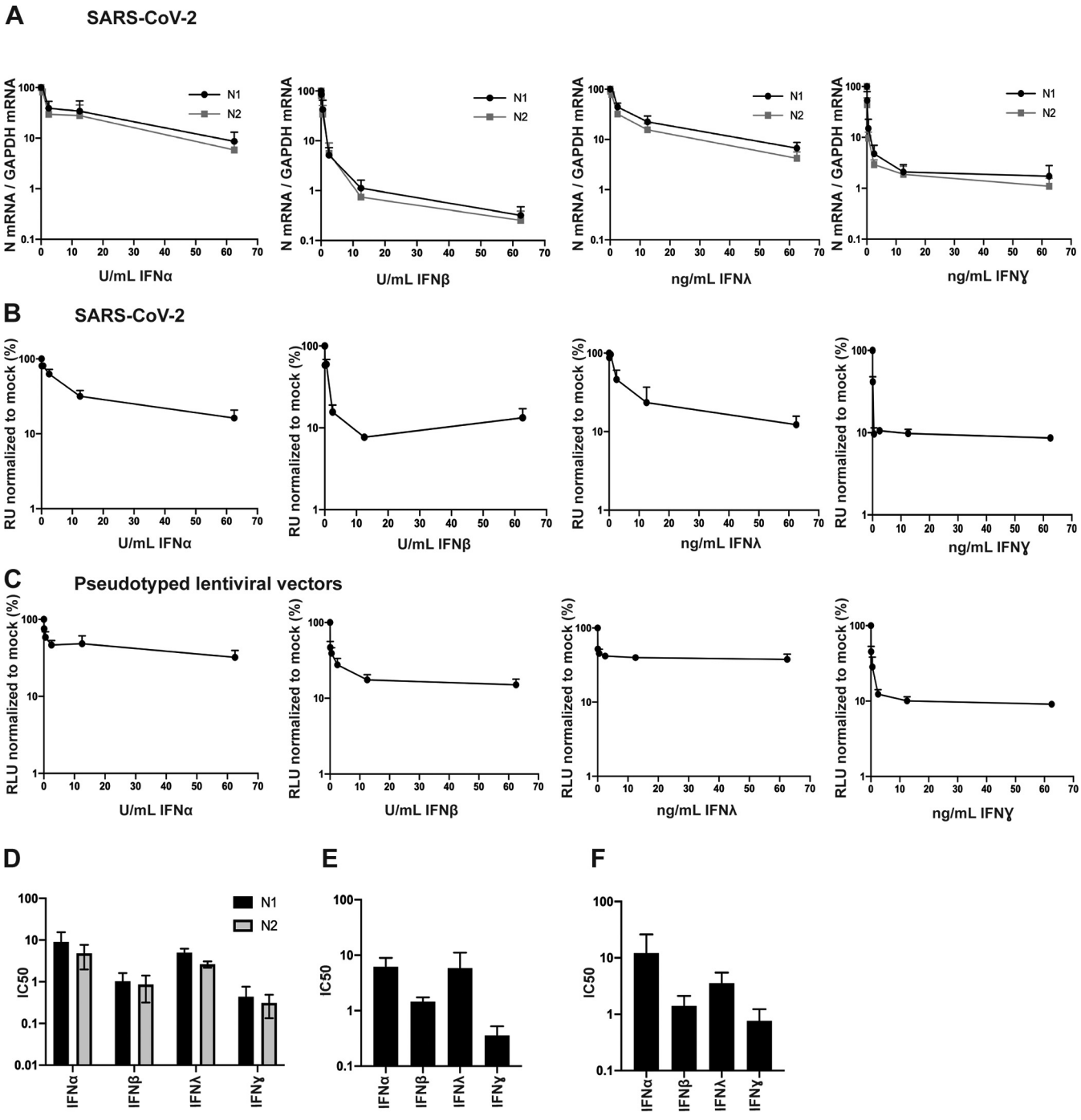

FIG 1 Entry of replication-competent SARS-CoV-2 and PLVs of SARS-CoV-2 is inhibited by IFN-β and IFN-γ. (A) A549-ACE2 cells were pretreated for 18 h with IFN-α, -β, -λ, or -γ and subsequently infected with replication-competent SARS-CoV-2 at an MOI of 0.005. Viral RNA was extracted 48 h later, detected with two sets of primers (N1 and N2) against nucleocapsid mRNA, and normalized to infection in mock-treated cells. (B) Supernatant from infected A549-ACE2 used for panel A was used to infect Vero E6 cells for 24 h. Vero E6 cells were then stained for nucleocapsid protein and normalized to mock-treated conditions. RU, relative units. (C) A549-ACE2 cells were pretreated for 18 h with IFN-α, -β, -λ, or -γ and transduced with PLVs of SARS-CoV-2 for 48 h. Infection was quantified by luciferase activity and normalized to mock-treated conditions. RLU, relative luminescence units. (D to F) IC_{50}s for panels A to C were calculated in Prism. All data are means and standard errors of the means (SEM) ($n = 3$).

Disease Control N1 and N2 primer probe sets (Fig. 1A and D). We found that SARS-CoV-2 is highly sensitive to IFN-β and IFN-γ, with very low half-maximal inhibitory concentrations (IC_{50}s), and is less sensitive but nonetheless still restricted by IFN-α and IFN-λ. In addition to measuring intracellular viral RNA abundance in the IFN-treated cells, we infected Vero E6 cells with the supernatant harvested from IFN-treated and

infected A549-ACE2 cells and quantified the expression of nucleocapsid (N) protein 24 h later. This assay measures the amount of infectious virus produced by the mock or IFN-treated cells and showed similar results (Fig. 1B and E), thus confirming previous studies showing that the virus is highly IFN sensitive, particularly to IFN-β and IFN-γ, and indicating that a number of ISGs have direct antiviral effects against SARS-CoV-2 (16, 18).

In order to address the activities of ISGs directed against spike-mediated entry, we first determined whether we could recapitulate the IFN phenotypes observed above using pseudotyped lentiviral vectors (PLVs). We generated PLVs containing SARS-CoV-2 spike bearing a luciferase reporter gene and tested them for sensitivity to IFNs on A549-ACE2. Similar to full-length SARS-CoV-2, we found that PLVs with SARS-CoV-2 spike are also highly sensitive to IFN-β and IFN-γ (Fig. 1C and F). While the early events of HIV-1 are known targets of IFN treatment in some cell lines, these data suggest that when we isolated the entry stage of SARS-CoV-2 infection, we observed inhibition by IFN-β and IFN-γ (22).

SARS-CoV-2 is sensitive to IFITM2, but not IFITM3, in A549-ACE2 cells. IFITMs are a family of ISGs that predominantly inhibit fusion of viral and cellular membranes (11, 14). Considering that our PLVs with SARS-CoV-2 spike demonstrated an extent of inhibition by IFNs similar to that of the full-length virus, we suspected that IFITMs, which have previously been reported to inhibit SARS-CoV-1 and more recently suggested to inhibit SARS-CoV-2, may contribute to this inhibition (5, 12, 19, 23).

To test the impact of each individual IFITM on SARS-CoV-2 infection, we generated stable A549-ACE2 cell lines expressing each human antiviral IFITM (Fig. 2A). Of note, cross-reactivity between antibodies targeting IFITM2 and IFITM3 is inevitable due to high homology between these proteins. We infected these cells with influenza A virus (IAV) and confirmed that, consistent with previous findings, overexpression of IFITM2 and IFITM3 inhibited IAV infection (Fig. 2B) (24, 25). Next, we infected these cells with PLVs and found that SARS-CoV-2 showed a small but significant sensitivity to IFITM1 and a greater sensitivity to IFITM2 (Fig. 2C). We recapitulated these phenotypes by challenging the A549-ACE2-IFITM cells with SARS-CoV-2 at MOI of 0.005, 0.01, and 0.05. We used the supernatants from these cells 48 h later to infect Vero E6 cells and measured viral infectivity by staining for N protein (Fig. 2D). At low MOI, SARS-CoV-2 was particularly sensitive to IFITM2 but not IFITM3, with an inhibitory effect seen with IFITM1, and these sensitivities were ameliorated at high viral inputs. As both single-round PLVs and the full-length virus essentially displayed similar phenotypic sensitivity to IFITM2, these results suggest that a predominant antiviral effect is mediated at cellular entry.

Both IFITM2 and IFITM3 predominantly localize to endosomal compartments but reach them via endocytosis from the cell surface, through the recruitment of the clathrin adaptor AP2 to a tyrosine-based endocytic signal (YXXΦ) in the IFITM2/3 cytoplasmic tail. We and others have previously demonstrated that mutating Y19 and Y20 to a phenylalanine in IFITM2 and IFITM3, respectively, results in their accumulation at the plasma membrane (13, 26). To test this, we stably expressed IFITM2 Y19F A549-ACE2 (Fig. 2E) and infected these cells with IAV (Fig. 2F). We found that infection of IFITM2-Y19F cells was slightly enhanced compared to that of IFITM2 cells. Similarly, infection of these cells with PLVs and replication-competent SARS-CoV-2 at an MOI of 0.005 revealed that infection was not inhibited but rather was enhanced by the presence of IFITM2-Y19F (Fig. 2G and H). Although it was surprising that mislocalization of IFITM2 resulted in enhancement of infection rather than simply an absence of restriction, these data are consistent with a recent report suggesting that similar mutants of IFITM3 enhance SARS-CoV-2 infection (27). These data suggest that the localization of IFITM2 to endosomes or its recruitment to clathrin-coated pits at the plasma membrane is key to its inhibition of SARS-CoV-2 entry.

The polybasic cleavage site determines sensitivity to IFITM2 in the presence or absence of TMPRSS2. A major difference between the spike protein of SARS-CoV-2 and that of the majority of the phylogenetically related bat sarbecoviruses, including SARS-CoV-1, is the presence of the polybasic cleavage site at the S1/S2 boundary (Fig.

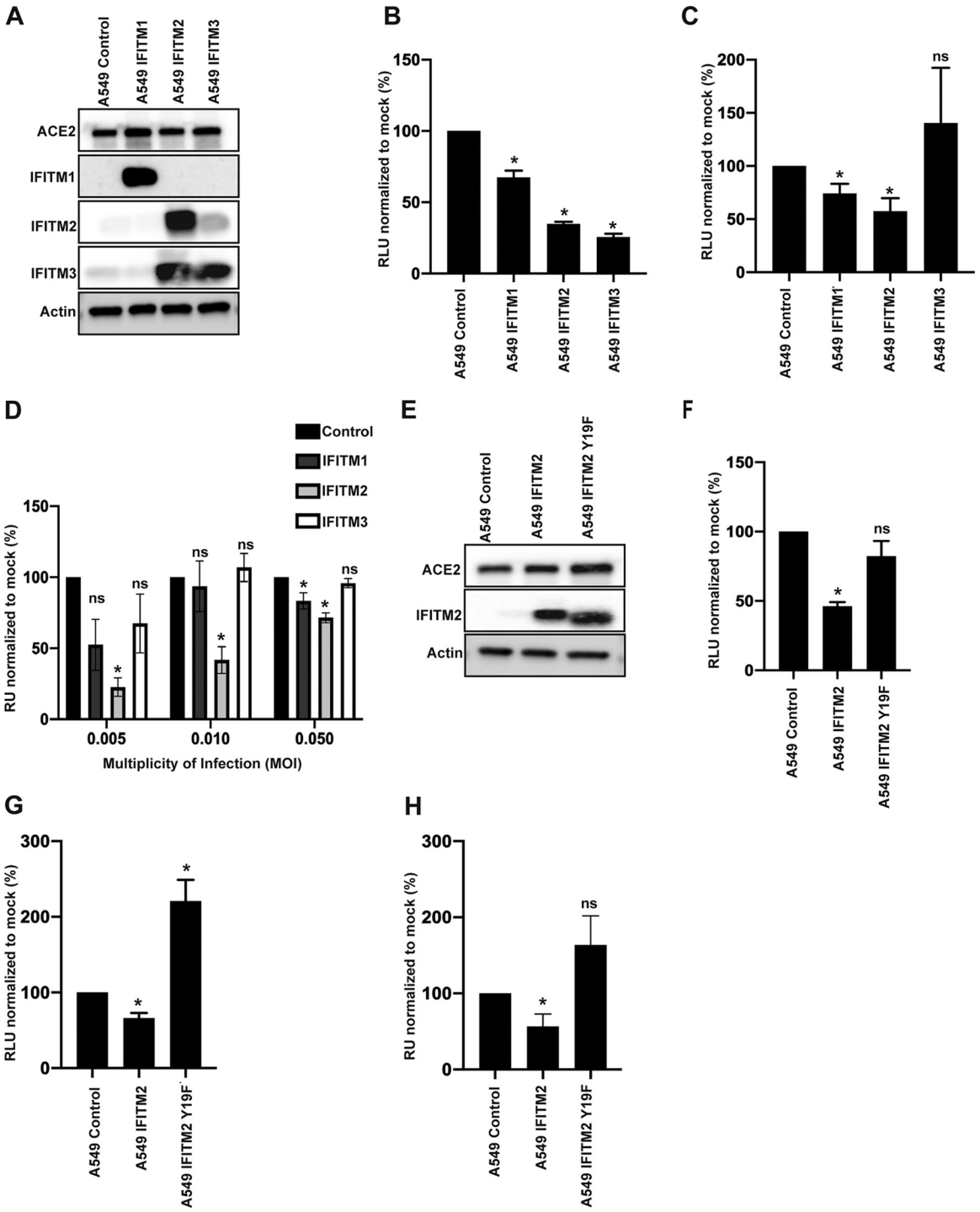

FIG 2 Replication-competent SARS-CoV-2 and PLVs of SARS-CoV-2 are inhibited by IFITM2 in A549-ACE2 cells. (A) Representative immunoblot of A549-ACE2 cells stably expressing IFITM1, IFITM2, and IFITM3. Of note, the antibody to IFITM2 and IFITM3 recognizes both proteins. (B) A549-ACE2-IFITM cells were infected with influenza A virus (IAV), and infection was quantified by luciferase activity 24 h later. (C) A549-ACE2-IFITM cells were transduced with SARS-CoV-2 PLVs for 48 h, and infection was quantified by luciferase activity. (D) A549-ACE2-IFITM cells were infected with replication-competent SARS-CoV-2 for 48 h at MOI of 0.005, 0.01, and 0.05. Supernatant was then used to infect Vero E6 cells for 24 h, and cells were stained for nucleocapsid protein. (E) Representative immunoblot of A549-ACE2 cells stably expressing IFITM2 and IFITM2 Y19F. (F) A549-ACE2 IFITM cells used for panel E were infected with IAV, and infection was quantified by luciferase activity 24 h later. (G) SARS-CoV-2 PLVs were used to transduce A549-ACE2-IFITM2 and the Y19F mutant, and infection was quantified 48 h later by luciferase activity. (H) Replication-competent SARS-CoV-2 was used to infect A549-ACE2-IFITM2 cells or A549-ACE2 cells stably expressing IFITM2 or IFITM2 Y19F at an MOI of 0.005. Supernatant was used to infect Vero E6 cells for 24 h, and cells were N stained as for panel C. RU, relative units; RLU, relative luminescence units. All data are means and SEM ($n = 3$). *, $P < 0.05$ (unpaired t test, calculated in Prism).

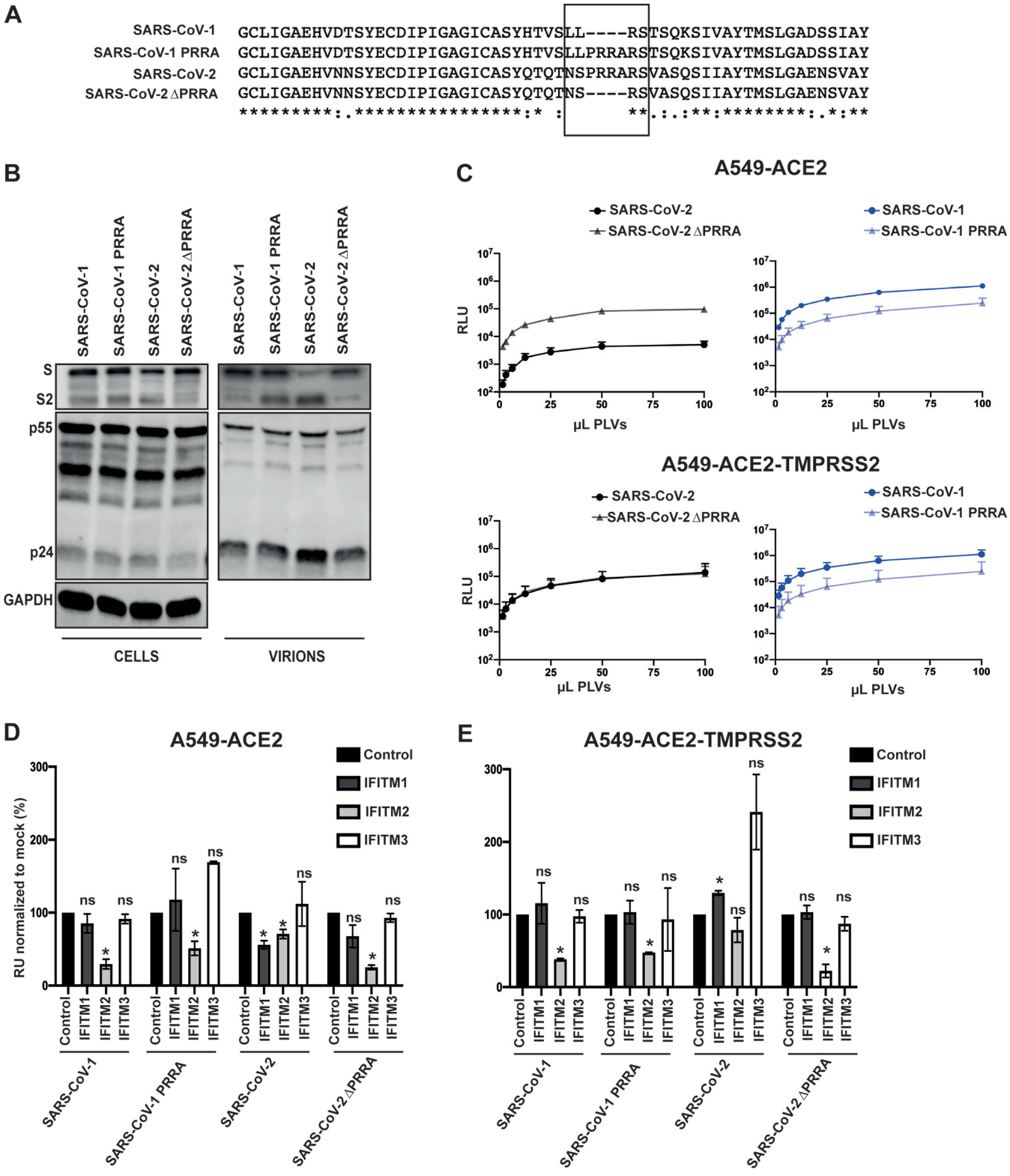

FIG 3 The presence or absence of a polybasic cleavage site determines sensitivity to IFITM2. (A) Alignment of the S1/S2 boundary in SARS-CoV-1 and SARS-CoV-2 with mutants where PRRA has been inserted/deleted. Alignment was created in Clustal Omega. (B) Representative immunoblot of PLVs of SARS-CoV-1, SARS-CoV-1 PRRA, SARS-CoV-2, and SARS-CoV-2ΔPRRA. (C) PLVs of SARS-CoV-1, SARS-CoV-1 PRRA, SARS-CoV-2, and SARS-CoV-2ΔPRRA were titrated on A549-ACE2 or A549-ACE2-TMPRSS2 cells, and infectivity was measured by luciferase assay 48 h later. (D and E) PLVs of SARS, as described for panels B and C, were used to transduce A549-ACE2-IFITM cells (D) or A549-ACE2-TMPRSS2-IFITM cells (E) for 48 h, and infection was measured by luciferase activity. Infection was normalized to empty vector cells. RLU, relative luminescence units. All data are means and SEM ($n = 3$). *, $P < 0.05$ (unpaired t test, calculated in Prism).

3A). This facilitates the processing of spike to S1/S2 during viral assembly in the producer cell rather than during entry into the target cell. As this feature has been proposed to be associated with the increased transmissibility of SARS-CoV-2, we hypothesized that it might affect the sensitivity of the virus to IFITM2. To investigate this, we deleted the polybasic cleavage site from SARS-CoV-2 (while preserving the adjacent RS serine protease cleavage site) and swapped the corresponding region from (P_{681}-A_{684}) SARS-CoV-2 into SARS-CoV-1, generating SARS-CoV-2ΔPRRA and SARS-CoV-1 PRRA, respectively (Fig. 3A). We made PLVs of these mutants and analyzed spike expression and virion incorporation by Western blotting using a polyclonal antibody against SARS-CoV-1/2 S2 (Fig. 3B). We found that all spike proteins were equivalently expressed in the transfected producer 293T-17 cells. As expected, the SARS-CoV-1 spike existed predominantly as the S1/2 precursor on pelleted virions in the supernatant. In contrast, processed S2 was the predominant species found on virions pseudotyped with SARS-CoV-2 spike, indicating furin-mediated cleavage during virion assembly. As expected, SARS-CoV-2ΔPRRA was not cleaved. Insertion of the SARS-CoV-2 cleavage site into SARS-CoV-1 was sufficient to lead to processed spike; however, this was not as efficient as in SARS-CoV-2, with virions incorporating both cleaved and uncleaved spike (Fig. 3B). In keeping with results from others in Vero E6 cells, in A549 cells SARS-CoV-2ΔPRRA PLVs had a marked increase in infectivity of approximately 50-fold in A549-ACE2 cells compared to the wild-type spike, approaching the infectivity of SARS-CoV-1 (Fig. 3C) (4). Addition of the PRRA site to SARS-CoV-1 slightly reduced titers. Since SARS-CoV-2 requires TMPRSS2 in the target cells to activate spike for entry, we overexpressed TMPRSS2 in A549-ACE2 cells by retroviral transduction. This specifically enhanced infection of SARS-CoV-2 PLVs, indicating that, in the absence of TMPRSS2 expression, much of the SARS-CoV-2 inoculum is not infectious in these cells.

We then tested IFITM sensitivity of these PLVs in A549-ACE2 cells with and without TMPRSS2 overexpression (Fig. 3D and E). As expected, SARS-CoV-2 PLVs were sensitive to both IFITM1 and IFITM2 in A549-ACE2 cells (Fig. 3D). SARS-CoV-1 PLVs were significantly more sensitive to IFITM2 but displayed no restriction by IFITM1, suggestive of distinct subcellular site of entry between SARS-CoV-1 and SARS-CoV-2. Interestingly, deletion of PRRA in SARS-CoV-2 rendered this spike as sensitive as SARS-CoV-1 to IFITM2 and slightly reduced the IFITM1 sensitivity. In contrast, the addition of a cleavage site to SARS-CoV-1 significantly reduced IFITM2 sensitivity, albeit not to the levels of the fully cleaved SARS-CoV-2 spike. When we overexpressed TMPRSS2, we found that while IFITM1 sensitivity of SARS-CoV-2 could be abolished, this was not sufficient to rescue SARS-CoV-2 or SARS-CoV-2ΔPRRA from IFITM2 (Fig. 3D). Thus, the presence of the polybasic cleavage site markedly reduces the sensitivity of SARS-CoV-2 S-mediated entry to IFITM2, suggesting that it affects the route of entry into the cell and distinguishes this virus from SARS-CoV-1.

To address the effects of spike cleavage on route of entry, we first determined the pH sensitivity of the spike cleavage mutants using concanamycin A (ConA), an inhibitor of the vacuolar ATPase in late endosomes (Fig. 4A). As expected, SARS-CoV-1 PLVs were exquisitely sensitive (1,000-fold) to ConA inhibition in A549-ACE2, indicating that entry occurred exclusively in a low-pH endosomal compartment. In the presence of TMPRSS2, SARS-CoV-1 pH sensitivity was reduced, but entry still remained 20- to 50-fold lower, suggesting that any enhanced S2′ processing was not sufficient to abolish pH-dependent entry. Similarly, while insertion of a partially processed polybasic cleavage site in SARS-CoV-1 reduced but did not abolish pH-dependent entry in either cell type. In contrast, entry of SARS CoV-2 PLVs was only mildly affected (2- to 3-fold) by ConA treatment irrespective of TMPRSS2 overexpression, indicating that most viral entry occurred at neutral pH and that TMPRSS2 enhanced entry at this point rather than elsewhere in the cell. Similar to SARS-CoV-1, deletion of the PRRA site from SARS-CoV-2 rendered PLVs strictly pH dependent without affecting titers. In keeping with these data, unlike SARS-CoV-2-, SARS-CoV-1-, and SARS-CoV-2ΔPRRA-mediated entry was inhibited by the endosomal cathepsin inhibitor E64D but not the TMPRSS inhibitor

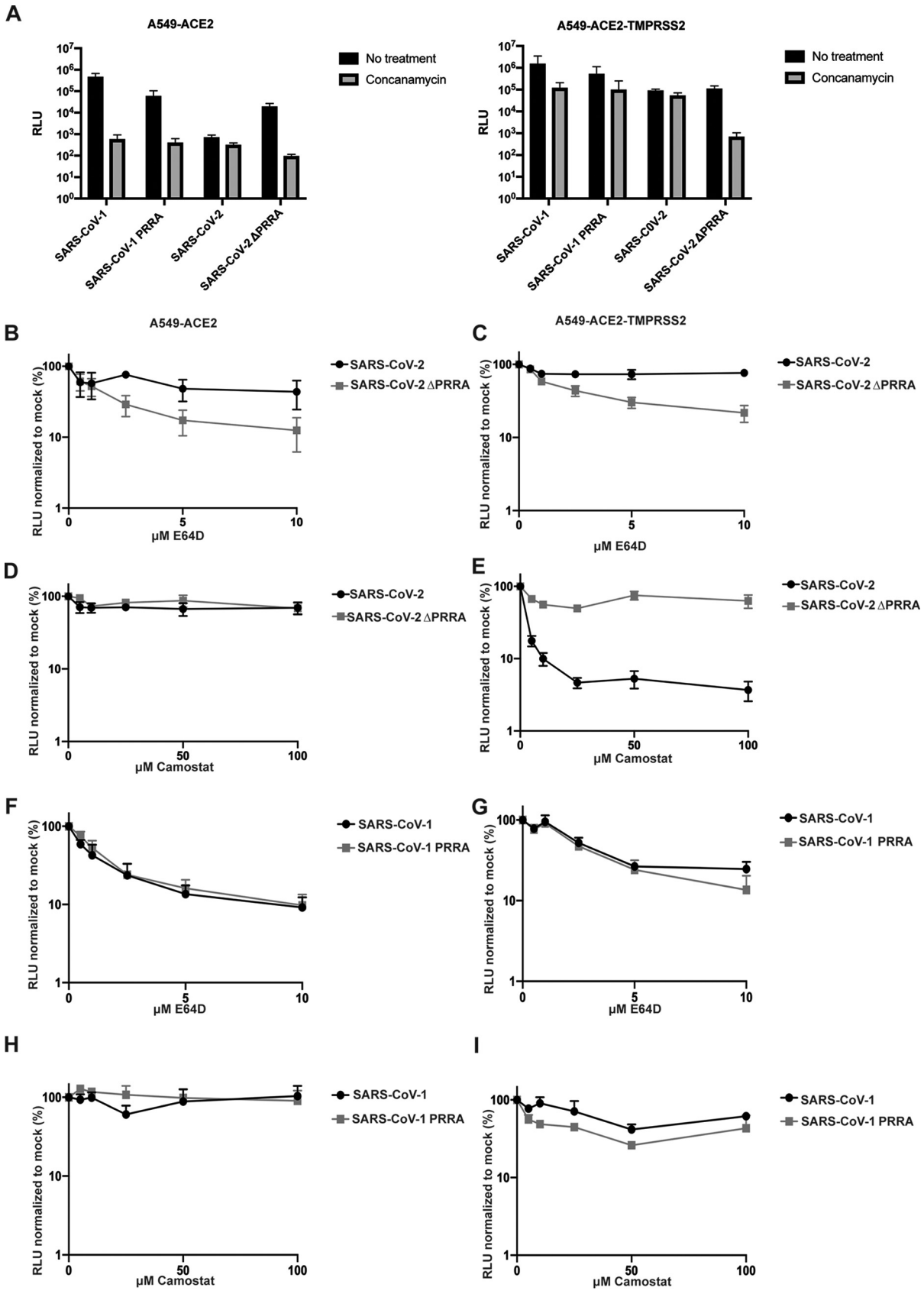

FIG 4 SARS-CoV-2 and SARS-CoV-2ΔPRRA differ in preferential route of entry. (A) A549-ACE2 and A549-ACE2-TMPRSS2 cells were treated with 100 nM concanamycin for 1 h and transduced with SARS PLVs. Infection was determined by luciferase activity 48 h later. Black,

(Continued on next page)

camostat (Fig. 4B to I). In contrast, SARS-CoV-2 was sensitive to E64D only in TMPRSS2-overexpressing cells. Together, these data suggest that S1/S2 cleavage by furin in the producer cell promotes TMPRSS2-mediated entry at the plasma membrane, or soon after internalization, and abolishes the requirement for cathepsin-mediated processing in the acidic endosomal compartments. The data further suggest that in the absence of abundant TMPRSS2 at the cell surface, the processed SARS-CoV-2 cannot efficiently enter through a low-pH compartment. Thus, the PRRA site dictates the route of entry into the cell and therefore its sensitivity to IFITM proteins that occupy different cellular locations.

IFITM2 contributes to the antiviral restriction of SARS-CoV-2 by IFN-β. Having established that IFITM2 can restrict SARS-CoV-2 depending on its mechanism of entry, we wanted to determine how much of the inhibition of replication-competent SARS-CoV-2 by IFN-β and IFN-γ could be attributed to IFITM2. We examined the expression of IFITM2 and IFITM3 in IFN-treated A549-ACE2 and observed a robust upregulation of both IFITM2 and IFITM3 following treatment with IFN-β. In contrast, while IFITM3 was also robustly induced by IFN-γ, IFITM2 was weakly induced (Fig. 5A). Using small interfering RNAs (siRNAs) against IFITM2 that rescued SARS-CoV-2 replication in A549-ACE2-IFITM2 cells (Fig. 5B and C), we then knocked down IFITM2 in the context of pretreating A549-ACE2 cells with IFN-β or IFN-γ and challenged the cells with SARS-CoV-2, measuring infectious virus output on Vero E6 cells 48 h later (Fig. 5D and E). IFITM2 depletion substantially relieved the inhibition of viral replication by IFN-β treatment, whereas that induced by IFN-γ was only modestly alleviated. This was reflected in the 20-fold increase in the IC_{50} of IFN-β, but only a 2-fold increase in IFN-γ, indicating that in these cells IFITM2 is a major component of the type I IFN-antiviral state protecting cells from SARS-CoV-2 (Fig. 5F). Furthermore, in A549-ACE2 cells overexpressing TMPRSS2, the knockdown of IFITM2 essentially abolished all the antiviral activity of pretreating the cells with IFN-β (Fig. 5G). Thus, IFITM2-mediated entry restriction is a major type I IFN activity that constitutes an antiviral state, blocking the replication of SARS CoV-2.

DISCUSSION

In this study, we provide evidence that IFITM2 has potent inhibitory activity against SARS-CoV-2 entry and constitutes at least part of the antiviral activity conferred by treatment of target cells with IFN-β. Furthermore, we find that the presence or absence of the polybasic cleavage site, which facilitates pH-independent entry of SARS-CoV-2, modulates the sensitivity of the virus to IFITM2. In contrast to SARS-CoV-1 and other related SARS-like CoVs in bats, SARS-CoV-2 is distinguished by the presence of a furin cleavage site at the S1/S2 boundary (4). This leads to the spike on SARS-CoV-2 virions being predominantly cleaved in the producer cell rather than by cathepsins during endocytic entry into the target cell and renders its entry pH independent, suggesting that fusion occurs at, or near, the cell surface. Recent evidence further indicates that furin cleavage generates a C-terminal ligand on S1 that interacts with neuropilin-1 (NRP-1) on the surface of target cells in the lung (28, 29). The role of NRP-1 is not completely clear, but there is some suggestion that it may stabilize the attachment of SARS-CoV-2 at the cell surface to facilitate either ACE2 interaction or processing of the S2′ site by TMPRSS2. Structural analyses of the SARS-CoV-2 spike trimer further show that furin-mediated cleavage facilitates at least one RBD to adopt an erect conformation that would further promote ACE2 interaction (9). Interestingly, deletion of the PRRA is not detrimental to SARS-CoV-2 entry in all cell types in culture, and in TMPRSS2-low Vero E6 cells, the furin cleavage site is rapidly lost upon passage, suggesting that it can actively hinder infection (6). Herein, we show that while wild-type

FIG 4 Legend (Continued)
nontreated; gray, concanamycin. (B to E) A549-ACE2 and A549-ACE2-TMPRSS2 cells were treated for 1 h with E64d or camostat and subsequently transduced with PLVs of SARS-CoV-2 or SARS-CoV-2ΔPRRA, and infection was detected by luciferase activity 48 h later. (F to I) A549-ACE2 or A549-ACE2-TMPRSS2 cells were treated with E64d or camostat for 1 h and transduced with PLVs of SARS-CoV-1 or SARS-CoV-1 PRRA, and infection was detected by luciferase activity 48 h later. RLU, relative luminescence units. All data are means and SEM (n = 3).

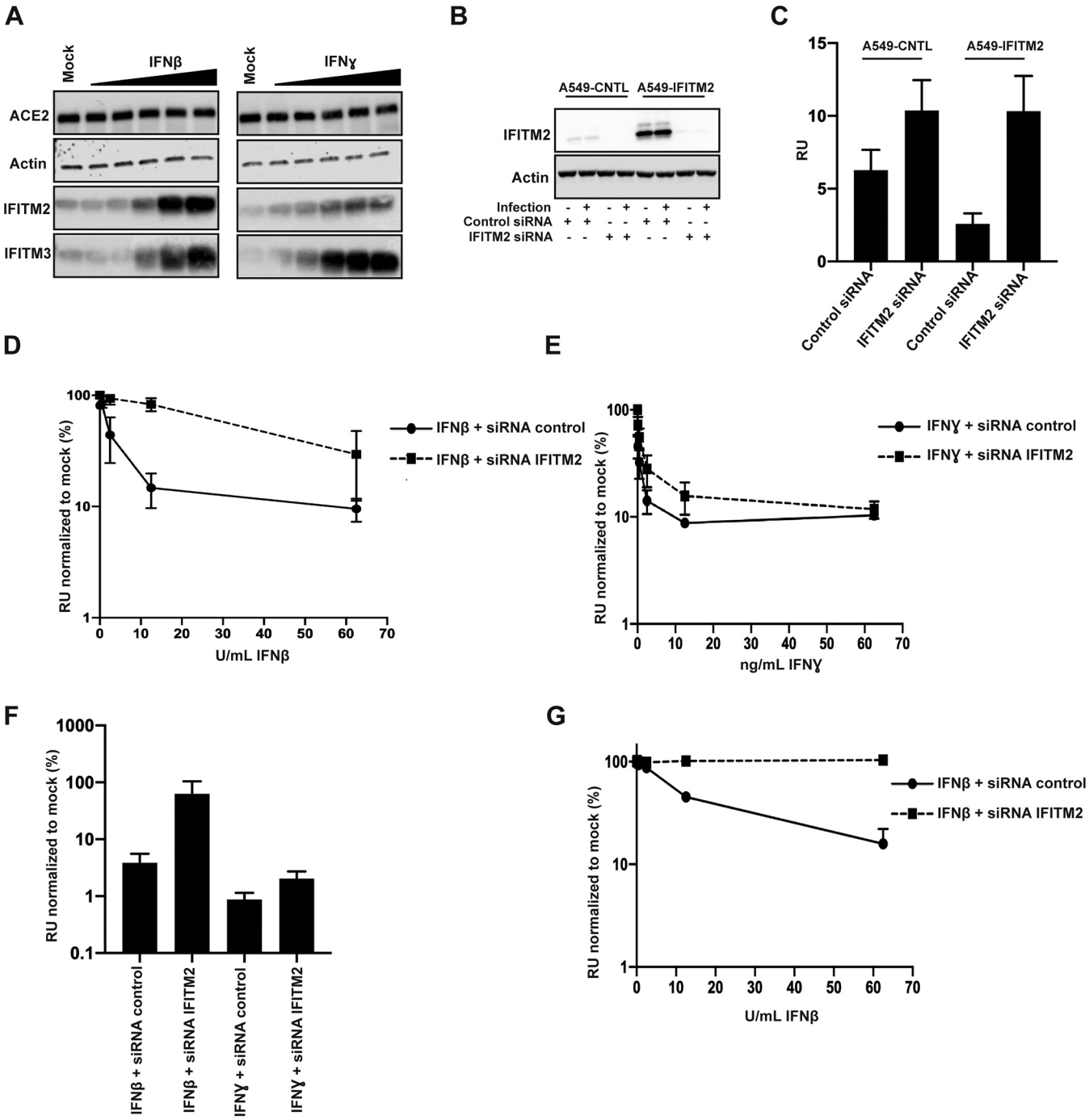

FIG 5 siRNA of IFITM2 rescues IFN-β-mediated restriction of replication competent SARS-CoV-2. (A) Representative immunoblot of A549-ACE2 treated with different amounts of IFN-β or IFN-γ for 18 h. (B and C) A549-ACE2 cells were transfected with siRNAs against nontargeting control or IFITM2; supernatants were used to infect Vero E6 cells for 24 h, and cells were stained for nucleocapsid protein. (D and E) A549-ACE2 cells were pretreated with IFN-β and IFN-γ for 18 h and infected with replication-competent SARS-CoV-2 at an MOI of 0.005. Infected supernatant was used to infect Vero E6 cells for 24 h, and cells were stained for N protein. (F) IC_{50}s for panels D and E were calculated in Prism. (G) A549-ACE2-TMPRSS2 were transfected with siRNAs against nontargeting control or IFITM2 when seeding and prior to IFN treatment. Cells were treated with IFN-β and infected with replication-competent SARS-CoV-2 at an MOI of 0.005 18 h later. Infected supernatant was used to infect Vero E6 cells for 24 h, and cells were stained for N protein. RU, relative units. All data are means and SEM (n = 3).

spike-mediated entry is insensitive to inhibition of endosomal pH, the cleavage mutant is strictly dependent on endosome acidification and cathepsins.

Interestingly, for efficient entry, SARS-CoV-2 requires high TMPRSS2 expression to activate the fusion mechanism by cleaving S2′. However, in cells where TMPRSS2 is limiting,

SARS-CoV-1 and SARS-CoV-2ΔPRRA entry is far more efficient. Thus, in its uncleaved form, SARS-CoV-2 spike can mediate entry in endosomes, but in its mature form, entry cannot be rescued in low-pH compartments of TMPRSS2-low cells. This implies that the cleaved spike is unstable at endosomal pH, and, interestingly, recent studies from the Kwong group indicate that conformational dynamics of the RBD are also pH sensitive (30). Despite this potential greater fragility of the SARS-CoV-2 trimer, the furin cleavage site appears to be essential for replication in primary airway epithelium and for transmission in ferret models (5). We suggest that one of the reasons pH-independent fusion at or near the cell surface is maintained is to mitigate the antiviral activity of IFITM proteins, particularly IFITM2. We note that insertion of the PRRA site into SARS-CoV-1 does not result in cleavage of spike to the same extent as in SARS-CoV-2 or fully rescue sensitivity to IFITM2. We expect that this is due to other differences in the structure of these spikes besides the S1/S2 boundary, such as in the RBD.

The localization of IFITMs largely defines which viruses they restrict. While they can be incorporated into nascent virion membranes and exert an antiviral effect there, their best-studied mechanism of action is to prevent fusion of an incoming virus at the target cell membrane (14). IFITM1 is predominantly found at the plasma membrane, whereas IFITM2 and IFITM3 occupy endosomal compartments by virtue of a conserved endocytic signal. Palmitoylation of the intracellular loop of the IFITM stabilizes their conformation in the membrane and promotes their homo- and heterotypic interactions (31). The current model for their action is that IFITM-IFITM interactions exert a level of positive curvature to the target membrane that arrests enveloped viral entry at the hemi-fusion stage (32). IFITM3 is particularly potent against influenza viruses, and its redistribution away from early endosomes by mutating the endocytic site in the cytoplasmic tail abolishes its antiviral activity (24, 33). Less is known about IFITM2, although it has been shown to inhibit a number of other enveloped viruses that enter in later endosomes (13, 23). Of note, human IFITM2 and -3 differ from each other by only 10 amino acids, and yet their restriction patterns are not interchangeable. While IFITM2 and -3 are localized in endosomal compartments, they traffic via the cell surface, and their recruitment into clathrin-coated pits would imply that they may have some activity at viral entry sites at the plasma membrane as well. However, our observations that IFITM2, but not IFITM3, in the A549 system inhibits SARS-CoV-1 and -CoV-2 suggests that neither virus fuses significantly in a cellular compartment occupied by IFITM3 in this cell type. It is not yet clear which cell type most accurately models the interactions of SARS-CoV-2 and IFITMs in the lung; however, it is likely that the choice of cell and whether overexpression of IFITMs is transient or stable affect the pattern of IFITM restriction of SARS-CoV-2. Furthermore, cell type specificity in IFITM localization (due to endocytic rate, etc.) and heterotypic interactions between IFITMs suggest that when all are coexpressed, they may form a more complex barrier to enveloped virus fusion than an individual IFITM alone.

Studies on SARS-CoV-1 and recent papers and preprints on SARS-CoV-2 have shown a variety of phenotypes with different IFITMs on both viral entry and cell-to-cell fusion mediated by the spike protein (5, 19, 34). IFITM1 appears to block syncytium formation between infected and uninfected cells, and this is overcome by TMPRSS2 expression, which is consistent with our observations that in stably expressing cells, small effects of IFITM1 on SARS-CoV-2 entry in A549-ACE2 cells can be abolished similarly (35). Other data have implicated IFITM3 and demonstrated that it can be enhancing if its expression is restricted to the cell surface (19). Most of these experiments were performed in transiently transfected 293T cells with PLVs, and while the known determinants of IFITM3 function are required, whether transient overexpression faithfully represents the localization and potency of IFITM2 and IFITM3 natural expression is unclear. Furthermore, in mouse embryo fibroblasts, murine IFITM3 was shown to impart an IFN-regulated block to SARS-CoV-2 infection. However, it should be borne in mind that human IFITM2 and IFITM3 are more closely related to each other than either of them is to mouse IFITM3. Given the amount of positive selection that has occurred

in the mammalian IFITM locus, species-specific differences in the spectrum of viruses restricted by mammalian IFITM orthologues should be expected (36).

Here, we find that stable ectopic expression of IFITM2 and to some extent IFITM1 restricts both the entry of PLVs and the replication of the SARS-CoV-2 virus itself in A549-ACE2 cells. The enhanced sensitivity of the PRRA mutant of SARS-CoV-2 and SARS-CoV-1 to IFITM2 is entirely consistent with their dependence on low-pH compartments for cathepsin cleavage. By restricting IFITM2 to the plasma membrane and the outside of clathrin-coated pits by abolishing AP2 interaction, we see enhancement effects similar to those seen by the Yount group with IFITM3 (34). Why this happens is not known, but given the effects that IFITMs have on membrane fluidity, this may be an indirect effect on the surface levels and distribution of entry cofactors at the plasma membrane. It also suggests why there may be an association of the rs12252-C polymorphism that expresses an N-terminally truncated IFITM3 with COVID-19 severity (37). Restriction by IFITM2 but not IFITM3 is surprising. This would suggest not only that IFITM2 localization is limited to later endosomes than IFITM3 but also that it may reside in distinct localizations at or near the plasma membrane dependent on its AP2-binding site.

In addition to examining the sensitivity of SARS-CoV-2 to individual IFITM proteins, we also showed that IFITM2 knockdown is sufficient to alleviate much of the antiviral effect of pretreating A549 cells with type I, but not type II, IFN. Studies from many groups have shown that while SARS-CoV-2 is a poor inducer of IFN responses in infected cells early in the replication cycle, it is highly sensitive to pretreatment of target cells by type I, II, and III IFNs (17, 18, 38). This suggests the potential for multiple ISGs to restrict SARS-CoV-2 replication and has raised the possibility of IFNs as possible treatments for COVID-19 (39). The role of IFNs in SARS-CoV-2 pathogenesis is complex. Genetic lesions in pattern recognition and IFN signaling as well as serum autoantibodies that neutralize type I IFNs are associated with risk of severe coronavirus disease 2019 (COVID-19) (40). However, dysregulated or delayed IFN responses driving systemic inflammation may underlie some of the pathology in COVID-19 (41). Understanding which aspects of the IFN response are antiviral against SARS-CoV-2 is thus of very high importance.

In A549-ACE2 cells, IFITM2 is more potently induced by IFN-β than IFN-γ, and its knockdown substantially reduces the sensitivity of the virus to IFN-β-induced restriction. The sequence similarity between IFITM2 and IFITM3 means that it is difficult to knock down one without affecting the other. The lack of IFITM3 restriction when expressed alone and its potent expression after both IFN-β and IFN-γ treatment would argue against IFITM3 playing the major role. However, given that IFITMs can interact with each other, we cannot rule out the possibility that IFITM1 or IFITM3 plays a role in potentiating IFITM2's antiviral activity after IFN induction. The former is a distinct possibility, as IFITM2 knockdown fully rescues SARS-CoV-2 from IFN-β treatment in cells overexpressing TMPRSS2. Since we found that the minor restriction conferred by IFITM1 alone is abolished by TMPRSS2 expression, a plausible explanation is that more robust S2′ activation of SARS-CoV-2 spike at the cell surface overcomes IFITM1inhibition by saturating its activity (42). While it is surprising that IFN-β has no effect in these cells when IFITM2 is knocked down, we would caution against interpreting that IFITM2 is the only ISG targeting SARS-CoV-2 replication. The rapidity and burst size of SARS-CoV-2 replication in culture may render other relevant antiviral proteins difficult to measure. Furthermore, the virus encodes a number of antagonists of antiviral pathways (43). As shown clearly by the IFN-γ phenotype, expression of other ISGs or their differential regulation may make a given antiviral more or less potent. Of note, the IFN-γ-mediated inhibition of SARS-CoV-2 has been demonstrated to be in part mediated through the zinc-finger antiviral protein (ZAP) (38).

Despite the sensitivity of SARS-CoV-2 to IFITM2, deletion of the PRRA cleavage site in spike substantially potentiates its antiviral activity. In most cells in culture expressing low levels of TMPRSS2, furin cleavage is detrimental to entry, and in A549 cells, this can be rescued to mutant levels of entry by ectopic expression of TMPRSS2. In primary

lung epithelial cells, however, the wild-type spike is clearly superior and outcompetes the mutant as well as being more transmissible in ferret models (5). Epithelial barrier tissues constitutively express a level of ISGs through the tonic activity of type I IFNs (44). Therefore, it is tempting to speculate that the selection pressure for maintaining this attribute in SARS-CoV-2 spike is in part to promote cell surface fusion in target cells that already express IFITM2. Interestingly, Peacock et al. have shown that an equivalent PRRA mutant virus can be rescued in lung epithelial cells by the antifungal drug amphotericin B, known to disrupt IFITM function (5). Addition of a partially active PRRA cleavage site is not sufficient to reduce the IFITM2 restriction of SARS-CoV-1 S to that of SARS-CoV-2, and thus, other determinants in spike are likely to modulate sensitivity.

In summary, we show that IFITM2 is a key antiviral protein targeting SARS-CoV-2 entry and its activity is modulated by the furin cleavage site in spike. These data therefore suggest that therapeutic strategies which upregulate IFITM2 in epithelial tissues or inhibit furin-mediated cleavage of spike may render the virus more sensitive to innate-immune mediated control.

MATERIALS AND METHODS

Cell lines and plasmids. 293T-17 (ATCC), A549-ACE2, A549-ACE2-TMPRSS2, Calu3 (ATCC), Vero E6, and A549-ACE2 cells expressing the individual IFITM proteins were cultured in Dulbecco's modified Eagle medium (DMEM) (Gibco) with 10% fetal bovine serum (FBS) (Invitrogen) and 200 μg/ml gentamicin (Sigma) and incubated at 37°C and 5% CO_2. Codon-optimized SARS-CoV-1 spike was synthesized by GeneArt, and codon-optimized SARS-CoV-2 spike and ACE2 were kindly provided by Nigel Temperton. Plasmid containing the TMPRSS2 gene was kindly provided by Caroline Goujon. The following mutants of spike or IFITMs were generated with a Q5 site-directed mutagenesis kit (E0554) following the manufacturer's instructions: SARS-CoV-2 spike ΔPRRA (AGAAGCGTGGCCAGCCAG, GCTATTGGTCTGGGTCTGGTAG), SARS-CoV-1 spike PRRA (AGAGCCCGGAGCACCAGCCAGAAA, TCTAGGCAGCAGAGACACGGTGTG), IFITM2 Y19A (GCCTCCCAACgctGAGATGCTCAAGGAGGAG, TGGCCGCTGTTGACAGGA), and IFITM2 Y19F (GCCTCCCAACtttGAGATGCTCAAGGAG, TGGCCGCTGTTGACAGGA).

A549 stable cell lines expressing ACE2 (pMIGR1-puro), TMPRSS2 (IRES-neoWPRE), and IFITMs (pLHCX) were generated through transducing cells with lentiviral or retroviral vectors packaged with HIV Gag-Pol (8.91) or murine leukemia virus (MLV) Gag-Pol and vesicular stomatitis virus G protein (VSV-G). Cells were incubated with lentiviral or retroviral vectors for 4 h. Corresponding antibiotic selection was added 24 h after transduction.

Production of PLVs and infection. 293T-17 cells were transfected with firefly luciferase-expressing vector (CSXW), HIV Gag-Pol (8.91), and spike at a ratio of 1.5:1:0.9 μg using 35 μl of PEI-MAX as previously described (45). Medium was changed 18 h later, and vectors were harvested through a 0.45-μm filter 48 h after transfection. Viral supernatant was then used to transduce each cell line of interest for 48 h, and readout was measured with a Promega Steady-Glo luciferase assay system (E2550).

Passage and titration of SARS-CoV-2. PHE England strain 02/2020 was propagated in Vero E6 cells, and titers were determined by plaque assay (46). Vero E6 cells were infected with serial dilutions of SARS-CoV-2 for 1 h. Subsequently, 2× overlay (DMEM, 2% FBS, and 0.1% agarose) medium was added, and infected cells were fixed and stained with crystal violet at room temperature 72 h later. Plaques were counted, and MOI was calculated for subsequent experiments.

Infection with replication-competent SARS-CoV-2. A549-ACE2 cells (1.5×10^5) were infected for 1 h at 37°C with replication-competent SARS-CoV-2 at an MOI of 0.005. Medium was replaced, and cells were incubated for 48 h at 37°C. Forty-eight hours later, cells were harvest for RNA extraction or protein analysis, and the supernatant was used to infect Vero E6 cells to measure virus infectivity.

Interferon assays. Cells were treated with different doses of IFN-α (Invitrogen; 111001) IFN-β (PBL Assay Science; 11415-1), IFN-γ (Peprotech; 300-02), or IFN-λ (Peprotech; 300-02L) for 18 h prior to infection. Medium was changed for virus or PLVs the following day, and the infection was measured by Steady-Glo assay, qPCR, or N staining 48 h later.

siRNA knockdown of IFITM2. A549-ACE2 cells (1×10^5) were reverse transfected using 20 pmol of nontargeting siRNA (Dharmacon catalog no. D-001206-13-20) or IFITM2 siRNA (Dharmacon catalog no. M-020103-02-0010) and 1 μl of RNAi Max (Invitrogen). Cells were incubated for 24 h prior to a second round of reverse transfection. Eight hours later, cells were treated with different doses of IFN-β or IFN-γ as described above.

Following 16 h of IFN treatment, cells were infected with replication-competent SARS-CoV-2 at an MOI of 0.005, as described above. Forty-eight hours after infection, cells were harvested for protein analysis, and the supernatant was used to measure virus infectivity by N staining.

RT-qPCR. RNA from infected cells was extracted using Qiagen RNeasy (Qiagen RNeasy minikit; 74106) following the manufacturer's instructions. One microliter of each extracted RNA was used to performed one-step RT-qPCR using TaqMan fast virus one-step master mix (Invitrogen). The relative quantities of nucleocapsid (N) gene were measured using a SARS-CoV-2 (2019-nCoV) CDC qPCR probe assay (IDT DNA Technologies).

SARS-CoV-2 N staining. Vero E6 cells (2×10^4) were infected for 1 h with 50 μl of undiluted or 1/10-diluted virus supernatant. Following infection, 50 μl of 2× overlay (DMEM, 2% FBS, and 0.1% agarose) medium was added to infected cells. Twenty-four hours later, cells were fixed using 4% paraformaldehyde for 30 min at room temperature. Fixed cells were permeabilized with 0.1% Triton for 15 min, blocked using 3% milk, and incubated for 45 min with anti-human anti-SARS-CoV-2 N (CR3009). Following incubation, cells were washed with 1× phosphate-buffered saline (PBS) and incubated with secondary antibody, goat anti-human IgG (Fc) peroxidase conjugate (Sigma A0170), for 45 min. Finally, the presence of N protein was determined using 1-Step Ultra TMB-ELISA substrate solution (Thermo Fisher).

Drug assays. Cells were pretreated with camostat mesylate (Sigma; SML0057), E64D (Sigma; E8640), or concanamycin (Cayman Chemicals; 80890-47-7) for 1 h at 37°C prior to transduction. Cells were then transduced with PLVs for 48 h, and infection was determined by luciferase activity.

Influenza A virus multicycle replication assay. Cells were infected with a NanoLuc luciferase-tagged influenza A virus (A/WSN/33), WSN-PASTN, a kind gift from Andrew Mehle (University of Wisconsin–Madison, Madison, WI, USA) (47). The inoculum was prepared in serum-free DMEM, and cells were inoculated at an MOI of 0.001 for 1 h at 37°C. After inoculation, cells were washed in PBS and grown in Opti-MEM (Gibco). NanoLuc expression was measured at 24 h postinfection using the Nano-Glo luciferase assay system (Promega) according to the manufacturer's instructions.

SDS-PAGE and Western blotting. Cellular samples were lysed in reducing Laemmli buffer at 95°C for 10 min. Supernatant samples were centrifuged at a relative centrifugal force (RCF) of 18,000 through a 20% sucrose cushion for 1 h at 4°C prior to lysis in reducing Laemmli buffer. Samples were separated on 8 to 16% Mini-Protean TGX precast gels (Bio-Rad) and transferred onto nitrocellulose membranes. Membranes were blocked in milk prior to detection with the following antibodies: 1:1,000 rabbit anti-ACE2 (Abcam; Ab108209), 1:1,000 rabbit anti-TMPRSS2 (Abcam; Ab92323), 1:2,000 mouse anti-actin (Abcam; Ab6276), 1:5,000 rabbit anti-GAPDH (Abcam; Ab9485), 1:5,000 mouse anti-HSP90 (Genetex; Gtx109753), 1:50 mouse anti-HIV-1 p24Gag (48), 1:1,000 mouse anti-spike (Genetex; Gtx632604), 1:3,000 mouse anti-IFITM1 (Proteintech; 60074-1-Ig), 1:3,000 rabbit anti-IFITM2 (Proteintech; 12769-1AP), and 1:3,000 rabbit anti-IFITM3 (Proteintech; 11714-1-AP). Proteins were detected using Li-Cor and ImageQuant LAS 4000 cameras.

ACKNOWLEDGMENTS

We are grateful to Nigel Temperton, Caroline Goujon, Andrew Davidson, Andrew Mehle, and Public Health England for reagents. We thank Michael Malim and Jose Jimenez-Guardeno for helpful advice. Finally, we thank all other members of the Neil and Swanson groups for help and good humor throughout a very difficult year.

This work was funded by Wellcome Trust Senior Research Fellowship WT098049AIA to S.J.D.N., MRC Project Grant MR/S000844/1 to S.J.D.N. and C.M.S., and funding from the Huo Family Foundation jointly to S.J.D.N. and K.J.D. MR/S000844/1 is part of the EDCTP2 program supported by the European Union. H.W. is supported by the UK Medical Research Council (MR/N013700/1) and is a King's College London member of the MRC Doctoral Training Partnership in Biomedical Sciences. We also benefit from infrastructure support from the KCL Biomedical Research Centre, King's Health Partners.

All SARS-CoV-2 and PLV experiments were performed by H.W., M.J.L., and A.C.R. C.B. performed influenza A virus experiments. S.P. and R.P.G. provided help in setting up the SARS-CoV-2 N immunostaining. C.K. provided help in preliminary data. K.J.D. and C.M.S. provided reagents, funding support, and advice. H.W., M.J.L., and S.J.D.N. analyzed the data and wrote the manuscript. All authors edited the manuscript and provided comments.

REFERENCES

1. Wu F, Zhao S, Yu B, Chen YM, Wang W, Song ZG, Hu Y, Tao ZW, Tian JH, Pei YY, Yuan ML, Zhang YL, Dai FH, Liu Y, Wang QM, Zheng JJ, Xu L, Holmes EC, Zhang YZ. 2020. A new coronavirus associated with human respiratory disease in China. Nature 579:265–269. https://doi.org/10.1038/s41586-020-2008-3.
2. Hoffmann M, Kleine-Weber H, Schroeder S, Krüger N, Herrler T, Erichsen S, Schiergens TS, Herrler G, Wu NH, Nitsche A, Müller MA, Drosten C, Pöhlmann S. 2020. SARS-CoV-2 cell entry depends on ACE2 and TMPRSS2 and is blocked by a clinically proven protease inhibitor. Cell 181:271–280.E8. https://doi.org/10.1016/j.cell.2020.02.052.
3. Andersen KG, Rambaut A, Lipkin WI, Holmes EC, Garry RF. 2020. The proximal origin of SARS-CoV-2. Nat Med 26:450–452. https://doi.org/10.1038/s41591-020-0820-9.
4. Hoffmann M, Kleine-Weber H, Pöhlmann S. 2020. A multibasic cleavage site in the spike protein of SARS-CoV-2 is essential for infection of human lung cells. Mol Cell 78:779–784.E5. https://doi.org/10.1016/j.molcel.2020.04.022.
5. Peacock TP, Goldhill DH, Zhou J, Baillon L, Frise R, Swann OC, Kugathasan R, Penn R, Brown JC, Sanchez-David RY, Braga L, Williamson MK, Hassard JA, Staller E, Hanley B, Osborn M, Giacca M, Davidson AD, Matthews DA, Barclay WS. 2020. The furin cleavage site of SARS-CoV-2 spike protein is a key determinant for transmission due to enhanced replication in airway cells. bioRxiv. https://doi.org/10.1101/2020.09.30.318311.
6. Davidson AD, Williamson MK, Lewis S, Shoemark D, Carroll MW, Heesom KJ, Zambon M, Ellis J, Lewis PA, Hiscox JA, Matthews DA. 2020. Characterisation of the transcriptome and proteome of SARS-CoV-2 reveals a cell passage induced in-frame deletion of the furin-like cleavage site from the spike glycoprotein. Genome Med 12:1–15. https://doi.org/10.1186/s13073-020-00763-0.

7. Liu Z, Zheng H, Lin H, Li M, Yuan R, Peng J, Xiong Q, Sun J, Li B, Wu J, Yi L, Peng X, Zhang H, Zhang W, Hulswit RJG, Loman N, Rambaut A, Ke C, Bowden TA, Pybus OG, Lu J. 2020. Identification of common deletions in the spike protein of SARS-CoV-2. J Virol 94:e00790-20. https://doi.org/10.1128/JVI.00790-20.
8. Sasaki M, Uemura K, Sato A, Toba S, Maenaka K, Hall WW, Orba Y, Sawa H. 2020. SARS-CoV-2 variants with mutations at the S1/S2 cleavage site are generated in vitro 1 during propagation in TMPRSS2-deficient cells 2 3. bioRxiv. https://doi.org/10.1101/2020.08.28.271163.
9. Wrobel AG, Benton DJ, Xu P, Roustan C, Martin SR, Rosenthal PB, Skehel JJ, Gamblin SJ. 2020. SARS-CoV-2 and bat RaTG13 spike glycoprotein structures inform on virus evolution and furin-cleavage effects. Nat Struct Mol Biol 27:763–767. https://doi.org/10.1038/s41594-020-0468-7.
10. Schoggins JW. 2019. Interferon-stimulated genes: what do they all do? Annu Rev Virol 6:567–584. https://doi.org/10.1146/annurev-virology-092818-015756.
11. Foster TL, Pickering S, Neil SJD. 2017. Inhibiting the ins and outs of HIV replication: cell-intrinsic antiretroviral restrictions at the plasma membrane. Front Immunol 8:1853. https://doi.org/10.3389/fimmu.2017.01853.
12. Zhao X, Li J, Winkler CA, An P, Guo JT. 2019. IFITM genes, variants, and their roles in the control and pathogenesis of viral infections. Front Microbiol 10:1–12. https://doi.org/10.3389/fmicb.2018.03228.
13. Foster TL, Wilson H, Iyer SS, Coss K, Doores K, Smith S, Kellam P, Finzi A, Borrow P, Hahn BH, Neil SJD. 2016. Resistance of transmitted founder HIV-1 to IFITM-mediated restriction. Cell Host Microbe 20:429–442. https://doi.org/10.1016/j.chom.2016.08.006.
14. Shi G, Schwartz O, Compton AA. 2017. More than meets the I: the diverse antiviral and cellular functions of interferon-induced transmembrane proteins. Retrovirology 14:1–11. https://doi.org/10.1186/s12977-017-0377-y.
15. Brass AL, Huang I, Benita Y, John SP, Manoj N, Feeley EM, Ryan B, Weyer JL, Van Der Weyden L, Fikrig E, Adams DJ, Xavier RJ, Farzan M, Stephen J. 2009. IFITM proteins mediate the innate immune response to influenza A H1N1 virus, West Nile virus and dengue virus. Genome 139:1243–1254. https://doi.org/10.1016/j.cell.2009.12.017.
16. Felgenhauer U, Schoen A, Gad HH, Hartmann R, Schaubmar AR, Failing K, Drosten C, Weber F. 2020. Inhibition of SARS–CoV-2 by type I and type III interferons. J Biol Chem 295:13958–13964. https://doi.org/10.1074/jbc.AC120.013788.
17. Stanifer ML, Kee C, Cortese M, Zumaran CM, Triana S, Mukenhirn M, Kraeusslich HG, Alexandrov T, Bartenschlager R, Boulant S. 2020. Critical role of type III interferon in controlling SARS-CoV-2 infection in human intestinal epithelial cells. Cell Rep 32:107863. https://doi.org/10.1016/j.celrep.2020.107863.
18. Lokugamage KG, Hage A, De Vries M, Valero-Jimenez AM, Schindewolf C, Dittmann M, Rajsbaum R, Menachery VD. 2020. Type I interferon susceptibility distinguishes SARS-CoV-2 from SARS-CoV. J Virol 94:e01410-20. https://doi.org/10.1128/JVI.01410-20.
19. Bozzo CP, Nchioua R, Volcic M, Wettstein L, Weil T, Krüger J, Heller S, Conzelmann C, Müller J, Gross R, Zech F, Schütz D, Koepke L, Stuerzel CM, Schüler C, Stenzel S, Braun E, Weiß J, Sauter D, Münch J, Stenger S, Sato K, Kleger A, Goffinet C, Sparrer KMJ, Kirchhoff F. 2020. IFITM proteins promote SARS-CoV-2 infection of human lung cells. bioRxiv. https://doi.org/10.1101/2020.08.18.255935.
20. Bailey CC, Zhong G, Huang IC, Farzan M. 2014. IFITM-family proteins: the cell's first line of antiviral defense. Annu Rev Virol 1:261–283. https://doi.org/10.1146/annurev-virology-031413-085537.
21. Hachim MY, Al Heialy S, Hachim IY, Halwani R, Senok AC, Maghazachi AA, Hamid Q. 2020. Interferon-induced transmembrane protein (IFITM3) is upregulated explicitly in SARS-CoV-2 infected lung epithelial cells. Front Immunol 11:1372–1379. https://doi.org/10.3389/fimmu.2020.01372.
22. Doyle T, Goujon C, Malim MH. 2015. HIV-1 and interferons: who's interfering with whom? Nat Rev Microbiol 13:403–413. https://doi.org/10.1038/nrmicro3449.
23. Huang IC, Bailey CC, Weyer JL, Radoshitzky SR, Becker MM, Chiang JJ, Brass AL, Ahmed AA, Chi X, Dong L, Longobardi LE, Boltz D, Kuhn JH, Elledge SJ, Bavari S, Denison MR, Choe H, Farzan M. 2011. Distinct patterns of IFITM-mediated restriction of filoviruses, SARS coronavirus, and influenza A virus. PLoS Pathog 7:e1001258. https://doi.org/10.1371/journal.ppat.1001258.
24. Feeley EM, Sims JS, John SP, Chin CR, Pertel T, Chen LM, Gaiha GD, Ryan BJ, Donis RO, Elledge SJ, Brass AL. 2011. IFITM3 inhibits influenza a virus infection by preventing cytosolic entry. PLoS Pathog 7:e1002337. https://doi.org/10.1371/journal.ppat.1002337.
25. Gerlach T, Hensen L, Matrosovich T, Bergmann J, Winkler M, Peteranderl C, Klenk H-D, Weber F, Herold S, Pöhlmann S, Matrosovich M. 2017. pH optimum of hemagglutinin-mediated membrane fusion determines sensitivity of influenza A viruses to the interferon-induced antiviral state and IFITMs. J Virol 91:e00246-17. https://doi.org/10.1128/JVI.00246-17.
26. Chesarino NM, McMichael TM, Hach JC, Yount JS. 2014. Phosphorylation of the antiviral protein interferon-inducible transmembrane protein 3 (IFITM3) dually regulates its endocytosis and ubiquitination. J Biol Chem 289:11986–11992. https://doi.org/10.1074/jbc.M114.557694.
27. Shi G, Kenney AD, Kudryashova E, Zani A, Zhang L, Lai KK, Hall-Stoodley L, Robinson RT, Kudryashov DS, Compton AA, Yount JS. 2020. Opposing activities of IFITM proteins in SARS-CoV-2 infection. EMBO J 40:e106501. https://doi.org/10.15252/embj.2020106501.
28. Cantuti-Castelvetri L, Ojha R, Pedro LD, Djannatian M, Franz J, Kuivanen S, van der Meer F, Kallio K, Kaya T, Anastasina M, Smura T, Levanov L, Szirovicza L, Tobi A, Kallio-Kokko H, Österlund P, Joensuu M, Meunier FA, Butcher SJ, Winkler MS, Mollenhauer B, Helenius A, Gokce O, Teesalu T, Hepojoki J, Vapalahti O, Stadelmann C, Balistreri G, Simons M. 2020. Neuropilin-1 facilitates SARS-CoV-2 cell entry and infectivity. Science 370:856–860. https://doi.org/10.1126/science.abd2985.
29. Daly JL, Simonetti B, Klein K, Chen KE, Williamson MK, Antón-Plágaro C, Shoemark DK, Simón-Gracia L, Bauer M, Hollandi R, Greber UF, Horvath P, Sessions RB, Helenius A, Hiscox JA, Teesalu T, Matthews DA, Davidson AD, Collins BM, Cullen PJ, Yamauchi Y. 2020. Neuropilin-1 is a host factor for SARS-CoV-2 infection. Science 370:861–865. https://doi.org/10.1126/science.abd3072.
30. Zhou T, Tsybovsky Y, Gorman J, Rapp M, Cerutti G, Chuang G-Y, Katsamba PS, Sampson JM, Schön A, Bimela J, Boyington JC, Nazzari A, Olia AS, Shi W, Sastry M, Stephens T, Stuckey J, Teng I-T, Wang P, Wang S, Zhang B, Friesner RA, Ho DD, Mascola JR, Shapiro L, Kwong PD. 2020. Cryo-EM structures of SARS-CoV-2 spike without and with ACE2 reveal a pH-dependent switch to mediate endosomal positioning of receptor-binding domains. Cell Host Microbe 28:867–879. https://doi.org/10.1016/j.chom.2020.11.004.
31. Yount JS, Karssemeijer RA, Hang HC. 2012. S-palmitoylation and ubiquitination differentially regulate interferon-induced transmembrane protein 3 (IFITM3)-mediated resistance to influenza virus. J Biol Chem 287:19631–19641. https://doi.org/10.1074/jbc.M112.362095.
32. Rahman K, Coomer CA, Majdoul S, Ding S, Padilla-Parra S, Compton AA. 2020. Homology-guided identification of a conserved motif linking the antiviral functions of IFITM3 to its oligomeric state. Elife 9:e58537. https://doi.org/10.7554/eLife.58537.
33. Jia R, Xu F, Qian J, Yao Y, Miao C, Zheng YM, Liu SL, Guo F, Geng Y, Qiao W, Liang C. 2014. Identification of an endocytic signal essential for the antiviral action of IFITM3. Cell Microbiol 16:1080–1093. https://doi.org/10.1111/cmi.12262.
34. Shi G, Kenney AD, Kudryashova E, Zani A, Zhang L, Lai KK, Hall-Stoodley L, Robinson RT, Kudryashov DS, Compton AA, Yount JS. 2021. Opposing activities of IFITM proteins in SARS-CoV-2 infection. EMBO J 40:e106501. https://doi.org/10.15252/embj.2020106501.
35. Buchrieser J, Dufloo J, Hubert M, Monel B, Planas D, Michael Rajah M, Planchais C, Porrot F, Guivel-Benhassine F, Van der Werf S, Casartelli N, Mouquet H, Bruel T, Schwartz O. 2020. Syncytia formation by SARS-CoV-2 infected cells. EMBO J 39:e106267. https://doi.org/10.15252/embj.2020106267.
36. Zhang Z, Liu J, Li M, Yang H, Zhang C. 2012. Evolutionary dynamics of the interferon-induced rransmembrane gene family in vertebrates. PLoS One 7:e49265. https://doi.org/10.1371/journal.pone.0049265.
37. Gómez J, Albaiceta GM, Cuesta-Llavona E, García-Clemente M, López-Larrea C, Amado-Rodríguez L, López-Alonso I, Melón S, Alvarez-Argüelles ME, Gil-Peña H, Vidal-Castiñeira JR, Corte-Iglesias V, Saiz ML, Alvarez V, Coto E. 2021. The interferon-induced transmembrane protein 3 gene (IFITM3) rs12252 C variant is associated with COVID-19. Cytokine 137:155354. https://doi.org/10.1016/j.cyto.2020.155354.
38. Nchioua R, Kmiec D, Müller JA, Conzelmann C, Groß R, Swanson CM, Neil SJD, Stenger S, Sauter D, Münch J, Sparrer KMJ, Kirchhoff F. 2020. Sars-cov-2 is restricted by zinc finger antiviral protein despite preadaptation to the low-cpg environment in humans. mBio 11:e01930-20. https://doi.org/10.1128/mBio.01930-20.
39. Haji Abdolvahab M, Moradi-Kalbolandi S, Zarei M, Bose D, Majidzadeh-A K, Farahmand L. 2021. Potential role of interferons in treating COVID-19 patients. Int Immunopharmacol 90:107171. https://doi.org/10.1016/j.intimp.2020.107171.
40. Bastard P, Rosen LB, Zhang Q, Michailidis E, Hoffmann HH, Zhang Y, Dorgham K, Philippot Q, Rosain J, Béziat V, Manry J, Shaw E, Haljasmägi L, Peterson P, Lorenzo L, Bizien L, Trouillet-Assant S, Dobbs K, de Jesus AA, Belot A, Kallaste A,

Catherinot E, Tandjaoui-Lambiotte Y, Le Pen J, Kerner G, Bigio B, Seeleuthner Y, Yang R, Bolze A, Spaan AN, Delmonte OM, Abers MS, Aiuti A, Casari G, Lampasona V, Piemonti L, Ciceri F, Bilguvar K, Lifton RP, Vasse M, Smadja DM, Migaud M, Hadjadj J, Terrier B, Duffy D, Quintana-Murci L, van de Beek D, Roussel L, Vinh DC, Tangye SG, HGID Lab, et al. 2020. Autoantibodies against type I IFNs in patients with life-threatening COVID-19. Science 370:eabd4585. https://doi.org/10.1126/science.abd4585.

41. Lucas C, Wong P, Klein J, Castro TBR, Silva J, Sundaram M, Ellingson MK, Mao T, Oh JE, Israelow B, Takahashi T, Tokuyama M, Lu P, Venkataraman A, Park A, Mohanty S, Wang H, Wyllie AL, Vogels CBF, Earnest R, Lapidus S, Ott IM, Moore AJ, Muenker MC, Fournier JB, Campbell M, Odio CD, Casanovas-Massana A, Obaid A, Lu-Culligan A, Nelson A, Brito A, Nunez A, Martin A, Watkins A, Geng B, Kalinich C, Harden C, Todeasa C, Jensen C, Kim D, McDonald D, Shepard D, Courchaine E, White EB, Song E, Silva E, Kudo E, DeLuliis G, Rahming H, Yale IMPACT Team, et al. 2020. Longitudinal analyses reveal immunological misfiring in severe COVID-19. Nature 584:463–469. https://doi.org/10.1038/s41586-020-2588-y.
42. Weston S, Czieso S, White IJ, Smith SE, Wash RS, Diaz-Soria C, Kellam P, Marsh M. 2016. Alphavirus restriction by IFITM proteins. Traffic 17:997–1013. https://doi.org/10.1111/tra.12416.
43. Xia H, Cao Z, Xie X, Zhang X, Chen JYC, Wang H, Menachery VD, Rajsbaum R, Shi PY. 2020. Evasion of type I interferon by SARS-CoV-2. Cell Rep 33:108234. https://doi.org/10.1016/j.celrep.2020.108234.
44. Broggi A, Ghosh S, Sposito B, Spreafico R, Balzarini F, Lo Cascio A, Clementi N, de Santis M, Mancini N, Granucci F, Zanoni I. 2020. Type III interferons disrupt the lung epithelial barrier upon viral recognition. Science 369:706–712. https://doi.org/10.1126/science.abc3545.
45. Grehan K, Ferrara F, Temperton N. 2015. An optimised method for the production of MERS-CoV spike expressing viral pseudotypes. MethodsX 2:379–384. https://doi.org/10.1016/j.mex.2015.09.003.
46. Mendoza EJ, Manguiat K, Wood H, Drebot M. 2020. Two detailed plaque assay protocols for the quantification of infectious SARS-CoV-2. Curr Protoc Microbiol 57:ecpmc105. https://doi.org/10.1002/cpmc.105.
47. Tran V, Moser LA, Poole DS, Mehle A. 2013. Highly sensitive real-time in vivo imaging of an influenza reporter virus reveals dynamics of replication and spread. J Virol 87:13321–13329. https://doi.org/10.1128/JVI.02381-13.
48. Chesebro B, Wehrly K, Nishio J, Perryman S. 1992. Macrophage-tropic human immunodeficiency virus isolates from different patients exhibit unusual V3 envelope sequence homogeneity in comparison with T-cell-tropic isolates: definition of critical amino acids involved in cell tropism. J Virol 66:6547–6554. https://doi.org/10.1128/JVI.66.11.6547-6554.1992.

AMERICAN SOCIETY FOR MICROBIOLOGY | Journal of Virology®

PATHOGENESIS AND IMMUNITY

The P681H Mutation in the Spike Glycoprotein of the Alpha Variant of SARS-CoV-2 Escapes IFITM Restriction and Is Necessary for Type I Interferon Resistance

Maria Jose Lista,[a,d] Helena Winstone,[a,d] Harry D. Wilson,[a,d] Adam Dyer,[a,d] Suzanne Pickering,[a,d] Rui Pedro Galao,[a,d] Giuditta De Lorenzo,[b] Vanessa M. Cowton,[b] Wilhelm Furnon,[b] Nicolas Suarez,[b] Richard Orton,[b] Massimo Palmarini,[b,d] Arvind H. Patel,[b,d] Luke Snell,[c] Gaia Nebbia,[c] Chad Swanson,[a] Stuart J. D. Neil[a,d]

[a]Department of Infectious Diseases, King's College London, London, United Kingdom
[b]MRC-University of Glasgow Centre for Virus Research, Glasgow, United Kingdom
[c]Centre for Clinical Infection and Diagnostics Research, Department of Infectious Diseases, Guy's and St Thomas' NHS Foundation Trust, London, United Kingdom
[d]UKRI Genotype-2-Phenotype Consortium, London, United Kingdom

Maria Jose Lista and Helena Winstone contributed equally to this work. The order of their authorship was agreed upon between the two authors.

ABSTRACT The appearance of new dominant variants of concern (VOC) of severe acute respiratory syndrome coronavirus type 2 (SARS-CoV-2) threatens the global response to the coronavirus disease 2019 (COVID-19) pandemic. Of these, the alpha variant (also known as B.1.1.7), which appeared initially in the United Kingdom, became the dominant variant in much of Europe and North America in the first half of 2021. The spike (S) glycoprotein of alpha acquired seven mutations and two deletions compared to the ancestral virus, including the P681H mutation adjacent to the polybasic cleavage site, which has been suggested to enhance S cleavage. Here, we show that the alpha spike protein confers a level of resistance to beta interferon (IFN-β) in human lung epithelial cells. This correlates with resistance to an entry restriction mediated by interferon-induced transmembrane protein 2 (IFITM2) and a pronounced infection enhancement by IFITM3. Furthermore, the P681H mutation is essential for resistance to IFN-β and context-dependent resistance to IFITMs in the alpha S. P681H reduces dependence on endosomal cathepsins, consistent with enhanced cell surface entry. However, reversion of H681 does not reduce cleaved spike incorporation into particles, indicating that it exerts its effect on entry and IFN-β downstream of furin cleavage. Overall, we suggest that, in addition to adaptive immune escape, mutations associated with VOC may well also confer a replication and/or transmission advantage through adaptation to resist innate immune mechanisms.

IMPORTANCE Accumulating evidence suggests that variants of concern (VOC) of SARS-CoV-2 evolve to evade the human immune response, with much interest focused on mutations in the spike protein that escape from antibodies. However, resistance to the innate immune response is essential for efficient viral replication and transmission. Here, we show that the alpha (B.1.1.7) VOC of SARS-CoV-2 is substantially more resistant to type I interferons than the parental Wuhan-like virus. This correlates with resistance to the antiviral protein IFITM2 and enhancement by its paralogue IFITM3. The key determinant of this is a proline-to-histidine change at position 681 in S adjacent to the furin cleavage site, which in the context of the alpha spike modulates cell entry pathways of SARS-CoV-2. Reversion of the mutation is sufficient to restore interferon and IFITM2 sensitivity, highlighting the dynamic nature of the SARS CoV-2 as it adapts to both innate and adaptive immunity in the humans.

KEYWORDS IFITM, SARS-CoV-2, type 1 interferon, VOC, furin cleavage site

Editor Stacey Schultz-Cherry, St. Jude Children's Research Hospital

Address correspondence to Stuart J. D. Neil, stuart.neil@kcl.ac.uk.

The authors declare no conflict of interest.

Received 10 August 2022
Accepted 10 October 2022
Published 9 November 2022

Both severe acute respiratory syndrome coronavirus type 1 (SARS-CoV-1) and SARS-CoV-2 enter target cells through the interaction of their S proteins with the angiotensin-converting enzyme 2 (ACE2) cell surface receptor. Upon attachment and uptake, the S glycoprotein trimer is cleaved by cellular proteases such as cathepsins and TMPRSS (transmembrane proteases serine subfamily) members at two positions—the S1/S2 junction and the S2′ site—to facilitate the activation of the fusion mechanism. Similar to more distantly related beta-CoVs, but so far unique in known sarbecoviruses, the SARS-CoV-2 glycoprotein contains a polybasic furin cleavage site (FCS) with a 681-PRRAR*S-685 sequence at the S1/S2 junction. This allows the S precursor to be additionally processed to the S1 and S2 subunits by furin-like proteases before viral release from the previously infected cell (1). This leads to a proportion of processed S being present on the virion before engagement with the target cell, allowing rapid activation and fusion at or near the cell surface by TMPRSS2. The importance of the FCS is highlighted by the observations that it enhances SARS-CoV-2 replication specifically in airway epithelial cells and that it is essential for efficient transmission in animal models (2).

The alpha variant of SARS-CoV-2 arose in the southeast of England in autumn 2020 and rapidly spread across the world in the first months of 2021. Various studies suggested that alpha had an increased transmissibility between individuals (3–5). Alpha contains nine amino acid residue changes in S, including a deletion of amino acid residues H and V in the N-terminal domain (NTD) at position 69/70 (thought to increase S incorporation into virions), a single amino acid deletion of Y144 (thought to assist NTD antibody neutralization escape), and an N501Y mutation in the receptor-binding domain (RBD), which enhances ACE2 binding affinity (6, 7). Together, these changes have been shown to reduce efficiency of neutralization by some antibodies (8), but compared to the later variants of concern (VOC) delta and omicron, it is not thought to be a major adaptive immune escape variant. Alpha also acquired a P681H change in the FCS, which has been proposed to increase the accessibility of the site by furin, leading to enhanced cleavage as well as more efficient cell-to-cell fusion and syncytium formation (9–12). Since early 2021, several other VOC have emerged with mutations in the FCS, including kappa, delta, and omicron (12, 13). Both kappa and delta contained the P681R mutation; however, only delta superseded alpha and became a globally dominant variant in the summer of 2021. In late 2021, the delta variant was in turn displaced by the omicron variant, which contains the P681H mutation in its FCS.

We and others have previously demonstrated that the ancestral SARS-CoV-2 is variably sensitive to entry inhibition by the interferon-regulated interferon-induced transmembrane protein (IFITM) family and that this can be modulated by the FCS (2, 14, 15). IFITM1, -2, and -3 are transmembrane proteins that exert antiviral activity against diverse enveloped viruses by blocking fusion of the viral and cellular membranes (16, 17). While IFITM1 localizes primarily to the plasma membrane, IFITM2 and IFITM3 are internalized via a conserved YxxΦ endocytic motif to occupy both distinct and overlapping endosomal compartments. However, it was demonstrated previously that the IFITM proteins can oligomerize with each other in heterologous complexes (18, 19). The sensitivity of a given virus to individual IFITM proteins is largely determined by its route of cellular entry. We showed previously that for a prototypic Wuhan-like SARS-CoV-2 isolate from early 2020, IFITM2 reduced viral entry and contributed to type I interferon (IFN-I)-induced inhibition in human cells (14). Sensitivity to IFITM2 could be markedly enhanced by deletion of the FCS, suggesting that furin processing ameliorated SARS-CoV-2 sensitivity to IFITM2 restriction at least to some extent. We therefore postulated that the altered cleavage site of VOC with mutations in the FCS may have consequences for their sensitivity to IFN-I and IFITMs. Here, we demonstrate that of the alpha, beta, gamma, kappa, delta, and omicron variants, only the S of the alpha variant is resistant to IFITM restriction in A549-ACE2-IFITM cells. We also demonstrate that the ΔCT (cytoplasmic tail) mutation commonly used in improving SARS-CoV-2 pseudotyped lentiviral vector (PLV) infectivity masks the IFITM resistance of alpha PLVs by conferring increased cathepsin dependence. Furthermore, we show that the alpha variant is

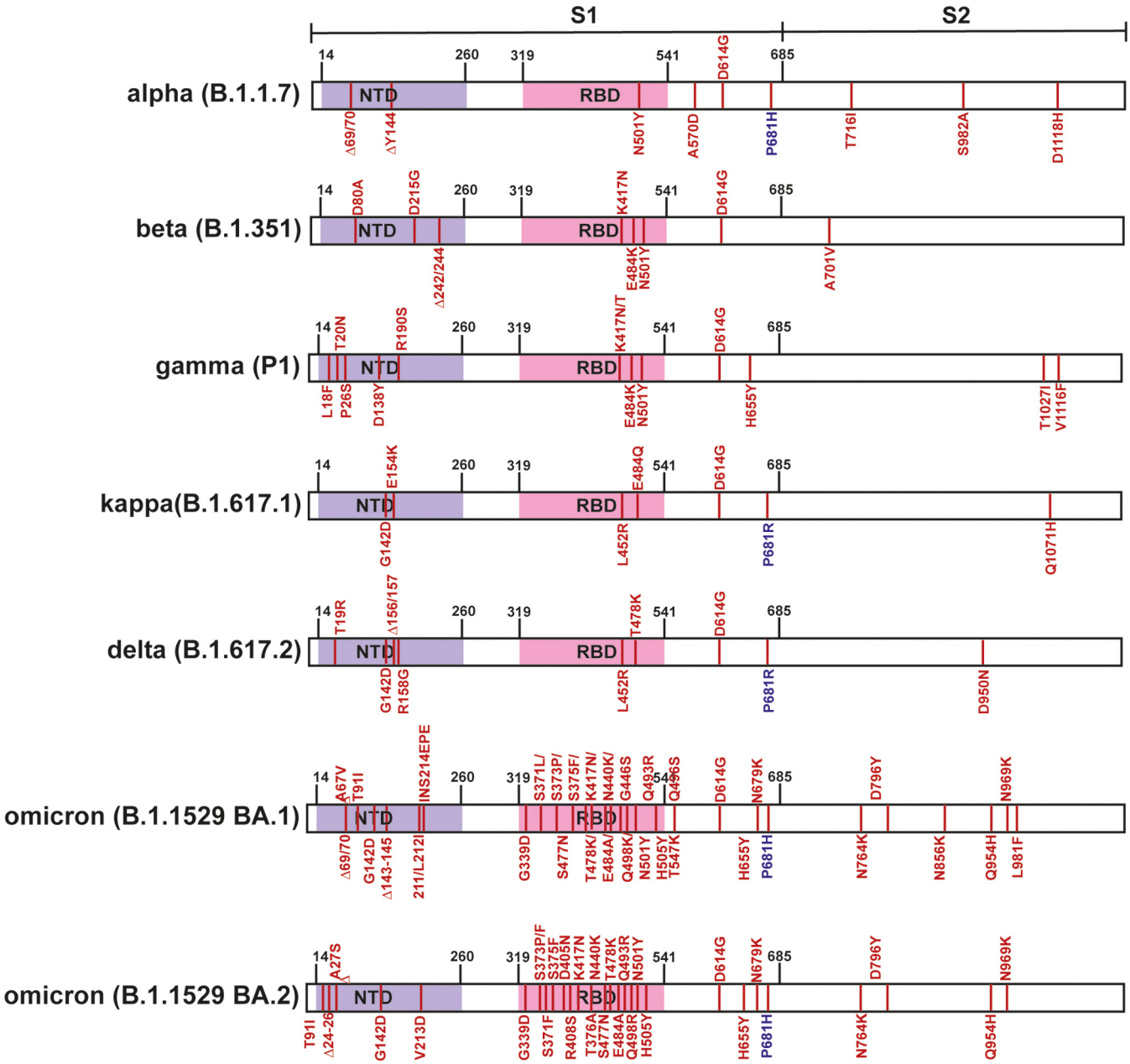

FIG 1 SARS-CoV-2 variants of concern spike sequences. Schematic of spike protein domains of the different variants of concern relative to the original Wuhan spike sequence: alpha, beta, gamma, delta, and omicron. The different mutations between the variants are represented in red.

resistant to IFN-β in both A549-ACE2 and Calu-3 cells, and this resistance can be abolished by reversion of the P681H mutation.

RESULTS

The S proteins of currently circulating variants display different sensitivities to IFITMs in A549-ACE2 cells. Over 2020 and 2021, several major VOC arose—alpha (B.1.1.7) in the United Kingdom, beta (B.1.351) in South Africa, gamma (P1) in Brazil, delta (B.1.617.2) in India, and most recently the omicron family (B.1.1.529) in South Africa (13). All of these variants have multiple changes in the S protein that could potentially affect the entry process (Fig. 1). Of particular interest, the alpha, delta and omicron variants contain mutations in the polybasic cleavage site which have been postulated to enhance S cleavage: P681H in alpha and omicron and P681R in delta (20–22). We therefore compared the sensitivity of PLVs bearing full-length, untruncated SARS-CoV-2

spike proteins of these VOC to entry inhibition the presence of IFITM proteins. As expected, all VOC PLVs produced were infectious on A549-ACE2 cells, although efficiency was variable (see Fig. S1A in the supplemental material). We then used these PLVs to infect A549-ACE2 cells stably expressing the individual IFITMs (Fig. S1B; Fig. 2A to I). The spike protein with the D614G mutation, which became dominant early in the first wave of the pandemic, displayed a sensitivity to IFITM2 similar to that of the previously characterized Wuhan-1 S but was resistant to both IFITM1 and IFITM3 (Fig. 2A and B) (14, 23). We then compared the IFITM sensitivities of alpha, beta, gamma, kappa, delta, and omicron (BA.1 and BA.2) as PLVs (Fig. 2C to I). The alpha S (Fig. 2C) appeared completely insensitive to IFITM1, -2, and -3, while beta, gamma, kappa, delta, and both omicron spikes retained some sensitivity to IFITMs 1 and/or 2. We noted that kappa and delta (Fig. 2F and G), which both contain the P681R mutation, retained some sensitivity to both IFITM1 and -2. Interestingly the alpha variant, and to some extent delta, also appeared to be significantly enhanced by IFITM3. Such enhancement by IFITMs has been previously documented in the human seasonal CoV OC43 and in SARS-CoV-2 under specific assay conditions when IFITM2 is knocked down postinfection in IFN-treated cells (24, 25). To confirm the enhancement we observed with alpha was due to IFITM3, we pretreated A549-ACE2-IFITM3 cells with cyclosporine H, a compound known to drive IFITM3 to ubiquitin-dependent degradation (9, 25, 26). We found that overnight treatment with CSH was able to reduce expression levels of all three IFITMs and led to specific abolishment of IFITM3 enhancement of alpha PLVs while having no effect on D614G PLVs (Fig. S1C to E).

The ΔCT mutation increases PLV infectivity but confers greater cathepsin dependence and IFITM2 sensitivity to D614G and alpha PLVs. Deleting the last 19 amino acids of SARS-CoV-2 spike increases spike incorporation and infectivity of PLVs and is common practice among many groups studying SARS CoV-2 (27, 28). Truncation of the cytoplasmic tail results in the deletion of a suboptimal endoplasmic reticulum retention signal (ERRS) and increased accumulation of the spike at the surface, where it is incorporated into PLVs. However, the site of coronavirus assembly is not at the plasma membrane, and the spike goes through considerable posttranslational modifications in the ER-Golgi apparatus intermediate compartment (ERGIC) (29). To test whether deletion of the last 19 amino acids affected IFITM phenotypes, we generated a D614GΔCT mutant and tested infectivity in A549-ACE2 cells of these PLVs relative to the full-length D614G spike as PLVs (Fig. 3A). The ΔCT mutant exhibited a 28-fold boost in infectivity (Fig. 3A). However, the D614GΔCT PLVs were 2-fold more sensitive to IFITM2 (Fig. 3B). This was consistent with an increase in sensitivity of these PLVs to E64d, an inhibitor of cathepsins B/L at both 2.5 μM and 10 μM (Fig. 3C). Next, to confirm if there were phenotypic differences in the spike of D614GΔCT spikes during PLV production, D614G and D614GΔCT PLVs were immunoblotted for spike and Gag in both the cell lysates and purified supernatant of PLV production (Fig. 3D). Intriguingly, the D614GΔCT mutant showed a 10-fold increase in S1/S2 processing (Fig. 3E). Although increased spike processing was surprising given an increased dependence on cathepsins B and L, it could be that, although it was more processed, the D614GΔCT spike is in a conformation where the second cleavage site is less accessible, resulting in increased cathepsin dependence. Finally, to confirm whether the ΔCT mutation is sufficient to overcome the IFITM2 resistance observed with the alpha spike, alphaΔCT was generated and its IFITM sensitivity was tested (Fig. 3F). Strikingly, the ΔCT mutation rendered the previously resistant alpha spike highly sensitive to IFITM2. Additionally, the 3-fold enhancement we previously found with alpha in this system was abolished by the ΔCT mutation. Overall, these data suggest that the ERRS plays a significant role in the posttranslational modifications of spike, and in turn, this has consequences for the route of viral entry and sensitivity to antiviral proteins. Given the significant effect of this mutation on IFITM sensitivity and route of entry of D614G and alpha viruses, we advise caution in interpreting data of phenotypes involving differential viral entry utilizing ΔCT spikes.

SARS-CoV-2 alpha variant is IFITM resistant. Next, we sought to confirm that the native alpha virus demonstrated a phenotype on our IFITM-expressing cells similar to that of the PLVs. We infected A549-ACE2 cells stably expressing the individual IFITMs with

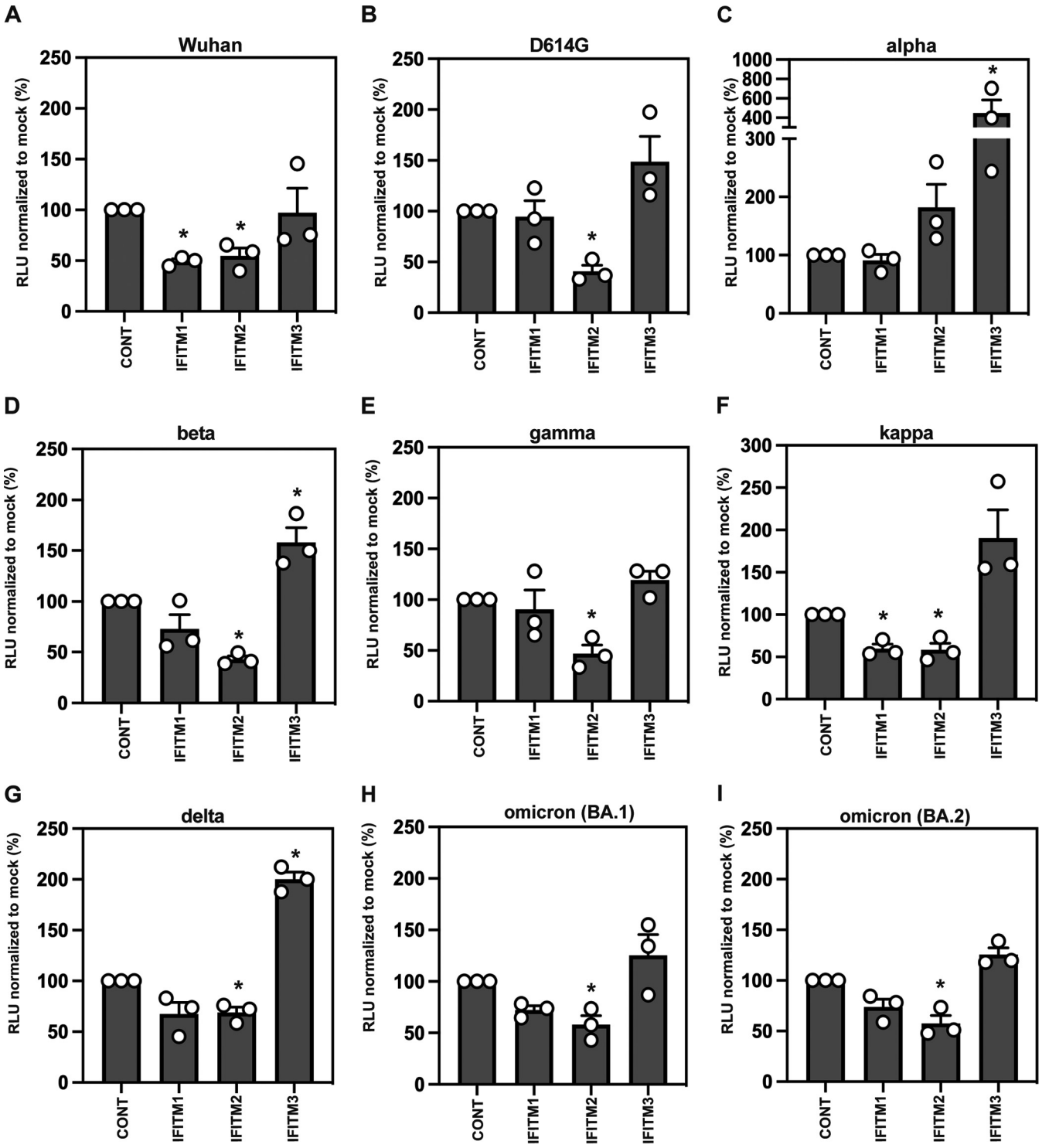

FIG 2 IFITM sensitivity of SARS-CoV-2 variants of concern. IFITM sensitivity of PLVs bearing full-length Wuhan, D614G, alpha, beta, gamma, kappa, delta, and omicron spike in A549-ACE2 cells stably expressing the individual IFITMs. PLV entry was quantified by luciferase activity 48 h after infection and normalized to control (CONT) cells. Data are means and standard errors of the means (SEM; $n = 3$). Statistics were calculated in Prism using analysis of variance (ANOVA). *, $P = 0.05$ relative to control values.

England-02, D614G, or alpha isolates and measured the percentage of N-positive cells by flow cytometry (Fig. 4A and B) and the level of intracellular E RNA by quantitative PCR (qPCR) (Fig. 4C) at 48 h postinfection. We found that England-02 and D614G isolates were IFITM2 sensitive, while alpha was insensitive to inhibitory effects of all three IFITMs. Also,

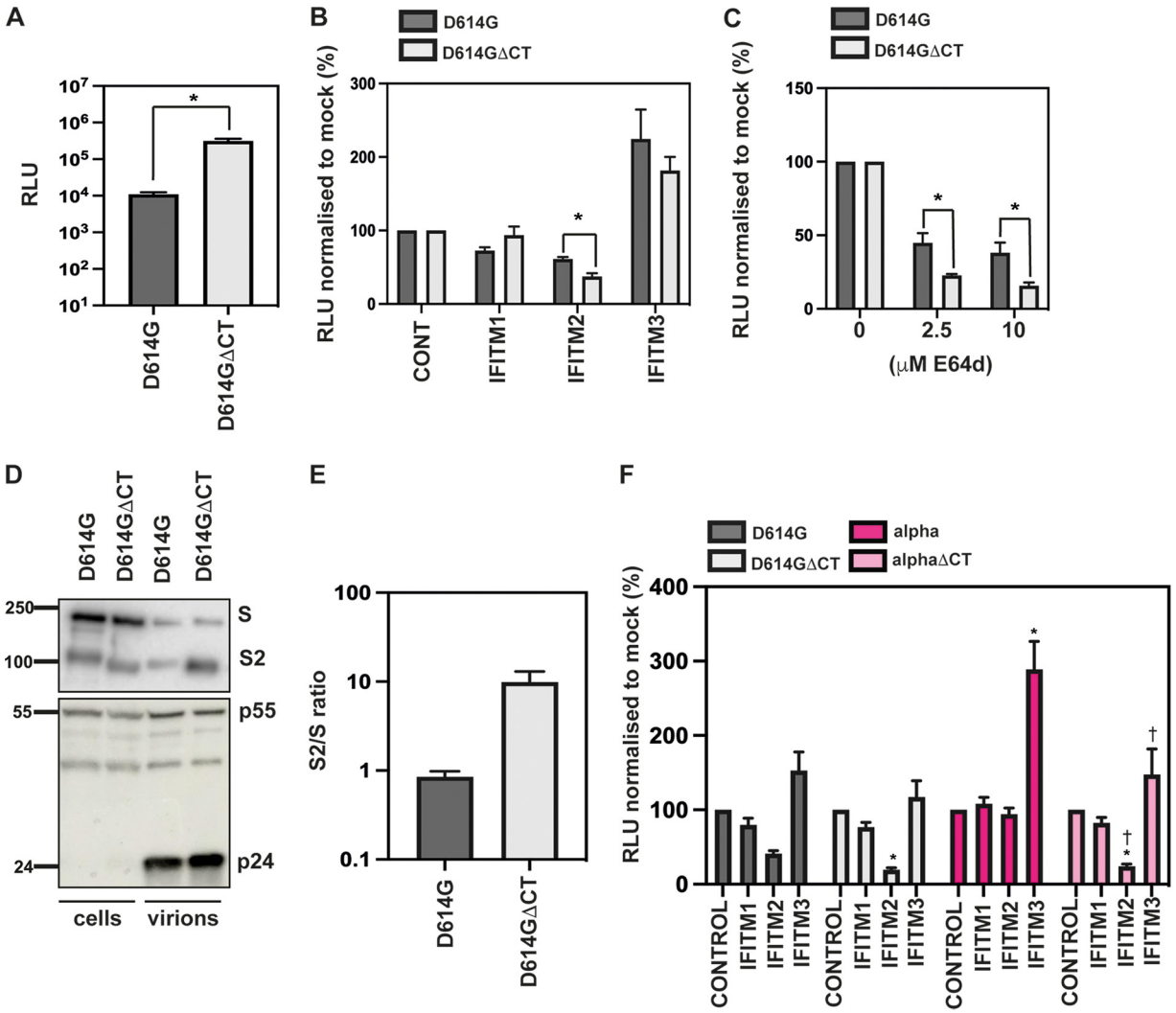

FIG 3 The ΔCT mutation in the D614G and alpha viruses confers IFITM2 sensitivity by increasing cathepsin dependence. (A) D614G or D614GΔCT PLVs were used to infect A549-ACE2 cells, and infectivity was measured by luciferase activity 48 h later. Raw relative light units (RLU) are shown. (B) D614G or D614GΔCT PLVs were used to infect A549-ACE2-IFITM cells, and infectivity was measured by luciferase activity 48 h later. Percent infection normalized to control values without IFITM is shown. (C) A549-ACE2 cells were pretreated with 2.5 μM or 10 μM E64d prior to infection with D614G or D614GΔCT PLVs for 48 h. Infection was measured by luciferase activity, and infection was normalized to mock-treated cells. (D) Representative immunoblot of cell lysates and supernatant from PLV production. Supernatant was purified through a 20% sucrose cushion for 1 h at 18,000 $\times$ *g* prior to lysis. (E) Quantification of the S2/S ratio in 3 independent immunoblots of the purified supernatant used for panel D. (F) D614G, ΔCT, alpha, or alpha ΔCT PLVs were used to infect A549-ACE2-IFITM cells for 48 h, and infection was quantified by luciferase activity. Infection is normalized to control values. Data are means and SEM (n = 3). Statistics were calculated in Prism using ANOVA. Asterisks and daggers indicate significance ($P < 0.05$) between control cells and cells expressing individual IFITMs and between different IFITM/drug conditions, respectively.

we again noted significant enhancement of infection in the presence of IFITM3, consistent with our PLV experiments. However, while alpha PLV is weakly enhanced by IFITM2, the native virus was enhanced by IFITM1. We concluded that IFITM1 and -2 can enhance alpha infection, but in a variable manner that may be due to the ability of IFITMs to cycle through multiple cell compartments. Furthermore, both delta and omicron viruses displayed sensitivity to both IFITM2 and IFITM3 (Fig. S2). Thus, the alpha variant of SARS CoV-2, unique among the current VOC, is fully IFITM resistant in A549-ACE2s. Furthermore, the IFITM3 enhancement of alpha infection is reproducible between PLVs and native virus.

The alpha variant is less sensitive to IFN-β than an early pandemic isolate. While previous data have indicated that the original Wuhan-like SARS-CoV-2 virus can delay pattern recognition of viral RNA in target cells, its replication is highly sensitive to exogenous IFN-I treatment in culture, in part determined by IFITM2 (30). Having confirmed that the

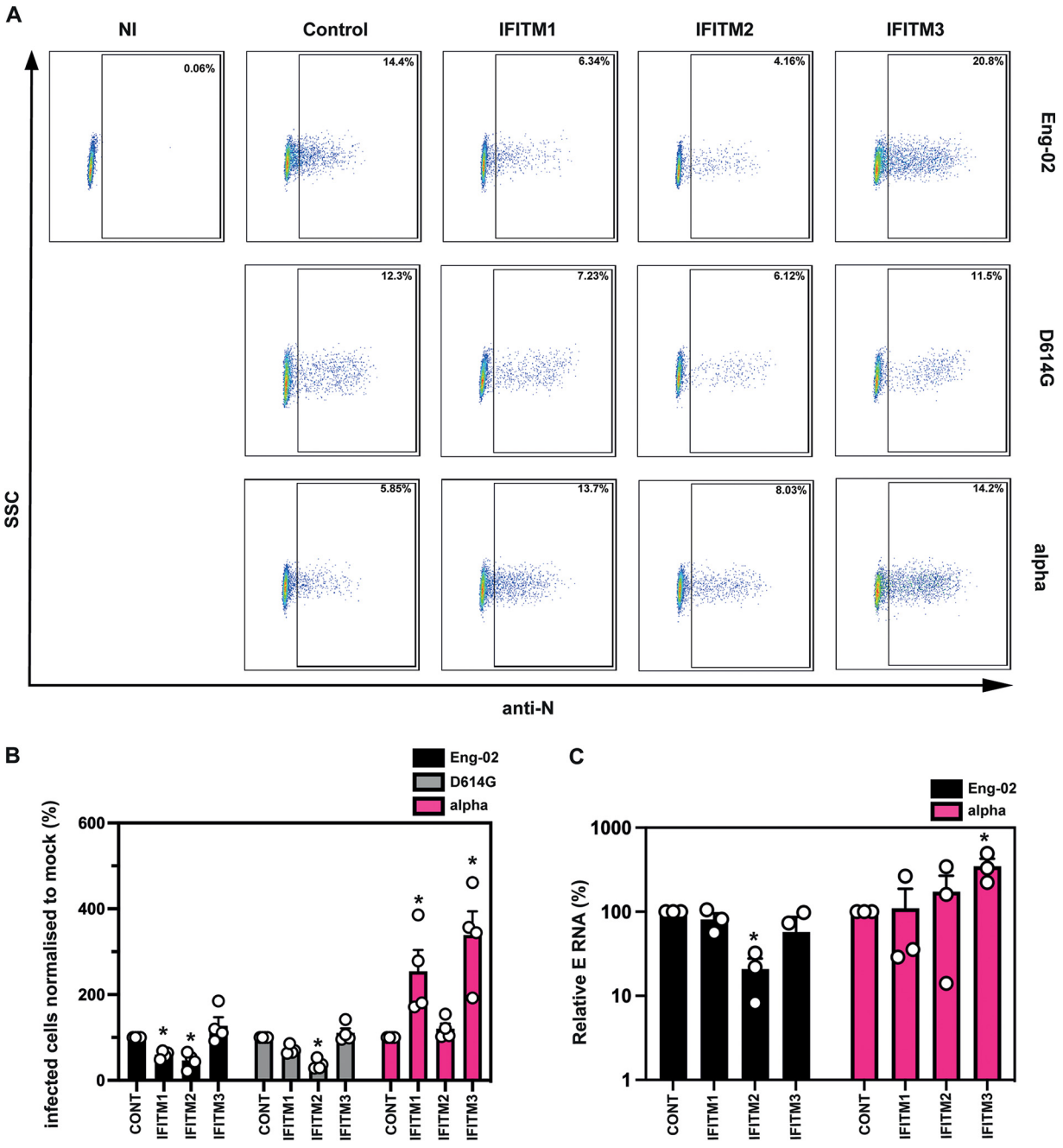

FIG 4 The alpha variant of SARS-CoV-2 is resistant to IFITMs. (A) Representative fluorescence-activated cell sorting plots of intracellular N staining of infected A549-ACE2-IFITM cells. NI, noninfected; SSC, side scatter. (B) Quantification of intracellular N staining by flow cytometry of A549-ACE2 IFITM cells infected with England-02, Wuhan D614G, and alpha. A549-ACE2 cells expressing the individual IFITMs were infected with England-02, D614G, or alpha isolates for 48 h. Infection was measured by determining the percentage of N-positive cells by flow cytometry. Data were analyzed in FlowJo. (C) Infection of A549-ACE2 stably expressing the individual IFITMs with England-02 and alpha viruses at an MOI of 0.01. Infection was quantified by RT-qPCR of E gene relative to GAPDH 48 h later; values are E mRNA levels relative to GAPDH. Data are means and SEM ($n = 3$). Statistics were calculated in Prism using ANOVA. Asterisks and daggers indicate significance ($P < 0.05$) between control cells and individual IFITMs and between different IFITM/drug conditions, respectively.

alpha variant is resistant to IFITM expression when ectopically expressed, we then tested if alpha was also more resistant to the effects of IFN-β, as suggested by others (31, 32). Indeed, we found from measuring supernatant viral RNA 48 h after infection of A549-ACE2 cells that alpha is more resistant than England-02 to pretreatment with increasing doses of IFN-β (Fig. 5A). Additionally, this was recapitulated in lung epithelial Calu-3 cells, which naturally express ACE2 and TMPRSS2 (Fig. 5B). We further extended these observations to two

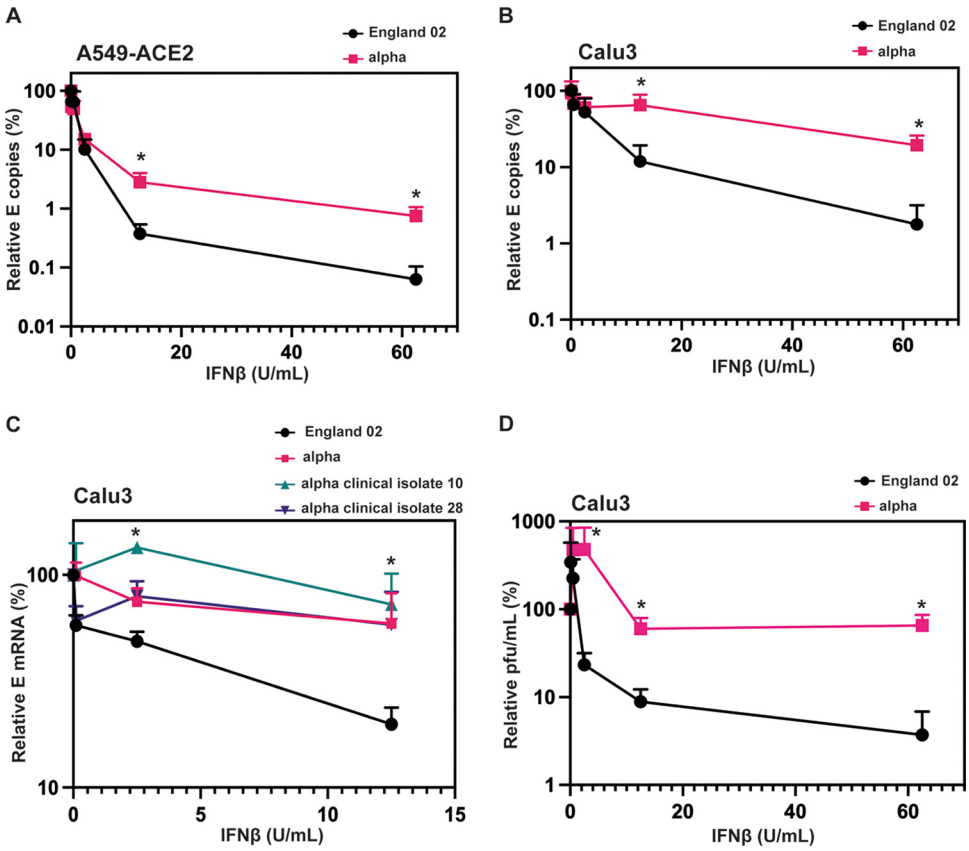

FIG 5 The alpha variant is resistant to IFN-β. (A) England-02 and alpha virus infection in A549-ACE2 cells pretreated with IFN-β. Cells were pretreated with increasing concentrations of IFN-β for 18 h prior to infection with either virus at 500 E mRNA copies/cell. Infection was quantified by RT-qPCR of E mRNA from the supernatant 48 h later and normalized to the untreated control. (B) England-02 and alpha virus infection in Calu-3 cells pretreated with IFN-β. Cells were pretreated with increasing concentrations of IFN-β for 18 h prior infection with either virus at 5,000 E copies/cell. Infection was quantified by RT-qPCR of E mRNA from the supernatant 48 h later and normalized to the untreated control. (C) England-02 and clinical isolates of alpha virus infection in Calu-3 cells pretreated with IFN-β and harvested as for panels A and B. Cells were pretreated with increasing concentrations of IFN-β for 18 h prior to infection with either virus at 5,000 E copies/cell. Infection was quantified by RT-qPCR of cellular E mRNA relative to GAPDH 48 h later and normalized to the untreated control. (D) Calu-3 cells were infected with England-02 or alpha as for panel B, and supernatant from infected cells was used to infect Vero-E6-TMPRSS2 cells for 72 h. The number of PFU per milliliter was determined by plaque assay. Data are means and SEM (n = 3). Statistics were calculated in Prism using a t test. *, $P < 0.05$ for the different viruses at individual IFN concentrations.

clinical isolates of alpha (clinical isolates 10 and 28) (Fig. 5C) and measured viral RNA in cell lysates. This confirmed that two further clinical isolates of alpha grown from patient swabs are also resistant to pretreatment with IFN-β. Finally, we showed that the alpha isolate is resistant to exogenous IFN-β pretreatment by taking the supernatant from infected Calu-3 cells pretreated with IFN-β and measuring the viral infectivity by plaque assay on Vero-E6-TMPRSS2 cells, confirming that the alpha variant still actively replicates in the presence of IFN-β to produce infectious virions (Fig. 5D). Thus, in comparison to a representative example of Wuhan-1-like SARS-CoV-2, the alpha variant has a marked resistance to IFN-I.

Discordance between the incorporation of furin-processed spike proteins into lentiviral particles and native virions. It has been postulated that the P681R and P681H mutations that have emerged in the delta, alpha, and omicron variants enhance spike processing, which facilitates a more cell surface-based route of entry (33). However, whether the P681R or P681H mutations confer a greater degree of S processing has been debated (20, 34). We had previously identified cleavage at the S1/S2 boundary in the Wuhan-1 virus as a factor in reduced IFITM2 sensitivity and therefore postulated that the P681H mutation may lead to increased S1/S2 cleavage and explain why alpha is IFITM resistant in A549-ACE2s. PLV particles assemble and bud at the plasma membrane (35) and

incorporate SARS-CoV-2 spike into virions, which reaches the cell surface by bulk anterograde transport because it escapes coatomer protein I (COPI)-mediated ER/Golgi retention (29), and this process is enhanced by removal of the C-terminal 19 amino acid (aa) of spike (36). In contrast, native CoV virions assemble at, and bud into, intracellular Golgi-derived membranes and are then secreted.

While most studies have compared the incorporation of furin-cleaved spike in PLVs to that of spike in lysates of SARS-CoV-2-infected cells, we compared S cleavage and incorporation into sucrose-pelleted virions for sequence-verified isolates of the major VOC and lentiviral pseudotypes made with the same spike (Fig. 6A to F). In contrast to the HEK293T cells producing PLVs, Vero-E6-TMPRSS2 cells infected with fixed doses of the Wuhan-1-like England-02, D614G, alpha, delta, and omicron isolates displayed marked differences in cleaved spike content in both cells and pelleted virions. Lysates of 30-h-infected Vero-E6-TMPRSS2 cells displayed markedly larger amounts of the S2 cleavage product as a proportion of uncleaved spike for the D614G mutant and the VOC than the England-02 isolate. While incorporation of spike into harvested virions (S levels in pelleted virions relative to N) was equivalent (Fig. 6A and C), virions produced from Vero-E6-TMPRSS2 reflected the cell lysate well, with alpha and omicron showing much higher relative cleaved spike incorporation than delta or D614G variants, which in turn was more pronounced than that of England-02 (Fig. 6A and B).

That these results contrast with data from other groups producing virus in other systems highlights the idea that the relative proportion of cleaved spike on SARS-CoV-2 virions is likely to be highly dependent on the cell line in which the virus is grown. In contrast, PLVs displayed clear differences with the native virus: while all spikes were similarly expressed in the cell lysates, there were clear differences in the level of PLV incorporation of between PLVs (6D-6F), indicating that PLVs may not give a true reflection of the spike incorporation or processed conformation on native virions. Discrepancies between lentiviral vectors and virus spike processing was also recently suggested by the Côté group (22), and it is likely that the cell type in which the viruses and PLVs are produced influences the observed spike processing and may explain some of the differences in the literature (22, 37). Given that the structural proteins E, M, and N are known to regulate S retention, assembly, and glycosylation (38), we suggest that differences in spike cleavage based solely on assays using spike-only PLVs be interpreted with caution. Furthermore, as demonstrated in Fig. 3, PLVs with a ΔCT result in both differential S1/S2 cleavage and cathepsin dependence, further confirming that this needs to be taken into account when determining consequences for spike cleavage.

Next, we tested if the alpha, delta, and omicron variants used the same route of entry given the polybasic cleavage site mutations. Other groups have suggested that the omicron variant, despite containing a P681H mutation, is more dependent on the endosomal route of entry because the receptor binding domain is more likely to be in the "down" conformation (27). This change in entry route may account for our observation that omicron retains IFITM2 sensitivity. We thus hypothesized that despite the P681H mutation, omicron, unlike alpha, would still require endosomal cathepsins for entry. To test this, we pretreated A549-ACE2 cells with the endosomal cathepsin inhibitor E64d and infected them with D614G, alpha, delta, and omicron PLVs. We found that, in line with what others have described, omicron displayed E64d sensitivity similar to that of the D614G mutant (Fig. 6G). The alpha or delta variants essentially showed no significant dependence on cathepsin-mediated S cleavage relative to the D614G variant. Overall, these results suggest that S1/S2 cleavage is highly cell-type dependent and does not necessarily correlate with viral entry route.

The P681H mutation is necessary for conferring IFITM and IFN-β resistance in alpha by promoting a cell surface route of viral entry. Our previous data indicated that IFITM sensitivity of SARS-CoV-2 spike can be increased by deletion of the polybasic cleavage site (14). Given that the alpha spike acquired the P681H mutation and we demonstrated that it is relatively insensitive to an inhibitor of endosomal entry (Fig. 6G), we hypothesized that P681H might be a determinant of resistance to IFN and IFITMs for the alpha spike. Using PLVs on A549-ACE2-IFITM cells, we first confirmed

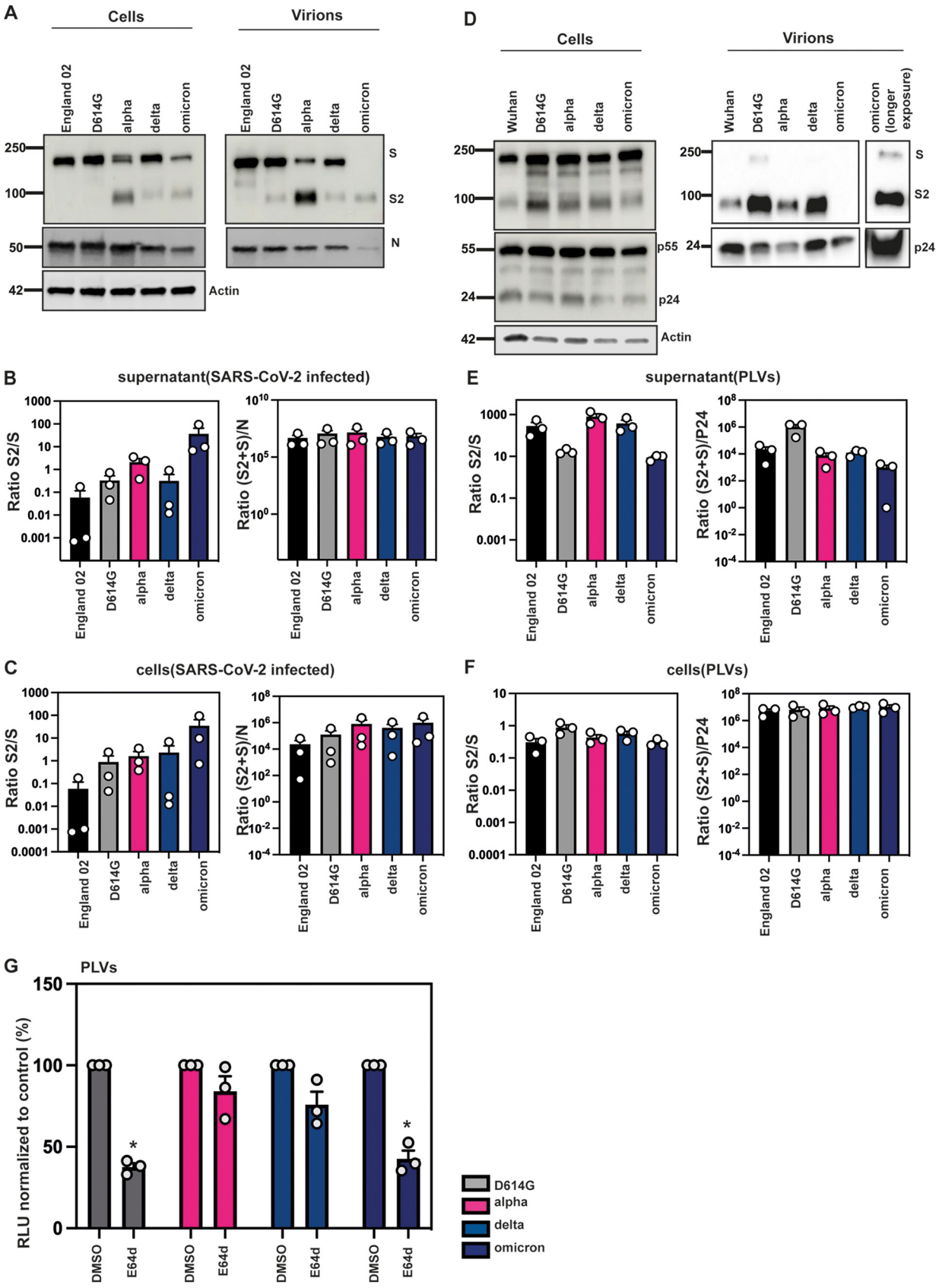

FIG 6 Spike is differentially cleaved across the major variants but not in PLVs. (A) Representative Western blot of spike protein in cell lysates and purified supernatants of infected Vero-E6-TMPRSS2 cells. Cells were infected with Wuhan, D614G, alpha, delta, or omicron isolates at an

(Continued on next page)

that ablation of the entire polybasic cleavage site increases IFITM2 sensitivity of the D614G mutant, as we have previously demonstrated for the Wuhan-1 spike (14). As expected, D614GΔPRRA is highly sensitive to IFITM2 and is not cleaved on PLV particles (Fig. 7A; Fig. S3C to E). Next, we tested if the same polybasic cleavage site deletion sensitized alpha to the IFITMs. Not only was the ΔHRRA mutant sensitive to IFITM2, but also, we abolished the IFITM3 enhancement phenotype observed with the alpha PLV (Fig. 7A; additional statistics are provided in Fig. S3A and B), suggesting that prior S1/S2 cleavage was essential for both of these phenotypes.

Having confirmed that alpha spike could be sensitized to IFITM2 by deletion of the HRRA site, we next tested whether the P681H mutation alone could confer IFITM resistance to D614G S, and vice versa. We found that the P681H mutation in the D614G background was sufficient to abolish IFITM2 sensitivity but was not able to confer the level of IFITM3-mediated enhancement that we observe with alpha. However, the H681P mutation in alpha sensitized the alpha PLV to IFITM2, although not to the same extent as the ΔHRRA mutation, and also reduced the IFITM3 enhancement of alpha. We noted that the H681P mutation did not revert the cleavage of the alpha spike in the context of PLVs (Fig. S3C to E); however, as suggested in Fig. 5, conclusions regarding spike cleavage drawn from observations with PLVs may not represent the real virus. We concluded that although the P681H mutation is necessary for IFITM resistance, it is likely that other contextual mutations in the alpha spike are required for this to be sufficient for IFITM3 enhancement. Next, we tested whether the P681R mutation in the D614G background alters IFITM sensitivity (Fig. S3F). Unlike the P681H mutation, the P681R mutation did not alter the IFITM sensitivity of the D614G virus. Additionally, reverting R861 to a P in the delta S had little impact on IFITM sensitivity (Fig. S3G), further suggesting that the P681R mutation itself cannot confer IFITM resistance.

We then wanted to confirm whether the P681H mutation confers IFITM resistance by reducing the dependence on endosomal entry in the A549-ACE2 system. Previously, we demonstrated that the alpha spike is relatively insensitive to the effects of the cathepsin inhibitor E64d. To test whether the increased IFITM sensitivity of the ΔHRRA and H681P mutants correlated with increased endosomal entry and therefore exposure to IFITM2, we pretreated cells with the cathepsin inhibitor E64d as before and infected them with PLVs (Fig. 7D). As expected, we found that the proteins with D614G and alpha polybasic cleavage site deletions were highly sensitive to E64d. Additionally, the H681P mutation conferred increased E64d sensitivity to alpha, suggesting that this mutant is more reliant on cathepsin-dependent entry and therefore more likely to encounter IFITM2 (Fig. 7B). As expected, the inverse P681H mutation in the context of D614G conferred decreased E64d sensitivity to the wild-type spike. This suggests that the P681H mutation alone is sufficient to confer increased preference for cell surface entry to a D614G-bearing PLV. In the context of the alpha spike, we further suggest that the P681H mutation is a determinant of route of viral entry and therefore of sensitivity to antiviral proteins that occupy endosomal compartments. Having established that the P681R mutation did not alter IFITM sensitivity, we hypothesized that this mutation alone would not reduce E64d sensitivity to a wild-type spike. Indeed, while the P681H mutation reduces cathepsin-dependence, the P681R mutation is indistinguishable from D614G in terms of E64d sensitivity (Fig. S3H). This suggests that the P681R mutation does not confer cell surface-mediated entry in the A549-ACE2 cells. Finally, to determine whether any of the other defining mutations in the alpha spike altered IFITM sensitivity, we generated single mutants with the Δ69/70 (Fig. 7C), Δ144

FIG 6 Legend (Continued)
MOI of 1 for 30 h. Virions were purified through a 20% sucrose gradient. (B) Quantification of spike in cell lysates of infected Vero-E6-TMPRSS2 cells after 30 h. (C) Quantification of spike in purified supernatant from infected Vero-E6-TMPRSS2 cells after 30 h. (D) Representative Western blot of spike protein in cell lysates and purified supernatants from PLVs. PLVs were produced in 293T/17 cells and immunoblotted 48 h after transfection. Virions were purified through a 20% sucrose gradient. (E) Quantification of spike in cell lysates of 293T/17 cells used to produce PLVs. (F) Quantification of spike in purified PLVs produced in 293T/17 cells. (G) E64d sensitivity of D614G, alpha, delta, and omicron PLVs. A549-ACE2 cells were pretreated with 10 μM E64d for 1 h prior to transduction, and infection was quantified on the basis of luciferase activity 48 h later. Data are means and SEM ($n = 3$). Statistics were calculated in Prism using a *t* test. *, $P < 0.05$ between control and drug.

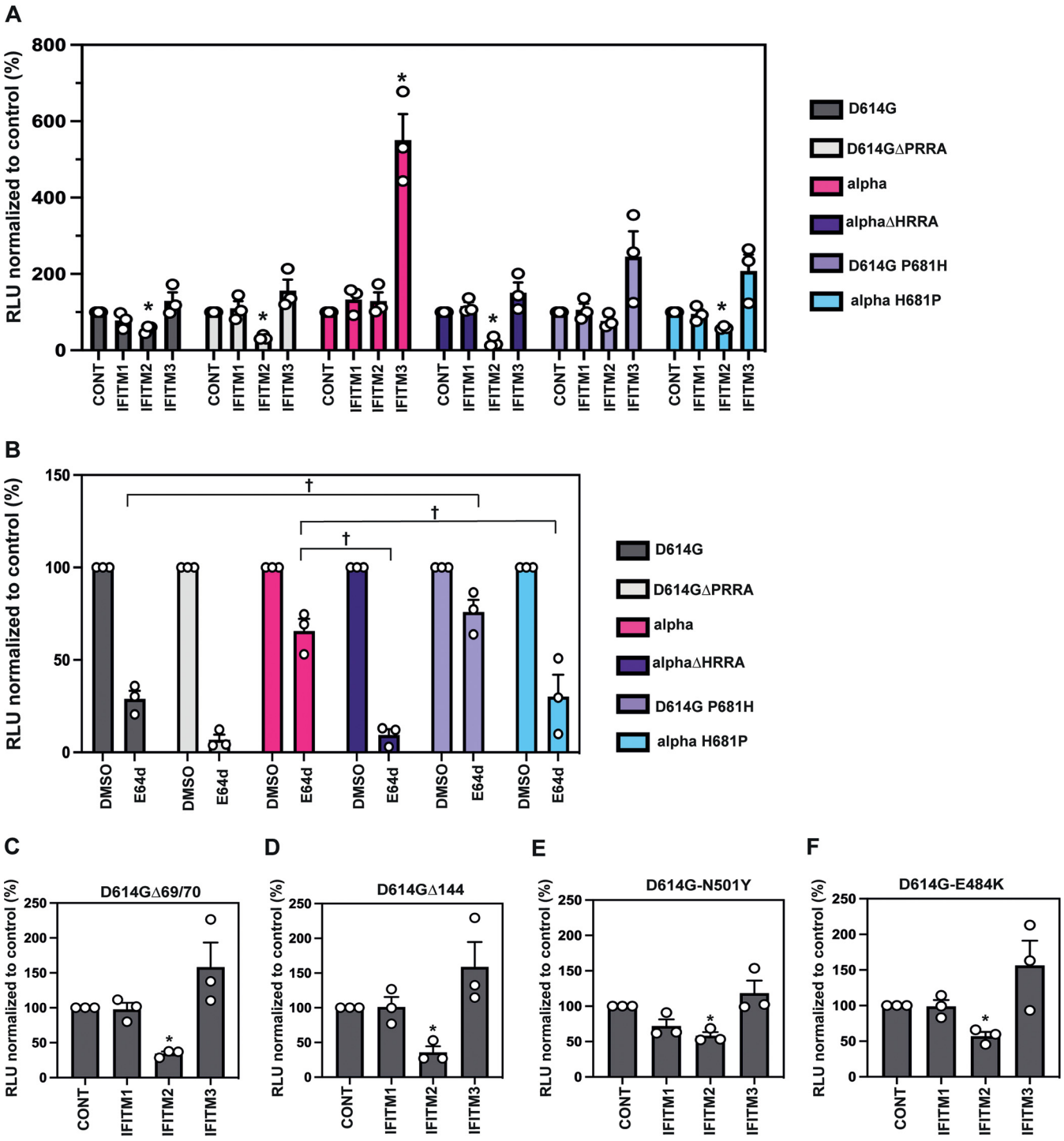

FIG 7 The P681H mutation confers IFITM resistance to a wild-type spike and a reduced dependence on E64d. (A) D614G, D614GΔPRRA, alpha, alpha-ΔHRRA, D614G P681H, and alpha H681P and PLV infection in A549-ACE2 cells stably expressing the individual IFITMs. PLV entry was quantified on the basis of luciferase activity 48 h later and normalized to control values. (B) E64d treatment of A549-ACE2 cells infected with PLVs. A549-ACE2s were pretreated with 10 μM E64d prior to transduction with D614G, alpha, delta, or omicron PLVs, and infection was quantified on the basis of luciferase activity 48 h later. (C to F) PLVs of individual mutations from alpha in the D614G background were used to infect A549-ACE2-IFITM cells, and infection was quantified on the basis of luciferase activity 48 h later. Infection normalized to control values from cells with no IFITM is shown. Data are means and SEM ($n = 3$). Statistics were calculated in Prism using ANOVA. Asterisks and daggers indicate significance ($P < 0.05$) between control cells and individual IFITMs or drug and between different IFITM/drug conditions.

(Fig. 7D), N501Y (Fig. 7E), and E484K (Fig. 7F) mutations, which emerged in several sublineages. None of these mutations significantly altered IFITM resistance.

Reversion of the P681H mutation sensitizes the alpha variant to IFN-β and IFITM2. Finally, we tested if the H681P reversion was sufficient to revert the overall IFN-β resistance phenotype of alpha. We constructed a recombinant molecular clone of SARS-CoV-2 Wuhan-1 encoding spike from the alpha variant. This virus essentially mimicked the resistance of the alpha variant itself to IFN-β in comparison to England-02, demonstrating that the alpha spike alone is sufficient to confer a level of IFN-I resistance in A549-ACE2 cells (Fig. 8A). Then, we reverted the amino acid residue H681 in this recombinant virus to a proline. Importantly, this single point mutation was sufficient to confer a significant sensitivity to IFN-β in Calu-3 cells, indicating that it was a major determinant of IFN resistance in alpha spike (Fig. 8B). Furthermore, we wanted to confirm whether small interfering RNA (siRNA) knockdown of IFITM2 was sufficient to rescue the Wuhan(B.1.1.7 spike H681P) virus from IFN-β-mediated inhibition. We confirmed that IFITM2 knockdown had no effect on expression of other interferon-stimulated genes (ISGs) and IFN-β signaling, measured by STAT1 phosphorylation and viperin expression (Fig. 8C). We showed that the H681P-reverted virus was rescued from IFN-β restriction by IFITM2 knockdown, while the Wuhan (B.1.1.7 spike) virus was unaffected, consistent with this virus being resistant to IFITM restriction (Fig. 8D). Thus, this confirmed that the S protein of the alpha variant of SARS-CoV-2 is a determinant of type-I IFN resistance, which is primarily modulated by IFITM2. Most importantly, the P681H mutation is necessary for this. Interestingly, when we immunoblotted purified virions of the Wuhan(B.1.1.7 spike) and Wuhan(B.1.1.7 spike-H681P), we found that, similar to the PLVs (Fig. 6B and C), the H681P reversion did not affect the cleavage of the alpha S (Fig. 8E). Thus, P681H adaptive mutation is a determinant of IFN type I resistance acquired in the alpha variant that evades IFITM2 restriction. It further appears to exert its activity independently of S1/S2 cleavage by altering the route of viral cell entry.

DISCUSSION

Here, we show that the spike protein of the alpha variant of SARS-CoV-2 is a determinant of viral resistance to IFN-I. This maps to the histidine residue adjacent to the polybasic cleavage site that has been mutated from the parental proline. While this has been shown to enhance spike cleavage at the S1/S2 boundary in a context-dependent manner (39), the H at this position in alpha rather than the cleavage itself appears to confer the IFN resistance phenotype. This is reinforced by the finding that deleting the last 19 amino acids of D614G spike results in enhanced S1/S2 cleavage but not enhanced IFITM resistance, further suggesting that cleavage *per se* is not the determining factor of the alpha variant's IFITM resistance. The P681H mutation correlates with the abolition of the residual sensitivity to endosomal cathepsin inhibitors, implying a change in viral entry route that distinguishes alpha from delta. This residue is also necessary to confer both resistance to IFITM2 and enhancement by IFITM3 and, as we demonstrated in our previous study (14), confirms that the polybasic cleavage site can modulate IFITM entry restriction. Furthermore, we demonstrate that this mutation alone in a wild-type D614G spike is sufficient to promote reduced IFITM sensitivity, while the delta P681R mutation is not. Furthermore, we note that infection by alpha is enhanced in the presence of IFITM3, and this is abolished by cyclosporine H, cytoplasmic tail deletion, and the H681P mutation. IFITM3 was reported previously to enhance the entry of the coronavirus OC43 and more recently was suggested to enhance the entry of hepatitis B and D viruses (24, 40). Although it is surprising that an antiviral protein can enhance infection, this phenotype in multiple viruses suggests a common mechanism of hijacking host factors for viral entry. We also saw enhancement by IFITM1 or IFITM2 a factor of 1 or 2 with the alpha virus and PLVs to a variable degree. We suggest that this may be a factor of the trafficking of IFITMs through multiple compartments and the occasional presence of IFITM1 and -2 in the compartment where IFITM3 usually resides. Enhancement of coronavirus entry by the mutant IFITM1Δ117-125 has been documented, suggesting that IFITM1 can enhance viral entry depending

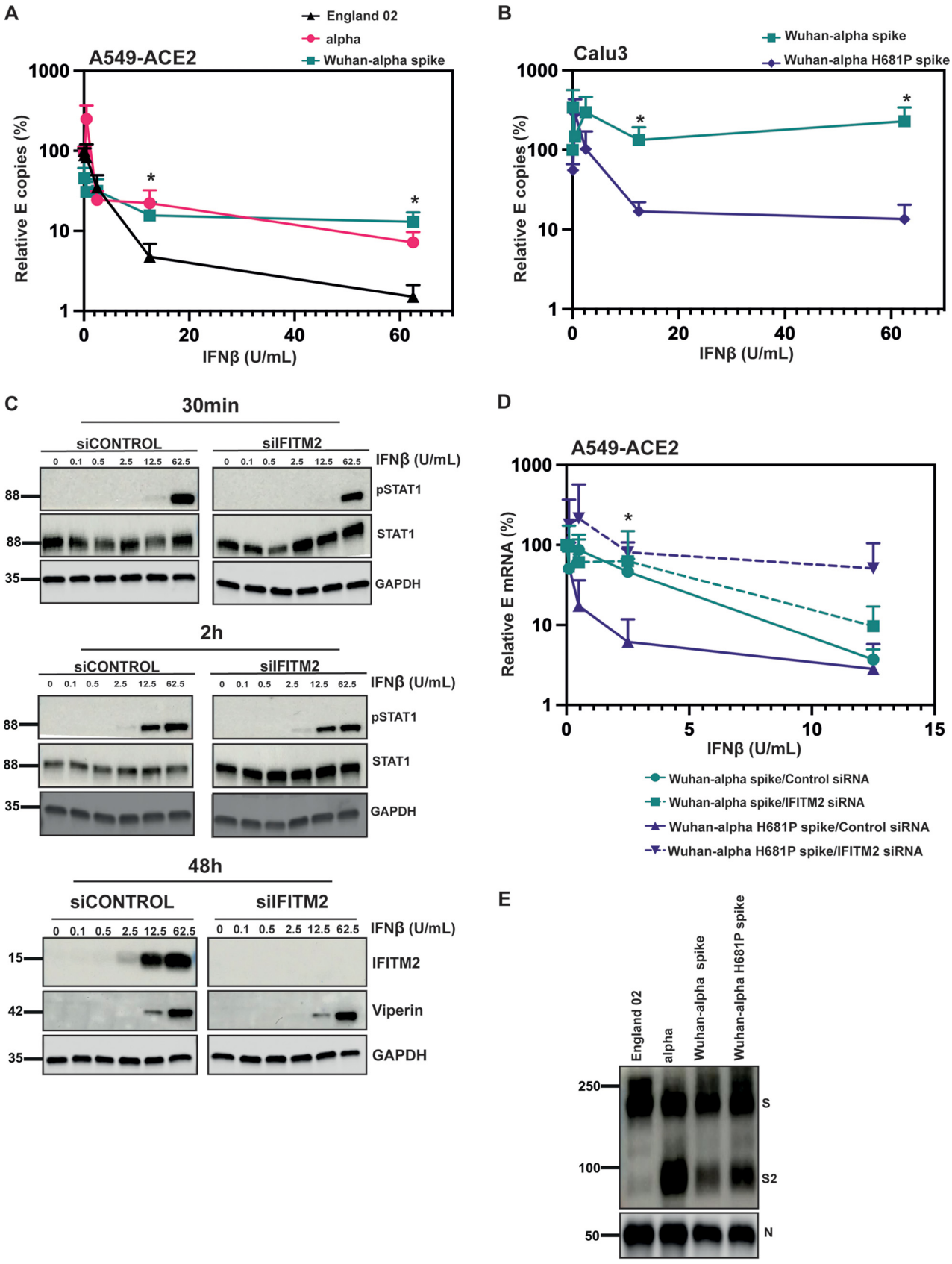

FIG 8 The P681H mutation is necessary and sufficient for IFN-β resistance. (A) England-02, alpha, and Wuhan(alpha spike) virus infection in A549-ACE2 cells pretreated with IFN-β. Cells were pretreated with increasing concentrations of IFN-β for 18 h prior to infection with either virus at 500 E copies/cell.

(Continued on next page)

on localization (41). We also showed previously that the Y19F mutation in IFITM2 results in enhancement of Wuhan entry, further suggesting that IFITM localization can alter its capacity to enhance coronavirus infection (14).

We suggest that the P681H change in alpha changes the site of viral fusion, thus avoiding the endosomal compartment where IFITM2 predominantly resides. Consistent with this, we showed that the alpha spike in a PLV is less sensitive to the cathepsin inhibitor E64d. Thus, we propose that these changes in the alpha spike have, in part, arisen to resist innate immunity. At least two studies suggest that variants of SARS-CoV-2 have begun to evolve further resistance to interferon-induced innate immunity (31, 42, 43). In one, viral isolates obtained over the course of the pandemic showed a reduced sensitivity to type I interferons in culture (42); in a second, the alpha variant showed a significantly reduced propensity to trigger pattern recognition in epithelial cells by cytoplasmic RNA sensors (31, 43). In contrast, another study found no difference in IFN sensitivity of the new variants in African green monkey Vero-E6 cells (11), although species specificity in viral sensitivity to ISGs is a well-characterized trait that could explain this discrepancy (44). The SARS-CoV-2 genome contains multiple mechanisms to counteract host innate immune responses, and much remains to be learned about the mechanisms deployed by this virus and its relatives. While many reports on SARS-CoV-2 evolution have naturally focused on the pressing concern of the potential for vaccine escape, it is very unlikely that all selective adaptations that we see arising in VOC can be due solely to escape from adaptive immunity. The alpha spike, for example, displays only a minor reduction in sensitivity to neutralizing antibodies (NAbs) (8, 45–47). However, this VOC had a considerable transmission advantage, giving rise to the suspicion that it may have arisen in an immunocompromised individual with a persistent infection, providing ample time for changes to be selected that further evade innate immunity, including those that target viral entry (48, 49).

In terms of IFITM resistance of VOC spike proteins, so far, we have seen a marked change in phenotype only in the alpha variant. This is despite the fact that both delta and omicron, variants that superseded alpha, also showed an adaptation for enhanced S1/S2 cleavage with a P681R and P681H change, respectively (20, 39). This suggests that cleavage of S1/S2 is necessary but not sufficient for IFITM resistance and that other mutations in each cognate spike act in concert to determine relative IFITM sensitivity. Despite the increased cleavage of a D614G-containing isolate in delta and omicron relative to England-02, these viruses are not IFITM resistant. This suggests that the P681H mutation confers IFITM resistance through a mechanism distinct from S1/S2 cleavage itself. We and others show that omicron is sensitive to E64d inhibition, and we suggest that this preference for endosomal entry correlates with omicron's IFITM sensitivity (27).

The spike of omicron contains 30 mutations, 12 of which are in the RBD and have been suggested to increase the affinity for ACE2 (50). The constellation of mutations in the RBD of omicron also promotes an "RBD down" closed conformation, which necessitates cathepsin-mediated cleavage in the endosome rather than surface TMPRSS2-mediated cleavage (27). This suggests that the up conformation of the RBD is required for H681 to exert its IFN resistance phenotype (27). Furthermore, omicron contains an H655Y mutation, which has been suggested to enhance endosomal entry (51). Despite delta containing a P681R mutation, we report that this spike is not IFITM resistant, nor is the kappa variant, which also bears a P681R mutation and was relatively short-lived as a variant. Despite the delta

FIG 8 Legend (Continued)
Infection was quantified by RT-qPCR of E mRNA in the supernatant 48 h later and normalized to the value for the mock-treated control. (B) Wuhan(alpha spike) and Wuhan(alpha spike H681P) virus infection in Calu-3 cells pretreated with IFN-β. Cells were pretreated with increasing concentrations of IFN-β for 18 h prior to infection with either virus at 5,000 E copies/cell. Infection was quantified by RT-qPCR of E mRNA in the supernatant 48 h later and normalized to the value for the mock-treated control. (C) Representative immunoblot of pSTAT1 and STAT1 in cell lysates with IFITM2 knocked down or a nontargeting control and subsequently treated with IFN-β. A549-ACE2 cells were transfected with siRNAs against nontargeting control or IFITM2 and then either treated with IFN-β for 30 min or 2 h and immunoblotted for pSTAT1 and STAT1 or treated for 24 h and blotted for viperin and IFITM2. (D) A549-ACE2 cells were transfected with siRNAs against nontargeting control or IFITM2 for 24 h and then treated with IFN-β for 18 h prior to infection with Wuhan(alpha spike) or Wuhan(alpha spike H681P) at 500 copies/cell. Infection was quantified by RT-qPCR of E gene relative to GAPDH 48 h later. Data are means and SEM ($n = 3$). Statistics were calculated in Prism using a t test. *, $P < 0.05$ for differences between the different viruses. (E) Representative immunoblot of England-02, alpha, Wuhan(alpha spike), and Wuhan(alpha spike) H681P viral stocks. England-02, alpha, Wuhan(alpha spike), and Wuhan(alpha spike H681P) viruses were purified through 20% sucrose and immunoblotted for spike and N proteins.

spike demonstrating E64d insensitivity, the P681R mutation alone does not result in reduced IFITM sensitivity or decreased E64d sensitivity to a D614G spike. This implies that there are other factors besides the P681R mutation governing delta's route of viral entry. Two recent papers have suggested that certain matrix metalloproteinases (MMPs) can mediate an alternative route of entry to TMPRSS2, and that this can be utilized by the delta variant (22, 52). It is possible that a combination of these viral entry routes is variably present in different cell types and may therefore explain differential IFITM sensitivities of VOC.

Finally, the delta variant also contains different RBD mutations than alpha, in particular the T478K and L452R mutations, which may also affect the RBD conformation and be a factor in delta's relative sensitivity to IFITMs. The mutations in the RBDs of delta and omicron have led to hypotheses that both of these variants were driven by antibody escape, suggesting that selection pressures on the alpha variant may have been more due to innate immunity. It is important to note that the discordance between virion-incorporated spike species in the native SARS-CoV-2 particle and lentiviral pseudotypes imply a degree of cell type dependency as well as cellular location of viral assembly in the relative presence of cleaved spike. We also demonstrate that this issue is of particular concern for those using C-terminal deletions of the COPI retention signal in spike. We would hesitate to ascribe some of the phenotypes associated with VOC spike protein simply to differences in furin cleavage efficiency or phenotypes observed with Δ19aa PLVs when the route of viral entry is implicit to the phenotype.

Viral glycoproteins are dynamic structures that shift through large-scale conformational changes while interacting with their cognate receptors mediating viral membrane fusion (53). Such context dependency is therefore likely to be complex and will arise under competing selective pressures. Indeed, we showed previously that the HIV-1 envelope glycoprotein of transmitted viruses is IFITM insensitive and that this contributes to their overall type I IFN resistance (54). As HIV-1 infection progresses over the first 6 months in an infected person, the circulating variants increase in IFN/IFITM sensitivity, and this is determined by adaptive changes in Env that resist the early neutralizing antibody response (55). Such escape has structural and functional implications for such dynamic proteins that may impact receptor interactions and route of entry into the target cell.

The mapping of IFN-I resistance to P681H to the polybasic cleavage site of alpha, combined with the observation of reversion of IFN-I sensitivity by the restoration of the P without affecting the cleavage of virion-associated spike, suggests that H681 exerts its effects on viral entry and IFITM/IFN-I sensitivity downstream of cleavage itself. While it is possible that this could be simply related to stability of the cleaved form, it is intriguing that the C-terminal RRAR of S1 has also been proposed as a ligand for neuropilin-1 (NRP-1), a receptor for furin-processed growth factors like vascular endothelial growth receptor A (VEGF-A). NRP-1 was found to promote the entry and replication of SARS-CoV-2 in an FCS-dependent manner (56, 57). Given the accumulating evidence that interprotomer interactions in the S trimer affect the accessibility of cleavage sites in spike (58), future studies will determine whether a role for NRP-1 in entry also governs sensitivity to IFITM restriction and IFN sensitivity.

While the polybasic cleavage site of the SARS-CoV-2 S reduces its IFITM sensitivity, other interferon-induced proteins may contribute to this phenotype. The guanylate binding protein family, and particularly GBP2 and GBP5, has been shown to have a general antiviral activity against enveloped viruses by dysregulating furin processing of diverse viral and cellular proteins (59). Similarly, IFITM overexpression in HIV-infected cells can lead to their incorporation into virions and in some cases promote defects in glycoprotein incorporation (60). Future studies will confirm whether either of these mechanisms is involved in the IFN resistance associated with the P681H mutation in alpha (27).

In summary, the spike protein of SARS-CoV-2 alpha increases resistance to IFN-I, and this correlates with the P681H mutation. Furthermore, it also correlates with IFITM resistance, as IFITM2 knockdown rescues the IFN-sensitive alpha H681P virus, but not alpha. Despite also containing P681R/P681H mutations, the delta and omicron variants

are not IFITM resistant in the A549-ACE2 system. We suggest that factors such as spike conformation and alternate routes of viral entry all act in concert to determine the relative sensitivities of spike proteins to antiviral proteins that affect viral entry.

MATERIALS AND METHODS

Cells and plasmids. HEK293T-17 (ATCC; CRL-11268), Calu-3 (ATCC; HTB-55), A549-ACE2, Vero-E6, Vero-E6-TMPRSS2, and A549-ACE2 cells expressing the individual IFITM proteins were cultured in Dulbecco's modified Eagle medium (DMEM; Gibco) with 10% fetal bovine serum (FBS; Invitrogen) and 200 μg/mL gentamicin (Sigma), and incubated at 37°C and 5% CO_2. Cells stably overexpressing ACE2, TMPRSS2, and IFITM were generated as previously described (14).

Codon-optimized SARS-CoV-2 Wuhan spike and ACE2 were kindly provided by Nigel Temperton. Codon-optimized variant spikes (alpha and beta) were kindly provided by Katie Doores. Codon optimized variant spikes (gamma, kappa, delta) were kindly provided by Wendy Barclay. Plasmid containing the TMPRSS2 gene was kindly provided by Caroline Goujon. Spike mutants were generated with Q5 site-directed mutagenesis kit (E0554) following the manufacturer's instructions and using the following forward and reverse primers: D614G (GCTGTACCAGGGCGTGAATTGCA, ACGGCCACCTGATTGCTG), B.1.351. Δ242-244 (ATTTCATATCTTACACCAGGC, ATGCAGGGTCTGGAATCTG), D614G P681H (GACCAATAGCCACAGAAGAGCC AGAAGC, TGGGTCTGGTAGCTGGCG), B117 ΔHRRA (AGAAGCGTGGCCAGCCAG, GCTATTGGTCTGGGTCTG GTAG), B117 H681P (GACCAATAGCcccAGAAGAGCCAG, TGGGTCTGGTAGCTGGCG), Δ69/70 (AGCGGCACC AATGGCACC, GATGGCGTGGAACCAGGTC), Y144 (CATAAGAACAACAAGAGC, ATAAACACCCAGGAAAGG), E484K (TAATGGCGTGAAGGGCTTCAATTGCTACTT, CACGGTGTGCTGCCGGCC), N501Y (CCAGCCTACCTACGGCGTGGGCT, AAGCCGTAGCTCTGCAGAG), and ΔCT (GTCCTGCTGCTGATGAGACGAGGACGACAGCG, CCACACGAACAACACCCT).

Stable A549 cell lines expressing ACE2 (pMIGR1-puro) and IFITMs (pLHCX) were generated and selected as described previously (14).

Production of PLVs and infection. HEK293T-17 cells were transfected with firefly luciferase-expressing vector (CSXW), HIV gag-pol (8.91), and spike plasmid with PEI-max as previously described (14). One hundred microliters of viral supernatant was then used to transduce each cell line of interest, and readout was measured as luciferase activity 48 h later (Promega Steady-Glo [E2550]).

Cyclosporin H assay. Cells were pretreated with 30 μM cyclosporine H (Sigma; SML1575) for 18 h. Cells were then infected with PLVs as described above, and viral entry was quantified on the basis of luciferase activity 48 h later.

E64d assay. A549-ACE2 cells were pretreated with 10 μM E64d (Sigma; E8640) for 1 h at 37°C prior to infection. Cells were transduced with PLVs, and infection was determined on the basis of luciferase activity 48 h later.

Passage and titration of SARS-CoV-2. PHE England strain 02/2020 and D614G isolate were propagated in Vero-E6-TMPRSS2 cells, and titer was determined by plaque assay (14). Plaque assays were performed by infecting Vero-E6-TMPRSS2 cells with serial dilutions of SARS-CoV-2 for 1 h. Subsequently, 2× overlay medium (DMEM with 2% FBS and 0.1% agarose) was added, and infected cells were fixed with 4% paraformaldehyde (PFA) 72 h after infection and stained with crystal violet. Plaques were counted and multiplicity of infection calculated for subsequent experiments. A replication-competent alpha variant was kindly provided by Wendy Barclay (Imperial College London) (61). The spike gene sequences of all virus stocks were confirmed at each passage to ensure no loss of the polybasic cleavage site.

Generation of recombinant full-length viruses. We used the previously described method of transformation-associated recombination (TAR) in yeast (62), with some modifications, to generate the mutant viruses described in this study. Briefly, a set of overlapping cDNA fragments representing the entire genomes of SARS-CoV-2 Wuhan isolate (GenBank accession no. MN908947.3) and the B.1.1.7 alpha variant were chemically synthesized and cloned into pUC57-Kan (Bio Basic Canada Inc. and Genewiz, respectively). The cDNA fragment representing the 5′ terminus of the viral genome contained the bacteriophage T7 RNA polymerase promoter preceded by a short sequence stretch homologous to the XhoI-cut end of the TAR-in-yeast vector pEB2 (63). The fragment representing the 3′ terminus contained the T7 RNA polymerase termination sequences followed by a short segment homologous to the BamHI-cut end of pEB2.

To generate Wuhan virus carrying the alpha variant spike, a mixture of the relevant synthetic cDNA fragments of the Wuhan and alpha variants was cotransformed with XhoI-BamHI-cut pEB2 into the *Saccharomyces cerevisiae* strain TYC1 (*MATα ura3-52 leu2Δ1 cyh2*^{r}, containing a knockout of DNA Ligase 4) (63) that had been made competent for DNA uptake using the $LiCl_2$-based yeast transformation kit (YEAST1-1KT; Merck). The transformed cells were plated on minimal synthetic defined (SD) agar medium lacking uracil (Ura) but containing 0.002% (wt/vol) cycloheximide to prevent selection of cells carrying the empty vector. Following incubation at 30°C for 4 to 5 days, colonies of the yeast transformants were screened by PCR using specific primers to identify those carrying plasmids with fully assembled genomes. Selected positive colonies were then expanded to grow in 200 mL SD-Ura dropout medium, and the plasmid was extracted. Approximately 4 μg of the extracted material was then used as the template to synthesize viral genomic RNA transcripts *in vitro* using the Ribomax T7 RNA transcription kit (Promega) and Ribo m7G cap analogue (Promega) as per the manufacturer's protocol. Approximately 2.5 μg of the *in vitro*-synthesized RNA was used to transfect ~6 $\times 10^5$ BHK-hACE2-N cells stably expressing the SARS-CoV-2 N and the human ACE2 genes (64) using the MessengerMax lipofection kit (Thermo Scientific) as per the manufacturer's instructions. Cells were then incubated until signs of viral replication (syncytium formation) became visible (usually after 2 to 3 days), at which time the medium was collected (P0 stock) and used further as a source of rescued virus to infect Vero-E6 cells to generate P1 and P2

stocks. Full genome sequences of viruses collected from P0 and P1 stocks were obtained in order to confirm the presence of the desired mutations and exclude the presence of other spurious mutations. Viruses were sequenced using Oxford Nanopore Technologies as previously described (65).

To generate Wuhan virus carrying the alpha spike gene with the H681P mutation, we first introduced this mutation into the relevant alpha variant cDNA fragment by site-directed mutagenesis. This fragment was combined with those described above, and the mixture was then used to generate plasmid pEB2 carrying the cDNA genome of Wuhan encoding the H681P alpha spike by the TAR-in-yeast procedure. The virus rescue and subsequent characterization were performed as described above.

Isolation and propagation of clinical viral isolates. Viruses were isolated on Vero-E6 cells (ATCC; CRL 1586) from combined naso-oropharyngeal swabs submitted for routine diagnostic testing by real-time reverse transcription-PCR (RT-PCR) and shown to be from the B.1.1.7 (alpha) variant by on-site whole-genome sequencing (Oxford Nanopore Technologies, Oxford, UK) (66). Infected cells were cultured at 37°C and 5% CO_2 in DMEM (Gibco, Thermo Fisher, UK) supplemented with 2% FBS (Merck, Germany), penicillin-streptomycin, and amphotericin B.

All work performed with full-length SARS-CoV-2 preparations, as well as isolation and propagation of viral isolates from swabs, was conducted inside a class II microbiological safety cabinet in a biosafety level 3 (BSL3) facility at King's College London.

Infection with replication competent SARS-CoV-2. A549-ACE2 cells (1.5×10^5) were infected for 1 h at 37°C with SARS-CoV-2 replication-competent viruses at a multiplicity of infection (MOI) of 0.01 or 500 E gene mRNA copies/cell. Calu-3 cells (2×10^5) were infected for 1 h at 37°C with SARS-CoV-2 replication-competent viruses at 5,000 E gene mRNA copies/cell. Medium was replaced, and cells were incubated for 48 h at 37°C, after which cells or supernatant was harvested for RNA extraction or protein analysis.

Intracellular N staining. A549-ACE2 IFITM cells (1.5×10^5) were infected for 1 h at 37°C with SARS-CoV-2 replication-competent VOC to achieve the same percentage of infected cells as under the mock-infection condition. After 24 h infection, cells were trypsinized and fixed with 4% PFA during 30 min at room temperature. Cells were permeabilized with 1× phosphate-buffered saline (PBS) plus 0.5% Triton during 10 min following blocking with 5% FBS in 1× PBS for 20 min. After blocking, cells were stained with anti-N antibody (CR3009, mouse) for 45 min at room temperature and washed once with 1× PBS. Next, cells were incubated with secondary anti-mouse immunoglobulin conjugated to Alexa Fluor 488 for 25 min. Finally, cells were washed with 1× PBS and analyzed on a BD FACSCanto II flow cytometer using FlowJo software.

Interferon assays. Cells were treated with different doses of IFN-β (PBL Assay Science; 11415-1) for 18 h prior to infection. The following day, medium was replaced, and the infection was performed as described above. Viral RNA levels in cells or supernatants were measured 48 h after infection by RT-qPCR.

siRNA knockdown of IFITM2. A549-ACE2 cells were reverse transfected using 20 pmol of nontargeting siRNA (D-001206-13-20) or IFITM2 siRNA (M-020103-02-0010) with 1 μL of RNAiMax (Invitrogen). Cells were incubated for 24 h prior to a second round of reverse transfection. Eight hours later, cells were treated with different doses of IFN-β. Following 18 h of IFN treatment, cells were infected with full-length viruses as previously described.

RT-qPCR. RNA from infected cells was extracted using a Qiagen RNeasy minikit (Qiagen; 74106) following the manufacturer's instructions. One microliter of each extracted RNA was used to performed one-step RT-qPCR using TaqMan Fast Virus one-step master mix (Invitrogen). The relative quantities of envelope (E) gene were measured using a SARS-CoV-2 (2019-nCoV) CDC qPCR probe assay (Integrated DNA Technologies [IDT]). Relative quantities of E gene were normalized to GAPDH mRNA levels (Applied Bioscience; Hs99999905_m1).

Supernatant RNA was extracted using RNAdvance viral XP (Beckman) following the manufacturer's instructions. Five microliters of each RNA was used for one-step RT-qPCR (TaqMan Fast Virus one-step master mix) to measured relative quantities of E and calibrated to a standard curve of E kindly provided by Wendy Barclay.

SDS-PAGE and Western blotting. Cellular samples were lysed in reducing Laemmli buffer at 95°C for 10 min. Supernatant or viral stock samples were centrifuged at a relative centrifugal force (RCF) of 18,000 through a 20% sucrose cushion for 1 h at 4°C prior to lysis in reducing Laemmli buffer. Samples were separated on 8 to 16% Mini-Protean TGX precast gels (Bio-Rad) and transferred onto nitrocellulose membranes. Membranes were blocked in milk or Bovine serum albumin (BSA) prior to detection with specific antibodies: 1:1,000 ACE2 rabbit (Abcam; Ab108209), 1:5,000 GAPDH rabbit (Abcam; Ab9485), 1:2,000 anti-GAPDH mouse (Proteintech; 60004-1-Ig), 1:5,000 HSP90 mouse (GeneTex; Gtx109753), 1:50 HIV-1 p24Gag mouse (67), 1:1,000 spike mouse (GeneTex; Gtx632604), 1:1,000 anti-SARS-CoV-2 N rabbit (GeneTex; GTX135357), 1:1,00 anti-pSTAT1 mouse (BD Transduction Laboratories; 612133), 1:1,000 anti-STAT1 rabbit (Cell Signaling; 9172S), and 1:1,000 anti-viperin mouse (Millipore; MABF106). Proteins were detected using LI-COR and ImageQuant LAS 4000 cameras.

Ethics. Clinical samples were retrieved by the direct care team in the Directorate of Infection, at St Thomas Hospital, London, United Kingdom, and anonymized before being sent to the King's College London laboratories for virus isolation and propagation. Sample collection and studies were performed in accordance with the UK Policy Framework for Health and Social Care Research and with specific Research Ethics Committee approval (REC 20/SC/0310).

SUPPLEMENTAL MATERIAL

Supplemental material is available online only.

SUPPLEMENTAL FILE 1, PDF file, 3.4 MB.

ACKNOWLEDGMENTS

We are grateful to Nigel Temperton, Caroline Goujon, Katie Doores, Wendy Barclay, and Public Health England for reagents. We acknowledge the G2P-UK National Virology consortium funded by MRC/UKRI (grant MR/W005611/1) and the Barclay Lab at Imperial College London for providing the alpha variant. We thank E. J. Louis, University of Leicester, for generously providing the TAR-in-yeast system. Finally, we thank all other members of the Neil and Swanson groups for their helpful advice and provision of sugar-based support.

This work was funded by Wellcome Trust Senior Research Fellowship WT098049AIA to S.J.D.N., MRC Project Grant MR/S000844/1 to S.J.D.N. and C.S., and funding from the Huo Family Foundation jointly to S.J.D.N., Katie Doores, Michael Malim, and Rocio Martinez Nunez. MR/S000844/1 is part of the EDCTP2 program supported by the European Union. H.W. is supported by the UK Medical Research Council (MR/N013700/1) and is a King's College London member of the MRC Doctoral Training Partnership in Biomedical Sciences. This work is supported by the UKRI SARS-CoV-2 Genotype-2-Phenotype consortium. We also benefit from infrastructure support from the KCl Biomedical Research Centre, King's Health Partners. Work at the CVR was also supported by the MRC MC_UU12014/2 and the Wellcome Trust (206369/Z/17/Z).

Experiments were performed by M.J.L., H.W., A.D., and H.D.W. S.P., R.P.G., L.S., and G.N. collected, sequenced, and isolated clinical viral isolates. M.P., A.H.P., G.D.L., V.M.C., W.F., N.S., and R.O. generated reverse genetics-derived viruses. M.J.L., H.W., A.D., and H.D.W. analyzed data. C.S. provided reagents, funding support, and advice. H.W. and S.J.D.N. wrote the manuscript. All authors edited the manuscript and provided comments.

REFERENCES

1. Hoffmann M, Kleine-Weber H, Pohlmann S. 2020. A multibasic cleavage site in the spike protein of SARS-CoV-2 is essential for infection of human lung cells. Mol Cell 78:779–784.E5. https://doi.org/10.1016/j.molcel.2020.04.022.
2. Peacock TP, Goldhill DH, Zhou J, Baillon L, Frise R, Swann OC, Kugathasan R, Penn R, Brown JC, Sanchez-David RY, Braga L, Williamson MK, Hassard JA, Staller E, Hanley B, Osborn M, Giacca M, Davidson AD, Matthews DA, Barclay WS. 2021. The furin cleavage site in the SARS-CoV-2 spike protein is required for transmission in ferrets. Nat Microbiol 6:899–909. https://doi.org/10.1038/s41564-021-00908-w.
3. Lindstrom JC, Engebretsen S, Kristoffersen AB, Ro GOI, Palomares AD, Engo-Monsen K, Madslien EH, Forland F, Nygard KM, Hagen F, Gantzel G, Wiklund O, Frigessi A, de Blasio BF. 2021. Increased transmissibility of the alpha SARS-CoV-2 variant: evidence from contact tracing data in Oslo, January to February 2021. Infect Dis (Lond) 54:72–77. https://doi.org/10.1080/23744235.2021.1977382.
4. Tanaka H, Hirayama A, Nagai H, Shirai C, Takahashi Y, Shinomiya H, Taniguchi C, Ogata T. 2021. Increased transmissibility of the SARS-CoV-2 alpha variant in a Japanese population. Int J Environ Res Public Health 18:7752. https://doi.org/10.3390/ijerph18157752.
5. Mok BW-Y, Liu H, Deng S, Liu J, Zhang AJ, Lau S-Y, Liu S, Tam RC-Y, Cremin CJ, Ng TT-L, Leung JS-L, Lee L-K, Wang P, To KK-W, Chan JF-W, Chan K-H, Yuen K-Y, Siu GK-H, Chen H. 2021. Low dose inocula of SARS-CoV-2 Alpha variant transmits more efficiently than earlier variants in hamsters. Commun Biol 4:1102. https://doi.org/10.1038/s42003-021-02640-x.
6. Meng B, Kemp SA, Papa G, Datir R, Ferreira IATM, Marelli S, Harvey WT, Lytras S, Mohamed A, Gallo G, Thakur N, Collier DA, Mlcochova P, Duncan LM, Carabelli AM, Kenyon JC, Lever AM, De Marco A, Saliba C, Culap K, Cameroni E, Matheson NJ, Piccoli L, Corti D, James LC, Robertson DL, Bailey D, Gupta RK, COVID-19 Genomics UK (COG-UK) Consortium. 2021. Recurrent emergence of SARS-CoV-2 spike deletion H69/V70 and its role in the Alpha variant B.1.1.7. Cell Rep 35:109292. https://doi.org/10.1016/j.celrep.2021.109292.
7. Chi X, Yan R, Zhang J, Zhang G, Zhang Y, Hao M, Zhang Z, Fan P, Dong Y, Yang Y, Chen Z, Guo Y, Zhang J, Li Y, Song X, Chen Y, Xia L, Fu L, Hou L, Xu J, Yu C, Li J, Zhou Q, Chen W. 2020. A neutralizing human antibody binds to the N-terminal domain of the Spike protein of SARS-CoV-2. Science 369:650–655. https://doi.org/10.1126/science.abc6952.
8. Graham C, Seow J, Huettner I, Khan H, Kouphou N, Acors S, Winstone H, Pickering S, Galao RP, Dupont L, Lista MJ, Jimenez-Guardeño JM, Laing AG, Wu Y, Joseph M, Muir L, van Gils MJ, Ng WM, Duyvesteyn HME, Zhao Y, Bowden TA, Shankar-Hari M, Rosa A, Cherepanov P, McCoy LE, Hayday AC, Neil SJD, Malim MH, Doores KJ. 2021. Neutralization potency of monoclonal antibodies recognizing dominant and subdominant epitopes on SARS-CoV-2 Spike is impacted by the B.1.1.7 variant. Immunity 54:1276–1289.E6. https://doi.org/10.1016/j.immuni.2021.03.023.
9. Mohammad A, Abubaker J, Al-Mulla F. 2021. Structural modelling of SARS-CoV-2 alpha variant (B.1.1.7) suggests enhanced furin binding and infectivity. Virus Res 303:198522. https://doi.org/10.1016/j.virusres.2021.198522.
10. Zhang L, Mann M, Syed Z, Reynolds HM, Tian E, Samara NL, Zeldin DC, Tabak LA, Ten Hagen K. 2021. Furin cleavage of the SARS-CoV-2 spike is modulated by O-glycosylation. bioRxiv. https://doi.org/10.1073/pnas.2109905118.
11. Rajah MM, Hubert M, Bishop E, Saunders N, Robinot R, Grzelak L, Planas D, Dufloo J, Gellenoncourt S, Bongers A, Zivaljic M, Planchais C, Guivel-Benhassine F, Porrot F, Mouquet H, Chakrabarti LA, Buchrieser J, Schwartz O. 2021. SARS-CoV-2 Alpha, Beta, and Delta variants display enhanced Spike-mediated syncytia formation. EMBO J 40:e108944. https://doi.org/10.15252/embj.2021108944.
12. Araf Y, Akter F, Tang Y-D, Fatemi R, Parvez MSA, Zheng C, Hossain MG. 2022. Omicron variant of SARS-CoV-2: genomics, transmissibility, and responses to current COVID-19 vaccines. J Med Virol 94:1825–1832. https://doi.org/10.1002/jmv.27588.
13. Ostrov DA, Knox GW. 2022. Emerging mutation patterns in SARS-CoV-2 variants. Biochem Biophys Res Commun 586:87–92. https://doi.org/10.1016/j.bbrc.2021.11.059.
14. Winstone H, Lista MJ, Reid AC, Bouton C, Pickering S, Galao RP, Kerridge C, Doores KJ, Swanson CM, Neil SJD. 2021. The polybasic cleavage site in SARS-CoV-2 spike modulates viral sensitivity to type I interferon and IFITM2. J Virol 95:e02422-20. https://doi.org/10.1128/JVI.02422-20.
15. Shi G, Kenney AD, Kudryashova E, Zani A, Zhang L, Lai KK, Hall-Stoodley L, Robinson RT, Kudryashov DS, Compton AA, Yount JS. 2021. Opposing activities of IFITM proteins in SARS-CoV-2 infection. EMBO J 40:e106501. https://doi.org/10.15252/embj.2020106501.
16. Bailey CC, Zhong G, Huang IC, Farzan M. 2014. IFITM-family proteins: the cell's first line of antiviral defense. Annu Rev Virol 1:261–283. https://doi.org/10.1146/annurev-virology-031413-085537.

17. Shi G, Schwartz O, Compton AA. 2017. More than meets the I: the diverse antiviral and cellular functions of interferon-induced transmembrane proteins. Retrovirology 14:53. https://doi.org/10.1186/s12977-017-0377-y.
18. Jia R, Pan Q, Ding S, Rong L, Liu S-L, Geng Y, Qiao W, Liang C. 2012. The N-terminal region of IFITM3 modulates its antiviral activity by regulating IFITM3 cellular localization. J Virol 86:13697–13707. https://doi.org/10.1128/JVI.01828-12.
19. Jia R, Xu F, Qian J, Yao Y, Miao C, Zheng Y-M, Liu S-L, Guo F, Geng Y, Qiao W, Liang C. 2014. Identification of an endocytic signal essential for the antiviral action of IFITM3. Cell Microbiol 16:1080–1093. https://doi.org/10.1111/cmi.12262.
20. Liu Y, Liu J, Johnson BA, Xia H, Ku Z, Schindewolf C, Widen SG, An Z, Weaver SC, Menachery VD, Xie X, Shi PY. 2021. Delta spike P681R mutation enhances SARS-CoV-2 fitness over Alpha variant. bioRxiv. https://doi.org/10.1101/2021.08.12.456173.
21. Liu Y, Liu J, Johnson BA, Xia H, Ku Z, Schindewolf C, Widen SG, An Z, Weaver SC, Menachery VD, Xie X, Shi P-Y. 2022. Delta spike P681R mutation enhances SARS-CoV-2 fitness over Alpha variant. Cell Rep 39:110829. https://doi.org/10.1016/j.celrep.2022.110829.
22. Benlarbi M, Laroche G, Fink C, Fu K, Mulloy RP, Phan A, Ariana A, Stewart CM, Prévost J, Beaudoin-Bussières G, Daniel R, Bo Y, Yockell-Lelièvre J, Stanford WL, Giguère PM, Mubareka S, Finzi A, Dekaban GA, Dikeakos JD, Côté M. 2022. Identification of a SARS-CoV-2 host metalloproteinase-dependent entry pathway differentially used by SARS-CoV-2 and variants of concern Alpha, Delta, and Omicron. bioRxiv. https://doi.org/10.1016/j.isci.2022.105316.
23. Korber B, Fischer WM, Gnanakaran S, Yoon H, Theiler J, Abfalterer W, Hengartner N, Giorgi EE, Bhattacharya T, Foley B, Hastie KM, Parker MD, Partridge DG, Evans CM, Freeman TM, de Silva TI, McDanal C, Perez LG, Tang H, Moon-Walker A, Whelan SP, LaBranche CC, Saphire EO, Montefiori DC, Sheffield COVID-19 Genomics Group. 2020. Tracking changes in SARS-CoV-2 spike: evidence that D614G increases infectivity of the COVID-19 virus. Cell 182:812–827.E19. https://doi.org/10.1016/j.cell.2020.06.043.
24. Zhao X, Guo F, Liu F, Cuconati A, Chang J, Block TM, Guo J-T. 2014. Interferon induction of IFITM proteins promotes infection by human coronavirus OC43. Proc Natl Acad Sci U S A 111:6756–6761. https://doi.org/10.1073/pnas.1320856111.
25. Prelli Bozzo C, Nchioua R, Volcic M, Koepke L, Krüger J, Schütz D, Heller S, Stürzel CM, Kmiec D, Conzelmann C, Müller J, Zech F, Braun E, Groß R, Wettstein L, Weil T, Weiß J, Diofano F, Rodríguez Alfonso AA, Wiese S, Sauter D, Münch J, Goffinet C, Catanese A, Schön M, Boeckers TM, Stenger S, Sato K, Just S, Kleger A, Sparrer KMJ, Kirchhoff F. 2021. IFITM proteins promote SARS-CoV-2 infection and are targets for virus inhibition in vitro. Nat Commun 12:4584. https://doi.org/10.1038/s41467-021-24817-y.
26. Petrillo C, Thorne LG, Unali G, Schiroli G, Giordano AMS, Piras F, Cuccovillo I, Petit SJ, Ahsan F, Noursadeghi M, Clare S, Genovese P, Gentner B, Naldini L, Towers GJ, Kajaste-Rudnitski A. 2018. Cyclosporine H overcomes innate immune restrictions to improve lentiviral transduction and gene editing in human hematopoietic stem cells. Cell Stem Cell 23:820–832.E9. https://doi.org/10.1016/j.stem.2018.10.008.
27. Mesner D, Reuschl A-K, Whelan MVX, Bronzovich T, Haider T, Thorne LG, Towers GJ, Jolly C. 2022. SARS-CoV-2 Spike evolution influences GBP and IFITM sensitivity. bioRxiv. https://doi.org/10.1101/2022.03.07.481785.
28. Chen H-Y, Huang C, Tian L, Huang X, Zhang C, Llewellyn GN, Rogers GL, Andresen K, O'Gorman MRG, Chen Y-W, Cannon PM. 2021. Cytoplasmic tail truncation of SARS-CoV-2 spike protein enhances titer of pseudotyped vectors but masks the effect of the D614G mutation. J Virol 95:e00966-21. https://doi.org/10.1128/JVI.00966-21.
29. Jackson CB, Farzan M, Chen B, Choe H. 2022. Mechanisms of SARS-CoV-2 entry into cells. Nat Rev Mol Cell Biol 23:3–20. https://doi.org/10.1038/s41580-021-00418-x.
30. Jouvenet N, Goujon C, Banerjee A. 2021. Clash of the titans: interferons and SARS-CoV-2. Trends Immunol 42:1069–1072. https://doi.org/10.1016/j.it.2021.10.009.
31. Thorne LG, Bouhaddou M, Reuschl A-K, Zuliani-Alvarez L, Polacco B, Pelin A, Batra J, Whelan MVX, Hosmillo M, Fossati A, Ragazzini R, Jungreis I, Ummadi M, Rojc A, Turner J, Bischof ML, Obernier K, Braberg H, Soucheray M, Richards A, Chen K-H, Harjai B, Memon D, Hiatt J, Rosales R, McGovern BL, Jahun A, Fabius JM, White K, Goodfellow IG, Takeuchi Y, Bonfanti P, Shokat K, Jura N, Verba K, Noursadeghi M, Beltrao P, Kellis M, Swaney DL, García-Sastre A, Jolly C, Towers GJ, Krogan NJ. 2022. Evolution of enhanced innate immune evasion by SARS-CoV-2. Nature 602:487–495. https://doi.org/10.1038/s41586-021-04352-y.
32. Guo K, Barrett BS, Mickens KL, Vladar EK, Morrison JH, Hasenkrug KJ. 2021. Interferon resistance of emerging SARS-CoV-2 variants. bioRxiv. https://doi.org/10.1073/pnas.2203760119.
33. Takeda M. 2022. Proteolytic activation of SARS-CoV-2 spike protein. Microbiol Immunol 66:15–23. https://doi.org/10.1111/1348-0421.12945.
34. Lubinski B, Fernandes MHV, Frazier L, Tang T, Daniel S, Diel DG, Jaimes JA, Whittaker G. 2021. Functional evaluation of the P681H mutation on the proteolytic activation the SARS-CoV-2 variant B.1.1.7 (Alpha) spike. bioRxiv. https://doi.org/10.1016/j.isci.2021.103589.
35. Ramdas P, Sahu AK, Mishra T, Bhardwaj V, Chande A. 2020. From entry to egress: strategic exploitation of the cellular processes by HIV-1. Front Microbiol 11:559792. https://doi.org/10.3389/fmicb.2020.559792.
36. Roy S, Ghani K, de Campos-Lima PO, Caruso M. 2021. A stable platform for the production of virus-like particles pseudotyped with the severe acute respiratory syndrome coronavirus-2 (SARS-CoV-2) spike protein. Virus Res 295:198305. https://doi.org/10.1016/j.virusres.2021.198305.
37. Kreutzberger AJB, Sanyal A, Saminathan A, Bloyet LM, Stumpf S, Liu Z, Ojha R, Patjas MT, Geneid A, Scanavachi G, Doyle C, Somerville E, Da Cunha Correira RB, Di Caprio G, Toppila-Salmi S, Makitie A, Kiessling V, Vapalahti O, Whelan SPJ, Balistreri G, Kirchhausen T. 2022. SARS-CoV-2 requires acidic pH to infect cells. bioRxiv.
38. Xu R, Shi M, Li J, Song P, Li N. 2020. Construction of SARS-CoV-2 virus-like particles by mammalian expression system. Front Bioeng Biotechnol 8:862. https://doi.org/10.3389/fbioe.2020.00862.
39. Peacock TP, Sheppard CM, Brown JC, Goonawardane N, Zhou J, Whiteley M, PHE Virology Consortium, de Silva TI, Barclay WS. 2021. The SARS-CoV-2 variants associated with infections in India, B.1.617, show enhanced spike cleavage by furin. bioRxiv. https://doi.org/10.1101/2021.05.28.446163.
40. Palatini M, Müller SF, Kirstgen M, Leiting S, Lehmann F, Soppa L, Goldmann N, Müller C, Lowjaga KAAT, Alber J, Ciarimboli G, Ziebuhr J, Glebe D, Geyer J. 2022. IFITM3 interacts with the HBV/HDV receptor NTCP and modulates virus entry and infection. Viruses 14:727. https://doi.org/10.3390/v14040727.
41. Zhao X, Sehgal M, Hou Z, Cheng J, Shu S, Wu S, Guo F, Le Marchand SJ, Lin H, Chang J, Guo J-T. 2018. Identification of residues controlling restriction versus enhancing activities of IFITM proteins on entry of human coronaviruses. J Virol 92:e01535-17. https://doi.org/10.1128/JVI.01535-17.
42. Guo K, Barrett BS, Mickens KL, Hasenkrug KJ, Santiago ML. 2021. Interferon resistance of emerging SARS-CoV-2 variants. bioRxiv. https://doi.org/10.1073/pnas.2203760119.
43. Thorne LG, Bouhaddou M, Reuschl AK, Zuliani-Alvarez L, Polacco B, Pelin A, Batra J, Whelan MVX, Ummadi M, Rojc A, Turner J, Obernier K, Braberg H, Soucheray M, Richards A, Chen KH, Harjai B, Memon D, Hosmillo M, Hiatt J, Jahun A, Goodfellow IG, Fabius J, Shokat K, Jura N, Verba K, Noursadeghi M, Beltrao P, Swaney DL, Garcia-Sastre A, Jolly C, Towers GJ, Krogan NJ. 2021. Evolution of enhanced innate immune evasion by the SARS-CoV-2 B.1.1.7 UK variant. bioRxiv. https://doi.org/10.1038/s41586-021-04352-y.
44. Schoggins JW. 2014. Interferon-stimulated genes: roles in viral pathogenesis. Curr Opin Virol 6:40–46. https://doi.org/10.1016/j.coviro.2014.03.006.
45. Planas D, Veyer D, Baidaliuk A, Staropoli I, Guivel-Benhassine F, Rajah MM, Planchais C, Porrot F, Robillard N, Puech J, Prot M, Gallais F, Gantner P, Velay A, Le Guen J, Kassis-Chikhani N, Edriss D, Belec L, Seve A, Courtellemont L, Péré H, Hocqueloux L, Fafi-Kremer S, Prazuck T, Mouquet H, Bruel T, Simon-Lorière E, Rey FA, Schwartz O. 2021. Reduced sensitivity of SARS-CoV-2 variant Delta to antibody neutralization. Nature 596:276–280. https://doi.org/10.1038/s41586-021-03777-9.
46. Mahase E. 2021. Covid-19: Novavax vaccine efficacy is 86% against UK variant and 60% against South African variant. BMJ 372:n296. https://doi.org/10.1136/bmj.n296.
47. Shen X, Tang H, McDanal C, Wagh K, Fischer W, Theiler J, Yoon H, Li D, Haynes BF, Sanders KO, Gnanakaran S, Hengartner N, Pajon R, Smith G, Glenn GM, Korber B, Montefiori DC. 2021. SARS-CoV-2 variant B.1.1.7 is susceptible to neutralizing antibodies elicited by ancestral spike vaccines. Cell Host Microbe 29:529–539.E3. https://doi.org/10.1016/j.chom.2021.03.002.
48. Kemp SA, Collier DA, Datir RP, Ferreira IATM, Gayed S, Jahun A, Hosmillo M, Rees-Spear C, Mlcochova P, Lumb IU, Roberts DJ, Chandra A, Temperton N, Sharrocks K, Blane E, Modis Y, Leigh KE, Briggs JAG, van Gils MJ, Smith KGC, Bradley JR, Smith C, Doffinger R, Ceron-Gutierrez L, Barcenas-Morales G, Pollock DD, Goldstein RA, Smielewska A, Skittrall JP, Gouliouris T, Goodfellow IG, Gkrania-Klotsas E, Illingworth CJR, McCoy LE, Gupta RK, COVID-19 Genomics UK (COG-UK) Consortium. 2021. SARS-CoV-2 evolution during treatment of chronic infection. Nature 592:277–282. https://doi.org/10.1038/s41586-021-03291-y.

49. Corey L, Beyrer C, Cohen MS, Michael NL, Bedford T, Rolland M. 2021. SARS-CoV-2 variants in patients with immunosuppression. N Engl J Med 385:562–566. https://doi.org/10.1056/NEJMsb2104756.
50. Lupala CS, Ye Y, Chen H, Su XD, Liu H. 2022. Mutations on RBD of SARS-CoV-2 Omicron variant result in stronger binding to human ACE2 receptor. Biochem Biophys Res Commun 590:34–41. https://doi.org/10.1016/j.bbrc.2021.12.079.
51. Yamamoto M, Tomita K, Hirayama Y, Inoue J-i, Kawaguchi Y, KaJ G. 2022. SARS-CoV-2 Omicron spike H655Y mutation is responsible for enhancement of the endosomal entry pathway and reduction of cell surface entry pathways. bioRxiv. https://doi.org/10.1101/2022.03.21.485084.
52. Yamamoto M, Gohda J, Kobayashi A, Tomita K, Hirayama Y, Koshikawa N, Seiki M, Semba K, Akiyama T, Kawaguchi Y, Inoue J-i. 2022. Metalloproteinase-dependent and TMPRSS2-independent cell surface entry pathway of SARS-CoV-2 requires the furin cleavage site and the S2 domain of spike protein. mBio 13:e00519-22. https://doi.org/10.1128/mbio.00519-22.
53. Garcia NK, Lee KK. 2016. Dynamic viral glycoprotein machines: approaches for probing transient states that drive membrane fusion. Viruses 8:15. https://doi.org/10.3390/v8010015.
54. Foster TL, Wilson H, Iyer SS, Coss K, Doores K, Smith S, Kellam P, Finzi A, Borrow P, Hahn BH, Neil SJD. 2016. Resistance of transmitted founder HIV-1 to IFITM-mediated restriction. Cell Host Microbe 20:429–442. https://doi.org/10.1016/j.chom.2016.08.006.
55. Fenton-May AE, Dibben O, Emmerich T, Ding H, Pfafferott K, Aasa-Chapman MM, Pellegrino P, Williams I, Cohen MS, Gao F, Shaw GM, Hahn BH, Ochsenbauer C, Kappes JC, Borrow P. 2013. Relative resistance of HIV-1 founder viruses to control by interferon-alpha. Retrovirology 10:146. https://doi.org/10.1186/1742-4690-10-146.
56. Cantuti-Castelvetri L, Ojha R, Pedro LD, Djannatian M, Franz J, Kuivanen S, van der Meer F, Kallio K, Kaya T, Anastasina M, Smura T, Levanov L, Szirovicza L, Tobi A, Kallio-Kokko H, Österlund P, Joensuu M, Meunier FA, Butcher SJ, Winkler MS, Mollenhauer B, Helenius A, Gokce O, Teesalu T, Hepojoki J, Vapalahti O, Stadelmann C, Balistreri G, Simons M. 2020. Neuropilin-1 facilitates SARS-CoV-2 cell entry and infectivity. Science 370:856–860. https://doi.org/10.1126/science.abd2985.
57. Daly JL, Simonetti B, Klein K, Chen K-E, Williamson MK, Antón-Plágaro C, Shoemark DK, Simón-Gracia L, Bauer M, Hollandi R, Greber UF, Horvath P, Sessions RB, Helenius A, Hiscox JA, Teesalu T, Matthews DA, Davidson AD, Collins BM, Cullen PJ, Yamauchi Y. 2020. Neuropilin-1 is a host factor for SARS-CoV-2 infection. Science 370:861–865. https://doi.org/10.1126/science.abd3072.
58. Qing E, Kicmal T, Kumar B, Hawkins GM, Timm E, Perlman S, Gallagher T. 2021. Dynamics of SARS-CoV-2 spike proteins in cell entry: control elements in the amino-terminal domains. mBio 12:e01590-21. https://doi.org/10.1128/mBio.01590-21.
59. Braun E, Hotter D, Koepke L, Zech F, Groß R, Sparrer KMJ, Müller JA, Pfaller CK, Heusinger E, Wombacher R, Sutter K, Dittmer U, Winkler M, Simmons G, Jakobsen MR, Conzelmann K-K, Pöhlmann S, Münch J, Fackler OT, Kirchhoff F, Sauter D. 2019. Guanylate-binding proteins 2 and 5 exert broad antiviral activity by inhibiting furin-mediated processing of viral envelope proteins. Cell Rep 27:2092–2104.E10. https://doi.org/10.1016/j.celrep.2019.04.063.
60. Tartour K, Appourchaux R, Gaillard J, Nguyen X-N, Durand S, Turpin J, Beaumont E, Roch E, Berger G, Mahieux R, Brand D, Roingeard P, Cimarelli A. 2014. IFITM proteins are incorporated onto HIV-1 virion particles and negatively imprint their infectivity. Retrovirology 11:103. https://doi.org/10.1186/s12977-014-0103-y.
61. Brown JC, Goldhill DH, Zhou J, Peacock TP, Frise R, Goonawardane N, Baillon L, Kugathasan R, Pinto AL, McKay PF, Hassard J, Moshe M, Singanayagam A, Burgoyne T, the ATACCC Investigators, PHE Virology Consortium, Barclay W. 2021. Increased transmission of SARS-CoV-2 lineage B.1.1.7 (VOC 2020212/01) is not accounted for by a replicative advantage in primary airway cells or antibody escape. bioRxiv. https://doi.org/10.1101/2021.02.24.432576.
62. Thi Nhu Thao T, Labroussaa F, Ebert N, V'kovski P, Stalder H, Portmann J, Kelly J, Steiner S, Holwerda M, Kratzel A, Gultom M, Schmied K, Laloli L, Hüsser L, Wider M, Pfaender S, Hirt D, Cippà V, Crespo-Pomar S, Schröder S, Muth D, Niemeyer D, Corman VM, Müller MA, Drosten C, Dijkman R, Jores J, Thiel V. 2020. Rapid reconstruction of SARS-CoV-2 using a synthetic genomics platform. Nature 582:561–565. https://doi.org/10.1038/s41586-020-2294-9.
63. Gaida A, Becker MM, Schmid CD, Buhlmann T, Louis EJ, Beck HP. 2011. Cloning of the repertoire of individual Plasmodium falciparum var genes using transformation associated recombination (TAR). PLoS One 6:e17782. https://doi.org/10.1371/journal.pone.0017782.
64. Rihn SJ, Merits A, Bakshi S, Turnbull ML, Wickenhagen A, Alexander AJT, Baillie C, Brennan B, Brown F, Brunker K, Bryden SR, Burness KA, Carmichael S, Cole SJ, Cowton VM, Davies P, Davis C, De Lorenzo G, Donald CL, Dorward M, Dunlop JI, Elliott M, Fares M, da Silva Filipe A, Freitas JR, Furnon W, Gestuveo RJ, Geyer A, Giesel D, Goldfarb DM, Goodman N, Gunson R, Hastie CJ, Herder V, Hughes J, Johnson C, Johnson N, Kohl A, Kerr K, Leech H, Lello LS, Li K, Lieber G, Liu X, Lingala R, Loney C, Mair D, McElwee MJ, McFarlane S, Nichols J, et al. 2021. A plasmid DNA-launched SARS-CoV-2 reverse genetics system and coronavirus toolkit for COVID-19 research. PLoS Biol 19:e3001091. https://doi.org/10.1371/journal.pbio.3001091.
65. da Silva Filipe A, Shepherd JG, Williams T, Hughes J, Aranday-Cortes E, Asamaphan P, Ashraf S, Balcazar C, Brunker K, Campbell A, Carmichael S, Davis C, Dewar R, Gallagher MD, Gunson R, Hill V, Ho A, Jackson B, James E, Jesudason N, Johnson N, McWilliam Leitch EC, Li K, MacLean A, Mair D, McAllister DA, McCrone JT, McDonald SE, McHugh MP, Morris AK, Nichols J, Niebel M, Nomikou K, Orton RJ, O'Toole Á, Palmarini M, Parcell BJ, Parr YA, Rambaut A, Rooke S, Shaaban S, Shah R, Singer JB, Smollett K, Starinskij I, Tong L, Sreenu VB, Wastnedge E, Holden MTG, Robertson DL, COVID-19 Genomics UK (COG-UK) Consortium, et al. 2021. Genomic epidemiology reveals multiple introductions of SARS-CoV-2 from mainland Europe into Scotland. Nat Microbiol 6:112–122. https://doi.org/10.1038/s41564-020-00838-z.
66. Pickering S, Batra R, Merrick B, Snell LB, Nebbia G, Douthwaite S, Reid F, Patel A, Kia Ik MT, Patel B, Charalampous T, Alcolea-Medina A, Lista MJ, Cliff PR, Cunningham E, Mullen J, Doores KJ, Edgeworth JD, Malim MH, Neil SJD, Galão RP. 2021. Comparative performance of SARS-CoV-2 lateral flow antigen tests and association with detection of infectious virus in clinical specimens: a single-centre laboratory evaluation study. Lancet Microbe 2:e461–e471. https://doi.org/10.1016/S2666-5247(21)00143-9.
67. Chesebro B, Wehrly K, Nishio J, Perryman S. 1992. Macrophage-tropic human immunodeficiency virus isolates from different patients exhibit unusual V3 envelope sequence homogeneity in comparison with T-cell-tropic isolates: definition of critical amino acids involved in cell tropism. J Virol 66:6547–6554.